
Practical Channel Hydraulics

Practical Channel Hydraulics

Roughness, Conveyance and Afflux

Donald W. Knight

The University of Birmingham, Birmingham, UK

Caroline Mc Gahey

HR Wallingford, Wallingford, Oxfordshire, UK

Rob Lamb

JBA Consulting, Skipton, North Yorkshire, UK

Paul G. Samuels

HR Wallingford, Wallingford, Oxfordshire, UK



CRC Press

Taylor & Francis Group

Boca Raton London New York Leiden

CRC Press is an imprint of the
Taylor & Francis Group, an **informa** business

A BALKEMA BOOK

CRC Press/Balkema is an imprint of the Taylor & Francis Group, an informa business

© 2010 Taylor & Francis Group, London, UK

Typeset by Vikatan Publishing Solutions (P) Ltd, Chennai, India.

Printed and bound in Great Britain by TJ International Ltd, Padstow, Cornwall

All rights reserved. No part of this publication or the information contained herein may be reproduced, stored in a retrieval system, or transmitted in any form or by any means, electronic, mechanical, by photocopying, recording or otherwise, without written prior permission from the publisher.

Although all care is taken to ensure integrity and the quality of this publication and the information herein, no responsibility is assumed by the publishers nor the authors for any damage to the property or persons as a result of operation or use of this publication and/or the information contained herein.

Published by: CRC Press/Balkema

P.O. Box 447, 2300 AK Leiden, The Netherlands

e-mail: Pub.NL@taylorandfrancis.com

www.crcpress.com – www.taylorandfrancis.co.uk – www.balkema.nl

Library of Congress Cataloging-in-Publication Data

Knight, Donald W.

Practical channel hydraulics : roughness, conveyance, and afflux /

Donald W. Knight ... [et al.]

p. cm.

Includes bibliographical references and indexes.

ISBN 978-0-415-54974-5 (hardcover : alk. paper) – ISBN 978-0-203-86418-0

(e-book) I. Channels (Hydraulic engineering) I. Title.

TC175.K55 2010

627'.042–dc22

2009026759

ISBN: 978-0-415-54974-5 (Hbk)

ISBN: 978-0-203-86418-0 (eBook)

Contents

<i>Foreword</i>	xi
<i>Acknowledgements</i>	xiii
<i>Notation</i>	xv
<i>Acronyms</i>	xxi
<i>Glossary of terms</i>	xxiii
I Introduction	I
1.1 Context and motivation for book	1
1.2 Scope of book and introduction to the CES-AES	6
1.3 Limitations of the CES-AES	7
1.4 Outline of book	8
1.5 Origin of the CES-AES	9
2 Practical and theoretical issues in channel hydraulics	15
2.1 Getting started with some practical examples on calculating flows in watercourses	15
2.2 Common difficulties in modelling flow in rivers and watercourses	24
2.2.1 Modelling flow in rivers and watercourses	25
2.2.2 Schematisation of channel geometry	26
2.2.3 Roughness and resistance	29

2.2.4	Energy and friction slopes	33
2.2.5	Velocity distributions and implications for 1-D modelling	37
2.2.6	Hydraulic structures and controls	42
2.2.7	Calibration data for river models	44
2.3	Flow in simple engineered channels	45
2.3.1	Flows in rectangular channels	50
2.3.2	Flows in trapezoidal channels	54
2.4	Inbank flow in natural rivers	57
2.5	Overbank flow in natural and engineered rivers	59
2.5.1	Overbank flow in an engineered river	60
2.5.2	Overbank flow in a natural river	64
2.6	Flows through bridges and culverts	69
2.6.1	Flows through bridges and contractions	69
2.6.2	Flows through culverts	77
2.6.3	Head-discharge and afflux relationships	77
2.6.4	Geometrical parameters affecting flow through bridges	78
2.7	Data sources used in this book	87
2.7.1	Conveyance data	87
2.7.2	Bridge afflux data	88
3	Understanding roughness, conveyance and afflux	93
3.1	Flow structures in open channel flow	93
3.1.1	Boundary shear	93
3.1.2	Vertical interfacial shear	95
3.1.3	Transverse currents	95
3.1.4	Coherent structures	97

3.1.5	Horizontal interfacial shear	100
3.1.6	Vorticity in rivers	102
3.1.7	Special features near structures	103
3.2	Governing equations	105
3.2.1	Roughness Advisor methods	105
3.2.2	Conveyance Estimation System methods	110
3.2.3	Summary of CES methods, outputs and solution technique	129
3.2.4	Backwater calculation methods	138
3.2.5	Afflux Estimation System methods	140
3.3	Dealing with uncertainty	161
3.3.1	Introduction to uncertainty	161
3.3.2	Risk, uncertainty, accuracy and error	162
3.3.3	Components of uncertainty in the CES	163
3.3.4	Representation and assessment of uncertainty	166
3.4	Introduction to the CES-AES software	169
3.4.1	Introduction to the Roughness Advisor	171
3.4.2	Introduction to the Conveyance Generator	175
3.4.3	Introduction to the Backwater Module	175
3.4.4	Introduction to the Afflux Estimation System	178
4	Practical issues – roughness, conveyance and afflux	183
4.1	An overview of the CES-AES use in practice	183
4.1.1	Single cross-section analysis	184
4.1.2	Single structure analysis (bridges and culverts)	186
4.1.3	Backwater profile analysis (no structures present)	188
4.1.4	Backwater profile analysis (structures present)	189

4.2	Estimating and using stage-discharge relationships and spatial velocities	189
4.2.1	Stage-discharge prediction for the River Trent at Yoxall, Staffordshire, UK	189
4.2.2	Stage-discharge and velocity prediction for the River Colorado, La Pampas, Argentina	192
4.2.3	Hierarchical approach to estimating roughness (and other flow parameters) for the River Main, County Antrim, UK	195
4.2.4	Stage-discharge, velocity and roughness predictions for the River Severn at Montford Bridge, UK	201
4.2.5	Investigating the influence of roughness, slope and sinuosity on stage-discharge for the River La Suela, Cordoba, Argentina	205
4.2.6	Application of the CES to a mountain stream with boulders	213
4.3	Use of backwater module for estimating water levels along the River Main	218
4.4	Estimating afflux at bridges	221
4.4.1	Field scale verification of bridge backwater analysis at Pea Creek, Alabama	221
4.4.2	Field scale bridge backwater analysis on the River Irwell, UK	227
4.5	Estimating afflux at culverts	233
4.5.1	Shallow culvert backwater analysis in a long reach	233
4.5.2	Exploratory culvert design and maintenance calculations in CES-AES	235
4.6	Dealing with vegetation and maintenance of weedy rivers	243
4.6.1	Exploration of cutting regimes for the River Cole	244
4.6.2	Exploration of different cutting regimes for the River Avon	249
4.6.3	Exploration of channel deepening for the River Hooke	252

5 Further issues on flows in rivers	255
5.1 Ecological issues	255
5.2 Sediment and geomorphological issues	258
5.3 Trash screen and blockage issues	263
5.4 Wider modelling issues	266
5.4.1 Types of model	266
5.4.2 Implications involved in model selection, calibration and use	273
5.4.3 The CES-AES software in context	275
5.5 Software architecture and calculation engines	276
6 Concluding remarks	283
6.1 Concluding remarks	283
6.2 Future developments	289
Appendix I The finite element approximations for the CES equations	295
Appendix 2 Summary of hydraulic equations used in the AES	299
Appendix 3 Cross-section survey data	301
<i>References</i>	305
<i>Author index</i>	331
<i>Subject index</i>	335
<i>Colour plates</i>	339

Foreword

Forty years ago as an MSc student studying Civil Engineering hydraulics, I read the excellent '*History of Hydraulics*' by Hunter Rouse and Simon Ince. I was impressed by two common strands to many of the advances in hydraulics over the centuries. First, developments were largely driven by the needs of society. Second, these developments were usually done by practical scientists and engineers who, while building on the scientific knowledge of that day, had a good understanding of engineering application and got involved in some inspiring experimental research – often at field scale.

There are elements of all the above in *Practical channel hydraulics* and its origins. With regard to societal need, the principal driver of the research and development covered by the book has been improved flood risk management in the United Kingdom. The subject matter is of course relevant to many other applications of open channel hydraulics throughout the world.

For effective design or management of the channels and structures associated with flood defence and land drainage, practitioners must be able to predict accurately the water level at the relevant flood or storm conditions. The local increase in water level (afflux effect) caused by flow constriction at bridges and culverts is particularly important as these structures are often located close to human settlement or some other important infrastructure or environmental features that will be affected by flooding. Key requirements that have driven the tools (the *Conveyance Estimation System or CES* and the *Afflux Estimation System or AES*) associated with this book are the ability (a) to understand the sensitivity of water level to the various physical parameters that determine it, and (b) to plan ‘interventions’ such as cutting vegetation in channels or installing a culvert that might reduce the required performance of the flood management or land drainage system.

Most rivers or watercourses in today’s world are multi-functional – as one might say ‘One river, many users’ – not least the flora and fauna who cannot speak for themselves! Fortunately their interests are covered in most countries by legislation, such as the Water Framework Directive in Europe, and by statutory and voluntary organisations and individuals. Channel management usually involves a dialogue with other users. A particular driver for the CES was the need to help those planning engineering works or management activities to provide evidence to, and to explore options with, others having different interests in the same channel.

Perhaps the strongest driver for the tools described in this book has been the consensus reached by the UK flood management community in 2000 that there would be significant benefit from developing new practical computer-based tools for the

estimation of water level in channels. Therefore the UK authorities, led by the Environment Agency but with support from the Scottish Government and Rivers Agency Northern Ireland, have funded the programme of R&D needed to draw together the advances in the underlying science and to make this available in a practical and useful form to practitioners. This national programme involving both researchers and practitioners was deemed necessary in order to bridge the so-called ‘implementation gap’ between the available science and its application.

To return to the *History of Hydraulics*, Antoine Chezy (who is a senior figure in hall of fame of channel hydraulicians) made an interesting and relevant comment to the French Academy of Sciences in the 1760s when he proposed his original formula for determining the required channel cross-section to convey a given discharge (in this case the water supply to Paris). He remarked that ‘... *It would also be interesting to have similar observations on different brooks and streams, but it is important to note that all these observations require the greatest care, that it is difficult to make them with sufficient precision, and that one should count only on those which are made by people known for giving the most scrupulous attention*’.

Practical channel hydraulics would certainly have pleased Chezy with the extent of data that it either contains or references through the related website (www.river-conveyance.net). I am sure that Chezy would also have approved of the care and scrupulous attention that has been given to the supporting programmes of research and development described in Section 1.5. The programme of research in the former UK Flood Channel Facility was world class and the scientific publications resulting from it have made a significant contribution to the literature. For promoting this as well as for the initiative to produce the book, we owe particular gratitude to Professor Donald Knight. However, I must also express gratitude to the other authors each of whom has contributed an important part of the book. They are all leaders in their respective fields. Chezy would have found them all to be the type of people he could count on!

Dr. Mervyn Bramley
OBE Engineer and Environmentalist,
Formerly Head of R&D Environment Agency
Bristol,
April 2009

Acknowledgements

With a book of this nature it will be only too evident that the Authors owe a considerable debt to many colleagues, research workers and practitioners who have contributed so much to its origin and present form. Several institutions have also been involved, notably the Environment Agency (EA) and the Engineering and Physical Sciences Research Council (EPSRC), both of whom funded the foundational research undertaken in the Flood Channel Facility (FCF) built at HR Wallingford, and related research carried out at various UK Universities. Other organisations include the Natural Environment Research Council (NERC), the Scottish Government, the Rivers Agency in Northern Ireland and the Association of Drainage Authorities. Especial thanks are due to Mervyn Bramley, formerly Head of R&D at the EA, who supported this collaborative work from the beginning and who has played a crucial role in getting this book to its present state.

The Authors gratefully acknowledge the EA team for their considerable efforts in bringing this book to fruition, namely Dr. Mitchell, Mr. Robinson, Dr. Baxter, Mr. Tustin and Ms. Eleanor. The views expressed in this book are, however, personal and the publication does not imply endorsement by either the EA or the Department for Environment, Food and Rural Affairs (Defra).

The Authors would like to thank various staff at HR Wallingford (Ms. Escarameia, Professor Bettess, Mr. Wills), Wallingford Software (Messrs. Fortune, Millington, Nex, Gunn and Body and Dr. Daniels) and JBA Consulting (Mr. Benn, Dr. Mantz, Dr. Atabay, Mr. Rose) who were involved in the original CES-AES development. In particular, Rob Millington has contributed substantially to the ongoing CES-AES software development as well as the documentation within this book. The CES-AES programme has also benefited from a wide range of valuable inputs outside of these organisations. Notably, the contributions of Ms. Fisher (Independent) and Drs. Dawson and O'Hare (CEH) on channel and vegetation roughness as well as Messrs. Evans, Pepper, Rickard, Spencer and Sisson, Drs. Ervine, Whitlow, Khatibi, Hamill and Riddell and Professors Pender and Wright.

The Authors would also like to acknowledge the input of many former research students at the University of Birmingham who provided much of the data referred to herein, notably Drs. Abril, Ayyoubzadeh, Brown, Chlebek, Macdonald, Mohammadi, Omran, Patel, Rezaei, Rhodes, Yuen, Professors Al-Hamid, Atabay and Lai, to name but a few. Those who led the first phase of work in the FCF at HR Wallingford, Professor Sellin, Drs. Myers and Wormleaton, together with their assistants, deserve special praise for their painstaking efforts.

Professor Shiono, of Loughborough University, whose outstanding work whilst collaborating with one of the Authors led to the development of the theoretical basis for the Shiono & Knight Method (SKM), deserves special mention. His continuing research into the nature of turbulent flow behaviour in open channels, sustained over many years, has advanced our understanding of turbulence phenomena significantly. Dr. Tang, of Birmingham University, also deserves recognition for his continued analysis and development of the SKM in recent years.

Finally, particular thanks are due to five individuals who kindly read the text and made critical and exceptionally helpful comments on it in the later stages of its preparation, namely Mr. Ramsbottom, Professor Bettess, Drs. Myers, Sterling, and Wormleaton. Without their valuable scrutiny the book would be less than it currently is. The Authors are, of course, responsible for any remaining errors and deficiencies.

Notation

A	cross-sectional area; coefficient in logarithmic velocity law, Eq. (2.49);	(m ²)
A_{ac}	Ackers' coefficient – function of D_{gr} , Table 5.2;	
a	coefficient for Colebrook-White equation, Eq. (3.12);	
B	amplitude, Eq. (5.14);	(m)
	channel width; coefficient in logarithmic velocity law, Eq. (2.49); barrel span;	(m)
B_{RD}	roadway width across channel above culvert or bridge;	(m)
b	channel base width; semi breadth; pier width;	(m)
b	coefficient for Colebrook-White equation, Eq. (3.12);	
C	Chezy coefficient, Eq. (2.23);	(m ^{1/2} s ⁻¹)
C	weir discharge coefficient, Eq. (3.60);	
C_{ac}	Ackers' coefficient – function of D_{gr} , Table 5.2;	
C_C	contraction energy loss coefficient applied upstream of bridge or culvert, Eq. (3.63);	
C_E	expansion energy loss coefficient applied downstream of bridge or culvert, Eq. (3.63);	
C_d	discharge coefficient, Eq. (3.59);	
COH	channel coherence (Ackers, 1991–93);	
C_{uv}	coefficient for sinuosity, Eqs. (3.29), (3.32) & (3.33);	
c	coefficient for Colebrook-White equation, Eq. (3.12);	
	wave celerity, Eq. (5.18);	(ms ⁻¹)
D	pipe diameter; culvert diameter; culvert depth when flowing full;	(m)
D	diffusion coefficient, Eq. (5.21);	(m ² s ⁻¹)
D_{gr}	dimensionless particle size number, Eq. (5.3);	
D_r	relative depth (= $(H - h)/H$), Figure (2.45) and Eq. (3.21);	
d	pipe diameter; sediment dimension;	(m)
d_{50}	median size diameter of sediment particles;	(m)
d_{90}	representative sediment size at 90% of distribution, Eq. (4.1);	(m)
E	specific energy, Eq. (2.12);	(m)
E_t	total energy, Eq. (2.39);	(m)
e	eccentricity, see Figure (2.66);	
F	force on fluid, Eq. (2.17);	(N)

F_g	force on sluice gate;	(N)
F_{gr}	particle mobility number, Eq. (5.2);	
Fr	Froude Number ($=U/(\sqrt{gA/T})$), Eq. (2.5);	
f	Darcy-Weisbach friction factor, Eqs. (2.24)–(2.27);	
f	local boundary friction factor in Eq. (2.58), adapted from Eq. (2.24) using U_d ;	
f, f_z, f_b, f_t	global, zonal, local and turbulent friction factors defined variously in Eq. (2.61);	
G_{gr}	sediment transport parameter, Eq. (5.1);	
g	gravitational acceleration; (ms^{-2})	
H	local water depth, Fig. (2.30) and Eq. (3.4); (m)	
H_i	water level above datum in some bridge afflux Figures, e.g. Fig. (2.53); (m)	
HWL_{ic}	Headwater level above datum for culvert under inlet control, Table (3.10); (m)	
HWL_{oc}	Headwater level above datum for culvert under outlet control, Table (3.10); (m)	
b	local water depth; (m)	
b_c	critical depth, see Eqs. (2.6)–(2.8) & (2.10); (m)	
b_f	head loss due to friction (m), Eq. (2.24); (m)	
b_{HW}	culvert head water depth, Fig. (3.48); (m)	
b_i	culvert inlet energy loss, Fig. (3.48); (m)	
b_n	normal depth, see Eqs. (2.2)–(2.4); (m)	
b_o	culvert outlet energy loss, Fig. (3.48); (m)	
b_{TW}	culvert tail water depth, Fig. (3.48); (m)	
Δh	water level difference (m); (m)	
I	inflow, Eq. (5.22) $(\text{m}^3\text{s}^{-1})$	
IL_i	culvert invert level above datum at the inlet, Fig. (3.48); (m)	
IL_o	culvert invert level above datum at the outlet, Fig. (3.48); (m)	
J_D	blockage ratio, Eq. (3.61);	
K	cross-sectional channel conveyance, Eq. (2.41); $(\text{m}^3\text{s}^{-1})$	
K_i	energy loss coefficient of i th mechanism, Eq. (3.2);	
k	roughness height (linked to k_s); (m)	
k_s	roughness height after Nikuradse (1933), as in Eqs. (2.26) & (2.30); (m)	
L	backwater length (m), as in Eq. (2.46); culvert or barrel length, length of bend; (m)	
L_C	contraction length upstream of bridge or culvert; (m)	
L_E	expansion length downstream of bridge or culvert; (m)	
L_W	culvert entrance length; (m)	
l	length of pipe or channel; (m)	
M	linear operator (FEM), as in Eq. (3.37);	
M	Momentum, as defined in Eq. (2.20); Manning Number ($=1/n$); $(\text{m}^{1/3}\text{s}^{-1})$	
M	bridge opening ratio ($=q/Q$), used in Section 2.6.1, see Figure (2.66);	

m_{ac}	Ackers' coefficient – function of D_{gr} , Table 5.2;	
n	Manning's resistance coefficient, Eq. (2.1);	$(\text{sm}^{-1/3})$
n_{ac}	Ackers' constant relating to grain size, Table 5.2;	
n_{clear}	Manning ' n ' when the channel is clear of vegetation;	$(\text{sm}^{-1/3})$
n_{irr}	unit roughness due to channel irregularities, Eq. (3.1);	$(\text{sm}^{-1/3})$
n_l	local or unit roughness, Eqs. (3.1) & (3.15);	$(\text{sm}^{-1/3})$
n_{sur}	unit roughness due to ground material, Eq. (3.1);	$(\text{sm}^{-1/3})$
n_{veg}	unit roughness due to vegetation, Eq. (3.1);	$(\text{sm}^{-1/3})$
O	outflow, Eq. (5.22);	$(\text{m}^3\text{s}^{-1})$
Q	total cross-section discharge;	$(\text{m}^3\text{s}^{-1})$
q	discharge per unit width ($=Q/B$ or Q/b), unit flow rate, Eq. (2.11); unfettered flow through a gap, as if the bridge or constriction was not in place	$(\text{m}^2\text{s}^{-1})$ $(\text{m}^3\text{s}^{-1})$
q^n	unit flow for iteration n (FEM);	$(\text{m}^2\text{s}^{-1})$
Δq^n	incremental change in q^n (FEM);	$(\text{m}^2\text{s}^{-1})$
q_s	volume of sediment transported per second per unit channel width;	$(\text{m}^2\text{s}^{-1});$
P	wetted channel perimeter; power as in Eq. (2.16);	$(\text{m}), (\text{W})$
per	percentage, Eq. (3.46);	$(\%)$
R	hydraulic radius ($=A/P$);	(m)
Re	Reynolds Number ($=UD/v$ for pipes and $4RU/v$ for open channels), Fig. (2.10);	
r	entrance rounding, see Figure (2.66);	(m)
S	longitudinal common uniform gradient in steady uniform flow, Eq. (2.41);	
S_e	longitudinal energy gradient, Eq. (2.40);	
S_f	longitudinal friction gradient, ($S_f = h_f/l$), Eq. (2.43);	
\bar{S}_f	reach-averaged friction slope, Eq. (2.44);	
S_{fx}	friction gradient in x -direction, Eq. (5.27);	
S_{fy}	friction gradient in y -direction, Eq. (5.27);	
S_o	longitudinal bed slope, see Figure (2.11);	
S_w	longitudinal water surface slope ($=\partial\eta/\partial x$), see Figure (2.11);	
S_y	local transverse bed slope, Eq. (3.6);	
s	channel side wall slope (1 : s , vertical : horizontal);	
T	top width of channel at water surface;	(m)
TW	tailwater depth;	(m)
t	time;	(s)
U	average cross-section velocity ($=Q/A$);	(ms^{-1})
U	velocity component in the x -direction (longitudinal), Eqs. (2.57);	(ms^{-1})
U_*	shear velocity ($=\sqrt{(\tau_o/\rho)}$, Eq. (2.31);	(ms^{-1})
U_d	depth-averaged streamwise velocity (x -direction), defined by Eq. (2.52);	(ms^{-1})
U_o	average cross-section velocity ($=Q/A$), Eq. (3.49);	(ms^{-1})

u	local velocity component in the x -direction (horizontal)	
	Eq. (2.47);	(ms ⁻¹)
u_{\max}	maximum velocity, as used in Eq. (2.55);	(ms ⁻¹)
u_*	local shear or friction velocity, Eq. (2.47);	(ms ⁻¹)
V	velocity component in the y -direction (lateral), Eq. (2.57) & (3.4);	(ms ⁻¹)
V	section mean velocity (in bridge afflux Figures from Hamill), Fig. 2.17);	(ms ⁻¹)
V_d	depth-averaged velocity (y -direction), Eq. (5.24);	(ms ⁻¹)
W	velocity component in the z -direction (vertical), Eq. (2.57);	(ms ⁻¹)
X_s	mass flux of sediment per mass flux of fluid, Eq. (5.6);	(ppm)
x	horizontal direction, streamwise in plan view;	(m)
x_s	unit mass sediment flux per unit mass of flow per unit time, Eq. (5.5);	(ppm)
\mathbf{x}	vector of all contributing functions that are independent of Δq^n (FEM);	
Y	water depth in some bridge afflux Figures, e.g. Fig. (2.62);	(m)
y	lateral direction across channel section;	(m)
y_o	tailwater depth downstream of culvert outlet;	(m)
z	vertical direction;	(m)
\bar{z}	distance of centre of area below water surface;	(m)
z_b	level of channel bed above datum;	(mAD)
z_o	roughness length ($=\gamma k_s$), Eq. (2.47);	(m)

Greek Alphabet

α	Coriolis or ‘kinetic energy’ correction coefficient, Eqs. (2.12), (2.53) & (3.54);	
β	Boussinesq or ‘momentum’ correction coefficient, Eqs. (2.17) & (2.54);	
Γ	secondary flow term for straight prismatic channels, Eq. (2.60);	
Γ_{ave}^*	average scaled secondary flow term, Eq. (3.24);	
$\Gamma_{\text{mc(trans)}}$	secondary flow term in the transitional main channel region, Eq. (3.28);	
Δ	increment, percentage change in;	(%)
γ	energy loss factor in Eq. (2.62); coefficient for z_o in Eq. (2.47);	
ε	eddy viscosity ($=\tau_{yx}/(\rho \partial U/\partial y)$);	(m ² s ⁻¹)
ε	weighting coefficient, Eq. (5.23);	
$\bar{\varepsilon}_{yx}$	depth-averaged eddy viscosity, Eq. (2.59);	(m ² s ⁻¹)
η	water level above datum ($=b + z$), Fig. (2.11);	(mAD)
κ	von Kármán’s constant, Eq. (2.47);	
λ	dimensionless depth-averaged eddy viscosity, Eq. (2.59) ($=\bar{\varepsilon}_{yx}/(U^*H)$);	
μ	dynamic viscosity;	(Nsm ⁻²)

ν	kinematic viscosity of the fluid ($=\mu/\rho$);	$(\text{m}^2\text{s}^{-1})$
ν_t	turbulent eddy viscosity, Eq. (3.4);	$(\text{m}^2\text{s}^{-1})$
ρ	fluid density;	(kgm^{-3})
σ	plan form channel sinuosity, length along river thalweg/length along valley slope;	
σ	blockage ratio ($=(B - b)/B$), Eq. (2.62), see Figure (2.66);	
τ_d, τ_{2d}	two-dimensional shear stress;	(Nm^{-2})
τ_o	boundary shear stress, Eq. (2.32);	(Nm^{-2})
τ_{yx}	Reynolds stresses on vertical plane, normal to y axis in x direction, Eq. (2.57);	(Nm^{-2})
$\bar{\tau}_{yx}$	depth-averaged value of τ_{yx} , Reynolds stresses on vertical plane, Eq. (2.59);	(Nm^{-2})
τ_{zx}	Reynolds stresses on horizontal plane, normal to z axis in x direction, Eq. (2.57);	(Nm^{-2})
ϕ	linear shape functions (FEM);	
ϕ_b	bend angle; skewness of bridge, see Figure (2.66);	$(^\circ)$
χ	relaxation factor, Eq. (3.36);	
ψ	projection onto plane due to choice of Cartesian coordinate system, Eqs. (3.4) & (3.6);	

Subscripts

ave	average;
fp	floodplain;
i	i th channel element;
mc	main channel;

Acronyms

AE	Aflux Estimator
AES	Aflux Estimation System
BM	Backwater Module
CAPM	Centre for Aquatic Plant Management
CES	Conveyance Estimation System
CFD	Computational Fluid Dynamics
CIRIA	Construction Industry Research and Information Association
CIWEM	Chartered Institution of Water and Environmental Management
CG	Conveyance Generator
COH	Coherence
COHM	Coherence Method
DCM	Divided Channel Method
Defra	Department for Environment, Food and Rural Affairs
DRF	Discharge Reduction Factor
DTi-SAM	System based Analysis and Management of flood risk
EA	Environment Agency
EC	European Commission
EPSRC	Engineering and Physical Sciences Research Council
EU	European Union
FCF	Flood Channel Facility
FE	Finite Element
FEH	Flood Estimation Handbook
FEM	Finite Element Method
FHWA	Federal Highways Administration
FRMRC	Flood Risk Management Research Consortium
HA	Hydrologic Atlas
HEC	Hydrologic Engineering Center (US Army Corps of Engineers)
HEC-RAS	HEC-River Analysis System (US Army Corps of Engineers)
HW	Head Water
ICE	Institution of Civil Engineers
InfoWorks RS	Hydrodynamic modelling software (Wallingford Software)
IPCC	Intergovernmental Panel on Climate Change
ISIS	Hydrodynamic modelling software (Halcrow)
ISO	International Standards Organisation
IWRS	InfoWorks RS (see above)

LiDAR	Light Detection And Ranging
LIFE	Lotic-invertebrate Index for Flow Evaluation
MAFF	Ministry of Agriculture, Fisheries and Food
MDSF	Modelling and Decision Support Framework
MIKE11	Hydrodynamic Modelling Software (Danish Hydraulic Institute)
NERC	Natural Environment Research Council
NIRA	Northern Ireland Rivers Agency
NIWA	National Institute of Water & Atmospheric research
NRA	National Rivers Authority
PAMS	Performance based Asset Management System
PDF	Probability Density Function
PHABSIM	Physical Habitat Simulator
RA	Roughness Advisor
RANS	Reynolds Averaged Navier-Stokes equations
RASP	Risk Assessment for Strategic Planning
RDL	Road Level
ReFEH	Revised Flood Estimation Handbook
RHABSIM	River Habitat Simulator
RHS	River Habitat Survey
SCM	Single Channel Method
SEPA	Scottish Environment Protection Agency
SFL	Soffit Level
SKM	Shiono & Knight Method
SMURF	Sustainable Management of Urban Rivers and Floodplains
SPL	Springer Level
SSSI	Site of Special Scientific Interest
TW	Tail Water
UE	Uncertainty Estimator
USBPR	United States Bureau of Public Roads
USGS	United States Geological Survey
VPMC	Variable Parameter Muskingum-Cunge method
WFD	Water Framework Directive
WSPRO	Water Surface Profile analysis

Glossary of terms

Accuracy	The precision to which measurement or calculation is carried out. Potentially accuracy can be improved by better technology.
Advection	The transfer of a property of the atmosphere or water, such as heat, cold, or humidity, by the horizontal movement of an air mass or current.
Afflux	Afflux by a partial obstruction such as a bridge or culvert is defined as the maximum difference in water level, for a specified discharge, if the structure were to be removed.
Aspect ratio	Ratio of channel breadth to depth, typically B/H .
Backwater	Backwater effects occur when sub-critical flow is controlled by the down stream conditions, for example, presence of an outfall, bridge constriction, dam, etc.
Bankfull	The maximum channel discharge capacity; further discharge spreads onto the floodplains.
Berms	(i) The space left between the upper edge of a cut and toe of an embankment to break the continuity of an otherwise long slope; (ii) The sharp definitive edge of a dredged channel such as in a rock cut; (iii) Natural levee where river deposits sediment.
Bias	A statistical sampling or testing error caused by systematically favouring some outcomes over others.
Biodiversity	The variability among living organisms from all sources including, <i>inter alia</i> , terrestrial, marine and other aquatic ecosystems and the ecological complexes of which they are part; this includes diversity within species, between species and of ecosystems.
Boundary layer	Region of fluid influenced in behaviour by the presence of a rigid boundary. Boundary layer theory enables the velocity distribution of a fluid to be established, showing a reduction in velocity within the boundary layer.
Braided	A braided channel is a channel that is divided into two or more channels, for example, flow around an island.
Calibration	Adjustment of a model to reach an acceptable degree of accuracy.

Chaotic	Description of a dynamic system that is very sensitive to initial conditions and may evolve in wildly different ways from slightly different initial conditions.
Compound channel	A channel whose width changes markedly at the bankfull level, typically increasing from the top width of the main river channel to the width of the river and any associated floodplains.
Convection	The transfer of heat in a fluid by the circulation of flow due to temperature differences, where a change in temperature at one location affects the temperature exclusively in the flow direction such that a point only experiences effects due to changes at upstream locations.
Conveyance	Measure of the discharge carrying capacity of a channel, $K(m^3 s^{-1})$ at a given depth and slope.
Control point	Point that controls the water surface profile in an upstream or downstream direction, typically associated with where the flow passes through the critical depth.
Critical depth	Depth at which the Froude Number equals one (i.e. $Fr = 1.0$), the energy is a minimum and where there is only one depth for a given specific energy ($h = h_c$).
Culverts	Pipes to enable the flow of water between parts of the catchment where roads and railways traverse the watershed.
Diffusive	Diffusion is the movement of a fluid from an area of higher concentration to an area of lower concentration by random fluctuations. In diffusive phenomena, such as heat conduction, a change in temperature at one location affects the temperature in more or less all directions.
Dispersive	Spreading by differential velocity field.
Discharge	The volume of water that passes through a channel section per unit time.
Emergent vegetation	Plants growing above the water but that are rooted below the surface or along the water edge.
Error	Errors are mistaken calculations or measurements with quantifiable differences.
Flow	A general term for the movement of volumes of water at a speed.
Geomorphology	The system of description and analysis of (physical) landscapes processes that change them; the study of landforms.
Habitat	An area in which a specific plant or animal naturally lives, grows and re-produces; the area that provides a plant or animal with adequate food, water, shelter and living space.
Inbank flow	Flow confined solely within the main river channel, with no flow over the floodplains.
Interpolation	Estimation of values based on a relationship within the limits of observation.
Invertebrate	An animal lacking a backbone or spinal column.

Irregularity	Channel irregularities represent variations in roughness from obstructions such as exposed boulders, trash, groynes etc or channel shape e.g. pools and riffles.
Manning's n	An engineering coefficient, n , that incorporates all losses i.e. losses due to local friction, secondary flows, form losses and lateral shear stresses (Chow, 1959). Derived for use in medium to large non-vegetated rivers with fully developed flow profiles.
Maximum depth	The vertical distance of the lowest point of a channel section from the free water surface.
Mean	The arithmetic average i.e. the sum of the data divided by the sample size.
Multi-thread	A multi-thread channel that is divided into two or more channels, for example, flow around an island. (≈braided)
Normal depth	The depth of flow that will occur in a channel of constant bed slope and roughness, provided the channel is sufficiently long and the flow is undisturbed.
Offset	Distance measured laterally across the channel, measured from the left-hand side of the cross-section when looking downstream.
Overbank flow	Flow that is sufficiently large to cause the floodplains to be inundated.
Pool	A point at which the stream is relatively unenergetic due to channel widening and deepening and sediment entrainment (the counterpart of riffle).
Rating curve	Relationship between depth of water and discharge.
Regression	Mathematical analysis of applying straight line principles to an observed relationship.
Resistance	As for roughness but defined as flow-, form-, frictional or turbulent, etc.
Reynolds Number	The Reynolds Number describes the ratio of the inertia forces to the viscous forces. In open channel flow, for $Re < 500$ laminar flow occurs, $Re > 2000$, turbulent flow occurs and for $500 < Re < 2000$ transitional flow occurs i.e. the flow is characterised by both laminar and turbulent effects.
Riffle	A point at which the stream is relatively energetic due to a constriction or steep gradient (the counterpart of pool).
Roughness	The effect of impeding the normal water flow of a channel by the presence of a natural or artificial body or bodies, which may be biotic for example vegetation; or abiotic/mineral for example bank and bed substrate.
Secondary flows	Flows that are typically transverse the main direction of flow, caused either by anisotropic turbulence or curvature of the mean flow (i.e. bends), manifested as slowly rotating vortices, as illustrated in Figures 2.14 & 3.12.

Shear layer	The region close to the boundary between a solid surface and the water or between two bodies of water moving at different mean velocities.
Siltation	The deposition of finely divided soil and rock particles on the bottom of streams, river beds and reservoirs.
Sinuosity	A measure of a channel's tendency to meander defined as the thalweg length over the valley length.
Stage	The vertical distance of the free surface from an arbitrary or defined datum.
Stream power	Rate of work required by a river to transport water and sediment.
Study reach	The length of a study reach or a section under investigation/measurement
Substrate	A generic term for a substance that underlies another; soil is the substrate for plants, while bedrock is the substrate for soil.
Surface material	Surface material encompasses the substrate on the bed, bank and floodplains. The roughness due to surface material includes, for example, sand, gravel, peat, rock, etc.
Thalweg	A line connecting the deepest points along a channel length.
Trash screens	Screens in front of structures (e.g. culverts) where rubbish is collected for removal.
Trend	A general tendency or inclination. To extend, incline, or veer in a specified direction.
Uncertainty	Uncertainty arises principally from lack of knowledge or of ability to measure or to calculate which gives rise to potential differences between assessment of some factor and its "true" value.
Unit roughness	Roughness due to an identifiable segment of boundary friction per unit length of channel.
Vegetation morphotype	Aquatic and marginal plant species of similar form or function in the riparian corridor.
Vena contracta	The <i>vena contracta</i> (Latin for <i>contracted vein</i>) is where the local water depth in a channel downstream of a sluice gate or similar structure is the lowest.
Vorticity	Circular motion of the fluid, often in the streamwise or planform directions; a vector measure of local rotation in a fluid flow, defined mathematically as the curl of the velocity vector.
Water course	Natural or man-made channel for the conveyance of drainage and flood water by gravity.
Wetland	Transitional habitat between dry land and deep water. Wetlands naturally occur in river valleys where drainage is impeded either by topography or soil structure. Wetlands include marshes, swamps, peatlands (including bogs and fens), flood meadows, river and stream margins.

Chapter I

Introduction

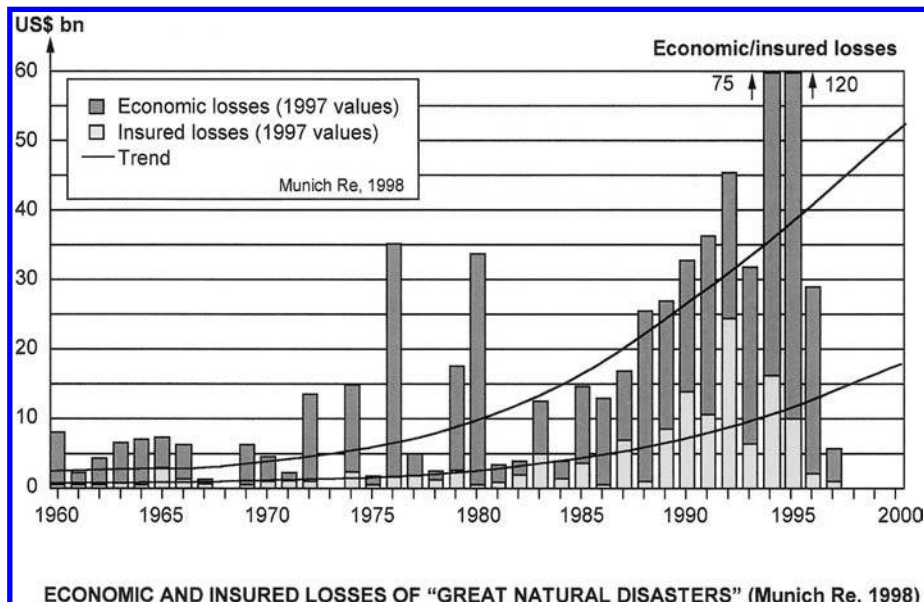
ABSTRACT

This chapter describes the wider issues related to flooding and flood risk management and how the concepts of conveyance, roughness and afflux are related to these issues. The context and motivation behind this book are outlined, together with a brief description of the origins of the Conveyance Estimation System (CES) and the Afflux Estimation System (AES). The CES-AES software incorporates five main components: a Roughness Advisor, a Conveyance Generator, an Uncertainty Estimator, a Backwater Module and an Afflux Estimator. These are introduced and briefly described, together with comments concerning key assumptions and some technical limitations. An outline of the structure of the book and how it might be used in conjunction with the software is also given.

1.1 CONTEXT AND MOTIVATION FOR BOOK

The origins of this book lie in a sequence of research projects and programmes commissioned within the UK since the 1980's. These focused on, and provided, increased scientific knowledge and understanding on the hydraulic factors that affect river flows and flood levels in particular. Some of these programmes brought together researchers from other countries, notably Japan and European (e.g. see Ikeda and McEwan, 2009; Knight and Shamseldin, 2006), and their work also focused on the behaviour of rivers in flood conditions.

The widespread nature of flooding at a global scale has been highlighted by Berz (2000), who has reminded the engineering community that flood disasters account for about a third of all natural disasters by number and economic losses, but are responsible for over half the deaths world-wide. Asian countries, in particular, are prone to flooding problems, with consequent high loss of life. The extent of flooding in Europe in the past decade has been highlighted by Knight and Samuels (2007), who give examples of some significant flood events, together with their causes and impacts. Figure 1.1 indicates the economic and insured losses of all types of natural disasters (floods, earthquakes, storms and others) and Figures 1.2–1.7 show some examples of fluvial flooding in various countries, and the impact that they have. Other examples of floods are given by Miller (1997), together with strategies for prevention. This book



ECONOMIC AND INSURED LOSSES OF "GREAT NATURAL DISASTERS" (Munich Re, 1998)

Figure 1.1 Trends in economic and insured losses arising from all types of disaster world-wide (floods, earthquakes, storms and others, after Berz, 2000) (See colour plate section).



Figure 1.2 Initial stages of floodplain inundation – River Severn, UK (courtesy HR Wallingford) (See colour plate section).

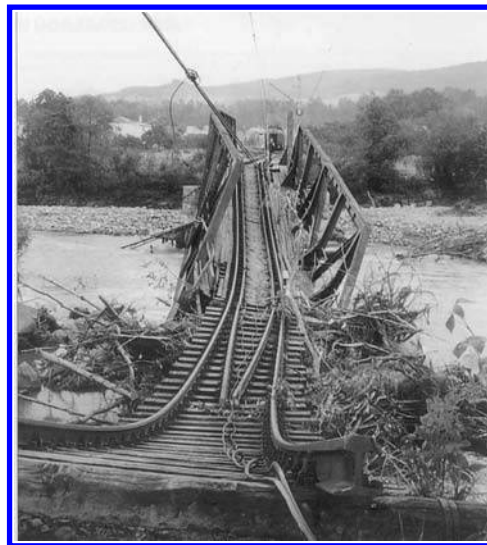


Figure 1.3 Flood damage to a bridge in the River Oder basin, Poland, July 1997 (courtesy IIHR) (See colour plate section).



Figure 1.4 Overtopping of a river flood defence wall, China, 2006 (courtesy H Liao). [Note height of river above ground level by scale of steps & buildings] (See colour plate section).

deals with three key aspects of river hydraulics and is aimed at all those professionals world-wide working in the field of flood risk management, river engineering and drainage.

National and international policy and practice have now generally moved from one of flood defence to a more encompassing approach of flood risk management. This



Figure 1.5 Flood damage to infrastructure and a railway line during floods in China, 2006 (courtesy H Liao) (See colour plate section).



Figure 1.6 Breach in a river embankment on the River Aire, UK, 2002 (courtesy Environment Agency) (See colour plate section).



Figure 1.7 River Severn in flood at Upton upon Severn, UK, 1990 (courtesy Environment Agency).

recognises that flooding cannot be eliminated, but that the influence of floods on people and the environment needs to be addressed in the context of broader sustainability (Samuels *et al.*, 2006). Although the policy objective has been broadened, that has not diminished the need to understand the fundamental fluvial processes that determine the depths, velocities and extent of flooding. These factors remain essential in reaching final decisions on the design of physical flood defences and on river maintenance.

In Europe, there has been a significant development of international policy with the entry into force in late 2007 of the European Directive on the assessment and management of flood risks (European Commission, 2007). As a result of this directive, each Member State of the EU must, within their boundaries, undertake a preliminary flood risk assessment, prepare flood risk maps and develop flood risk management plans for each river basin. Clearly an understanding of the way floods propagate within a river basin is important in carrying out these responsibilities. To this end, the European Commission recently sponsored an ‘Advanced Study Course’ on ‘River basin modelling for flood risk mitigation’, which gave a broad but integrated view of flood risk management at a river basin scale (Knight and Shamseldin, 2006).

Furthermore, the WFD – the European Water Framework Directive – (European Commission, 2000) also requires an assessment of the flow conditions in rivers, although the primary environmental objectives of the WFD are in particular to achieve by 2015 “good ecological and good chemical status” for surface water bodies in general or good ecological potential for the specific case of heavily modified and artificial water bodies. The WFD also seeks that in general “no deterioration” in status of the water body and this will require the management of the quality, quantity and structure of aquatic environments. However, in the area of “hydromorphology”, derogations from some of the WFD requirements are possible under Article 4 (7) for flood management operations, but only when specific criteria and conditions are met. These need a full justification through analysis of the alternatives.

In the UK, under the national policy of “Making Space for Water” there is a strong emphasis on understanding the performance of flood defence “assets”, that is channels, floodplains, embankments, structures and other infrastructure to make decisions on their effective and efficient management. For river channel and floodplains this requires an assessment of their combined capacity to convey floods and how routine maintenance, upgrading of defences or construction of new works will influence this. Thus estimation of river channel conveyance and the afflux at river structures are core components of flood risk management through water level prediction and flood defence design.

As the executive agency responsible for flood risk management works on main rivers in the UK, the Environment Agency (EA) has a commitment to use sound science in undertaking its activities. The EA is assisted in these activities at a local level by internal drainage boards and local authorities, who have new statutory responsibility following the Pitt review (2008). It is usual practice to undertake assessments of river flows and flood conditions using computational models, with a process of model construction, calibration and verification, and then application to the particular issue of concern. All such assessments require the estimation of the discharge involved, estimation of the capacity of the watercourse to carry that discharge, and the degree and extent of influence of any structures on the watercourse. Discharge estimation is a core activity in hydrology and lies beyond the scope of this book, which concentrates

on the capacity of a watercourse to discharge water as the water level varies (this is known as its ‘conveyance’) and on the water level increases caused by bridges and culverts (that is their ‘afflux’). These two technical terms are defined in the glossary and dealt with in detail in [Chapters 2 & 3](#).

All river modelling software includes one or more methods for conveyance estimation, usually based upon methods dating from research completed more than 50 years ago, with little or no account taken of more recent advances in knowledge and understanding. Hence the Environment Agency, with support from the Scottish Government and the Northern Ireland Rivers Agency, commissioned the development of new methods for the calculation of conveyance that incorporate the latest scientific knowledge on the topic. Likewise the Agency commissioned a review of methods for assessing the effects of river structures on flood levels and this work on afflux and blockage was incorporated into a single modelling tool alongside the new work on conveyance estimation.

1.2 SCOPE OF BOOK AND INTRODUCTION TO THE CES-AES

This book provides a stand-alone introduction to the principles and processes of hydrodynamics in open channel flows, set in the context of the Conveyance and Afflux Estimation System (CES-AES), developed from certain Environment Agency R&D projects outlined in Section 1.5. It aims to give the technical background to each of the components of the CES-AES, together with illustrations of their use. The five main components of the CES-AES are:

- The Roughness Advisor,
- The Conveyance Generator,
- The Uncertainty Estimator,
- The Backwater Module, and
- The Afflux Estimator.

The Roughness Advisor incorporates a database of information on the hydraulic roughness of different surfaces including descriptions, photographs and unit roughness values for a range of natural and man-made roughness types. These were sourced from over 700 references (including the UK based River Habitat Survey) and include aquatic vegetation, crops, grasses, hedges, trees, substrates, bank protection and irregularities (Defra/EA, 2003b). The Roughness Advisor also includes information on seasonal variations in vegetation roughness, the effects of weed cutting in river maintenance activities and has suggested re-growth patterns following cutting.

The Conveyance Generator estimates the channel conveyance based on the roughness information and the shape of the cross-section. The calculation considers the lateral distribution of velocity across the section and the overall flow is then determined by integrating the velocity across the river section. The outputs available include the variation with depth of important hydraulic parameters, such as: water level, flow,

rating curves, velocity, area, wetted perimeter, Froude Number, Reynolds Number, etc. It is also possible to obtain lateral distributions (across a section) of velocity, boundary shear stress and shear velocity, which may be used in assessments of sediment movement and other environmental factors.

The Uncertainty Estimator provides upper and lower “credible” scenarios, providing some measure of the range of the uncertainty associated with each predicted water level. These values are derived from the upper and lower roughness estimates from the Roughness Advisor. However, they do not have any precise statistical interpretation nor do they represent any upper or lower limits on the water level for all possible conditions. They are scenarios of what can occur based on the observations in the roughness database and some expert assessments where field data were unavailable.

The Backwater Module includes a standard calculation of the backwater profile upstream of a control, i.e. a point of known stage and flow. This is based on a basic balance of work done against the river resistance to the loss of potential energy as the water flows downstream. The calculation covers only subcritical (or tranquil) flow; it works from downstream to upstream and includes the option to incorporate the variation of velocity head in non-uniform channels (i.e. changes in the bulk kinetic energy of the flow). The module can be used to simulate the change in water level between structures.

The Afflux Estimator models the influence on water level of arch and beam bridges with up to 20 openings, and pipe, box and arch culverts with up to 10 identical barrels. This calculation is embedded within the bridge and culvert units in the CES-AES model and, combined with the Backwater Module, produces a longitudinal water surface profile along a watercourse taking account of channel shape, roughness and hydraulic structures.

1.3 LIMITATIONS OF THE CES-AES

In any technical assessment it is important to understand the limitations of the methods being used. For the use of the CES-AES, the most important limitations are:

- Steady flow (i.e. negligible attenuation);
- Fixed bed (i.e. no scour or deposition);
- Fixed roughness (i.e. uninfluenced by velocity);
- Small to medium sized channels and rivers (say 0.5 to 500 m width, 0.2 to 10 m depth, gradients 10^{-2} to 10^{-4} approximately), low to moderate sinuosity;
- Unobstructed bridges and culverts (i.e. not partially blocked by debris or sediments).

The assumption of steady flow arises in the Backwater Module and is appropriate for many practical purposes. The main implication is that the Backwater Module, through its simple model of the watercourse, must not be used for the assessment of the effects of changes in flood storage. It may be used with confidence to investigate the sizing of river and drainage channels, the dimensioning of structures and the assessment of maintenance works through vegetation cutting regimes and dredging. The calculation of conveyance as a characteristic property of the channel cross-section is

not affected by the assumption of steady flow; the conveyance calculations can be used in unsteady flow simulations.

The assumption of a fixed bed means that the variation of the shape of the section is not taken into account in any of the components of the CES-AES. This restriction is important in any watercourse that is morphologically active, especially where changes in section dimensions occur over the course of a flood. In such cases the conveyance should be estimated for the initial and final dimensions of the sections or a full sediment transport model should be employed. This limitation is likely to be of importance in flash flood cases, such as the flood in Boscastle (Cornwall, UK) that occurred in August 2004.

The assumption of fixed roughness can be significant in several circumstances. For channels where the bed material is fine or is easily transported, the effective roughness may depend upon the flow velocity as ripples or dunes appear on the river bed or are washed out. Such alluvial friction processes currently lie outside the scope of the CES-AES and are not covered in this book. The limitation probably only affects the use of the CES-AES on the lower reaches of larger rivers and these are more often in the tidal zone anyway (Tagg and Samuels, 1989).

The limitation to small and medium sized channels reflects the range of cases used in the development and validation of the CES. Mc Gahey *et al.* (2008) report that the new methods included in the CES are appropriate for all except the largest or the steepest rivers in the international data assembled. It is possible that for the largest rivers the assumption (as above) of fixed roughness independent of velocity is not appropriate, and in steep mountain rivers the roughness from boulders (which are large in comparison with the flow depth) is not well-represented by the current resistance equations in the code, although an alternative is suggested.

The Afflux Estimation System component of the CES-AES applies only to fixed dimensions of the hydraulic structures, and there is no transient allowance for the changes in effective shape and area through blockages that may form during a flood (Mantz and Benn, 2009). There are a range of opening types available in the CES-AES for bridges and culverts, with some flexibility to define the shapes of the openings; however more complex types such as multiple culvert openings with different shapes and invert levels or bridges with relief culverts cannot be represented directly.

1.4 OUTLINE OF BOOK

The book has been written so that the various topics are introduced initially at a simplified level, and then again progressively at more complex levels in later chapters. In this way it is hoped that the reader can learn about certain practical and theoretical aspects of river engineering early on, without recourse to all the details normally required when actually modelling a particular river in earnest. Thus, [Chapter 2](#) deals with some basic theoretical concepts in open channel flow, illustrated via simple examples, followed by certain practical issues illustrated via case studies. These are largely based on the Shiono and Knight (1988 & 1991) method of analysis (SKM), a pre-cursor to the CES methodology described in detail in [Chapter 3](#). [Chapter 2](#) deals with inbank and overbank flows in simple engineered channels, flows in natural channels, afflux at bridges and culverts, roughness, hydraulic resistance and data sources. In [Chapter 3](#) further details

of the scientific issues related to flow structures, their mathematical representation, governing equations and assumptions are provided, expanding on what was initially presented in Chapter 2. Having now fully established these concepts, full details of the CES-AES methods related to roughness, conveyance and afflux are given, together with an introduction to uncertainty and the CES-AES software. Chapter 4 then deals with the application of the CES-AES software, covering many practical issues such as estimating and using stage-discharge relationships, assessing lateral distribution of velocities and boundary shear stress, estimating afflux at bridges and dealing with vegetation. These issues are again illustrated via case studies and examples, and serve to demonstrate the wide range of application of the CES-AES software. Chapter 5 considers how the CES and AES methodologies can be used more broadly in assessments covering ecological issues, habitats, sediment and geomorphology and some more generic issues in river modelling.

The CES-AES stand-alone software is available to all as a free download at the CES-AES Website: www.river-conveyance.net. It is also available to the Environment Agency of England and Wales staff through their internal Corporate Information Services. The CES conveyance calculation and roughness information has also been made available through the 1-D hydrodynamic modelling software InfoWorks RS (Version 6.5 and onwards) and ISIS Flow (Version 2.3 and onwards), providing an alternative to the Manning equation for evaluating cross-section conveyance. Information and documentation from the original CES and AES development projects may be found at: www.river-conveyance.net/ces and www.river-conveyance.net/aes respectively. For up-to-date information on the CES-AES software including documentation, training, Frequently Asked Questions and contact details for provision of feedback, please visit the CES-AES Website.

1.5 ORIGIN OF THE CES-AES

The scientific basis of the Conveyance Estimation System and Afflux Estimation System (CES-AES) was formulated in UK funded research that was undertaken in the decade 1985–1995. It was focused on the conveyance capacity of river and floodplain systems, and involved a programme of large-scale experiments on the conveyance of compound channels in the Flood Channel Facility (FCF) at HR Wallingford. The experimental programme, which included straight, skewed and sinuous cases with a variety of geometries, roughness conditions and flow conditions, is summarised by various authors, notably Knight and Sellin (1987), Knight and Shiono (1990), Sellin *et al.* (1993) and Knight (2008a). Figures 1.8–1.11 illustrate some of the fixed bed experimental geometries that were used in Phases A & B of this work. In a later phase (Phase C), a loose boundary was employed and sediment re-circulated in both straight and meandering channels. The observations explored systematically discharge capacity, boundary shear stresses and turbulence stresses in the body of the flow. The data and further details of the FCF experimental programme may be found at www.flowdata.bham.ac.uk. These data produced greater physical insight into the fluid mechanics of these flows and various research papers indicated that traditional methods of analysing these flows could have large uncertainties of the order of 30% or

more. However, this improved knowledge of the processes of flood propagation was not taken up readily into practice.

The former National Rivers Authority in England and Wales (1994) commissioned the derivation of hand calculation methods for assessing the conveyance of straight and compound channels based upon the research undertaken in the first two phases of the experimental programme of the Flood Channel Facility (Ackers, 1992b and James and Wark, 1992). Although these methods performed well in tests against experimental measurements and those from real rivers, these methods remained largely unused. Potential reasons for this slow take-up of the research were deemed to be:

- changes in the profession away from hand calculation to much greater reliance on standard computational models;
- the lack of a pathway into use for research in internal procedures from the principal end user.

A key issue addressed by the joint research programme into Flood and Coastal Defence established by the former Ministry of Agriculture, Fisheries and Food (MAFF)



Figure 1.8 Straight channel with two symmetric smooth floodplains in FCF (courtesy HR Wallingford).



Figure 1.9 Skewed channel in FCF with smooth floodplains (courtesy HR Wallingford).



Figure 1.10 Meandering natural channel in FCF with sinuosity of 2.043 (courtesy HR Wallingford).

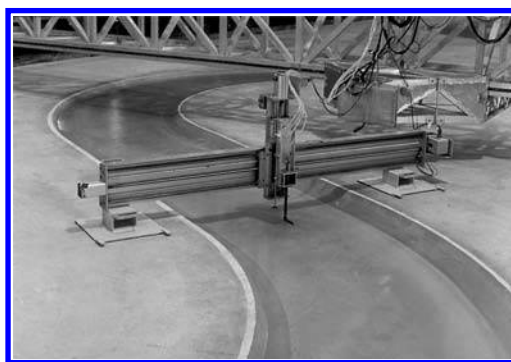


Figure 1.11 Dispersion experiments in FCF with a trapezoidal meandering channel with a sinuosity of 1.374 (courtesy HR Wallingford).

and the Environment Agency in 2000 was the improved dissemination and implementation of the outputs of research. See, for example, Leggett and Elliott (2002) and Townend *et al.* (2007).

In 2000 the Engineering and Physical Sciences Research Council (EPSRC), together with the Government Department for Food and Rural Affairs (Defra) and the Environment Agency (EA) established a joint research network on river and floodplain conveyance in the UK, with over 60 academics and practicing river engineers participating. Following the extensive flooding in the UK in the autumn and winter of 2000 to 2001, the Institution of Civil Engineers Presidential Commission on flood management issues identified the importance of improving the application of technical knowledge on the hydraulics of flood level calculation and the supporting models in practical use (ICE, 2001; Fleming, 2002). An early action resulting from the joint EPSRC/Defra/EA network was the commissioning by the Environment Agency of a Scoping Study on reducing uncertainty in river flood conveyance calculation. The setting up of the CES project was supported by the Natural Environment Research Council (NERC), the Rivers Agency in Northern Ireland and the Scottish Government. The Environment

Agency was particularly concerned that the Scoping Study should address the whole of flood risk management as the end objective, not just the design function (as had been the case in the earlier work of the National Rivers Authority). In addition, the Scoping Study needed to reconcile the needs for both research openness and the supply of commercial software systems for simulation of river flow.

The objective of the scoping study was to identify a programme of work to synthesise current knowledge and how to fill in the gaps, in order to improve the tools available for river management practice. The project involved directly, and through consultation, recognised academic experts and researchers, operational staff and consulting engineering practices. The Scoping Study included a questionnaire targeted at specific individuals and distributed more broadly within the UK and internationally. The industry and academic communities were involved through workshops on the user needs and to validate the draft of the research recommendations.

The study also included the preparation of a series of expert review papers on flow measurements (field and experimental), effects of vegetation, conveyance calculation methods in 1-D models, implications for 2-D and 3-D models and the use of remote sensing. These expert papers were prepared by members of the EPSRC network and the texts are contained in an annex to the final report (Defra/EA, 2001). This documentation on the state-of-the-art underpinned many of the scoping study research recommendations. The subsequent research involved a partnership between academic researchers, experts and end-users. Particular emphasis was placed on issues of concern, such as: the effects of riverine vegetation, the influence of natural shaped (and re-naturalised) channels and the interaction between river channels and floodplain flows. The output from this programme was the novel Conveyance Estimation System (CES) and its inclusion in several modelling packages. The CES also includes a Roughness Advisor (RA) to facilitate access to the wide body of knowledge on the estimation of fluvial resistance. These are described in detail in [Chapters 3 & 4](#).

At the same time, the Environment Agency acted on the need to provide similar guidance and methods for estimating the effects of river structures on flood conditions. [Figures 1.12–1.15](#) illustrate some of the effects of flood flows on bridges. First of all, a study collected information on current knowledge and practice (Defra/EA, 2003a) and this was followed by the development of the Afflux Estimation System (AES) to operate with the CES and the Afflux Advisor (originally begun as just an MS Excel



Figure 1.12 Elliptical arch bridge with river level close to the soffit (courtesy HR Wallingford).



Figure 1.13 Multiple arch bridge with inundation of approach road (courtesy HR Wallingford).



Figure 1.14 Multiple arch bridge with debris beginning to collect around central pier (courtesy University of Birmingham).



Figure 1.15 Arch bridge with a parapet destroyed by flood debris.

spreadsheet application). The AES project was also supported by others, including the Scottish Government. A particular impetus to the CES-AES project was provided by the report on ‘Sediment transport and alluvial resistance in rivers’ by Bettess (2001), that helped to demonstrate to practitioners and funders the relevance of drawing together existing knowledge for an improved tool on conveyance.

The main purpose of developing the AES was to improve the tools available in engineering practice to simulate the effects of bridges and culverts on flood water levels at high flows, particularly for the representation of afflux (the increase in upstream water levels attributable to the structure). The project researched a range of methods of calculating afflux, to determine their applicability to the various types of bridges and culverts found in UK channels and incorporated the most appropriate methods and algorithms, following detailed testing, into the AES software (Defra/EA, 2004a&b). The development again involved close collaboration between academic researchers, experts and practitioners.

The CES and the AES have now been integrated into a single software module so that they can operate separately, or together where needed, to estimate water levels along an open channel reach containing bridge or culvert crossings. For completeness, the software includes backwater calculations along a watercourse as a basic model of open channel flow.

Chapter 2

Practical and theoretical issues in channel hydraulics

ABSTRACT

This chapter is an introduction to the many practical and theoretical issues that need to be considered when attempting to model the flow of water in open channels and rivers. These issues are illustrated through several worked examples, as well as a number of case studies on actual rivers. Consideration is also given to several related topics, such as: how to schematise a river cross-section or reach, the difficulty of estimating hydraulic roughness and resistance, the hydraulic characteristics of inbank and overbank flows, and flows through bridges and culverts. The data requirements for effective modelling are also considered.

2.1 GETTING STARTED WITH SOME PRACTICAL EXAMPLES ON CALCULATING FLOWS IN WATERCOURSES

The flow of water in a river, water course or drainage system is governed by physical laws related to the conservation of mass, energy and momentum. Their application to open channel flow is the subject of this book. Although these physical laws and principles are sometimes difficult to apply to all types of fluid flow in river engineering, as well as other areas in engineering and science, mainly due to the difficulty of accounting for energy degradation, some physical characteristics of open channel flow may be readily understood and are surprising. In order to appreciate some key features of open channel flow, the following 5 examples are given to get started on some practical problems. They also help to introduce and define certain terms and parameters, as well as illustrating certain issues addressed in later sections. Examples 1 to 3 are concerned with a freely flowing small-sized river or drainage channel, and Examples 4 & 5 are concerned with flow in a reach where the channel has some hydraulic controls. Although these examples are straightforward for those familiar with hydraulic principles and text books (e.g. Chadwick *et al.*, 2004; Chanson, 1999; Chow, 1959; Cunge *et al.* 1980; Henderson, 1966), they should be worked through none-the-less as they serve to illustrate some basic topics and issues in modelling mentioned later. They introduce parameters such as specific energy, momentum, roughness, resistance to flow and energy losses, as well as the notation used in this book.

Example 1

A river has a simple trapezoidal cross section with a bed width, b , of 15.0 m, side slopes, s , of 1:1 (vertical : horizontal), a Manning's n of 0.030 and a longitudinal bed slope, S_o , of 3.0×10^{-4} . Determine the discharge in the channel when the depth of flow, h , is 1.5 m, using Manning's equation (1891), given as Eq. (2.1). Figures 2.1(a) & (b) illustrate typical river channels that might be considered to be approximately trapezoidal in shape, but with different roughnesses.

$$Q = AR^{2/3}S_o^{1/2}/n \quad (2.1)$$

(a) low Manning n value (~0.03)(b) high Manning n value (~0.30)

Figure 2.1 Two trapezoidal channels with different Manning n roughness values.

Answer & comment

$$\text{Area, } A = (b + sh)b = (15 + 1.0 \times 1.5) \times 1.5 = 24.75 \text{ m}^2.$$

$$\text{Wetted perimeter, } P = b + 2h\sqrt{(1 + s^2)} = 15 + 2 \times 1.5\sqrt{(1 + 1^2)} = 15 + 3\sqrt{2} = 19.243 \text{ m.}$$

$$\text{Hydraulic radius, } R = A/P = 24.75/19.243 = 1.286 \text{ m.}$$

$$\text{Discharge, using Eq. (2.1), } Q = 24.75 \times 1.286^{2/3} \times 0.0003^{1/2}/0.030 = 16.90 \text{ m}^3\text{s}^{-1}.$$

Note that the discharge is given explicitly by the Manning equation, because the depth, h , is specified, and the whole cross section is used. For a long reach, with a constant slope and roughness, this depth is referred to as the 'normal depth' and often given the symbol h_n . Since the whole section is used, this is essentially a 'single channel' method of analysis, employing a simple 'one-dimensional' (1-D) approach that gives the discharge, but no other information about the velocity distribution within the channel (i.e. across the width or over the depth). For further details on the background to the Manning equation, see Yen (1991).

Example 2

If the discharge in Example 1 is now reduced to $10 \text{ m}^3\text{s}^{-1}$, determine the new depth of flow (normal depth), b_n , and the ‘critical depth’, b_c . Also determine the ratio of normal to critical depth, b_n/b_c , the Froude Number and whether the flow is ‘subcritical’ or ‘supercritical’.

Answer & comment

[Equation \(2.1\)](#) may be re-arranged with all known parameters on one side and all the geometric parameters involving depth on the other side. Noting that $R = A/P$, then:

$$Qn/S_o^{1/2} = A^{5/3}/P^{2/3} \quad (2.2)$$

Since h occurs both in the area and wetted perimeter, whose constituent equations depend on the shape of the cross section, it is generally now not possible to obtain an answer for the depth in explicit form using Manning’s equation. Pivoting around the highest power of h , a numerical method, such as fixed-point iteration, may be shown to give a new value for the normal depth, b_{j+1} , in terms of a previous value, b_j , as:

$$b_{j+1} = \left[\frac{Qn}{S_o^{1/2}} \right]^{3/5} \frac{[b + 2b_j\sqrt{1+s^2}]^{2/5}}{(b + sh_j)} \quad (2.3)$$

[Equation \(2.3\)](#) may be solved numerically for b_{j+1} , by assuming initially that $b_j = 0$, and then by repeated iteration until b_{j+1} is sufficiently close to b_j , giving ultimately $b_n = 1.095 \text{ m}$. The normal depth of flow for the discharge of $10 \text{ m}^3\text{s}^{-1}$ is therefore 1.095 m .

[Equation \(2.3\)](#) may also be formulated into a dimensionless form, convenient for other purposes, as

$$\frac{b_{j+1}}{b} = \left[\frac{Qn}{b^{8/3}S_o^{1/2}} \right]^{3/5} \frac{[1 + (2b_j/b)\sqrt{1+s^2}]^{2/5}}{(1 + sh_j/b)} \quad (2.4)$$

[Figure 2.2](#) shows the solution for b for flows in trapezoidal channels and circular culverts or pipes running part full, to illustrate the influence of each dimensionless group. These types of flow are commonly found in engineering design and feature in this book in relation to simple shaped rivers, culverts and drainage conduits.

The critical depth, b_c , is given when $Fr = 1.0$, where the Froude Number, Fr , is defined by

$$Fr = \frac{U}{\sqrt{gA/T}} \quad (2.5)$$

in which U = section mean velocity ($= Q/A$) and T = top width of channel (i.e. at the free surface). At the critical depth and ‘critical flow’, $Fr = 1$, and the energy is

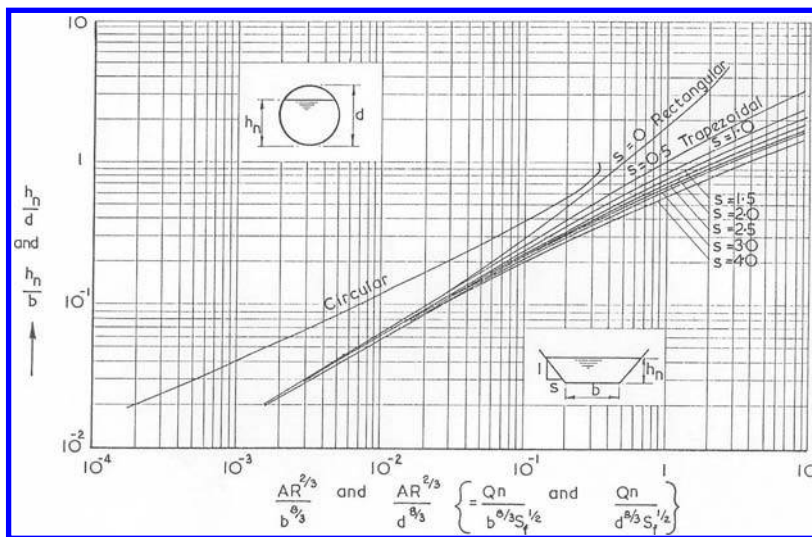


Figure 2.2 Uniform depth relationships based on Eq. (2.4), and equivalent equation for circular culverts running part full, showing influence of individual parameter groups.

also a minimum, as may be deduced later from Eq. (2.12). The condition necessary for critical flow then follows from Eq. (2.5) and may be written in the general form for channels of any cross sectional shape, as

$$\frac{Q^2 T}{g A^3} = 1 \quad (2.6)$$

In order to calculate h_c , a similar numerical procedure to the normal depth calculation method is required. In this particular example, with a trapezoidal channel, $T = b + 2sh$, which is a function of depth and therefore initially unknown. Re-arranging Eq. (2.6) for fixed-point iteration yields

$$h_{j+1} = \left[\frac{Q^2}{g} \right]^{1/3} \frac{[b + 2sh_j]^{1/3}}{(b + sh_j)} \quad (2.7)$$

This may also be put into a dimensionless form again, convenient for other purposes, as:

$$\frac{h_{j+1}}{b} = \left[\frac{Q}{g^{1/2} b^5} \right]^{2/3} \frac{[1 + 2sh_j/b]^{1/3}}{(1 + sh_j/b)} \quad (2.8)$$

Using Eq. (2.7) iteratively, assuming initially again that $h_j = 0$, gives $h_c = 0.354$ m. Thus $h_n/h_c = 1.0952/0.3537 = 3.096$ (i.e. $h_n > h_c$, therefore subcritical flow. See Fig. 2.12)

At the new normal depth, $A = (b + sh)h = (15 + 1.0 \times 1.0952) \times 1.0952 = 17.628 \text{ m}^2$.

Top width, $T = b + 2sh = 15 + 2 \times 1.0 \times 1.0952 = 17.190 \text{ m}$.

$$U = Q/A = 10.0/17.6275 = 0.567 \text{ ms}^{-1}$$

$$Fr = 0.5673/(9.807 \times 17.6275/17.1904)^{1/2} = 0.179.$$

Hence, since $Fr < 1.0$ the flow is confirmed as being subcritical.

Note that an iterative approach is required to solve Eq. (2.1) because this is the inverse problem to Example 1, in which the discharge is given and not the depth. Since $h_n > h_c$, this means that the flow is subcritical, a fact confirmed by the Froude Number being less than 1.0. The general form of the Froude Number, Eq. (2.5), should always be used in open channel work, and distinguished from the particular form adopted in channels with a rectangular cross section. In that particular case, since $A = bh$ and $T = b$, the Froude Number is given by

$$Fr = \frac{U}{\sqrt{gb}} \quad (\text{rectangular channel only}) \quad (2.9)$$

and the critical depth may be readily obtained from Eq. (2.6) in the form

$$h_c = \sqrt[3]{q^2/g} \quad (\text{rectangular channel only}) \quad (2.10)$$

where the discharge per unit width, q , is defined by

$$q = Q/b \quad (2.11)$$

The discharge per unit width is a useful concept, used widely in designing channel transitions, and also in a depth-averaged form of the Reynolds Averaged Navier-Stokes equations (RANS) which form the basis of the CES system described more fully in Chapter 3.

Example 3

If the river in Example 1 is re-graded, maintaining the same bed width and side slopes, but with a Manning's $n = 0.025$, what bed slope is required to convey $30 \text{ m}^3\text{s}^{-1}$ at a depth of 1.5 m? What will be the increase in water level for $Q = 30 \text{ m}^3\text{s}^{-1}$, if subsequently the roughness of the river reverts back to its original Manning's n value, with S_o remaining as calculated?

Answer & comment

$A = 24.75 \text{ m}^2$; $P = 19.243 \text{ m}$; $R = 1.286 \text{ m}$ as before, then solving for slope: Bed slope, using Eq. (2.1), $S_o = [30 \times 0.025/(24.75 \times 1.2862^{2/3})]^2 = 6.565 \times 10^{-4}$. For original $n = 0.030$, depth will increase. Using Eq. (2.3) gives $h_n = 1.673 \text{ m}$. Increase in water level = 0.173 m.

Note that with reduced roughness, but the same depth, the bed slope is increased because the specified discharge has increased from $16.9 \text{ m}^3\text{s}^{-1}$ to $30 \text{ m}^3\text{s}^{-1}$. With the original roughness, depth, new discharge but reduced bed slope, the depth is increased. This illustrates how useful the Manning equation is in relating the 4 basic parameters $\{Q, b, S_o, n\}$ that commonly occur in many design problems in river engineering. Furthermore, Eq. (2.1) also shows how easy it is to calculate changes in any one parameter that are governed by the other three.

Example 4

This example is based on the physical situation shown in Figure 2.3, and the corresponding diagrams in Figure 2.4. A horizontal channel with a rectangular cross section is 4.5 m wide and conveys $13.5 \text{ m}^3\text{s}^{-1}$. A vertical sluice gate is incorporated in the channel and the gate is regulated until the depth of flow just upstream is 3.0 m. Assuming no energy loss during the passage of water under the gate, find the depth of flow just downstream of the gate. Figure 2.3 shows a picture of this type of flow in the laboratory, and Figure 2.4 shows the corresponding depth versus specific energy (b v E) and depth versus specific momentum (b v M) diagrams. The depth at section 2 is known as the *vena contracta* (Latin for *contracted vein*), i.e. where the depth in the channel is the lowest. The flow with a hydraulic jump is covered in Example 5.

Answer & comment

This example requires one to understand the concept of specific energy, E , defined by

$$E = b + \alpha \frac{U^2}{2g} \quad (2.12)$$



Figure 2.3 Flow under a laboratory vertical sluice gate with a hydraulic jump downstream.

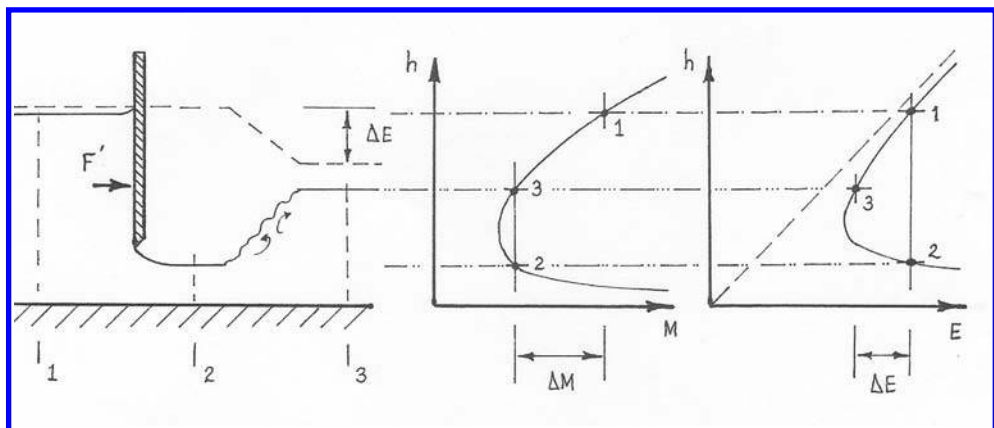


Figure 2.4 Schematic diagrams of specific energy and momentum for flow under a vertical sluice gate with a hydraulic jump downstream.

where E = specific energy per unit weight, α = kinetic energy correction coefficient, taken here as 1.0 in order to simplify the problem. The technical definition of α , and the corresponding momentum correction coefficient, β , are dealt with more fully in Section 2.2.5.

Equation (2.12) may be developed for flow in a rectangular channel of breadth, b , with $\alpha = 1.0$, as a cubic equation in h

$$E = b + \frac{q^2}{2gb^2} \quad (2.13)$$

Thus with $q = Q/b = 13.5/4.5 = 3.0 \text{ m}^3\text{s}^{-1}\text{m}^{-1}$, then $E_1 = 3.0 + 3.0^2/(2 \times 9.807 \times 3.0^2) = 3.051 \text{ m}$.

Assuming no energy loss across the sluice gate, as shown in Figure 2.4, then $E_1 = E_2$ and the depth downstream of the gate, h_2 , may be obtained from

$$E_2 = h_2 + \frac{q^2}{2gh_2^2}$$

Solving this for $E_2 = 3.051 \text{ m}$ gives $h_2 = 0.417 \text{ m}$. Hence $A_2 = 4.5 \times 0.4174 = 1.878 \text{ m}^2$ and $U_2 = 13.5/1.8783 = 7.187 \text{ ms}^{-1}$. Also, from Eq. (2.10), $h_c = 0.972 \text{ m}$, indicating that $h_2 < h_c$.

Checking that the value of h_2 gives the same specific energy, the kinetic head at section 2 = $U_2^2/2g = 7.1874^2/(2 \times 9.807) = 2.6337 \text{ m}$ and hence $E_2 = 0.4174 + 2.6337 = 3.0511 \text{ m} (\approx E_1)$.

Note that for a given specific energy there are generally two possible depths of flow, h_1 and h_2 , known as ‘alternate depths’, one subcritical ($Fr < 1$) and the other

supercritical ($Fr > 1$). These are denoted in [Figure 2.4](#) by the two points 1 & 2 in the h v E diagram, where a vertical line for the given value of E intersects the curve for a given q . Note the value of $U_2^2/2g$, and how the sluice gate changes the flow from subcritical to supercritical flow. The point on the h v E curve where the energy is a minimum, and where there is only one depth for a given energy, is where critical flow occurs (i.e. $Fr = 1.0$). The depth there is known as the critical depth, h_c , as already defined by [Eq. \(2.6\)](#), and is associated usually with the transition from subcritical to supercritical flow. It should also be noted that the downstream depth, h_2 , is seen to be much smaller than the upstream depth h_1 and is defined by h_1 and q , not the gate opening, h_g . The flow downstream is also confirmed to be supercritical since $h_2 < h_c$. The contraction coefficient, $C_c (= h_2/h_g)$, may be calculated for the sluice gate if h_g is known. Typically, C_c is around 0.61 for such sluice gates. Alternatively, if h_g , C_c and q are known, then the upstream depth, h_1 , may be calculated.

Example 5

If a hydraulic jump occurs downstream of the sluice gate in Example 4, as shown in [Figures 2.3 & 2.4](#), determine the maximum tail water level which could be tolerated before the sluice gate becomes ‘drowned out’, i.e. when the downstream depth begins to affect the depth of flow upstream of the gate. Also determine the height of the jump and the energy and the power lost in the jump.

Answer & comment

The standard equation for a hydraulic jump in a rectangular channel (Chow, 1959) is as follows:

$$\frac{h_2}{h_1} = \frac{1}{2} \left[\sqrt{(1 + 8Fr_1^2)} - 1 \right] \quad (2.14)$$

where h_1 and h_2 are the depths before and after the jump, known as ‘conjugate depths’. These should not be confused with the two ‘alternate depths’ defined in Example 4 in relation to specific energy. Applying [Eq. \(2.14\)](#) to sections 2 & 3, where section 2 is upstream of the jump and section 3 downstream, then:

From [Eq. \(2.9\)](#), $Fr_2 = 7.1874/(9.807 \times 0.4174)^{1/2} = 3.552$.

From [Eq. \(2.14\)](#), with appropriate notation changes, $h_3/h_2 = 1/2 [(1 + 8 \times 3.552^2)^{1/2} - 1] = 4.549$.

Hence $h_3 = 4.5487 \times 0.4174 = 1.899$ m.

Thus the height of the jump = $h_3 - h_2 = 1.898 - 0.417 = 1.481$ m.

The maximum tail water level to prevent drowning of the sluice gate is thus around 1.90 m.

In order to determine the energy loss, one needs to calculate E_3 .

Downstream of the jump, $U_3 = Q/A_3 = 13.5/(1.8986 \times 4.5) = 1.580$ ms⁻¹.

Hence $E_3 = 1.8986 + 1.5801^2/(2 \times 9.807) = 2.026$ m.

The specific energy lost in the jump = $E_2 - E_3 = 3.051 - 2.026 = 1.025$ m.

This may also be determined from the standard relationship for a jump in a rectangular channel (see Chow, 1959), where again b_1 and b_2 are the depths before and after the jump

$$\Delta E = (b_2 - b_1)^3 / (4b_1 b_2) \quad (2.15)$$

Thus between sections 2 & 3, $\Delta E = (1.8986 - 0.4174)^3 / (4 \times 0.4174 \times 1.8986) = 1.024$ m.

The power lost is given by

$$P = \rho g Q \Delta E \quad (2.16)$$

Hence power loss = $1000 \times 9.807 \times 13.5 \times 1.0251 = 135713$ Watts {or 135.7 kW}.

Note how the specific energy and momentum vary between sections 1, 2 & 3. The value of b_3 in Figure 2.4 is seen to be much less than b_1 , indicating an energy loss somewhere between 1 & 3. Most of this loss is known to occur as a result of the intense mixing and turbulence within the hydraulic jump. Between 1 & 2, across the sluice gate, it was therefore assumed that $\Delta E = 0$ and $\Delta M \neq 0$, whereas across the hydraulic jump, between 2 & 3, it was assumed that $\Delta E \neq 0$ and $\Delta M = 0$. Since both energy and momentum feature later with regard to hydraulic structures, the momentum function, M , is now introduced. Applying Newton's 2nd law for flow in an open channel

$$F_1 - F_2 + F = \beta \rho Q (U_2 - U_1) \quad (2.17)$$

where F_1 & F_2 are the hydrostatic forces acting on upstream and downstream cross sections ($= \rho g A \bar{z}$), \bar{z} is the distance below the water surface to the centre of area of the cross section, F is any additional force acting on the fluid in the direction of flow and β = momentum correction coefficient. Then in general for 1-D flow

$$\rho g A_1 \bar{z}_1 - \rho g A_2 \bar{z}_2 + F = \beta \rho Q (U_2 - U_1) \quad (2.18)$$

Re-arranging terms in Eq. (2.18), dividing by ρg and assuming here for simplicity that $\beta = 1$, then

$$\left\{ \frac{Q^2}{gA_1} + A_1 \bar{z}_1 \right\} - \left\{ \frac{Q^2}{gA_2} + A_2 \bar{z}_2 \right\} + \frac{F}{\rho g} = 0 \quad (2.19)$$

Defining the momentum function as

$$M = \frac{Q^2}{gA} + A \bar{z} \quad (2.20)$$

then the force acting on the fluid in the flow direction between any two sections is

$$\frac{F}{\rho g} = M_2 - M_1 \quad (2.21)$$

For the special case of a rectangular channel, with $\bar{z} = b/2$, Eq. (2.20) shows that the momentum function is related to the specific force ($= F/b$, i.e. force per unit width) by

$$M = b \left[\frac{q^2}{gb} + \frac{b^2}{2} \right] \quad (2.22)$$

Equation (2.22) has certain similarities with the Eq. (2.13) as already shown in Figure 2.4. Thus in Example 4, the force acting on the sluice gate, F_g , ($= -F$) may be calculated from Eq. (2.21), giving

$$M_1 = 4.5 \times [3^2/(9.807 \times 3.0) + 3^2/2] = 4.5 \times [0.3059 + 4.5] = 21.627 \text{ m}^3.$$

$$M_2 = 4.5 \times [3^2/(9.807 \times 0.4174) + 0.4174^2/2] = 4.5 \times [2.1986 + 0.0871] = 10.286 \text{ m}^3.$$

$$F = 1000 \times 9.807 \times (10.2858 - 21.6266) = -111218.98 \text{ N or } -111.22 \text{ kN.}$$

$F_g = -F = +111.22 \text{ kN}$ (i.e. force is positive and therefore acts in the direction of flow).

It should be also noted that in the derivation of Eq. (2.14) it is assumed that the frictional force, F_f , on bed under the short length of the jump is negligibly small. This is equivalent to stating that in Eq. (2.17) the force $F = -F_f = 0$. However, in straight channels where there may be blocks, or forward and rearward facing steps present (as shown in Figure 2.22), the relevant forces have to be specified in Eq. (2.17) in order to produce an equation equivalent to Eq. (2.14). Where supercritical flow occurs in channels with bends, care must be taken in dealing with the high super-elevation that might occur and any cross waves that may develop as a result of a hydraulic jump forming in the channel. See Chow (1959) for further details on these topics.

2.2 COMMON DIFFICULTIES IN MODELLING FLOW IN RIVERS AND WATERCOURSES

The five examples in Section 2.1 were selected to illustrate simple flow behaviour in channels where the geometry of the cross section is prismatic, i.e. a constant cross sectional shape in the flow direction, the roughness is uniformly distributed around the wetted perimeter and characterised by the Manning equation, and there are no complex hydraulic structures, vegetation or sediment within the channel. In reality, in most rivers and watercourses, all of these issues are generally of concern and must be modelled appropriately.

The previous pages and some of the examples have highlighted the three physical laws related to the conservation of mass, energy and momentum. In each example the flow was considered to be steady, with no additional discharge being introduced with distance along the channel, thus always ensuring mass conservation ($Q_1 = Q_2$).

The conservation of energy was assumed in the analysis of the vertical sluice gate ($E_1 = E_2$), allowing the depths either side to be determined, whereas the force acting on the fluid (or the reaction on the gate) was shown to be related to the change in momentum (i.e. $M_1 \neq M_2$). In the case of the hydraulic jump, an energy loss occurred (i.e. $E_2 \neq E_3$), but momentum was conserved ($M_2 = M_3$). Dealing with energy losses is, as shown later, one of the key issues to be considered in modelling flows in rivers.

Although the same three physical principles outlined in Section 2.1 apply to flow in natural watercourses, the flow structure is typically three-dimensional and unsteady. The geometry of the river itself is also generally more complex and highly variable in the streamwise direction. All of this makes the modelling of flow in rivers and watercourses more difficult. Furthermore, there is often little or no data concerning channel roughness or resistance, which are typically flow and season dependent. Many of the hydraulic structures that have been built in rivers are often outflanked by the flow in flood conditions, or built to non-standard conditions, thus creating uncertainties in the application or interpretation of various national or international codes of practice. There are also scale issues to consider when modelling at basin, reach, or cross-section scales, and even the schematisation of a short stretch of river requires careful consideration. Hydraulic controls may also vary with flow conditions, due to changing channel resistance, the behaviour of particular hydraulic structures or even human input. For these reasons, some of the common difficulties and issues in modelling actual river flows are now considered.

2.2.1 Modelling flow in rivers and watercourses

The use of models in investigating and solving practical river engineering problems is now so commonplace, that it is easy sometimes to overlook their origin, nature and purpose. There are different types of model that are now routinely used to analyse both general flow behaviour patterns and also particular hydraulic issues, such as the extent of flooding, sediment deposition or erosion patterns, pollution incidents, vegetation control and habitat biodiversity. A wide range of hydrodynamic tools are also frequently used in developing optimum design strategies for dealing with specific practical problems. For example, these tools might include models for flood risk mapping, or models that simulate dispersion phenomena, sediment movement, bank erosion or general flow behaviour. Such tools are typically based on a mathematical representation of the physical processes (sometimes incorrectly referred to as a ‘model’), contain advanced numerical procedures, and employ complex computer techniques to carry out not only all the routine calculations, but also to present the results in a convenient form to the end-user, typically in graphical as well as numerical format.

The origin of modern, computer-based, river modelling began in the 1960’s and the background to this is described by Abbot (1991), Cunge *et al.* (1980) and Nakato & Ettema (1996). Some of the key steps involved in modelling flow behaviour may be summarized as follows:

- Identify the nature of the practical problem requiring solution;
- Identify the physical processes involved;
- Develop some mathematical representation of the physical processes;
- Understand any limitations to the mathematical representation;

- Replace the (simplified) mathematical governing equations with a set of alternative equations based, for example, on finite difference, finite element or finite volume equations;
- Define the ‘domain’ of the river to be studied and represent it by a suitable mesh or grid. This process is sometimes known as the ‘schematization’;
- Define the boundary conditions to the domain, e.g. flows, velocities or water levels at specified boundaries;
- Solve the set of equations using appropriate numerical techniques;
- Check the answers by solving any ‘benchmark’ test cases to similar problems and compare the solutions;
- Calibrate the model for the particular problem in hand, optimizing key features such as water levels, velocity distributions, flow capacity, etc. by appropriate selection of any calibration coefficients;
- Check on the values and range of any calibration coefficients used, preferably by direct measurement or by comparison with other values in similar circumstances, with reference to their physical meaning;
- Optimize the design or analysis by repeated use of the model.

The word ‘model’ is now used frequently in a broader sense, not just for the mathematical equations governing the physical processes, but to describe the whole modelling process, as described above, often encapsulated in a particular software ‘package’. A good example of the development from ‘physical processes’ to a conceptual ‘theoretical model’ is shown in the work of the ASCE Task Force on River Width Adjustment (Thorne *et al.*, 1998; Darby *et al.*, 1998). Another example showing the development from initial data on overbank flow, through to conceptual thinking, model development and calibration issues is described by Knight (2008a&b).

Modelling thus involves not only selecting the right ‘tool’ for the right ‘job’, but also being aware of the various steps involved, particularly concerning the limitations and uncertainties in the chosen methodology. It is quite possible that, for example, the numerical procedures may vary between models even of the same type. Furthermore, most models use empirical coefficients that have to be selected carefully at the calibration stage, often without adequate field measurements on the particular river in question. Turbulent parameters are also often based on inadequate full-scale measurements, sometimes even on flows other than in rivers, and in some cases on flows not even amenable to experimental scrutiny at all. See Nezu & Nakagawa (1993) and Ikeda & McEwan (2009) for further details.

The use of resistance coefficients to account for roughness effects is particularly problematic, as indicated by Yen (1991) and Morvan *et al.* (2008) and described later in more detail in Section 2.2.3 and in [Chapter 3](#). The engineer is thus faced with some considerable difficulty in blending theoretical and empirical knowledge together in a pragmatic manner in order to simulate river processes and develop any type of ‘model’ at all. See Ikeda & McEwan (2009), Knight (1996 & 2008a&b) and Wang (2005) for further details.

2.2.2 Schematisation of channel geometry

The schematisation of river geometry may be relatively straightforward where the cross section is of a simple shape and prismatic. [Figure 2.5](#) illustrates a trapezoidal



Figure 2.5 River Main, with compound trapezoidal cross section (i.e. a prismatic channel).



Figure 2.6 River Severn in flood at Upton upon Severn, February 1990 (See colour plate section).

compound section, an ‘engineered’ channel, which forms part of a specially constructed flood relief scheme for the River Main in Northern Ireland. Between 1982 and 1986, an 800 m reach of the channel was reconstructed and realigned to form a double trapezoidal channel from Lisnafillan Weir to the junction with the Braid River. The cross-section comprises a main channel with a bankfull depth of $\sim 0.9\text{--}1.0$ m, a top width of 14 m, two berms covered with heavy weed growth, making a total width, inclusive of floodplains, of 27.3–30.4 m. The floodplains slope towards the main channel with a 1:25 gradient. The reach-averaged longitudinal bed slope is 0.00297. The river bed consists of coarse gravel, with a d_{50} of the order 10–20 mm and the main channel side slopes consist of quarry stone (0.5 tonne weight, 100–200 mm size). This reach has been closely monitored (Myers & Lyness, 1989) and subsequently modelled extensively, as discussed later.

Many natural rivers, particularly in times of flood, exhibit much more variability in both cross section shape and plan form geometry than engineered channels. Figure 2.6 shows the lower reaches of the River Severn during extensive flooding in February 1990, with the town of Upton upon Severn at the centre of inundation. In this case the river has overflowed its banks and occupied part of its floodplain. Figure 2.6 thus illustrates the need to include sufficient floodplain area, together with



Figure 2.7 River Severn in flood at Worcester, February 1990. Note land use management (See colour plate section).

embankments, bridges and urban areas in any numerical model for effective flood risk mapping and management. Figure 2.7 shows an example of why it is important to include flood plain storage elements into any model. The flooded racecourse in the foreground will make a positive contribution towards reducing flooding, as it provides additional short-term storage whenever particular floods occur. This illustrates a good example of integrated policy on land use. The reclaimed land in the centre, on the other hand, may indicate poor land use policy, since it demonstrably restricts the flood plain width and hence exacerbates flooding locally.

The severe economic damage that such flooding causes to infrastructure, the loss of life and the potential impact of climate change, have forced many politicians to re-consider land use policy. The global scale of the impact of flooding is described by Knight (2006a) and the impact of climate change is dealt with by Bronstert (2006a&b), Green *et al.* (2009) and Oshikawa *et al.* (2008). Examples of the impact of recent flooding in 7 European countries are described by Knight & Samuels (2007). The European Parliament ratified the Flooding Directive in 2007 (European Commission, 2007) that requires the following for every river basin district:

- Preliminary flood risk assessment to identify areas for subsequent investigation;
- Flood risk maps;
- Flood risk management plans.

The role of numerical models is therefore likely to play a significant part in all of these activities. As described elsewhere by Knight (2006c), the schematisation of a river, including its floodplain, is an important element in constructing a successful mathematical simulation model. It should not be treated merely as an exercise in digitising numerous survey data, but rather as an art: that of blending the geometry and the hydraulic flow features together in parallel. General rules for the location of cross-sections and the data requirements for 1-D models are given in Samuels (1990 & 1995), Cunge *et al.* (1980), Casellarin *et al.* (2009) and Defalque *et al.* (1993), summarized below:

- At model limits (boundary conditions)
- Either side of structures (for afflux or energy loss calculations)

- At all flow and level measuring stations (for calibration purposes)
- At all sites of prime interest to the client
- Representative of the channel geometry
- About $20B$ apart (as a first estimate only), where B = bankfull width
- A maximum of $0.2H/S_o$ apart
- A maximum of $L/30$ apart where L is the length scale of the physically important wave (flood or tide)
- The area for successive sections lies between $2/3$ and $3/2$ of the previous section.
- The conveyance for successive section lies between $4/5$ and $5/4$ of the previous sections.

The overall plan form geometry of a river, and its associated floodplain boundaries, as well as other large topographical features, will inevitably steer the flow into certain patterns and produce large scale or macro flow structures. For example, dense bankside vegetation or clumps of trees/hedges on the floodplain will create plan form vorticity that will govern lateral momentum transfers and mixing processes. The variation in the shape of the main river channel around a meander bend likewise causes significant variation in the longitudinal flow pattern. Convective accelerations and decelerations along the channel will not only affect turbulence levels and resistance, but the balance of terms in the 1-D equation also. Likewise, non-prismatic floodplains will produce transverse fluxes of mass and momentum which need to be considered (see for example Bousmar, 2002; Bousmar & Zech, 1999; Bousmar *et al.*, 2004; Chlebek & Knight, 2008; Chlebek, 2009; Elliott & Sellin, 1990; Rezaei, 2006; Sellin, 1995). The degree of sinuosity, as well as the depth of flow and the aspect ratio of the river channel, will affect the position of the filament of maximum velocity, and thus influence where bank erosion might take place (Okada & Fukuoka, 2002 & 2003). Such knowledge is clearly required before designing bank protection works, targeting maintenance work or estimating flood wave speed (Tang *et al.*, 2001).

Although survey data are collected routinely at particular cross-sections, it should be remembered that the hydraulic equations are generally applied to a reach (Laurensen, 1985; Samuels, 1990) and that energy losses are quantified over a specific distance. Although care may be taken in identifying reaches that are approximately prismatic, there will inevitably be some longitudinal variation in shape and energy gradient that will cause changes in hydraulic parameters in the streamwise direction. An example of the use of 1-D models to determine the appropriate ‘bankfull discharge’ along a series of river reaches is given by Navratil *et al.* (2004).

2.2.3 Roughness and resistance

Although it is relatively straightforward to obtain digital terrain data, it is much harder to obtain the corresponding roughness data to go with the terrain data to the same level of detail (Defra/EA, 2003b; Hicks & Mason, 1998). For this reason the CES includes a Roughness Advisor that allows the modeller to select appropriate roughness values for various substrates, types of vegetation and seasonal growth patterns. Figures 2.1(a) & (b) have already shown the variation that can occur in lowland and upland rivers. To illustrate seasonal growth of instream and bankside vegetation,

Figures 2.8 & 2.9 show two reaches of the River Blackwater in Hampshire, near Coleford bridge. The effect of this vegetation on the roughness coefficient and conveyance capacity of the river throughout the year is documented by Sellin & van Beesten (2004).

A distinction should be made between ‘roughness’, which denotes a surface textual property and ‘resistance’, which is the cumulative effect of the roughness resisting any hydraulic flow over or through a particular type of roughness. The meaning of the term ‘roughness’ in the field of fluvial hydraulics, and how it is often formulated as a ‘resistance to flow’ term in 1-D, 2-D & 3-D numerical models, is described elsewhere more fully by Morvan *et al.* (2008). The Manning formula (1891), which was introduced in Section 2.1, is but one of a number of equations that attempt to quantify hydraulic resistance to flow. Although it is well founded and popular with river engineers (Yen, 1991), it should be recognized that there are a number of alternative formulations that describe resistance. A brief review of these and related topics is now given.



Figure 2.8 River Blackwater, showing seasonal growth (Winter to Summer) in a narrow reach (See colour plate section).



Figure 2.9 River Blackwater, showing seasonal growth in a meandering reach (See colour plate section).

One of the earliest resistance equations was that by Chezy (1768), who expressed the discharge in an open channel in terms of a roughness ‘constant’, C , where

$$Q = CAR^{1/2} S_o^{1/2} \quad (2.23)$$

This was followed by the Darcy-Weisbach equation (1857), which gave the head loss, h_f , over a length, l , in either a circular pipe or open channel as

$$h_f = \frac{f \ell U^2}{2gd} = \frac{f \ell U^2}{8gR} \quad (2.24)$$

where h_f = head loss, f = friction factor, l = length of pipe or channel, d = pipe diameter, R = hydraulic radius ($= A/P = d/4$ for pipe running full), U = section mean velocity ($= Q/A$), and S_f = friction slope ($= h_f/l$). When the friction slope, S_f , is equal to the bed slope, S_o , (see Section 2.2.4 for further details), then Eq. (2.24) may be expressed in a similar way to Eq. (2.23) as

$$Q = \left(\frac{8g}{f} \right)^{1/2} AR^{1/2} S_o^{1/2} \quad (2.25)$$

The Colebrook-White equation (Colebrook, 1939; Colebrook and White, 1937) clarifies how f varies in smooth and rough pipes, conduits running part full and open channels. The variation of f is usually expressed in terms of two parameters, the relative roughness, k_s/d and the Reynolds Number, Re ($= 4UR/v$). For clarity, two forms of the Colebrook-White equation are given, one for pipes and another for channels, but these are essentially the same, since $d = 4R$:

$$\frac{1}{\sqrt{f}} = -2.0 \log \left[\frac{k_s}{3.71d} + \frac{2.51}{(ud/v)\sqrt{f}} \right] \text{(pipes \& culverts running full)} \quad (2.26)$$

$$\frac{1}{\sqrt{f}} = -2.0 \log_{10} \left[\frac{k_s}{14.8R} + \frac{2.51}{(4UR/v)\sqrt{f}} \right] \text{(open channels and pipes part full)} \quad (2.27)$$

The variation of f with k_s/d and Re is often shown plotted in the form of the so-called ‘Moody diagram’ (1944), as illustrated in Figure 2.10. The roughness of any surface is now characterised by k_s , the so-called Nikuradse equivalent sand roughness size (see Nikuradse, 1933), a measure of the size of excrescences, k , on a flat surface that would yield the same resistance as that in a circular pipe roughened with uniform grains of sand. The Colebrook-White equation is physically well founded, since it tends towards two theoretically limiting cases, described elsewhere by Schlichting (1979). For example, for very smooth surfaces, as $k_s \rightarrow 0$, then Eq. (2.27) becomes the Prandtl ‘smooth law’, in which f depends solely on Reynolds Number, Re , giving:

$$\frac{1}{\sqrt{f}} = 2.0 \log_{10}(Re\sqrt{f}) - 0.80 \quad (2.28)$$

On the other hand, as $Re \rightarrow \infty$, Eq. (2.27) becomes the fully ‘rough law’, in which f is independent of Re and depends solely on the ratio of surface roughness, k_s ,

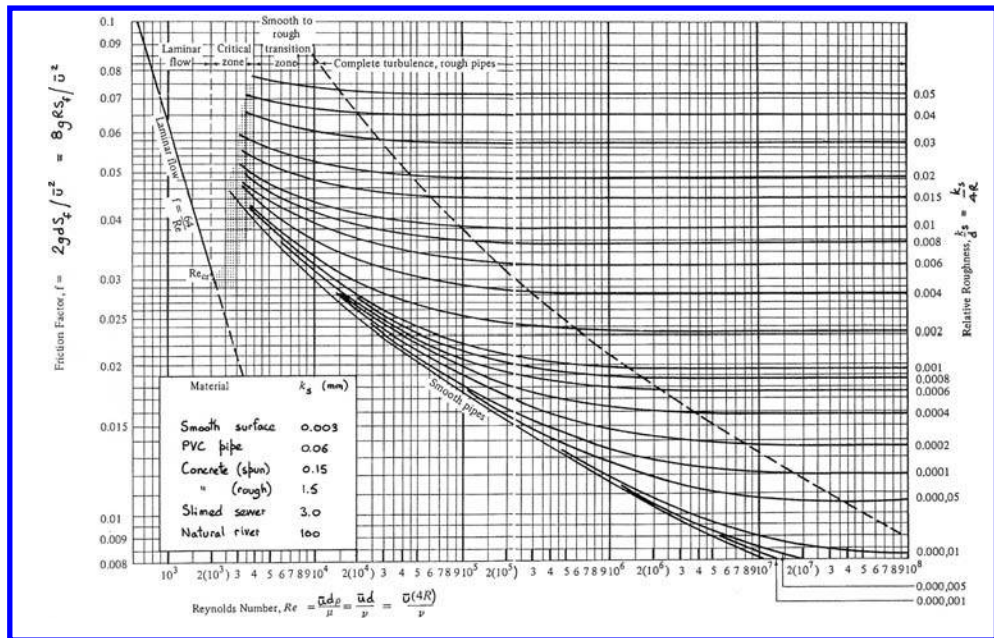


Figure 2.10 Variation of friction factor, f , versus Re and k_s/d or $k_s/4R$ (Moody, 1944).

to hydraulic radius, R , i.e. $k_s/4R$, giving:

$$\frac{1}{\sqrt{f}} = -2.0 \log_{10} \left[\frac{k_s}{14.8R} \right] \quad (2.29)$$

This is particularly important in river engineering as it may be shown that this links Manning's n in Eq. (2.1) with k_s , in Eq. (2.27), by the relationship:

$$n = k_s^{1/6} \left[\frac{(R/k_s)^{1/6}}{18 \log(11R/k_s)} \right] \quad (2.30)$$

The Colebrook-White equation essentially expresses the transition region from '*hydraulically smooth*' to '*hydraulically rough*' flow. Technically these terms are defined by the shear Reynolds Number, (U_*k_s/ν) , as

Hydraulically smooth $(U_*k_s/\nu) < 5$

Transitional flow $5 < (U_*k_s/\nu) < 70$

Hydraulically rough $(U_*k_s/\nu) > 70$

where U_* is known as the shear velocity, defined by

$$U_* = \sqrt{\tau_o/\rho} \quad (2.31)$$

with τ_o = boundary shear stress and ρ = fluid density. The shear stress and shear velocity are important parameters in open channel flow as they frequently used when dealing with sediment transport and erosion issues (Chang, 1988). The boundary shear stress may be shown to be related to geometric parameters as follows.

Consider a short length of a prismatic channel, Δx in length, with a cross-sectional area, A , then in uniform flow, there will be a balance between the weight force acting down the channel bed slope ($=mg\sin\theta$, where m = mass, θ = channel bed slope and $\tan\theta = S_o$), with the resisting force acting on the wetted area ($=\tau_o P\Delta x$, where τ_o = mean boundary shear stress, and P = wetted perimeter). For small channel bed slopes ($< \sim 0.1$), since $\theta \approx \sin\theta \approx \tan\theta = S_o$, then for uniform flow $\rho g A \Delta x S_o = \tau_o P \Delta x$, noting that $R = A/P$, the mean boundary shear stress is given by

$$\tau_o = \rho g R S_o \quad (2.32)$$

This is essentially the momentum principle applied to this particular case. For practical purposes, and in order to provide a link between shear stress and velocity (or discharge), the energy principle needs to be invoked. If the shear stress, τ_o , is assumed to be proportional to the square of the velocity (for dimensional reasons), then this suggests that

$$\tau_o \propto \rho U^2 \quad (2.33)$$

The constant of proportionality must then be $f/8$, where f is the friction factor, in order to satisfy Eq. (2.24). Hence

$$\tau_o = \frac{f}{8} \rho U^2 \quad (2.34)$$

It may then be observed that by equating Eqs. (2.31) & (2.34), the Darcy-Weisbach friction factor, f , is simply the ratio of two velocities, U_* and U , since

$$f = 8 \left(\frac{U_*}{U} \right)^2 \quad (2.35)$$

2.2.4 Energy and friction slopes

So far, two longitudinal slopes have been introduced, the bed slope, S_o , and the friction slope, S_f ($= h_f/l$) via Eqs. (2.1) or (2.23) and (2.24) respectively. These only have the same value when the depth and velocity do not change with distance, x , along the channel, i.e. uniform flow exists and $h = h_n$. Although this is an important type of flow, often used when calculating conveyance capacity, as shown in the worked Examples 1–3, natural river flows are frequently affected by upstream or downstream controls. This makes the flow non-uniform, that is to say, the depth and velocity now vary with distance x along the channel, as well as possibly with time, t , if the flow is also unsteady. See Figure 2.11 for general non-uniform flow behaviour and notation.

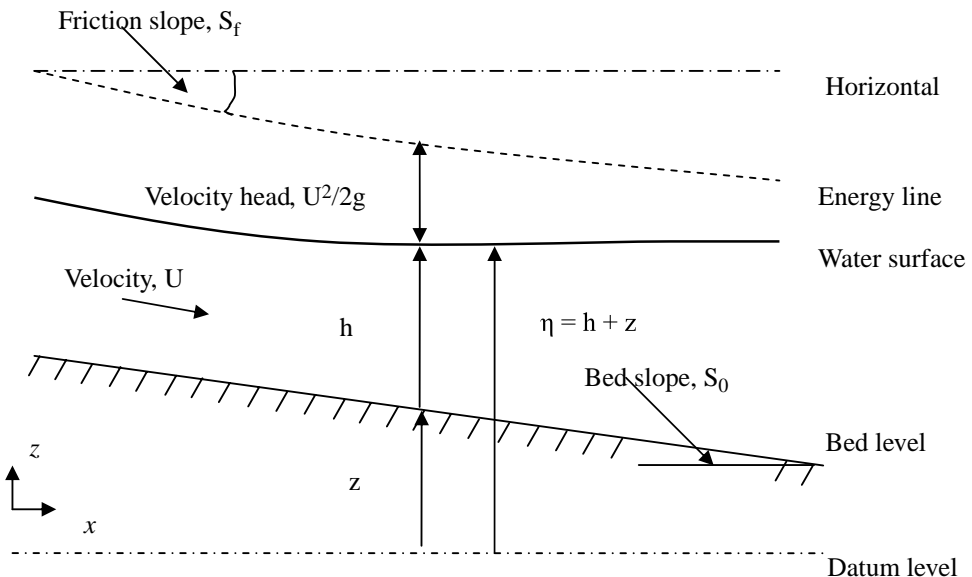


Figure 2.11 General non-uniform flow behaviour, with notation.

Under these circumstances, the friction slope is given by the following 1-D equation

$$S_f = S_o - \left[\frac{\partial h}{\partial x} + \frac{U}{g} \frac{\partial U}{\partial x} + \frac{1}{g} \frac{\partial U}{\partial t} \right] \quad (2.36)$$

in which $\{h \& U\}$ vary as functions of distance and time $\{x \& t\}$. Since the first two terms on the right hand side are equivalent to the water surface slope, S_w , ($=\partial\eta/\partial x$), then Eq. (2.36) may be simplified and expressed in a form useful for field measurements, as

$$S_f = \frac{\partial \eta}{\partial x} - \frac{U}{g} \frac{\partial U}{\partial x} - \frac{1}{g} \frac{\partial U}{\partial t} \quad (2.37)$$

Equation (2.36) is important in extending rating curves (h v Q relationships), since it may be combined with Manning's equation, in which S_f replaces S_o in Eq. (2.1) for non-uniform flow. The discharge in unsteady non-uniform flow, Q , in terms of the discharge for steady flow at the same depth, based on the same Manning roughness coefficient, Q_n , is then given by

$$Q = Q_n \left[1 - \frac{1}{S_o} \frac{\partial h}{\partial x} - \frac{U}{g S_o} \frac{\partial U}{\partial x} - \frac{1}{g S_o} \frac{\partial U}{\partial t} \right]^{1/2} \quad (2.38)$$

The concept of specific energy that was introduced via Eq. (2.12) relates the depth and kinetic energy of the flow relative to the bed (invert) of the channel. If the level of the channel bed (invert) above a horizontal reference frame is given by z_b , then the

total energy, E_t relative to this reference frame is

$$E_t = z_b + h + \alpha \frac{U^2}{2g} = z_b + E \quad (2.39)$$

The gradient of total energy in the downstream direction, S_e , is then given by

$$\frac{\partial (E_t)}{\partial x} = \frac{\partial (z_b + E)}{\partial x} = -S_e \quad (2.40)$$

in which the bed slope $S_o = -\partial z_b / \partial x$. In steady uniform flow, all three slopes, S_o , S_f & S_e have the same value, S , and normal flow occurs ($h = h_n$). Under these circumstances, the conveyance of a channel, K , is defined as

$$Q = KS^{1/2} \quad (2.41)$$

Conveyance is thus a quantitative measure of the discharge capacity of a water-course, relating the total discharge, Q (m^3s^{-1}) to a measure of the gradient or slope of the channel. By comparing Eqs. (2.1) & (2.41), it may be seen that K (m^3s^{-1}) is essentially related to the geometry and roughness of the channel. For example, when Manning's equation is used

$$K = A^{5/3} / (nP^{2/3}) \quad (2.42)$$

For steady non-uniform flow, Eq. (2.36) may be reduced to an ordinary differential equation

$$\frac{dh}{dx} = \frac{S_o - S_f}{1 - Fr^2} \quad (2.43)$$

Equation (2.43) may be solved to give the variation of depth, b , with distance, x , along a channel. The local depth is seen to depend on the longitudinal variation of 3 parameters, the bed slope, S_o , the friction slope, S_f and the Froude Number, Fr . For a reach of length, Δx , then the average friction slope, \bar{S}_f , is required (Laurensen, 1985), and Eq. (2.43) is commonly written in the form

$$\Delta x = \frac{\Delta E}{S_o - \bar{S}_f} \quad (2.44)$$

Equation (2.43) is usually known as the 'gradually varied flow' (GVF) equation, and leads to a way of classifying longitudinal water surface profiles in open channels. For a wide rectangular channel, such that $b \gg h$, then $R \approx h$ and Eq. (2.43) may be written as

$$\frac{db}{dx} = \frac{S_o[1 - (b_n/b)^{10/3}]}{1 - (b_c/b)^3} \quad (2.45)$$

This shows that water surface profiles depend upon values of S_o , b_n and b_c . Traditionally, these profiles have been divided into 5 classes, depending on the bed slope,

and each class is further sub-divided depending on the depth of water, h , relative to the normal and critical depths, h_n and h_c . For a given shape of cross section, discharge, bed slope and roughness, the values of h_n and h_c may be determined, as shown previously, and these will effectively divide the flow space into 3 depth zones. The water surface, being disturbed from its equilibrium normal depth, may lie in any of these 3 depth zones. Flow profiles are then classified by denoting the type of channel bed slope by a letter and the depth zone by a number. For example, an M3 profile would imply that the channel bed slope is mild (M) and that the flow was in zone 3, i.e. supercritical. Since there are 5 classes of channel slope: horizontal (H), mild (M), critical (C), steep (S) and adverse (A), one might expect 15 possible profiles. In fact 2 are inadmissible (H1 and A1) and C2 is technically uniform flow with $h_n = h_c$, so there are only 12 distinct gradually varied flow profiles.

Of most interest to river engineers are those on mild or horizontal slopes, illustrated in Figures 2.12 & 2.13 respectively. In Figure 2.12, the left hand side indicates the 3 depth zones, with schematic M1, M2 and M3 water surface profiles sketched in relation to imaginary h_n and h_c lines drawn parallel to the bed. On the right hand side of the Figure, the smaller diagrams (a) to (f) represent some examples of where such profiles might typically occur in practice. For mild slopes ($h_n > h_c$), the backwater profile (M1) is frequently encountered, particularly in relation to bridges and control structures, as shown later in Section 2.6. An estimate of the length of a backwater profile has been given by Samuels (1989b), as

$$L = 0.7h/S_o \quad (2.46)$$

where L = the distance upstream over which the water depths are disturbed by more than 10% from their equilibrium condition ($h = h_n$). The actual water surface profile may be determined by numerical solution of the GVF equation, using the ‘standard step’ method for non-prismatic channels, or the ‘direct step’ method for prismatic channels. See Chow (1959) and Henderson (1966) for further details of these so called

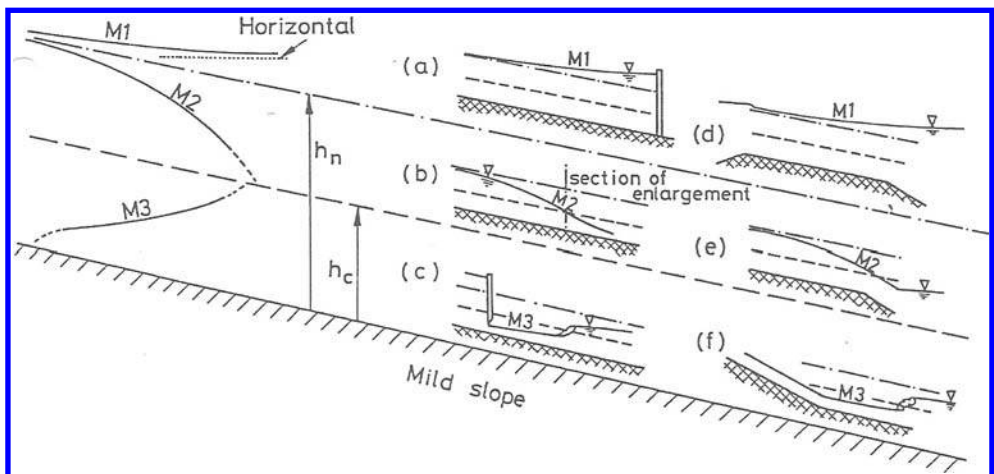


Figure 2.12 Gradually varied flow profiles on a mild slope.

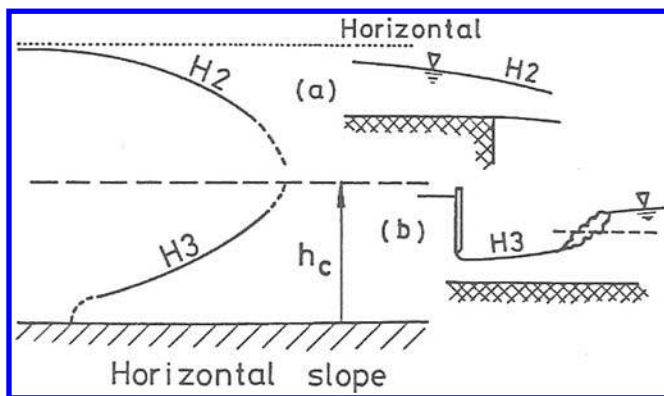


Figure 2.13 Gradually varied flow profiles on a horizontal slope.

'step' methods. Since there is a widespread need to calculate backwater lengths or profiles, a backwater routine is included within the CES and further details are given in Chapters 3 & 4 (Sections 3.2.4 & 4.3 respectively).

In addition to the bed slope and friction slope, the energy slope, S_e , is also important. Since this involves the kinetic energy correction coefficient, to account for the 3-D nature of most flow fields in rivers, the next section considers a number of issues related to the velocity distributions within channels and their implications for 1-D modelling.

2.2.5 Velocity distributions and implications for 1-D modelling

Up until now, the flow has been considered as one-dimensional (1-D), with the section mean velocity, U ($= Q/A$) being the only one used in all resistance equations and water surface profile relationships. As mentioned earlier, this has certain implications with respect to energy, kinetic head, and approximating 3-D effects into a lateral distribution model such as is used in the CES. Figure 2.14 shows a typical velocity field for inbank flow in a simple trapezoidal channel, taken from the work of Yuen (1989). Figure 2.15 shows how the flow field becomes even more complex when overbank flow occurs, partly due to the strong interaction that may develop between the flows in the main river channel and on the floodplain(s). Since 3-D concepts and flow structures are described in more detail in Section 3.1, only those that are relevant to the velocity field are introduced now, hopefully enabling the reader to understand more about modelling flows in rivers.

The first issue to appreciate is the 3-D nature of the flow, even in straight channels. Figure 2.14 shows a typical isovel pattern, secondary flow cells (Einstein & Li, 1958; Nezu & Nakagawa, 1993) and the resulting distribution of boundary shear stress around the wetted perimeter (Knight *et al.*, 1994). The maximum velocity may be at the free surface for a wide river, as shown, but very often is just below the surface, particularly in channels with a low aspect ratio (b/h). Boundary layers (Schlichting, 1979) develop from the bed and sides of the channel, with the local velocity, u , being zero at every solid/liquid interface around the wetted perimeter (i.e. a boundary condition

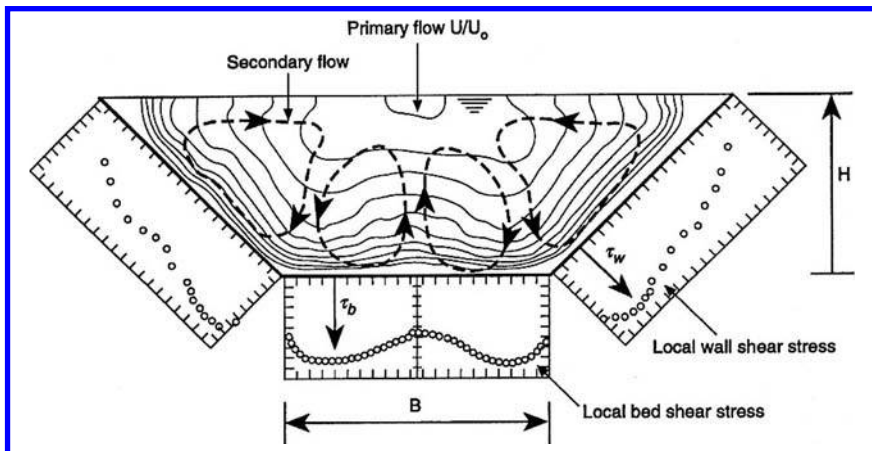


Figure 2.14 Isovels and boundary shear stresses for inbank flow in a trapezoidal channel (after Knight et al, 1994).

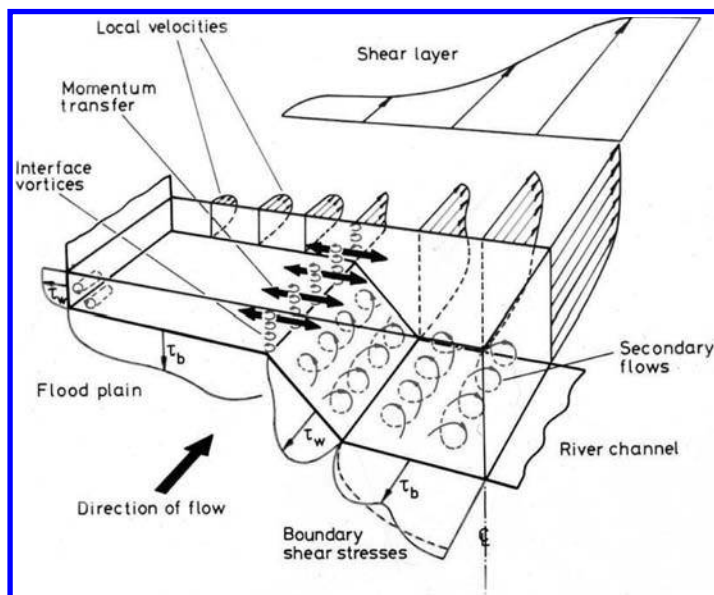


Figure 2.15 Flow structures in a straight two-stage channel (after Knight & Shiono, 1996).

of $u = 0$). If the channel is wide (large aspect ratio, b/h), then the velocity distribution over a vertical at the centre-line position may be assumed to be approximately logarithmic, described by Prandtl's logarithmic velocity law for a rough surface as

$$\frac{u}{u_*} = \frac{1}{\kappa} \ln \left(\frac{z}{z_0} \right) \quad (2.47)$$

where u = velocity a distance z above the bed, u_* is the local shear velocity, κ is von Karman's constant, $z_0 = \gamma k_s$, γ = constant and k_s is the Nikuradse equivalent sand roughness size. Thus z_0 is assumed to be proportional to the size of the roughening excrescences, k_s , as for smooth surfaces. Early experiments gave values of $\gamma = 1/30$ and $\kappa = 0.40$ (now taken as ~ 0.41). Hence the velocity distribution law for rough surfaces is often assumed to be governed by an equation of the form

$$\frac{u}{u_*} = 2.5 \ln\left(\frac{z}{k_s}\right) + 8.5 \quad \text{or} \quad \frac{u}{u_*} = 5.75 \log_{10}\left(\frac{z}{k_s}\right) + 8.5 \quad (2.48)$$

The corresponding equation for velocity distribution over a smooth surface is of the general form

$$\frac{u}{u_*} = A \ln\left(\frac{z}{k_s}\right) + B \quad (2.49)$$

where A & B are constants. Experiments show that B is a function of $(u_* k_s / v)$, given by

$$B = 2.5 \log_{10}\left(\frac{u_* k_s}{v}\right) + 5.5 \quad (\text{only valid for } (u_* k_s / v) < 5.0) \quad (2.50)$$

Combining Eqs. (2.49) & (2.50), and using Prandtl's original constants, gives the corresponding velocity distribution over a smooth surface as

$$\frac{u}{u_*} = 2.5 \ln\left(\frac{u_* z}{v}\right) + 5.5 \quad \text{or} \quad \frac{u}{u_*} = 5.75 \log_{10}\left(\frac{u_* z}{v}\right) + 5.5 \quad (2.51)$$

The second issue is to consider the implications of using a depth-averaged model. The depth-averaged velocity, U_d , is defined as

$$U_d = \frac{1}{b} \int_0^b u dz \quad (2.52)$$

Typical lateral distributions of U_d across a channel are shown in Figure 2.16. As might be expected, $U_d = 0$ at the two edges and increases towards the central region. The presence of secondary flows may mean that the maximum value of U_d does not actually occur at the centerline of the channel.

The third issue is to consider how a 3-D velocity field might be included in a 1-D formulation of energy or momentum. As noted earlier in Eqs. (2.12) & (2.17), this is usually achieved by use of the kinetic energy and momentum correction coefficients, α and β , here formally defined as

$$\alpha = \frac{1}{U^3 A} \int_A u^3 dA \quad (2.53)$$

$$\beta = \frac{1}{U^2 A} \int_A u^2 dA \quad (2.54)$$

These coefficients are introduced to ensure that the energy flux ($= 1/2 \rho A U^3$) or momentum flux ($= \rho A U^2$) based on the area, A , and section mean velocity, U ,

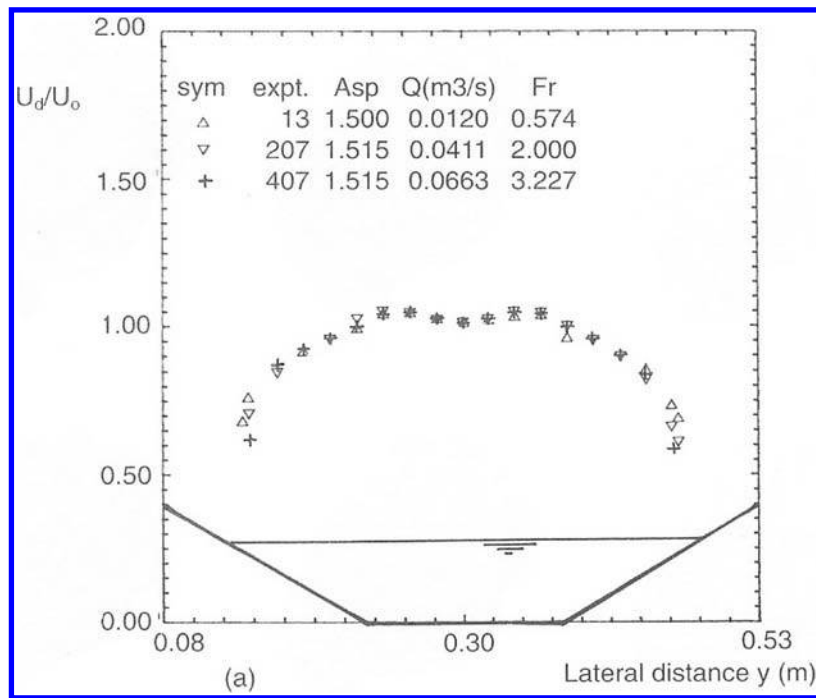


Figure 2.16 Variation of U_d with lateral distance across a trapezoidal channel (Knight et al., 1994).

Table 2.1 Typical values of kinetic energy and momentum correction coefficients.

Correction coefficient	Prismatic channels	Rivers	Using the seventh power law, Eq. (2.55)
α	1.15	1.30 (and higher)	1.045
β	1.05	1.10 (and higher)	1.016

agree with the actual energy and momentum fluxes ($= \int_A \frac{1}{2} \rho u^3 dA$ and $= \int_A \rho u^2 dA$) obtained by summing over the whole area, using local velocities, u , applied to each individual element of area, dA . This effectively allows one to use the section mean velocity, U , rather than knowledge of the complete velocity field ($u = f\{y, z\}$), which can be obtained from measurement or 3-D computational fluid dynamics (CFD) and integrating over the areal surface. The use of these two correction coefficients has great practical merit in that only section mean velocities are used, and these are generally known. Typical values of α and β are shown in Table 2.1.

As indicated in Table 2.1, a seventh power law is sometimes used to represent the distribution of velocity over a vertical in turbulent open channel flow, rather than the more complex logarithmic laws, expressed earlier as Eqs. (2.48) & (2.51), on account

of its simplicity and closeness of fit to logarithmic distributions. This distribution may be written as

$$\frac{u}{u_{\max}} = \left(\frac{z}{h}\right)^{1/7} \quad (2.55)$$

When this is inserted into Eq. (2.52), to obtain the depth-averaged value, it gives

$$U_d = \frac{7}{8} u_{\max} \quad (2.56)$$

Although Eq. (2.55) has the advantage that it is a simpler relationship to use than Eqs. (2.48) & (2.51), it has the disadvantage from an engineering perspective that it needs the maximum velocity, u_{\max} to be known, as well as its position within the cross section. If it is assumed that u_{\max} occurs at the free surface, then it may be shown that U_d occurs at approximately $z = 0.4 h$, regardless of which equation, Eq. (2.48), (2.51) or (2.55), is used. This is helpful, since it forms the basis of river gauging in open channels.

The fourth issue following on from the third, is the application of these α and β coefficients to flows in natural channels. As already indicated in Eq. (2.12), the kinetic head term based on the section mean velocity, $U^2/2g$, needs to be multiplied in every energy relationship by α . In a similar way, wherever the momentum equation is used, the term $\rho Q U$ should be multiplied by β , as indicated in Eq. (2.18), to give the correct force-momentum relationship. The energy line (or surface) may be conceived as an imaginary line drawn a distance $\alpha U^2/2g$, above the water surface, as already indicated by the dotted line in Figure 2.4. This is now shown more clearly in Figure 2.17 for flow in a section of open channel in which there is a constriction, such as arising from bridge piers or a measuring flume. Upstream of the bridge, the velocities are

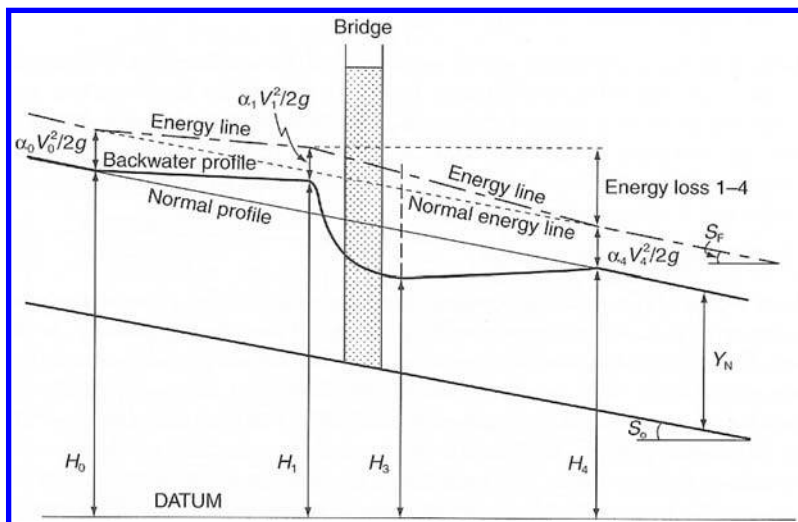


Figure 2.17 Illustration of variation of kinetic heads and energy losses through a bridge (after Hamill, 1999).

lower and so the energy line is closer to the water surface than downstream where the velocities are larger. Note that the afflux is the increase in water level upstream of a bridge, above the water level that would occur in the absence of the bridge, and should not be confused with the energy loss across the whole bridge structure.

In Figure 2.17 water surface dips as it passes through the section with a reduced width, on account of the increase in velocity from considerations of continuity ($Q = U_1A_1 = U_2A_2$). Since the frictional losses are proportional to the square of the velocity, the frictional losses in the narrow section will be larger than those in the channel upstream. Because of the change in cross section, there may also be additional energy losses in the contraction and expansion regions, with the losses in any expansion region generally being larger than those in a contracting region. The overall losses are then the sum of the frictional and additional energy losses, with the overall energy line indicating the total budget of energy and how it is degraded. A distinction should therefore be made between the energy and friction gradients, S_e and S_f .

2.2.6 Hydraulic structures and controls

A particular difficulty in modelling water surface profiles in rivers arises from the wide variety of hydraulic structures that are commonly used in river engineering. These range from weirs and flumes (Ackers *et al.*, 1978; Bos *et al.*, 1984), to bridges and culverts (Neill, 1973; Ramsbottom *et al.*, 1997), gates and sluices (Franke & Valetin, 1969; Kolkman, 1994; Larock, 1969; Rajaratnam & Subramanya, 1969; Rajaratnam & Humpries, 1982), siphon spillways (Novak *et al.*, 1996) and free overfalls (Chow, 1959). Each structure will cause a change in water level across the structure and should be modelled accordingly. For bridges, the ‘head loss’ may be different from the ‘afflux’, as considered further in Section 2.6.

Wherever the flow changes from subcritical to supercritical there exists a unique relationship between h & Q , and this may form one or two ‘control points’. For example, in the case of the sluice gate, illustrated in Figures 2.3 & 2.4 (Example 4 in Section 2.1), the control point on the upstream side of the gate controls all the water levels in the upstream direction, i.e. in the subcritical part of the flow. This is referred to as a backwater profile and, if the sluice gate were sited in a mildly sloping channel,



Figure 2.18 Bridge arches in flooding River Avon (courtesy University of Birmingham) (See colour plate section).



Figure 2.19 Scour in channel with bridge (courtesy HR Wallingford) (See colour plate section).

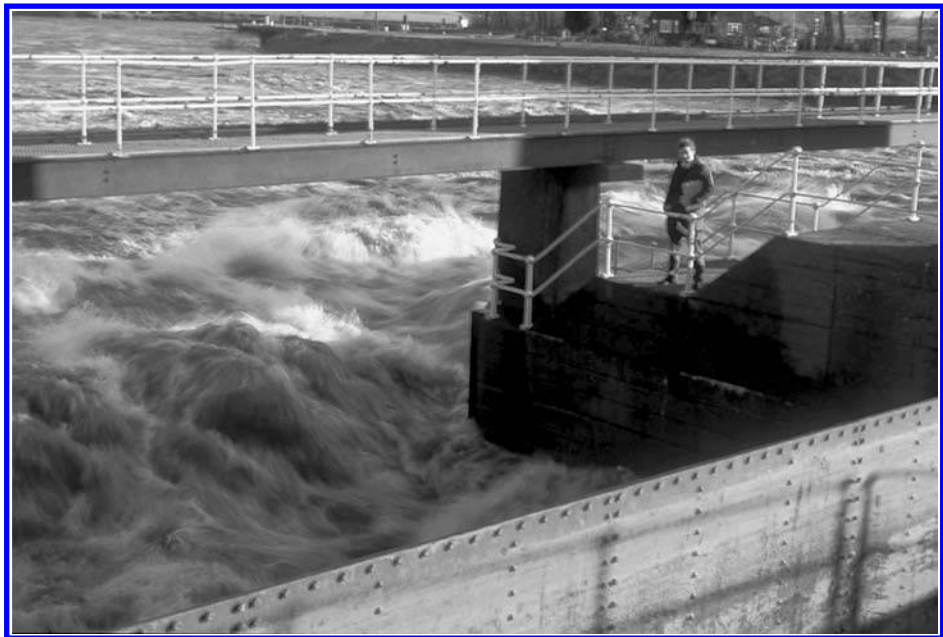


Figure 2.20 Flow downstream of the Holme sluices, River Trent (courtesy University of Birmingham) (See colour plate section).

it would be an M1 profile (see [Figures 2.12\(a\) & \(c\)](#)). On the downstream side of the gate, at the *vena contracta*, the control point controls all the water levels in the downstream direction, i.e. in the supercritical part of the flow, creating the H3 profile in Example 4.1 or an M3 as shown in [Figure 2.12\(c\)](#) if the channel has a mild slope. Knowledge about where control points occur, or rules about where they form, are a pre-requisite for deciding which of the 12 gradually varied flow profiles will occur and for modelling any water surface profiles in open channels. Some examples of flow through bridges and some typical control structures are shown in [Figures 2.18–2.22](#).

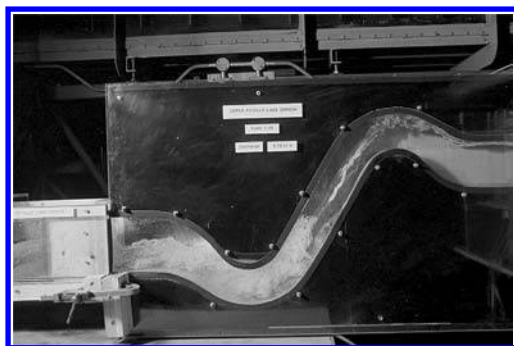


Figure 2.21 Model of air regulated siphon Figure (model scale 1:10) (See colour plate section).



Figure 2.22 Siphon outlet, showing flow over energy reducing blocks (See colour plate section).

2.2.7 Calibration data for river models

One of the main difficulties frequently experienced in the development of a mathematical model of a river is the lack of suitable field data for calibration, especially that related to channel roughness, water surface behaviour and turbulence parameters under extreme flow conditions. Despite hydrometric survey work being routinely carried out in the UK, there are generally never enough gauging stations in the right position, or indeed any monitoring of other key hydraulic parameters at all. This has two main consequences: that of making the model less useful than it might have been and, secondly, the model results will have larger uncertainties associated with them than perhaps originally hoped for. This issue has been discussed by several authors (e.g. Anastasiadou-Partheniou & Samuels, 1998; Knight, 2008a&b; Seed *et al.*, 1993; Vidal *et al.*, 2007) many of whom stress the need for a proportion of any modelling budget to be spent on acquiring appropriate data. Well focussed physical model studies, such as those undertaken in the UK Flood Channel Facility (Knight & Sellin, 1987; website www.flowdata.bham.ac.uk), are sometimes the only source of data at sufficiently comprehensive spatial and temporal scales to be used in the effective calibration of numerical models of river flow. These, and other sources of data, will be explored further in Section 2.7.

In addition to the hydraulic variables, there are many meteorological, hydrological and hydro-geological factors that affect the discharge in a river and also influence its variability. Such factors might be related to rainfall-runoff issues, precipitation and snow melt issues, groundwater issues, the underlying geology of the river basin, the number of tributaries and the behaviour of individual sub-catchments. The Flood Estimation Handbook (FEH, 1995) and the revised version (ReFEH, 2007) contain much of this information that should be consulted by all modellers requiring further details.

2.3 FLOW IN SIMPLE ENGINEERED CHANNELS

This section, and subsequent sections in [Chapter 2](#), now explores briefly the more complex flow conditions that can occur in actual rivers and watercourses and how they might be modelled successfully. A full explanation of the scientific basis behind the CES-AES software is given in [Chapter 3](#), and more examples illustrating further practical issues are given in [Chapter 4](#).

The modelling strategy used within the CES is largely based on the Shiono & Knight Method (SKM) of analysis, which gives the lateral distribution of depth-averaged velocity, U_d across channels of any prismatic shape. It is applicable to inbank and overbank flows in straight channels, and may be extended to flows in meandering channels by adding an additional term. The method captures certain 3-D flow effects and embodies them into a simpler 1-D approach. A full explanation of the methodology is given in [Chapter 3](#), and further details of the model may be found in Shiono & Knight (1988 & 1991), Knight & Abril (1996), Abril & Knight (2004), Mc Gahey (2006), Knight, Omran & Tang (2007), Knight & Tang (2008), Mc Gahey *et al.* (2006 & 2009) and Tang & Knight (2009). A brief introduction to the SKM approach is now given, using H = water depth to make the notation appropriate to the CES method (see [Figure 2.23](#)).

The equations which govern the behaviour of fluids in motion are known as the Reynolds Averaged Navier-Stokes (RANS) equations. See Schlichting (1979) and Drazin and Riley (2006) for further details on the RANS equations. The governing Reynolds Averaged Navier-Stokes equation for the streamwise motion of a fluid element in an open channel, with a plane bed inclined in the streamwise direction, may be combined with the continuity equation to give

$$\rho \left[\frac{\partial}{\partial y} (UV) + \frac{\partial}{\partial z} (UW) \right] = \rho g S_o + \frac{\partial \tau_{yx}}{\partial y} + \frac{\partial \tau_{zx}}{\partial z} \quad (2.57)$$

where $\{UVW\}$ = velocity components in the $\{xyz\}$ directions, x -streamwise parallel to the channel bed, y -lateral and z -normal to the bed, ρ = fluid density, g = gravitational acceleration, S_o = channel bed slope, and $\{\tau_{yx}, \tau_{zx}\}$ = Reynolds stresses in the streamwise direction on planes perpendicular to the y and z directions respectively. [Figure 2.23](#) indicates these stresses, the notation and some of the key terms used. A physical interpretation of Eq. (2.57) would be: Secondary flows (streamwise and planform) = Weight force + Reynolds stresses (lateral + vertical).

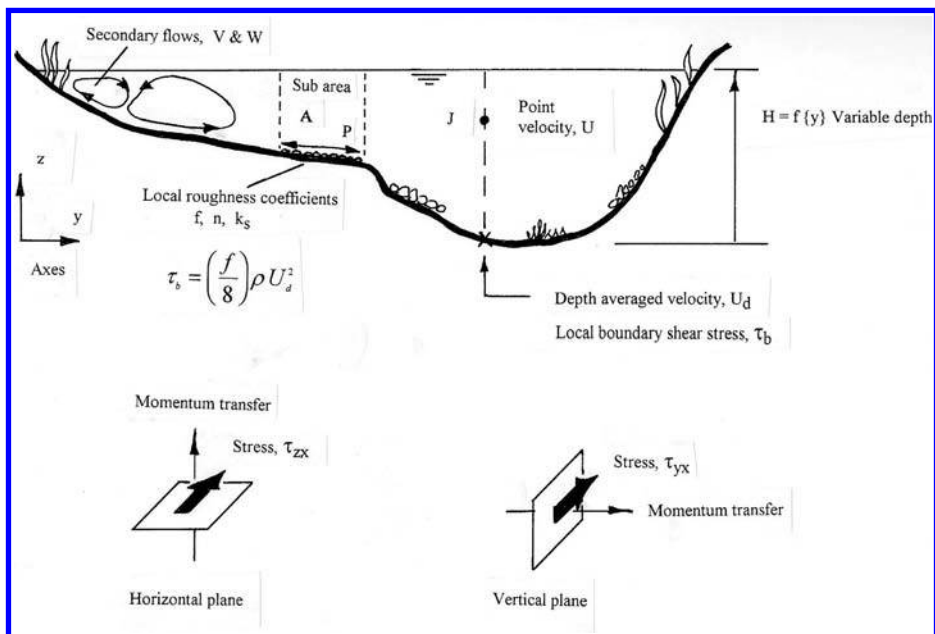


Figure 2.23 Flow in a natural channel and the various terms used in SKM and the CES.

Shiono and Knight (1991) obtained a depth-averaged velocity equation by integrating (2.57) over the flow depth (\$H\$), to give

$$\rho g H S_o - \rho \frac{f}{8} U_d^2 \left(1 + \frac{1}{s^2}\right)^{1/2} + \frac{\partial}{\partial y} \left\{ \rho \lambda H^2 \left(\frac{f}{8}\right)^{1/2} U_d \frac{\partial U_d}{\partial y} \right\} = \frac{\partial}{\partial y} [H (\rho UV)_d] \quad (2.58)$$

where \$f\$ = Darcy-Weisbach friction factor; \$\lambda\$ = dimensionless eddy viscosity; \$s\$ = the channel side slope of the banks (1:\$s\$, vertical: horizontal) and \$U_d\$ = the depth-averaged velocity. Solving Eq. (2.58) yields \$U_d\$ as a function of \$y\$, the lateral co-ordinate. Other terms are defined by:

$$U_d = \frac{1}{H} \int_0^H U dz; \quad \tau_b = \left(\frac{f}{8}\right) \rho U_d^2; \quad \bar{\tau}_{yx} = \rho \bar{\varepsilon}_{yx} \frac{\partial U_d}{\partial y}; \quad \bar{\varepsilon}_{yx} = \lambda U_* H \quad (2.59)$$

where \$U_* = (\tau_b/\rho)^{1/2}\$ = shear velocity. Eq. (2.58) thus includes the effect of secondary flows (streamwise vorticity about horizontal axes) and planform vorticity (vorticity about vertical axes). Both these types of vortex structure are important in many open channel problems, and particularly so in overbank flow, as shown schematically in Figure 2.15. Based on experimental results, the term \$(\rho UV)_d\$ is assumed to vary approximately linearly, and therefore of the form

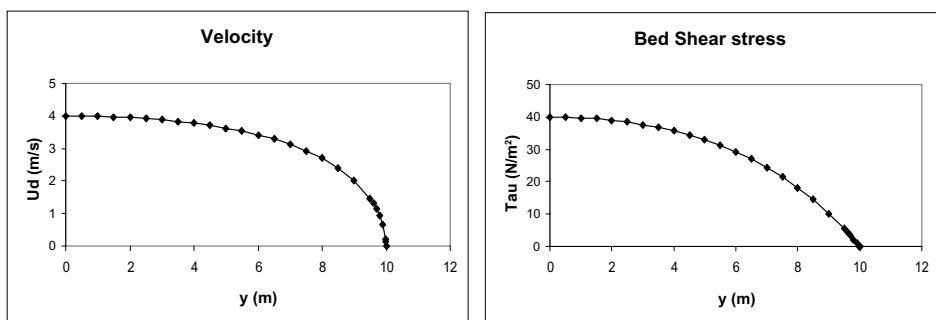
$$\frac{\partial}{\partial y} [H (\rho UV)_d] = \Gamma \quad (2.60)$$

where Γ is the lateral gradient of the advective term. In essence the SKM method allows values of the three calibration parameters (f , λ and Γ) to be assumed for each part of the flow and then Eq. (2.58) to be solved either numerically or analytically. In order to illustrate its use, some simple examples are now given, beginning with flow in straight channels.

Since the two simplest types of cross section that commonly occur, or are used in modelling, are rectangular and trapezoidal, these are used first to demonstrate the modelling strategy. See Figure 2.24 for examples of natural channels, and Figures 2.25–2.29 for examples of laboratory channels used in refined calibration studies (Chlebek & Knight, 2006; Chlebek, 2009; Knight *et al.*, 2007; Liao & Knight, 2007a&b; Omran *et al.*, 2008; Sharifi *et al.*, 2009; Tominaga *et al.*, 1989).



Figure 2.24 Inbank flows in approximately rectangular and trapezoidal river channels.



(a) Lateral distribution of depth-averaged velocity, U_d

(b) Lateral distribution of bed shear stress, τ_b

Figure 2.25 Velocity and bed shear stress results for flow in one half of a 20 m wide rectangular channel (single panel results, with $y = 0$ at centreline).

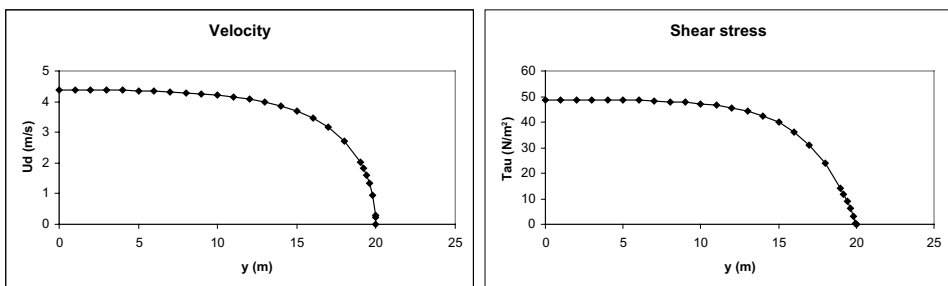
(a) Lateral distribution of depth-averaged velocity, U_d (b) Lateral distribution of bed shear stress, τ_b

Figure 2.26 Velocity and bed shear stress results for flow in one half of a 40 m wide rectangular channel (single panel results, with $y = 0$ at centreline).

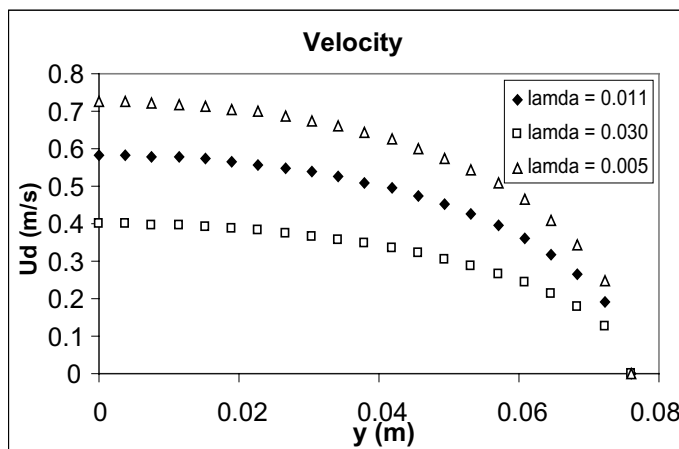


Figure 2.27 Effect of λ on lateral distribution of velocity in a rectangular channel.

The cross section of a rectangular channel may be treated singly or sub-divided into any number of panels, each of equal depth, but with varying flow parameters (f , λ and Γ) set for each panel. A trapezoidal channel may likewise be sub-divided, but this time the panels will be of different depths if they are on the sloping side region, and constant in the flat bed region. In this case, the least number of panels to model the whole channel would be 2, one for each region, as shown in Figure 2.30 later. The choice concerning the number of panels is important and may affect the results in a number of ways. If the flow and cross section are symmetric, as maybe sometimes for certain flows in straight channels with rectangular and trapezoidal cross sections, then only half the channel requires analysis.

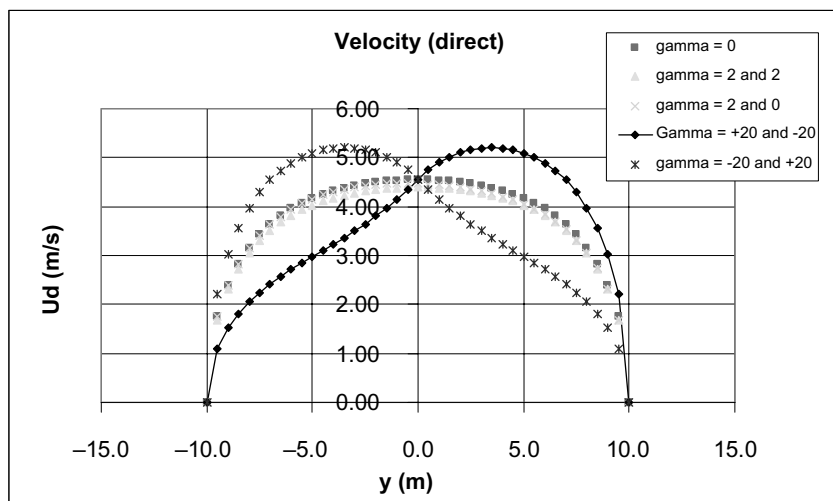


Figure 2.28 Simulated bend flow in a rectangular channel (variable Γ).

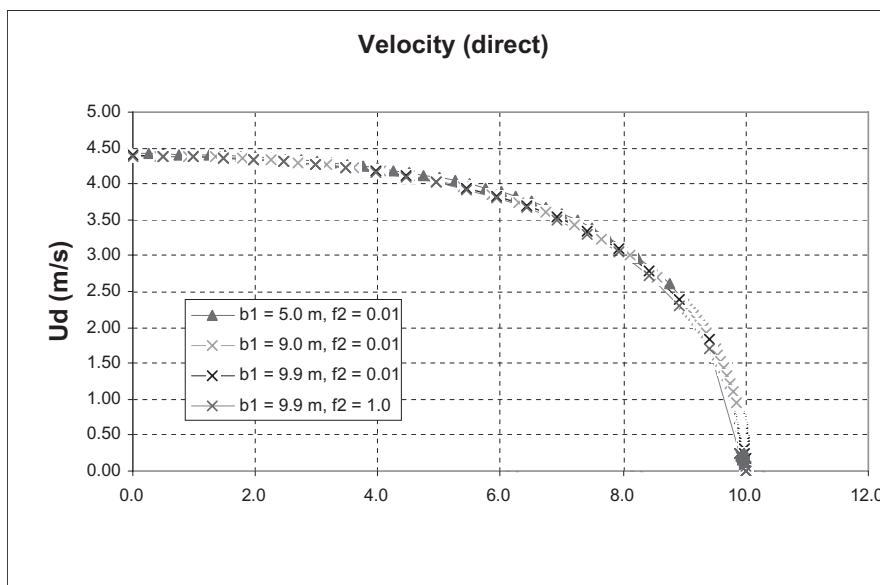


Figure 2.29 Flow in a 20 m wide rectangular channel with variable panel widths (2 panels, with $y = 0$ at centreline).

The philosophy adopted within SKM is to choose the minimum number of panels, commensurate with obtaining the maximum useful output from the results. Any greater accuracy is unwarranted since it should be remembered that the method itself is an approximate one. However, there are a number of principles that

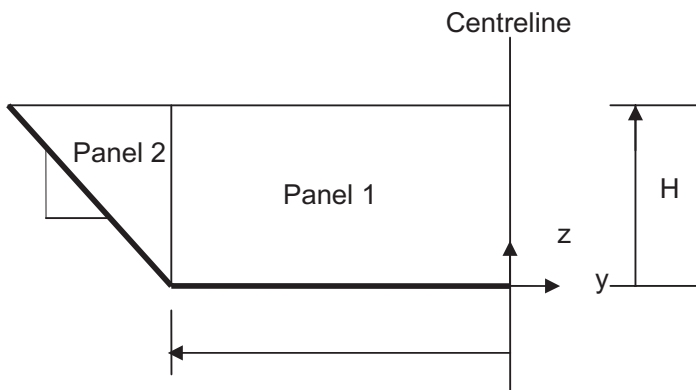


Figure 2.30 Cross-section of trapezoidal channel, schematized with two panels.

should be followed concerning panel selection that are described in detail in [Chapter 3](#). For the present purposes, the following examples are restricted to single or, at most, a small number of panels.

2.3.1 Flows in rectangular channels

Example 6

Determine the discharge and velocity distribution in a 20 m wide rectangular channel that flows at a depth of 5.0 m at a bed slope of 0.001, assuming a Darcy f of 0.02, and constant values for λ and Γ of 0.07 and 0.15 respectively.

Answer & comment

Consider only half the channel so one panel has a width of 10 m. The results are as shown in [Figure 2.25](#) at 0.5 m intervals for $y = 1\text{--}9 m, then at 0.1 m intervals to 9.9 m and finally at closer intervals near the wall. It can be seen that $U_d = f\{y\}$ for the one panel, even though the three calibration parameters (f , λ and Γ) are constant. The distribution of U_d is physically realistic, in that $U_d = \text{maximum}$ at the centreline ($y = 0$) and zero at the wall ($y = 10$ m). The method thus mimics the anticipated shear layer, and also gives the bed shear stress distribution since, once U_d is known, values of τ_b may be calculated from [Eq. \(2.59\)](#). Both distributions are hyperbolic, and this illustrates how some details of the flow have now been calculated, in a way that was not possible using the simple 1-D Manning resistance equation, [Eq. \(2.1\)](#).$

Having determined the lateral distribution of U_d , the individual values may be multiplied by the appropriate area of each sub-panel and the discharge obtained. This gives $Q = 330 \text{ m}^3\text{s}^{-1}$, which is somewhat different from the value of $362 \text{ m}^3\text{s}^{-1}$ calculated below, on the basis of using the same value of f in [Eq. \(2.25\)](#).

From Eq. (2.25):

$$U = (8gRS_o/f)^{1/2} = (8 \times 9.807 \times 3.3333 \times 0.001/0.02)^{1/2} = 3.616 \text{ ms}^{-1}.$$

$$Q = UA = 3.616 \times 20 \times 5 = 361.6 \text{ m}^3\text{s}^{-1}.$$

The same value of Q should not in fact be expected, despite Eq. (2.25) being essentially a single channel method (SCM), since the influences of the other two parameters (λ and Γ) have not yet been considered. For example, halving the value of λ (i.e. less lateral shear) and putting $\Gamma = 0$ (no secondary flow) in Eqs (2.58) & (2.59) gives $Q = 364 \text{ m}^3\text{s}^{-1}$ which is much closer to the value of $362 \text{ m}^3\text{s}^{-1}$ calculated using Eq. (2.25).

The lateral distribution of velocity in Figure 2.25(a) is seen to give $U_{\max} = 4.0 \text{ ms}^{-1}$ at the centreline and a mean value of $U \approx 3.2 \text{ ms}^{-1}$. The mean value is again slightly different from the value calculated from Eq. (2.25), $U = 3.616 \text{ ms}^{-1}$, for the reasons given above. The centre-line value of bed shear stress in Figure 2.25(b) is seen to be approximately $\tau_b \approx 40.0 \text{ Nm}^{-2}$, which is lower than the mean bed value based on assuming two-dimensional flow, ($\tau_{b2d} = \rho g H S_0$) and higher than the mean boundary shear stress for the whole cross-section ($\bar{\tau}_o = \rho g R S_o$). This is to be expected, since:

$$\tau_{b2d} = 1000 \times 9.807 \times 5.0 \times 0.001 = 49.03 \text{ Nm}^{-2}.$$

$$\bar{\tau}_o = 1000 \times 9.807 \times 3.3333 \times 0.001 = 32.69 \text{ Nm}^{-2}.$$

The value of maximum bed shear stress will approach the two-dimensional value ($\tau_b = \rho g H S_0$) as the channel is widened. For example if the width is now doubled to 40 m, and assuming the same values for the parameters (f , λ and Γ) as before, gives the distributions shown in Figure 2.26. In this case, the centre-line bed shear stress, τ_b , is now much closer to the two-dimensional value of 49.03 Nm^{-2} , since the aspect ratio of the channel (width/depth) has risen to $40/5 = 8$. This is still not technically a ‘wide’ channel as the simulation results here are some way from those for a wide channel (see Figure 9 of Knight & MacDonald (1979), Knight *et al.* (1992 & 1994) and Al-Hamid (1991) for further details). For practical purposes the aspect ratio needs to be at least >10 to get within 95% of τ_{b2d} and generally >25 .

Figure 2.26(a) shows $U_d = f\{y\}$ for the 40 m wide channel, varying from $U_{\max} = 4.38 \text{ ms}^{-1}$ at centerline to zero at the wall. Integrating across the width gives $Q = 774.9 \text{ m}^3\text{s}^{-1}$. This is less than the value of $Q = 792.24 \text{ m}^3\text{s}^{-1}$ below, based on Eq. (2.25):

$$U = (8gRS_o/f)^{1/2} = (8 \times 9.807 \times 4.0 \times 0.001/0.02)^{1/2} = 3.9612 \text{ ms}^{-1}.$$

$$Q = UA = 3.9612 \times 40 \times 5 = 792.24 \text{ m}^3\text{s}^{-1}.$$

Lowering λ to 0.035 causes the values of U_d to rise, especially nearer the walls, giving $Q = 810.3 \text{ m}^3\text{s}^{-1}$, now above the value of $792.3 \text{ m}^3\text{s}^{-1}$. This example has shown that the individual values of the parameters λ and Γ , as well as f , will also influence the discharge, and so this is explored further in the next example.

Example 7

Using only one panel to represent half of a rectangular channel, explore the combined influence of all 3 parameters (f , λ and Γ).

Answer & comment

In order to test the methodology further, data are needed on channels where both velocity and boundary shear stress distributions have been measured with known accuracy. Since such data are rare at full scale in large channels, recourse has to be made to data from small scale laboratory channels where it had been possible to measure both parameters accurately. One set of data that is suitable is highlighted by Chlebek & Knight (2006), taken from experiments in a series of small rectangular channels. Further discussion on data and availability are given in Section 2.7.

The general effect on Q of varying all 3 parameters and the percentage of shear force on the channel walls, $\%SF_w$, is shown in [Table 2.2](#), based on numerical simulations of all the experimental results from the various channels, covering a wide range of aspect ratios. The $\%SF_w$ values were obtained by integrating the bed shear stresses over the semi width of the channel, determining the overall shear force on the bed, SF_b , and then subtracting it from the overall mean shear force for the whole channel, $(\tau_o \times P)$ to give SF_w , which is then expressed as a percentage of the total (bed and both walls).

[Figure 2.27](#) shows the effect of varying λ on the lateral distribution of U_d , while holding f and Γ constant for one particular simulation. In this case, the experimental channel had a width of 152 mm, a depth of 200 mm, a Q of 13.78 l/s with a value of $\%SF_w$ of 73.08%. The $\%SF_w$ value is understandably high, given the narrowness of the channel (aspect ratio of only 0.76). In general, it was found that for a given depth, when λ was increased, with fixed f & Γ , it caused Q to decrease and $\%SF_w$ to increase. The reverse occurred when λ was decreased. [Tables 2.2 & 2.3](#) illustrate these changes quantitatively, based on this one depth ($H = 200$ mm) with reference values of $Q = 13.78 \text{ ls}^{-1}$ and $\%SF_w = 73.08\%$ for which $f = 0.018$, $\lambda = 0.011$ and $\Gamma = 0.47$ gave the closest approximation to the experimental data, using just one panel.

The results in rows 2 & 3 of [Table 2.3](#) indicate that the effect of varying f from 0.040 to 0.005 (from optimum of 0.018) is to change Q from 13.78 ls^{-1} to 10.46 and

Table 2.2 Effect of varying one calibration parameter, holding the other two constant.

Variable parameter	Fixed parameters	+/-	Q	$\%SF_w$
f	$\lambda & \Gamma$	increase	decreases	decreases
	$\lambda & \Gamma$	decrease	increases	increases
λ	$f & \Gamma$	increase	decreases	increases
	$f & \Gamma$	decrease	increases	decreases
Γ	$f & \lambda$	increase	decreases	increases
	$f & \lambda$	decrease	increases	decreases

Table 2.3 Effect of varying parameters f , λ and Γ on values of Q and $\%SF_w$ (Highlighted row shows closest simulation to the experimental data, i.e. optimum values).

f	λ	Γ	Q (litres sec $^{-1}$)	$\%SF_w$ (%)
0.018	0.011	0.047	13.78	73.08
0.040	0.011	0.047	10.46	65.23
0.005	0.011	0.047	20.52	83.08
0.018	0.030	0.047	9.36	87.54
0.018	0.005	0.047	17.35	57.44
0.018	0.011	0.500	11.97	79.68
0.018	0.011	0.000	13.95	72.93

20.52 ls $^{-1}$ respectively, and to change $\%SF_w$ from 73.08% to 65.23% to 83.08%. The effect of varying λ from 0.030 to 0.005 (from optimum value of 0.011) is shown in rows 4 & 5, and the effect of varying Γ from 0.500 to 0.000 (from optimum value of 0.047) is shown in rows 6 & 7. This example highlights the need to consider the combined effect of all 3 calibration parameters on two objective functions (discharge and a boundary shear force, i.e. Q and $\%SF_w$). Before considering this in detail, and using substantive sets of data outlined in Section 2.7, the influence of the secondary flow term, Γ , as well as the appropriate number of panels to be used to represent the channel cross section, also need to be investigated. These are now considered together in Example 8.

Example 8

A rectangular channel is 20 m wide, 3.0 m deep and has a bed slope of 0.001. Using two panels to represent half of this channel, investigate the influence of the secondary flow term, Γ , and panel selection on the flow results, assuming $f = 0.01$ and $\lambda = 0.10$ for all panels.

Answer & comment

In the absence of suitable full scale data, particularly those in which Γ has been measured, this exercise on secondary flow effects and the number of panels that should be used has to be a purely numerical one. Detailed numerical simulation of multi-panels is reserved for an example in Section 2.3.2, using laboratory data for both U_d and $\%SF_w$ and examples in Chapter 3 using river data, for which data exists on U_d but not on boundary shear stress distributions.

Figure 2.28 shows the results of these simulations for a 20 m wide channel in which two panels of equal width ($b = 10$ m) make up the total width of the rectangular channel. This is equivalent to modelling half the channel with just a single panel 10 m wide. The results show that for $\Gamma = 0$, the distribution of U_d is symmetric, as expected. For $\Gamma = 2$, in all panels the velocities are diminished slightly. When Γ is changed in sign for each panel either side of the centerline, i.e. $\Gamma_1 = +20$ on one side and $\Gamma_2 = -20$ on the other side, then the velocity distribution is no longer symmetric, but

biased towards one side or another. Such a distribution is that which might occur in a left-handed or right-handed bend, with a higher velocity on the outside of the bend. Not surprisingly this is seen to be produced here by altering the secondary flow term, Γ . As shown later in [Chapter 3](#), there are other ways of attempting to simulate flow in meandering channels.

[Figure 2.29](#) shows the effect of splitting a single panel into a number of sub-panels. In this case, a single panel of width b , equivalent to half of the channel width, is divided further into 2 sub panels, of widths b_1 and b_2 , to make up half of a rectangular channel of semi-width, b , thus making $b_2 = b - b_1$. The width of one panel, b_1 , is altered progressively from 5.0 m to 9.9 m in order to see if the smaller panel adjacent to the wall captures the very high shear in that region. As can be seen, with $b_1 = 9.9$ m and $b_2 = 0.1$ m the results compare quite well with the simulation undertaken with two equal sized panels. The effect of increasing the roughness in the smaller panel adjacent to the wall by a factor of 100 is seen to reduce the velocity in that region, thus indicating a possible way of refining any calibration to fit data. This is dealt with more thoroughly in the next section that deals with flows in trapezoidal channels.

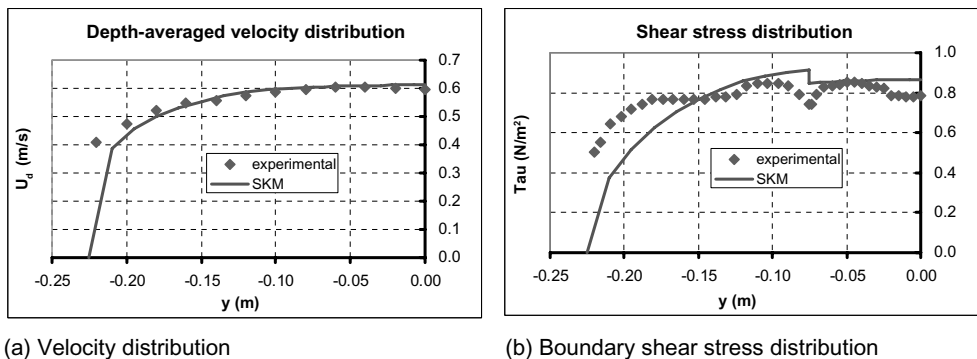
Example 9

Attempt some of these exercises using the CES software, which is based on the SKM, and compare your answers with those given in this Chapter. All the results in Examples 6–8 were obtained using spreadsheets to evaluate the analytical solutions to [Eq. \(2.58\)](#) directly.

2.3.2 Flows in trapezoidal channels

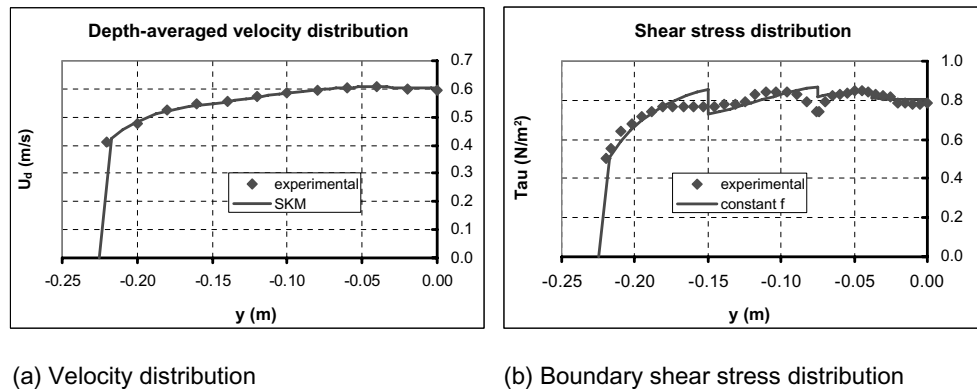
The previous examples have indicated some general features of the SKM for flows in rectangular channels. The use of multi-panels is now explored more thoroughly, using data from laboratory experiments undertaken by Yuen (1989) and Tominaga *et al.* (1989). [Figure 2.30](#) shows a typical schematization for a trapezoidal channel, based initially on just two panels. [Figure 2.31](#) shows the results of a simulation based on using such a schematization, together with some experimental data. Although [Figure 2.31\(a\)](#) shows that the lateral distribution of U_d is reasonably well simulated, [Figure 2.31\(b\)](#) shows that the corresponding lateral distribution of boundary shear stress, τ_b , is not simulated as well. A much better simulation for the latter is obtained when each of the previously used 2 panels are sub divided further, making 4 panels in all, as shown by the results in [Figures 2.32\(a\) & \(b\)](#). It was found by Omran (2005) that 4 panels are normally quite adequate for practical purposes when modelling most types of flow in trapezoidal channels.

In particularly demanding cases, where even greater precision is required, such as when attempting to simulate the boundary shear stress distribution very accurately in



(a) Velocity distribution (b) Boundary shear stress distribution

Figure 2.31 Results of velocity and boundary shear stress simulations of flow in a trapezoidal channel (2 panels). [Exp.16, Yuen, 1989, with $f_1 = 0.0185$, $f_2 = 0.020$, $\lambda_1 = \lambda_2 = 0.07$, $\Gamma_1 = 0.5$, $\Gamma_2 = -0.2$].



(a) Velocity distribution (b) Boundary shear stress distribution

Figure 2.32 Results of velocity and boundary shear stress simulations of flow in a trapezoidal channel (4 panels, Exp 16, Yuen), after Knight, Omran & Tang (2007).

corner regions, then 6 panels may be required. Under these circumstances, the number, pattern and strength of the secondary flow cells should be taken into account, as shown in [Figure 2.33](#) by Tominaga *et al.* (1989). The results of simulating the same experiment shown in [Figures 2.31 & 2.32](#) are shown in [Figure 2.34](#). It can be seen that by using 6 panels the sharp decrease in boundary shear stress in the corner region ($y = 0.075$ m) is much better simulated. Another feature that is important when dealing with boundary shear stress with multiple panels of different roughness is to include some lateral smoothing into the friction factor, f , in order to overcome any discontinuity in τ_b that arises from use of a depth-averaged approach based on [Eqs \(2.34\) & \(2.52\)](#). This is shown in [Figure 2.34](#), where lateral distributions of boundary shear stress, τ_b , are shown for constant f values (saw tooth plot, 4 panels), linearly varying f values

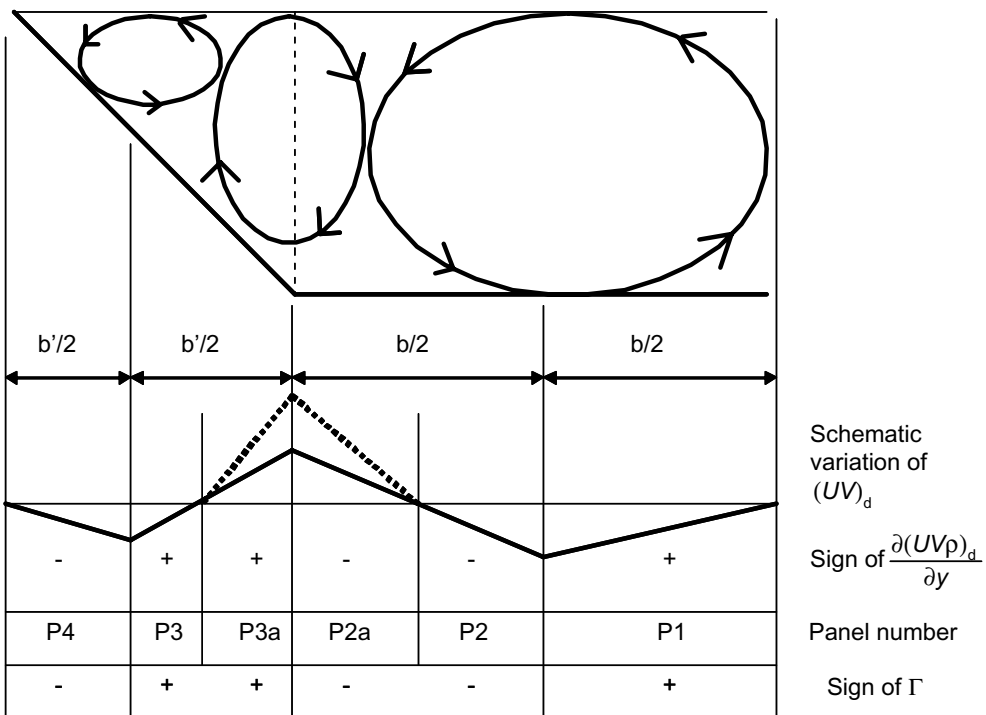


Figure 2.33 Secondary flow cells in a trapezoidal channel, after Tominaga (1989) and Omran (2005).

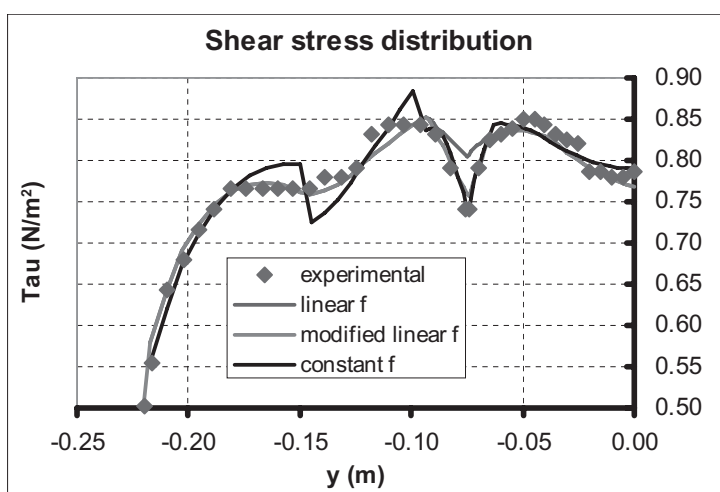


Figure 2.34 Results of boundary shear stress simulations of flow in a trapezoidal channel (6 panels, with variable λ , Exp. 16, Yuen), after Omran (2005).

(4 panels) and modified linearly varying f values (6 panels). Further details of this and related issues may be found in Omran (2005), Omran & Knight (2006), Knight *et al.* (2007) and Omran *et al.* (2008). Figures 2.31–2.34 thus indicate that the main issues that need to be considered are the number of panels and the values of each parameter within individual panels.

2.4 INBANK FLOW IN NATURAL RIVERS

The previous section has shown some of the background to modelling flows using SKM/CES approaches, applied to simple prismatic channels, and how useful some laboratory data might be for validation purposes. However, river engineers are usually concerned with flows in natural rivers, where the cross-section is generally irregular in shape, not necessarily prismatic, the distribution of roughness more varied around the wetted perimeter, and other practical issues such as vegetation, culverts and bridges need to be considered. This section and subsequent ones now address all of these concerns and illustrates them via several case studies.

Figure 2.23 shows that the flow in a natural channel is more complex than those cases considered in Section 2.3. Firstly the irregular cross section has to be schematised using survey data to create multiple panels, and should be undertaken with some knowledge of the flow characteristics. Secondly, because there is often a lack of knowledge concerning the velocity distributions from suitable field data, care needs to be taken over the choice of the 3 calibration parameters (f , λ and Γ) to be used in each panel. Arising from this, a measure of uncertainty in the predicted results also needs to be established. These features are now illustrated using the CES applied to an actual river, the River Ngunguru in New Zealand.

The example of the River Ngunguru at Drugmores Rock has been deliberately chosen to illustrate inbank flow in a natural channel that has many of the difficult features cited above. It will also serve to highlight further modelling issues, and is totally unlike any of the previous examples, based on simple prismatic laboratory channels. Furthermore, one particular reach has been subject to ongoing measurements since 1969 (Hicks & Mason, 1998). The Ngunguru River drains a catchment area of 12.5 km^2 , has a mean annual flood discharge of $61 \text{ m}^3\text{s}^{-1}$ and an average flow rate of $0.41 \text{ m}^3\text{s}^{-1}$. Water level and discharge measurements were taken at three cross-sections along an 80 m reach, with a gentle bend in the downstream portion. The sections were approximately 12 m wide and 2 m deep. The water surface slope varied from 0.0037 at low depths to 0.0064 at large depths. The river bed consists of gravel and cobbles and the banks are lined with grazed grass and scattered brush, as shown in Figure 2.35. The observed Manning n values vary with depth in the range 0.051 to 0.160, with the values increasing substantially at lower depths. The cross section is shown in Figure 2.36.

The cross section was divided into 100 panels or elements and values of the 3 calibration parameters (f , λ and Γ) chosen for each panel, based on the rules outlined in Chapter 3. The CES software was then used at a specified depth to solve for the lateral distribution U_d v y , which was subsequently integrated laterally to give the discharge at that same value of depth. Repeated application over a range of depths led to the stage-discharge relationship (H v Q) shown in Figure 2.37. As can be seen in



(a) looking upstream

(b) looking downstream

Figure 2.35 River Ngunguru at Drugmores Rock looking upstream and downstream from the mid-reach section (Hicks & Mason, 1998).

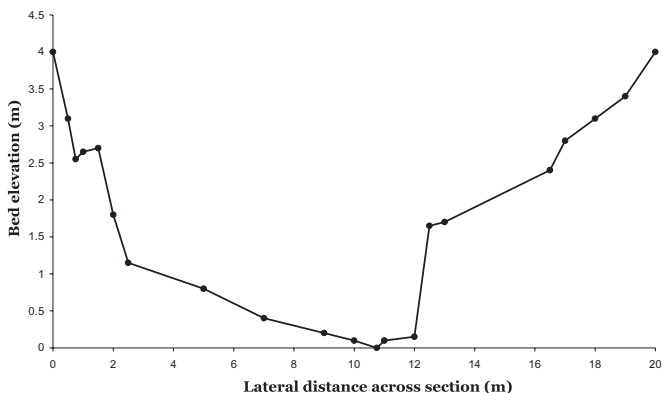


Figure 2.36 Surveyed cross-section geometry for the River Ngunguru at Drugmores Rock (Hicks & Mason, 1998).

Figure 2.37, although the CES stage-discharge prediction and data agree well for the majority of flows, there is some discrepancy at shallow depths. This is related to the physical representation of the large roughness in the river (Manning's $n = 0.1$ to 0.16), a topic which is discussed further in Chapter 3 when dealing with boulder roughness. Figure 2.38 shows the actual measured Manning n values, together with those back calculated from the CES. The back calculated values agree well with the data for depths in excess of 0.9 m. This Figure also demonstrates how Manning n often varies with depth in rivers, decreasing from a high value at low depths. This is a key feature, that indicates that roughness coefficients (n , C , f or k_s) should always be plotted in a similar manner and checked when calibrating a numerical model. Other examples are given by many authors (e.g. Chow, 1959; Hicks & Mason, 1998; Knight, 1981; and

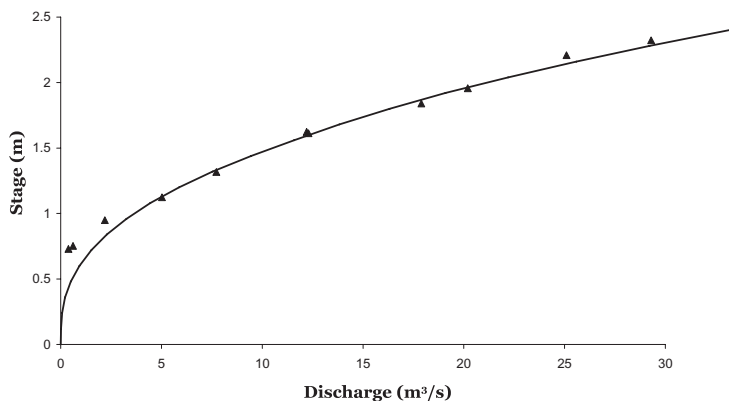


Figure 2.37 CES stage-discharge prediction and data for the River Ngunguru at Drugmores Rock (Hicks & Mason, 1998; Mc Gahey, 2006).

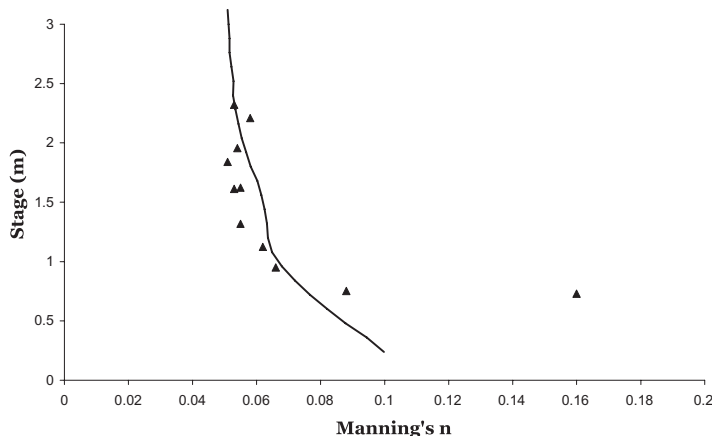


Figure 2.38 Back-calculated CES Manning n values and measured Manning n values from the River Ngunguru at Drugmores Rock (Hicks & Mason, 1998; Mc Gahey 2006).

Yen, 1991). Following consideration of resistance in overbank flow (see for example Fig. 2.47), roughness is considered further in Sections 3.2.1 & 3.4.1.

2.5 OVERBANK FLOW IN NATURAL AND ENGINEERED RIVERS

Overbank flow is somewhat different in a number of respects from inbank flow. The key difference is that more complex three-dimensional (3-D) flow structures

may be present (Ashworth *et al.*, 1996). When overbank flow occurs, and floods occupy the floodplains, there are a number of issues that require special consideration, dealt with more fully by Knight & Shiono (1996). These are summarised here as follows:

- use of hydraulic radius, R , in calculations (abrupt change at bankfull stage);
- interaction between main river and floodplain flows (strong lateral shear);
- proportion of flow between sub-areas is important (e.g. river and floodplains);
- heterogeneous roughness (differences between river and floodplains);
- vegetation zone (effect on flow, plan form vortices);
- unusual resistance parameters (global, zonal and local);
- significant variation of resistance parameters (with depth and flow regime);
- distribution of boundary shear stresses (affects sediment, mixing and erosion);
- sediment transport (rate, equilibrium shape, deposition, etc.);
- flood routing parameters (wave speed and attenuation parameters are affected);
- critical flow (definition and control points);
- valley and channel slopes and sinuosities (may be different for meandering channels);
- greater plan form variations in geometry (due to meandering patterns).

Many hydraulic equations, such as [Eq. \(2.1\)](#), were developed primarily for inbank flows and are based on a mean velocity, U , applied to the whole of the cross-section area, A . Manning's equation is therefore classed as a single channel method (SCM). Other methods divide the area into zones in which the roughness and flow might vary within the cross-section, giving rise to the so-called divided channel methods (DCM). There are several categories of DCMs, as shown by many authors, e.g. Huthoff *et al.* (2008); Knight & Demetriou (1983); Knight (2006b&c); Lambert & Myers (1978); Myers & Lyness (1997); Wormleaton (1988 & 1996); Wormleaton & Merrett (1990); Wormleaton *et al.* (1982, 1985) and Yen (1991). A variant on this theme is the 'coherence method' (COHM) of Ackers (1991, 1992a&b & 1993a&b), which deals with heterogeneous roughness and shape effects. The 'coherence', COH, is defined as the ratio of the basic conveyance, calculated by treating the channel as a single unit with perimeter weighting of the friction factor, to that calculated by summing the basic conveyances of the separate zones. All of these simple sub-division methods, and the composite roughness methods given in Chow (1959), are now known to be inappropriate for simulating overbank flow accurately (Wormleaton & Merrett, 1990). The CES, on the other hand, was designed specifically with overbank flows in mind, as shown by the following examples.

2.5.1 Overbank flow in an engineered river

A good example of an engineered channel is that of the River Main, already shown as [Figure 2.5](#), details of which are also given in Section 2.2.2. The main channel cross section is approximately trapezoidal, and so links in with the previous laboratory examples, and the floodplains are prismatic. [Figure 2.39](#) shows the survey data at Bridge End bridge.

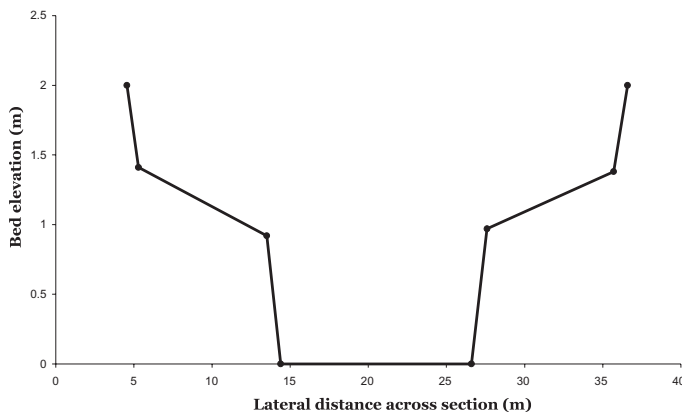


Figure 2.39 Surveyed cross-section geometry for the River Main at Bridge End bridge (Myers & Lyness, 1989).

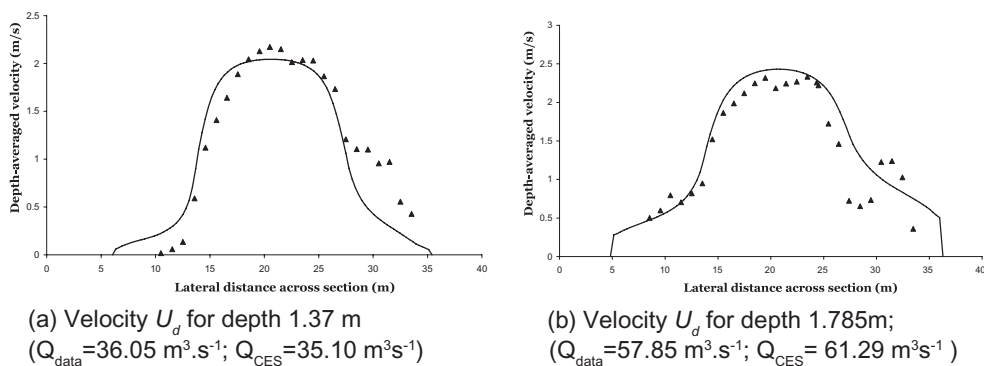


Figure 2.40 Comparison of lateral distributions of velocity by CES with data (Myers & Lyness, 1989; Mc Gahey, 2006).

The CES was used to simulate the lateral distribution of U_d for a number of flow depths and discharges. Two of these are shown in Figure 2.40 for flow depths of 1.37 m and 1.79 m, together with the field data (Myers & Lyness, 1989). The depth-averaged velocity profiles are reasonably well simulated, but there appears to be a small degree of skew in the velocity data at low depths. This may result from the effects of the upstream bend circulations being transported downstream. Since the channel bed material is gravel, with no vegetation present, these higher velocities are plausible but are not captured by the CES where the effect of the slightly higher calibrated bank side roughness is present. Subsequent integration of these, and all the data sets, produced the predicted stage-discharge curve shown in Figure 2.41. The H v Q relationship is well simulated, including the bankfull variations around the depth of ~ 0.95 m. The differences between CES predicted and all data flow values are shown in Figure 2.42,

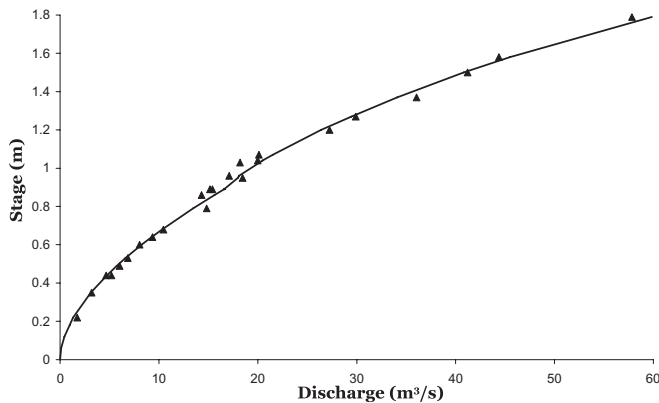


Figure 2.41 CES stage-discharge prediction and data for the River Main at Bridge End Bridge (Myers & Lyness, 1989; Mc Gahey, 2006).

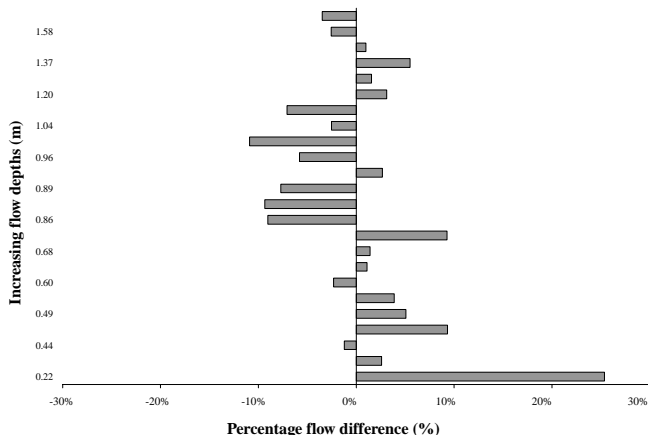
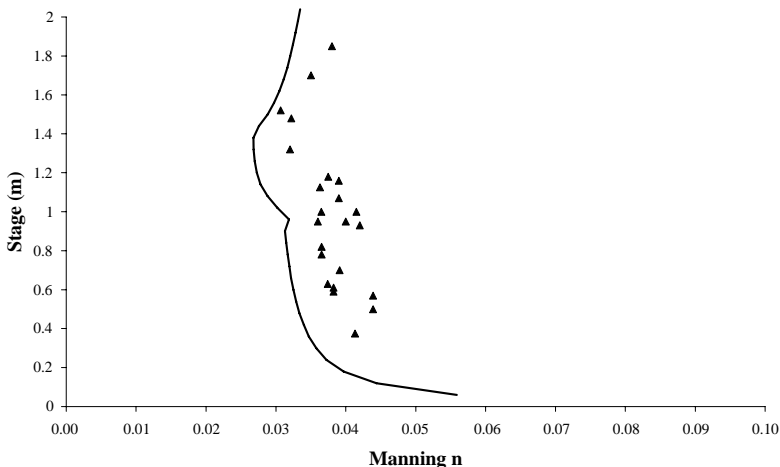


Figure 2.42 Differences between CES predicted and data flow values for the River Main at Bridge End Bridge (Mc Gahey, 2006).

giving an average difference of 5.6% and a standard deviation value of 7.6%. These differences obviously depend on the technical capability of the model, the accuracy of the measured data and the calibration parameters used in the numerical model, especially on the unit roughness which is the most significant parameter. These roughness values and equivalent roughness heights, k_s , are shown in Table 2.4, together with the Manning's n values suggested by previous authors. It is instructive to note that the various author estimates vary substantially. The large CES unit roughness, n_l , (defined by Eq. (3.15) in Chapter 3) on the left floodplain is explained by the dense vegetation immediately below the bridge, where the measurements were taken. The

Table 2.4 Calibrated roughness values for the River Main at Bridge End Bridge (Mc Gahey, 2006).

Roughness parameter	Left floodplain	Left Bank	Main channel	Right bank	Right floodplain
n_l	0.0750	0.0350	0.0300	0.0350	0.0450
k_s (m)	2.225	0.316	0.172	0.316	0.713
Author	Manning's n values				
Myers et al (1999) based on measurement	0.0380				
Ackers (1991)	0.0200				
Wark (1993)	0.0400				

Figure 2.43 Back-calculated CES Manning n values and measured Manning n values from for the River Main at Bridge End Bridge (Myers & Lyness, 1989; Mc Gahey, 2006).

CES back-calculated Manning's n values are shown in Figure 2.43, illustrating a reasonable distribution with depth, albeit $\sim 15\%$ lower than the measured data. Further details of this simulation are given in Mc Gahey (2006).

This example serves to show how sensitive the solution is to roughness, even apart from other parameters, and how compromises sometimes have to be made with regard to fitting both individual data sets (such as U_d v y) and overall relationships (H v Q or H v n). It is for these reasons that an Uncertainty Estimator (UE) has been incorporated into the CES to assist modellers at the calibration stage. An example showing the sensitivity to roughness is given after the next example which illustrates some other important technical issues associated with overbank flow.

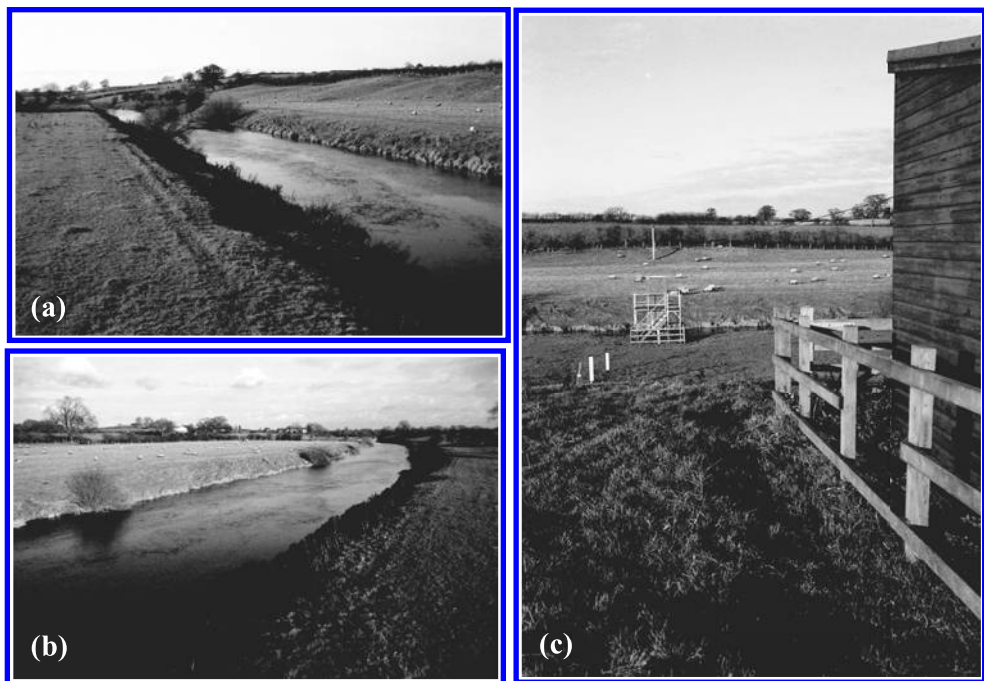


Figure 2.44 The River Severn at Montford Bridge (a) looking upstream from right bank, (b) looking downstream from the cableway and (c) the cable way at the bridge (Courtesy HR Wallingford).

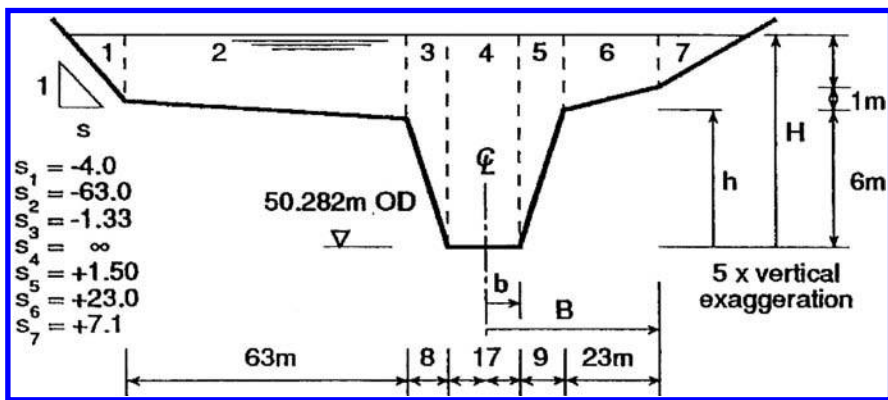


Figure 2.45 Cross-section of River Severn at Montford Bridge (after Knight et al., 1989).

2.5.2 Overbank flow in a natural river

A reach of the River Severn at Montford Bridge (Figure 2.44) has been extensively monitored for practical hydrometry and research purposes, providing a large body of accurate current metering data. It is a natural cross-section with a cableway extending

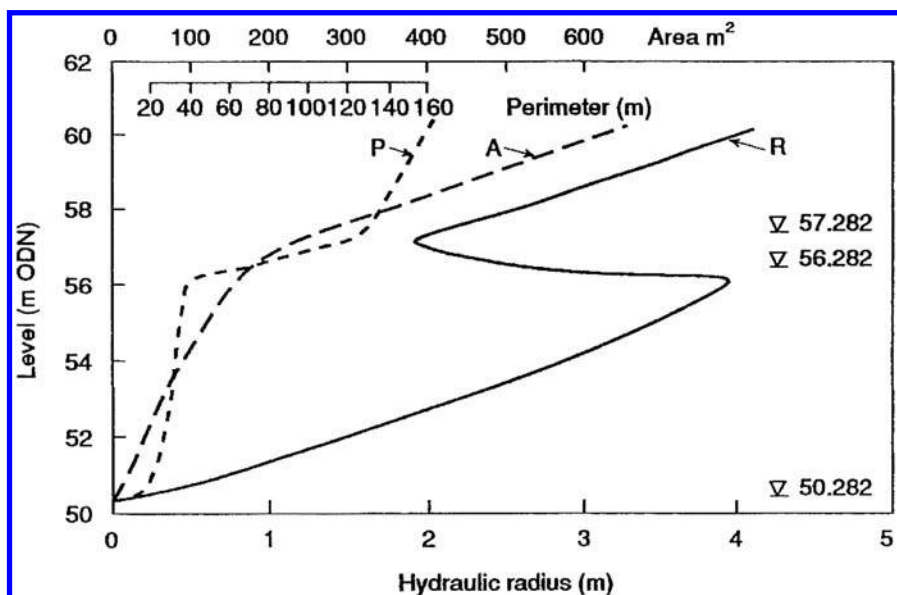


Figure 2.46 Variation of hydraulic parameters with level, River Severn at Montford Bridge (after Knight et al., 1989).

over the full width, including the floodplains. The bankfull width and depth are 40 m and 6.3 m respectively. The total width, including the floodplains, is approximately 120 m and the reach-averaged longitudinal bed slope is 0.000195. The floodplains are grass-covered and the gauged station is on a straight section of the river. The measured data includes water surface slope, water levels, velocity and discharge.

The cross section, shown schematically in Figure 2.45, indicates a bankfull depth of around 6.0 m and two flood plains of differing widths. This section was modelled by Knight *et al.* (1989) prior to the development of the CES, and undertaken analytically using the 7 panels shown to represent the geometry and the secondary flow term ignored. It was later modelled numerically by Abril & Knight (2004) with all the terms included. The variation of area, wetted perimeter and hydraulic radius with depth are shown in Figure 2.46, which serves to illustrate a key problem when dealing with 1-D modelling of overbank flow and the use of standard 1-D resistance laws based on the hydraulic radius, R . When the flow rises just above the bankfull level (56.282 m OD), the hydraulic radius ($R = A/P$) changes markedly, since for a small change in depth there is little change in A but a significant increase in P . As a result, R decreases sharply, unlike inbank flow in which R generally increases with depth monotonically. This can have certain implications when applying resistance laws to sub-regions of the flow, as indicated in Figure 2.47.

Figure 2.47 shows that if the river is treated as a single channel, then the overall or composite n value decreases with increasing depth from 0.036 to 0.030 at the bankfull level, as might be expected from the trends shown in Figures 2.38 & 2.43 for inbank flows. However, with further increase in water level above the bankfull level,

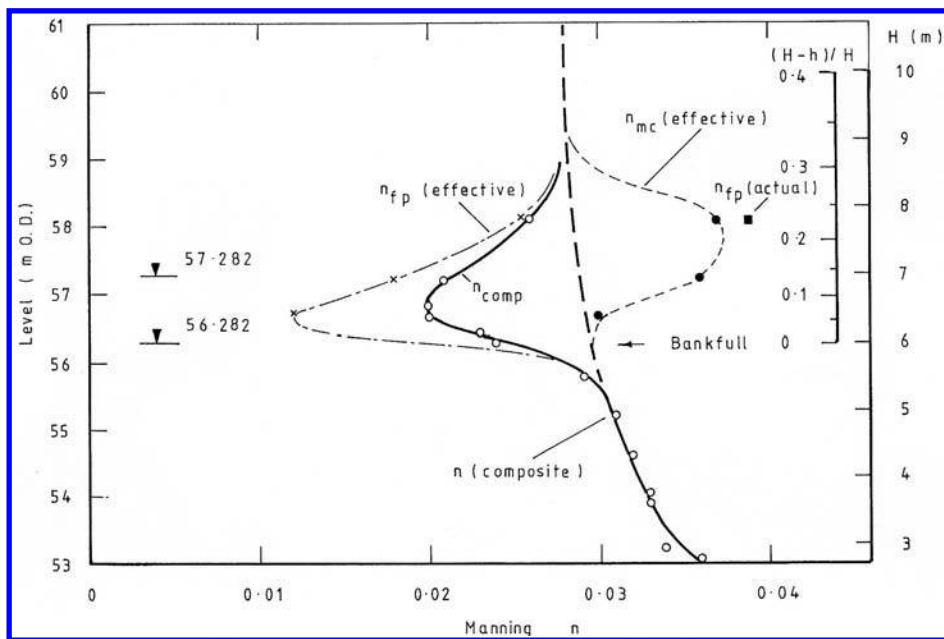


Figure 2.47 Variation of Manning's n resistance coefficient for overbank flow at Montford Bridge, River Severn (after Knight *et al.*, 1989).

n_{comp} appears to decrease sharply to around 0.020, before increasing again to join the characteristic smooth H v n relationship at $n \sim 0.029$. This apparent reduction in overall resistance coefficient is entirely fictitious, and due to the changes in R noted in Figure 2.46. In fact the overall resistance of the river actually increases when overbank flow occurs, due to the effects of bankside and floodplain vegetation. Using measured water surface slope and velocity data, Knight *et al.* (1989) showed that when the channel was divided into 3 zones, the LH floodplain (panels 1 & 2), the main channel region (panels 3–5) and the RH floodplain (panels 6 & 7), then the effective n value for the main channel n_{mc} (effective), based on the main channel area, appeared to increase from 0.030 to around 0.038, and the effective n value for the floodplains n_{fp} (effective), based on the inundated floodplain areas, appeared to decrease from 0.030 to 0.012. This is despite the actual floodplain roughness being estimated as ~ 0.04 , as shown in Figure 2.47.

The physical explanation for this seeming anomaly is straightforward. By dividing the channel into separate zones, typically using vertical lines that form panel boundaries, then using measured U_{mc} , A_{mc} and S_f values, the resulting zonal Q_{mc} takes no account of the retarding effects of the shear layers between the slower moving floodplain flows and the faster moving main channel flow. Consequently, to match the observed Q_{mc} a larger ‘resistance’ is apparently needed. The reverse is true of the zonal floodplain flow, Q_{fp} , where it appears that an impossibly low resistance value is required to account for the accelerating effects of the main channel flow on the floodplain flow (0.012 compared with the actual value of ~ 0.040). This highlights

one of the main difficulties that all the divided channel methods (DCMs), mentioned in the introduction, have had to deal with. Many of them attempted to insert the apparent shear forces between zones or panels, based on arguments about transverse shear and secondary flows. The CES approach considers this issue from first principles and is based on extensive experimental data and observations.

When using resistance coefficients, care needs to be taken to distinguish between the section-mean velocity, U_A , the zonal velocity U_z , the depth-mean velocity, U_d , and any local near bed velocity, u , used in the ‘law of the wall’ in a turbulence model. It is also important to distinguish between ‘global’, ‘zonal’ and ‘local’ friction factors used in 1-D, 2-D & 3-D river models, where:

$$\begin{array}{lll} \tau_o = \left(\frac{f}{8}\right) \rho U_A^2; & \tau_z = \left(\frac{f_z}{8}\right) \rho U_z^2; & \tau_b = \left(\frac{f_b}{8}\right) \rho U_d^2; \\ (\text{global}) & (\text{zonal/sub-area}) & (\text{local/depth-averaged}) \\ 1\text{-D model} & (\text{quasi 1-D model}) & 2\text{-D model} \end{array} \quad \tau_b = \left(\frac{f_t}{8}\right) \rho u^2 \quad 3\text{-D model} \quad (2.61)$$

It should be noted here that, within the CES, the third option is used, with the shear stress on the bed assumed to be in the same streamwise direction as U_d . The topic of how resistance is represented in numerical models is addressed more fully by Morvan *et al.* (2008). Some of the errors involved in using DCMs are highlighted by Knight & Demetriou (1983), Knight (2006b&c), Lambert & Myers (1998), Myers (1978) and Wormleaton (1996).

The same reach of the River Severn, as well as other rivers, were modelled by Abril & Knight (2004), who also put forward a novel link between boundary shear and the secondary flow parameter, Γ . As a result, certain rules were formulated for the variation of the 3 calibration parameters (f , λ and Γ) in different zones (main channel

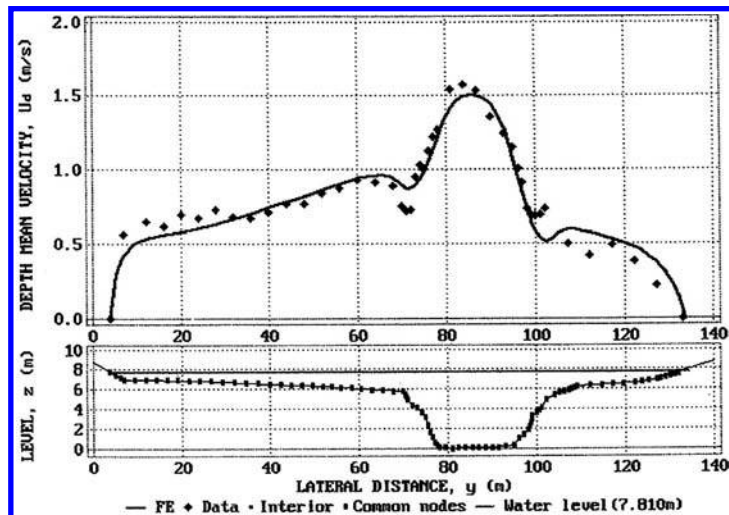


Figure 2.48 Finite element simulation of the lateral distribution of depth-averaged velocity in the River Severn at Montford Bridge (after Abril & Knight, 2004).

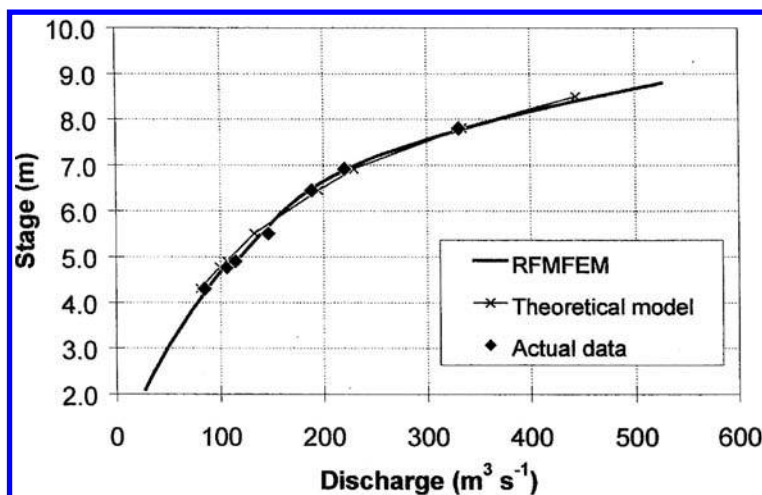


Figure 2.49 Stage-discharge prediction for the River Severn at Montford Bridge (after Abril & Knight, 2004).

Table 2.5 Percentage change in flow rate as a result of change in unit roughness for the River Main and River Severn at Montford Bridge (adapted from Mc Gahey, 2006).

Percentage change in n_l	Depth (m)	Percentage change in flow rate (%)						
		-50%	-30%	-10%	0%	+10%	+30%	+50%
River Main	1.785	+92	+40	+10	0	-8	-21	-31
River Severn	7.805	+69	+30	+8	0	-6	-16	-23

and floodplains). These are described and utilized in [Chapters 3 & 4](#) in relation to several other rivers. The results of one simulation of the River Severn at Montford bridge at a depth of 7.81 m are shown in [Figure 2.48](#). Lateral integration of these U_d values with the corresponding elemental areas gave the total discharge for this particular depth. Repeated simulations over a range of depths gave the complete stage-discharge relationship, shown in [Figure 2.49](#). The H v Q relationship may also be obtained analytically for steady inbank and overbank flow for certain shapes of open channel, as shown by Liao & Knight (2007a&b). See also the relevant International Standards, ISO 1100-1 (1996) and ISO 1100-2 (1998). Unsteady flows require special treatment, as indicated by Schmidt & Yen (2008), and also by [Eq. \(2.38\)](#).

Since the outputs from any model are especially sensitive to the input roughness values used, two examples are now given to illustrate the sensitivity of discharge to roughness value. These are based on the River Main and River Severn, which have been illustrated already in [Figure 2.41](#) (River Main) and [Figure 2.49](#) (River Severn). [Table 2.5](#) illustrates the percentage change in flow rate as a result of changes in n_l of ±10, 30 and 50% at the two particular depths, 1.785 and 7.805 m, used previously. The variation in discharge is seen to be from +92% to -31% for the River Main

and from +89% to -23% for the River Severn. This highlights the importance of estimating the roughness as accurately as possible when modelling flows in rivers. As noted from Eq. (2.61), the resistance coefficients have to be carefully defined for overbank flows, and may differ considerably depending upon whether global, zonal or local situations are being considered. For further details on resistance of compound channels see Myers & Brennan (1990) and Myers *et al.* (1999).

2.6 FLOWS THROUGH BRIDGES AND CULVERTS

In addition to the energy losses caused by channel resistance, energy losses also occur at river control structures such as bridges, culverts and weirs. Since these may affect water levels in any simulation model, the Afflux Estimator (AE) is included within the CES, together with a backwater module. For detailed information on flow through bridges, culverts, flumes and weirs, reference should be made to papers, textbooks, manuals and international standards, such as Ackers *et al.* (1978), Benn & Bonner (2001), Biery & Delleur, (1962), Biglari & Sturm (1998), Bos *et al.* (1984), Brown (1985 & 1988), Chow (1959), Hamill (1999), Henderson (1966), Kaatz & James (1997), Knight & Samuels (1999), Mantz & Benn (2009), May *et al.* (2002), Ramsbottom *et al.* (1997), Seckin *et al.* (1998, 2007 & 2008a&b), ISO 4374 (1990), ISO 4377 (2002) and ISO 1438 (2008). The AE concentrates particularly on flows through bridges and culverts, since these are often more difficult to model accurately than flows through weirs and flumes and they are frequently encountered.

2.6.1 Flows through bridges and contractions

The flow of water through bridges and contractions is illustrated in Figures 2.50 & 2.51. The cross-sections 1.4 have been positioned at those places that are frequently adopted in the analysis of flow through constricted waterways. Section 1 is traditionally taken upstream of the bridge, prior to the commencement of any contraction of the streamlines due to the bridge. Section 2 is generally taken on the upstream face of the bridge, with Section 3 either on the downstream face or at the position of the *vena contracta*. Section 4 is taken some distance further downstream, typically at the end of the expansion of the streamlines, where the flow returns to normal depth conditions in the river channel. Note the differences between afflux, head loss and energy loss. The afflux is defined as the increase in water level upstream of a bridge above the water depth that would occur in the absence of the bridge, here indicated by the normal depth at section 1, and should not be confused with the energy loss across the whole bridge structure, i.e. between sections 1 & 4. See Mantz & Benn (2009) for further details of computation of afflux ratings and water surface profiles through bridges and culverts.

Figure 2.52 shows a typical variation in water surface profile through a laboratory scale model bridge, taken from Atabay & Knight (2002). Figures 2.53 & 2.54 illustrate how such experiments were conducted in a compound channel at the University of Birmingham, and Figures 2.55–2.58 illustrate some actual flows through bridges with piers and arches of various shapes. Figures 2.18 & 2.19 have already shown some actual bridges during or after a flood event.

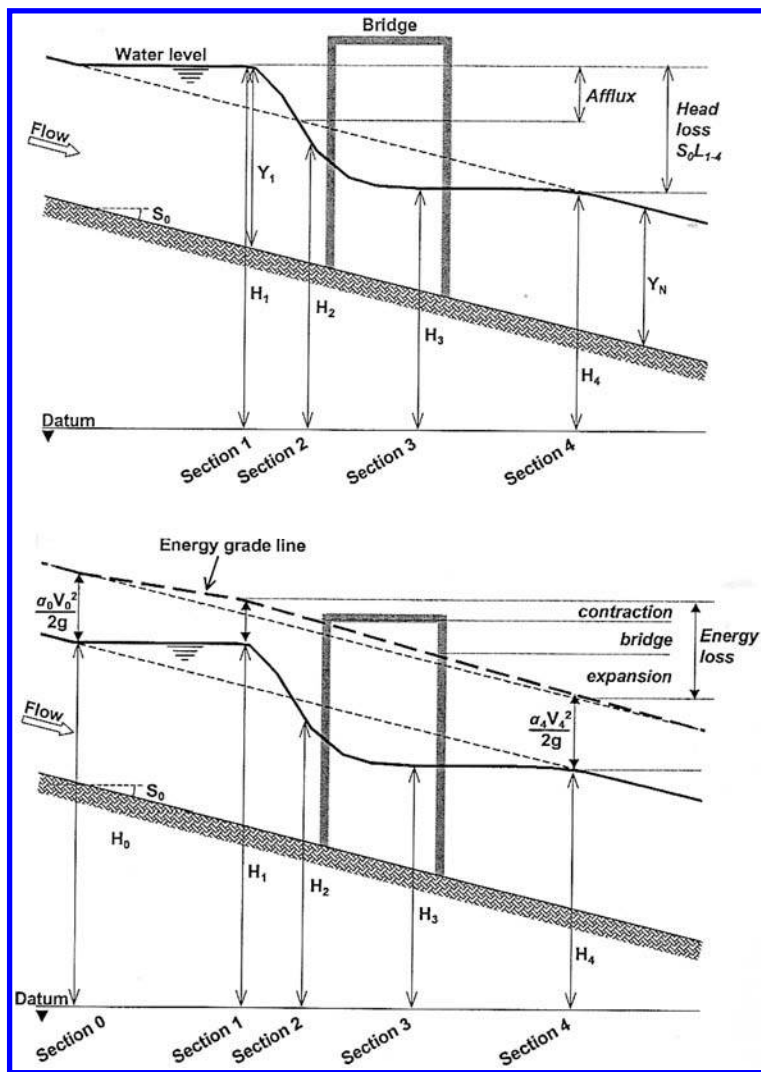


Figure 2.50 Definition of afflux, head loss and energy losses at a bridge (after Hamill, 1999).

There are a number of different methods for determining afflux, the main ones being:

- Energy equation method (various authors);
- Momentum equation method (various authors);
- USGS method;
- USBPR method;
- FHWA WSPRO method;
- HR method (arch bridges);

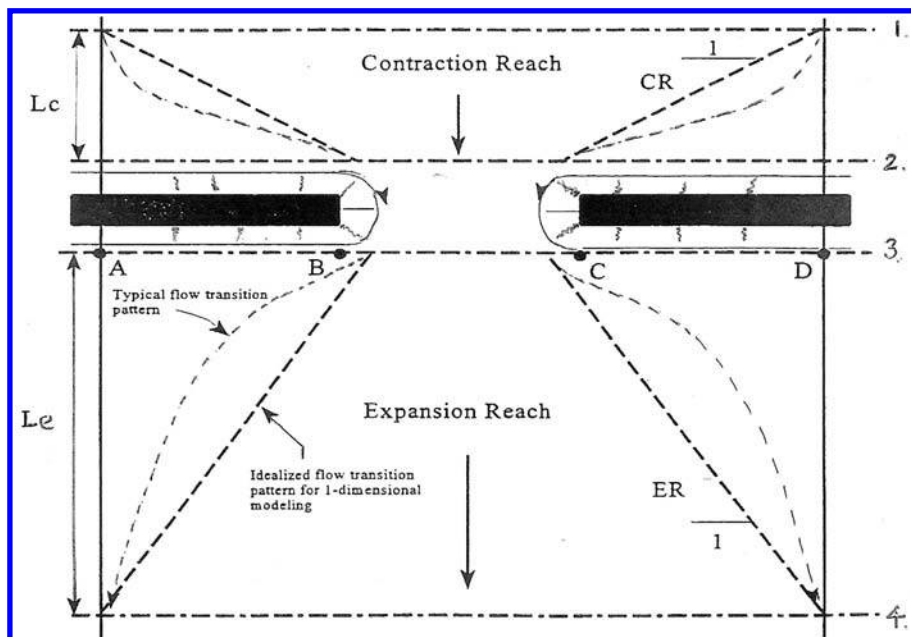


Figure 2.51 Plan view of flow though a bridge or constriction (as in HEC-RAS R&D, 1995, but with reversed notation to make it compatible with standard practice and the USBPR method).

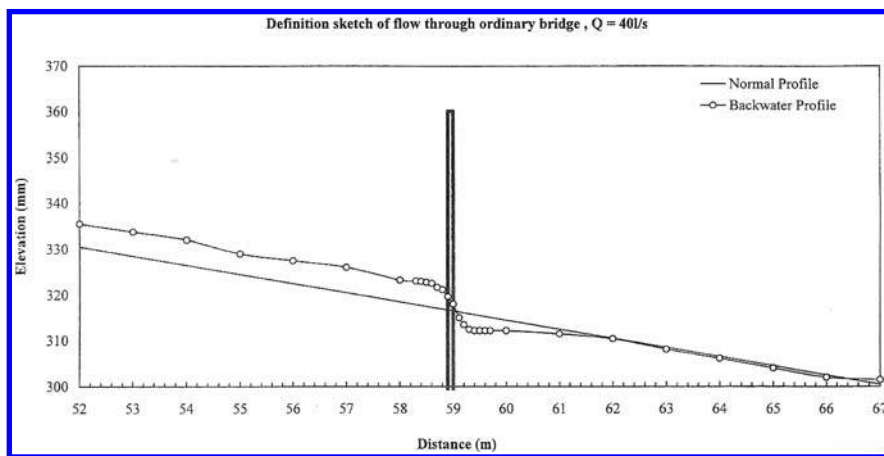


Figure 2.52 Observed water surface profile through a model bridge in the laboratory (Atabay & Knight, 2002).

- Biery & Delleur method (arch bridges);
- Pier loss methods – Yarnell, Nagler and d'Aubuisson.

Although it is not appropriate to reproduce details of these methods here, since they are well documented elsewhere (Defra/EA, 2004), it should be appreciated that



Figure 2.53 Flume with model bridge set in a compound channel with smooth floodplains (University of Birmingham) (See colour plate section).

there are several conceptual differences between them, so that the affluxes computed by the various methods will differ according to the method used, the coefficients adopted, and the expertise of the user in applying the method to both standard and non-standard situations. In the same way, methods for analyzing flows through culverts have also been well documented, see for example, Bradley (1978), Chow (1959), CIWEM (1989), Hamill (1999), HEC-RAS (1996 & 2008), Henderson (1966), Miller (1994) and Ramsbottom *et al.* (1997).

Figure 2.59 illustrates schematically the various types of flow that may occur through a bridge, and how a distinction needs to be drawn between free, submerged and drowned flow. At low discharges, with the channel controlling the flow, the flow is referred to as an open channel type flow, as shown for a subcritical state in Figure 2.59(a). When the discharge and upstream water level reach a value at which submergence of the upstream face occurs, then the hydraulic behaviour switches from a free flow state to a sluice gate-like flow state, as shown in Figure 2.59(b).

If re-attachment occurs on the underside of the bridge soffit, then the contraction effect within the bridge opening will be affected, typically causing the whole area at the outlet to become a flow area and thereby changing the longitudinal pressure gradient,



Figure 2.54 Model double arch bridge in a flume with roughened floodplains (University of Birmingham) (See colour plate section).

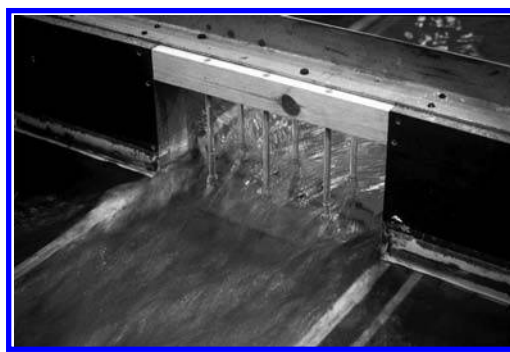


Figure 2.55 Flow through a model bridge with multiple piers (See colour plate section).

as shown in [Figure 2.59\(c\)](#), Type 2. The flow is now referred to as a drowned orifice type flow, with both the structure and the channel controlling the flow. Depending on the tailwater level, the downstream face of the structure might also become submerged, as shown in [Figure 2.59\(c\)](#), Type 1. At very large discharges, some flow may also occur



Figure 2.56 Flow through a model bridge with single elliptical arch (See colour plate section).



Figure 2.57 Flow through a model double arch bridge (viewed from upstream).

over the bridge parapet or roadway, leading to overtopping or bypassing of the structure. In this case the flow is part orifice-like, through the bridge opening, and part weir-like, over the bridge parapet and any adjoining embankments. The simulation of these different types of flow during a flood event must, therefore, be reproduced in any numerical model, using different algorithms, and the transition from one type of flow to another clearly linked to key water levels relative to the structure. Another way of categorising flows through bridges, different to that shown in Figure 2.59, is given in the USBPR method, based on the work of Bradley (1978). Since this is one of the most widely used methods for determining the afflux through a constricted waterway, this is summarised as follows:

- Type I subcritical flow throughout a constriction;
- Type II A critical at throat only, i.e. choking at throat;
- Type II B critical for a short distance downstream, then a jump and subcritical flow further downstream;
- Type III choking at throat, then supercritical flow downstream.

Should supercritical flow occur, then bridges have to be treated particularly carefully as the depth of flow will increase in the constriction (i.e. the opposite to that

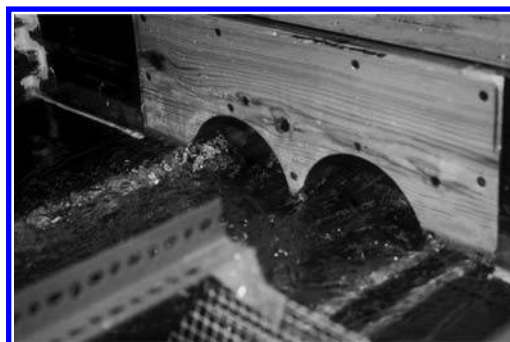


Figure 2.58 Flow through a model double arch bridge (viewed from downstream).

shown in Figure 2.59(a)). Under these circumstances the water level may reach the soffit, and a hydraulic jump forms on the upstream side of the bridge, thereby creating a new control point. Where bridges are sited on bends with supercritical flow, then splitter walls may be required to reduce the super-elevation so that the water surface does not reach the level of the bridge soffit. Since bridges are often sited in two-stage or compound channels, with the embankments crossing part or whole of the floodplain, then particular care needs to be taken over the definition of sub and supercritical flow in such channels. It is sometimes possible for rivers with floodplains to have sub and supercritical flow co-existing within the same cross section, and therefore the Froude Number, Fr , as defined by Eq. (2.5), is no longer appropriate for defining critical flow in such channels with a complex geometry. Further information on this is given by Blalock & Sturm (1981) and Yuen & Knight (1990).

Since flow conditions upstream of bridges are sometimes not dissimilar from the flow conditions upstream of other types of hydraulic structure (e.g. vertical sluice gates, Tainter gates and other similar structures), then technical knowledge concerning the drowning characteristics of these other types of structure may also be relevant (e.g. Escarameia *et al.* (1993), Knight & Samuels (1999) and Rajaratnam (1977)). In the same manner, technical information on contraction and expansion losses in other types of fluid flow are also relevant and should not be overlooked (e.g. Cebeci & Bradshaw (1977), Chow (1959), Henderson (1966), Reynolds (1974) and Schlichting (1979)).

The flow through a constriction may be dominated by ‘choking’, a phenomenon that may be readily explained by reference to specific energy, E , as defined in Eq. (2.12). Since the specific energy, depth and discharge per unit width relationship is theoretically fixed for a particular shape of cross section, the flow within a constriction may become critical if the gap width is too small. Further reduction in the gap width will only maintain the hydraulic control at that point, but cause the water level upstream to rise. Standard hydraulic theory applied to flow in a rectangular channel of breadth B , in which a single pier of width b is placed, will lead to the following equation for choking

$$\sigma^2 = \frac{27Fr_1^2}{\gamma^3(2 + Fr_1^2)^3} = M_L^2 \quad (2.62)$$

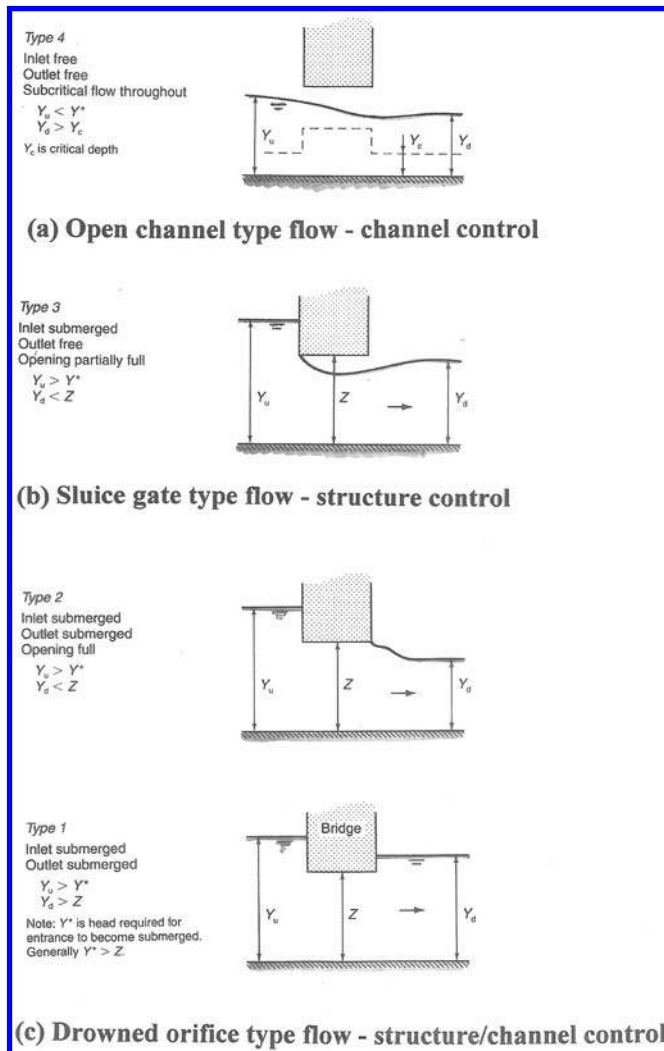


Figure 2.59 Types of flow through a bridge crossing (after Hamill, 1999).

where $\sigma = (B - b)/B$, Fr_1 is the upstream Froude Number and γ is a factor to account for any energy loss between the upstream section (1) and the throat (2), such that $\gamma E_1 = E_2$, where $\gamma < 1$ and E refers to the specific energy. It should be noted that despite the use of b as defined here for the pier width, and not the gap width, σ becomes the same as the bridge opening ratio, M . The bridge opening ratio, M , is defined as a ratio of discharges, $M = q/Q$, where here q = unfettered flow through the gap as if the bridge or constriction was not in place and Q = total flow in the river. Thus for known B , Fr , and γ , the value of σ , and hence the width of the bridge pier, b , or limiting opening ratio, M_L , that will cause choking may be determined. Eq. (2.62) is

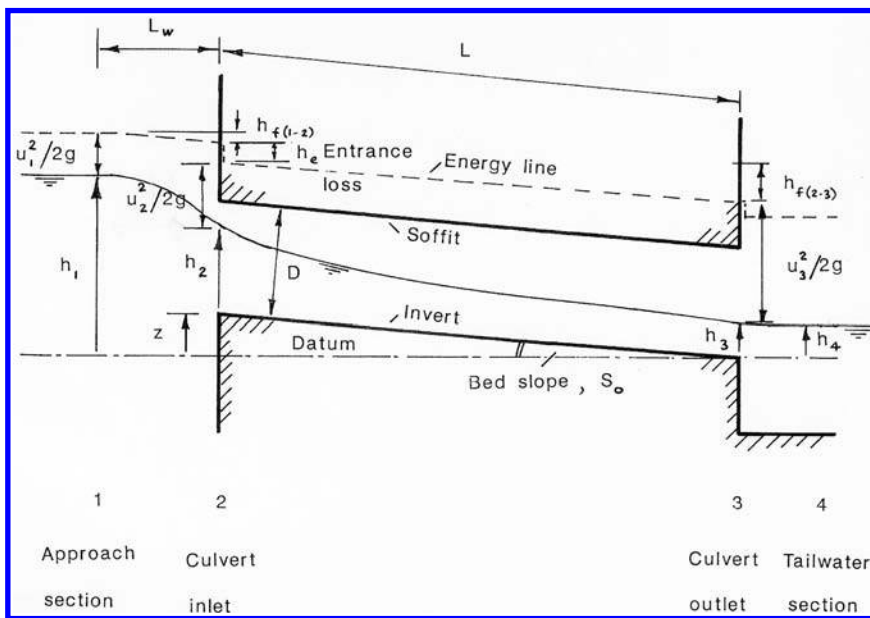


Figure 2.60 General characteristics of flow through a culvert, with notation.

similar to that presented by Hamill (1999), but with the energy loss term included. Many alternative equations may be produced, based on similar principles (e.g. Wu & Guo, 2002; Wu & Molinas, 2001), but these are more complex to use than Eq. (2.62).

2.6.2 Flows through culverts

The flow of water through a culvert is somewhat similar to that under a bridge. It depends on whether the hydraulic control is at the inlet or outlet and also on upstream and downstream water levels. The general features of flow through a culvert are shown in Figure 2.60, together with notation. It should be noted that bridges are defined as structures with a small length to the opening size ratio ($L/D < 1$), whereas culverts are structures with typically much larger L/D values. The various types of flow through culverts are shown in Figures 2.61 & 2.62.

The head-discharge, and hence afflux, relationships depend on the type of flow. These are dealt with in Section 2.6.3 and the various geometrical parameters that affect the flow are dealt with in Section 2.6.4. Further details are reserved until later Chapters, where worked examples are also given, along with a description of the AES.

2.6.3 Head-discharge and afflux relationships

The head-discharge relationships for all the types of flow, identified in Figures 2.59–2.62 for flow through bridges and culverts, are inevitably complex (see Chapters 3 & 4). The afflux relationships, together with worked examples, are likewise given later.

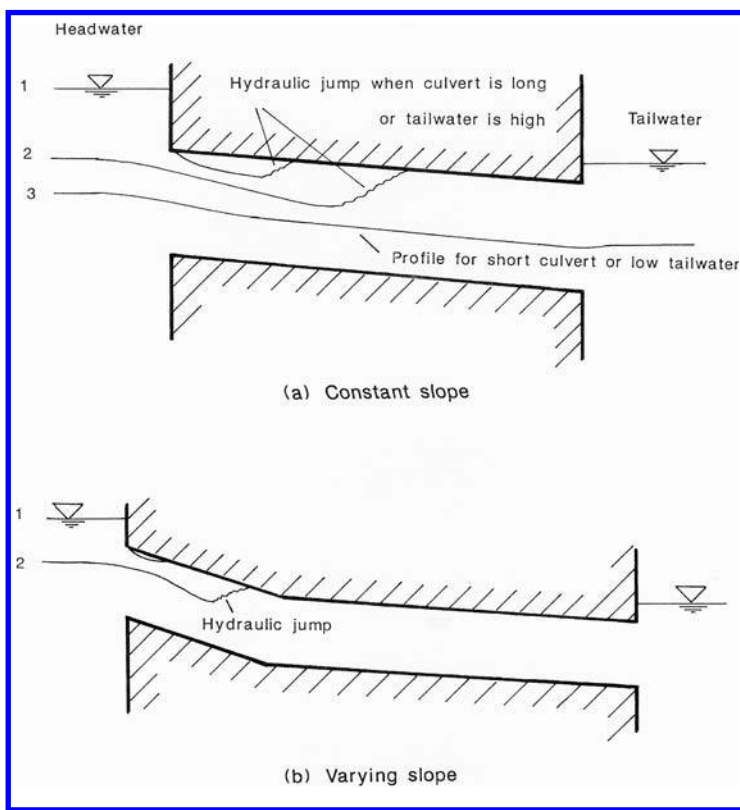


Figure 2.61 Several modes of flow in a partially filled culvert (Type 6 flow, as in Figure 2.62).

In general terms it may be noted that when a bridge is flowing ‘free’, the discharge–head relationship is given by $Q \sim \Delta h^2$, where Δh = water level difference between upstream and downstream sections, but when flowing like an orifice, it changes to $Q \sim \Delta h^{1/2}$. The transition from one type of flow to another is an important feature to model correctly and governed by many factors, further details of which may be found in Ramsbottom *et al.* (1997) and Hamill (1999). In order to understand the impact that certain geometric parameters have on the flow through bridges and contractions, the following section describes their influence and the related issues that need to be considered by the modeller.

2.6.4 Geometrical parameters affecting flow through bridges

The principal parameters that govern the flow of water through bridges and constrictions are illustrated in Figure 2.63. These parameters have traditionally been grouped under two major headings, geometric and flow, although as will be shown later, this distinction is somewhat blurred. They are, however, presented and discussed briefly here under a number of different headings.

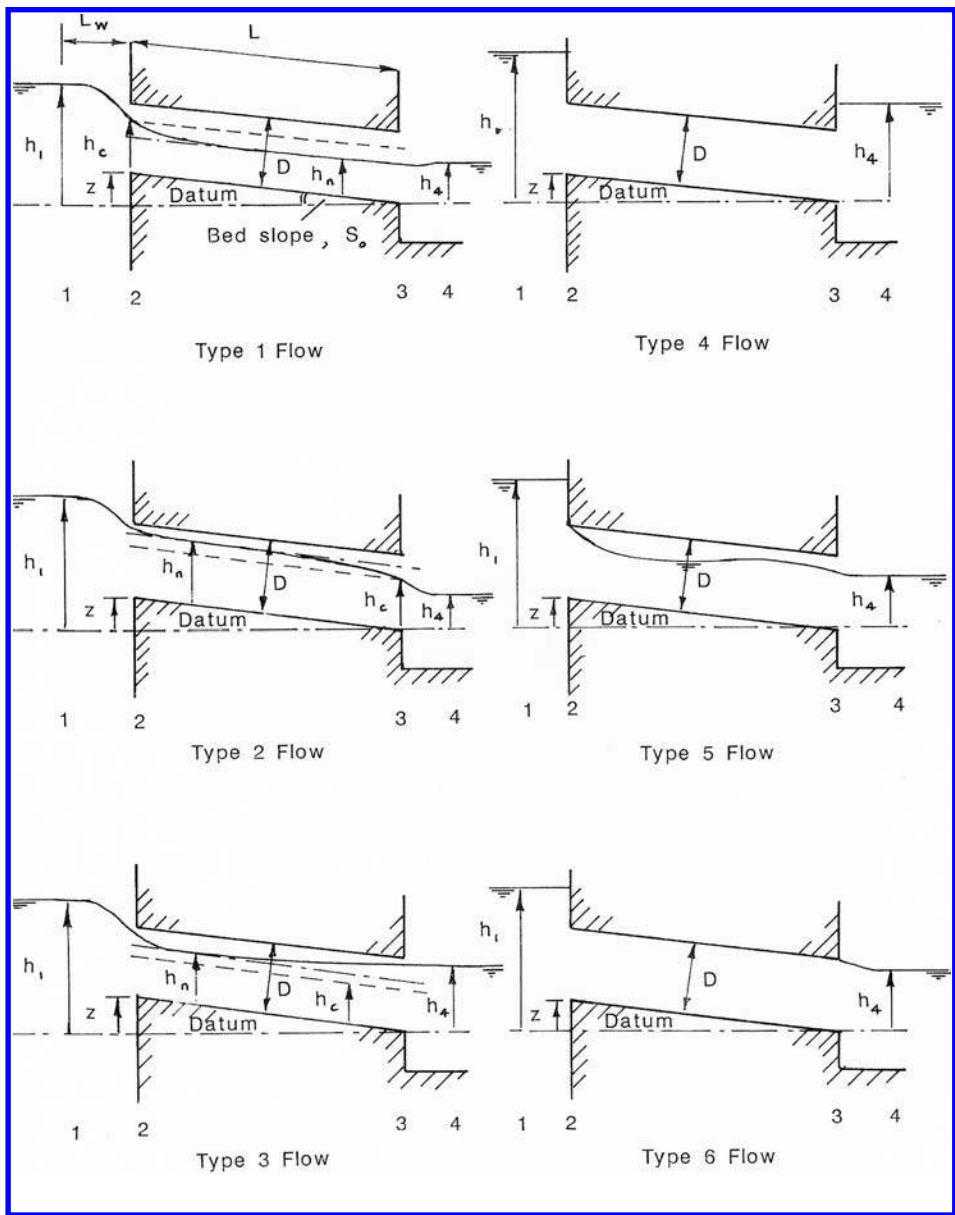


Figure 2.62 Standard types of flow through a culvert.

2.6.4.1 Bridge opening ratio, M

The bridge opening ratio, M , is defined as a ratio of discharges, $M = q/Q$, where q = unfettered flow through the gap as if the bridge or constriction was not in place and Q = total flow in the river. Thus $M = 1.0$ when there is no effect arising from a constriction, and $M < 1.0$ when there is an effect, see Figure 2.63(a). The bridge

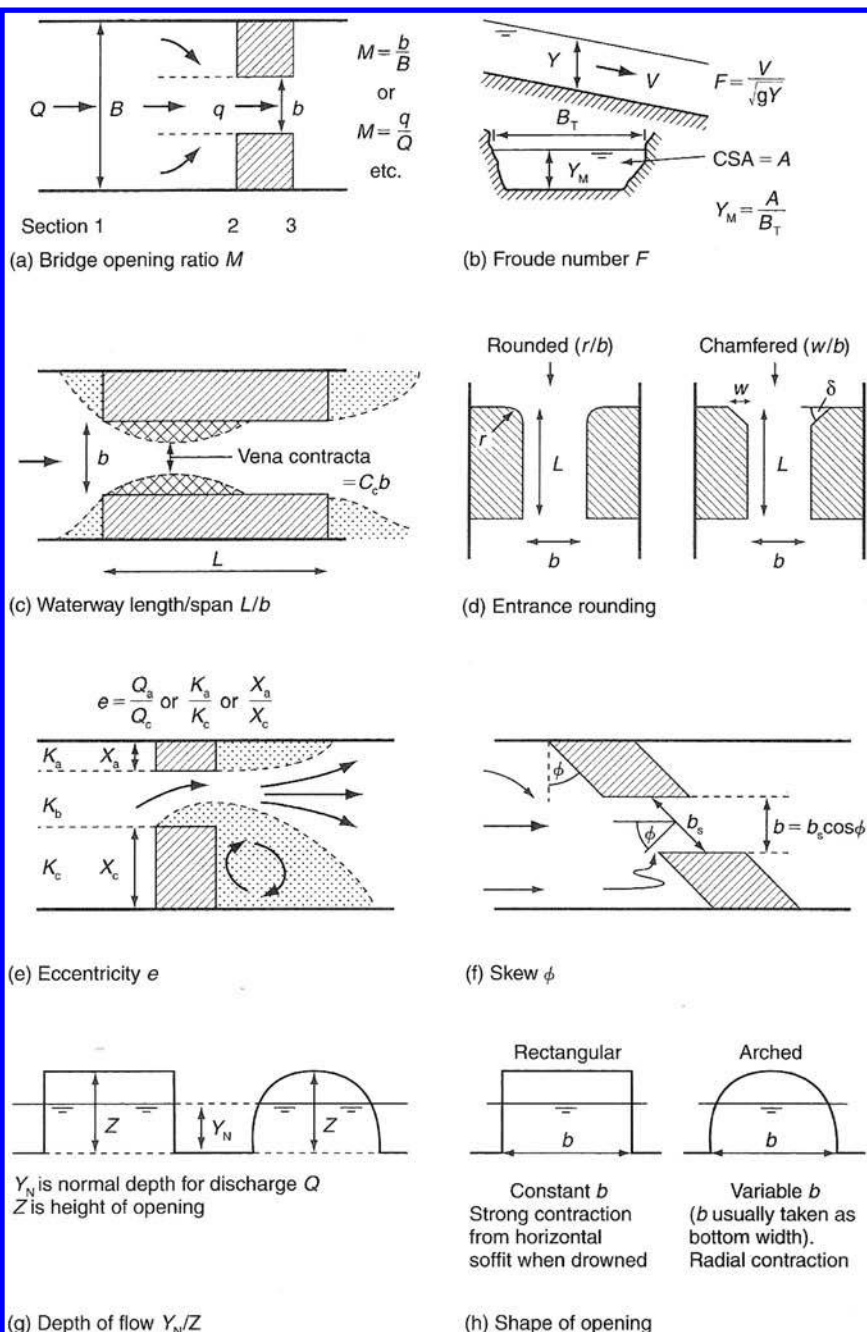


Figure 2.63 Principal hydraulic variables affecting flow through bridges (after Hamill, 1999). (a) bridge opening ratio, M ; (b) Froude Number, Fr ; (c) waterway length span, L/b ; (d) entrance rounding; (e) eccentricity, e ; (f) skew, ϕ ; (g) depth of flow, h/Z ; (h) shape of opening.

opening ratio should be distinguished from the blockage ratio, m , commonly defined as $(1 - q/Q)$, giving $m = 0$ when there is no blockage, $m = 1.0$ for full blockage. It should be noted here that in evaluating q , the depth is usually taken to be the normal depth in the river, b_n , and the width, b , is associated with that particular portion of the river occupied by the bridge opening. The value of M is, therefore, strictly dependent on the flow distribution within the river channel, which in turn is generally influenced by the geometric shape of the river channel, the roughness distribution and the upstream flow conditions. Thus the proportion of total flow occurring in a given width, located at an arbitrary lateral position within a river cross-section, is governed by the 3-D nature of the flow, as illustrated earlier in this Chapter. Technically M should therefore be regarded as a flow parameter, and not a purely geometric one.

Most ‘standard’ textbooks dealing with the issue of afflux do not consider the 3-D nature of the flow, and assume that in a simple rectangular channel, M is simply equivalent to the width ratio, b/B , (i.e. $M = b/B$), where b = waterway opening and B = total channel width. It should be noted that even for a rectangular channel, this is never strictly true because of the boundary layers that develop from both sides and the bed of the channel, as shown in [Figure 2.25](#). The value of M would vary from a minimum when the opening b is located near the walls, to a maximum when b is located at the channel centreline. The numerical values of M would also vary with depth (i.e. discharge), since as the aspect ratio of the channel changes from a large value at low depths to a lower value at high depths (discharges), the proportion of flow in any sub-region or zone would also vary. In the case of a compound channel M might correspond to the percentage of the total flow occurring in the main river channel, $\%Q_{mc}$, i.e. excluding the flow on the floodplains, which again has to be known.

2.6.4.2 Eccentricity, e

The alignment of the flow with the bridge/channel boundary is also important, as shown in [Figure 2.63\(e\)](#). Some consideration must be given to the macro flow field, as well the local flow field immediately adjacent to the bridge or culvert. The effect of the macro flow field is traditionally simulated somewhat crudely by two parameters, the eccentricity, e , and the skewness, ϕ , shown in [Figures 2.63\(e\)&\(f\)](#) respectively. The very local or micro flow field is traditionally simulated by a rounding parameter, r , or chamfering parameter, w , shown in [Figure 2.63\(d\)](#).

To some extent the eccentricity parameter, e , which equals the ratio of the bridge abutment lengths intruding from either side of the channel, X_a/X_c , is one traditional attempt at accounting for some of the 3-D effects of flow distribution on the coefficient of discharge. The eccentricity, e , was originally regarded as a purely geometric parameter (e.g. Kindsvater *et al.*, 1953), but later assumed by some (e.g. Matthai, 1967) to be equal to the ratio of flow discharge occurring either side of the bridge opening, Q_a/Q_c , in direct proportion to the specified lengths, in a somewhat similar way to the parameter M . However, from the comments made earlier, it should be clear that the link between discharge and length is not a simple linear one.

Experimental work in rectangular shaped channels by Kindsvater & Carter (1955), Matthai (1967) and Bradley (1978) indicate that when $e > 0.12 – 0.2$, or when one embankment length is less than 5 to 8 times the other, there is little reduction in

discharge performance. For $e = 0$, the USGS method states that the discharge reduction is only around 5%. However, it should be noted that the eccentricity parameter, e , does not strictly deal with all possible geometries and flow conditions. For example, it is possible to have $X_a = 0$ in [Figure 2.63\(e\)](#), but different values of X_c , all giving $e = 0$. In the case of $X_a = 0$, i.e. when there is no embankment on one side of the channel, the *vena contracta* effect would be suppressed on that side, leading to a smaller contraction laterally and therefore an increase in discharge, provided X_c is not too large. However, when $X_a = 0$ and X_c is large, or even for some very small values of e , the flow from one side towards the gap would cause a very large contraction, reduce the discharge capacity, increase the afflux, and might even be sufficient to produce supercritical flow locally. It would therefore seem sensible to redefine the eccentricity in such a way that introduces the ratio of gap width to embankment length, b/X_c or b/X_a in addition to the ratio X_a/X_c . It should be noted that e is usually defined in such a way that it never exceeds unity, the longer embankment length always being placed in the denominator.

In the case of flow in prismatic channels with two floodplains, the link between proportionate discharge and floodplain width will be especially complex, due to the lateral exchange of momentum between the main river channel and its associated floodplains. At flow constrictions, where typically embankments extend across the full width of both floodplains, the momentum exchange is further complicated by the flow spilling off the floodplain upstream of the bridge and onto the floodplain downstream of the bridge. These flow exchanges, which also occur in compound channels with converging or diverging floodplains, will directly affect the momentum-force balance and introduce additional energy losses, as shown by Bousmar (2002), Rezaei (2006), Chlebek (2009), Chlebek & Knight (2008) and Sellin (1995). The theoretical determination of e , based on flow proportioning, is therefore especially difficult for overbank flow in natural channels with floodplains.

2.6.4.3 Skewness, ϕ

For cases where the bridge crossing is not normal to the predominant flow direction, an angle of skew, ϕ , is traditionally introduced, as shown in [Figure 2.63\(f\)](#), where $\phi = 0^\circ$ when the embankments are perpendicular to the flow. As illustrated in [Figure 2.64](#), the gap width normal to the mean direction of river flow is then given by $b = b_s \cos \phi$, where b_s is the span width of the opening between the abutments of a skewed bridge, as measured along the highway centreline. It should be noted that the width b will have an impact on the determination of q (and hence M), and again highlights the confusion between geometric and flow parameters in traditional approaches. The alignments of the ends of the abutments also become important, as illustrated in [Figure 2.64](#) for skewed opening Types 1, 2 & 3.

In the case of a skewed opening of type 1A, the water level will be higher on the left-hand side of the channel (looking downstream), since a dead zone will develop there. The lower velocities in that region will give a smaller velocity head term, causing the water surface to be closer to the energy line or energy surface in this case. A second dead zone, larger than the upstream one, will occur on the right-hand side of the channel immediately downstream of the right-hand embankment. Since the water level in the upstream dead zone on the left-hand side will generally be higher than the average water level in the main river channel upstream, due to the recovery of the

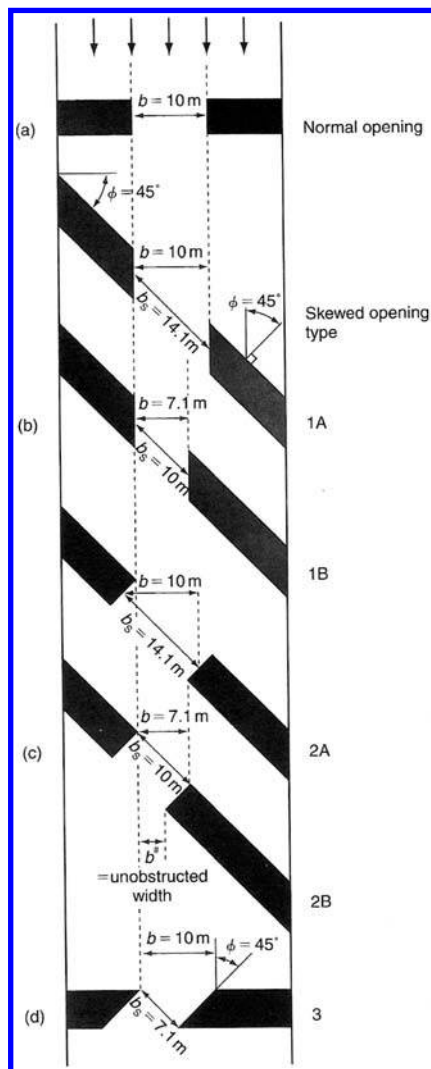


Figure 2.64 Comparison of normal and skewed crossing (after Hamill, 1999). (a) normal crossing; (b) type 1 skew with abutments parallel to the flow; (c) type 2 skew with abutments at 90° to approach abutments; (d) type 3 skew with abutments at an angle ϕ to both flow and approach abutments.

velocity head, it may, therefore, have consequences for the onset of submergence, as this generally occurs on the side that has the higher upstream water level.

The hydraulic efficiency of the waterway crossing is affected by skewness in a number of ways. Although the span width, b_s , increases with ϕ , the flow now has to turn through an angle in order to enter the gap. Furthermore, the orientation of the ends

of the abutments may cause flow separation resulting in additional eddying, as well as contraction effects downstream, if the alignments of the end faces are unsuitable. See [Figure 2.64](#), in which $b = 10$ m for the normal opening ($\phi = 0^\circ$), as well as in 1A and 2A, giving $b_s = 14.1$ m for $\phi = 45^\circ$ in both 1A and 2A. The flow through skewed openings is, therefore, complex. In 1A and 2A the afflux will be less relative to the afflux through the normal opening, but not in direct proportion to b_s/b , arising from the effects of changing the direction of the flow normal to the waterway opening, b_s , as well as the effects of separation due to possible differences in the alignment of the ends of the abutments. In 1B and 2B there will be a corresponding increase in afflux relative to the afflux through the normal opening, but again not in proportion to b/b_s . It should be remembered that it is not uncommon for a river course to change its direction during a flood, and therefore the alignment of the bridge abutments and mean skew angle of the river flow to the embankments will vary and will need to be considered as well.

Experimental results by Matthai (1967) indicate that the effect of skewness is most significant when ϕ is around 45° , producing a possible 30% reduction in discharge for the same upstream water level. Once a crossing is fully submerged, the influence of skewness is, however, reduced, as the opening then behaves more like an orifice, with the flow separating strongly from the underside of the bridge (soffit or deck) causing the flow to contract strongly in a vertical plane rather than the horizontal plane. In these circumstances the discharge capacity is then related to b_s , the width of the opening between the abutments, and is less dependent on ϕ . It thus appears that the ‘effective discharge width’ of a skewed crossing is complex, and care should be taken in evaluating the 3-D flow field under free or submerged conditions.

2.6.4.4 Rounding of piers, entrances to bridges or culverts

The introduction of a corner radius, r , or a chamfer length, w , into a waterway crossing is illustrated in [Figure 2.63\(d\)](#). It is known that the upstream rounding of piers and entrances to both bridges and culverts significantly influences the flow characteristics of such structures, by preventing or delaying flow separation at the changes in geometry. Small local changes, such as rounding or chamfering, will, therefore, generally reduce the contraction effect, increase the discharge capacity, and this increase is usually related to the parameter M . The increase is particularly large when the structure is operating under submerged conditions, i.e. orifice flow. The bridge opening ratio, M , is usually calculated for simple geometrical shapes, such as arch bridges, by assuming that the flow is wholly normal to the structure and that the flow area is identical to the geometric area. On this basis equations for the variation of M with depth for various types of arch bridge may be produced (e.g. Hamill, 1999).

The influence of r/b and w/b on the discharge coefficient, and hence the discharge capacity, is given by Kindsvater *et al.* (1953), Kindsvater & Carter (1955) and Hamill (1997). The USGS results indicate that the greatest increase in discharge capacity through entrance rounding will occur in narrow waterways (e.g. discharge increase of 20% for $M = 0.2$ & $r/b = 0.14$). As in all hydraulic flows, the streamlining of the macro and micro flow fields is important for enhancing discharge capacity and reducing energy losses. In the context of bridge crossings, streamlining is especially difficult to ensure throughout the full depth range, as the direction of the approaching

flow may change significantly as the floodplains become inundated upstream of the bridge.

2.6.4.5 Length to breadth ratio, L/b

The length to breadth ratio, L/b , of a waterway crossing is shown in Figure 2.63(c), where L is the length between the upstream and downstream faces of the constriction, or waterway length, and b is the width of the bridge opening or a characteristic height dimension of the culvert. The length to breadth ratio, L/b , is important for distinguishing between bridges and culverts, and common practice dictates that a culvert is defined by having an integral invert and $L/b > 1$, so that the flow conditions become similar to those in a pipe with 6 main categories of flow (Chow, 1959; CIWEM, 1989; Ramsbottom *et al.*, 1997). The length is important in determining where re-attachment of the flow to the sides or soffit of a bridge takes place, which generally enhances the discharge capacity. The USGS results indicate that the increase in discharge is strongly related to L/b and M values and may be as high as 30%. A large culvert is taken here to mean $b > 1.5$ m (or an equivalent height or diameter), and provided $L/b < 1$ it will behave in a similar manner to a bridge.

2.6.4.6 Channel shape

For a single waterway opening, the cross-section shape of the river channel is important as it will affect the length of piers subjected to drag resistance, the choking behaviour, the kinetic energy correction coefficient values, as well as the determination of Q , the conveyance capacity, q , the zonal conveyance capacity corresponding to the width b without the bridge present, the normal and critical depths of flow, etc. Although these considerations are important, it should be remembered that in many cases, even without an integral invert, the shape of the waterway opening is often configured into a relatively simple shape by the structure. The customary convergence and acceleration of the flow towards a constriction generally helps to re-distribute the velocity and reduce the turbulence. Arch bridges will generally affect the flow more than those with rectangular openings, due to the separation and contraction effects produced by the upper surface once the water level is above the springing of the arch.

The traditional method for dealing with the channel shape and 3-D influences in standard 1-D open channel theory is to account for it by including kinetic energy and momentum correction coefficients. However, these are unlikely to be appropriate when dealing with complex flows through bridges. Since most of the experimental work on bridges and culverts has been conducted in channels of simple prismatic shape, generally rectangular or trapezoidal, there is a need to break away from this traditional approach and to investigate more realistic cross-sectional shapes. The most obvious one is to consider bridges in natural channels with floodplains. A considerable number of bridges in the UK fall into this category (e.g. see Pool bridge, River Wharfe, given as Figure 1 by Knight & Samuels, 1999), in which the general river shape is a compound channel and the embankments are perched higher, giving multiple openings at different invert levels. Apart from the experiments at the University of Birmingham (Atabay & Knight, 2002), there is a dearth of investigative work on bridge crossings in compound channels.

2.6.4.7 Multiple openings

For a waterway crossing with multiple openings, the division of flow has to be determined or assumed prior to any analysis. Where there are multiple openings with different invert and drowning characteristics, this will be problematic. As already commented upon, the answer lies in estimating the flow field, by using 2-D depth averaged models that give both the magnitude and the direction of the approaching flow, or by using full 3-D CFD modelling. An example of a single opening culvert with a square headwall with no rounding of the corners is shown in [Figure 2.65](#). A multiple opening culvert, with inverts at different levels is shown in [Figure 2.66](#). Note the tendency for silt to deposit and block the entrance to the right hand side opening.

2.6.4.8 Blockage

One remaining geometric issue concerning the shape of the opening is that of blockage. However this is conceptualised in any modelling process, the discharge characteristics and any additional head loss will be affected by the debris. Blockage may occur through floating debris trapped against the deck or soffit, trash against piers, ice accumulation, siltation or other types of trash, such as shopping trolleys, cars and even sometimes caravans. Modelling these by simply decreasing the waterway area is not always appropriate, and other methods should be attempted such as those that proportion the area to the floating debris (i.e. varying the proportion of the flow area that is blocked depending on the distance from the water surface downwards), those that include vertical or horizontal strips of blockage, those that consider random blocked area patches and those that mimic siltation by reducing the area from the invert upwards. Care needs to be taken in recognising the impact that these different geometric changes might have on the hydraulic behaviour and functioning of the structure. Some attention should also be paid to collecting evidence of where bridges have failed, due to debris accumulation, impact forces (overturning moments) and scour. There is very little experimental data on measured forces on bridges with which to check any momentum-force balance approach, and what are available often



Figure 2.65 Pre-cast concrete box culvert with one cast in-situ headwall (Ramsbottom et al., 1997).



Figure 2.66 Cast in-situ twin box culvert with invert lower to carry normal flow (Note deposition on right side entrance).

relates to specific case studies, such as required in low cost bridge crossings in India or Australia (e.g. Roberts *et al.*, 1983).

2.7 DATA SOURCES USED IN THIS BOOK

2.7.1 Conveyance data

This Chapter began by emphasising the physical principles of fluid flow, theoretical concepts and how these ideas are encapsulated into mathematical models of river flow and the CES-AES in particular. The various case studies have shown the wide range of issues and some of the difficulties in developing, validating and calibrating any numerical model, particularly for overbank flow. As a result, empirical evidence from different sources was introduced, both from the field and laboratory. The laboratory data were found to play an essential part in elucidating flow mechanisms and turbulence parameters, albeit at small scale, that are virtually impossible to obtain at full scale at appropriate spatial and temporal scales on the grounds of cost and control. Figure 2.67 shows some views of the experimental arrangements used in the Phase A & B studies in the Flood Channel Facility (FCF). See Knight & Sellin (1987) and Knight & Shiono (1990 & discussion in 1991) for further details of these studies. The FCF was built at HR Wallingford for the Engineering and Physical Sciences Research Council (EPSRC) for joint collaborative work between 10 UK universities. These data, as well as many other data sets related to overbank flow studies and bridge flow may be found at www.flowdata.bham.ac.uk. Recent work by HR Wallingford is given at www.river-conveyance.net and should be consulted for further details.

The recent UK Foresight project, the recent European Commission (EC) Flood-site and Peseta projects on climate issues all indicate the strength of activity in flood research (see Table 2.6 for links to the various websites). The EC has in fact funded

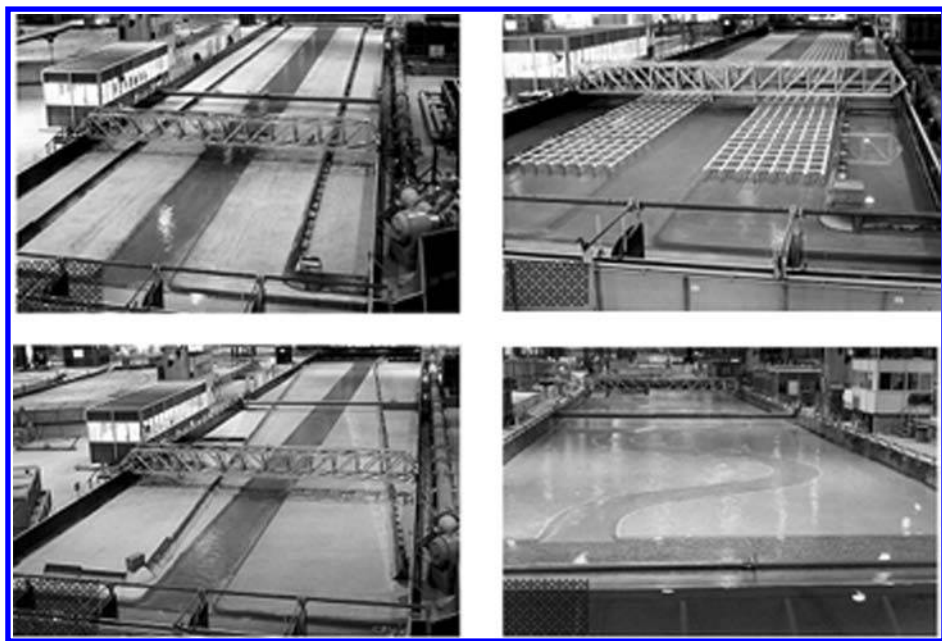


Figure 2.67 FCF flumes showing Phase A with (a) smooth and (b) roughened floodplains and (c) the skewed channel layout and (d) Phase B with a sinuosity of 1.374 (Courtesy HR Wallingford).

over 100 research projects on flooding since the early 1980s, and these are itemised in a report by the University of Birmingham (see actif-ec.net website in [Table 2.6](#)).

2.7.2 Bridge afflux data

[Table 2.7](#) summarises the most significant data sets for bridge afflux and their suitability (and availability) for use in development of the methods described in [Chapter 3](#) of this book. Much of the early twentieth century data is inaccessible and often specific to certain types of bridge found in the USA, but not common in the UK.

After careful review, it was concluded (Mantz *et al.*, 2007, Lamb *et al.*, 2006) that the most relevant measurements for development of the AES were contained within two data sets, the HEC (1995) field scale numerical model results and the recent University of Birmingham laboratory measurements of Atabay and Knight (2002) and Seckin *et al.* (2007 & 2008a&b). Both data sets provide detailed water surface elevation data for some distance upstream and downstream of a bridge. Additionally, the USGS (1978) field survey data were used in testing the AES. These measurements are for wide (~ 100 to ~ 1000 m), rough, vegetated floodplains with low bed slopes, are very detailed and remain the most comprehensive field measurements available for bridges on wide vegetated floodplains.

Table 2.6 Links to useful flood studies websites.

Project	Link
RIBAMOD	http://www.hrwallingford.co.uk/projects/RIBAMOD/index.html
RIPARIUS	http://www.nwl.ac.uk/ih/www/research/briparius.html
MITCH	http://www.hrwallingford.co.uk/Mitch/default.htm
IMPACT	http://www.samui.co.uk/impact-project
University of Birmingham	http://www.actif-eu.net/library/review_EU_flood_projects.pdf http://www.flowdata.bham.ac.uk
MDSF	http://www.mdsf.co.uk
SMURF	http://www.smurf-project.info
RASP	http://www.rasp-project.net
CES	http://www.river-conveyance.net
PAMS	http://www.pams-project.net
FORESIGHT	http://www.foresight.gov.uk
FLOODSITE	http://www.floodsite.net
DTI-SAM	http://www.dti-sam.co.uk
PESETA	http://peseta.jrc.es
EU directive	http://europa.eu.int/comm/environment/water/flood_risk/index.htm
FRMRC/EPSRC	http://www.floodrisk.org.uk

The University of Birmingham data were measured in a laboratory flume, as illustrated in Figures 2.53–2.59. Subject to appropriate scaling they provide the detailed information needed for a rigorous analysis of afflux. A total of 325 afflux measurements were made for arch bridge types of single and multiple openings, and beam bridges with or without piers. An important feature is that the tests were made for a compound channel and for bridges at various skew angles. Multiple bridge and channel roughness configurations were tested in a fixed bed, compound channel, as follows:

- 15 tests with an elliptical arch bridge (designated ASOE) using three different roughness conditions;
- 20 tests with a semi-circular arch bridge (designated ASOSC) using four different roughness conditions;
- 15 tests with a twin semi-circular arch bridge (designated AMOSC) using three different roughness conditions;
- 45 tests with a single span beam bridge (designated BEAM) using three different roughness conditions and three different bridge spans;
- 50 tests with a beam bridge having three piers (designated PBEAM) using four different roughness conditions and three different bridge spans;
- 180 afflux measurements, were made for bridges located at an angle to the flow direction ('skew bridges').

In 1978–79 the USGS published detailed field data for bridge afflux analysis in the 'Hydrologic Investigations Atlas' series numbers HA-590 to HA-611. These surveys were conducted for 35 floods at 22 bridge sites in southern USA, and they

Table 2.7 Sources of data for bridge afflux.

Source	Date	Details	Available	Notes
Rehbock	1922	Over 2000 laboratory experiments		
Nagler	1918	256 laboratory experiments on 34 different bridge models		
Yarnell	1934	2600 laboratory experiments with pier bridges		
Kindsvater, Carter and Tracy	1953	Laboratory data from the Georgia Institute of Technology		
Biery and Delleur	1962	Laboratory study on arched bridges		
Matthai	1967	Verified the Kindsvater et al. (1953) method with data from 30 field sites		
Bradley	1978	Laboratory experiments, Colorado State University	No	
USGS	1978, 1979	Hydrologic Investigations Atlases. Observed water surfaces for 35 flood events, 22 field sites	Paper maps.	I
HR Wallingford	1988	Laboratory study, arched bridges, 203 tests (see Brown, 1988)		
HR Wallingford	1985	Field data from bridges in the UK, 66 data sets (see Brown).	Yes, (partial records)	2
Hamill	1993	Field observations from Canns Mill bridge, Devon (see Hamill, 1999)	Yes	3
HEC	1995	Two dimensional numerical model results for 5 real and 76 idealised cases.	Yes	I
Atabay and Knight	2002	University of Birmingham laboratory tests in compound channels, 145 measurements, bridges normal to flow direction		
Seckin, Knight, Atabay and Seckin	2004 2008	Extension of University of Birmingham lab tests in compound channels, 225 measurements, skewed bridges	Yes	4

Notes

1 Digitised and used in development of AES.

2 Archives reviewed for AES development but not suitable for use.

3 Provided subjective checks for AES but not calibration data.

4 Used in development of AES.

have been described in detail by Kaatz and James (1997). Of the surveyed floods, 17 events at 13 bridge sites have previously been satisfactorily modelled using HEC-RAS (HEC, 1995) although some bridge sites were eliminated because of inadequate water level data near to the bridge. The modelling has been repeated more recently at JBA Consulting in development of the Afflux Estimation System using the HEC-RAS software. In the AES development, 15 events at 11 bridge sites could be satisfactorily modelled. The rivers and bridges from the USGS (1978) surveys that were used in development of AES are listed in [Table 2.8](#) and their locations shown in [Figure 2.68](#).

The US Army Corps of Engineers Hydrologic Engineering Center (USACE HEC) used data from three of the USGS Hydrologic Atlas field sites in an investigation of flow transitions in bridge backwater analysis (HEC, 1995) based on two dimensional (2-D) numerical modeling. To extend the scope of the study, HEC (1995) also created

Table 2.8 Bridges in the USGS (1978) Hydrologic Atlas (HA) series used with AES.

HA series no.	River	Bridge span (m)	Floodplain width (m)
591	Bogue Chitto	230	1360
596	Okatoma Creek	65	560
600	Alexander Creek	75	285
601	Beaver Creek	80	560
603	Cypress Creek	40	240
604	Flagon Bayou	70	480
606	Tenmile Creek	160	640
607	Buckhorn Creek	80	280
608	Pea Creek	78	340
609	Poley Creek	62	400
610	Yellow River	78	400

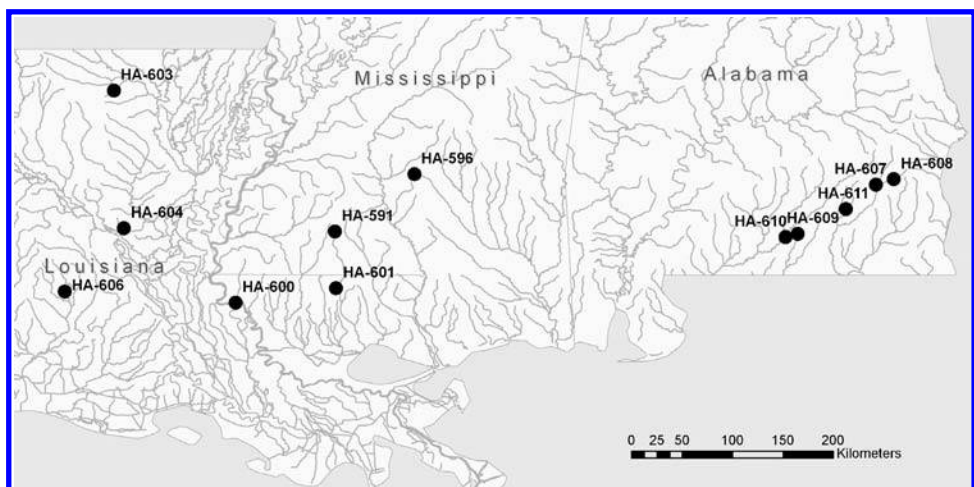


Figure 2.68 USGS Hydrologic Atlas (HA) field surveys used with the AES.

2-D models of an idealized bridge crossing based on a uniform compound channel of 305 m width with 76 different combinations of opening width, discharge, slope and roughness.

The HEC (1995) numerical model data, USGS (1978) field surveys and Birmingham University laboratory data provide a basis for analysis over a range of scales from ~ 1 m to ~ 1000 m, and a wide range of roughness conditions. There is a lack of measured field data for a scale of ~ 100 m. Field measurements from UK rivers were used in the HR Wallingford (Brown, 1988) work on arch bridges. However, the field data proves very difficult to use in practice because it gives estimates of head loss rather than the water surface profiles and channel survey data are needed to recover afflux estimates. Additionally, there is scant information to determine the exact locations of the measurements or the flow conditions. The bridges were not originally instrumented for the study of afflux and so these limitations are not surprising. Only one detailed set of measurements exists for afflux analysis at this scale, which is the data of Hamill (1999) at Canns Mill in Devon. Paper records were available to make subjective checks in the development of AES methods. Whilst the laboratory measurements made under careful scaling principles are very useful in calibrating and testing afflux calculation methods, there remains a gap in the data at the field scale.

Chapter 3

Understanding roughness, conveyance and afflux

ABSTRACT

This chapter is an introduction to the roughness, conveyance and afflux concepts and governing equations as adopted in the CES-AES in 2005/06. The topics also include the backwater calculation, the method assumptions and limitations and the numerical solution techniques. Where the science has subsequently advanced, references are given which may be used for future evolution of the CES-AES. The issue of uncertainty is introduced and a pragmatic approach is set-out for dealing with this when estimating water levels in practice. The CES-AES software components are presented with a description of the overall modular interaction and example screen shots.

3.1 FLOW STRUCTURES IN OPEN CHANNEL FLOW

Identifying and understanding the various flow features is critical to estimating the overall channel flow capacity. The flow structure influences the energy dissipation, boundary shear stresses, resistance to flow and hence the overall conveyance (Knight, 2001). The flow features are defined here as ‘energy transfer mechanisms’, which typically convert the energy from one form to another through the development of vortex structures on a variety of length scales. Once vorticity is created, its rotational energy cascades down in length scale into increased turbulence intensity until it dissipates as heat through viscosity. The streamwise translational kinetic energy may, for example, be transferred in part to rotational kinetic energy, which no longer contributes to the streamwise channel conveyance. It is possible to identify different situations in which vorticity is created in open channel flow.

3.1.1 Boundary shear

Vorticity may be generated from boundary shear due to surface roughness (Nezu & Nakagawa, 1993), the bursting phenomenon (Reynolds, 1974; Grass *et al.*, 1991) as described below or a combination of these two mechanisms.

In uniform open channel flow, the boundary layer is fully developed and extends from the channel boundary throughout the flow depth. It includes a viscous laminar sub-layer adjacent to the boundary, a transitional zone characterised by both viscous

and inertia effects and a turbulent zone where the inertia forces dominate. The effect of boundary resistance is felt throughout this layer, and is closely linked to the channel velocity distribution (Stokes, 1845). A hydraulically smooth boundary condition (Figure 3.1a) occurs where the boundary roughness elements are submerged within the viscous sub-layer. The streamlines adjacent to the bed are therefore parallel to the bed, and separation is unlikely to occur. A hydraulically rough boundary condition occurs where the roughness elements (height k_s) penetrate through the viscous sub-layer (Figure 3.1b). The boundary velocities adjacent to the bed tend to accelerate over the crest of the roughness elements and come to an abrupt standstill between them, substantially reducing the velocity and resulting in flow separation. Hydraulically rough boundary conditions are present in most rivers.

Bursting may also occur on smooth and rough beds. Bursting is a randomly occurring event comprising gradual local lift-up of the fluid in the area of low velocity parallel to the channel bed, causing sudden oscillations and ejection of fluid away from the boundary (Kline *et al.*, 1967). This is usually stimulated by an inrush or “sweep” event (Figure 3.1), where high velocities move in close to the boundary, intensifying near wall vorticity by lateral spanwise stretching and generating new vorticity which is subsequently transported away by the ejections. Theodorsen (1952) first proposed a simple horseshoe vortex model (Figure 3.2) as the central element of the turbulence generation in shear flows.

Lighthill's (1963) explanation for the bursting phenomenon is that it represents the only means by which the very large gradients in mean vorticity present at the wall in turbulent boundary layers can be maintained against the corresponding outward diffusion and transport of vorticity by viscous and ejective action. This argument applies independently of wall roughness. More recently, Grass *et al.* (1991) undertook experiments to establish the full three-dimensional form of these turbulence structures over rough boundaries, and found that the horseshoe vortex structures are a central feature and play an important role in rough wall flows.

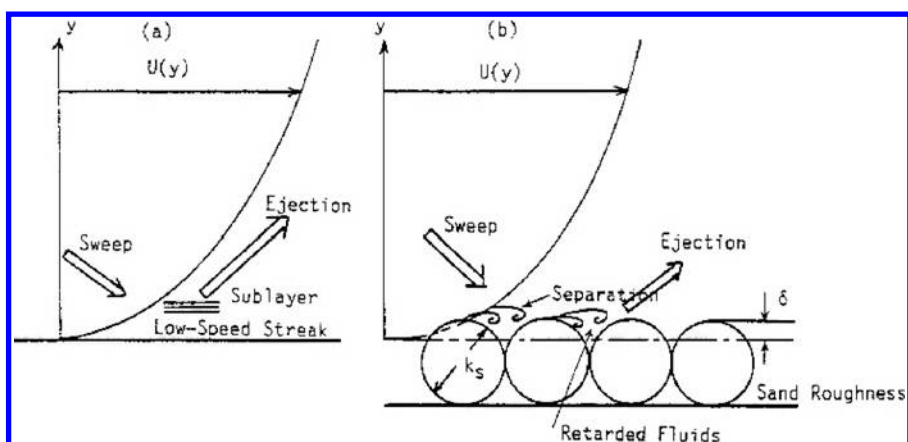


Figure 3.1 Turbulent flow over (a) smooth and (b) rough beds (Nezu & Nakagawa, 1993).

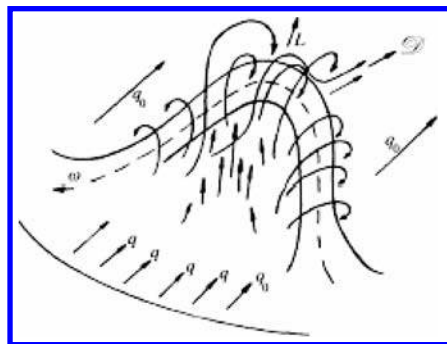


Figure 3.2 Horseshoe vortex model first proposed by Theodorsen (1952).

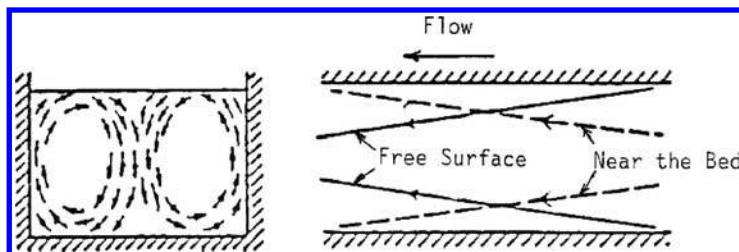


Figure 3.3 Schematic flow pattern of secondary currents in a narrow open channel (Gibson, 1909).

3.1.2 Vertical interfacial shear

Small-scale vorticity is generated from vertical interfacial shear in straight channels due to the steep velocity gradients at the main channel floodplain interface. These eddy structures tend to be smallest at the floodplain bed (i.e. at a relative depth of zero), and they expand gradually through to the water surface. These interfacial vortices are shown in Figure 2.15, Section 2.2.5.

3.1.3 Transverse currents

More than a century ago, river engineers (e.g. Stearns, 1883) first inferred the presence of secondary or “transverse” currents, as the maximum streamwise velocity occurred well below the free surface in open channel flow. Gibson (1909) first envisaged the flow pattern depicted in Figure 3.3 and estimated that the transverse velocities would be about 5% of the mainstream velocities. This simple pattern was later suggested to repeat itself across wide channels (Vanoni, 1946; Karcz, 1966), supported by the cyclical variations in spanwise sediment concentration.

Prandtl (1925) categorised the two types of secondary flows into flows of the first kind, derived from mean flow skewing, and those of the second kind, caused by inhomogeneity of anisotropic wall turbulence.

- Flows of the first type are driven by the channel geometry, which may affect non-uniform flow in the streamwise direction and hence the generation of streamwise vorticity through vortex stretching. In curved or meandering channels, the centrifugal driving force results in secondary currents in both laminar and turbulent flows with magnitudes typically 20–30% of the mainstream velocity (Rozovskii, 1957; Nezu & Nakagawa, 1993).
- Flows of the second type are generally smaller in magnitude and arise in straight channels due to the transverse gradients of the Reynolds stresses and anisotropy between the fluctuating velocity component (Prandtl, 1925; Brundrett & Baines, 1964; Perkins, 1970; Hinze, 1973). The production and suppression mechanisms for this vorticity are perhaps best understood through detailed examination of the terms in the vorticity equations, derived from the cross-differentiation of the Reynolds-Averaged Navier-Stokes equations in the y - and z -directions, to eliminate the pressure term (Perkins, 1970; Nezu & Nakagawa, 1993; Shiono & Muto, 1998). Detailed measurements of the various vorticity production terms (Perkins, 1970) suggest that the normal stresses do play an essential role (Figure 3.4).

Regions of flow confined by two perpendicular boundaries, for example, the corner of a rectangular (Figure 3.3) or trapezoidal (Figure 2.14, Section 2.2.5) channel are characterised by spontaneously occurring secondary flows of Prandtl's second kind. These circulations are only present in non-circular sections in turbulent flows, and the circulation is oriented towards the corners along the bisector line. In open channel flow, this secondary flow pattern alters slightly, in that a larger "free vortex" is formed near the surface and a smaller "bottom vortex" is formed at the channel bed, both still oriented along the bisector line (Nezu & Nakagawa, 1993). These transverse flows are small in comparison to the primary flow, in the order of 1%. They affect

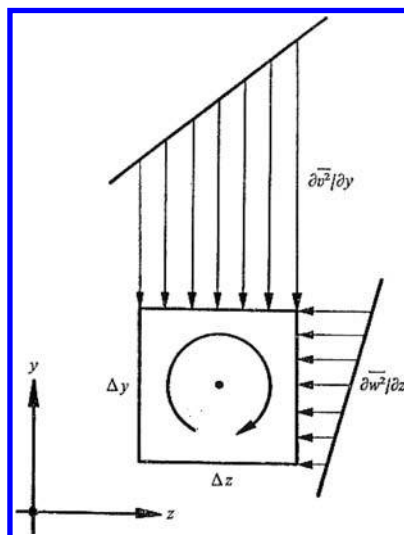


Figure 3.4 Mechanism of vorticity production by the direct stresses (Perkins, 1970).

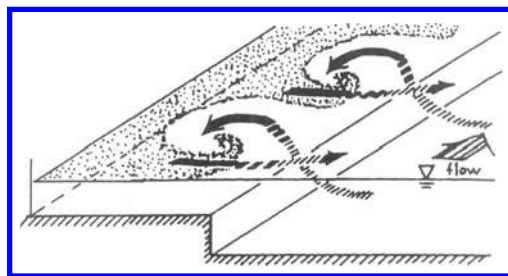


Figure 3.5 Transverse currents in a straight two-stage channel (Fukuoka & Fujita, 1989).

the isovel and boundary shear stress distributions significantly (Knight *et al.*, 1994; Tominaga & Knight, 2004), resulting in the maximum shear stress and velocity no-longer occurring at the channel centre line and free surface (Figure 2.14, Section 2.2.5). The number and orientation of these secondary flows have been related to the peaks and troughs in the lateral shear stress and mean velocity profiles (Imamoto & Ishigaki, 1989; Omran, 2005).

Post 1960, researchers still attribute the position of the maximum velocity filament to these secondary currents (e.g. Rajaratnam & Muralidhar, 1969). The cause of this velocity dip may be related to the aspect ratio (Nezu & Rodi, 1985), giving two channel types:

- i narrow channels with small aspect ratios ($b/h < 6$) where the velocity dip is caused by the free surface effect, which dampens the vertical velocity fluctuations, resulting in a different turbulent anisotropy from that in closed channels; and
- ii wide channels with large aspect ratios ($b/h > 6$) where the side-wall effects are not felt so much in the channel centre, and a series of secondary circulations occurs across the channel width. This results in low- and high-speed streaks, where the maximum velocity filaments in the high-speed streaks are below the free surface, but not always located at the centre of the channel.

Secondary currents of Prandtl's second kind can also be observed (Fukuoka & Fujita, 1989) along the flood plain main channel interface in compound channels (Figure 3.5). These transverse currents vary with relative depth, changing in orientation as the flow moves from inbank to low overbank and then to high overbank flow.

In skewed or meandering channels, secondary flows of the first kind are largely dominated by the additional contribution of the primary shear stresses. Toebees and Sooky (1967) observed that these secondary flow rotations change direction before and after inundation at the bend apex, which is supported by the detailed three-dimensional velocity measurements of Muto (1997), Shiono and Muto (1998) and Shiono *et al.* (1999b). Here, the influence of the secondary flows on eddy viscosity was found to be significant.

3.1.4 Coherent structures

Large plan form eddies or coherent structures are generated by shear instability (Ikeda & Kuga, 1997) in regions of high velocity gradient, for example, at the

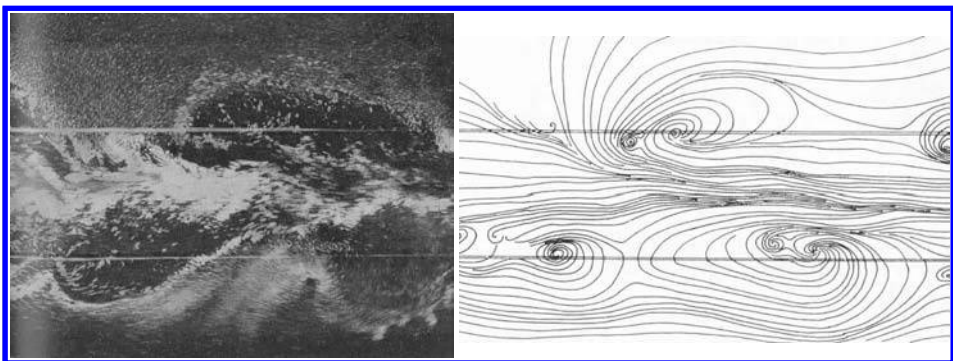


Figure 3.6 Surface velocity patterns and streamlines relative to a moving camera (Sellin, 1964).

main channel flood plain interface. Sellin (1964) identified these flow features in a two-stage experimental channel by scattering aluminium powder on the free water surface (Figure 3.6). The 4.6 m long channel was designed to maximise the flood plain main channel interaction through having vertical main channel side slopes. A strong vortex structure in the region of contact between the flood plain flow and that in the main channel was revealed (Figure 3.6a), with the surface streamlines providing further evidence of these large eddy structures (Figure 3.6b). Ikeda *et al.* (2002) carried out laboratory experiments for two-stage channels with varying relative depths (D_r). The presence of these coherent structures at low relative depths (e.g. 0.180, Figure 3.7a) was identified, however at higher relative depths (e.g. 0.344, Figure 3.7b) the periodic plan form vortices disappeared and active intermittent boils were observed. Nezu *et al.* (1997, 1999) observed that these boils actually grew stronger with increasing relative depth.

A vortex street may develop along the interfacial zone, and in compound channels the effect of these tends to vary if the parallel vortex streets are in or out of synchronisation with one-another, tending to increase the energy transfers for the in synchronisation case. Where adverse streamwise pressure gradients are present, this may result in flow separation. These patterns are further influenced by the channel aspect ratio. A large aspect ratio results in more lateral freedom for these eddies, allowing increased momentum transfer to the outer banks. Figure 3.8 provides an example of these coherent structures as observed in 1981 during a flood in the River Tone, Japan (Kitagawa, 1998).

Ikeda *et al.* (2002) undertook experiments in a two-stage curvilinear channel. Here, large-scale coherent structures were observed on both the inside and outside of the bend (e.g. Figure 3.9, $D_r = 0.5$).

Van Prooijen (2003 & 2004) considered the plan form rotation structure, highlighting the additional energy transfers due to the expansion and contraction of the flow as it rotates into and out of the main channel (Figure 3.10). In meandering channels, this rotational structure is further complicated, since the co-existence of plan form vortices with opposite rotations has been observed near the inner bank of a two-stage



Figure 3.7 Visualisation of the free surface in a straight two-stage channel with $D_r = 0.180$ and $D_r = 0.344$ (Ikeda et al., 2002).

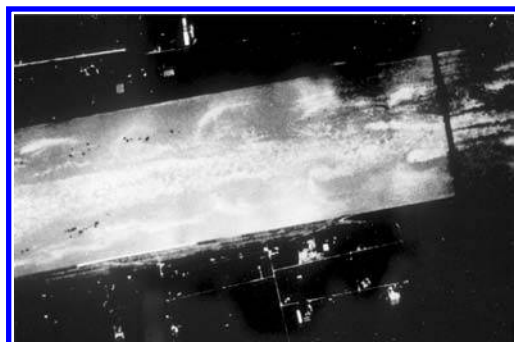


Figure 3.8 Horizontal vortices observed in the River Tone, Japan, during the 1981 flood. The flow is from left to right. (Courtesy of the Ministry of Construction of Japan).

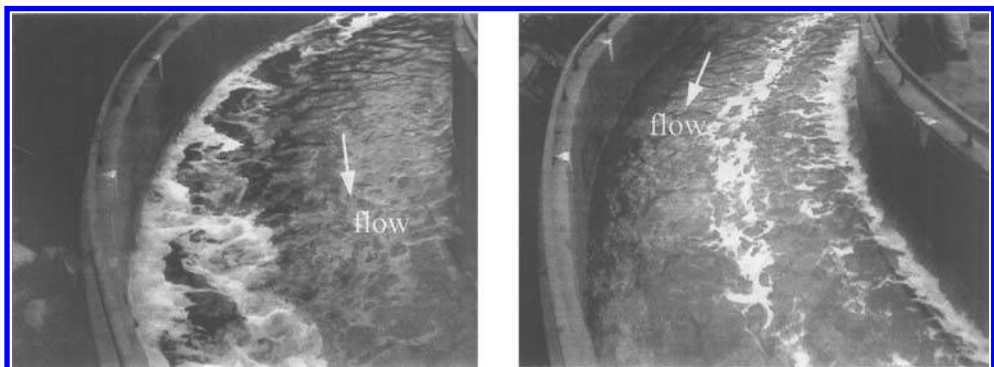


Figure 3.9 Flow visualisation of the free surface in a curvilinear two-stage channel ($D_r = 0.5$) at the outer bank and inner bank (Ikeda et al., 2002).

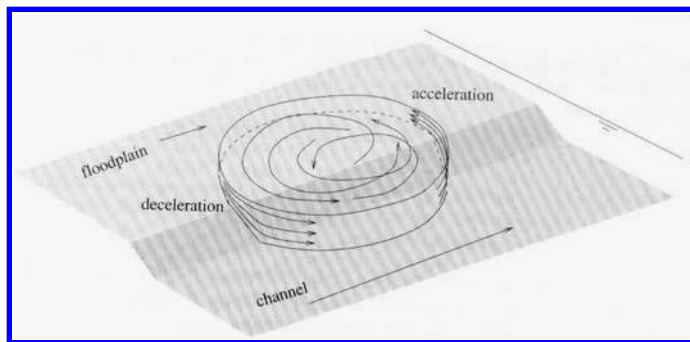


Figure 3.10 Large-scale coherent structure at the main channel-floodplain interface in a two-stage channel (van Prooijen, 2003).

curvilinear channel (Figure 3.9). In doubly meandering channels, the vortex path may be further influenced by the phasing of the main channel sinuosity relative to that of the flood plain levees. In rivers, these are rarely in phase. Fukuoka and Fujita (1989) show that the effect of this levee alignment on flow characteristics, i.e. on the position of maximum velocity filament and velocity distribution, is small compared to other influences and the main channel sinuosity has a dominant impact.

The lateral transport of fluid momentum associated with horizontal vortices becomes relatively greater, compared with that by secondary flows, as the water depth becomes shallower. If the channel curvature increases, the secondary flows transferring momentum to the outer banks increases, and this influences the strength of the horizontal vortices to induce still more momentum transport to the outer bank. The result is that the horizontal vortex structures are generally larger at the main channel-floodplain interface on the outer bend relative to those at the inner bend.

3.1.5 Horizontal interfacial shear

Vorticity may be generated from horizontal interfacial shear due to steep velocity gradients at the main channel to floodplain interface. Here, the two water bodies may be oriented with different bulk flow directions, typically observed in meandering channels (Elliott & Sellin, 1990; Shiono & Muto, 1998). Figure 3.11 illustrates this with a flow visualisation technique. At low relative depths (e.g. $D_r = 0.15$), the out-of-bank main channel flow tends to follow the main channel flow direction. At high relative depths (e.g. $D_r = 0.25$), the out-of-bank flow direction is parallel to the flood plains. Water moving from the flood plain into the main channel shears over the main channel flow, and the relative magnitude and direction of this interfacial shear may enhance or retard the main channel rotations. Typically, the main channel rotational structures expand into the bend in a helical shape, and gradually dissipate beyond the bend where the shearing is no longer present. The orientation of the main channel rotations or secondary currents changes before and after the bend (Figure 3.12), since the angle of the floodplain relative to the main channel changes the magnitude and

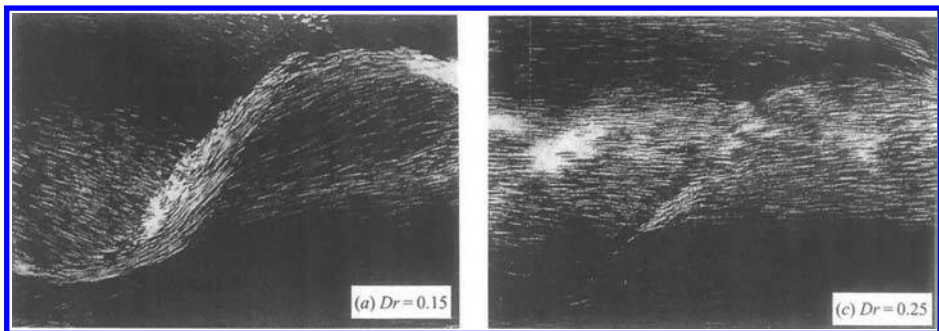


Figure 3.11 Flow visualisation using sawdust showing (a) flow in the streamwise direction ($D_r = 0.15$) and (b) parallel to the floodplain ($D_r = 0.25$) (Shiono & Muto, 1998).

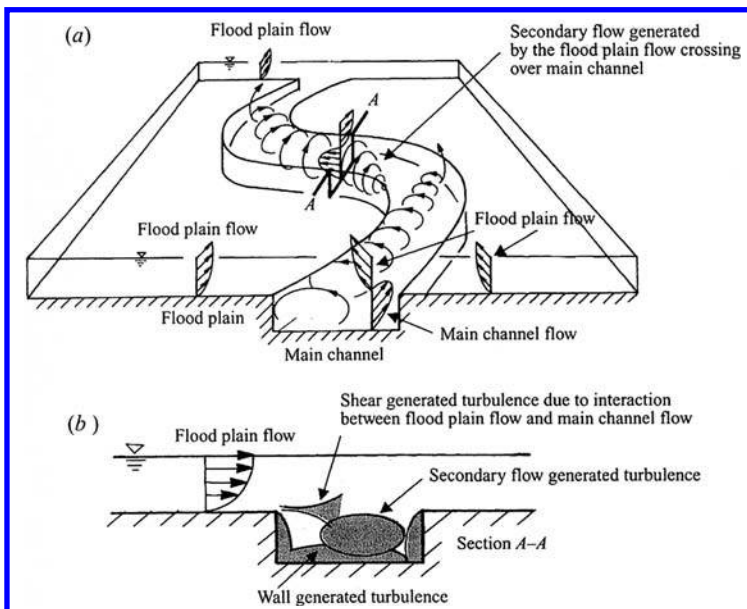


Figure 3.12 Flow mechanisms in a compound meandering channel (Shiono & Muto, 1998).

direction of the horizontal interfacial shear. These examples are taken from idealised laboratory flow where the floodplains are relatively smooth. In nature, the floodplains are typically more rough, offering greater resistance, and thus the interfacial shearing is less intense and the centrifugal accelerations are not always carried through to the next downstream apex.

If the floodplain flow entering the main channel region is slowed, for example, through roughness, it may result in less or no vorticity as the relative velocity is low.

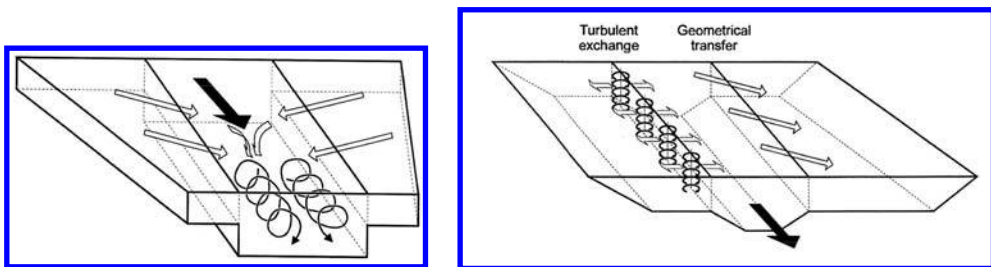


Figure 3.13 Non-prismatic channels with (a) converging and (b) diverging flow (Bousmar, 2002).

This may result in the in channel circulation occurring along the centre of the main channel, rather than the channel edges (Elliott & Sellin, 1990).

Horizontal interfacial shearing may also occur in converging (narrowing floodplains) and diverging (enlarging floodplains) channel geometries (Bousmar, 2002; Rezaei, 2006; Chlebek, 2009):

- For converging flow, the floodplain flow moves over the main channel flow, causing a horizontal shearing action and main channel eddies that rotate with a different orientation to straight prismatic channels. The flow plunges to the channel bed along the main channel centreline, and then rotates back out towards the main channel edges, forming a rotating helical structure in the streamwise direction (Figure 3.13a).
- For diverging flow, there is a transfer of momentum from the main channel to the flood plain flow (Figure 3.13b). This is similar to the skewed compound channel, where the water on the enlarging floodplain is accelerated due to the faster main channel velocities passing onto the floodplain, through a smaller depth of flow, resulting in increased lateral momentum transfer relative to that in a straight channel.

3.1.6 Vorticity in rivers

The various instances in which vorticity may occur are closely related to the nature of the channel geometry i.e. a simple or compound, straight or meandering, depth and nature of flow etc. Experimental set-ups tend to idealise flow conditions to restrict the number of unknown parameters. Purpose-made river-measurements are often based on sections with idealised shapes e.g. River Main (Section 2.2.2). Vorticity in rivers, with non-idealised section shapes, may differ from those outlined thus far, for example:

- *Asymmetry of floodplains or berms* – Asymmetric channels (e.g. one floodplain or berm present) will have different in channel circulations as the flood plain flow will only influence one side of the main channel.
- *Multiple berms* – A main channel cross-section with multiple berms will affect the secondary flow structure and orientation with flow depth.

- *Braiding* – A braided channel with common floodplains may result in the floodplain flow structures (e.g. coherent vortices) overlapping and hence interacting. This may influence the stability of the vortex pattern, where a decreased stability (i.e. the vortex patterns of the two channels are out of synchronization with one-another) is characterized by flow separation.
- *Shape* – Natural rivers have large width to depth ratios, resulting in non-homogenous turbulence. The flow is affected by bottom generated small-scale isotropic “wall turbulence”, scaled by depth, and “free turbulence” from the large-scale horizontal eddy structures which have lateral freedom (Ikeda, 1999). These large-scale vortices constitute more than 75% of the lateral fluid momentum transport in rivers with large aspect ratios.
- *Bank vegetation* – Main channel banks may have thick vegetation. This may reduce or eliminate the vertical interfacial turbulent exchanges, acting as a streamwise vertical barrier between the main channel and flood plain flow. This may reduce the overall conveyance as the vegetation provides increased flow resistance or enhance the conveyance as less lateral momentum exchange takes place.
- *Floodplain features* – Clumps of trees or urban form may generate additional streamwise vorticity through stream drag or alternatively suppress the large-scale horizontal eddy structures.
- *Structures* – Hydraulic structures such as bridges or weirs may initiate a vortex street, the affect of which may be felt some way downstream (Section 3.1.7).
- *Pools and riffles* – Meandering channels in nature invariably have a pool and riffle sequence. These undulations result in localised head losses, which are larger in low overbank flows. Riffles occur at the cross-over point between consecutive bends. The pools generally occur at the bend apex in regions of maximum bend velocities. It is possible to determine the position of these maximum velocity filaments, through a flow classification based on sinuosity and relative depth (Okada & Fukuoka, 2002). The secondary currents in these pool and riffle sequences are convergent and divergent respectively, providing deposition or erosive properties.

It is possible to formulate some general rules for the occurrence and development of secondary cells. The classic rectangular channel case is effectively half a square duct, hence the symmetry in the circulations. The cells are always stronger in the corners, to either side of the bisector line. Weaker cells develop across the channel width, with the cell orientation changing for each adjacent cell, resulting in pairs of circulation with a radius similar to half the depth of flow. Trapezoidal channels have additional cells in the top corners. For two-stage channels, the flow in the main channel is similar to inbank flow and additional cells develop at the sharp floodplain edges. These are generally weaker in rivers whereas the plan form vortices have a far greater effect than in laboratory channels, for example, in the River Tone the planform eddies are up to 300 m wide (Kitagawa, 1998).

3.1.7 Special features near structures

The nature and orientation of vortices changes near hydraulics structures such as weirs, bridges, groynes and culverts. In-line weirs (e.g. broad crested, vertical, V-notch) obstruct the main flow direction, forcing the flow through a smaller cross-sectional

area above the structure. This results in the higher velocities initiating a slowly rotating vortex upstream of the structure, with a horizontal axis (Figure 3.14).

Flow structures around bridge abutments and piers are closely related to the size, shape and orientation of the structure. For example, as flow approaches circular bridge piers, a bow wave forms at the free surface on the upstream side. Along the sides of the pier, the free surface is drawn down as the flow accelerates around it. Wake vortices (with a vertical axis of rotation) are formed and shed downstream of the pier as the flow about either side of the pier separates from the structure (Figure 3.15).

Bridge abutments typically occupy more cross-sectional area than bridge piers and commonly result in a contraction of the flow through the bridge (converging streamlines) and flow expansion further downstream. Abutments occur in variety of shapes, see, for example, Hoffmans and Verheij (1997). Consider a simple vertical-wall abutment. As the flow comes into contact with the bridge abutment, the velocity is reduced to zero and the resulting pressure gradient causes a downflow on the upstream face of the abutment. Downstream of the abutment, the main flow is separated from a large slowly rotating vortex in the lee of the abutment by a vortex-street. The flow

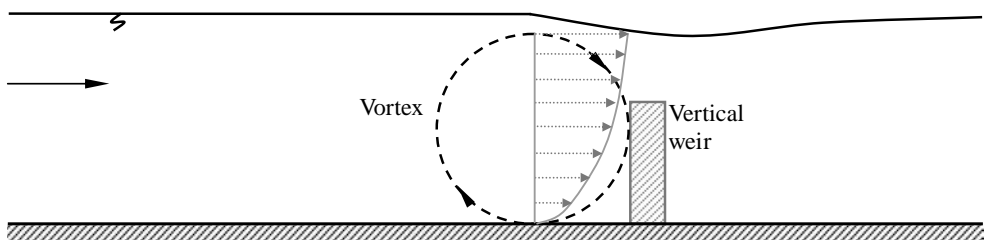


Figure 3.14 Vortex prior to a vertical weir (long-section view).

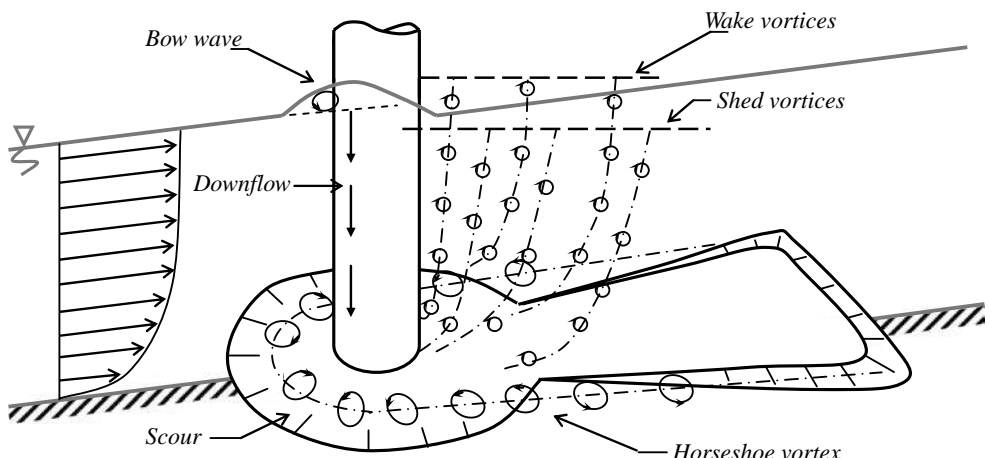


Figure 3.15 Flow patterns and vortex structures at a cylindrical pier (adapted from Raudkivi, 1998).

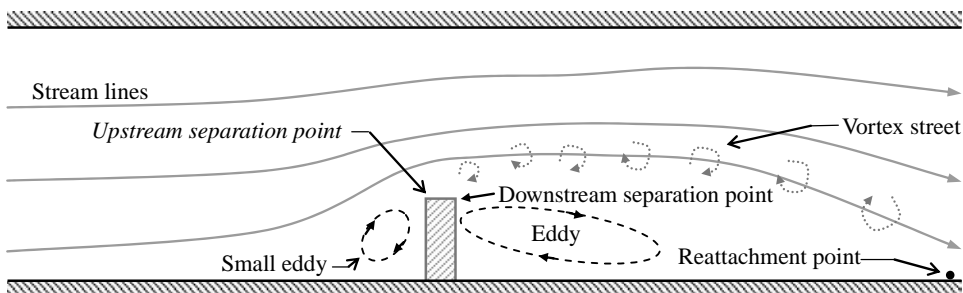


Figure 3.16 Flow patterns around a vertical-wall abutment (plan view).

decelerates over a significant distance downstream and normal depth is re-established further downstream beyond the reattachment point (Figure 3.16). Where the bridge has two similar abutments on opposite river banks, this pattern is symmetrical.

For further reading on vorticity, flow structures and other issues that need consideration, see Ashworth *et al.* (1996), Nezu & Nakagawa, (1993), Knight (1996) and Anderson *et al.* (1996).

3.2 GOVERNING EQUATIONS

3.2.1 Roughness Advisor methods

Roughness characterisation of channels and their associated floodplains is essential to water level estimation. Roughness reduces the discharge capacity through energy expenditure from boundary generated turbulence (Section 3.1.1) as well as physical blockages due to vegetation.

Traditionally, flow resistance datasets are based on average values of Manning's n , Chezy C or Darcy f for whole river sections (Chapter 2). These include the influence of bed material, vegetation and large-scale topographic effects. Table 3.1 provides a summary of some of the approaches for estimating n , C and f from the literature and used in practice today. These include methods for establishing lateral distributions of equivalent 'local' values for non-homogenous roughness across a channel section. Important assumptions of these approaches are steady, uniform flow conditions and a fixed channel bed.

The flow of water in a river, water course or drainage system is described by certain physical laws related to the conservation of mass, energy and momentum. The CES conveyance calculation requires a lateral and depth distribution of the friction factor f (Section 3.2.2). Due to the widespread use of Manning's equation, most resistance advice in the literature is expressed in terms of Manning n (Table 3.1). The Roughness Advisor (RA) is based therefore, on an input unit roughness n_l with similar units ($\text{sm}^{-1/3}$) to Manning n , rather than the friction factor f , to maintain user familiarity and confidence. This unit roughness describes identifiable segments of boundary friction only and the additional turbulence generation due to cross-section and plan

Table 3.1 Approaches for estimating Manning n , Chezy C and Darcy f .

No.	Approach	Description
Manning n		
1	Direct solution of the Manning (1889) equation from measurements (Eq. 2.1)	River survey to measure flow, depth, cross-section topography and longitudinal water surface (or bed) slope.
2	Photographic sources	The most widely used reference is Chow (1959). Others include Barnes (1967) and Hicks & Mason (1998), which are based on American and New Zealand channels respectively.
3	Tabular sources	An extensive list of typically used Manning's n values is available in Chow (1959) and Yen (1991).
4	Formulae for evaluating composite Manning n for non-homogenous roughness (e.g. main channel, banks & floodplain)	These include, for example, the methods of: <ul style="list-style-type: none"> - Pavlovskii (1931) - Horton (1933) and Einstein (1934) - Lotter (1933) - Krishnamurthy and Christensen (1972) - Einstein and Banks (1950) which vary in their assumptions relating to local shear force, velocity and hydraulic radius.
5	Formulae for evaluating composite Manning n due to multiple resistance sources (e.g. vegetation, meandering)	Cowan's (1956) additive approach evaluates the total Manning's n resistance value from multiple sources. The standard Manning n -value (e.g. Chow, 1959) is inflated by the additional resistance due to surface irregularities, channel shape and size, obstructions and vegetation and the total is then multiplied by a factor for channel curvature.
6	Formulae for evaluating Manning n where large boundary elements are present (e.g. sediments, cobbles)	<ul style="list-style-type: none"> - Strickler (1923) relates Manning's n to the average sediment diameter d (ft) for flow in channels with cobble beds - The Manning-Strickler formula relates Manning's n to Nikuradse's size k_s and the hydraulic radius R. - Ackers (1958) provides a simple approximation for the Manning Strickler in the range $5 < R/k_s < 500$.
Chezy C		
7	Direct solution of the Chezy (1768) equation from measurements (Eq. 2.23)	River survey to measure flow, depth, cross-section topography and longitudinal water surface (or bed) slope.
8	Formulae	A number of formulae exist for determining this coefficient, see for example Ganguillet & Kutter (1869), Bazin (1897) and Powell (1950).
Darcy f		
9	Direct solution of Darcy (1857) – Weisbach (1845) equation from measurement (Eq. 2.24)	This requires estimates of flow, hydraulic radius and longitudinal water surface (or bed) slope. This is typically used in open channel flow by setting the flow depth equal to 4 times the radius (Chow, 1959).

(Continued)

Table 3.1 (Continued).

No	Approach	Description
10	Blasius (1913) equation	Applicable for smooth turbulent pipe flows where the flow conditions are dominated by the viscous forces, typically used for experimental flumes ($4000 < Re < 105$).
11	Kármán-Prandtl (1925) equation	For use at higher Reynolds Numbers, where the Blasius equation under-predicts f . See Schlichting (1979).
12	Hazen-Williams equation	Derived for pipe flow.
13	Iterative solution of the Colebrook-White (1937) equation from measurements (Eq. 2.26)	This requires estimates of flow, roughness size, hydraulic radius and approximate cross-section shape. Many studies have been undertaken to establish shape coefficients for open channel flow (Table 3.3, Section 3.2.2).
14	Moody (1944) diagram (Figure 2.10)	A drawback in application of the Colebrook-White equation is that it is implicit in f . Moody sought to overcome this through developing a diagram for pipe resistance (Figure 2.10), where the pipe diameter can be replaced by four times the hydraulic radius R (m) for open channel flow. The diagram relates f to the relative roughness R/k_s and the Reynolds' Number for laminar, transitional and fully turbulent flow through a family of curves.
15	Direct solution of Barr (1975 & 1979) and Yen's (1991) form of the Colebrook-White equation from measurements	Barr (1975 & 1979) provides an alternative explicit equation to the Colebrook-White formula for pipe flow, which Yen (1991) has provisionally adapted for wide open channels where $Re > 30,000$ and $R/k_s > 20$. This requires estimates of flow, roughness size, hydraulic radius and approximate cross-section shape.
16	Approaches for establishing the lateral variation of f	Power Law approach (Shiono & Knight, 1991; Rhodes & Knight, 1995). Relates the ratio of Darcy f on the floodplain f_{fp} and main channel f_{mc} , to the relative depth by a power of 3/7. Calibrated relationships (Abril, 1995; Knight & Abril, 1996). Relates the main channel resistance f_{mc} to the floodplain resistance f_{fp} by an empirically derived factor R_f .

form shape is explicitly represented in the conveyance calculation (Section 3.2.2). The unit roughness n_l is then converted to an equivalent turbulence length scale k_s and thence to a friction factor f by an iterative procedure (due to velocity dependence) for input to the conveyance calculation (Section 3.2.2).

The unit roughness values are notionally associated with a depth of 1.0 m, selected as a ‘representative’ depth of flow for UK channels and one at which roughness elements (e.g. sand, pebbles, weeds) are normally small relative to flow depth i.e. the roughness does not vary rapidly with depth. This then excludes cases where the roughness is comparable with the flow depth (e.g. boulders, emergent vegetation), for which special rules may be introduced.

The unit roughness is comprised of three component values: surface material n_{sur} (e.g. sand, bedrock), vegetation n_{veg} (e.g. reeds, crops) and irregularities n_{irr} (e.g. tree roots, urban trash) and is evaluated from:

$$n_l = \sqrt{n_{\text{veg}}^2 + n_{\text{sur}}^2 + n_{\text{irr}}^2} \quad (3.1)$$

The “root sum of the squares” approach is adopted as the roughness is squared before being combined since the energy loss is related to the square of the local velocity. This approach highlights the contribution of the largest component roughness, for example, a tree would have more influence than a grain of sand.

The RA provides advice on the component unit roughness values, including minimum, maximum and expected values. This is based on an extensive literature review of over 700 references (Defra/EA, 2003b), and where possible, gives descriptions accompanied by photographs. The RA values, descriptions and advice are used together with information from the site to evaluate n_{sur} , n_{veg} and n_{irr} for a given cross-section or portion of cross-section (e.g. bank, channel bed). Where known, the seasonal variations in plan form aquatic vegetation coverage and n_l are provided as well as advice on expected regrowth patterns following cutting. These are derived from previous measurements and expert knowledge, giving a series of embedded rules for

Table 3.2 Unit roughness values for twelve vegetation morphotypes (Defra/EA, 2003b).

	<i>Aquatic vegetation by RHS vegetation type</i>	<i>Unit roughness n_l</i>		
		<i>Min</i>	<i>Mean</i>	<i>Max</i>
1	None – if no vegetation visible			
2	Free-floating plants typically algae or duckweeds, medium deep drainage channel [depth = 1.1 to 2.5 m, velocity = 0.1 to 0.6 ms ⁻¹]	0.010	0.030	0.040
3	Filamentous algae attached shallow nutrient rich waters [depth = 0.05 to 0.5 m, low velocities]	0.000	0.015	0.050
4	Mosses attached to bed or banks [depth ≈ 1 m]	0.000	0.015	0.030
5	Trailing bank-side plants [depth = 0.5 to 3+ m]	0.000	0.050	0.100
6	Emergent reeds, rushes, flag and large grasses	0.020	0.150	0.200
7	Floating-leaved typically water lilies in deeper slower waters	0.030	0.100	0.140
8	Emergent broad-leaved rooted plants, water cress or water parsnip	0.050	0.150	0.50+
9	Submerged broad-leaved, pondweeds [depth = 0.06 to 1.2 m, velocity 0.2 to 0.9 ms ⁻¹]	0.020	0.100	0.200
10	Submerged fine-leaved, shallow rivers, chalk streams, water crowfoot, pondweeds [depth = 0.2 to 0.6 m, velocity = 0.2 to 0.7 ms ⁻¹]	0.020	0.300	0.45+
11	Submerged fine-leaved, medium depth rivers, regular management [depth = 0.6 to 1.2 m, velocity = 0.3 to 0.8 ms ⁻¹]	0.021	0.100	0.249
12	Submerged fine-leaved, medium to deep rivers, some management [depth > 1.2 m, velocity = 0.3 to 1.0 ms ⁻¹]	0.010	0.080	0.120

regrowth pending vegetation type (and hence biomass), time of year and percentage cut (Defra/EA, 2003b).

In the absence of any survey data or channel description, the RA provides advice using data obtained through the UK national River Habitat Survey (RHS) (Raven *et al.*, 1998). Sample locations were sere selected within a 10 by 10 km square grid. At each location, observations were made at 10 cross-sections spaced at 50 m intervals. This enables provision of advice on expected in-channel and bank-side aquatic vegetation based on the UK grid reference for a study reach.

The Roughness Advisor includes values for:

- natural surface materials e.g. bedrock, cobbles, gravel, sand, silt, peat, earth, bare ploughed soil;
- man-made surface materials e.g. sheet/wood piling, stone block, hazel hurdles, concrete, rip-rap;

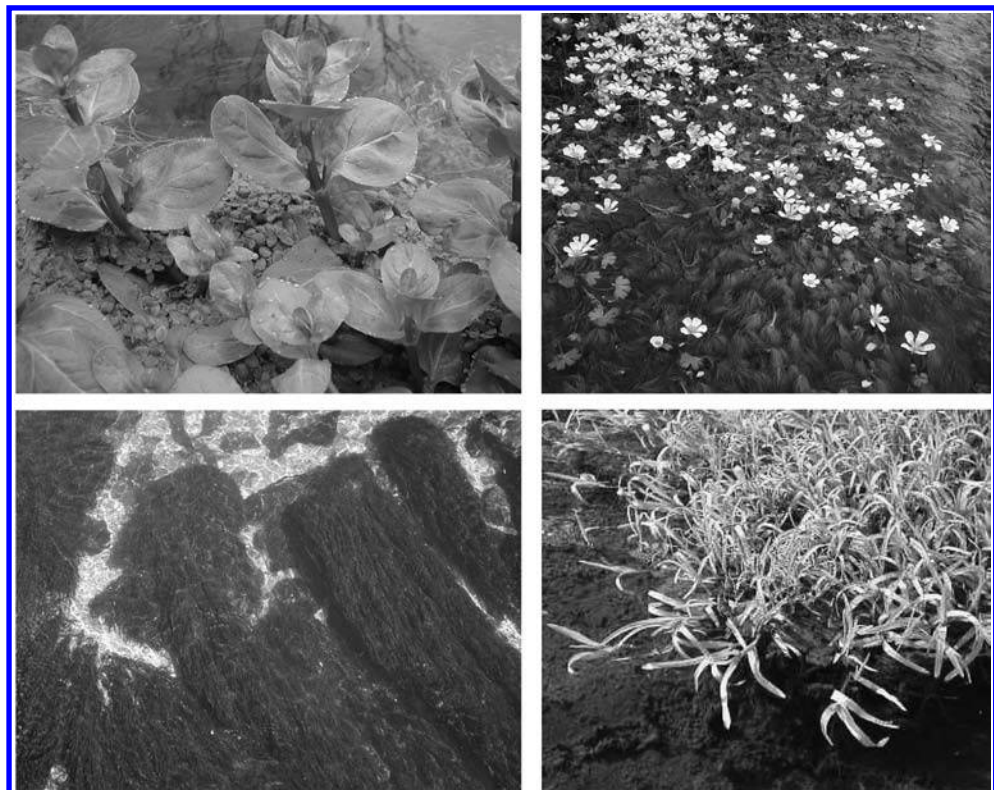


Figure 3.17 Example vegetation morphotypes including (top left) emergent broad-leaved brooklime *Veronica beccabunga*, (top right) submerged fine-leaved pond water crowfoot *Ranunculus peltatus*, (bottom left) willow moss *Fontinalis antipyretica* and (bottom right) trailing bank-side sweet grass *Glyceria* (See colour plate section).

- natural vegetation covering 12 morphotypes (Table 3.2, Figure 3.17) which are closely linked to the RHS categories;
- vegetation subject to human intervention e.g. grass, hedges, trees, shrubs and crops such as maize;
- natural irregularities e.g. groynes, exposed boulders, undulations on the floodplain and obstructions such as debris deposits, exposed stumps, logs and isolated boulders;
- man induced irregularities e.g. urban trash.

A more complete description of the information sources for the RA is provided in the Roughness Review (Defra/EA, 2003b). See also related work by Baptist (2005).

3.2.2 Conveyance Estimation System methods

Conveyance (Chapter 2, Section 2.2.4) relates total discharge to a measure of the gradient or slope of the channel under normal flow conditions, giving

$$Q = KS^{1/2} \quad (2.41)$$

where K (m^3s^{-1}) is the conveyance, Q (m^3s^{-1}) is the discharge and S is the common uniform gradient. For normal flow there is no ambiguity about this slope since the water surface slope S_w , the bed slope S_o and the so-called “energy” or “friction” slope S_f all coincide. In practice, this is approximated from the water surface slope (e.g. in numerical models) or bed slope.

Conceptual and chronological development of conveyance

The approaches to quantifying conveyance have varied throughout the late nineteenth and twentieth century. These may be broadly divided into five categories, reflecting the basis of their derivation (Figure 3.18):

- 1 *Hand calculation methods* – commonly termed Single (SCMs) and Divided Channel Methods (DCMs) where the channel cross-section is treated as a single unit or divided into more than one flow zone, respectively. These vary in terms of the number and nature of the sub-divisions (Figure 3.19) and the assumptions

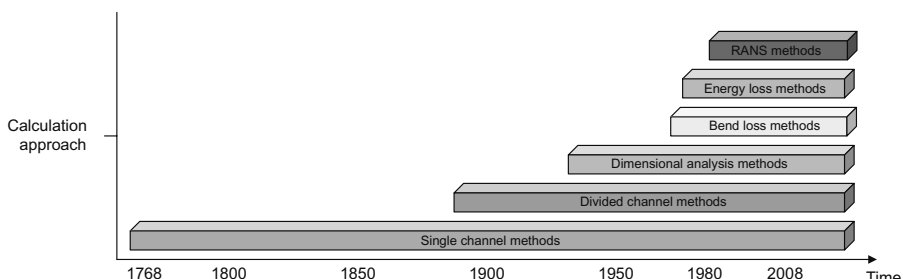


Figure 3.18 An approximate timeline of conveyance estimation approaches (Mc Gahey et al., 2008).

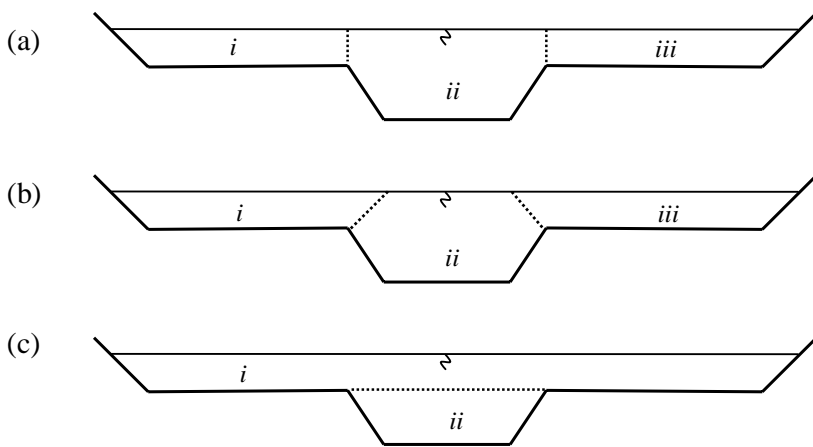


Figure 3.19 Example of (a) vertical, (b) diagonal and (c) horizontal division of a compound channel (Mc Gahey, 2006).

regarding velocity, shear stress and momentum transfer – including the so-called apparent shear force methods. These include, for example, the methods of Chezy (1768), Manning (1889), Lotter (1933), Yen and Overton (1973), Ervine and Baird (1982), Knight and Demetriou (1983), Knight, Demetriou & Hamed (1984), Wormleaton and Merrett (1990), Ackers (1991), Lambert and Myers (1998) and Knight and Tang (2008).

- 2 *Dimensional analysis approaches* – where channel properties likely to affect channel conveyance are identified and grouped into dimensionless combinations such as relative roughness, Froude Number and Reynolds Number. A regression analysis is applied to ascertain the value of any coefficients and the relationships are evaluated for scale models and assumed similar for the prototype e.g. Ackers (1991), Shiono *et al.* (1999a), Rameshwaran and Willetts (1999).
- 3 *Additional energy losses due to bends* – methods which account for the additional losses around channel bends, for example, the Soil Conservation Service and Linearised Soil Conservation Service approach and the methods of Rozovskii (1957), Leopold *et al.* (1960), Toebees and Sooky (1967), Argawal *et al.* (1984), Chang (1983 & 1984) and James (1994).
- 4 *Energy ‘loss’ methods* – which are based on an extension of the early DCMs, with consideration for the true flow mechanisms present within each sub-area. These assume that the energy transfers within each flow zone (e.g. main channel or floodplain region) are proportional to the square of the local flow velocity and they are mutually independent and hence the principle of superposition can be applied:

$$\sum_{i=1}^n K_i \frac{U_i^2}{2g} = S \text{ (straight); } \sum_{i=1}^n K_i \frac{U_i^2}{2g} = \frac{S_o}{\sigma} \text{ (meandering)} \quad (3.2)$$

where K_i represents the energy loss coefficient. Well known methods include those of Irvine and Ellis (1987), Greenhill (1992), James and Wark (1992), Shiono *et al.* (1999b), Bousmar and Zech (1999) and van Prooijen (2003 & 2004).

- 5 *Reynolds Averaged Navier-Stokes (RANS) approaches* – which are based on the depth-integration of the RANS equations for flow in the streamwise direction. These equations are derived from the equations of fluid flow and are therefore physically based and theoretically sound. The unit flow rate q (m^2s^{-1}) or depth-averaged velocity U_d (ms^{-1}) is solved for at discrete locations across the channel, and then a lateral integration provides the overall flow rate Q (m^3s^{-1}) i.e.

$$Q = \int_0^B q \, dy = \int_0^B U_d \, dA \quad (3.3)$$

where y is the lateral distance across the channel cross-section (m) and B is the total channel width (m). The various approaches differ in their assumptions, emphasis on different terms, the processes that are modelled rather than directly evaluated, the calibration coefficients and the turbulence model selected for closure. Significant research contributions include Shiono and Knight (1988), Wark (1993), Abril and Knight (2004), Spooner and Shiono (2003), Bousmar and Zech (2004), van Prooijen *et al.* (2005) and Tang and Knight (2009).

Methods adopted in practice

Industry practice in Europe and the United States still adopt variations of the early hand-calculation methods such as the Manning and Chezy equations. These equations are attractive due to their simplicity, limited data requirements, transparency of outputs and the ease with which they can be embedded in modelling systems. For example:

- *ISIS Flow* – developed by Wallingford Software and Halcrow incorporates the Manning equation with the Lotter (1933) approximation for non-homogenous roughness.
- *InfoWorks RS* – developed by Wallingford Software incorporates the Manning equation with the Lotter (1933) approximation for non-homogenous roughness.
- *HEC-RAS* – developed by the US Army Corps of Engineers incorporates the Manning equation with the Horton (1933) and Einstein (1934) approximation for non-homogenous roughness.
- *MIKE11* – developed by the Danish Hydraulic Institute incorporates the Manning and Chezy equations.

Today, with new research substantially improving our understanding of the flow behaviour, the advent of computing power allowing for more sophisticated solution techniques and the availability of flow measurements on a range of scales providing a sound basis for method testing (e.g. the EPSRC Flood Channel Facility at HR Wallingford, purpose-made river measurements) – it is feasible to consider alternatives

to these early methods. For example, the CES conveyance calculation is now incorporated in the UK modelling software ISIS Flow and InfoWorks RS, providing an alternative to the more traditional Manning equation.

The CES conveyance calculation

The CES conveyance calculation is derived from the depth-integration of the Reynolds-Averaged Navier-Stokes (RANS) equations at specified sections along the water course. See Schlichting (1979) and Drazin and Riley (2006) for further details of the RANS equations. The underpinning theory stems from the original Shiono Knight method (1988, 1990–91), and subsequent evolutions of this, for example, Abril (1997, 2001), Abril and Knight (2004), Knight and Abril, (1996), Ervine *et al.* (2000), Defra/EA (2003a) and Mc Gahey (2006). A complete description of the derivation from first principles is available in Mc Gahey (2006). Here, the method is described from the depth-averaged form of the RANS equation for flow in the x -direction, with x orientated streamwise in the x - y plane (or plane with normal z , Figure 3.20):

$$\rho g H \left(\frac{\partial H}{\partial x} - S_o \right) - \psi \tau_o + \frac{\partial}{\partial y} \left(H v_t \frac{\partial U_d}{\partial y} \right) - \frac{\partial}{\partial y} \rho [H(UV)_d] = 0 \quad (3.4)$$

(i) (ii) (iii) (iv)

where ρ (kgm^{-3}) is the fluid density, ψ is the projection onto plane due to choice of Cartesian coordinate system, τ_o (Nm^{-2}) is the boundary shear stress, v_t ($\text{m}^2 \text{s}^{-1}$) is the turbulent eddy viscosity and H implies $H(y)$ i.e. the local depth at any point within the cross-section. The remainder of this section describes the derivation of the four terms in Eq. 3.4:

- i Hydrostatic pressure term
- ii Representation of turbulence due to boundary friction
- iii Representation of turbulence due to transverse currents effecting vertical interfacial shear
- iv Representation of turbulence due to secondary circulations

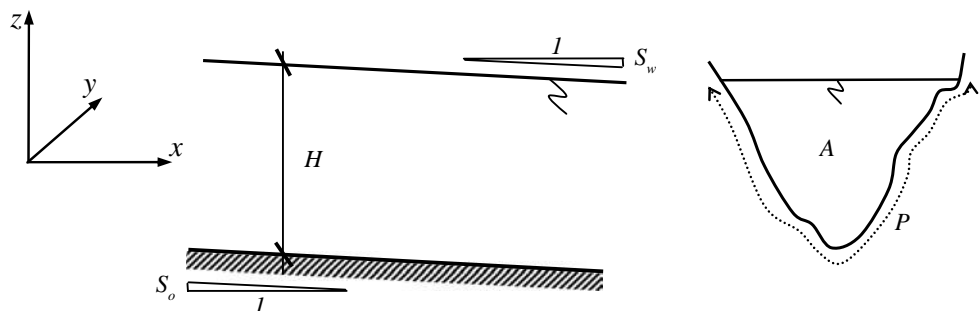


Figure 3.20 Definition of the co-ordinate system.

culminating in a system of equations that represent the complete CES conveyance methodology. An important theme is the extension of theoretically or experimentally derived models and coefficients for application in the field. This involves consideration of effects of scale, transferability of application extents, applicability of parameter values for field studies and, in particular, the potential of a depth-averaged model for predicting meandering channel flow conditions.

Term (i) – Hydrostatic pressure term

The first term in Eq. 3.4 represents the variation in hydrostatic pressure along the reach. As the flow depth H is assumed uniform along the representative reach, dH/dx is considered negligible, giving the expression for the hydrostatic pressure as

$$\rho g H S_o \quad (3.5)$$

The reach-averaged longitudinal bed slope, S_o , is a parameter based on the available reach information. Where water level measurements are present, it may be approximated by the longitudinal water surface slope. This latter option is a significant improvement as it is influenced by both bed slope and changes in water level and it will thus reduce any implications of the steady, uniform flow assumption.

Term (ii) – Representation of turbulence due to boundary friction

The second term in Eq. 3.4 represents the turbulence generated due to boundary friction and it comprises the primary balance of momentum for Term (i). The slope projection parameter ψ may be evaluated directly from (Wark, 1993)

$$\psi = \sqrt{1 + S_y^2 + S_o^2} \quad (3.6)$$

where the estimated lateral distribution of S_y is improved with increased density of channel survey data, particularly in areas of rapidly varying cross-section shape. For vertical channel banks, ψ tends to infinity as S_y tends to infinity (albeit it at a slower rate). The nature of the quasi-2D discretisation (see solution technique), whereby the surveyed data points must increase laterally, limits S_y to be a finite large number, the size of which is dependent on the grid resolution. Ideally, the force on the vertical bank should be evaluated.

The boundary shear stress τ_o (Nm^{-2}), can be related to the shear velocity u_* (ms^{-1}) (Prandtl, 1925), by (re-arrange Eq. 2.31)

$$\tau_o = \rho u_*^2 \quad (3.7)$$

The shear velocity is commonly related to the depth-averaged velocity by a dimensionless local friction factor f , giving (re-arrange Eq. 2.35)

$$u_* = \left(\frac{f}{8} \right)^{1/2} U_d \quad (3.8)$$

While this provides a useful expression for evaluating the shear velocity for cases of low slope, this relation originates from equating the shear stress in a uniform wide channel (Eq. 2.32) i.e.

$$\tau_o = \rho g R S \quad (3.9)$$

with the Darcy-Weisbach equation (re-arrange Eq. 2.24)

$$S_f = f U^2 / 8gR \quad (3.10)$$

for total channel flow, with cross-section all-encompassing resistance parameters. These parameters take account of, for example, shape effects and shear generated turbulence, rather than a local friction factor f . The wide channel assumption implies that the lateral velocity distribution is uniform and hence the lateral shear affects are not considered. Knight (2001) advocates this approach, on the basis that the local friction parameter is being related to a local depth-averaged velocity and a local boundary shear stress. Term (ii) can thus be expressed as

$$-\psi \rho \frac{f}{8} U_d^2 \quad (3.11)$$

It is worth noting that equating Terms (i) and (ii) in [Eq. 3.4](#) results in an equation similar to the Darcy-Weisbach equation ([Eq. 3.10](#)).

Evaluating the local friction factor f

The local friction factor is essentially a parameter that relates the local boundary shear stress to the depth-averaged velocity, and as such, it should consider the full three-dimensional flow effects throughout the depth of flow. This concept is incorporated through the use of the Colebrook-White equation,

$$\frac{1}{\sqrt{f}} = -c \log_{10} \left[\frac{k_s}{aR} + \frac{b}{Re\sqrt{f}} \right] \quad (3.12)$$

which evaluates a lateral distribution of f , at each depth of flow, based on an iterative estimate of the local depth-averaged velocity. Here, Re is the Reynolds Number and R (m) is the hydraulic radius ($= A/P$). This equation is preferred in contrast to, for example, the Chezy or Manning equation, as it covers smooth-turbulent, transitional and rough-turbulent flows; it has a strong physical basis in that it is derived from the logarithmic velocity profile together with the channel geometry; and it incorporates the variation of roughness with depth. It is therefore believed that this model will cover the experimental and prototype cases.

[Table 3.3](#) provides a summary of the advised Colebrook-White coefficients (a , b , c) which are based on channel shape, experimental findings and experience. The CES conveyance methodology has adopted values of 12.27, 3.09 and 2.03 for a , b and c respectively. The value of c is based on a value of 0.41 for the von Kármán constant, κ . The values of a and b are based on c and assuming a trapezoidal cross-section

Table 3.3 Values of constants for Colebrook-White type formula in steady uniform flow with rigid impervious boundary (after Yen, 1991).

Researcher	c	a	b	Description
Colebrook & White (1937)	2.00	14.83	2.52	Full circular pipe
Zegzhda (1938)	2.00	11.55	0.00	Rectangular with dense sand
Keulegan (1938)	2.03	12.27	3.41	Wide & smooth flow channel
Keulegan (1938)	2.00	12.62	2.98	Wide & fully rough channel
Keulegan (1938)	2.03	12.27	3.09	Smooth trapezoidal channel
Keulegan (1938)	2.00	13.99	2.27	Rough trapezoidal channel
Rouse (1946)	2.03	10.95	1.70	Wide channels
Thijsse (1949)	2.03	12.20	3.03	Wide channels
Sayre & Albertson (1961)	2.14	8.89	7.17	Wide channels
Reinius (1961)	2.00	12.40	3.40	Wide channels
Reinius (1961)	2.00	14.40	2.90	Rectangular – width/depth = 4
Reinius (1961)	2.00	14.80	2.80	Rectangular – width/depth = 2
Henderson (1966)	2.00	12.00	2.50	Wide channels
Graf (1971)	2.00	12.90	2.77	Wide channels

shape. In reality, river cross-section shapes are irregular except for a small percentage of heavily urbanised waterways. A trapezoidal shape was adopted as one more closely representative of an irregular shaped river section with sloping side banks than, for example, a narrow or wide rectangular section with vertical banks. The implication of this assumption is considered minor in that all three coefficients (a , b and c) are close to the average (12.40, 3.17 and 2.02) of the available values (Table 3.3) which cover a range of possible shapes.

The values in Table 3.3 were derived based on treating the cross-section as a whole whereas the intended application is to derive a localised value of f . The predicted values of f were compared therefore to localised f -values back-calculated from high quality boundary shear stress and velocity measurements in a two-stage trapezoidal channel from the Flood Channel Facility (www.flowdata.bham.ac.uk). This indicated good agreement over a range of depths, including both inbank and out-of-bank flow (Defra/EA, 2003a). Ideally further testing should be undertaken for a range of natural channel shapes, for which both local depth-averaged velocity and boundary shear stress measurements are available.

Conversion of n_l to k_s

Eq. 3.12 contains a further unknown, the absolute roughness size k_s , a parameter not widely used in river engineering practice. It is therefore necessary to relate the unit roughness n_l (Section 3.2.1) to the roughness size k originally defined in terms of the sand grain dimension (Nikuradse, 1933). Here, k_s is interpreted as an ‘equivalent’ turbulence length scale i.e. a measure of the turbulent eddy size. This length scale may be greater than the water depth, for example, willow trees and large boulders, as it represents the horizontal mixing action, whereby eddies may be larger in plan than the local water depth. An upper limit on k_s may be defined as the full channel width, where the large-scale roughness essentially represents a different physical process, with very low velocities or blockage.

Knight and MacDonald (1979) classified six categories of flow patterns over strip roughness, and illustrated the importance of the roughness element's shape, size and spacing on the overall resistance. Here, all three are wrapped into the k_s dimension. The equivalent k_s value can be determined from (variation of Strickler, 1923; Ackers, 1958),

$$n = 0.0342 k_s^{1/6} (ft) = 0.0417 k_s^{1/6} (m) \quad (3.13)$$

which is applicable to a limited range of R/k_s ($5 < R/k_s < 500$) with an accuracy range of 10%. This conversion is suitable for use in flow conditions under which the equation was derived, in particular, application to a whole cross-section or reasonably smooth channels. For application to natural channels with large-scale roughness elements, two issues arise:

- A solution is required locally at each point across the section, and hence, for a given location, the local roughness height may be equivalent to a large fraction of the depth or in some cases, exceed it, for example, emergent floodplain vegetation.
- Large typically-used Manning n values, and the corresponding unit roughness n_l – values, result in highly inflated k_s values. For example, should the bed material be characterised by large boulders, with an equivalent n_l value of 0.5, this would produce a k_s value of over 2,000 km. Values of this magnitude are meaningless in terms of flow depth, river width and reach length.

The CES conveyance method, therefore, incorporates an alternative conversion approach for natural channels. This is based on the rough-turbulent component of the Colebrook-White law, given by the first term in Eq. 3.12,

$$\frac{1}{\sqrt{f}} = -2.03 \log_{10} \left[\frac{k_s}{12.27H} \right] \quad (3.14)$$

And the expression for f given by relating the Darcy-Weisbach and Manning equations:

$$f = \frac{8gn_l^2}{H^{1/3}} \quad (3.15)$$

Hence, at a depth of 1.0 m, the depth associated with the unit roughness n_l values, k_s is given by

$$k_s = 12.27H10^{\left[\frac{H^{1/6}}{\sqrt{8gn_l(-2.03)}} \right]} = 12.27 \times 10^{\left[\frac{1}{\sqrt{8gn_l(-2.03)}} \right]} \quad (3.16)$$

An alternative approach for relating n_l to f would be the direct use of Eq. 3.15. This would eliminate the use of the Colebrook-White rough law to convert n_l to k_s and the iterative solution of the full Colebrook-White law in evaluating f at each of depth of flow. This direct approach has not been adopted for two reasons:

- Eq. 3.15 is derived from relating the Manning and Darcy-Weisbach resistance equations, which are intended for analysis of the total cross-section resistance rather than the localised boundary friction factor.

- Use of the full Colebrook-White equation allows for smooth and rough turbulent flow conditions i.e. the influence of the Reynolds Number on the flow; solution of the lateral and depth-varying distribution of f ; and the use of equation coefficients which capture the cross-section shape effects. To use this approach, the rough turbulent conversion (Eq. 3.16) is required to evaluate k_s .

Although Eq. 3.15 is not used directly, it is still embedded within Eq. 3.16, and it will therefore still have an influence on the results, albeit reduced from the influence of a more direct application.

The n_l predictions based on Eq. 3.13 and 3.16 are plotted in Figure 3.21 for a typical range of n_l values. As n_l approaches infinity, the bracketed term in Eq. 3.16 approaches zero, and k_s is asymptotic to 12.27, the coefficient in the Colebrook-White law. In the Ackers' approach, as n_l increases to ~ 0.1 , k_s tends to infinity. For the region $0.01 < n_l < 0.025$, both laws predict a similar relationship. Neither approach is strictly correct for experimental flumes where the smooth-turbulent law dominates. For example, the values of k_s for $n_l \leq 0.01$ decrease rapidly. In the absence of an alternative approach, the CES conveyance methodology incorporates Eq. 3.13 for this conversion in experimental flumes. Experimental conditions are generally characterised by smooth-turbulent flow conditions, and thus a lower limit for k_s is set, $k_s \geq 0.1$ mm, which corresponds to a minimum n_l of 0.009. This is reasonable since the final f distribution is based on solution of the full Colebrook-White law (Eq. 3.12), within which the rough-turbulent term will have a virtually insignificant contribution, and the distribution of f will be largely based on the viscous effects. For natural channels, the CES conversion is based on Eq. 3.16.

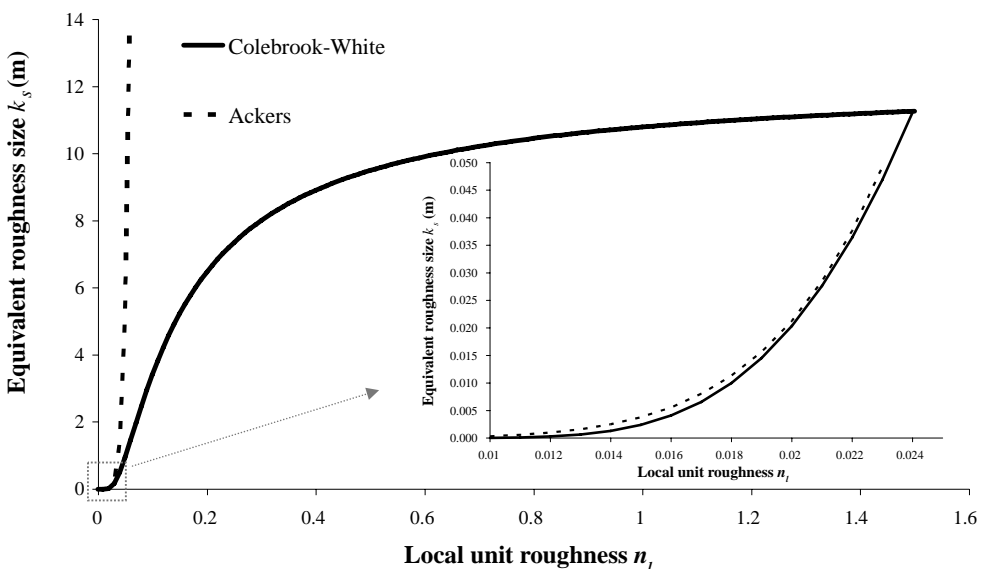


Figure 3.21 Conversion or n_l to k_s for a typical range of n_l values (Mc Gahey et al., 2008).

Conversion of k_s to f

The full Colebrook-White law (Eq. 3.12) is used to evaluate the lateral distribution of local values of f at each depth of flow, which assumes k_s is constant with depth. Eq. 3.12 was originally derived for pipe flow with small-scale roughness features, and when applied elsewhere, it can provide unrealistically large values of f if the k_s/H ratio is large, for example, in natural channels where the roughness size may be comparable with the depth, as with boulders.

Thus, at high k_s/H ratios a power law (Samuels, 1985) is introduced as the mathematical formulation of the velocity distribution in the overlap region of the boundary layer (i.e. between regions dominated by either viscous or inertia forces) is typically of the logarithmic or power law form. The former (the basis for Eq. 3.12) is generally favoured as it covers a wider range of Reynolds Numbers. The CES power law coefficients are derived from ensuring both laws are continuous in f and the derivative of f with respect to depth, df/dH , giving (Mc Gahey & Samuels, 2004):

$$f = \frac{8}{41.3015} \frac{k_s}{H} \quad (3.17)$$

At $k_s/H = 1.66$, these laws coincide. An upper limit of f is set at $k_s/H = 10$, which corresponds to an f -value of 1.937. This upper limit restricts the value of f from approaching infinity, as H approaches zero for shallow flows. The maximum predicted f in Nikuradse's (1933) experiments is approximately 0.125 in the laminar region and the entire turbulent region falls well below a value of 0.100. In practice, this large value of f would occur in regions with extremely shallow water relative to the roughness elements, which are expected to have a negligible contribution to the overall conveyance. Thus, the exact upper limit of f carries little practical significance.

Figure 3.22 illustrates the combined friction laws for an n_l value of 0.05, with the k_s/H ratio determining the applicable friction law. The Colebrook-White equation gives a rapidly increasing value of f below a stage of 0.5 m, i.e. the region where the k_s/H ratio approaches 12.27. The power law replaces the Colebrook-White law in this region, and the predicted value is restricted to 1.937 for $k_s/H > 10$.

The complete CES methodology for estimating the lateral distribution of f for a given depth of flow, based on the local n_l values provided by the Roughness Advisor is shown in Figure 3.23.

Term (iii) – Representation of turbulence due to transverse currents

The third term in Eq. 3.4 represents the turbulence generated due to transverse currents effecting vertical interfacial shearing. This typically occurs in regions characterised by steep velocity gradients such as the main channel floodplain interface and adjacent to river banks. To evaluate this term, a turbulence closure model is required for the eddy viscosity $\nu_t (\text{m}^2\text{s}^{-1})$. The CES methodology incorporates the approach of Cunge *et al.* (1980),

$$\nu_t = \lambda u_* H \quad (3.18)$$

where λ is the dimensionless eddy viscosity and the depth $H(\text{m})$ represents the characteristic length scale for the mixing layer. Ideally this model should separate out the

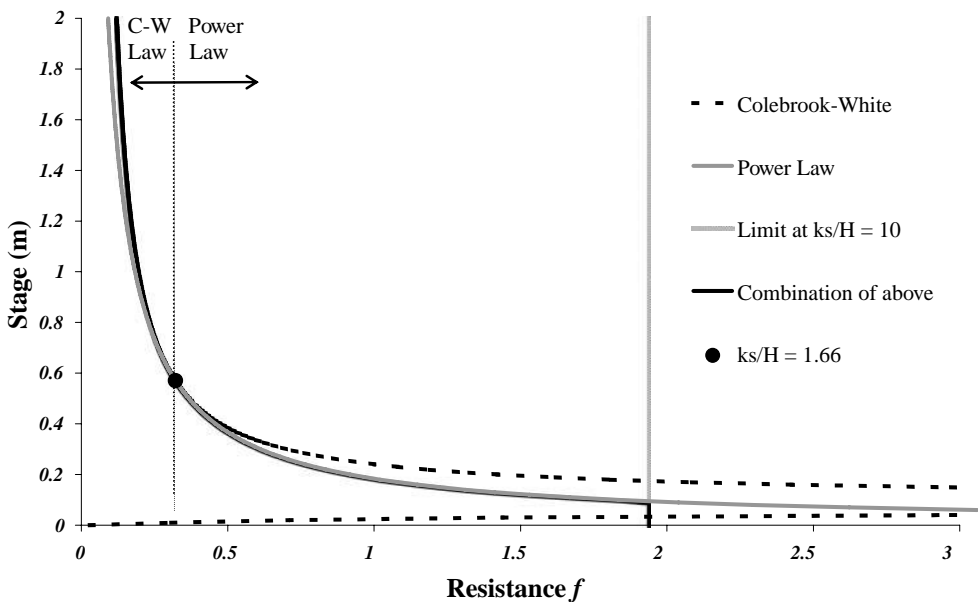


Figure 3.22 Graphical representation of the combined friction laws for $n_l = 0.05$ (Mc Gahey & Samuels, 2004).

boundary and shear generated effects (Wormleaton, 1988). This is not practicable in that the model is intended for a variety of rivers, for which shear layer information may not be readily inferred (Section 3.4). Substituting Eq. 3.18 and 3.8 into Term (iii) of Eq. 3.4 gives,

$$\frac{\partial}{\partial y} \left(\rho \lambda H^2 U_d \left(\frac{f}{8} \right)^{1/2} \frac{\partial U_d}{\partial y} \right) \quad (3.19)$$

Evaluating the dimensionless eddy viscosity λ

The CES methodology incorporates a recently proposed model (Abril, 2001; Abril and Knight, 2004) for estimating the lateral distribution of λ on the floodplain,

$$\lambda = \lambda_{mc} (-0.2 + 1.2 D_r^{-1.44}) \quad (3.20)$$

Here, the relative depth D_r is defined as,

$$D_r = \frac{H}{H_{\max}} \quad (3.21)$$

to enable application to inbank flow and D_r tends to 1.0 for the deepest part of the inbank section. The main channel dimensionless eddy viscosity λ_{mc} is 0.07 (Ikeda, 1981) for experimental channels and 0.24 (Elder, 1959; Cunge *et al.*, 1980) for natural

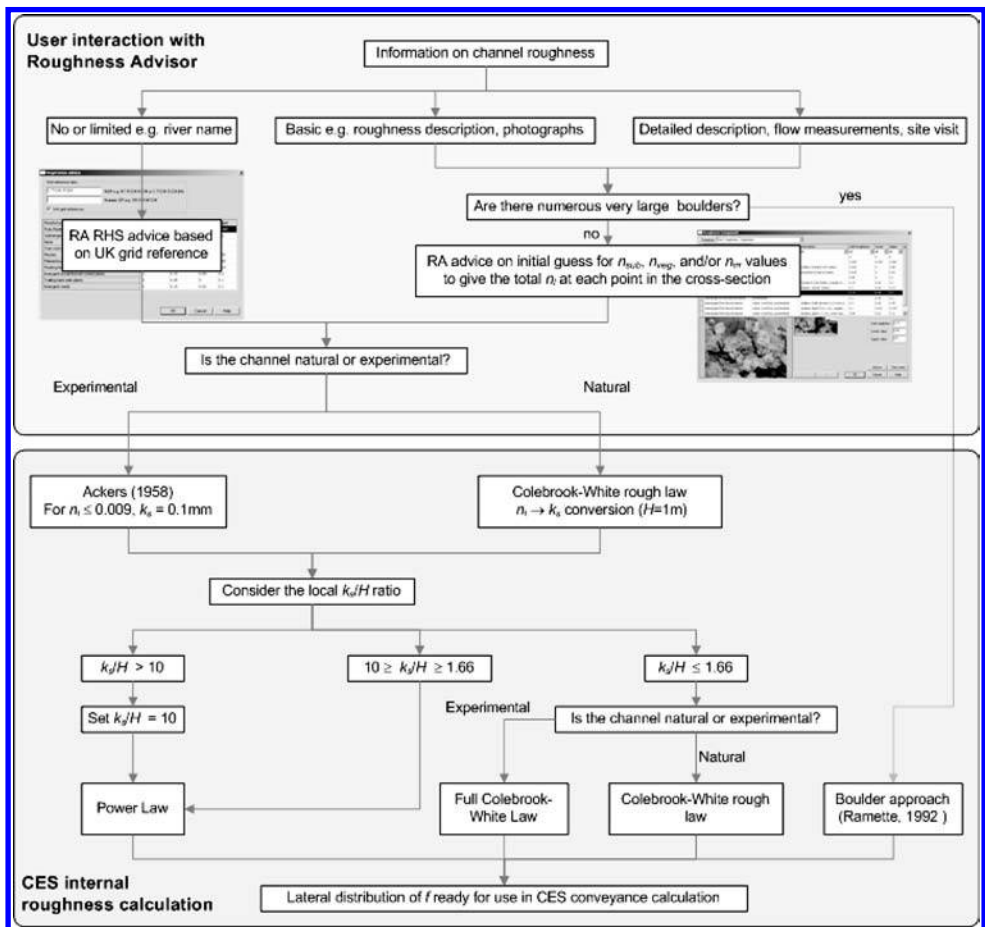


Figure 3.23 Summary of the CES methodology for estimating the friction factor f (Mc Gahey *et al.*, 2009).

channels. The 0.07 value is supported by experimental measurements of the viscosity distribution with depth (Nezu & Nakagawa, 1993), where the depth-averaged value is ~ 0.07 . The measured wind tunnel dispersion coefficient value is ~ 0.13 (Rhodes & Knight, 1995). The values in natural channels are generally larger as the rougher banks and longitudinal irregularities result in more boundary generated turbulence and stronger lateral shearing than in laboratory channels. Elder (1959) suggests a value of ~ 0.23 for uniform flow in a wide open channel. Main channel and floodplain values as high as 0.5 and 3.0 respectively, have previously been adopted (Knight *et al.*, 1989; James & Wark, 1992).

The original derivation of Eq. 3.20 was based on Flood Channel Facility experimental measurements (www.flowdata.bham.ac.uk) for a two-stage channel, with two distinct flow depths for the main channel and floodplain. The area of variable depth

between the main channel and floodplain was not considered and Eq. 3.21 would therefore provide two distinct values, of which one was always $D_r = 1.0$ (main channel). In practice, Eq. 3.21 will predict a range of relative depth values across the channel, and thus Eq. 3.20 requires an upper limit for λ , since at the channel edges, as D_r approaches zero, λ approaches infinity. These large λ values result in unrealistic boundary layer effects and the CES approach has adopted an upper limit on λ of 5.

Term (iv) – Representation of turbulence due to secondary circulations

The fourth term in Eq. 3.4 represents the energy transfers generated through transverse currents, coherent structures and horizontal interfacial shear (Knight *et al.*, 2007; Omran *et al.*, 2008; Tang & Knight, 2009). As this term contains an additional unknown, the lateral velocity V , a model is required for closure. The CES evaluation of this term is based on a hypothesised approach for combining two models, one for transverse currents in straight prismatic channels (Shiono & Knight, 1990; Abril & Knight, 2004) and one for the helical-type transverse currents characteristic of meandering channels (Ervine *et al.*, 2000). The contributions of these two models vary with the degree of plan form sinuosity σ (Figure 3.24), defined as the thalweg length over the valley length, where the straight model is applied for a sinuosity of 1.0, the meandering model is applied for a sinuosity greater than 1.015 and a combination of both models is applied in the low sinuosity or transition zone ($1.000 < \sigma < 1.015$) i.e.

$$\frac{(1.015 - \sigma)}{0.015} \text{ [straight approach]} + \frac{(\sigma - 1)}{0.015} \text{ [meandering approach]} \quad (3.22)$$

This summation method is an arbitrary choice to provide a working model.

It should be noted that predictions based on a depth-averaged model applied to meandering channel flow conditions should be interpreted with caution. In meandering channels, the flow is fully three-dimensional, and the lateral velocity component V has a substantially larger role than in a straight channel. For the CES, x is defined as the horizontal flow direction i.e. in the horizontal x - y plane. In the main channel, the flow direction and hence orientation of x varies throughout the vertical, from being parallel to the main channel banks for inbank flow to being parallel to the valley direction

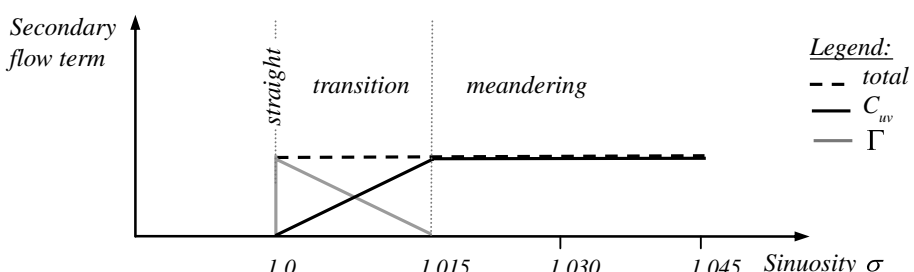


Figure 3.24 Contributions from the two models with increasing sinuosity (Defra/EA, 2003a).

for out-of-bank flow. The depth-averaging assumption is thus not strictly valid, and the validity decreases with increasing sinuosity. Despite this, previous application of the proposed model has provided reasonable stage-discharge and depth-averaged velocity predictions for a range of sinuosity values (Ervine *et al.*, 2000; Guan *et al.*, 2002; Spooner & Shiono, 2003). Thus, in the absence of an alternative model within the depth-averaging framework, this model has been adopted for the current (2004) version of the CES.

Secondary flow model for straight prismatic channels

The secondary flow model for straight channels is based on that of Shiono and Knight (1990) in which a secondary flow term Γ is defined as

$$\Gamma = \frac{\partial}{\partial y} [H(UV)_d] \quad (3.23)$$

This is a calibration parameter that varies laterally across the section and with relative depth. The laterally averaged boundary shear stress τ_{ave} (Nm^{-2}), and the two-dimensional shear stress τ_d ($= \rho g H S_o$) (Nm^{-2}) can be related for areas of constant depth, and the average scaled secondary flow term, Γ_{ave}^* , is thus (Abril & Knight, 2004),

$$\Gamma_{ave}^* = \rho g S_o (1 - k_\Gamma) \quad (3.24)$$

a novel approach for linking boundary shear stress and the secondary flow term. For overbank flow (Abril & Knight; 2004),

$$\Gamma_{mc} = 0.15 \rho g H_{mc} S_o \quad (3.25)$$

$$\Gamma_{fp} = -0.25 \rho g H_{fp} S_o \quad (3.26)$$

and for inbank flow,

$$\Gamma_{mc} = 0.05 \rho g H_{mc} S_o \quad (3.27)$$

The coefficients 0.15, -0.25 and 0.05 are calibrated values based on observed distributions derived from the Flood Channel Facility data (Shiono & Knight, 1991) for different relative depths in a straight compound channel. The applicability of these models for natural channels has not been widely tested, in part, as a result of limited availability of suitable river data. More recently (Omran, 2005; Omran *et al.*, 2008), the variation of Γ has been linked to the local nature and orientation of the secondary circulations within the channel section.

For practical application, a key difficulty is that natural channels are not readily divided into distinct regions with a main channel portion and two floodplains with identical bed elevations. For this reason, the CES requires the user to provide information on the estimated top-of-bank positions i.e. where the floodplain sections commence. This information is used to divide the flow domain into distinct flow regions (Figure 3.25), equivalent to those originally defined in Abril and Knight's model. Where the two floodplain bed elevations differ in level or for asymmetrical

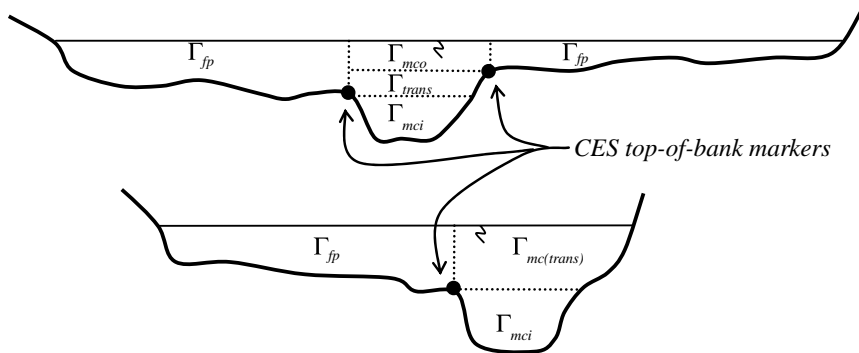


Figure 3.25 Example of natural channels with transitional secondary flow regions (Mc Gahey, 2006).

channels (i.e. only one floodplain present) a linear transition for Γ is applied in the main channel flow region. This allows for an averaging of the secondary flow effects based on the area of influence of the floodplain main channel vertical interface, which drives the magnitude and orientation of the transverse currents. The transitional main channel secondary flow term, $\Gamma_{mc(trans)}$, is given by (Mc Gahey, 2006),

$$\Gamma_{mc(trans)} = \frac{(\Gamma_{mco} - \Gamma_{mci})}{(Z_H - Z_L)} (h_l - Z_L) + \Gamma_{mci} \quad (3.28)$$

where the suffixes i and o denote inbank and overbank flow, respectively, Z_H and Z_L (mAD) are the bed elevations of the higher and lower floodplain top-of-bank marker, respectively, and h_l (mAD) is the water surface level for the given depth of flow. The $\Gamma_{mc(trans)}$ region may be compared to Regions 1 and 2 in the Coherence Method (COHM – Ackers, 1991–93), where the discharge initially drops (due to the interaction and resistance offered by the floodplains) and then increases above bankfull. Here, however, the non-symmetrical floodplain effects are averaged within the main channel portion and the flow over the single floodplain is treated independently, whereas the COHM is based on a symmetrical compound channel. An alternative approach would be the use of vertically layered models i.e. to incorporate two (symmetrical case) or three (non-symmetrical) layer models.

The extent of the lateral shear layer where these secondary circulations are present is important. In practice, these shear layers extend across the entire main channel region (Samuels, 1988) and over a portion of the flood plain. The flood plain extent of Γ_{fp} is, therefore, approximated in the CES based on the lesser of the main channel width and ten times the average bankfull depth.

Secondary flow model for meandering channels

The meandering secondary flow model is based on the work of Ervine *et al.* (2000), where the secondary currents are related to the depth-averaged velocity by

$$(UV)_d = C_{uv} U_d^2 \quad (3.29)$$

Substituting this expression into Term (iv) of Eq. 3.4 gives

$$-\frac{\partial}{\partial y} [\rho H C_{uv} U_d^2] \quad (3.30)$$

Ervine *et al.* (2000) applied this model within the main channel portion of the cross-section, with the C_{uv} coefficient attaining a single value related to sinuosity, relative depth and relative roughness. The effect is to introduce a non-symmetrical lateral profile for the depth-averaged velocity U_d in the main channel region and a corresponding decrease in the overall flow capacity.

Expanding Eq. 3.30, assuming C_{uv} is constant across the main channel, gives

$$-\rho C_{uv} \frac{\partial}{\partial y} (H U_d^2) = -\rho C_{uv} U_d \left[2H \frac{\partial U_d}{\partial y} + U_d \frac{\partial H}{\partial y} \right] \quad (3.31)$$

The expected distributions of the various bracketed terms for a simple trapezoidal channel are plotted in Figure 3.26, illustrating in particular the various non-symmetrical influences. Thus, evaluation of the right hand side of Eq. 3.31 produces a skewed main channel velocity profile, damping the velocity on falling lateral slopes (i.e. increasing lateral depths of flow $dH/dy > 0$), having little or no effect for horizontal channel beds and enhancing the velocity on rising slopes (i.e. decreasing lateral depths of flow $dH/dy < 0$).

The magnitude and sign of C_{uv} influences the size and orientation of the resulting skew, respectively. Figure 3.27 illustrates the effect of increasing positive C_{uv} values on the depth-averaged velocity profile, for a trapezoidal channel. On the laterally rising channel side slope, the aforementioned velocity enhancement causes an unrealistic increase or ‘spike’ in the depth-averaged velocity. However, on the laterally falling side slope, the main channel ‘skew’ effect is similar to that observed in real meandering channel data. Based on this observation, the CES methodology only incorporates the Ervine *et al.* (2000) model in main channel areas where the lateral slopes are less than or equal to zero. More recently, some limitations of this approach have been shown (Tang & Knight, 2009) which will be considered for future versions of the CES.

Evaluating the meandering channel coefficient C_{uv}

The CES evaluation of C_{uv} is based on the plan form sinuosity σ . Previous research (Ervine *et al.*, 2000) has identified an additional dependence of C_{uv} on relative roughness (i.e. main channel versus floodplain roughness) and relative depth. In natural channels, the relative roughness is not easily determined as it requires determination of the two reference locations (e.g. main channel and floodplain), which may not be obvious for an arbitrary shaped channel with heterogeneous roughness. Since there is uncertainty with respect to use of the meandering model within the depth-averaged framework, and coupled with this there is limited available calibration data for testing these dependencies, the CES approach for estimating C_{uv} is based on sinuosity alone.

A simple regression exercise based on 12 cross-sections taken at the bend apex for a small range of channel sinuosities (1.0; 1.0038; 1.012; 1.1; 1.18; 1.374; 2.04)

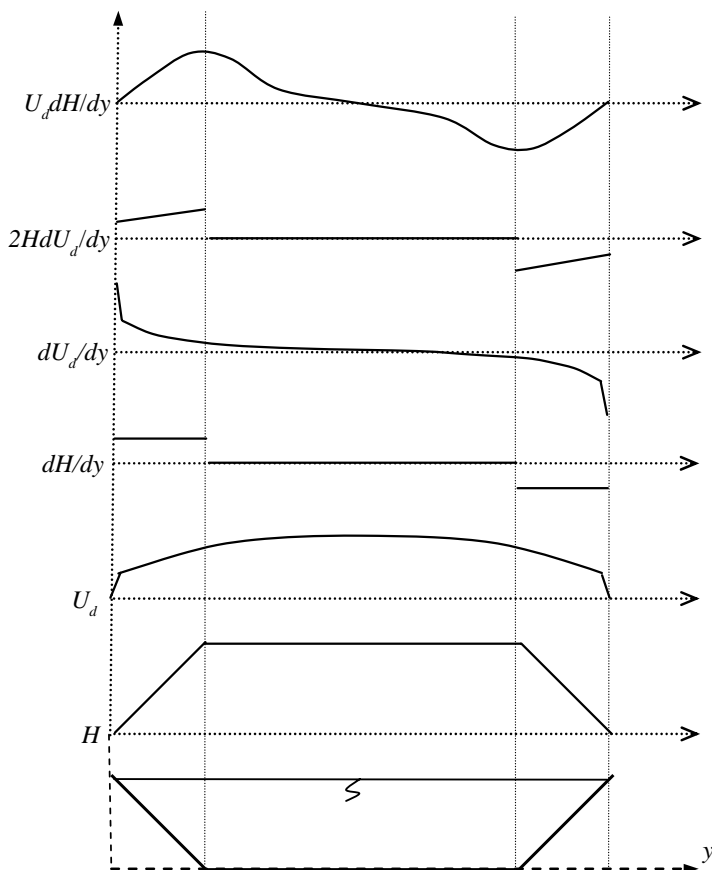


Figure 3.26 Example of meandering flow term lateral distributions in a trapezoidal channel (Mc Gahey, 2006).

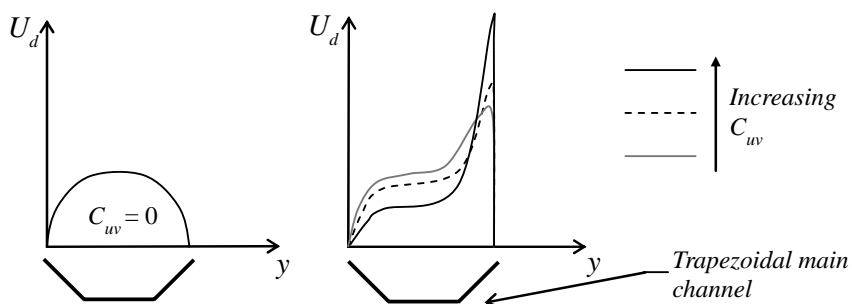


Figure 3.27 Effect of the meandering secondary flow term on the depth-averaged velocity profile in a simple trapezoidal channel (Mc Gahey & Samuels, 2004).

and best-fitting the overall flow rate and depth-averaged velocity profile (Defra/EA, 2003a) for inbank flow gives,

$$C_{uv} = 4.33\sigma^2 - 7.87\sigma + 3.540 \quad [1.0 < \sigma \leq 2.5 \text{ i.e. } 0\% < C_{uv} \leq 11\%] \quad (3.32)$$

with a regression fit of $R^2 = 0.99$, and for overbank flow

$$C_{uv} = 7.17\sigma - 6.626 \quad [1.0 < \sigma \leq 2.5 \text{ i.e. } 0.5\% < C_{uv} \leq 11\%] \quad (3.33)$$

with a regression fit of $R^2 = 0.9755$. Here, inbank flow is defined as flow below the average elevation of the top-of-bank markers, i.e. $(Z_L + Z_H)/2$. An upper limit of 2.5 is provided for the sinuosity as due to the regression approach, the provided equations should only be used within the range for which they were derived. This is not a significant restriction as a channel with a sinuosity greater than 2.5 is very uncommon in nature.

Figure 3.28 illustrates typically observed depth-averaged velocity profiles in meandering channels for inbank and out-of-bank flow conditions. It is apparent that the velocity ‘skew’ changes orientation from inbank to out-of-bank flow, and for this reason, the sign of C_{uv} is reversed above bankfull flow. This has a marginal impact

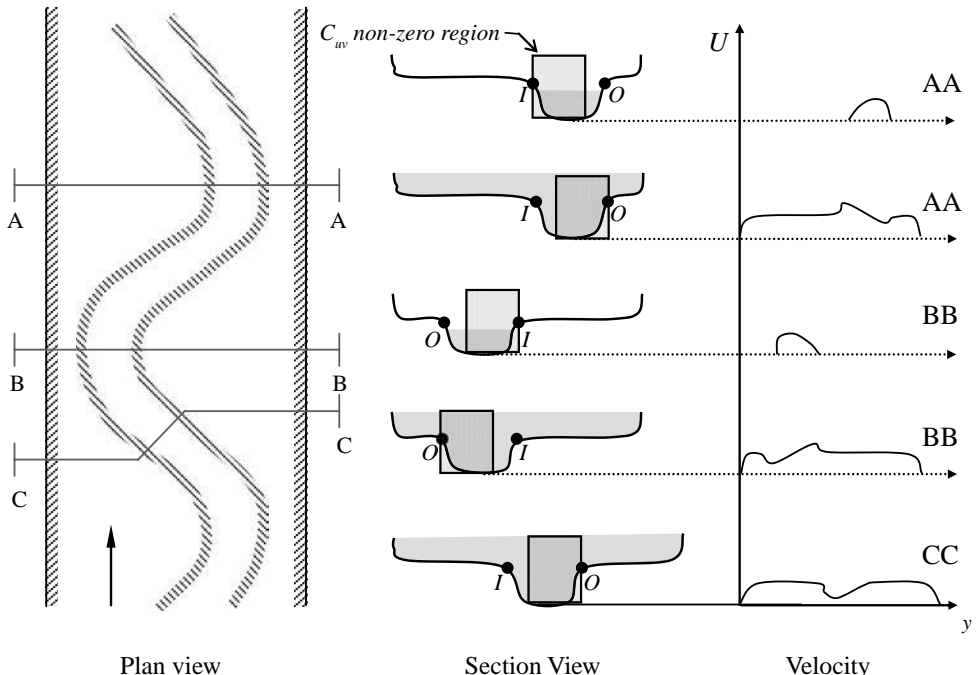


Figure 3.28 Sketch of typical depth-averaged velocity profiles observed in the Flood Channel Facility in a meandering two-stage channel for inbank and overbank flows illustrating inside “I” and outside “O” of bend top-of-bank markers and corresponding non-zero C_{uv} regions (Defra/EA, 2003a).

on the overall flow rate, except in cases where the main channel geometry is highly non-symmetrical, with bank slopes that differ substantially i.e. a large impact on the dH/dy term.

Practical considerations for evaluating C_{uv}

The CES requires additional user input to aid evaluation of C_{uv} . This includes the sinuosity magnitude, a directly measurable parameter, and the orientation of the meander bend or channel skew. This information is inferred through labelling the top-of-bank markers as “inside” or “outside” of bend (Figure 3.28). In instances where the cross-section is taken in a cross-over reach, these labels should assume the orientation of the previous bend, as the flow effects from the upstream bend are typically still present.

Practical considerations for secondary flow models in braided channels

In river modelling, a common application for conveyance estimation is in braided channels. The CES methodology calculates flow in braided channels through evaluating the conveyance within each individual channel at low depths, and then applying a simple summation (Figure 3.29).

For the case of overbank flows, where common floodplains or inundated islands are present, the island is treated as an additional floodplain when evaluating the secondary flow term Γ (Figure 3.30).

For the case of overbank flows in channels with varying sinuosity (Figure 3.31), the sinuosity and bend orientation for each channel is provided. For low sinuosities in the transitional range $1.0 < \sigma < 1.015$, the linear summation for the secondary flow models (Eq. 3.22) is applied, and the contributions from each channel in the common floodplain is averaged.

Practical modelling of low velocity regions

Rivers and their floodplains may be characterised by regions of low or zero velocity. Examples of low velocity regions include slowly rotating plan form eddies upstream or

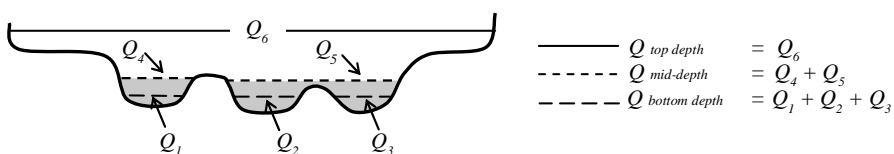


Figure 3.29 Addition of flow in braided channels (Defra/EA, 2003a).

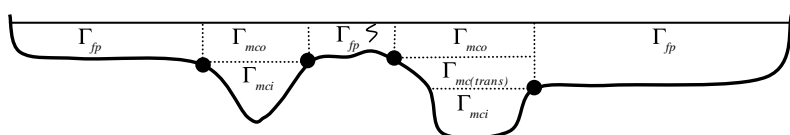


Figure 3.30 Example of straight secondary flow model Γ in a braided channel (Defra/EA, 2004b).

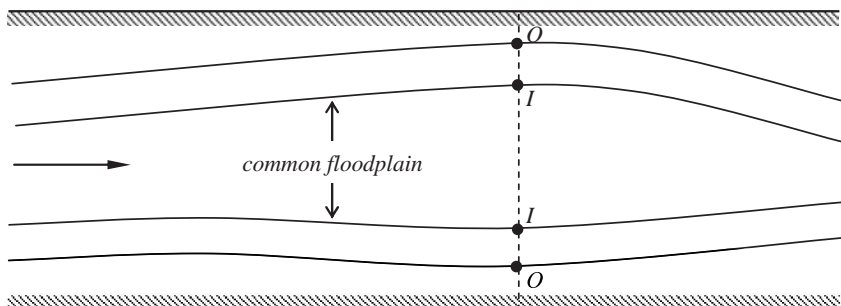


Figure 3.31 Plan view example of a braided channel with low sinuosity, a common floodplain and the appropriate top-of-bank marker labels (Defra/EA, 2004b).

immediately downstream of narrow flow constrictions and areas within the floodplain such as water trapped between hedges or garden fences perpendicular to the bulk flow direction, off-line natural reservoirs, buildings where the water enters through doors and windows etc. In standard 1-D modelling software such as HEC-RAS or InfoWorks RS, these regions are typically termed “non-conveyance regions”; however, this term is avoided to prevent confusion.

The CES methodology incorporates a simple approach for modelling the low velocity regions within a cross-section. As with current 1-D modelling practice, the user identifies apparent low velocity regions, for example, a portion of floodplain area where the flow is trapped behind a low wall perpendicular to the bulk flow direction. The CES assigns an extremely high roughness value to this region, which significantly reduces the conveyance associated with this region. The equations are then solved at each point in the section, however, when integrating the unit flow rate across the section to determine the overall flow rate (Eq. 3.3), only the conveyance portions are included. The result is that low velocity areas are effectively storage volumes that exert some resistance on the principal flow, but do not contribute to the overall cross-section conveyance. This approach assumes low velocity regions comprise static rotations or storage and does not take account of instances where separation occurs, resulting in the generation of vortices which are swept further downstream.

3.2.3 Summary of CES methods, outputs and solution technique

Complete system of CES equations

The previous sections have detailed the CES methodology for evaluating Terms (i) to (iv) in Eq. 3.4.

$$\rho g H \left(\frac{\partial H}{\partial x} - S_o \right) - \psi \tau_o + \frac{\partial}{\partial y} \left(H v_t \frac{\partial U_d}{\partial y} \right) - \frac{\partial}{\partial y} \rho [H(UV)_d] = 0 \quad (3.4)$$

(i) (ii) (iii) (iv)

Previous research (Samuels, 1989a; Knight *et al.*, 2004) advocates the solution of the unit flow rate, q (ms^{-2}), over the depth-averaged velocity U_d , due to the strong continuity properties of q with variations in depth, for example, across a vertical face or ‘step’ in an engineered channel cross-section. The unit flow rate is defined here as,

$$q = \int_0^H u dz = HU_d \quad (3.34)$$

Thus, back-substituting the derived expressions for Terms (i) to (iv) in Eq. 3.4 and expressing the depth-averaged velocity in terms of the unit flow rate q , gives the final equations adopted within the CES conveyance methodology as:

Final CES conveyance equations

$$gHS_o - \psi \frac{f}{8} \frac{q^2}{H^2} + \frac{\partial}{\partial y} \left(\lambda \left(\frac{f}{8} \right)^{1/2} Hq \frac{\partial}{\partial y} \left(\frac{q}{H} \right) \right) - \left(\frac{(1.015 - \sigma)}{0.015} \Gamma \right. \\ \left. + \frac{(\sigma - 1.0)}{0.015} C_{uv} \frac{\partial}{\partial y} \left(\frac{q^2}{H} \right) \right) = 0$$

$$\sigma = 1.0 \text{ inbank; } 1.0 \leq \sigma \leq 1.015 \text{ overbank}$$

$$gHS_o - \psi \frac{f}{8} \frac{q^2}{H^2} + \frac{\partial}{\partial y} \left(\lambda \left(\frac{f}{8} \right)^{1/2} Hq \frac{\partial}{\partial y} \left(\frac{q}{H} \right) \right) - C_{uv} \frac{\partial}{\partial y} \left(\frac{q^2}{H} \right) = 0$$

$$\sigma > 1.0 \text{ inbank; } \sigma > 1.015 \text{ overbank} \quad (3.35a\&b)$$

Eq. 3.35a&b are evaluated to determine the lateral distribution of the unit flow rate q and the total flow rate Q (m^3s^{-1}) is evaluated from:

$$Q = \int_0^B q dy = \int_0^B U_d dA \quad (3.3)$$

Table 3.4 provides a summary of the expressions for evaluating the unknown input parameters in Eq. 3.35a&b. Figure 3.32 provides an example of typical lateral distributions for f , λ , Γ and C_{uv} in a two-stage trapezoidal channel.

The CES method assumptions

The CES method derivation includes various assumptions. Table 3.5 provides a hierarchical summary of the assumptions made prior to developing the depth-averaged RANS equations (Eq. 3.4), identifying those which may have a significant impact on

Table 3.4 Summary of parameter evaluation for the final CES equations (Eq. 3.35a&b).

Parameter	Evaluation technique	Eq. no.
Gravitational acceleration g	9.81 ms^{-2}	
Longitudinal bed slope S_o	User input taken from best available measurements e.g. OS maps, water levels measurements, model outputs	
Lateral bed slope S_y	Evaluated from the surveyed cross-section	
Cartesian projection parameter ψ	$\psi = \sqrt{1 + S_y^2 + S_o^2}$	3.6
Friction factor f	$\frac{1}{\sqrt{f}} = -2.03 \log_{10} \left[\frac{k_s}{12.27R} + \frac{3.09}{Re\sqrt{f}} \right] k_s/H < 1.66$ $f = \frac{8}{41.3015 H} k_s/H > 1.66$ Upper limit $f = 1.937$; Lower limit $k_s = 0.0001 \text{ m}$	3.12 3.17
Dimensionless eddy viscosity λ	$\lambda = \lambda_{mc} (-0.2 + 1.2D_r^{-1.44})$ $\lambda_{mc} \text{ experimental} = 0.07; \lambda_{mc} \text{ rivers} = 0.24$	3.20
Straight secondary flow term Γ	$\Gamma_{mci} = 0.05\rho g H S_o$ $\Gamma_{mco} = 0.15\rho g H S_o$ $\Gamma_{fp} = -0.25\rho g H S_o$ $\Gamma_{mc(\text{trans})} = \frac{(\Gamma_{mco} - \Gamma_{mci})}{(Z_H - Z_L)} (h_l - Z_L) + \Gamma_{mci}$	3.27 3.25 3.26 3.28
Sinuosity σ	User input. Measured from OS map.	
Meandering secondary flow term C_{uv}	$C_{uv} = 4.3274\sigma^2 - 7.8669\sigma + 3.5395 \text{ inbank}$ $C_{uv} = 7.1659\sigma - 6.6257 \text{ out-of-bank}$	3.32 3.33

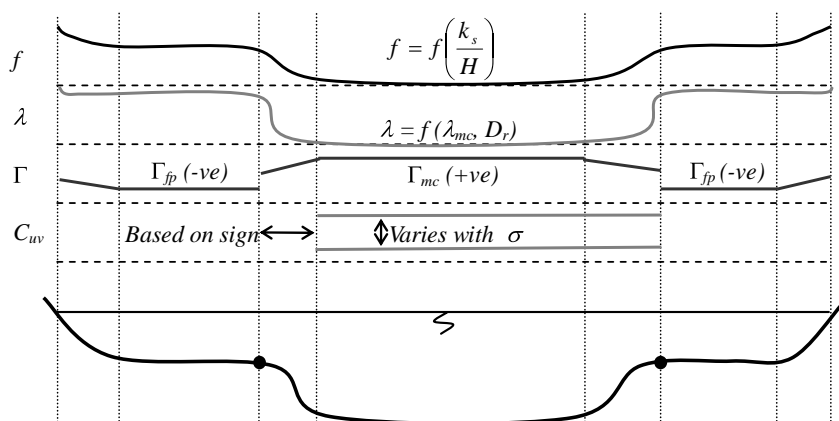
Figure 3.32 Example of lateral distributions for f , λ , Γ and C_{uv} in a typical two-stage channel.

Table 3.5 Summary of derivation assumptions, the implications and their significance.

Assumption	Implication	Significance to CES applications
<i>Standard global</i>		
The density is constant throughout the flow domain	i Air entrainment may vary the density and/or depth of flow. ii Sediment concentration may affect density. iii Tidal water is saline e.g. estuaries. iv Heat dissipation in rivers at power stations.	Low
The flow is incompressible	Density is constant.	Low
Hydrostatic pressure distribution	i Angle of longitudinal bedslope with horizontal is sufficiently small such that the vertical depth of flow is not significantly different from the depth measured perpendicular to the channel bed. ii The longitudinal bedslope is not curved in a convex/concave manner. iii Flow does not pass over any obstructions or areas of bedslope sufficiently steep for air entrainment to occur.	Low
The flow is steady	Cannot model event hydrograph, capture the change in water slope for the rising and falling hydrograph limbs or incorporate flood attenuation.	Medium
Coriolis forces resulting from the rotation of the earth about its own axis are considered small relative to other body forces	i <12 mm change in water level in UK rivers. ii Up to 3.5 m in the tidal range between the Irish and Welsh coastline.	Low High
Gravity is the only body force acting on the fluid		Low
Surface forces due to wind shear	Significant force may occur at gale force winds. These depend on the 'fetch' length in, for example, tidal areas and straight drains. In rivers, these may cause set-up and affect pump drainage.	Medium
Centrifugal forces due to streamline curvature in meander bends are small relative to other body forces		Medium
Isothermal flow	Temperature variations in open channel flow are small relative to other influences.	Low
Velocity adjacent to the channel bed is zero	Velocity at bed should average to zero over time i.e. may be instantaneously positive or negative.	Low
The fluid is isotropic		Low

(Continued)

Table 3.5 (Continued).

<i>Assumption</i>	<i>Implication</i>	<i>Significance to CES applications</i>
<i>3-D to 1-D simplification</i>		Low
Streamlines are approximately parallel		Medium
The flow is uniform	The cross-section is representative of a reach length, where the section shape (and water surface slope) is the same throughout the reach. In reality, non-engineered river channels vary in section shape.	Medium
Eddy viscosity	The 3-D eddy viscosity is depth-averaged in the vertical, reach-averaged in the longitudinal and only assumed to vary transversely across the channel.	Medium
The momentum equation is applied in the streamwise direction only	Ignores any large transverse or vertical currents i.e. lateral velocity movements. [Here, an energy balance approach would have included the various meandering effects.]	High
Vertical accelerations are negligible		Low
<i>Detailed method specific</i>		
Rigid bed	Most UK rivers are not alluvial in nature, however the cross-section shape may change over time.	Low-medium
Depth-averaging	i Is not stratified ii Does not change direction in the vertical (strong meanders) iii Is well-mixed in the vertical.	Medium
Turbulence modelled through RANS approach	Complete modelling of the physical properties.	Medium

the predicted output. Based on these, the CES conveyance calculation is not strictly applicable for:

- flow in alluvial channels with large bedforms;
- fully three-dimensional flows such as major confluences, strongly meandering channels and adjacent to structures such as bridges, weirs and culverts (See Section 3.2.5 on afflux estimation); and
- for determining the stage through major flood hydrographs where the water surface slope is unknown. This may be handled in 1-D hydrodynamic software such as InfoWorks RS, where the changing surface water slope is calculated with time and the conveyance is based on the embedded CES calculation.

There is further work in progress addressing some of the more important assumptions.

Additional CES conveyance calculation outputs

The CES conveyance calculation is primarily focused on evaluating the stage-conveyance and stage-flow relationship. Additional outputs are also evaluated (Table 3.6) for each depth of flow for the whole cross-section, including:

- Average velocity U (ms^{-1})
- Cross-sectional area A (m^2)
- Perimeter P (m)
- Width W (m)
- Back-calculated, all-encompassing Manning n
- Froude Number Fr
- Reynolds Number Re

Table 3.6 Summary of additional CES conveyance outputs and their evaluation.

Output	Equation	Comment
U	$U = Q/A$	
A	$A = \sum_i^n A_i$	This area A_i of each integration slice is summed. These areas are a trapezoidal or rectangular shape other than the triangular end slices.
P	$P = \sum_i^n P_i$	The boundary perimeter P_i of each integration slice is summed. This is the section linking successive points.
W		Top width i.e. width at the water level being evaluated.
n	$n = \frac{AP^{2/3}s^{1/2}}{Q}$	This is based on the overall cross-sectional area i.e. floodplains and main channel and the user entered slope. The 'n' value is equivalent to the all-encompassing Manning n value, which takes account of plan form and cross-section shape and turbulence due to lateral shear and secondary currents.
Fr	$Fr = \frac{U}{\sqrt{g(A/W)}}$	Here, A/W represents the hydraulic mean depth.
Re	$Re = \frac{4U(A/P)}{v}$	Here, A/P represents the hydraulic radius.
B_o	$B_o = \frac{\sum_i^n U_{di}A_i^2}{UA^2}$	The Boussinesq or momentum coefficient provides a measure of the local velocity variations across a section compared to the average values. B_o is never less than 1.0, is equal to 1.0 if the flow is uniform across the section and rarely exceeds 1.05.
C_o	$C_o = \frac{\sum_i^n U_{di}A_i^3}{UA^3}$	The Coriolis or energy coefficient provides a measure of the local velocity variations across a section compared to the average values. C_o is never less than 1.0, is equal to 1.0 if the flow is uniform across the section, rarely exceeds 1.15 in simple channels and is ~ 2.0 for two-stage channels.
U_d	$U_d = \frac{1}{h} \int_0^h u dz \quad (\text{Eq. 2.47})$	Depth-averaged velocity derived from the unit flow rate.
τ_o	$\tau_o = \frac{f}{8} \rho U_d^2 \quad (\text{Eq. 2.34})$	Boundary shear stress derived from the depth-averaged velocity and friction factor.
u_*	$U_* = \sqrt{\tau_o/\rho} \quad (\text{Eq. 2.31})$	Shear velocity derived from the boundary shear stress.

- Boussinesq coefficient B_o
- Coriolis coefficient C_o

An advantage of the chosen conveyance approach is that it also determines the lateral variation across the section of the following flow parameters:

- Depth-averaged velocity U_d (ms^{-1})
- Boundary shear stress τ_o (Nm^{-2})
- Shear velocity u_* (ms^{-1})

These parameters are important for the consideration of wider issues such as geomorphology and ecology (Chapter 5).

The CES conveyance calculation solution technique

Eq. 3.35a&b form a set of non-linear, elliptic, second order partial differential equations. The CES employs a numerical solution based on the Finite Element Method (FEM) (Zienkiewick, 1977; Davies, 1980), which is well suited to the solution of elliptic equations. The cross-sectional area of flow represents the solution domain, which is discretised laterally into a number of elements (Figure 3.33). The variable q is replaced with piecewise linear approximations or ‘shape functions’. The result is a system of discrete equations, which can be linearised, assigned boundary values and solved iteratively.

Linearising the system of equations

Eq. 3.35a&b is linearised by expressing the unit flow rate ‘ q ’ for iteration $n + 1$ in terms of the unit flow rate of the previous iteration n ,

$$q^{n+1} = q^n + \chi \Delta q^n \quad (3.36)$$

where χ is the relaxation factor and Δq^n is the incremental change in q^n to improve the previous estimate. The initial estimate for q^n is based on the Manning equation applied locally to each fluid element, and thereafter q^n is a known quantity based on the previous iteration. Substituting Eq. 3.36 into Eq. 3.35a&b and expressing the result as a system of linear equations for the solution of Δq^n , yields

$$\mathbf{M}[\Delta q^n] = \mathbf{x} \quad (3.37)$$

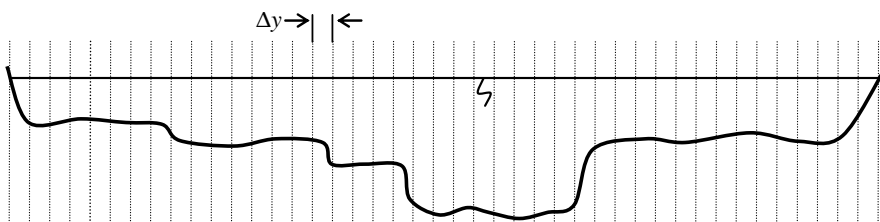


Figure 3.33 Example of the cross-section discretisation (Mc Gahey, 2006).

where \mathbf{M} is the linear operator defined by

$$\mathbf{M}[\Delta q^n] = A \frac{\partial^2 \Delta q^n}{\partial y^2} + g \left(\frac{\partial \Delta q^n}{\partial y}, \Delta q^n, y \right) \quad (3.38)$$

and \mathbf{x} is the vector of all contributing functions that are independent of Δq^n .

Incorporating piecewise functions

The FEM provides an approximate solution for $\Delta q^n(y)$ through piecewise functions in a total of E_e elements. Thus for a general element i , an approximation is sought in such a manner that outside i (Davies, 1980),

$$\Delta q_i^n(y) = 0 \quad i = 1, \dots, E_e \quad (3.39)$$

It follows that

$$\Delta q^n(y) = \sum_{E=1}^{i=1} \Delta q_i^n(y) \quad (3.40)$$

Linear shape functions ϕ are introduced where,

$$\Delta q_i^n(y) = \sum \Delta q_i^n \phi_i(y) \quad (3.41)$$

and ϕ is linear in y . Linear shape functions are the lowest order polynomials used in FEMs. A FEM using linear shape functions is similar to second order finite difference schemes. Higher order polynomials provide the option for fewer elements as they describe the parameter distribution more closely within each element. However, for the case of river channels, there is value in having more elements to capture the local variations in the input unit roughness and cross-section geometry. Thus, the CES is set to a default 100 elements and the linear shape functions are considered sufficient to capture the parameter variations across each of these elements.

Similar approximations can be introduced to describe the f , H and ψ distributions. Eq. 3.37 is integrated over the flow domain R_d ,

$$\int_{R_d} M[\Delta q^n] \phi(y) dy - \int_{R_d} x \phi(y) dy = 0 \quad (3.42)$$

Substituting the piecewise linear functions into Eq. 3.38 yields,

$$\sum_{E_e} \mathbf{M} \left(\sum \Delta q_i^n \phi_i(y) \right) \phi_j(y) - \sum_{E_e} \left(\sum x_i \phi_i(y) \right) \phi_j(y) = 0 \quad (3.43)$$

The numerical integration is based on Gauss-Legendre quadrature (Zienkiewick, 1977) with two sampling points on each flow element. Δq^n is evaluated for each element, q^n is then updated and the procedure is repeated until a specified tolerance on Δq^n is satisfied.

Boundary conditions

The Dirichlet boundary condition, $q = 0$, is prescribed at the boundary nodes at the edges of the flow domain. The nature of the numerical solution ensures continuity of q , i.e.

$$q_i = q_{i+1} \quad (3.44)$$

at the element boundaries. Knight *et al.* (2004) considered the boundary conditions applied at panels for the analytical solution of the SKM approach. As with Samuels (1989a), the continuity of q rather than U_d is advocated where the channel geometry has a vertical interface or ‘step’. The numerical FEM solution intrinsically implies continuity of force at each element interface, as the cross-section discretisation results in any vertical interfaces being approximated through a near vertical wall (i.e. almost 90 degrees). For the analytical solution, the boundary conditions between elements or panels are prescribed and thus vertical interfaces should be treated with care. Knight *et al.* (2004) illustrate the importance of including the shear force on the vertical wall in the force balance to achieve continuity in the unit flow rate.

Iteration strategy

The iterative procedure for determining q^{n+1} is based on Eq. 3.36 with a default relaxation of 1.0. The solution is designed to converge nearly quadratically. It is therefore unlikely to take more than 5–7 iterations to reach the iteration tolerance of $\Delta q \leq 0.001 \text{ m}^2\text{s}^{-1}$. In rare instances, for example, sections with a steep lateral roughness gradient, the solution may take longer to converge. Thus, to reduce the iteration requirement in achieving the solution tolerance, an approximate function for f at iteration $n + 1$,

$$f^{n+1} = f^n + \frac{\partial f^n}{\partial q^n} \Delta q^n \quad (3.45)$$

is substituted into Eq. 3.35a&b. The $\partial f / \partial q$ term is approximated through numerical differentiation (Newton’s Method, 1664),

$$\left(\frac{df}{dq} \right)^n \approx \frac{f((1 + per) \cdot q) - f(q)}{per \cdot q} \quad (3.46)$$

where the percentage ‘per’ is in the range $0 < per \leq 0.5\%$.

Relaxation strategy

As outlined above, the iterative procedure for determining q^{n+1} is based on Eq. 3.36. If the following condition occurs,

$$\Delta q^n < 0 \text{ and } |\Delta q^n| \geq q^n \quad (3.47)$$

then q^{n+1} will be negative. The interpretation of $q^{n+1} \leq 0$ (or flow leaving the system) is that the previous ‘ q^n ’ estimate was too high and thus the solution is overcorrecting.

This typically occurs at low flow depths, for example, floodplain depths just above bankfull. The implication for the CES methodology is that in the Colebrook-White equation (Eq. 3.12), where $Re = f(q^n)$, the logarithm (base 10) term is zero or a negative number leading to an infinite number. Two possible solutions are identified: (i) set q^n as a small positive number or (ii) alter the value of the relaxation parameter χ . The first is not easily applied, as it requires interpretation of what ‘small’ is. The CES relaxation strategy is therefore based on the second.

The final system of equations is solved directly with a tri-diagonal matrix solver (Press *et al.*, 1996) appropriate for the resulting diagonally dominant and well-conditioned matrix coefficients. This solves linear simultaneous equations using Gaussian elimination and back-substitution. The equations and their finite element approximations are provided in Appendix 1.

3.2.4 Backwater calculation methods

Backwater profiles occur upstream of structures such as reservoirs, weirs, bridges and free outfalls where the upstream flow is controlled by the downstream structure. The backwater extends from where the control or disturbance to normal depth occurs to the upstream location where normal depth is re-established. These lengths may be tens of kilometres long (e.g. Table 3.7), having a substantial impact on flow depths far upstream of the control point (e.g. a new housing development or a flow gauging weir). A range of methods exist for determining backwater profiles using direct, graphical or numerical integration, for example, the direct or standard step methods (see Chow, 1959; Henderson, 1966). The CES adopts a simple iterative (as the velocity head is incorporated) energy balance approach to estimate the backwater profile.

The backwater calculation starts at the downstream control of known depth and flow rate and moves upstream, applying energy balances at each consecutive cross-section. The backwater effect is present until $\sim 99\%$ of normal depth is achieved at some backwater length L (m) upstream of this downstream control (Figure 3.34). Where either the flow rate or the flow depth is known, the CES backwater approach

Table 3.7 Backwater lengths for some UK Rivers (Samuels, 1989b).

River	Location	Depth (m)	Slope S_0	Backwater length (km)
Avon	Pershore	4.2	0.46	6.90
Cleddau	Haverfordwest	2.5	1.70	1.00
Lagan	Dunmurry	2.5	1.20	1.40
Lagan	Lisburn	3.0	0.29	7.20
Lagan	Banoge	2.0	1.30	1.10
Little Ouse	Lakenheath	2.5	0.05	35.00
Rhymney	Llanedeyrn	2.0	2.20	0.64
Severn	Shrewsbury	4.5	0.50	6.90
Severn	Tewkesbury	8.5	0.10	59.50
Soar	Loughborough	3.5	0.25	9.80
Stour	Christchurch	4.5	1.0	3.20
Taff	Cardiff	6.0	2.5	1.70
Wharfe	Otley	2.0	1.8	0.76

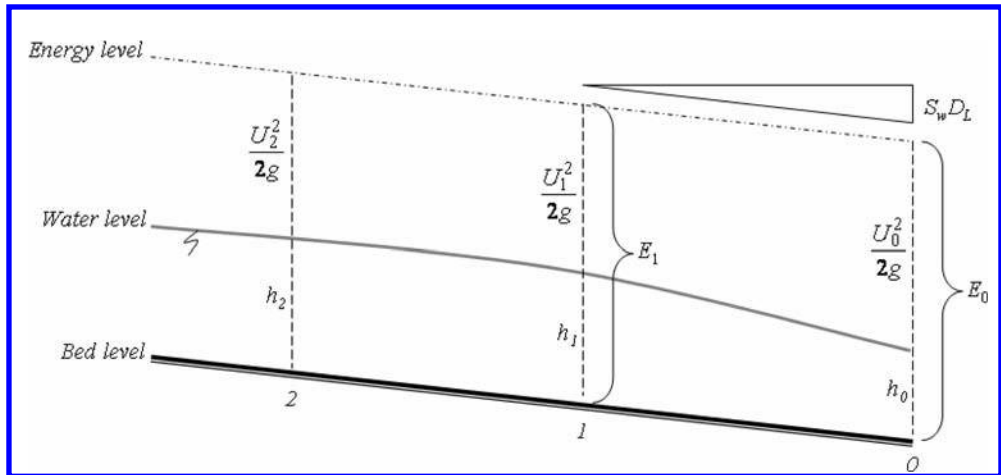


Figure 3.34 Backwater calculation method from downstream (cross-section 0) to upstream (cross-section 2).

may be used to calculate the corresponding normal depth of flow or discharge, respectively. This is then used as the downstream control.

At the control point, the flow Q (m^3s^{-1}) and corresponding depth h_0 (m) is known. The conveyance for this depth of flow, K_0 (m^3s^{-1}), is estimated for the downstream cross-section with the CES conveyance calculation (Section 3.2.2). The water surface slope S_w is approximated from

$$S_w = \left(\frac{Q}{K_0} \right)^{1/2} \quad (3.48)$$

The section average velocity U_0 is calculated from

$$U_0 = \frac{Q}{A_0} \quad (3.49)$$

The total downstream energy level E_0 is determined from

$$E_0 = h_0 + \frac{U_0^2}{2g} \quad (3.50)$$

The surface water slope is extrapolated to predict the energy level E_1 for the upstream cross-section i.e.

$$E_1 = E_0 + S_w D_L \quad (3.51)$$

where D_L is the streamwise chainage between the two cross-sections. The upstream depth of flow h_1 is then solved iteratively using a Newton-Raphson Solver i.e.

- set h_1 as E_1 for the initial estimate
- calculate the cross-section area A_1 (by-product of the CES calculation)

- calculate the velocity U_1 ([Eq. 3.49](#))
- calculate the energy level E_1 from ([Eq. 3.51](#))
- if E_1 (step above) is equal to E_1 ([Eq. 3.51](#)) within a tolerance of ± 0.001 m stop, if not update $b_1 = b_1 - E_o/E_1$ and repeat. Note, if $E_1 < 0.0$, then update $b_1 = 1.1 * E_1$.

The conveyance K_1 is then estimated for this upstream cross-section and the procedure is repeated moving progressively further upstream ([Figure 3.34](#)).

The CES backwater approach assumes:

- subcritical flow (for subcritical flow where the channel bed is steep, the calculation may result in a negative upstream energy head, and hence a negative depth, being calculated);
- single reaches i.e. no branches, confluences, junctions, loops or spills into floodplain storage areas;
- steady flow conditions i.e. the flow rate is constant with time.

3.2.5 Afflux Estimation System methods

The AES methods for bridge and culvert structures are designed to model

- discharge through the structure,
- upstream and downstream transition reaches,
- free surface flow through the structure,
- pressurised flow through the structure when it is flowing full,
- overtopping flow when the structure is drowned.

The AES methods are based on a one dimensional analysis, which is a simplification of the physics observed in reality, as discussed in [Chapter 2](#). The analysis is based on estimation of energy losses as water flows through the structure. This simplification of the physics requires the use of empirical or semi-empirical approximations, many of which are derived from previous work reviewed in [Chapter 2](#) and references cited therein. The AES methods incorporate both re-analysis of some existing data sets (HEC, 1995) and also new data (Atabay and Knight, 2002, Seckin *et al.*, 2008b) to provide the best available empirical support. [Figure 3.35](#) illustrates the longitudinal schematisation adopted in the AES (note that the order of numbering for cross sections differs from some other presentations). [Figure 3.35](#) includes a normal depth profile for the ‘unobstructed stream’, representing uniform flow conditions in the channel that would exist if the structure were not present. Section 1 is interpreted as the location where the water surface profile downstream of the bridge would depart from the normal depth.

There are many methods available for calculation of afflux or head loss at bridges. One of the practical difficulties can be deciding which calculation approach is most suitable. In many cases, there will be several formulae that are relevant, especially when there is a need to analyse a wide range of flows in a channel from low flow through to extreme flood conditions. The AES software combines calculations for flows through and, where necessary, over a structure.

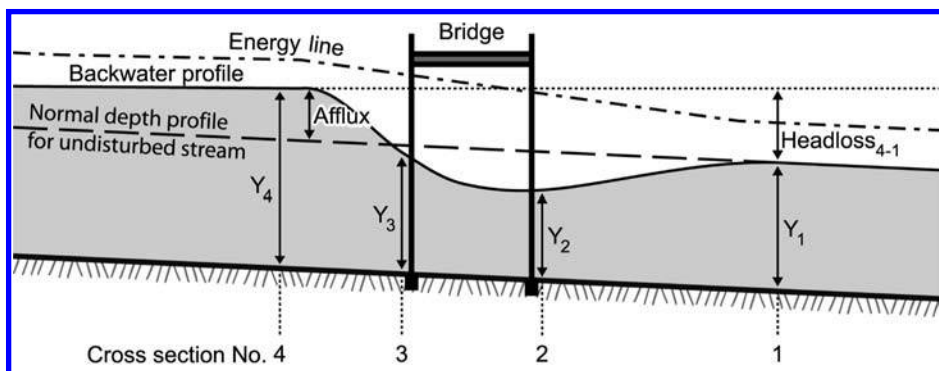


Figure 3.35 Long section profile schematic for the Afflux Estimation System bridge analysis.

Bridge flow modes represented in the AES

At least nine modes of flow may occur through a bridge structure, depending on the flow depth and the upstream and downstream conditions. Figure 3.36 illustrates these modes of flow. The flow modes are generally subdivided as sub-soffit flows and super-soffit flows. For the case where a bridge deck has an underlying girder, the soffit is taken as the elevation at the bottom of this girder. And for the case where a bridge deck has an overlying parapet, the road elevation is taken as that at the top of the parapet. (These overtopping elevations may also sometimes be called the ‘relief elevation’). The following modes are illustrated in order of increasing water level at the bridge structure:

Mode 1 – Supercritical flow occurs when the flow is shallow relative to the normal depth and is associated with a Froude Number (Fr) greater than unity. For this flow, the afflux is theoretically zero since no backwater can exist. There will, however, be a local bridge energy loss due to form drag. If this mode is encountered in the AES, then the flow is set to critical depth by default.

Modes 2 and 3 – When critical flow occurs at the structure, the flow is said to be choked. This is because critical flow is a condition of minimum energy at constant discharge, and any increase in potential energy upstream will increase the upstream water level but not increase the critical flow level. This may occur, for example, when the bridge entry becomes partially blocked by debris. The longitudinal water surface profile may change gradually (Mode 2) or rapidly (Mode 3 as a hydraulic jump) downstream. Where supercritical flow is detected between the upstream and downstream faces of the bridge, the flow defaults to critical depth in the AES.

Mode 4 – Flow throughout the structure is subcritical and is modelled using a backwater calculation.

Mode 5 – Sluice gate flow occurs when the upstream water level is greater than the soffit level and the downstream soffit level is not submerged. The upstream soffit is effectively acting as a sluice gate, and associated sluice gate equations are used. In common with the Water Surface Profile Program (WSPRO, 1986), sluice gate flow is not modelled in the AES as the mode only occurs over a small region of the discharge rating.

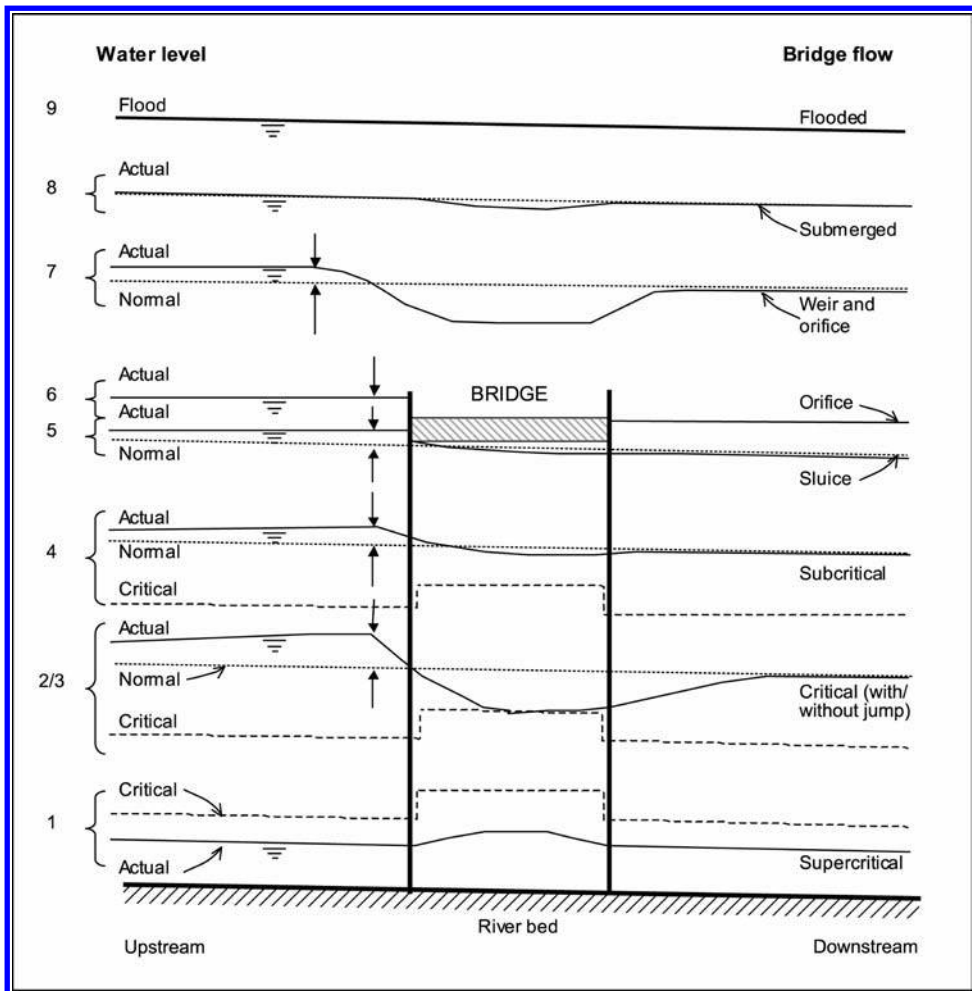


Figure 3.36 Modes of flow for a bridge.

Mode 6 – When the downstream soffit level is submerged, the flow under the bridge becomes fully pressurised. Since the bridge length is rarely much greater than the flow depth, the pressurised flow acts more like a submerged orifice than a closed conduit. The flow is therefore described by orifice flow equations in the AES.

Mode 7 – Once the upstream water level is above the road or parapet, a weir flow will ensue. If the weir flow submergence (downstream water level above road level divided by upstream water level above road level) is less than about 85%, then the weir flow is modular, and its discharge coefficient is determinable (Ackers *et al.*, 1978). Note that pressure flow is still occurring beneath the bridge (provided it is not totally obstructed). The simultaneous weir flow and pressure flow are calculated in the AES using an iterative procedure.

Mode 8 – As the downstream flow level increases further, the weir becomes submerged and the flow becomes a non-modular weir flow. This occurs for a submergence of between 85% and 95%, and the discharge coefficient is accordingly reduced. As for Mode 7, the simultaneous weir flow and pressure flow are calculated in the AES using an iterative procedure.

Mode 9 – When a submergence of about 95% is reached, the weir is drowned and the structure is assumed to act in effect as a feature of the river bed profile. As for Mode 7, the flow through the structure continues to be calculated.

In summary, the AES computes solutions for the most important flow modes, that is Mode 4 (subcritical), Mode 6 (orifice) and Modes 7, 8 and 9 (modular, submerged and drowned weir respectively). Supercritical flow (Modes 1, 2 and 3) defaults to critical depth. The detail of the computational limits used for each mode is given in [Table 3.8](#).

Culvert flow modes represented in the AES

The AES incorporates a culvert calculation module that automates methods set out for hand calculation in the CIRIA Culvert Design Guide (CIRIA, 1997) and the Federal Highway Administration (FHWA, 2001) manuals. As for bridges, the AES computes overtopping weir flows for culverts to allow the user to obtain a full upstream rating curve.

Culvert flow may be controlled by high resistance to flow at the inlet structure or at the outlet due to a long barrel structure. If the inlet structure allows the least discharge for the same upstream energy as applied to the outlet, then the culvert is under inlet control and the flow is usually supercritical. If the culvert outlet allows the least discharge for the same upstream energy as applied to the inlet, then the culvert is under outlet control and the flow is usually subcritical. Since the flow control determines the computation of a water surface profile, it must first be determined for both free and full flow conditions.

Table 3.8 Computational limits for bridge modes in the AES.

Flow mode	Bridge flow	Start condition	Finish condition	Constraints
1	Supercritical	$Fr > 1$ upstream	$Fr = 1$ upstream	Flow defaults to critical depth
2–3	Critical	$Fr = 1$ within bridge		Flow defaults to critical depth
4	Subcritical	Minimum river level	Section 3 level > soffit level	Supercritical flow defaulted to critical
6	Orifice flow	Section 3 level > soffit level < road level	Section 3 level > road level	
7	Weir and orifice	Section 3 level > road level	Submergence > 0.85	Defaults to critical depth at downstream face
8	Submerged weir and orifice	Submergence > 0.85	Submergence > 0.95	Defaults to critical depth at downstream face
9	Drowned weir and orifice	Submergence > 0.95	Maximum river level	

The AES initially calculates the inlet control energy using the FHWA (2001) methods for either an unsubmerged or submerged inlet condition, depending on the flow conditions. If both the inlet and outlet are submerged and the culvert is flowing under inlet control, a hydraulic jump and possible instability in the water surface profile may occur in the culvert. This is not a flow mode that would be designed for and is ignored in the AES for simplicity. The AES calculates the outlet control energy (for the same discharge) using the standard step backwater method to model the water surface profile through the culvert barrel. The higher of the two energies determines the control of the culvert flow for any given combination of discharge and tailwater depth. When the culvert outlet is nearly submerged under outlet control, the culvert flow becomes equivalent to that of full conduit flow. When the culvert inlet water level reaches the road level, modular weir flow, submerged and drowned weir flow can occur sequentially with increased flow elevation.

The AES therefore computes a total of eight culvert flow modes, as illustrated in [Figure 3.37](#) and described below.

Modes 1 and 2 – Inlet control condition (submerged or free inlet flow). The high friction at the culvert entry causes a high energy loss and water level fall. The FHWA (2001) formulae are used to calculate the energy loss at the inlet.

Mode 3 – Drawdown outlet control. The outlet water level is below the culvert normal depth, and thus a drawdown profile is developed within the culvert, returning to normal depth upstream for a long culvert. In the AES, the water surface profiles are computed using the standard step method.

Mode 4 – Backwater outlet control. The outlet water level is above the culvert normal depth, and thus a backwater profile develops within the culvert, which may revert to normal depth upstream for a long culvert.

Mode 5 – Submerged inlet, full flow, outlet control. It has been empirically shown by FHWA (2001) that when the outlet water level is greater than $(d_c + D)/2$, where d_c is the culvert critical depth and D is the barrel depth (see [Figure 3.48](#)), then the culvert friction loss is the same as if it were in full flow. This criterion is therefore used as an outlet condition in the AES if the associated outlet depth is less than D and $(d_c + D)/2$.

Mode 6 – Inlet water level above road level, weir flow. If the weir flow submergence (downstream water level above road level divided by upstream water level above road level) is less than about 85%, then the weir flow is modular, and its discharge coefficient is determinable (as for the bridge flow). Pressure flow is still occurring within the culvert. The simultaneous weir and pressure flow are calculated for each discharge rating in the AES using an iterative procedure.

Mode 7 – Non-modular weir flow. This occurs for submergence between 85% and 95%, and the discharge coefficient is accordingly reduced (as for the bridge flow). The AES continues to solve for the pressure flow through the culvert.

Mode 8 – Drowned weir. For submergence of 95%, the weir is drowned. See bridge Mode 9 above.

The AES assumes that the culvert is of uniform slope, dimensions, material and condition. Under these assumptions, culverts of any length can be computed. A minimum culvert rise or span of 0.45 m is recommended and the culvert invert slope is assumed to be equal to the river channel slope.

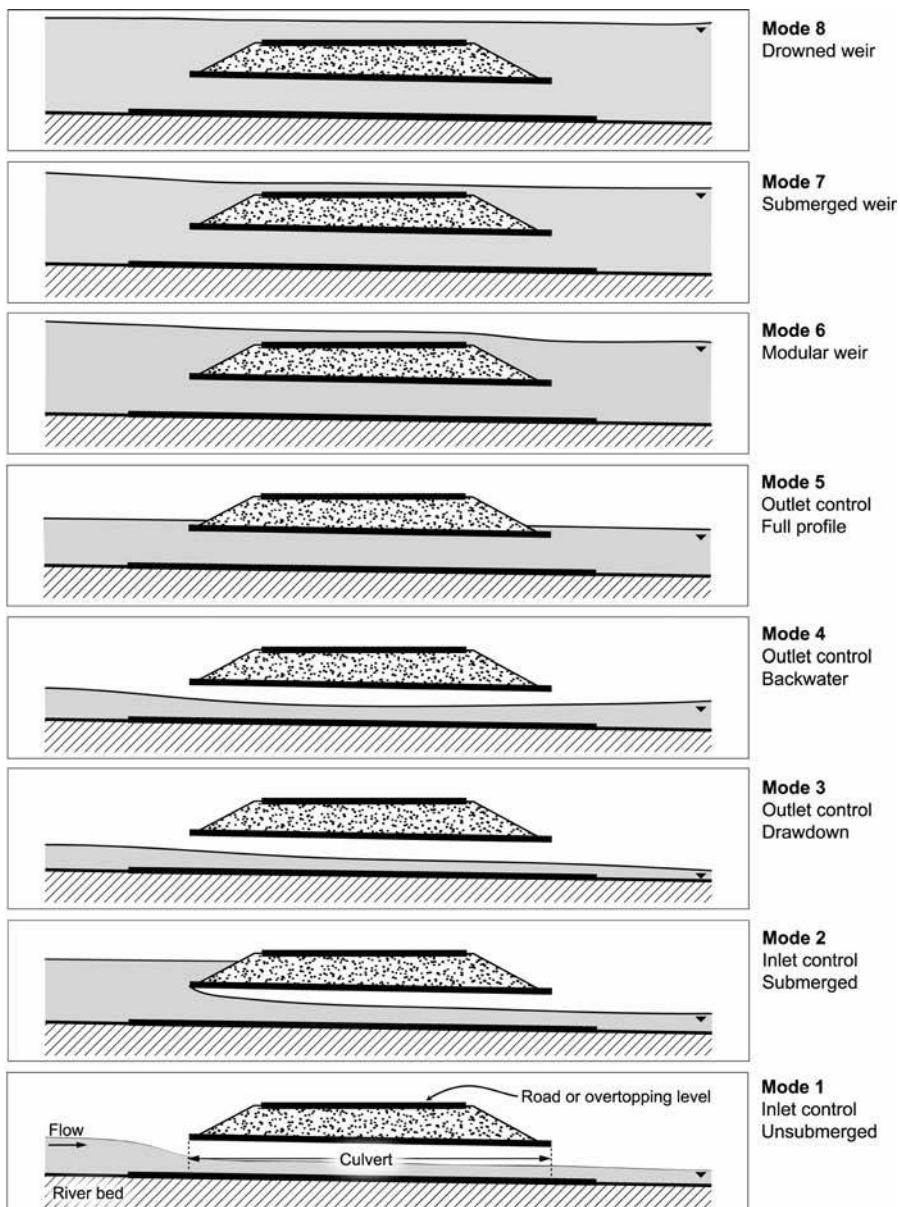


Figure 3.37 Culvert flow modes.

Channel conveyance

In the 1-D view adopted by the AES, afflux is related to the energy losses that occur when a channel is obstructed by a bridge or culvert. To determine the afflux from measured data, it is necessary to analyse both the flow conditions for the obstructed

channel and those that would exist without the structure. Hence it is necessary to model the conveyance through the channel with and without the structure.

The AES uses the divided channel method to calculate channel conveyance. Figure 3.38 illustrates a channel cross-section similar to the River Main in Northern Ireland (Section 2.2.2). Eight offset-elevation points have been used to draw the geometry, and the cross-section may be vertically subdivided into seven areas (A1-7) for any of the incremental depths from zero to 5 m, which is the maximum side boundary elevation.

The cross section is divided into three panels, the left floodplain, main channel (MC) and right floodplain, separated by location markers at left overbank (LOB) and right overbank (ROB) positions. The wetted perimeter (P) and top width (T) can also be calculated for each of the sub-areas.

The AES sums A , P and T for each of the sub areas at each flow depth, and computes A , P and T for each of the left floodplain, main channel and right floodplain panels. Manning's equation is then used to compute the conveyance (K) for each flow panel as follows:

$$K = [A(A/P^{2/3})/n] \quad (3.52)$$

where n is the Manning friction coefficient for each panel. The channel conveyance curve is derived as the relationship between the sum of the panel conveyances and the water surface elevation. Additionally, the kinetic energy coefficient (α) is computed as:

$$\alpha = \sum (K_i^3/A_i^2)/(K^3/A^2) \quad (3.53)$$

where K_i and A_i are the panel conveyance and flow area respectively, and K and A are the total cross section conveyance and flow area.

The use of Manning's equation rather than the CES method is expedient for three reasons. Firstly the CES and AES developments were parallel projects and so final outputs of the CES research were not available from the outset in developing the AES. The second reason is that although the CES method could in principle be applied for

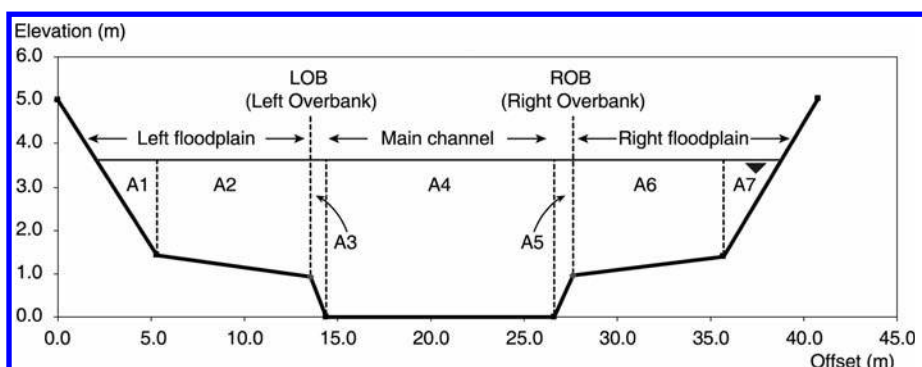


Figure 3.38 Divided channel method for the River Main.

channel conveyance, it does not yet handle the range of cross section geometries needed for the AES such as arches and pipes (see Section 6.2 on future developments). The third reason is that the AES development required numerous 1-D hydraulic models to be built to enable analysis of laboratory and field data for calibration. The USACE software HEC-RAS was used for this purpose, in part for consistency with earlier analysis of field scale data. The conveyance calculations in HEC-RAS are based on Manning's equation.

Bridge conveyance

The AES includes five bridge opening types. There are three arch bridge types, with parabolic, elliptical or semi-circular arch geometry, which are specified by the user in terms of the springer and soffit positions (offset and elevation). There is a 'custom' arch geometry, which allows a user to specify an arbitrary symmetrical arch profile. There is also a beam bridge type, which represents a beam bridge with continuous piers that are assumed to extend from upstream to downstream for the complete bridge length and to be of constant cross section. In all cases, the AES allows for multiple openings, which may have different shapes and sizes. The bridge conveyance calculation requires a Manning friction coefficient, which is assumed to be the same for all openings for a bridge with multiple spans. The recommended values have been adapted from the CIRIA (1997) recommendations for culvert surfaces.

Channel conveyance adjacent to the faces of an arch bridge is calculated within four vertical 'panels' defined in terms of the water level as follows:

- *Minimum elevation (Z_{min}) to springer level (SPL):* Conveyance is computed for the obstructed channel cross section (including bridge abutments/piers and using a roughness coefficient for the combined structure and channel)

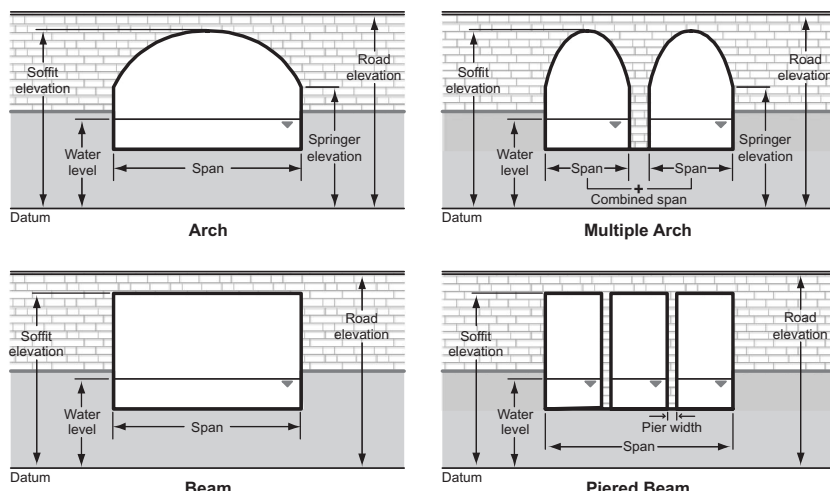


Figure 3.39 Generic bridge opening types in the AES showing variables used to define the bridge geometry.

- *Springer level (SPL) to soffit level (SFL):* Flow within the arch. As the water level rises within the arch, the rate of increase in flow area with water level reduces due to the shape of the arch. At the same time, the wetted perimeter increases and so the conveyance can decrease as the water level rises towards the soffit, resulting in an inflection in the conveyance rating curve.
- *Soffit level (SFL) to road level (RDL):* Orifice flow. This flow begins when the water surface reaches the soffit level.
- *Road level (RDL) to maximum elevation (ZMAX):* Orifice flow and above-road weir flow. Above RDL, orifice flow occurs through the bridge openings in combination with weir flow through the uncontracted channel cross sectional area above the bridge.

The conveyance for a beam bridge opening is calculated in a similar way, omitting the panel between springer and soffit. The roadway is assumed to be horizontal and flow by-passing the bridge is not represented within the CES-AES.

The AES conveyance rating for a single parabolic arch example is compared with the conveyance curve calculated by HEC-RAS (version 3.1), also using a three panel divided channel method, in [Figure 3.40](#). There are differences as expected between AES and HEC-RAS ratings because AES includes a friction coefficient for the structure and represents the reduction in conveyance when the water surface approaches the soffit, as noted above.

AES water surface profile calculation

The AES calculates the water surface profile through or over the structure in a similar way for both bridges and culverts. Firstly, the conveyance rating curves for the river channel at sections 1 to 4 in [Figure 3.35](#) are estimated using the divided channel method. Then the structure geometry is added to sections 2 and 3, giving additional cross sections named 2D and 3U representing the downstream and upstream openings of the structure. Complete conveyance curves for these sections are then computed from the structure geometry as described above.

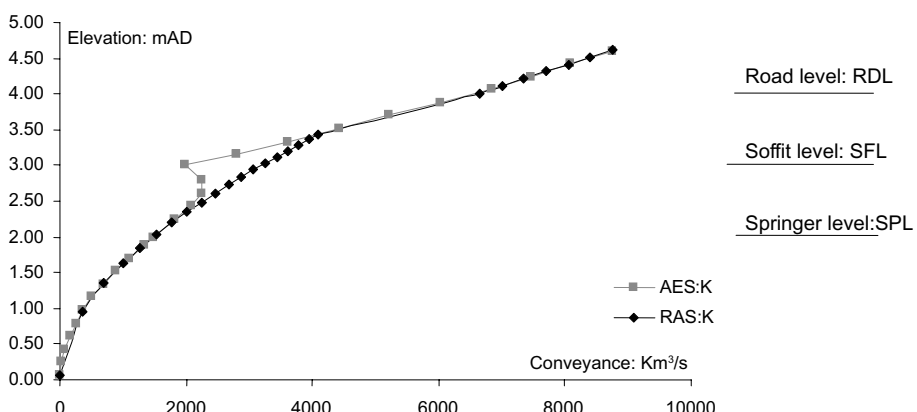


[Figure 3.40](#) Example conveyance curves for a parabolic arch, comparing AES and HEC-RAS (version 3.1).

Upstream (contraction) and downstream (expansion) lengths are estimated based on the required flow conditions, as discussed in more detail below. The standard step backwater method is then applied for the three different flow types:

- Free surface flows below soffit level;
- Free surface flows in the channel combined with pressurized orifice flow through the structure when the upstream water level is between the soffit and road level;
- Overtopping weir flow combined with orifice flow when the upstream water level is above the road level, including modular, non-modular and drowned weir flow.

i Free surface flow through bridges

For the subcritical, free surface flow modes through the bridge or culvert, the AES uses the standard step backwater method (Sturm, 2001; Montes, 1998). Like the backwater method used in the CES, the AES backwater calculation is based on conservation of energy between cross sections representing discrete channel reaches.

The method assumes that channels can be modelled by section reaches which have relatively small variations in bed slope. Consider the reach illustrated in [Figure 3.35](#). Conservation of energy between a downstream section (subscript 1) and an upstream section (subscript 2) can be expressed as

$$z_2 + \alpha_2 \frac{U_2^2}{2g} = z_1 + \alpha_1 \frac{U_1^2}{2g} + h_e \quad (3.54)$$

where z is the water surface elevation, U is the section average velocity and g is gravitational acceleration. The term $\alpha U^2/2g$ is then the kinetic energy for the section and h_e represents energy losses. The CES backwater calculation is able to make use of the CES quasi-2-D conveyance calculation in its estimation of water surface slope ([Eq. 3.48](#)) whereas in the AES it is necessary to specify a kinetic energy correction factor α that accounts empirically for non uniform velocity distribution.

The α coefficient is computed for a section from an abbreviated form of Manning's equation given by

$$Q = AR^{2/3}S^{1/2}/n = KS^{1/2} \quad (3.55)$$

where Q is a steady flow discharge, n is the Manning friction coefficient, A is the cross section area, R is the cross section hydraulic radius (flow area divided by wetted perimeter) and S is the channel energy gradient due to the frictional loss (i.e. the friction slope). The α coefficient can be calculated in terms of K , the conveyance, from [Eq \(3.53\)](#) as

$$\alpha = \sum (K_i^3/A_i^2)/(K^3/A^2) \quad (3.56)$$

where now K_i and A_i are the subsection (left or right overbank and channel) conveyance and flow areas respectively. Note that both K and α can be computed for a cross section without knowledge of the friction slope.

The energy loss h_e is assumed to consist of both a channel friction loss (h_f) and a transition loss (h_t) caused by changes in cross section shape and velocity profile, and

can be written

$$h_e = h_f + h_t = LS_f + C \left| \alpha_2 \frac{U_2^2}{2g} - \alpha_1 \frac{U_1^2}{2g} \right| \quad (3.57)$$

where S_f represents an average friction slope for the reach of length L , and C is a loss coefficient. Within the AES, the loss coefficient C is important in the transition reaches upstream and downstream of the bridge. Hence there are two such transition loss coefficients, $C = C_c$ the upstream contraction loss coefficient and $C = C_E$, the downstream expansion loss coefficient. It is assumed that Manning's equation for uniform flow can be applied to the total conveyance for between sections, thus

$$Q = K_1 S_1^{1/2} = K_2 S_2^{1/2} \quad (3.58)$$

where $S_1 = Q^2/K_1^2$ is a friction slope for Section 1, $S_2 = Q^2/K_2^2$ is a friction slope for Section 2 and K is the sum of panel conveyances for a given water level. Thus a reach of, say, adverse slope can be approximated to a uniform reach of similar friction and geometry (K) with a bed slope equal to the friction slope ($S = Q^2/K^2$). The average friction gradient for the reach, S_f , can be approximated by the arithmetic ($(S_1+S_2)/2$), geometric ($(S_1 S_2)^{0.5}$) or harmonic ($2S_1 S_2 / (S_1 + S_2)$) mean of the upstream and downstream sections. It has been shown by Montes (1998) that the arithmetic mean is the most accurate approximation for mild slope, subcritical profiles that are expected within the AES.

The solution to the above implicit energy equation is obtained by iteration, as for the CES backwater profile (Section 3.2.3). The solution to the iteration can sometimes produce supercritical flow within the bridge or culvert structure. In these cases, the AES defaults to critical depth to allow the computation to proceed and generates a warning.

ii Pressure flow

The AES switches to orifice flow when the upstream water level is between the structure soffit and the road level. In this case, the orifice equation in USBPR (1978) is used, which relates the discharge Q to the difference in water surface elevation across the bridge, Δh , as

$$Q = C_d b_N Z (2g \Delta h)^{1/2} \quad (3.59)$$

where b_N is the net width of waterway (excluding piers), Z is the water depth at soffit level and the coefficient of discharge, C_d , is approximately constant at $C_d = 0.8$. This orifice equation is solved explicitly for Δh in the AES. The upstream depth of flow at Section 3, Y_u , is then computed as a function of Δh using the dimensionless relationship given in USBPR (1978) and shown in Figure 3.41, where the depths are scaled by Y_{bar} , the normal flow depth at the bridge determined using Manning's equation.

In summary, for pressure flow the above algorithm is used to solve for the orifice flow depth at Section 3 (upstream face of the structure) and the standard step method for profiles upstream and downstream of the structure.

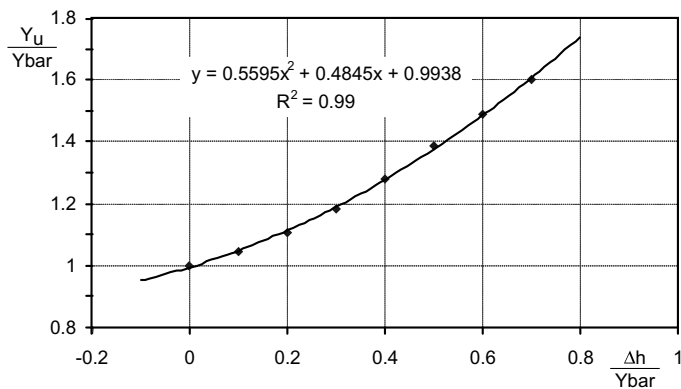


Figure 3.41 Dimensionless relationship between bridge headloss Δh and upstream depth Y_u (after USBPR, 1978).

iii Overtopping flow when the structure is drowned

The AES assumes weir flow over the structure when the upstream water level is above the supplied road level. The standard weir flow equation is given as

$$Q = CB_{RD}H^{3/2} \quad (3.60)$$

where Q is the total discharge, C the discharge coefficient, B_{RD} the road length across the floodplain, and H the total head upstream measured relative to the road level. Orifice flow through the bridge occurs in addition to the weir flow, and AES iterates both the weir and orifice flow equations until both solutions provide the same upstream energy level.

The major unknown variable in the weir equation is the weir coefficient C . The coefficient varies according to the weir type (broad crested or rectangular) and increases with B_{RD} . Values are summarised in HEC (2004), and vary from about 1.5 to 1.7. In the AES, the roadway length is taken as the distance between the extremities of the floodplain at the road elevation, hence no special allowance is made for approach roads or embankments. The modular weir coefficient is assumed to be 1.6. The modular weir flow coefficient is used until the submergence (the ratio of upstream and downstream water levels above the road) exceeds 85%.

Submerged or non-modular weir flow is taken to begin for a submergence of 85% and ends at a 95% submergence. The same weir flow equation and iterative method are used as for the modular flow, but the weir discharge coefficient is reduced by a discharge reduction factor (DRF) following USBPR (1978), see [Figure 3.42](#).

Transition reaches

The transition energy loss coefficients that appear in the water surface profile calculation relate to energy losses caused by acceleration within the flow as it contracts upstream and expands downstream of the structure.

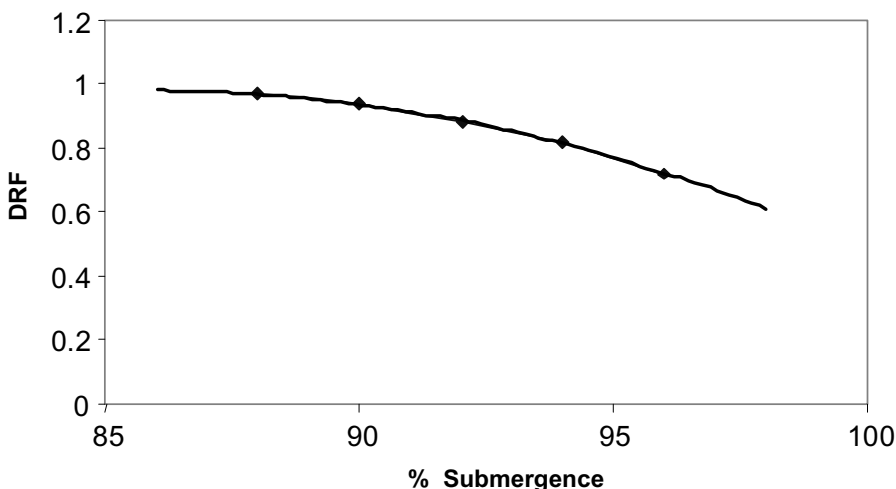


Figure 3.42 Discharge reduction factor for submerged weir flow (after USBPR, 1978).

Section 4 is assumed to be the position of the afflux in Figure 3.35, where the largest difference exists between the water surface profile affected by the structure and normal depth for the unobstructed channel. The flow contracts towards the structure between Sections 4 and 3 for a contraction length L_C . It then exits the structure and expands between Sections 2 and 1 for an expansion length L_E . Section 1 is assumed to be located where the water surface profile influenced by the structure would depart from normal depth for the channel.

For both transitions, the effective lengths vary according to the flow conditions and the geometry and roughness of the structure. The transition lengths affect the appropriate choice of location for cross sections in a backwater model that includes a bridge or culvert. Suitable choices for transition lengths and energy loss coefficients are, therefore, required for an accurate water surface profile calculation through a bridge. For the AES, these parameters have been calibrated using two data sets for flows below soffit level, as follows:

- University of Birmingham laboratory data for bridges in compound channels, described in Chapter 2,
- HEC (1995) two dimensional numerical model data that simulated field data for fixed bed channels.

The data summarized above is considered to be the most suitable, accurate set of records available at the time of the AES development for the analysis of bridge afflux. It comprises detailed measurements of discharge rates and water surface profiles or transition lengths for compound channels and floodplains of varying roughness conditions, for multiple bridge types and skew angles, and at scales ranging across three orders of magnitude (from ~ 1 m to ~ 100 m).

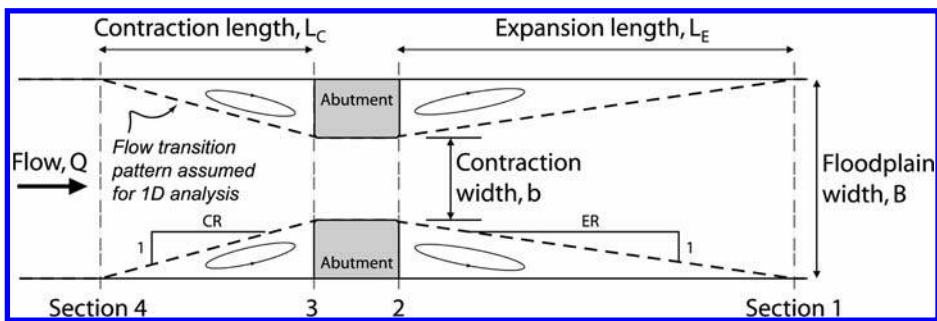


Figure 3.43 Plan view of flow transition reaches. CR is the contraction ratio, ER is the expansion ratio. The structure length is the distance between sections 3 and 2.

i Transition length analysis

Ideally, it is recommended to estimate transition lengths from field observations during high flow conditions (HEC, 1996), but this can rarely be done and so empirical formulae are often used instead. HEC (1995) investigated criteria for estimating transition lengths as a function of the total length of the side constriction caused by the structure abutments, $B - b$, where B is the floodplain width and b the width of the opening across the stream (Figure 3.43). In development of the AES, a dynamic similarity analysis was carried out for dimensionless transition lengths using the Froude Number of the downstream channel flow for scaling. The Froude Number was obtained either from the laboratory data or from numerical model data, in which case the undisturbed stream was replicated using HEC-RAS (version 3.1).

The similarity analysis was based on methods developed by Raju *et al.* (1983) and later used by Brown (1988) in the development of the 'Hydraulics Research Arch Bridges method' in the UK. In simple terms the analysis involves expressing the transition lengths L_C and L_E as follows:

$$L_{(C,E)}/D_N = f(Fr, J_D, B) \quad (3.61)$$

where D_N is the normal flow depth without the presence of the structure, Fr is the Froude Number of the flow without the presence of the structure and J_D is a blockage ratio to the flow caused by the structure. The blockage ratio J_D is defined as the area of flow blocked by the downstream bridge section divided by the total flow area in the unobstructed channel. The floodplain width, B , is introduced to accommodate information from both the laboratory scale model experiments (Chapter 2) and field scale modeled data from the HEC (1995) study.

From the compound channel laboratory experiments there are measured values of contraction length for 145 tests and expansion length from 130 tests. For some of the experiments, supercritical flow conditions occurred through the structure and thus a flow control was located at the structure as well as downstream. For some cases, a hydraulic jump occurred and the water surface profile was also unsteady. An expansion length cannot be measured for these conditions. For the remaining tests, water levels in the presence of the bridge were compared with the normal depth profile at 0.1 m

increments downstream of the bridge in cases where there were large water surface gradients, such as at standing waves, and at 1.0 m increments for smoother profiles. All water level measurements were made along the channel centerline. In each case, a two-point moving average was fitted to the measured water surface to smooth local variations, and to establish an objective intersection with the normal water level profile.

The measured contraction lengths are approximately constant at 0.5 m (± 0.02 m at 95% confidence level). The dimensionless quantity L_C/D_N is weakly related to the undisturbed flow Froude Number and blockage ratio, with a quadratic relationship able to predict L_C/D_N as a function of Froude Number and blockage ratio with a coefficient of determination of approximately 0.6. The relationship appears physically meaningful with L_C approaching zero as the Froude Number approaches zero (i.e. still water) and as the blockage ratio approaches 1.0 (i.e. total blockage). Since the average obstruction length $(B - b)/2$ was approximately 0.4 m for the laboratory data, the contraction ratio $2L_C/(B - b)$ was about 1.25, which is a value similar to that suggested by HEC (1995).

Measurements of expansion length L_E derived from the Birmingham University laboratory data vary more strongly with the unobstructed channel flow Froude Number. Figure 3.44 shows the dimensionless expansion length (scaled by the downstream normal depth) derived from the laboratory measurements and the Froude Number for the unobstructed channel. The data in Figure 3.44 include variation in the blockage ratio, J_D . A quadratic relationship is able to describe the variation in L_E/D_N as a function of Fr and J_D with a coefficient of determination of approximately 0.9.

For larger physical floodplain scales, HEC (1995) estimated transition lengths in data produced using a two dimensional numerical model based on data from three real bridge sites and 76 idealized bridge and channel configurations with a floodplain width of approximately 305 m. The data included various combinations of bridge opening width (b), discharge, overbank and main channel Manning coefficients and bed slopes.

The method for estimating transition lengths reported by HEC (1995) was a visual examination of modelled velocity vector fields, rather than comparison of water surface profiles as for the Birmingham University laboratory data. The limit of the

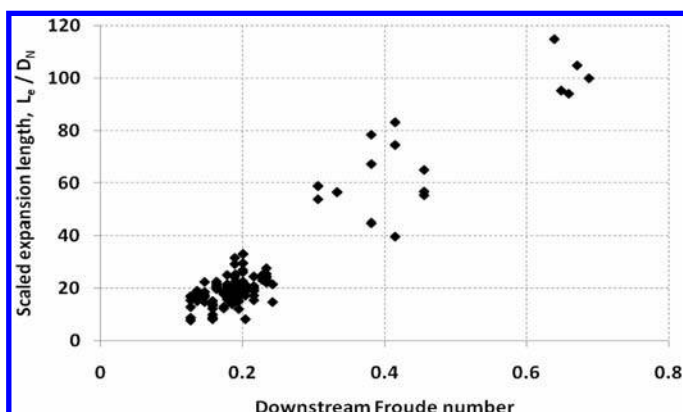


Figure 3.44 Relationship between dimensionless expansion length and Froude Number for compound channel laboratory data for all bridge types tested (see Chapter 2).

expansion reach was defined by HEC (1995) to be just upstream of the location where the velocity vectors became essentially parallel to the channel. This placed the expansion reach limit a small distance upstream of the location where normal depth is re-established (Section 1 in Figures 3.35 and 3.43). However, the two sets of measurements were accepted in development of the AES as alternative approximations of the same physical quantity. For the HEC (1995) data, the relationship found by fitting a model of the form of Eq. 3.61 to the data is similar to that identified from the laboratory data, but with a smaller coefficient of determination.

The AES estimates transition lengths using a composite of the quadratic best fit curves for both the laboratory scale ($B \approx 1$ m) and field scale ($B \approx 300$ m) data sets, described by

$$\frac{L_{(C,E)}}{D_N} = b_0 + b_1 Fr + b_2 J_D + b_3 Fr^2 + b_4 J_D^2 + b_5 Fr J_D \quad (3.62)$$

where the set of coefficients b_0, \dots, b_5 are defined separately for contraction and expansion, and are of the form $b_i = k_{i,1} B + k_{i,2}$. The fitted estimates are given in Table 3.9.

Figure 3.45 shows data estimated using Eq. 3.62 for expansions and contractions plotted on a common scale against the original experimental values derived from the University of Birmingham laboratory measurements and HEC (1995) two dimensional numerical models. The AES model is shown to approximate the experimental data over the range of flow conditions and scales described in the preceding discussion with little evidence of bias.

ii Transition energy loss coefficients

The transition loss coefficient introduced in Eq. 3.57 is defined as $C = C_C$ for contraction reaches and $C = C_E$ for expansion reaches. The transition coefficients scale the energy losses associated with changes in velocity head over the transition reaches. Their effect is to modify the afflux resulting from the backwater profile calculation through a bridge structure. Figure 3.46 shows comparisons between measured and modelled afflux for the University of Birmingham laboratory experiments that had subcritical flows below soffit level. In Figure 3.46(a) the afflux has been modelled using the standard step backwater method with the transition coefficients C_C and C_E both set to zero. It can be seen that the afflux is systematically underestimated by the model, particularly for the higher flows where the velocity heads in Eq. 3.57 would become

Table 3.9 Polynomial coefficients for AES transition lengths.

Coefficient	Contraction		Expansion	
	$k_1(m^{-1})$	k_2	$k_1(m^{-1})$	k_2
b_0	0.0190	-8.9	0.0712	-26.2
b_1	-0.2130	50.8	-0.2940	197.8
b_2	0.1900	26.6	0.0569	15.2
b_3	0.5650	-36.2	-0.8720	-22.2
b_4	-0.1700	-20.4	0.0170	9.9
b_5	0.4180	-39.1	0.3940	-2.8

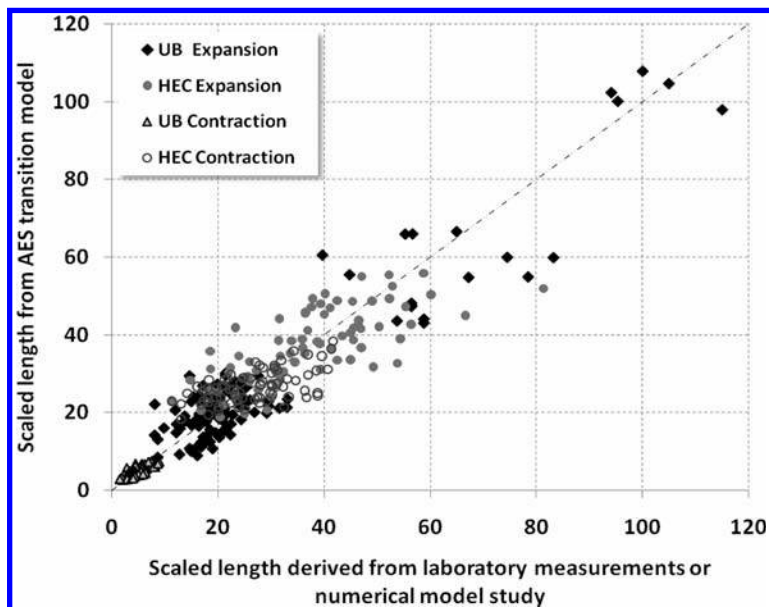


Figure 3.45 Dimensionless transition lengths (scaled by the downstream unobstructed normal depth) showing values estimated from the AES transition length model (Eq. 3.62) plotted against experimental data from University of Birmingham (UB) laboratory flume measurements and HEC (1995) field scale two dimensional numerical modelling.

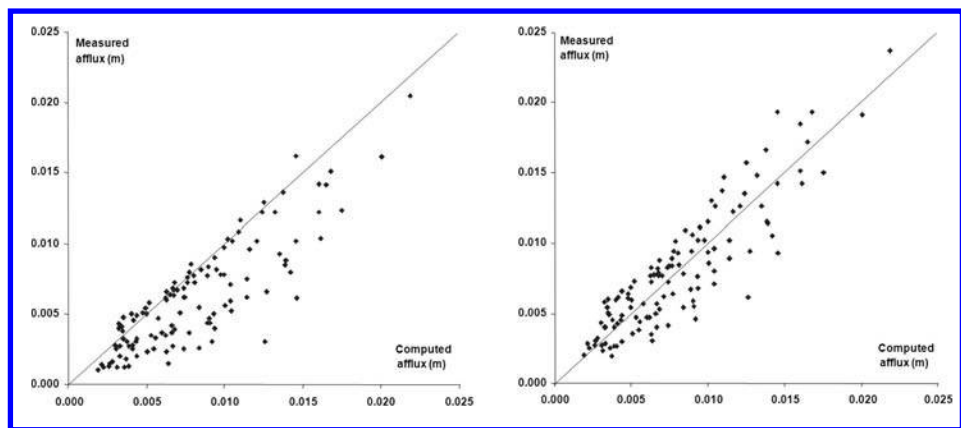


Figure 3.46 Comparison of measured and modelled afflux before (a, left panel) and after (b, right panel) calibration of laboratory scale transition energy loss coefficients.

more important. Correction of this bias therefore provides a convenient method for calibration of the transition energy loss coefficients. An approximate calibration of $C_C = C_E = 0.1$ was adopted, as shown in Figure 3.46(b), giving an ensemble parity of 0.98 for the afflux data with coefficient of determination of 0.80.

When supercritical flow occurs within the AES, the flow depth is set equal to critical depth. Critical flow first occurs at a bridge exit section, if both entry and exit sections have nearly equal conveyance. Upstream levels are solved using the critical condition in effect as a new boundary condition. Defaulting to critical depth at the bridge section increases the water level. The data used for calibration of transition losses did not include cases where critical flow conditions were observed. However, the University of Birmingham bridge data contains 26 critical flow profiles. When the associated afflux is computed using AES with the transition energy losses at the calibrated values for subcritical flow then there is an approximately 10% error in the computed afflux. When the transition energy losses are neglected ($C_C = C_E = 0$) then the results for critical flows agree closely with the experimental measurements, with approximately a 2% bias and a coefficient of determination of 0.9.

The energy loss coefficients were also calibrated using the field scale HEC (1995) data, and the following mean values with their 95% confidence limits were obtained:

$$C_C = 0.12 \pm 0.01 \quad \text{and} \quad C_E = 0.027 \pm 0.03 \quad (3.63)$$

These values were rounded to $C_C = 0.1$ and $C_E = 0.3$ for subcritical flows beneath soffit level. The calibrated field scale value for the contraction energy loss coefficient is consistent with the laboratory scale data, whilst the expansion loss appears to be greater.

The similarity analysis of transition reach lengths would suggest that the transition energy loss coefficients might also be related to undisturbed Froude Number, blockage ratio and the floodplain scale but it is difficult to establish a useful relationship, which is also as reported by HEC (1995). For the available laboratory and field scale data, the blockage ratio varies in the range 0.1 to 0.9, undisturbed Froude Number from about 0.05 to 0.7 and the floodplain width from ~ 1 m to ~ 305 m. The mean of the floodplain width values, $B^* = 153$ m, was used as a convenient reference scale and the resulting dimensionless floodplain scale variable B/B^* varies from about 0.01 to 2.0. The variation in floodplain scale is therefore significant in the functional relationship and so C_E is interpolated in the AES as a linear function of floodplain scale between a minimum of $C_E = 0.1$, calibrated using laboratory data, up to the maximum of $C_E = 0.3$, calibrated using field scale data from numerical modeling, such that

$$C_E = \min \left\{ 0.3, 0.1 \frac{B}{B^*} + 0.1 \right\} \quad (3.64)$$

The contraction loss coefficient was set to $C_C = 0.1$, which was found to be a reasonable value for both laboratory and field scale data. For supercritical flow $C_C = C_E = 0$, as determined for the 26 critical flow profiles observed in the laboratory measurements.

Culvert energy losses

The computation of a water surface profile for a culvert structure in the AES is made in a similar way to that for a bridge structure. Firstly, the rating curves for the four

surveyed river sections (S1, S2, S3 and S4) are estimated using the divided channel method. The culvert geometry is then added to the upstream and downstream structure sections (S2 and S3) and conveyance rating curves are computed using the same principles as for a bridge, including extension of the conveyance over the culvert road level, and the indeterminate rating between culvert soffit and road level. The standard step water surface profile method is then applied as for a bridge, taking the downstream boundary condition from S1.

For a culvert there are energy losses associated with the inlet and outlet structures, which, in the AES, are applied to the corresponding transition reaches in the backwater calculation. The inlet structure energy losses are calculated using the design formulae and coefficients given in CIRIA (1997) for certain standard culvert inlet configurations. In the CIRIA guide, the inlet control design coefficients and head loss coefficient depend on the shape, type, material and edge form of the inlet structure. [Figure 3.47](#) illustrates the choices available in the AES.

The culvert energy loss variables are defined in [Figure 3.48](#) and the calculation algorithm is summarised in [Table 3.10](#). The AES omits some details of the CIRIA (1997) and FHWA (2001) methods for simplicity, notably energy losses for bends and junctions. Culverts that contain complex features such as junctions and significant changes in cross section should be analysed using more sophisticated modelling software. However, the AES does automatically handle the full range of flow conditions from subcritical flow through the barrel to combined pressure and overtopping flow.

Integration with the CES backwater model

In the combined CES-AES software, the AES appears as a bridge or culvert placed ‘within’ a channel backwater profile between two CES cross sections, which can

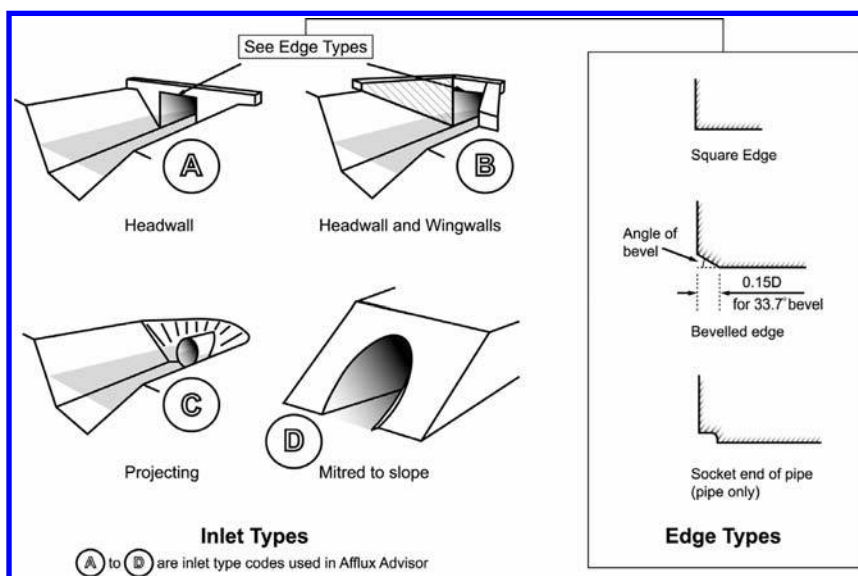
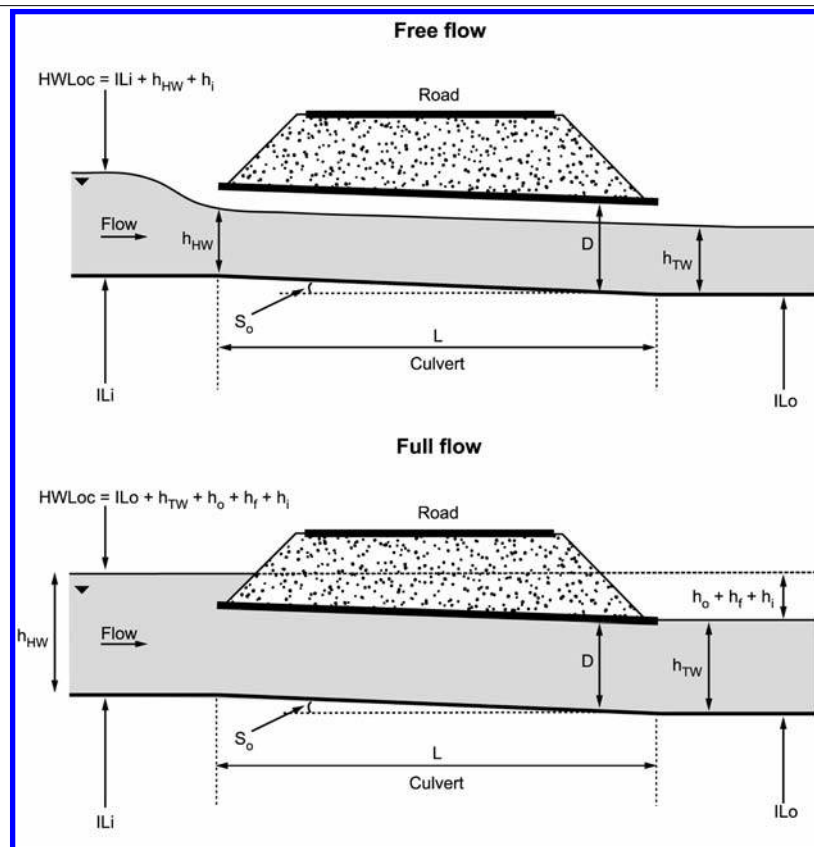


Figure 3.47 Inlet and edge types for culverts (after CIRIA, 1997).



HWLoc	Headwater elevation (outlet control)	h_{TW}	Tailwater depth
h_{HW}	Headwater depth	ILo	Invert elevation at barrel outlet
ILi	Invert elevation at barrel inlet	h_i	Energy loss at culvert inlet
D	Barrel depth	h_f	Friction loss in barrel for full flow
L	Barrel length	h_o	Energy loss at culvert outlet
S_o	Barrel bed slope		

Figure 3.48 Culvert analysis variables used in the CIRIA (1997) and AES methods.

be called CESd for the downstream section and CESu for the upstream section (Figure 3.49). If the CESu and CESd cross sections were located at the appropriate transition reach lengths along the stream, it would be possible simply to use the CES backwater depth at CESd as the downstream boundary condition for the AES model of the bridge or culvert. In the same way, it would then be simple to use the AES water surface results upstream of the bridge as a new downstream boundary for the remaining CES water surface profile calculation.

Table 3.10 Summary of the AES algorithm for culvert hydraulics, based on CIRIA (1997).

Symbol	Free flow	Full flow
<i>Inlet control</i>		
HWLic	An inlet structure design table is used to calculate the headwater elevation under inlet control.	
<i>Outlet control</i>		
h_{TW}	Tailwater depth (h_{TW}) is the maximum of the downstream depth or critical depth for the culvert, h_c .	If the downstream depth (h_{TW}) is less than $(h_c + D)/2$ then use FHWA (2001) approximate backwater assumption, $h_{TW} = (h_c + D)/2$.
h_o	The outlet head loss is calculated from the difference in velocity heads between the culvert barrel and the downstream channel.	
h_i	An inlet structure design Table is used to calculate the inlet head loss.	
h_{HW}	Water depth just inside the culvert barrel entrance is calculated by backwater analysis.	The upstream depth is determined from the inlet, friction and outlet head losses. The friction head loss (h_f) is calculated using Manning's equation.
HWLoc	The headwater elevation under outlet control is calculated as: $\text{HWLoc} = \text{ILo} + h_{TW} + h_o + h_i$	The headwater elevation under outlet control is calculated as: $\text{HWLoc} = \text{ILo} + h_{TW} + h_o + h_f + h_i$

1 If HWLoc > HWLic then use outlet control, else use inlet control. Headwater level is the maximum of HWLic or HWLoc.

2 Inlet control is computed for the entire discharge rating.

3 For inlet control, if the discharge ratio value $1.811Q/AD^{0.5}$ is between 3.5 and 4, then the HWLoc rating is linearly interpolated.

4 Free flow begins at the lowest flow elevation and ends when the flow depth in the barrel is greater than the soffit depth at the culvert inlet.

5 When the head water level is above the road level, the flow is computed sequentially as a modular weir, submerged weir and a drowned weir, each with the appropriate inlet or outlet controlled culvert flow. The weir elevation is computed iteratively since flow continues through the culvert.

6 Energy losses due to flow at culvert bends and at trash screens are omitted for simplicity.

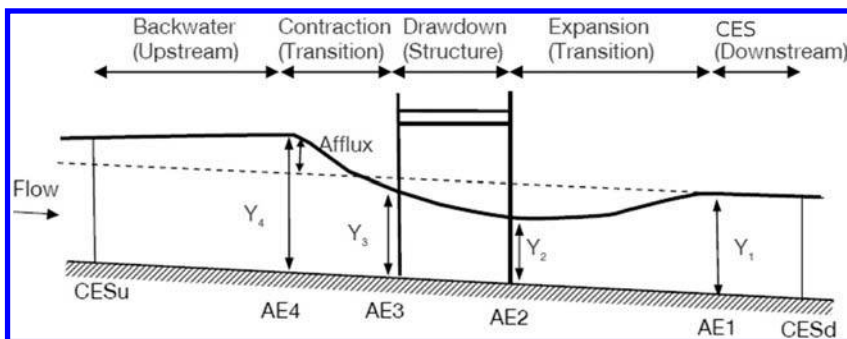


Figure 3.49 Placement of AES calculations within a CES backwater profile.

However, it is unlikely that surveyed channel cross sections will generally be available at the transition lengths (especially because those lengths are themselves a function of the flow conditions, as implied by the presence of the Froude Number in Eq. 3.62, and hence are not fixed). When the surveyed CESu and CESd sections are located

beyond the lengths of the AES transition reaches then the CES-AES software introduces interpolated sections in the AES at the transition lengths. The latter are computed by linear interpolation of the cross section geometry between the nearest surveyed cross sections to the structure. If the transition lengths for subcritical sub-soffit flow exceed the distance to the nearest CES cross section or if the structure is drowned then the software currently defaults to use the actual CES_u and CES_d cross section locations.

3.3 DEALING WITH UNCERTAINTY

3.3.1 Introduction to uncertainty

Uncertainty analysis is required in order to understand the implications for decision makers of limited data, model uncertainties, changes in the flooding system over the long term, incommensurate scales of appraisal and potentially conflicting decision objectives (see Hall *et al.*, 2008; Hall & Solomatine, 2008).

Flood level predictions based on existing hydrodynamic modelling software (e.g. ISIS, HEC-RAS, InfoWorks RS) provide no indication of the associated uncertainty. In fact, in practice uncertainty analysis and the use of the results are not widespread as Hall *et al.* (2008) points out:

- There is a bewildering proliferation of uncertainty methods published in the academic literature.
- Uncertainty analysis takes time, so adds to the cost of risk analysis, options appraisal and design studies.
- The data necessary for quantified uncertainty analysis are not always available, so new data collection campaigns (perhaps including time-consuming expert elicitation exercises) may need to be commissioned.
- The additional requirements for analysis and computation are rapidly being (more than) compensated for by the availability of enhanced computer processing power. However, computer processing power is only part of the solution, which also requires a step change in the approach to managing data and integrating the software for uncertainty calculations.

The uncertainty in water level prediction for channels arises from many factors including approximations to the fluid mechanics, natural variability in river resistance and the use of judgement or experience in applying models. These all produce differences between the assessment of river channel capacity and its “true” value.

The potential economic benefits of the use of improved methods for conveyance estimation will come from altering design, operation and maintenance practice as the degree of uncertainty is reduced. Strategic decisions made early in the project life cycle can have far reaching consequences and it is at this early stage that uncertainties in information and data are greatest. There is a close relationship between uncertainty and risk in that the greater the uncertainty the greater the probability of the project or maintenance activity not achieving its objective. This is linked to the confidence on the performance of the scheme or process to meet its intended objectives. Thus, optimisation of performance and the confidence with which performance can be delivered are linked inexorably with understanding and controlling uncertainty.

3.3.2 Risk, uncertainty, accuracy and error

Uncertainty has always been inherent in flood defence engineering. Traditionally it was treated implicitly through conservative design equations or through rules of thumb, for example by introduction of freeboard allowances. In recent years the emphasis in the UK has moved from Flood Defence to Flood Risk Management. The introduction of risk-based approaches has enabled more rational treatment of natural variability in loads and responses. It also paved the way for more explicit treatment of uncertainty in the evidence that is used to support risk-based decision making (Hall *et al.*, 2008). A difficulty with the language of risk (Defra/EA, 2002; Gouldby *et al.*, 2005) is that it has been developed across a wide range of disciplines and activities. It is common to describe risk as a combination of the chance of a particular event (i.e. a flood), with the impact that the event or hazard would cause if it occurred. Risk therefore has two components: the chance (or *probability*) of an event occurring and the impact (or *consequence*) associated with the event. The consequence of an event may be either desirable or undesirable. Generally, however, flood management is concerned with protecting society and hence a risk is typically concerned with the likelihood of an undesirable consequence and our ability to manage or prevent it. In some, but not all cases, therefore a convenient measure of the importance of risk is given by the “equation”:

$$\text{Risk} = \text{Probability} \times \text{Consequence}$$

The *Probability* refers to the chance of a particular consequence occurring. The *Consequence* refers to the undesirable outcome of harm that would arise should a risk be realized.

One system model that can be used to identify and assess risks is based upon the causative sequence of sources, pathways and receptors (Sayers *et al.*, 2002; Samuels, 2006). For a risk to arise, there must be a hazard that consists of a source or initiator event (e.g. high rainfall); a receptor (e.g. flood plain properties); and a pathway between the source and receptor (i.e. flood routes including defences, overland flow or landslide). Thus, the source describes the origin of the hazard in terms of the forcing or loading on the system. The source will be attributed quantitative values such as millimetres of rainfall, river discharge or be described in terms of probability of occurrence or exceedance. The receptor is the asset, individual, community, business or habitat etc. that could experience harm if affected by hazard. Whilst contained, the hazard does no damage, for harm and damage to occur a pathway is needed to transmit the source of the hazard to the receptor. However, the identification of a hazard does mean that there is a possibility of harm occurring. Once the receptor has experienced the hazard then adverse consequences occur. For practical analysis it must be recognized that there are likely to be multiple sources, pathways and receptors.

Evaluating risks involves identifying the hazards associated with the risk issue, i.e. what in a particular situation could cause harm or damage, and then assessing the likelihood that harm will actually be experienced by a particular population and what the consequences would be. Thus to evaluate the risk, it is necessary to consider the three generic components:

- the nature and probability of the hazard;

- the degree of exposure of people and assets to the hazard;
- the vulnerability of the people, assets etc to damage should the hazard be realised.

In describing each of these there is likely to be an element of imprecision depending upon the data available and methods employed. For further details on risk and uncertainty in flood management, see Samuels (2006).

Most engineering “failures” (such as those leading to flooding) arise from a complex and often unique combination of events and thus statistical information on their probability and consequence may be scarce or unavailable. Under these circumstances the practitioner has to resort to models and expert judgement. Models will inevitably be an incomplete representation of real life and so will generate results, which are uncertain. Similarly, human expert judgement is subjective and thus uncertain as it is based on mental models and personal experience, understanding and belief about a situation. So in practice every measure of risk has uncertainty associated with it. Uncertainty arises mainly from lack of knowledge or of ability to measure or to calculate and gives rise to potential differences between assessment of some factor and its “true” value. Understanding this uncertainty within our predictions and decisions is at the heart of understanding risk. Within uncertainty it is possible to identify:

- knowledge uncertainty from lack of knowledge of the behaviour of the physical world;
- natural variability from the inherent variability of the real world; and
- decision uncertainty from the complexity of social and organisational values and objectives.

However, this classification is not rigid or unique. For example, uncertainty on weather or climate will be taken as “natural variability” within flood risk management but as “knowledge uncertainty” in the context of climate simulation. It is helpful also to consider the differences between accuracy, error and uncertainty. Accuracy and error differ from uncertainty as defined above but limitations in accuracy or the possibility for human error will contribute to the overall uncertainty.

- Accuracy deals with the precision to which measurement or calculation is carried out; potentially, accuracy can be improved by better technology.
- Errors are mistaken calculations or measurements with quantifiable and predictable differences.

3.3.3 Components of uncertainty in the CES

Principal influences

The uncertainties in conveyance estimation are principally due to natural variability and knowledge uncertainty. Two contributions are normally recognised in knowledge uncertainty; these are:

- Process model uncertainty in any deterministic approach used in the assessment;
- Statistical uncertainty arising from the selection and fitting of statistical distributions and parameters from data within the assessment.

In the CES no use is made of statistical modelling and so issues of statistical uncertainty do not arise. However, in the overall estimation of flood risk there will be an important component of statistical uncertainty arising from any hydrological estimation procedures for flow.

The important components of process model uncertainty in the estimation of conveyance are:

- process model uncertainty arising from the selection and approximation of physical processes and from parameterisation made in the definition of conveyance;
- representation of topography through the density of discrete survey points and interpolation rules between them, i.e. the difference between the profile of the river and of the physical features on the flood plain as represented in the calculations and the river in “real” life;
- uncertainty related to data accuracy from limitations of the survey methods used;
- uncertainties arising from parameter estimation – particularly the experience and expertise of the modellers who set up and calibrate computational models of river flows; and
- uncertainties from the model calculation methods, approximations and rules. These are the domain of traditional numerical analysis.

The contributions to uncertainty from natural variability include

- seasonality of plant growth from variation in temperature, light and nutrients (and hence resistance of vegetation in channels);
- “memory” in the system e.g. from vegetation or river bed conditions being changed by a flood or through episodic input of sediments into the river system washed off the land surface;
- secondary influences of temperature on water viscosity and hence Reynolds Number and flow and sediment transport capacity of channels.

Importance of contributions

i Physical processes

In the development of the CES, a specific mathematical process model has been adopted based upon the fundamental equations of fluid mechanics with empirical models for the effects of river meanders and the variation of the water depth across the section. This process model accounts for a greater diversity of the physics of the water movement in rivers than the methods previously used in standard modelling packages. Thus it is to be expected that the contribution of the process model uncertainty due to the formulation of the physics of the flow has been reduced.

ii Topographic representation

Previous research on the representation of river topography, Defalque *et al.* (1993) indicated that the uncertainties from this source could be controlled by an adequate frequency of survey information. This is achieved through normal survey specifications (e.g. as undertaken by the Environment Agency of England and Wales).

iii Data accuracy

The development of the CES did not consider specifically the uncertainties from the typical accuracy of the topographic data sources; however, it is expected that these will

be similar to their influence on the uncertainty when using the traditional calculation methods. This has been analysed for the procedures in the US for the prediction of the 100-year flood by Burnham and Davis (1990). With the availability of new data sources (e.g. LiDAR) it would be appropriate to examine the influence of the typical accuracy of these measurements and formulate guidance on the density of the data grid on the consequent flood levels.

iv Model parameters

The parameters in a model are the “constants”, chosen to represent the chosen context and scenario. In general the following types of parameters can be recognised:

- Exact parameters, which are universal constants, such as the mathematical constant π .
- Fixed parameters, which are well determined by experiment and may be considered exact, such as the acceleration of gravity (approximately 9.81 ms^{-2}).
- A-priori chosen parameters, which are parameters that may be difficult to identify by calibration and are assigned certain values. The values of such parameters are associated with uncertainty that must be estimated on the basis of experience, for example from detailed measurements.
- Calibration parameters, which must be established to represent particular circumstances. They are determined by calibrating model results for historical data on both input and output. Parameters are generally chosen to minimise the difference between model results and measurement for the same event. The parameter set for a “satisfactory” calibration is unlikely to be unique.

The CES contains several a-priori chosen parameters in the model of velocity variation across the river channel although there is an option which allows the “expert” user to vary these ([Chapter 5](#)). The CES also contains calibration parameters – these are the values of river resistance which are either determined by systematic variation to match observed flow conditions or estimated from the Roughness Advisor (i.e. calibrated against vegetation type or spatial location).

v Calculation methods

The CES contains several numerical methods to generate (approximate) solutions of the mathematical model for any water depth or flow rate. These include an automatic division of the cross-section into a computational grid which is sufficiently fine to ensure that the uncertainty associated with the differences between the numerical solution and the “true” solution of the mathematical model are much smaller than the uncertainties in the selection of the model parameters.

vi Natural variability

The Roughness Advisor includes some account of the typical seasonal variation in resistance due to the growth and decay of vegetation. This generic information has been established from a variety of sources and includes an element of professional judgement. There is no guarantee that any particular year will match the average but the user can explore scenarios of advancing or delaying the seasonal growth-decay cycle and include the effects of river “maintenance” activities. No information can be given on the probability of the seasonality.

Other factors classified as natural variability are not incorporated in the standard version of the CES; however, there is an “expert” option for researchers to explore the effects of temperature in experimental facilities. Thus the CES has not reduced the uncertainties in conveyance arising from the erosion, transport or deposition of sediments, system “memory” or temperature.

3.3.4 Representation and assessment of uncertainty

There are many approaches to quantifying and assessing uncertainty. An important distinction is the difference between the gross uncertainties associated with unknowns (e.g. climate, socio-economic growth) and the lesser uncertainties associated with method, model and data. The former are typically handled through scenario analysis to assess the performance of options in terms of robustness, adaptability and sustainability (e.g. Evans *et al.*, 2004; IPCC 2001; Hine & Hall, 2007; de Bruijn *et al.*, 2008) whereas the latter are dealt with through interval probability theory, combined distribution analysis, Monte Carlo or variance-based sensitivity analysis (e.g. see Gouldby & Kingston (2007) for an approach in the context of flood risk). For the case of the CES, only a sub-set of the uncertainties are under consideration rather than the interpretation relying on defined probabilities for all parameters as required for a probabilistic approach. This is appropriate as the outputs are not being used for a detailed economic appraisal but are more likely to inform management practice (e.g. [Table 3.11](#)). More detailed approaches such as Monte Carlo are data hungry and computationally expensive.

A key decision in developing advice and estimates of uncertainty was on how the information should be presented. Several approaches are possible as described above but some require considerable additional information and analysis to generate the results. Thus an appropriate starting point was to consider the users of the CES and how they might incorporate information on uncertainty into their decisions. This led to some requirements of the method in practice, it should:

- express uncertainty in water level;
- link to and inform other risk approaches;
- be understandable to the user to facilitate better, more informed decisions in the situations they are responsible for;
- be as simple as possible in presentation;
- not require significant computational resources;
- ideally not require any additional input data; and
- be credible by being based on existing scientific methods for uncertainty where possible.

The potential direct and indirect users of the CES information have different needs for information on uncertainty in the decisions and plans they need to make. [Table 3.11](#) provides an indication of the potential use of the information.

In terms of presenting quantitative information on uncertainty the important choices are whether to:

- recommend the use of Monte-Carlo testing; and/or
- assign probabilities to the information given uncertainty.

It was decided not to recommend either of these because making statements on probability would give an appearance of confidence in the quantification of information which is partly subjective in origin. In addition:

- Monte Carlo testing requires considerable computation, particularly if the testing is embedded in a large flow simulation model;
- the underlying information is not available for the probability distribution of river resistance values which is required by Monte Carlo testing;
- the information on river resistance is not homogeneous in origin;
- the effects of residual process model uncertainties cannot be quantified in any probabilistic manner; and
- some information in the Roughness Advisor came from expert opinion rather than measurement.

However, it is important that the CES includes some quantitative statement on the effects of uncertainty even if probability (or likelihood or frequency) cannot be given. This has been achieved by illustrating the uncertainty in the relationship between water level and discharge through presenting a central estimate and credible upper and lower cases of water level for a given flow rate. The stage discharge curve is usually expected to lie within the upper and lower scenario bands, which may not be symmetrical about the mean. These bands should not be interpreted as minimum/maximum envelopes, but rather ‘soft’ boundaries within which the ‘true’ value is likely to occur.

The central estimate represents the “best” assessment without any particular definition of “best”. It is important to note that the upper and lower cases.

- are not necessarily equally distributed about the central estimate (i.e. not just $\pm x\%$);
- are not upper or lower bounds (i.e. it is possible for some real cases to lie outside the range);
- are not for any specific confidence limits (e.g. $\pm 95\%$); and
- are not simply related to the standard deviation of measured data.

Instead they represent a practical choice of a degree of variability to include in the analysis for flood risk management applications, based upon the range of values found in the compilation of data on river roughness. The concentration of the scenarios on the influence of uncertainty in river roughness is justified in terms of the sensitivity analysis undertaken in the testing phase of the CES research.

The dominant factor to be used in the analysis of the estimation of conveyance is the unit roughness as distributed across the section. A thorough review of the sensitivity of water level, to both the a-priori chosen and calibration parameters, identified roughness as having the most significant contribution to uncertainty in conveyance (Khatibi *et al.*, 1997; Latapie, 2003; Mc Gahey, 2006). The parameters considered were roughness, elevation of the floodplain and main channel, cross-chainage, planform sinuosity, temperature, longitudinal bed-slope and position of top-of-bank markers. The uncertainty of the input survey data depends largely on the method of measurement. The a-priori chosen parameters were the dimensionless eddy viscosity λ , the secondary flow

Table 3.11 Summary of uncertainty users, consequences and potential use of information.

User community	Consequences of uncertainty	Uncertainty information and use	Importance	Suitable presentation of uncertainty
Scheme design	Under capacity of defences leading to potential failure below the design standard or over capacity potentially leading to morphological problems or lower economic return than planned; Over estimation of capacity of defences leading to lack of implementation schemes due to excessive cost.	Change in water level for given flow rate (moving towards probabilistic optimisation for describing uncertainty). Undertake a sensitivity analyses and add a freeboard to allow for under capacity.	Medium to high	Upper and lower estimates Potentially probabilistic information for a full risk-based design appraisal of a major scheme
Strategic planning	Development of conservative strategies which potentially over compensate on data and method uncertainty rather than focussing on the more gross uncertainties associated with the medium to long-term.	Evaluating and comparing options against criteria such as effectiveness, efficiency, robustness, performance.	High	Upper and lower estimates
Maintenance	Inadequate or excessive maintenance activities, possibly unnecessary disruption to aquatic and riparian habitats or insufficient capacity of the watercourse leading to increased flood risk.	Timing, scheduling and prioritisation of vegetation cutting and dredging.	Low to medium	Upper and lower estimates or nothing
Flood forecasting and warning	Under- (over-) estimation of lead times, inexact inundation extent, and incorrect retention times of floods.	Issue a warning? Operational decisions Implement real-time updating procedures.	Low	Possibly an upper estimate of flood level (and early estimate of arrival time)
Hydrometry	Incorrect discharges with potentially large errors, influences flood forecasting and statistical estimation of flood flows for design, impacts upon cost-benefit assessment and decisions to promote flood defence schemes.	Flow rate for a given depth (influences other stakeholders) Undertake a sensitivity analyses and add a freeboard to allow for under capacity.	Medium to high	Upper/lower estimates Probabilistic
Regulation, insurance	Indicative Flood Mapping (IFM) in error – inadequate tool for planning and information on possible flood risk, inadequate (or over-necessary) development control, loss of professional and public confidence in the operating authorities technical abilities.	Water levels, flood outlines, indicative flood risk mapping.	High	Upper/lower estimates

coefficient Γ and the number of lateral divisions for integration. Other possible sources of uncertainty include non-modelled processes such as form losses, vertical accelerations through sudden local changes in depth, energy dissipation from sediment movement over mobile channel beds and lateral variations in surface water level around bends.

As a pragmatic approach it is recommended that the overall uncertainty in a model application may be estimated from an analysis similar to that of Samuels (1995). The uncertainty in water level Δh_u is given by the “root sum of the squares” of the uncertainties in water level due to different parameters (which may be justified for independent Gaussian processes)

$$\Delta h_u = [\Delta h_r^2 + \Delta h_s^2 + \Delta h_c^2 + \Delta h_{\Delta x}^2 + \Delta h_Q^2 + \dots]^{1/2} \quad (3.65)$$

where the subscripts are:

- r for roughness where little or no calibration data exist
- s for survey data depending upon the method of survey
- c for calibration and extrapolation away from the calibrated state
- Δx for numerical error (grid resolution and physical method)
- Q for flow estimation (outside the use of the CES)
- and ... represents any other commensurate factor.

The assumptions behind this type of formulation are that the sources of uncertainty are mutually independent and that they are roughly normally distributed. The numerical uncertainty $\Delta h_{\Delta x}$ is small (order of magnitude smaller than the other parameters) and well controlled because the grid can be refined to ensure this i.e. cross-section spacing. The flow estimation or uncertainty due to the hydrometric analysis Δh_Q is outside the scope of the CES, but experience shows that this is a key factor in scheme design, contributing about 40% of the overall uncertainty. The remaining factors are thus Δh_r , Δh_s and Δh_c .

Calibration of the flow resistance alters the uncertainty in the estimation of conveyance. Calibration data for flow resistance should supersede the generic, non-site specific information in the Roughness Advisor. Calibration may result in a different value for the central estimate of water level for the calibration flow rate and there is no guarantee that a single roughness value will achieve a perfect calibration for water levels and flow rates observed on different occasions (due to natural variability). However, once the model has been calibrated, Δh_r and Δh_s are likely to decrease, narrowing the range of uncertainty but the exact PDFs for the calibrated and uncalibrated cases will be difficult to determine.

3.4 INTRODUCTION TO THE CES-AES SOFTWARE

Having been introduced to the CES-AES methods, a brief introduction to the software ([Figure 3.50](#)) is provided here. The CES-AES Website (www.river-conveyance.net) is recommended as an up-to-date source of information, software and tutorials.

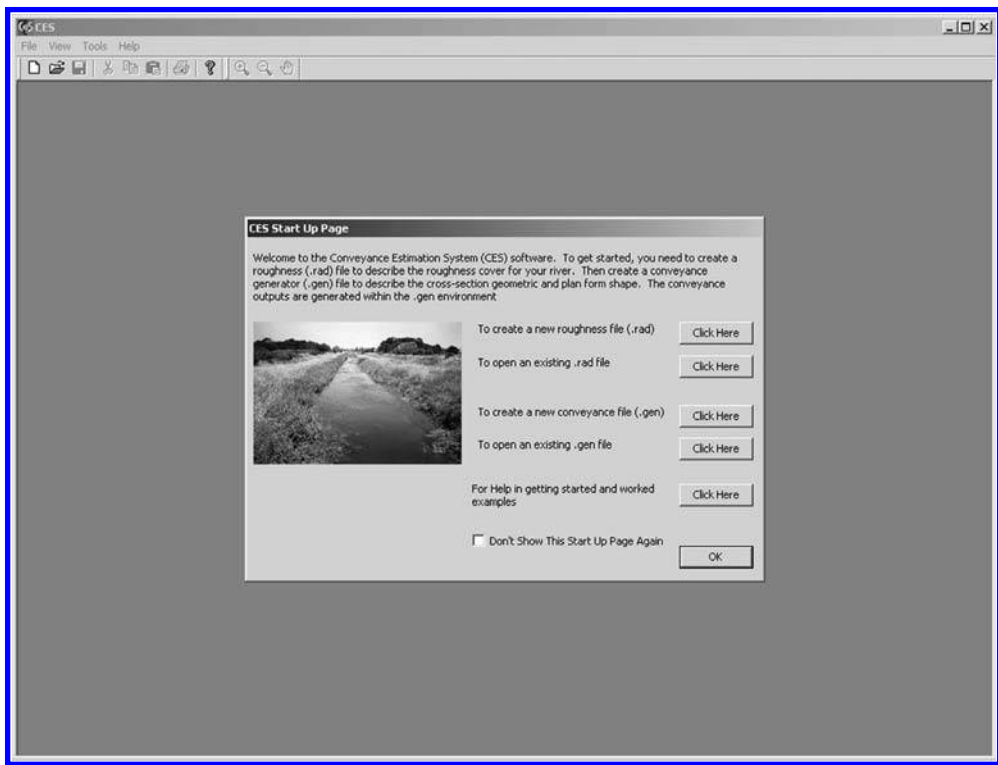


Figure 3.50 CES-AES software introductory page.

The CES-AES software comprises four modules (Figure 3.51):

- *Roughness Advisor* – which is a database of roughness information (Section 3.2.1) including descriptions, photographs and information on seasonal vegetation, cutting and regrowth.
- *Conveyance Generator* – which incorporates the conveyance calculation (Section 3.2.3), giving section-averaged water level (and associated uncertainty, Section 3.4), flow, conveyance, velocity, area, perimeter and Froude and Reynolds Numbers for each flow depth as well as lateral distributions of depth-averaged velocity, boundary shear stress and shear velocity.
- *Backwater Module* – which incorporates the energy-driven backwater calculation (Section 3.2.4) for determining the water surface profile upstream of a control point.
- *Afflux Estimator* – which calculates the afflux upstream of bridges and culverts as well as the energy losses through these structures (Section 3.2.5). It includes arch and beam bridges with up to 20 openings, and pipe, box and arch culverts with up to 10 identical barrels.

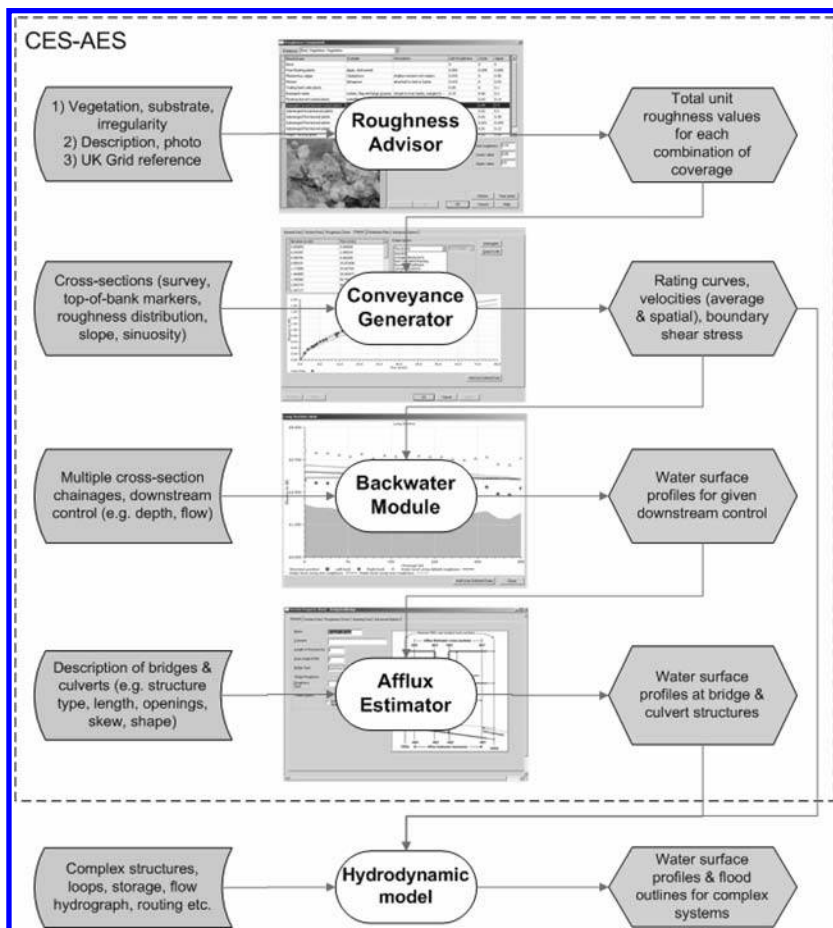


Figure 3.51 Description of CES-AES software user interaction and how it may link to a 1-D hydrodynamic model (See colour plate section).

Despite the complexity of the underlying calculations (Section 3.2), a key feature of the CES-AES tool is that the user input is straightforward and not dissimilar to existing 1-D river modelling software such as InfoWorks RS or HEC-RAS. Figure 3.51 describes the inputs and outputs for each calculation module and how these may feed into a more complex 1-D hydrodynamic model. The CES-AES tool is also embedded within ISIS and InfoWorks RS, providing flexibility to switch between this and the more traditional Manning calculation.

3.4.1 Introduction to the Roughness Advisor

The Roughness Advisor (RA) aids the user in building roughness zones which comprise plan form areas of the flood risk system with uniform unit roughness values

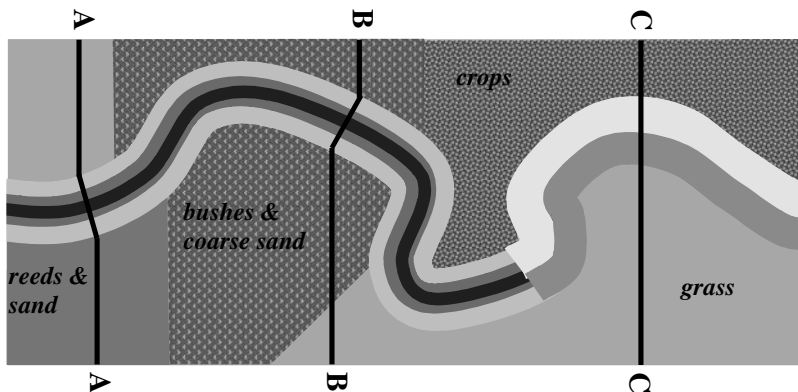


Figure 3.52 Example plan view of roughness zones (See colour plate section).

(Figure 3.52). The system may be divided into as many zones as required to describe the channel and floodplain cover, including within a channel cross-section i.e. non-homogenous roughness. Each zone may have up to three component roughness values i.e. n_{sur} , n_{veg} , and/or n_{irr} and the RA then evaluates the total unit roughness n_l (Section 3.2.1, Eq. 3.1) for each zone.

The RA advice is designed for use in a hierarchical manner based on the level of available information, for example:

- *Extensive information* – the user has been to the site and has access to local survey, bed material, information on plant type and cover, detailed measurements for one or more sections (flow, velocity, water surface profile) etc. Here, the RA is used to determine the initial unit roughness values for each zone and thereafter these values are refined based on calibration with measured data. Figures 3.53 and 3.54 provide examples of the substrate and vegetation advice for clay and emergent broad-leaved rooted plants respectively. Figure 3.55 provides an example of the seasonal variation in roughness for submerged fine-leaved plants.
- *Some information* – the user has access to site descriptions, photographs, approximate longitudinal bed slope, roughness types and limited survey data. Here, the RA is used together with the descriptions and photographic evidence to estimate the unit roughness value for each zone. Where additional information is present, e.g. historic flood outlines, these may be used to improve confidence in the RA values.
- *No information for sites located in the UK* – the user has no information for sites located in the UK and only knows the location of the channel reach from Ordnance Survey maps. Here, the UK grid reference is provided (e.g. Figure 3.56) and the RA provides advice on which aquatic vegetation is most likely to be present.

The RA roughness zones and descriptions are saved in a .RAD roughness files for use within the conveyance calculation.

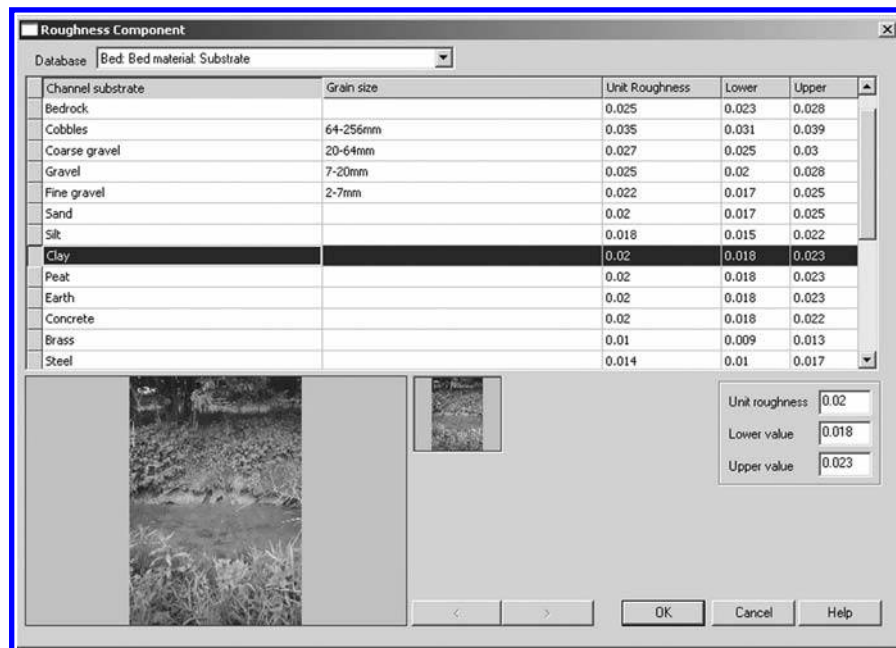


Figure 3.53 Example of RA advice for channel bed substrate (clay) (See colour plate section).

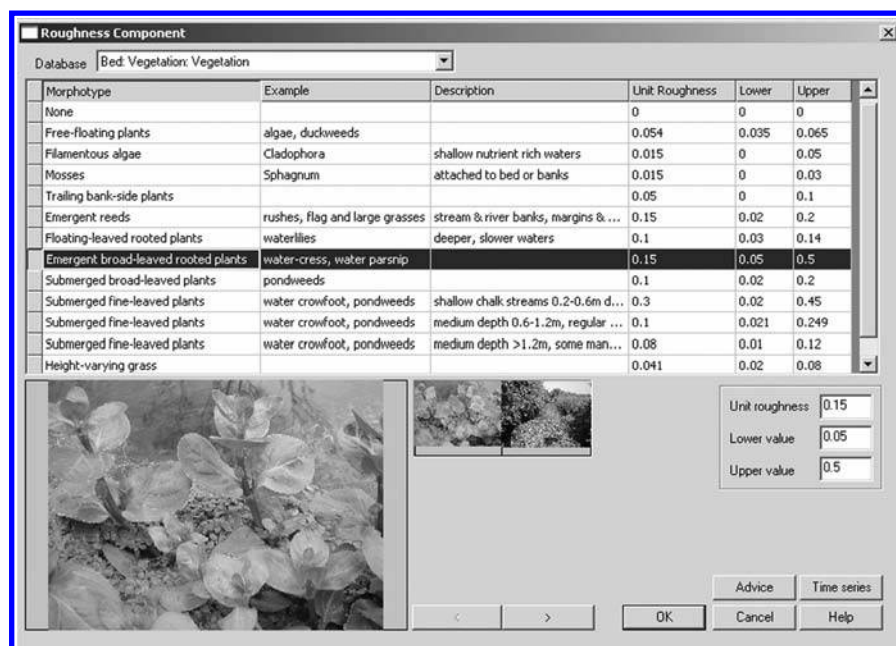


Figure 3.54 Example of RA advice for channel bed aquatic vegetation (emergent broad-leaved plants) (See colour plate section).

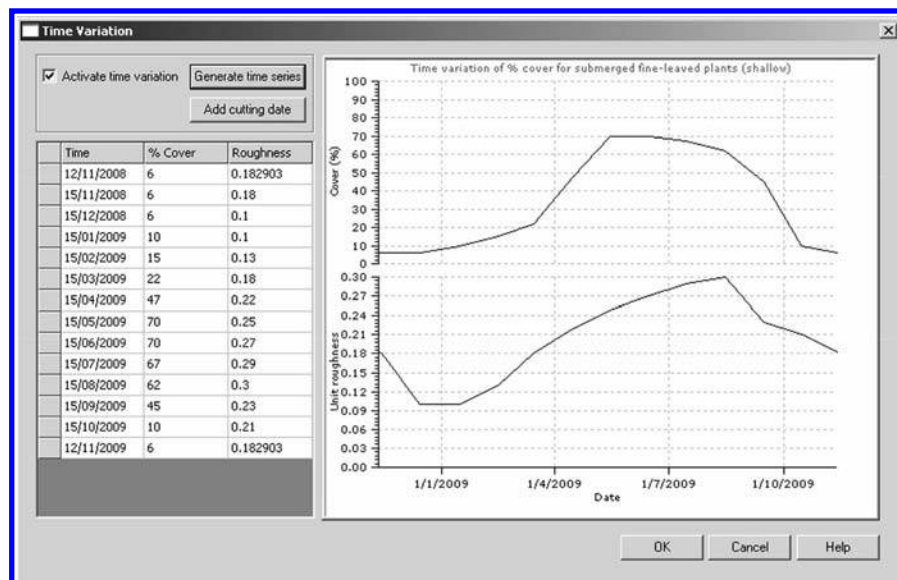


Figure 3.55 Example of RA advice for seasonal variations in vegetation roughness (submerged fine-leaved plants).

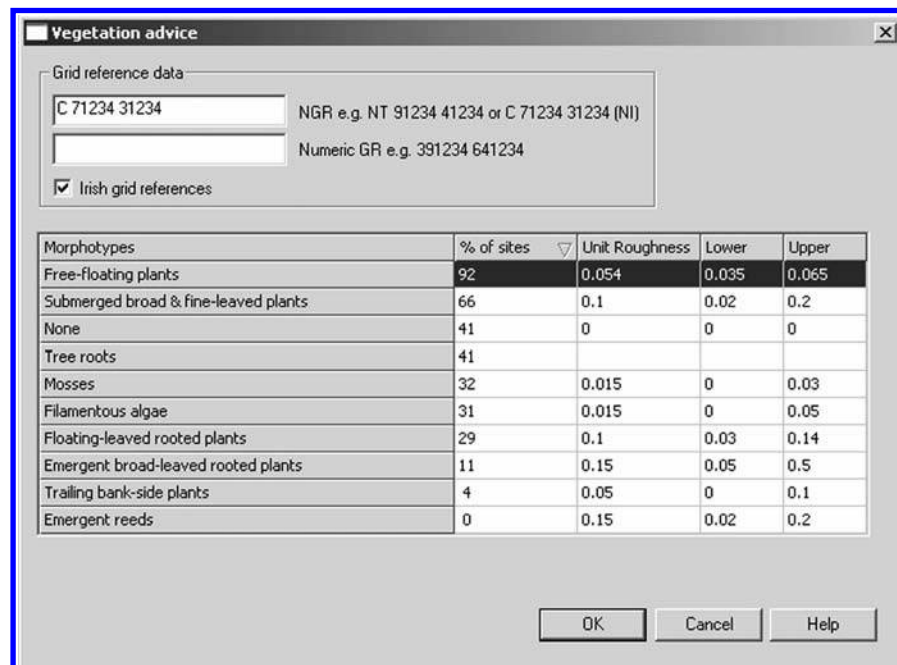


Figure 3.56 Example of RA advice based on River Habitat Survey information for a given UK grid reference.

3.4.2 Introduction to the Conveyance Generator

The Conveyance Generator (CG) aids the user in calculating stage-discharge relationships for individual channel cross-sections. As with traditional 1-D modelling, the user provides information on cross-section survey, top-of-bank positions and longitudinal bed (or water surface) slope (Figure 3.57). The conveyance .GEN file is linked to the relevant roughness .RAD file, enabling the user to match the previously created roughness zones to the cross-section survey (Figure 3.58). For meandering channels, the user indicates the degree of meandering through the plan form sinuosity and assigns inside of bend and outside of bend labels to the top-of-bank markers.

The CG enables the user to explore the various section-averaged (Figure 3.59) and spatially distributed outputs (Figure 3.60) and to compare these to measured data. Outputs include the upper and lower credible scenarios derived from the upper and lower unit roughness values.

The CG allows the user to alter the default calculation parameters through the Advanced Options (Chapter 5), for example, the number of calculation depths, the cross-section discretisation, the value of the main channel lateral eddy viscosity λ_{mc} , etc.

3.4.3 Introduction to the Backwater Module

The Backwater Module (BM) aids the user in calculating the surface water profile upstream of a control i.e. known flow and level. As with 1-D modelling, the user creates

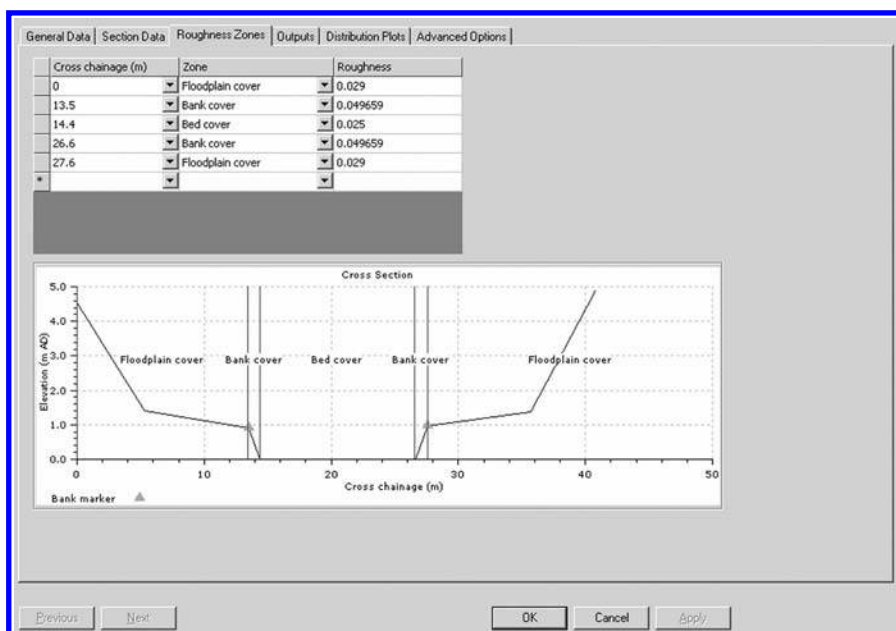


Figure 3.57 Example from Conveyance Generator showing a cross-section with allocated roughness zones for the River Main in at Bridge End Bridge in County Antrim.

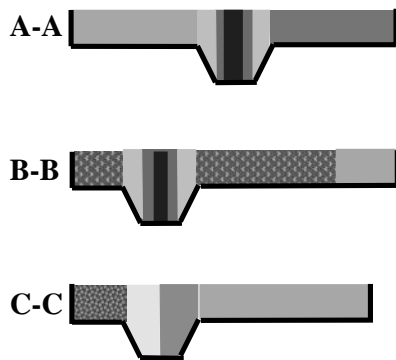


Figure 3.58 Plan form roughness zones from Figure 3.52 allocated to specific cross-sections (See colour plate section).

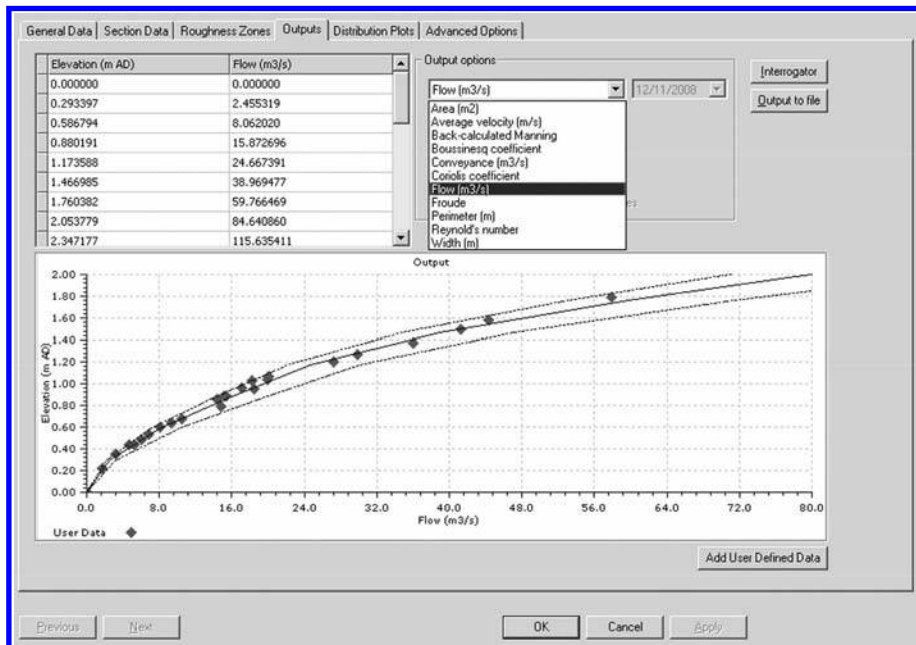


Figure 3.59 Example from Conveyance Generator of predicted flow for the River Main in at Bridge End Bridge in country Antrium and comparison to measured data (red) (See colour plate section).

multiple cross-sections along the channel reach and provides the chainage between these (Figure 3.61). The user provides the downstream depth and the inflow flow to the reach and the backwater is then calculated (Figure 3.62 and 3.63).

The user may impose normal flow conditions at the downstream end. Here, the flow is provided and the corresponding normal flow depth is evaluated at the downstream end and used as the starting point for the backwater calculation.

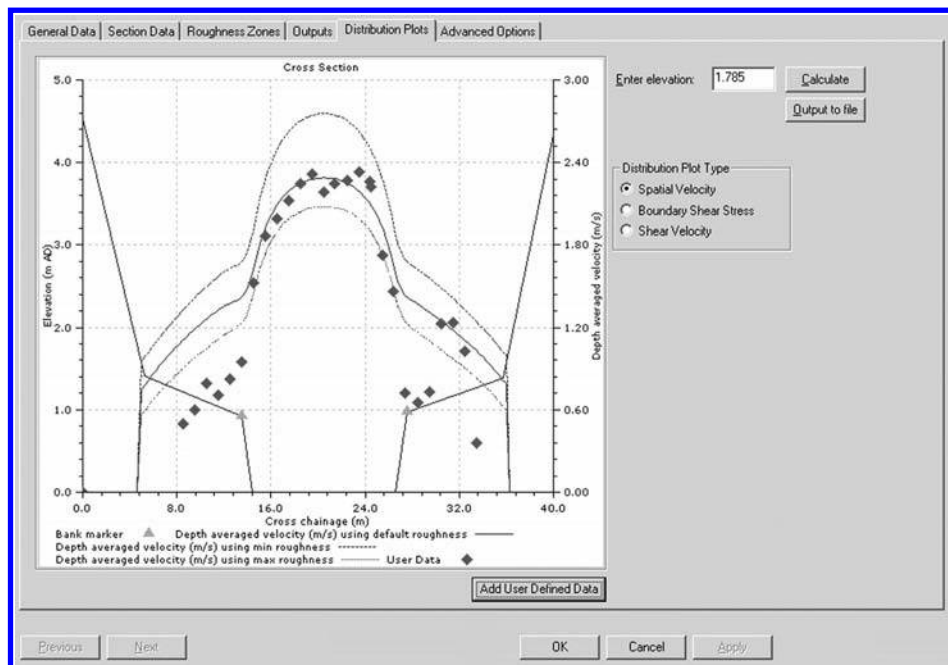


Figure 3.60 Example from Conveyance Generator of predicted velocity for the River Main in at Bridge End Bridge in County Antrim and comparison to measured data (red) (See colour plate section).

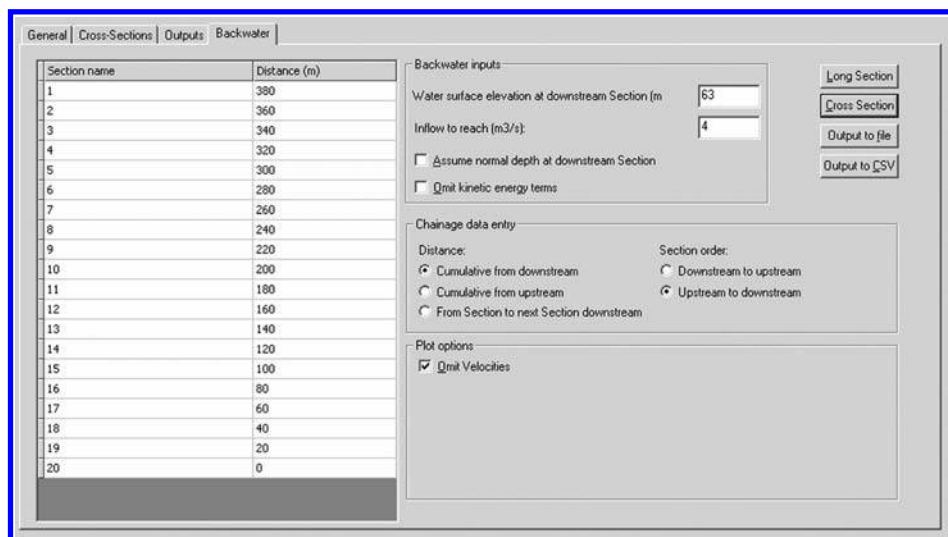


Figure 3.61 Example from Backwater Module showing multiple cross-sections and their associated chainages for the River Blackwater in Hampshire.

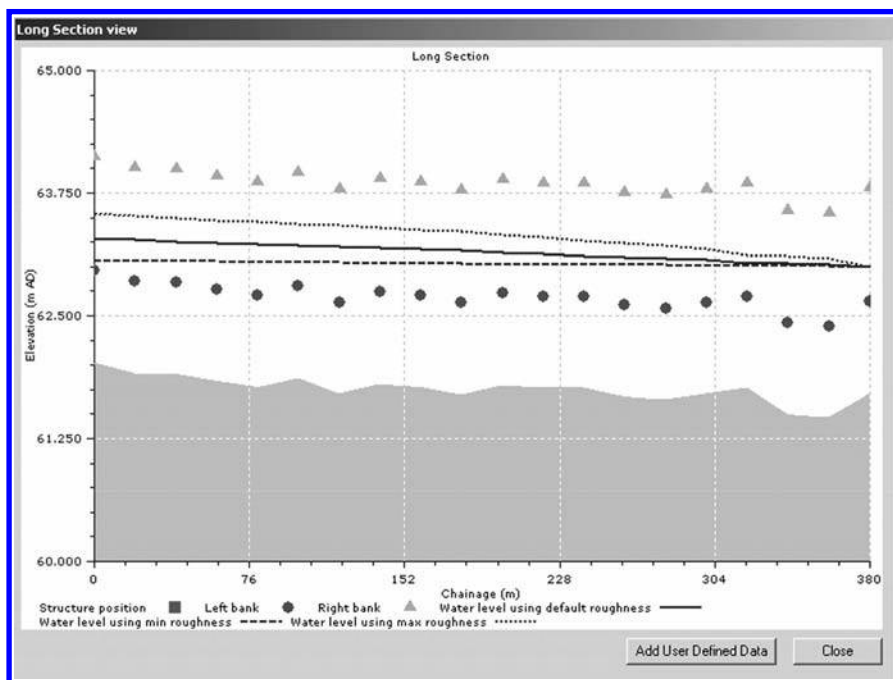


Figure 3.62 Example from Backwater Module showing a long-section with the predicted water surface profiles based on minimum, maximum and expected roughness for the River Blackwater in Hampshire.

The user may elect to omit the velocity term in the energy balance equation (Section 3.2.4). This is a useful alternative for shallow flows, reaches where the velocity changes rapidly along the reach or where the flow in a sub-reach may be supercritical.

3.4.4 Introduction to the Aflux Estimation System

The Aflux Estimator (AE) enables the user to add bridge or culvert units into a CES backwater model. In both cases, the unit appears within the CES software as a single entity containing data entry forms for the channel and structure cross section data at upstream and downstream faces. Figure 3.64 shows opening data for a bridge with identical upstream and downstream faces. Figure 3.65 shows opening data for a culvert. In common with CES river sections, the bridge or culvert data is stored in the CES .GEN file, which is linked to roughness values specified in a .RAD file.

The Aflux Estimator produces section averaged rating curve outputs, in the same way as they are displayed by the Conveyance Generator, for parameters such as conveyance, flow discharge and flow area. Figure 3.66 shows an example conveyance curve for a twin arch bridge. Outputs include upper and lower credible scenarios which are derived from upper and lower roughness ranges for the structure.

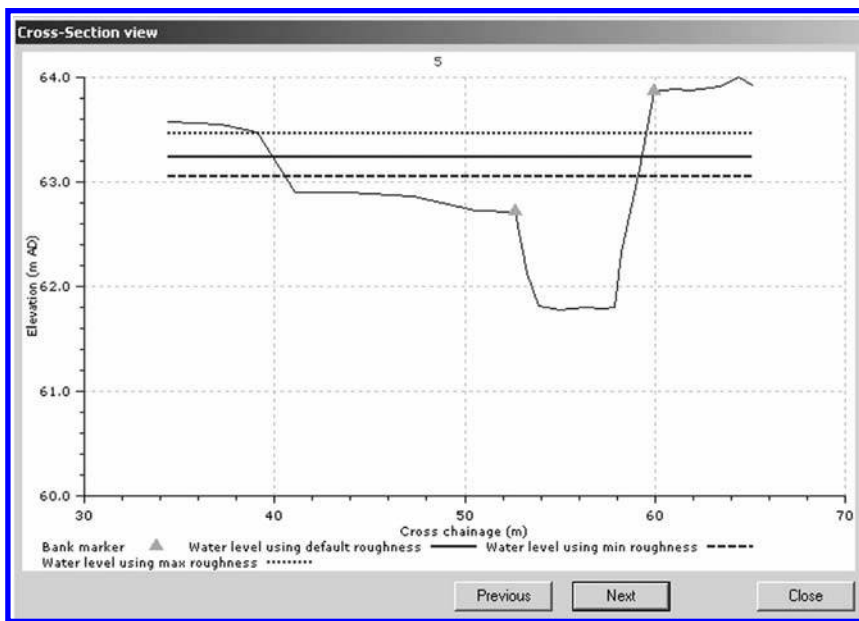


Figure 3.63 Example from Backwater Module showing a long-section with the predicted water surface profiles based on minimum, maximum and expected roughness for the River Blackwater in Hampshire.

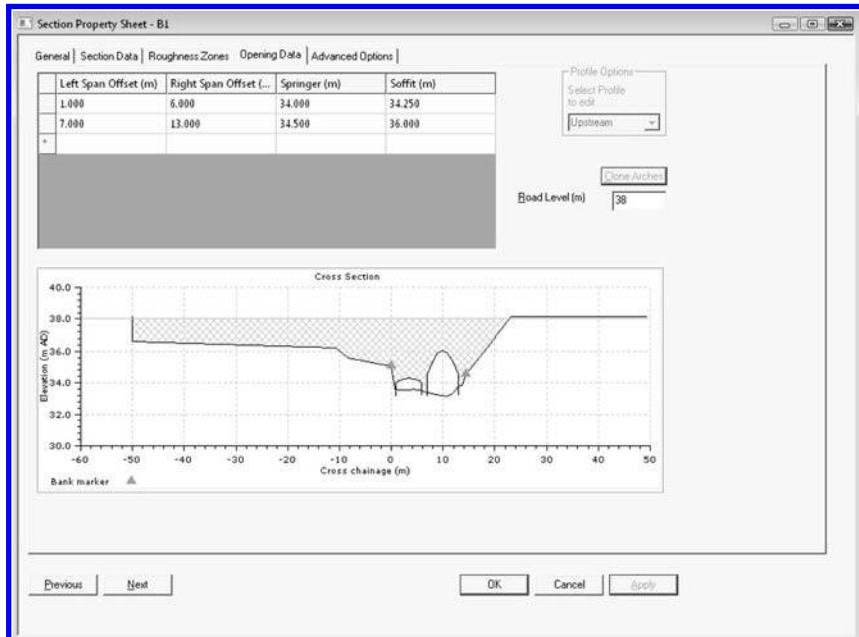


Figure 3.64 Bridge section opening data (See colour plate section).

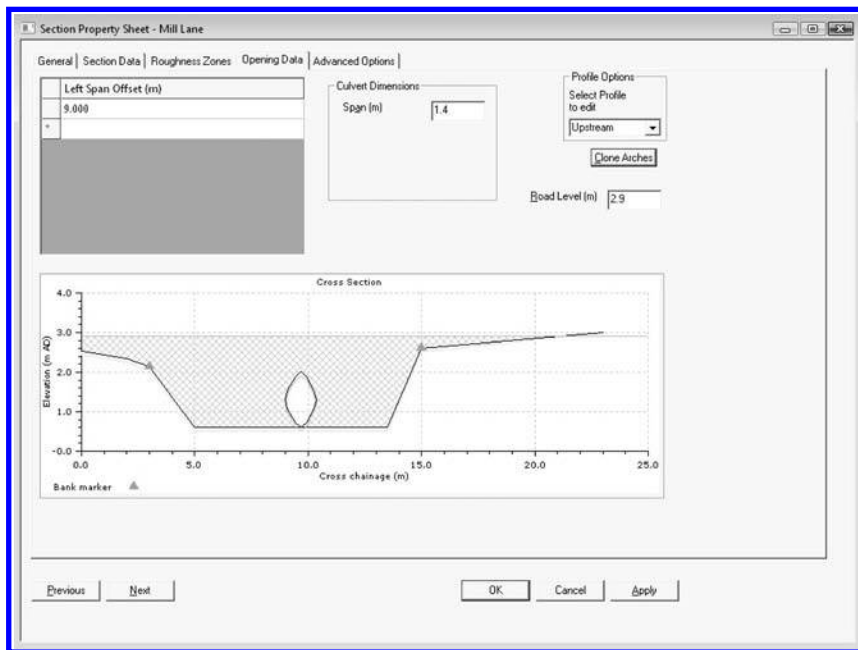


Figure 3.65 Culvert section opening data (See colour plate section).

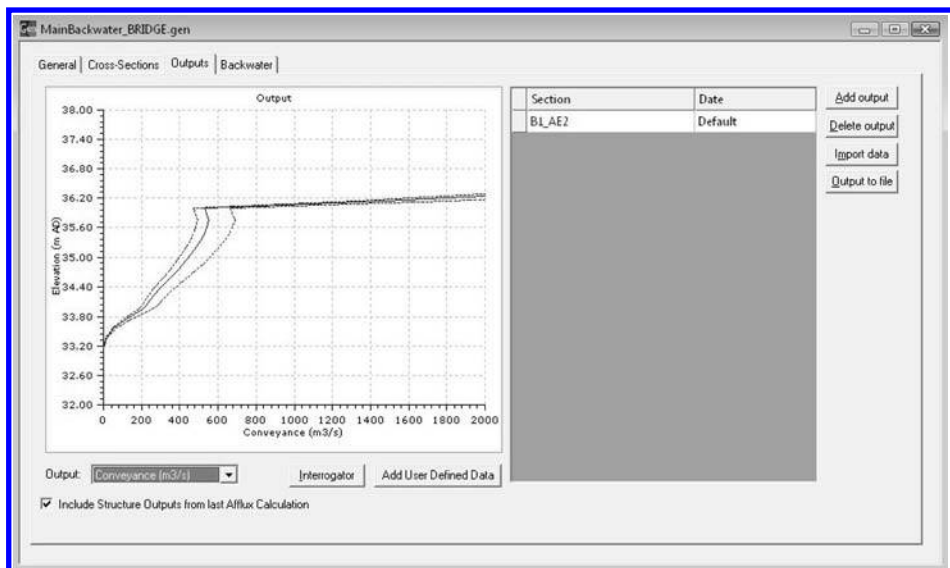


Figure 3.66 Bridge section conveyance curve output (See colour plate section).

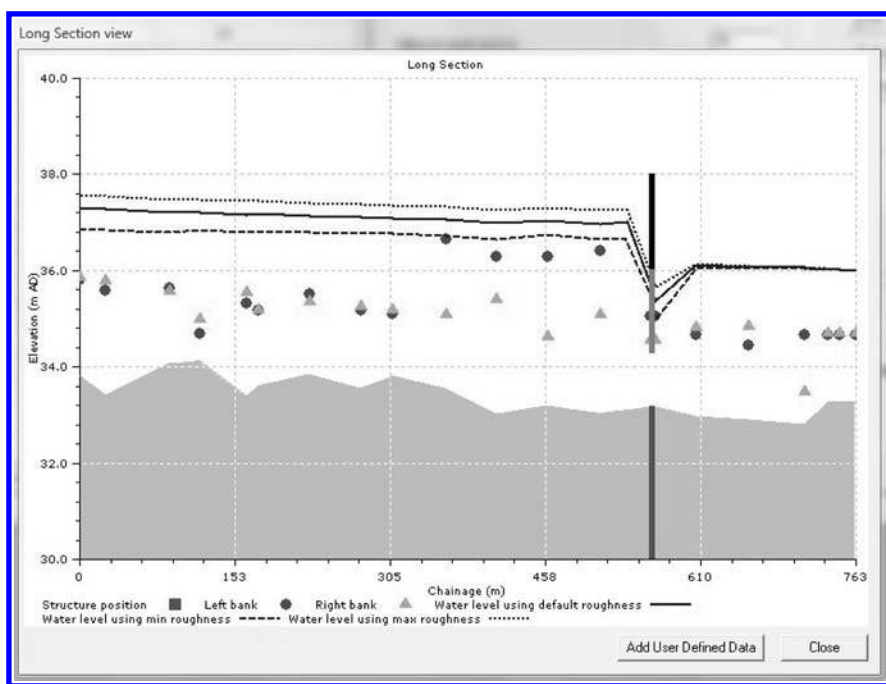


Figure 3.67 Long section backwater reach including bridge or culvert (See colour plate section).

When a backwater profile is computed by the CES-AES software, the Afflux Estimator calculates the water surface upstream of the structure and passes this information into the upstream backwater reach, where it is used in effect as a new boundary condition. Figure 3.67 shows an example where a twin arch bridge has been placed into a reach. The water surface profile dips through the arches and then rises upstream of the structure. The plot displays the profile for the defined roughness conditions, plus bounds based on credible limits for the roughness. Velocity data may also be displayed, along with a hypothetical water surface profile for the undisturbed stream (enabling the afflux to be calculated). The vertical grey bar shows the range of bridge soffit levels and the elevation between the highest soffit and the parapet (or ‘roadway’) level is shown as a black vertical bar.

Chapter 4

Practical issues – roughness, conveyance and afflux

ABSTRACT

This chapter illustrates the use of the CES-AES methods through a series of practical examples involving stage-discharge, velocity, backwater and afflux prediction for a range of channel types (size, shape, cover). Generic guidance on the use of the CES-AES for different flood risk management activities is provided, with specific examples relating to availability of site information, vegetation maintenance and dredging. A series of ‘what-if’ scenarios is explored to demonstrate the sensitivity of the CES-AES outputs to changes in input data (roughness, slope, sinuosity). An approach for estimating roughness in mountain streams with boulders is presented.

The survey data for the examples are provided in Appendix 3.

4.1 AN OVERVIEW OF THE CES-AES USE IN PRACTICE

The CES-AES software supports practitioners concerned with a range of flood risk management as well as other wider activities through, for example:

- Calculating water levels, flows and velocities for rivers, watercourses and drains;
- Providing upper and lower uncertainty scenarios;
- Assessing flood or extreme water levels, and the sensitivity of these to channel adaptation or management options (particularly dredging and plant management);
- Assessing the impact of timing and nature of vegetation cutting;
- Assessing the impact of blockage due to vegetation or debris;
- Understanding the influence of in-stream structures on water levels;
- Finding holistic solutions which address both environmental and flood risk management or land drainage objectives;
- Implementing guidance and procedures for channel maintenance.

The use of the CES for channel maintenance and flood risk management activities is recognised in Sir Michael Pitt’s review following the 2007 widespread flooding (Pitt, 2008):

“7.66 ... To progress its understanding of how seasonal variation in vegetation affects the way in which watercourses behave, the Environment Agency has

recently developed a tool called the Conveyance Estimation System (CES), which will help to deliver an improved maintenance programme. . .”

The Association of Drainage Authorities and Natural England's Biodiversity Manual – Integrating Wildlife and Flood Risk Management (Buisson *et al.*, 2008) recognises the potential use of the CES in identifying preferred channel management techniques:

“In choosing the best technique to apply it is essential to examine the effect on flood conveyance in the specific location and circumstances that the technique would be used. This will require judgment informed by experience and one of the available flood risk modelling tools. In many circumstances, the Conveyance Estimation System (www.river-conveyance.net) may provide the information needed. Modelling allows prediction of the effects of management techniques on conveyance and storage and can identify the additional capacity needed to offset any reduction in conveyance caused by additional wildlife habitat created, such as a wider uncut marginal strip of vegetation in the channel.”

Table 4.1 provides a summary of some of the core flood risk management activities, the type of hydrodynamic modelling associated with these and advice on the interpretation of outputs for specific activities. Outputs from the CES-AES may be used in modelling types (a) through to (f) in the table, which support a range of activities including strategic planning, scheme design, flood forecasting, flood mapping for regulation and insurance, hydrometry and maintenance.

For all of these activities, the basic building blocks within the CES-AES software include:

- a single cross-section analysis;
- a single structure analysis i.e. bridges and culverts;
- a backwater profile analysis with no structures present;
- a backwater profile analysis with structures present e.g. bridges, culverts; and
- the use of the CES-AES within a 1-D modelling environment (see [Chapter 5](#)).

4.1.1 Single cross-section analysis

A single cross-section analysis typically involves one or more of the following steps:

- 1 *Data gathering* – Gather all available data and information about the site, including where possible, survey; water level, discharge and velocity measurements; water surface slope; photographs; channel and floodplain cover; and any historical flood data.
- 2 *Initial stage-discharge analysis* – In the absence of flow data, apply the CES methodology using default parameters and the Roughness Advisor unit roughness information. Essential information is the surveyed cross-section geometry and the longitudinal water surface slope (ideally) or bed slope. Photographs, site descriptions and UK grid references may be used to assist in selecting the unit roughness values.

Table 4.1 Flood risk management tasks (adapted from EA/Defra, 2002a and Defra/EA, 2004).

Type of modelling	Activity						Comments/ Use
	a) I-D modelling	b) Routing models	c) Backwater models	d) Rating curves	e) Rating surfaces	f) Single levels/flows	
Strategic planning	x	x	x	x	x		Evaluate and compare options against criteria such as effectiveness, efficiency, robustness and performance. Where small changes in input parameters effect large changes in water level, devote additional resources to understanding and potentially reducing the cause.
Scheme design	x	x	x	x			New schemes ideally based on a calibrated I-D model. Alternatively, undertake a cost-benefit analysis for multiple cases with different site roughness values.
Flood forecasting & warning	x	x	x	x	x		Examine the sensitivity of flood wave speed to river resistance using a flood routing model such as that which is available in ISIS/InfoWorks RS(CES embedded). Additionally, undertake an offline analysis to examine where the flood peaks change significantly with channel roughness.
Flood mapping for regulation/insurance	x	x	x		x		For broad-scale mapping, inform Agency Development Control that approach is indicative not accurate. Examples of CES use in national flood mapping include the Second Generation Flood Maps for Scotland (Mc Gahey <i>et al.</i> , 2005; SEPA, 2006) and Northern Ireland (NIRA, 2005).
Hydrometry	x		x	x			Typically users have high quality calibration data. This may be used for model calibration & extension of ratings.
Maintenance			x	x	x		Detailed local site knowledge (including seasonal vegetation variations). Use CES to predict flow and local velocities.

- 3 *Calibration using stage-discharge measurements* – If flow data are available, calibrate the stage-discharge curve by varying the n_l values, as the flow rate is particularly sensitive to this parameter. The top-of-bank markers may also be varied within a realistic range (e.g. ± 0.25 m for rivers) to capture the bankfull variations.
- 4 *Calibration using stage-discharge and velocity measurement* – If velocity data are available, refine the lateral distribution of roughness, in particular, the in channel, bank and berm n_l values. Here, it is necessary to ensure the changes in n_l for a given depth apply to all depths i.e. the calibrated stage-discharge curve is preserved. If historic flood data are available, this is a useful means of calibrating the top-end of the rating curve, and establishing the floodplain n_l values.
- 5 *Expert calibration using internal model parameters* – Expert users may wish to vary the values of the main channel dimensionless eddy viscosity λ_{mc} (via the CES-AES Graphical User Interface, [Chapter 5](#)) and the secondary flow term Γ (via the source code, [Chapter 5](#)) based on local site knowledge, for example, reducing λ_{mc} if bankside vegetation reduces the mixing at the main channel floodplain interface. Note: this is advocated for research or expert users only as inexperienced application of this multi-parameter calibration approach may lead to wider uncertainty bounds than alternative calculation methods.
- 6 *Meandering channels* – For meandering channels, Steps 1 to 4 are identical, except there are two additional inputs, the plan form sinuosity, σ , and the bend orientation i.e. left or right hand bend. The σ value should only be varied if there is uncertainty associated with the true value, to gauge the sensitivity for the site. The bend orientation is a fixed input which is assigned to the top-of-bank markers.

[Figure 4.1](#) provides an example of a simple CES application to a two-stage cross-section located in a straight reach of the River Penk at Penkridge. The effect of n_l , λ and Γ on the depth-averaged velocity profile is shown and a small sinuosity is introduced to illustrate what the affect of C_{uv} would be. The calibrated n_l values are 0.033 and 0.060 for the main channel and floodplains respectively. The default λ and Γ models are used and an example sinuosity σ of 1.05 ($C_{uv} \approx 1\%$) is introduced.

4.1.2 Single structure analysis (bridges and culverts)

A single structure analysis typically involves one or more of the following steps:

- 1 *Data gathering* – Information is required to characterise both the structure and the channel surrounding it. Channel cross section information is required as in Section 4.1.1. If the bridge structure has abutments or other modifications of the surrounding channel then these need to be included in the cross section survey. Ideally, the structure should be surveyed (both upstream and downstream faces) to provide number of openings and elevation data for springer levels, soffit levels and road or parapet levels. The material and condition of the structure should be observed, if possible, bearing in mind that the material and condition of the structure at the opening might not always be representative of conditions throughout its downstream length. For culverts, the entrance structure type and shape should be recorded. Consideration should be given to the condition of the culvert barrel

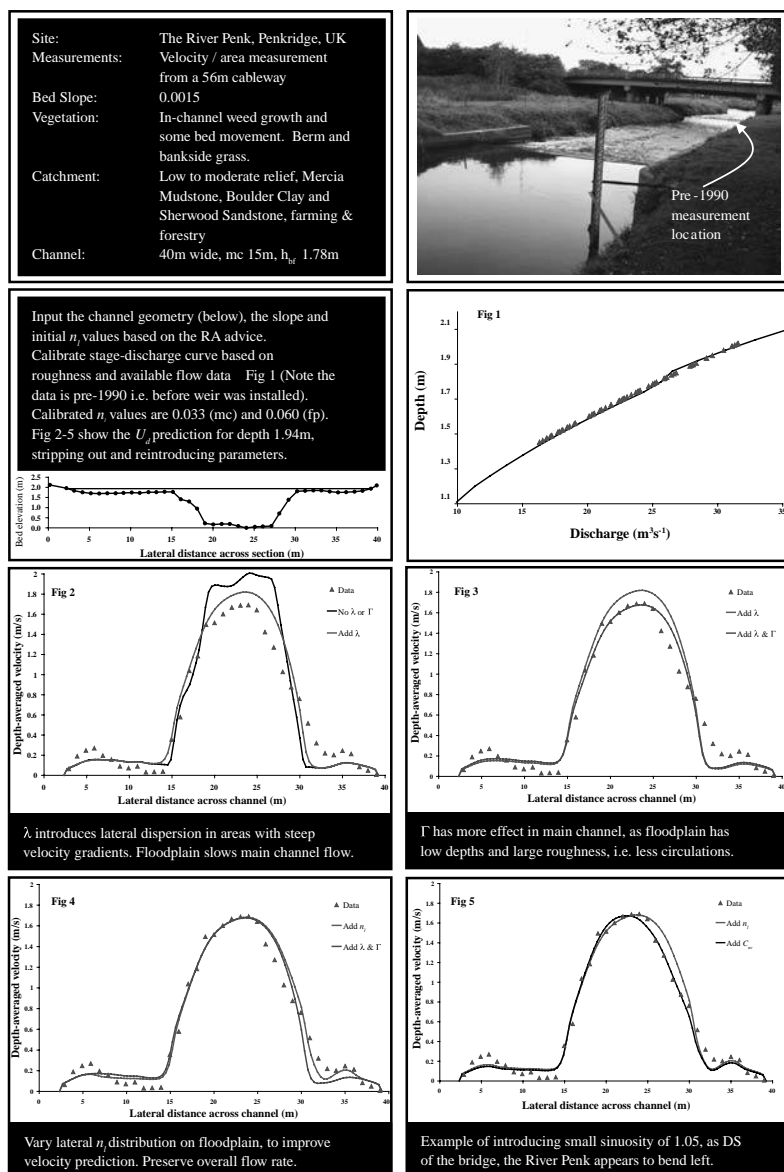


Figure 4.1 Example CES applications for the River Penk at Penkridge (Mc Gahey, 2006) (See colour plate section).

throughout its length, although this may not be known without a full inspection or CCTV survey.

- 2 *Initial structure analysis* – The AES includes certain typical bridge and culvert types (e.g. arch and beam bridge, pipe and box culvert). However some structures

may not fit exactly into the defined types. Where this is the case, the closest match should be used. The user defined arch bridge type allows greatest flexibility for opening shapes. For culverts with multiple barrels, the AES standard types allow identically sized openings to be specified. It may be possible to model a culvert with complex openings as a bridge unit if the barrel friction is thought likely to be the hydraulic control in most circumstances.

- 3 *Data entry* – Care is required in adding bridges or culverts to a CES model. There are a number of geometric and procedural rules enforced by CES-AES. These include:
 - a Openings for bridges and culverts must have valid coordinates within the channel cross section. This means, for example, that culvert openings should not extend below ground level and springer levels for arches must be above ground elevation at a given cross section offset (i.e. arches should not spring directly from ground level at the side of a cross section).
 - b Road elevations must be contained within the cross section.
 - c The CES river cross sections immediately upstream and downstream of a bridge or culvert should have three roughness zones.
 - d In the CES-AES backwater module, the upstream openings of a bridge or culvert are placed at the chainage implied by the reach length downstream of the previous section.
 - e In the CES-AES backwater module, the reach length downstream from the bridge section to the next CES river section is taken to include the bridge length.
- 4 *Cross section analysis* – The CES-AES software requires a backwater profile to be calculated in order to generate information on conveyance and flow ratings at the bridge or culvert opening sections. The ‘Outputs’ tab of the software requires the user to check a box ‘Include Structure Outputs from last Afflux Calculation’ to include data from the structure cross sections.
- 5 *Calibration* – Bridges and culverts can have a single roughness value (expressed in terms of Manning’s n) for the structure, which is combined with the channel and overbank roughness values at the structure sections when computing the conveyance. Should there be measurements available to assist with calibration then they may be used as for a normal CES river section. Note, as above, that a backwater profile must be computed to generate conveyance or water level results for bridges or culverts.

4.1.3 Backwater profile analysis (no structures present)

Backwater profiles are evaluated where there is a downstream control (i.e. known head and flow). A backwater analysis typically involves the following steps:

- 1 *Data gathering* – Information (similar to the single cross-section analysis, Section 4.1.1) for multiple cross-sections is required. An important question is how far upstream of the control the cross-sections are required. A useful rule

of thumb (Samuels, 1989b) based on the downstream depth and reach-averaged longitudinal slope may be used to estimate this. Additional inputs include the distance between each cross-section, the downstream water level and the inflow(s) to the reach. Additional measurements or historic data may include, for example, water levels along the reach for a given inflow.

- 2 *Initial single section analysis* – Steps 1 to 4 of the single section analysis (Section 4.1.1) are followed for any cross-sections where (i) measurements are available and (ii) the water level measurements are not dominated by the downstream control. The adopted/calibrated roughness values may then be assigned to the remainder of the reach cross-sections in accordance with the available descriptions.
- 3 *Backwater analysis* – The downstream control and inflow to the reach are assigned and the backwater calculation is implemented, providing the water surface profile and average velocities along the reach.
- 4 *Backwater calibration* – The backwater predictions may then be compared to water level and velocity measurements along the reach and these may guide further roughness calibration.

4.1.4 Backwater profile analysis (structures present)

The process for backwater profile analysis when a bridge or culvert is included is the same as above for a reach without structures. As described in [Chapter 3](#), the AES models the water surface profile through a structure using cross sections supplied by the user at the structure entrance and exit, these are labelled AE2 and AE3 in the output files exported by CES-AES following a backwater analysis. Interpolated upstream and downstream sections are also used where the transition lengths surrounding the structure require it. These sections AE1 and AE4 are also reported in the output files.

4.2 ESTIMATING AND USING STAGE-DISCHARGE RELATIONSHIPS AND SPATIAL VELOCITIES

4.2.1 Stage-discharge prediction for the River Trent at Yoxall, Staffordshire, UK

Aim

To predict the stage-discharge and upper and lower uncertainty scenarios for the River Yoxall site using the CES-AES software and available site information. The outputs are compared with measured data to instil confidence in the results.

The Yoxall site on the River Trent

The Yoxall site ([Figure 4.2](#)) is located on a gentle bend of the River Trent, in Yoxall, Staffordshire, immediately downstream of Yoxall road-bridge. The cross-section is 80 m wide, including a 35 m berm, and a cableway for measuring inbank flows is situated across the main channel. The site is bypassed through two flood relief culverts, the flows of which are measured under Yoxall Bridge. There are four overbank gauged



Figure 4.2 Electromagnetic gauging station on the River Trent (a) downstream of Yoxall bridge and (b) an upstream view showing Yoxall Bridge (Courtesy of the EA).

flows, of which two were recorded before and two after the construction of a training bank. The inbank flow measurements are generally considered more reliable than overbank flows (EA, 2005). Measurements from the Environment Agency's gauge station (Station 28012) include water level, discharge and velocity. The reach-averaged longitudinal slope at bankfull is ~ 0.001 , increasing to 0.00275 at a depth of 0.5 m. The channel bed material includes gravels and summer weed growth and the floodplains consist of grasses with occasional bushes.

Roughness and cross-section definition

Based on the description and photographs, the Roughness Advisor values include (Figure 4.3):

- *Channel bed* – The RA coarse gravel is adopted ($n_{\text{sur}} = n_l = 0.027$). This may be refined to gravel or fine gravel through calibration. The larger gravel option is incorporated for the initial guess i.e. a conservative approach.
- *Channel banks* – The RA height-varying grass ($n_{\text{veg}} = 0.041$) and sand ($n_{\text{sur}} = 0.02$) is adopted giving the total unit roughness $n_l = 0.0456$.
- *Floodplain* – The RA turf ($n_{\text{veg}} = 0.021$) and sand ($n_{\text{sur}} = 0.02$) is adopted giving $n_l = 0.029$. The reasoning is that bank-side vegetation appears thicker and taller (i.e. height-varying grass) than the floodplain grass (i.e. turf).

Results for the Yoxall site

Figure 4.4 provides the CES stage-discharge prediction using these RA roughness values and the measured data. The data are fairly scattered but tend to fall within the upper and lower credible scenarios, defined by the upper and lower roughness values. The data move away from the curve at high overbank flows which may be attributed to the reduced accuracy in flow gauging during times of flood together with uncertainty regarding the floodplain vegetation. A further factor may be the variation in longitudinal water surface slope with depth, which is subject to local topographic

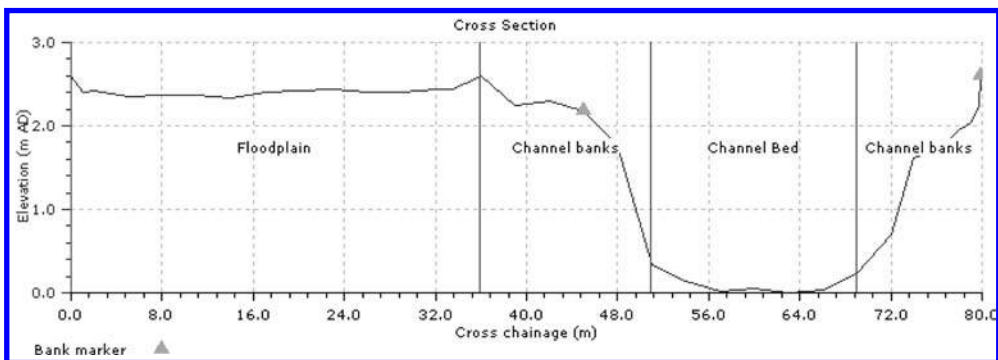


Figure 4.3 River Trent cross-section, roughness zones and top-of-bank marker locations.

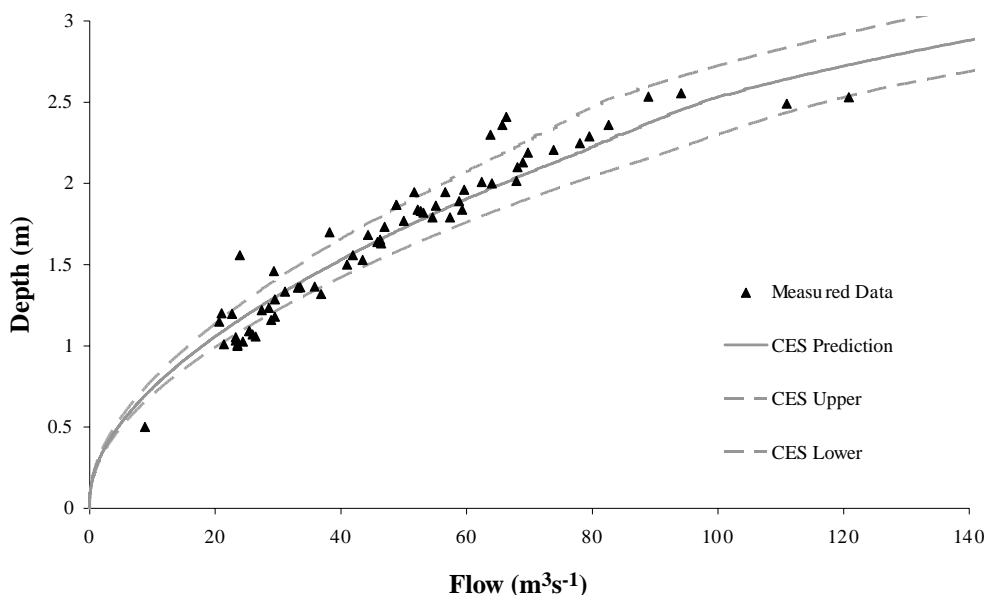


Figure 4.4 Stage-discharge prediction for the River Trent at Yoxall.

variations at low flows, ~ 0.001 at bankfull (as used in the CES simulation) and more closely linked to the overall valley slope at high flows. This issue may be overcome if the backwater module is used for the reach, as the variations in surface water slope are implicit. Similarly, where the CES is incorporated in a full 1-D model the depth specific surface water slope is incorporated. The stand-alone cross-section analysis is useful in determining and validating the unit roughness values to be adopted for the remainder of the reach.

4.2.2 Stage-discharge and velocity prediction for the River Colorado, La Pampas, Argentina

Aim

To predict a stage-discharge curve and velocity distributions for different flow depths for the River Colorado site using the CES-AES software and available site information. The outputs are compared to measured (flow and velocity) data throughout the depth range to instil confidence in the results.

The River Colorado site

The River Colorado provides a useful example of a wide, rigid bed, simple channel with large flows. It is 885 km long, rising in the Andes and flowing south-east across southern central Argentina to the Atlantic Ocean. It marks the northern limit of Patagonia. It is also a rough boundary between the commercial agriculture to the north and ranching to the south. The main channel is 60 m wide and 3.6 m deep, with a reach-averaged longitudinal bed slope of 0.0013. Typical flow rates are of the order $400\text{--}600 \text{ m}^3\text{s}^{-1}$ and the river often overflows its banks in Spring. Water level, discharge and depth-averaged velocity measurements are available; however, information on channel roughness is limited to the photographic evidence ([Figure 4.5](#)).

Roughness and cross-section definition

Based on the photographs, the Roughness Advisor values include ([Figure 4.6](#)):

- *Channel bed* – The RA bedrock ($n_{\text{sur}} = 0.025$) and 0–20% boulder coverage ($n_{\text{irr}} = 0.017$) are adopted, giving $n_l = 0.030$. Bedrock is assumed due to the apparent hard cut-out of the channel side-banks ([Figure 4.5](#)) and some boulders are included due to the presence of boulders near the right bank ([Figure 4.5c](#)).
- *Channel banks* – The RA bedrock ($n_{\text{sur}} = 0.025$) and height-varying grass ($n_{\text{veg}} = 0.041$) are adopted giving $n_l = 0.048$. Although the vegetation is not visible on all banks, the added influence of the height varying grass on the banks is likely to be minimal in terms of the overall channel width and hence capacity.
- *Floodplain* – The RA bedrock ($n_{\text{sur}} = 0.025$) and turf ($n_{\text{veg}} = 0.021$) are adopted giving $n_l = 0.033$.

Results for the Colorado site

[Figure 4.7](#) shows the CES stage-discharge predictions with these roughness values. The flow is described reasonably well throughout the range of depths other than near bankfull (3.6 m), where there is a sharp step or ‘kick’ in the curve. This is caused by the embedded secondary flow model, which takes the change in orientation and magnitude of the secondary flow circulations from inbank to out-of-bank flow into account, identified in the model by the bank markers ([Figure 4.6](#)). The step is sharp as the change in geometry from in-channel vertical banks to floodplain horizontal banks is sudden. As survey data were only available for the in-channel section, the floodplain topography is based on the photographic evidence (e.g. [Figure 4.5b](#)). The discrepancy

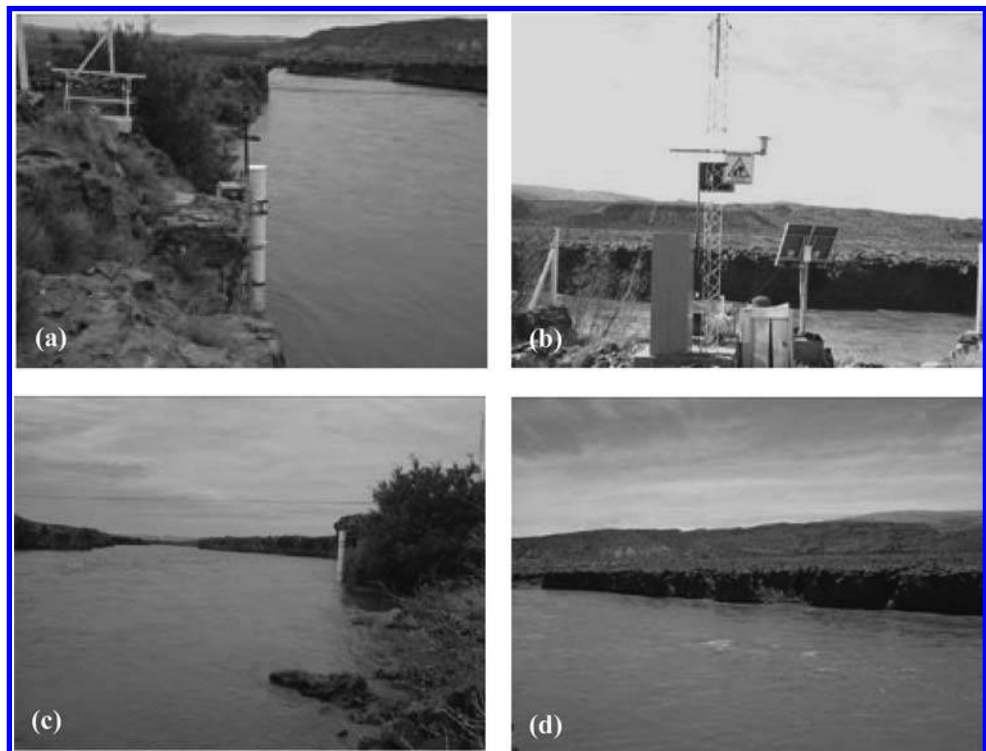


Figure 4.5 The River Colorado gauge site showing the instrumentation (a) & (b) and looking (c) downstream and (d) across the full width of the river (Courtesy of Leticia Tarrab).

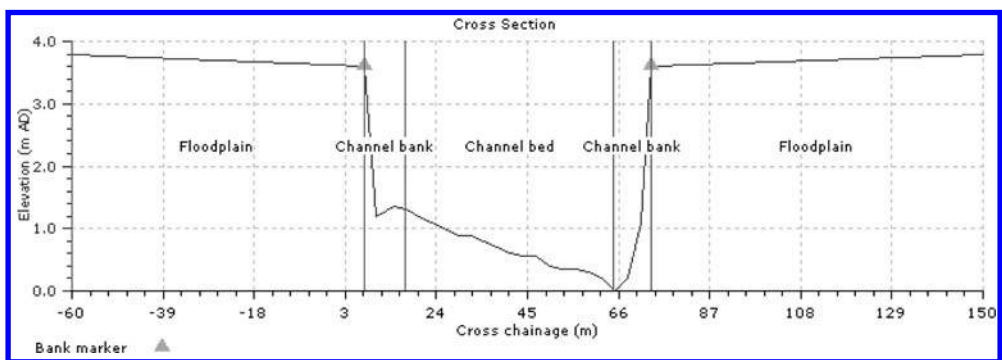


Figure 4.6 River Colorado cross-section, roughness zones and top-of-bank marker locations.

between the measured and predicted flows suggests that, in reality, the change from inbank to out-of-bank is perhaps more gradual.

Figure 4.8 provides the depth-averaged velocity predictions for a range of flow depths and the corresponding measured data. The CES tends to under-predict the high

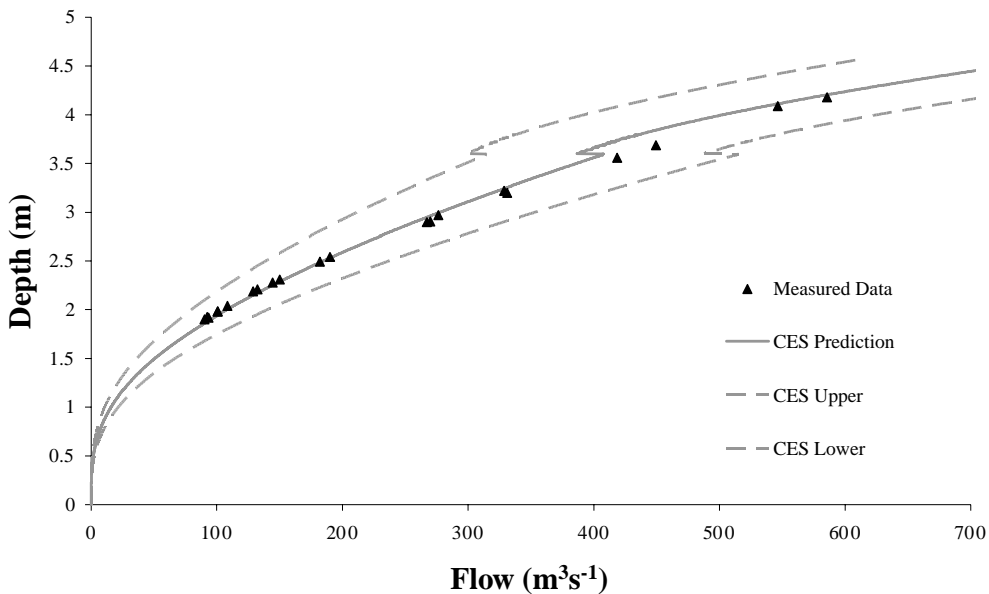


Figure 4.7 Stage-discharge prediction for the River Colorado, Argentina.

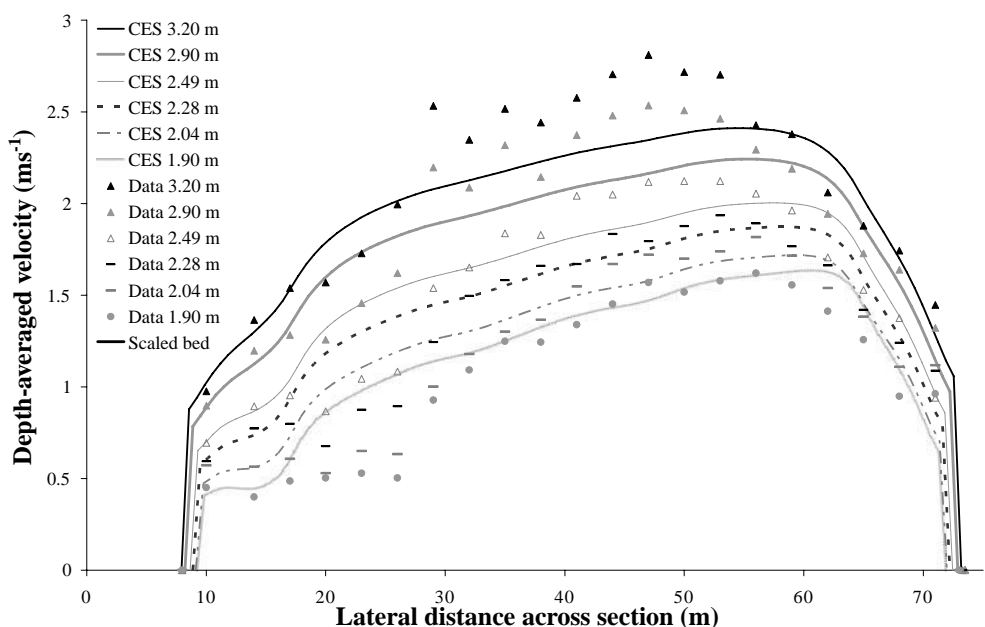


Figure 4.8 Depth-averaged velocity prediction for the River Colorado at various flow depths and comparison to measured data.

velocities (channel centre) at large flow depths and slightly over-predict the velocities at lower depths. This may be a short-coming in the CES approach for adequately resolving the variation of roughness with depth for this wide channel, where bed generated turbulence has a dominant role and the channel banks have less influence. The distribution may be further influenced by the presence of individual boulders (e.g. Figure 4.5c).

4.2.3 Hierarchical approach to estimating roughness (and other flow parameters) for the River Main, County Antrim, UK

Aim

This example is intended to demonstrate the hierarchical approach to estimating roughness within the CES i.e. no information (use of River Habitat Survey); some information (use of Roughness Advisor descriptions); and detailed information (use of photos and measurements to calibrate roughness). The hierarchical approach is based on stage-discharge predictions. Once the detailed information has been used, additional flow parameters are simulated with the CES including velocity, back-calculated Manning n , Froude Number and Reynolds Number.

The River Main site

The River Main in County Antrim was introduced in Chapter 2, Section 2.2.2. The reach of interest was reconstructed and realigned in the 1980s to form a double trapezoidal channel. The CES is used here to demonstrate its use in predicting various flow parameters at Bridge End Bridge based on available information. Although this includes survey (Figure 4.9), bed slope (0.00297), roughness, photographs (Section 2.2.2) and detailed measurements; this example is set-up to illustrate the RA use with varying degrees of roughness information i.e.:

- *No information* – for the main channel (use of RA RHS advice);
- *Some information* – for the main channel (use of RA based on descriptions);
- *Detailed information* – for the main channel (use of RA including calibrating roughness values to best-fit measurements and use of photographs).

Roughness and cross-section definition and results for the River Main

i No information

For this case it is assumed there is no information on in-channel cover other than the quarry stone on the channel banks (0.5 tonne weight, 100–200 mm size) – incorporated during the re-design of the channel. Three roughness zones are set-up in the RA:

- *Channel bed* – The UK Grid reference for the River Main is 350100 411000 (NI). Based on this, the RHS suggests the most likely vegetation is filamentous algae ($n_{veg} = 0.015$). This is adopted with sand ($n_{sur} = 0.02$) as a basic substrate giving $n_l = 0.025$.

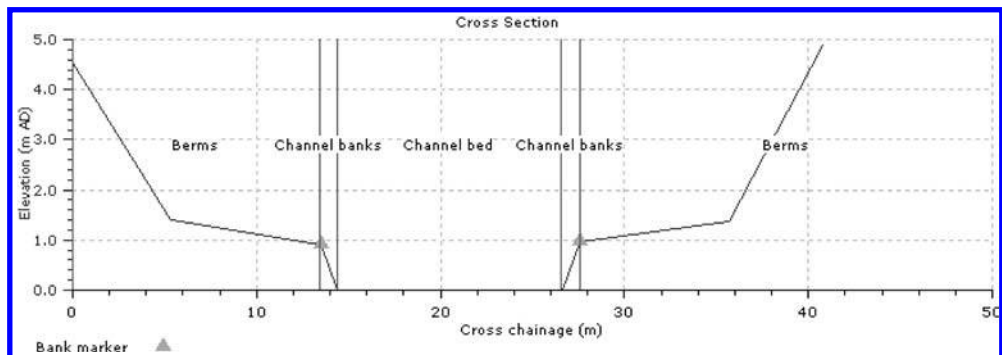


Figure 4.9 River Main cross-section, roughness zones and top-of-bank marker locations.

- *Channel banks* – The RA rip-rap option is adopted for the quarry stone ($n_{\text{sur}} = 0.045$) augmented with the RHS suggested filamentous algae, giving $n_l = 0.047$.
- *Berms* – Based on the available floodplain information, the RA height-varying grass ($n_{\text{veg}} = 0.041$) option is adopted with sand ($n_{\text{sur}} = 0.02$) as the basic substrate. This gives the total unit roughness $n_l = 0.046$.

The RA roughness zones are combined with the cross-section and slope information to predict the stage discharge (Figure 4.10). These include the upper and lower credible scenarios which are based on the upper and lower roughness values. The measured data falls within these scenarios (which are wide); however the curve based on the expected roughness falls below the data.

ii Some information

For this case there is additional information on the roughness cover including: no vegetation present at the channel bed which consists of coarse gravel and thick grass protruding through the quarry stone on the banks. As before, three roughness zones are set-up in the RA composed of:

- *Channel bed* – The RA coarse gravel is adopted ($n_{\text{sur}} = n_l = 0.027$).
- *Channel banks* – The RA rip-rap option is adopted for the quarry stone ($n_{\text{sur}} = 0.045$) together with the RA turf ($n_{\text{veg}} = 0.021$) to simulate the thick grass. This gives the total unit roughness $n_l = 0.050$.
- *Berms* – The values are unaltered i.e. a total unit roughness $n_l = 0.046$.

A revised flow prediction is made based on the updated roughness values (Figure 4.11). The curve based on the expected roughness value still falls below the measured data albeit closer. A notable difference is the reduced range of uncertainty i.e. the credible upper and lower scenarios are much narrower. This is largely due to eliminating the filamentous algae and heavy weed growth, which have considerable associated uncertainties. Some data now fall outside of these scenarios, which is

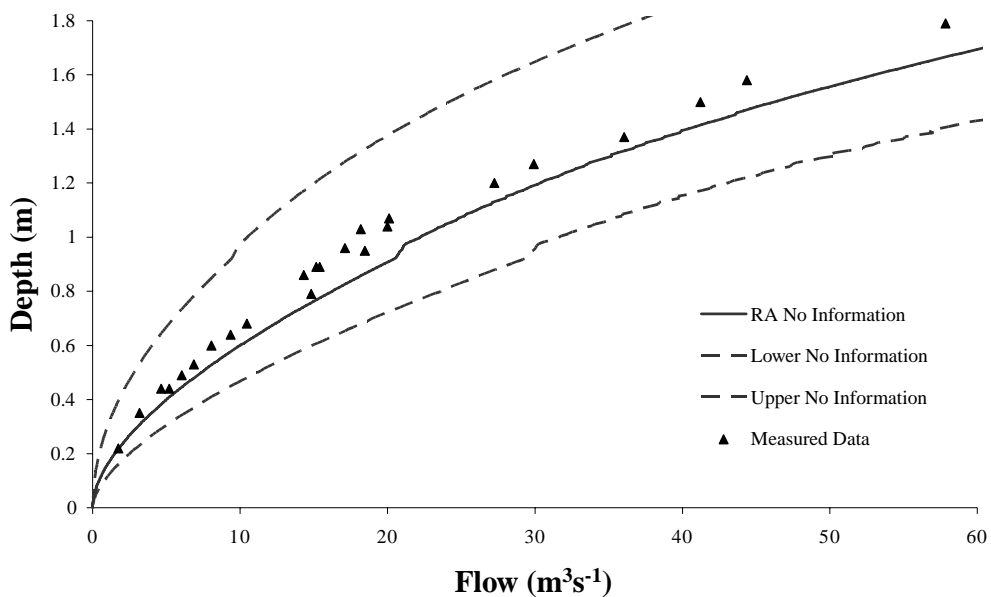


Figure 4.10 Stage-discharge prediction for the River Main with no in-channel information.

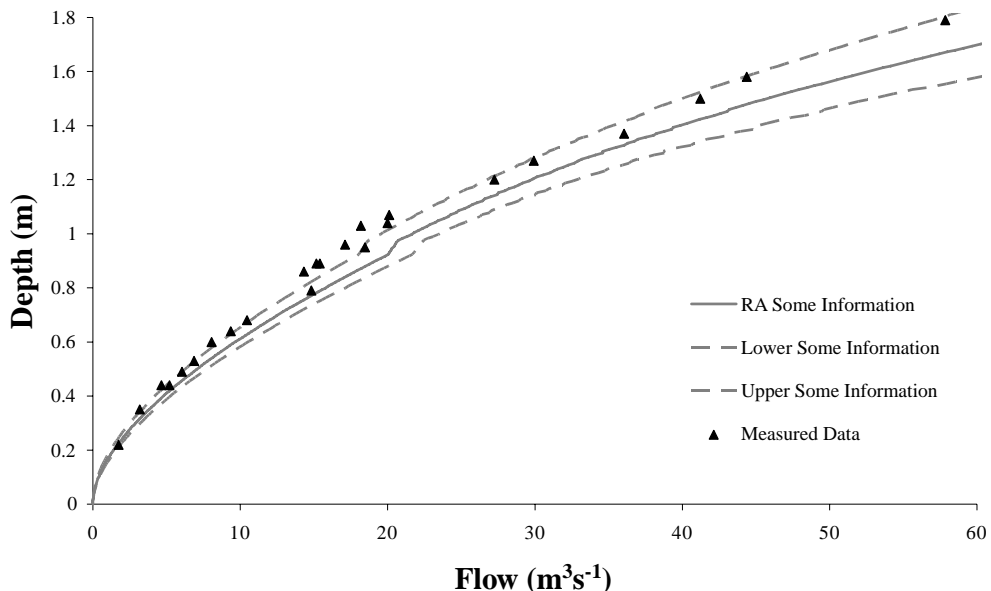


Figure 4.11 Stage-discharge prediction for the River Main with some roughness information.

plausible as these are not confidence intervals or envelopes (Chapter 3, Section 3.3) – they simply indicate the area where the data is likely to fall.

iii Detailed information

For this case there is detailed information available including photographs and measurements (flows and velocities), which can be used to improve the CES simulations. From Figure 4.11 it is apparent that the RA is under-estimating the roughness as the measured data are above the curve, and in some instances, above the upper credible scenario. The photographic evidence (Figure 2.5) suggests that the coarse gravel is very large with cobbles present. The RA unit roughness value for coarse gravels and cobbles are 0.027 and 0.035 respectively, a substantial difference. Here, steered by the measured data and photographic evidence, a value of 0.032 is adopted. Figure 4.12 provides the resulting stage-discharge prediction which follows the measured data well – including the variations at bankfull (~ 0.95 m). The ‘no information’ curves are added to illustrate the reduction in uncertainty and improved stage-discharge predictions where more detailed information is available.

These calibrated roughness values are used to predict the depth-averaged velocities for a range of flow depths (Figure 4.13). The predictions follow the data profile reasonably well for greater depths; however, at lower depths the main channel velocity is under-predicted. There appears to be a small degree of skew in the velocity data at low depths, which may arise from the effects of the upstream bend circulations being transported downstream. Since the channel bed material is gravel, with no vegetation present, these higher velocities are plausible but are not captured by the CES where

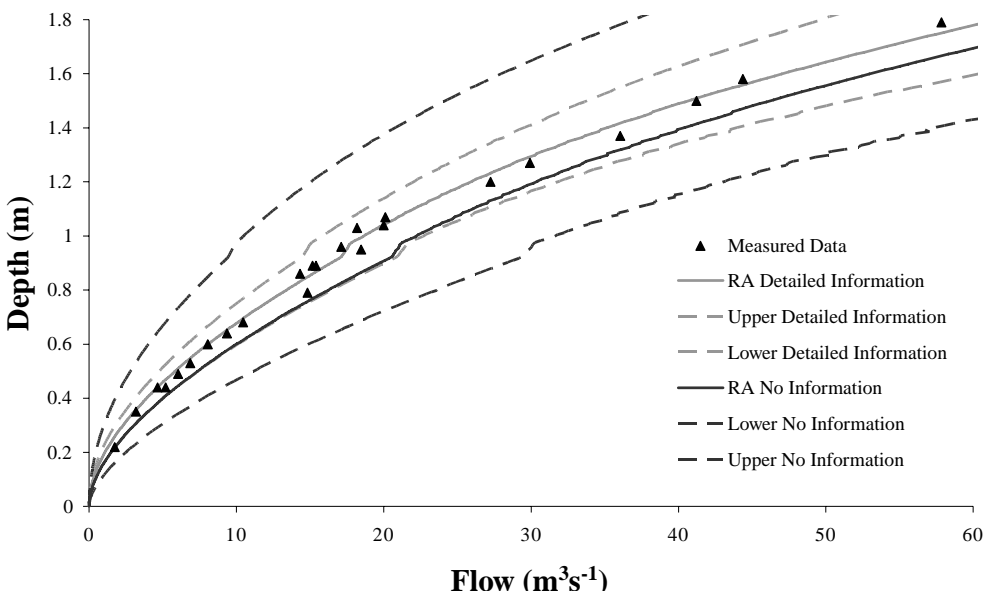


Figure 4.12 Stage-discharge for the River Main with detailed roughness information (and the no information case).

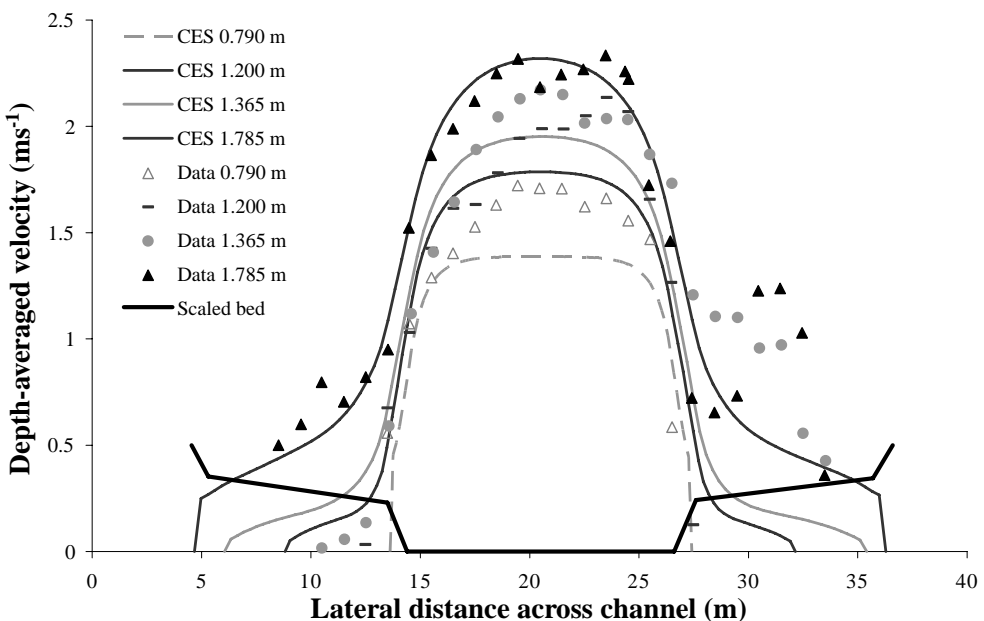


Figure 4.13 Depth-averaged velocity predictions for the River Main at various flow depths and comparison to measured data.

the effect of the slightly higher calibrated bank side roughness ($n_l = 0.050$) is present even at low flows.

Exploration of additional CES flow parameters

The CES enables users to back-calculate an equivalent Manning n resistance parameter. In modelling practice, a Manning n value is assigned to the channel bed, banks and berms, which is constant for all flow depths. In the field, measurements show how Manning's n varies with flow depth (e.g. Chow, 1959), with a greater resistance at low depths where roughness size is comparable with flow depth. Figure 4.14 provides the CES back-calculated and measured Manning n values with depth. These show a reasonable correlation throughout the depth albeit with the predictions ~15% lower than the measured data.

Figure 4.15 shows the CES predicted Froude Number with depth. The Froude Number is well below 1.0 throughout the depth, indicating subcritical flow conditions, as expected for natural channels. In some instances, supercritical flow may occur, for example, in steep mountain streams, rapidly varied flow downstream of structures or localised supercritical flow in parts of the cross-section. Engineers have also been known to design supercritical channels through cities i.e. steep heavily modified concrete conduits designed to convey floods over shorter distances than the natural plan form channel profile. For the River Main, the Froude Number increases away from the channel bed, reflecting the higher velocities at greater depths. The shape of

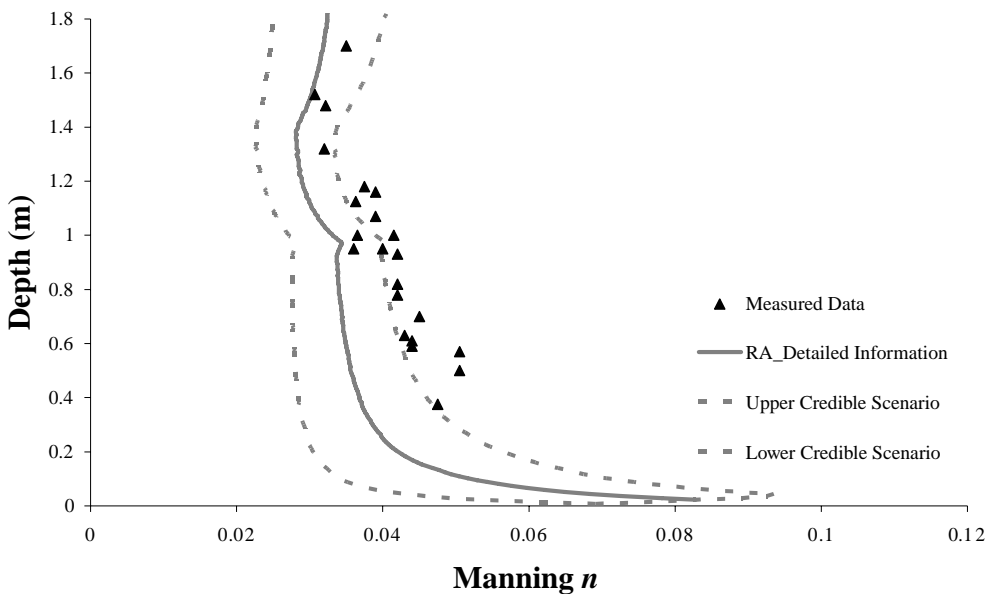


Figure 4.14 CES back-calculated and measured Manning n values for the River Main.

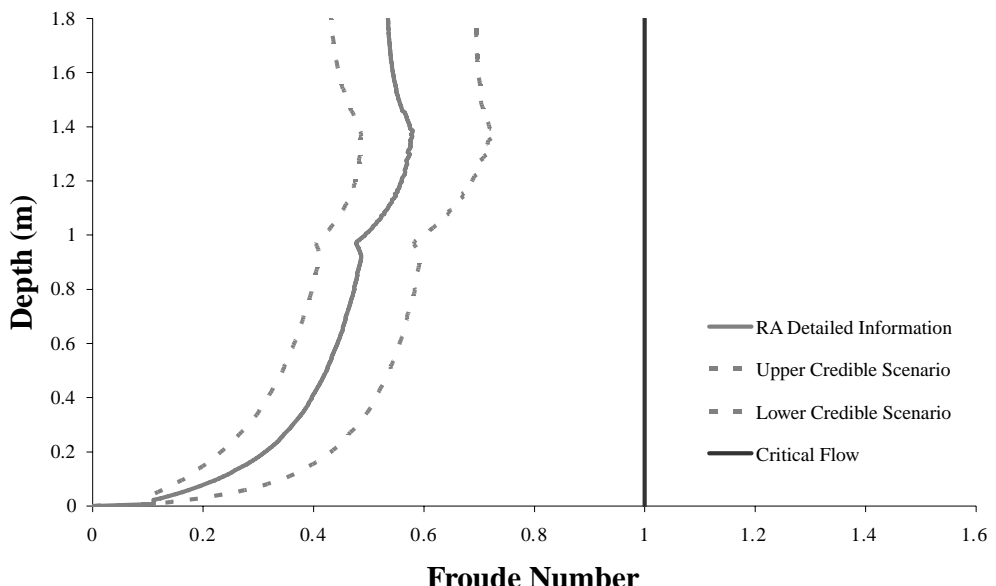


Figure 4.15 CES predicted Froude Number with depth for the River Main.

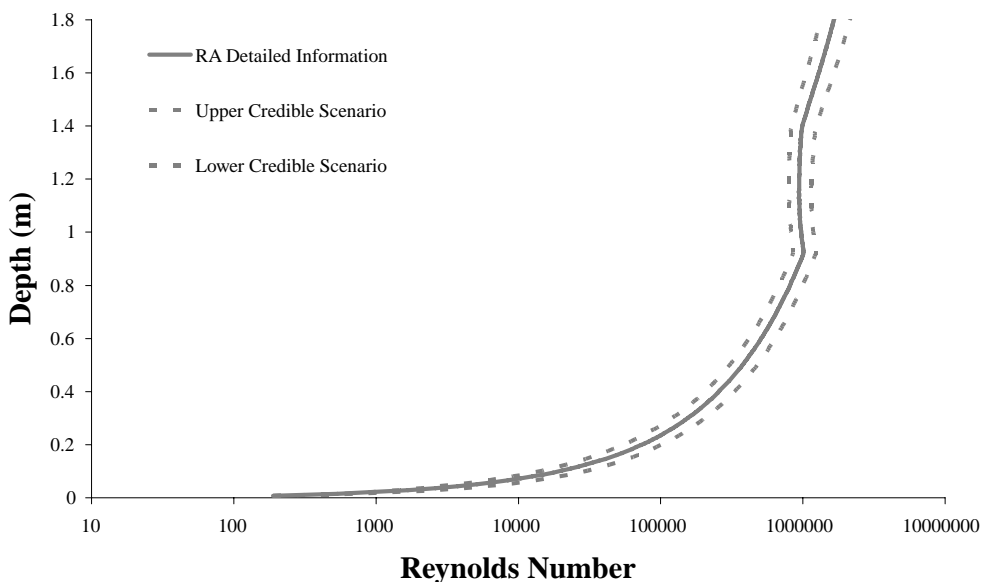


Figure 4.16 CES predicted Reynolds Number with depth for the River Main.

the curve changes as the channel flow moves out of bank onto the berms and again as it comes into contact with the distant berm edges, as these boundaries influence the velocity distribution.

Turbulence occurs at high Reynolds Numbers, where the flow incorporates a three-dimensional eddying or mixing action. Turbulence is dispersive, diffusive, chaotic, and contrary to viscosity, it is a property of the flow and not of the fluid (Reynolds, 1974; Nezu & Nakagawa, 1993). Figure 4.16 shows the CES predicted Reynolds Number with depth which is of the order 10^3 to 10^6 for most of the depth column i.e. characteristic of fully turbulent flow ($Re > 10^3$). Near the channel bed, the Reynolds Number drops substantially indicating the potential for laminar flow close to the boundary (although this is unlikely to occur in natural channels with sizable roughness elements e.g. cobbles).

This single cross-section analysis is a useful means to establish the calibrated rating curve and hence the roughness values to be used for the whole reach. These roughness values are adopted in Section 4.3, where different backwater profiles are explored for the River Main.

4.2.4 Stage-discharge, velocity and roughness predictions for the River Severn at Montford Bridge, UK

Aim

To improve confidence in high flow predictions required for a Flood Risk Assessment climate change scenario. This is achieved through simulating stage-discharge

and velocity distributions which capture the measured data at lower and intermediate flows, with the bed slope playing an important role. The back-calculated Manning n values are also compared to measured values to improve confidence. This is achieved using the CES software and available site information.

The Montford Bridge site on the River Severn

The Montford Bridge site along the River Severn is introduced in [Chapter 2](#), Section 2.5.2. To fulfil the requirements of a Flood Risk Assessment climate change scenario, it is necessary to determine the depth at a flow rate well above the available flow measurements. The scenario is to model the 100 year return period, $Q_{100} = 330 \text{ m}^3\text{s}^{-1}$, +20% flow to satisfy Defra's Project Appraisal Guidance on indicative sensitivity ranges for peak river flows in 50–100 years time, giving $Q = \sim 400 \text{ m}^3\text{s}^{-1}$. The available site information includes survey, flow and velocity measurements. The description of the floodplains is limited to grass-cover together with some photographic evidence.

Roughness and cross-section definition

Based on the site description, the RA values include ([Figure 4.17](#)):

- *Channel bed* – The RA sand ($n_{\text{sur}} = n_l = 0.02$) is adopted as the bed material.
- *Channel banks* – The RA sand ($n_{\text{sur}} = 0.02$) and medium grass 0.75–1.0 m ($n_{\text{veg}} = 0.08$) is adopted giving $n_l = 0.082$.
- *Floodplain* – The RA sand ($n_{\text{sur}} = 0.02$) and turf ($n_{\text{veg}} = 0.021$) is adopted giving $n_l = 0.029$.

Results for the River Severn at Montford Bridge

For this site, there are measurements available for the water surface slope at each depth of flow, with an average value of 0.0002 at greater depths (>6 m) and the slope decreasing down to as low as 0.00006 for depths of 2–6 m. The initial CES stage-

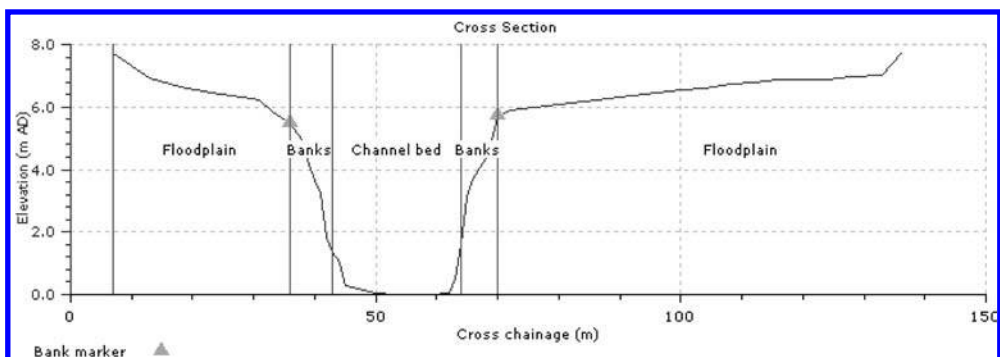


Figure 4.17 River Severn cross-section, roughness zones and top-of-bank marker locations.

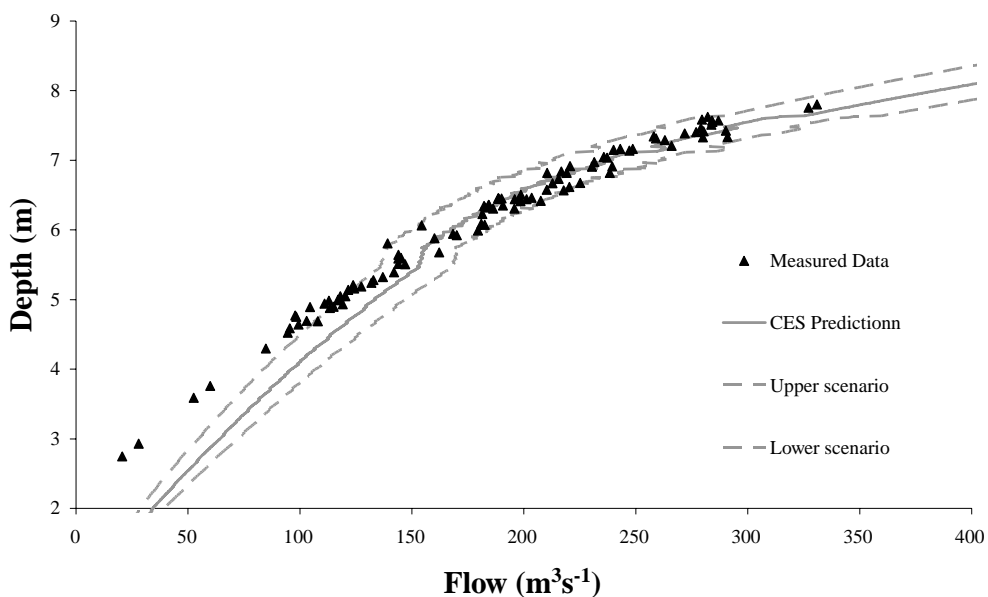


Figure 4.18 Stage-discharge prediction for the River Severn (slope = 0.000195).

discharge predictions (Figure 4.18) are based on the value 0.000195 giving reasonable predictions above 5 m, including the bankfull variations, and reducing the slope to 0.00015 (Figure 4.19) marginally improves the simulation magnitude at lower depths. The shape of the curve in the shallower region is poor, which may be related to the seasonal vegetation. Low flows typically occur in the summer months when the channel vegetation is dense, resulting in reduced conveyance and large flow depths.

Figure 4.20 shows the depth-averaged velocity predictions and measured data for a range of flow depths. The data are captured reasonably well, other than the very high velocities in the centre region of the channel. This may indicate that the CES model is over-representing the lateral shear (i.e. λ_{mc} is too high), resulting in an increased retarding effect of the slower floodplain flow on the main channel flow. This parameter may be altered in the CES-AES software (Chapter 5).

Figure 4.21 shows the CES back-calculated Manning's n values together with the seasonal data measurements. The CES simulates the average through the scattered data, capturing the slight increase in roughness where the depth drops from 6.5 m (out of bank) to 5.5 m (inbank). At lower flow depths, the CES under-predicts the roughness. This is not unexpected due to the uncertainty about the in-channel vegetation in the summer low-flow months.

As the flow, velocity and roughness information has been reasonably simulated, the stage-discharge curve (slope = 0.000195) can be extended with reasonable confidence to determine the flow depths for the climate change scenario of $Q_{100} + 20\% = 400 \text{ m}^3 \text{s}^{-1}$, giving 8.10 m depth with an uncertainty range of 7.9–8.4 m. Note that the uncertainty on water level is typically smaller than that associated with flow, due to the shape of the rating curve.

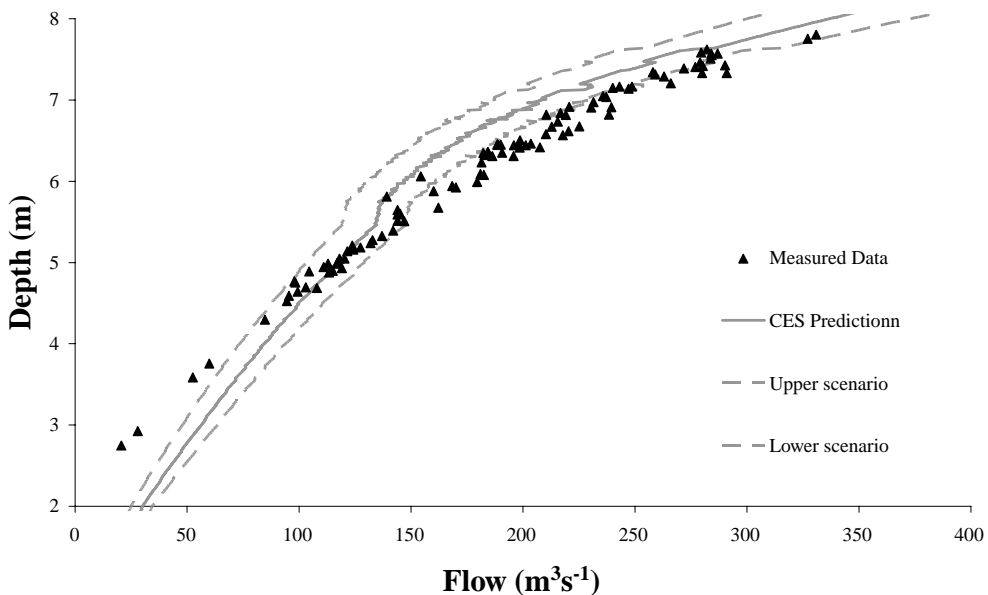


Figure 4.19 Stage-discharge prediction for the River Severn (slope = 0.00015).

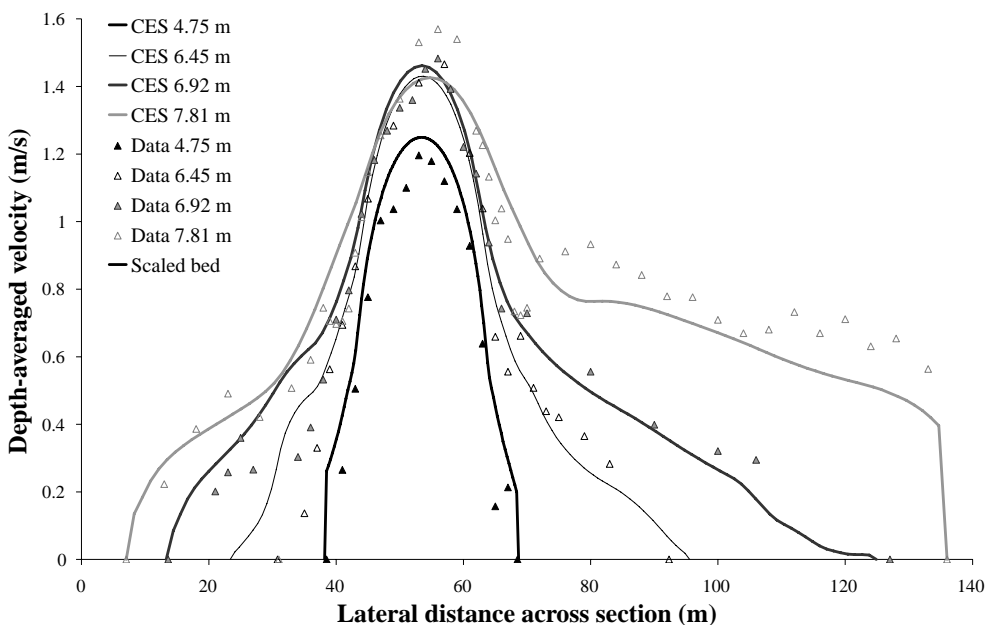


Figure 4.20 Depth-averaged velocity predictions for the River Severn at various flow depths and comparison to measured data (with depth 4.75 m based on slope = 0.00015).

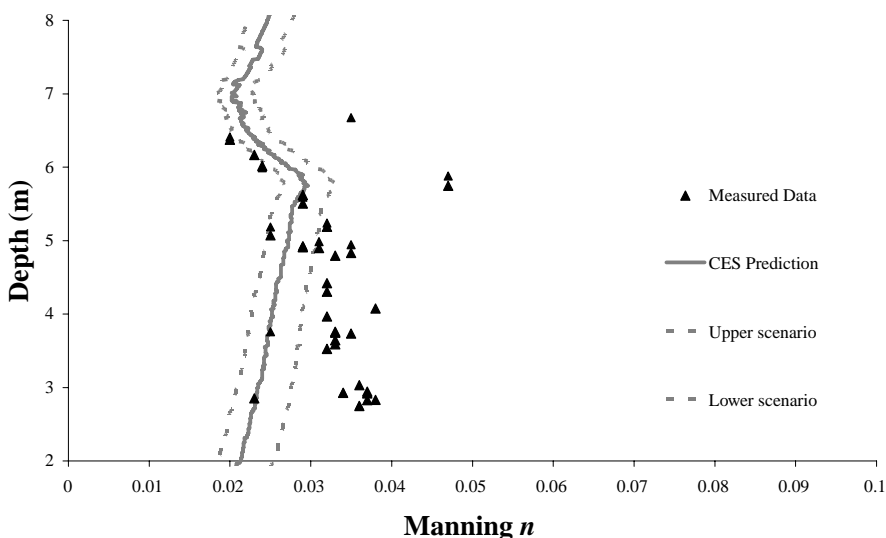


Figure 4.21 CES back-calculated and measured Manning n values for the River Severn.

4.2.5 Investigating the influence of roughness, slope and sinuosity on stage-discharge for the River La Suela, Cordoba, Argentina

Aim

To explore a series of ‘what-if’ scenarios for a simple channel and establish the sensitivity of the CES flow and velocity predictions to roughness, slope and sinuosity. This makes use of the CES-AES software and the available information for the La Suela river site and the outcomes are therefore specific to this site.

The River La Suela site

The River La Suela is a small river situated north-east of Cordoba, Argentina, with approximate dimensions of 25 m wide, 2 m deep and a reach-averaged longitudinal bed slope of 0.001355. Typical flow rates are in the range $50\text{--}70 \text{ m}^3\text{s}^{-1}$. Available measurements include water level, discharge and depth-averaged velocity profiles. Little is known about the roughness other than it consists of gravels, is alluvial in places and there is sparse bank-side vegetation.

Roughness and cross-section definition

Based on the description and a calibration using the unit roughness values, the final assigned roughness values include (Figure 4.22):

- Channel bed – the RA coarse gravels ($n_{\text{sur}} = 0.027$) and pools ($n_{\text{irr}} = 0.020$) giving $n_l = 0.034$.

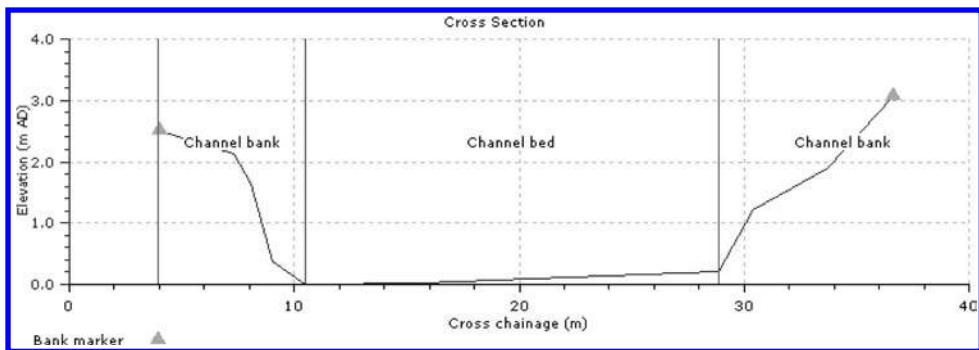


Figure 4.22 River La Suela cross-section, roughness zones and top-of-bank marker locations.

- *Channel banks* – the RA coarse gravels ($n_{\text{sur}} = 0.027$) and height-varying grass ($n_{\text{veg}} = 0.041$) giving $n_l = 0.049$.

Results for the River La Suela

Figure 4.23 shows the resulting stage-discharge predictions and the measured data – which provide a reasonable fit due to calibration. Figure 4.24 shows the depth-averaged velocity prediction for 1.52 m depth. For both cases the data fall largely within the credible upper and lower uncertainty scenarios.

Exploring what-if scenarios for the River La Suela

As little is known about this river, the La Suela provides a useful example to explore different ‘what-if’ scenarios for the predicted depths, flows and velocities. The aim is to improve understanding of how the channel behaves through testing the sensitivity of the CES flow predictions to changes in the input parameters. For example:

- 1 What happens if the channel bed roughness is doubled i.e. $n_l = 0.068$?
- 2 What happens if the channel bed roughness is halved i.e. $n_l = 0.017$?
- 3 What happens if the channel bank roughness is doubled i.e. $n_l = 0.1$?
- 4 What happens if the channel bank roughness is halved i.e. $n_l = 0.025$?
- 5 What happens if the channel is lined with concrete i.e. $n_l = 0.02$?
- 6 What happens if the concrete-lined channel is made rectangular?
- 7 What happens if the bed slope is doubled i.e. slope = 0.00271?
- 8 What happens if the bed slope is halved i.e. slope = 0.000678?
- 9 What happens if the channel is meandering with a sinuosity of 1.5?
- 10 What happens if the channel is meandering with a sinuosity of 2.5?

Exploring these scenarios provides some insight into the input parameters which are driving the predictions, for example, the importance of survey versus roughness. This may help direct the effort when obtaining improved local information. For a more detailed CES sensitivity analysis of numerous experimental and natural channels, see Latapie (2003) and Mc Gahey (2006).

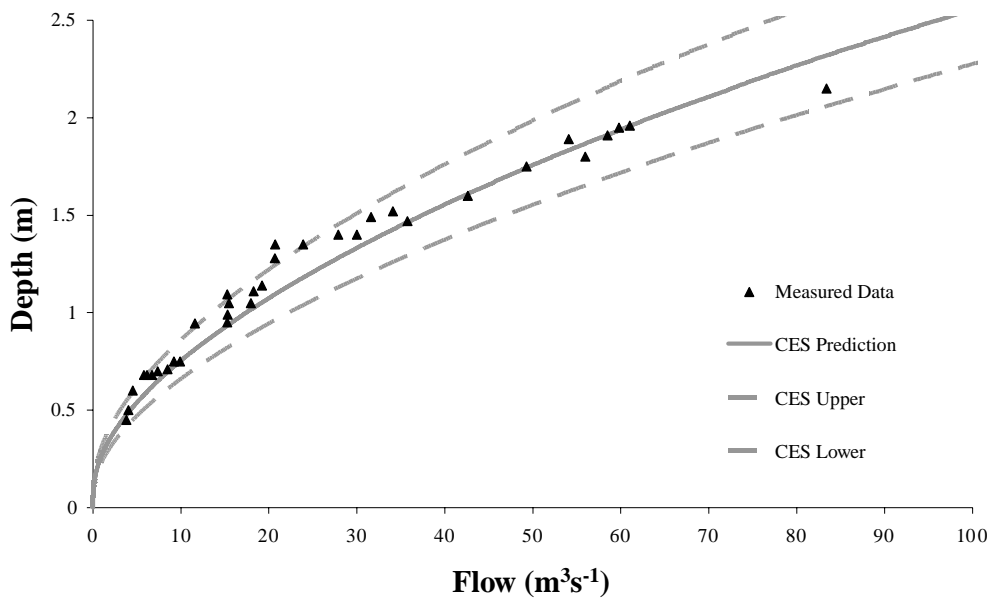


Figure 4.23 Stage-discharge prediction for the River La Suela.

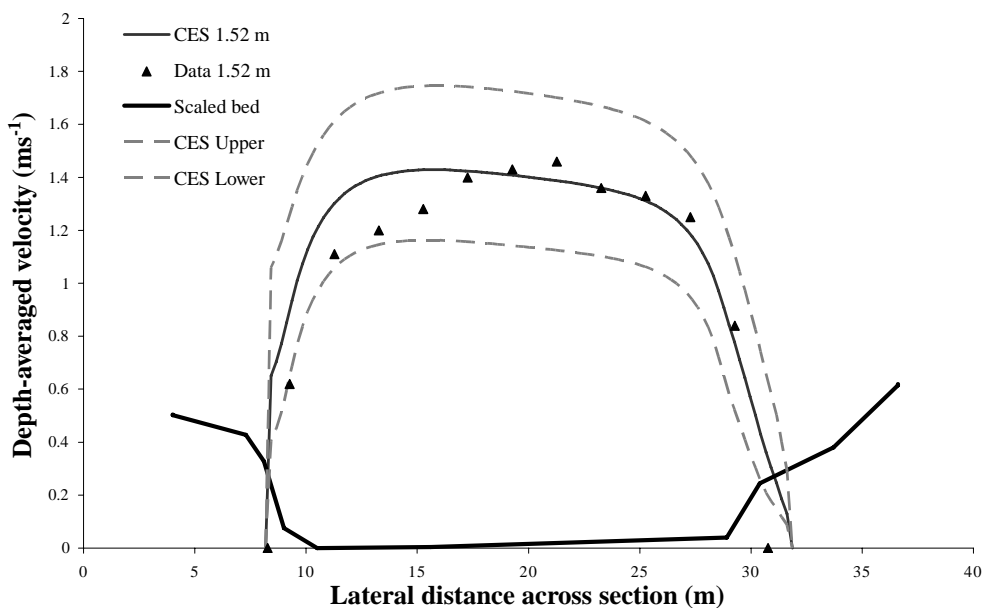


Figure 4.24 Depth-averaged velocity prediction for 1.52 m flow depth showing the uncertainty scenarios ($Q_{\text{CES}} = 38 \text{ m}^3\text{s}^{-1}$; $Q_{\text{data}} = 34 \text{ m}^3\text{s}^{-1}$).

i Results for what-if 1 to 6

What-if scenarios 1 to 6 are designed to improve understanding of the influence of channel roughness on flow within the channel. This includes the magnitude of the roughness (e.g. double or half the calibrated roughness value, concrete-lined) and the distribution of the roughness (e.g. the importance of bank cover versus bed cover). The outcomes are peculiar to the La Suela River and should only be considered as indicative for other channels of similar size, shape and roughness.

Figure 4.25 shows the CES predicted stage-discharge, measured data and the revised stage-discharge predictions based on scenarios 1 to 6. Intuitively, any increase in roughness results in a decrease in flow and vice versa for all depths. To this end, the results of scenarios 1 and 2 are both shown in solid lines and the results of scenario 3 and 4 are both indicated with dashed lines. Some observations can be made:

- bed roughness has a greater influence on flow than a change in bank roughness;
- a change in bed roughness influences the curve throughout the depth range;
- a change in bank roughness has little influence at low flow depths and increasing influence with increasing depth of flow;
- concrete-lining ($n_l = 0.02$ for the banks and floodplain) increases the flow capacity of the channel to a similar magnitude as scenario 2 (n_l bed = 0.017) as may be expected;
- the rectangular shape appears to improve conveyance; however this is only an artefact of the change in area for a given flow depth (here, the change in area is only zero at 1.52 m);
- there is a large amount of scatter in the measured data, particularly at flow depths of 1.3 to 1.5 m, and none of the predicted curves capture this.

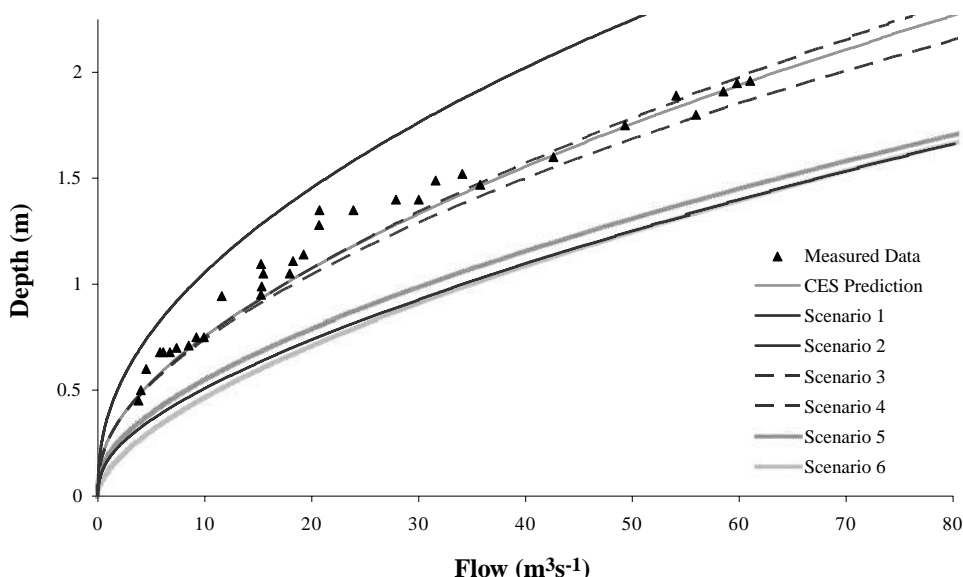


Figure 4.25 Scenario 1 to 6 stage-discharge prediction for the River La Suela.

[Figure 4.26](#) shows the corresponding predicted velocities for scenarios 1 to 4 for a 1.52 m depth together with the measured data. The observations include:

- the change in bank roughness influences the velocity profile close to the channel banks;
- the point at which the altered velocity due to the change in bank roughness returns to the original velocity profile mid-stream may differ for different degrees of bank roughness;
- the change in bed roughness has a significant impact on the mid-stream velocity profile which weakens towards the channel banks.

[Figure 4.27](#) shows the predicted velocities for scenarios 5 and 6 for 1.52 m depth (i.e. zero change in area) together with the measured data and scaled rectangular geometry. The observations include:

- increased velocities due to the concrete lining for both scenarios;
- change in velocity profile as a result of the change in channel shape.

The main findings for the River La Suela are that altering bed roughness has a more significant impact on the channel conveyance than altering the bank roughness; and that concrete-lining improves the conveyance capacity from that of a natural channel – as expected. These outcomes may well differ for very narrow channels where the channel banks have a more influential role on the mid-stream velocities. Similarly, for very wide channels, it is likely the channel banks will have little influence.

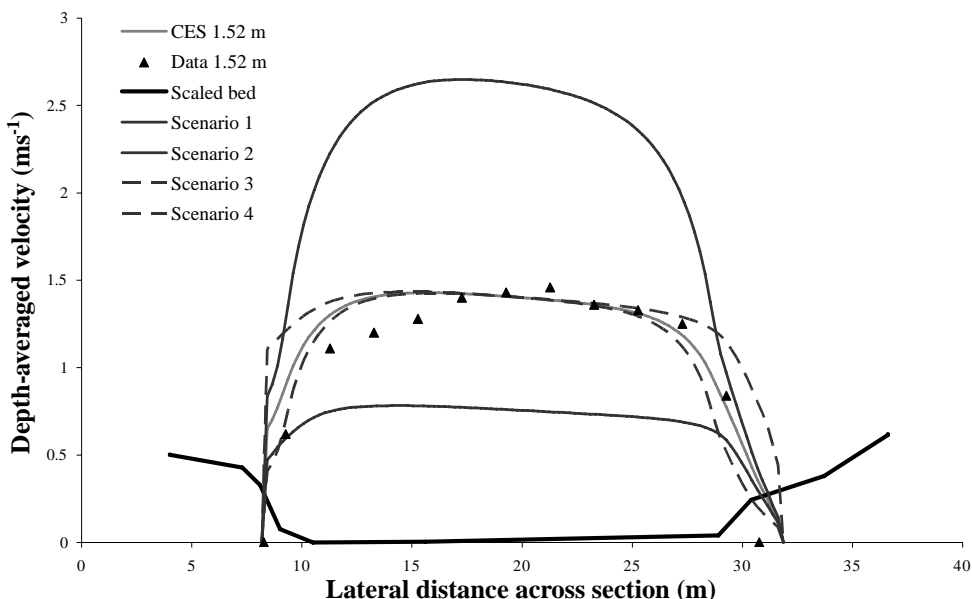


[Figure 4.26](#) Scenario 1 to 4 depth-averaged velocity predictions for 1.52 m flow depth ($Q_{CES} = 38 \text{ m}^3\text{s}^{-1}$; $Q_{data} = 34 \text{ m}^3\text{s}^{-1}$; Scenarios $Q_1 = 22 \text{ m}^3\text{s}^{-1}$; $Q_2 = 69 \text{ m}^3\text{s}^{-1}$; $Q_3 = 38 \text{ m}^3\text{s}^{-1}$; $Q_4 = 41 \text{ m}^3\text{s}^{-1}$).

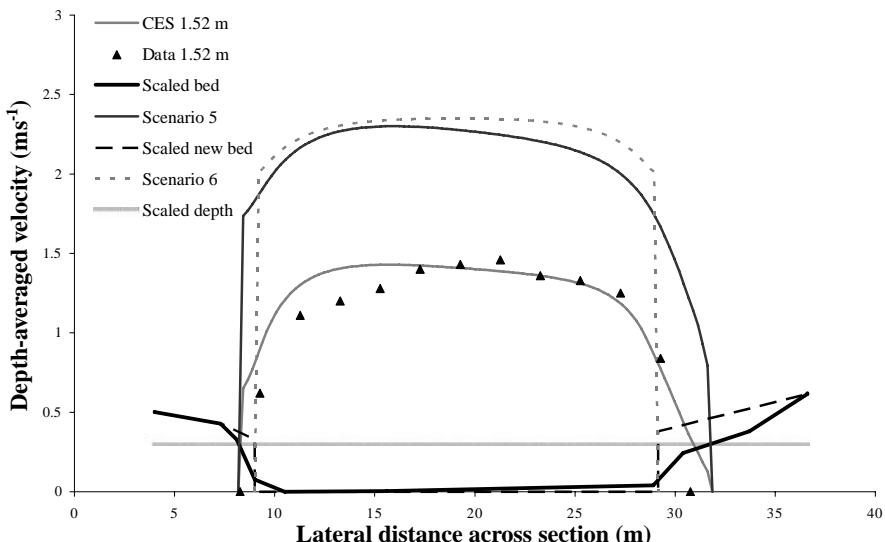


Figure 4.27 Scenario 5 and 6 depth-averaged velocity predictions for 1.52 m flow depth ($Q_{CES} = 38 \text{ m}^3 \text{s}^{-1}$; $Q_{data} = 34 \text{ m}^3 \text{s}^{-1}$; Scenarios $Q_5 = 65 \text{ m}^3 \text{s}^{-1}$; $Q_6 = 69 \text{ m}^3 \text{s}^{-1}$).

ii Results for what-if 7 and 8

What-if scenarios 7 and 8 are designed to improve our understanding of the influence of longitudinal bed slope on channel flow capacity. The scenarios involve doubling (slope = 0.00271) and halving (slope = 0.000678) the bed slope. Figure 4.28 provides the resulting stage-discharge distributions. From this it is apparent that obtaining the correct bed slope is imperative to determining the flow rate ($-30\% > \% \text{ change} > +45\%$, Table 4.2).

The calculation of conveyance using the CES approach requires the bed slope as an input as it solves for the unit flow rate (Chapter 3). As conveyance is independent of slope, the conveyance is calculated by dividing the final flow rate by the slope $K = Q/S_o^{1/2}$. Figure 4.29 provides the calculated conveyance for the CES prediction and scenario 7 and 8 as well as the values obtained from the measured data. Here, it is apparent that the conveyance has little dependence on slope and is therefore a robust measure of the channel capacity. For further details on slope testing see Mc Gahey (2006).

iii Results for what-if 9 and 10

What-if scenarios 9 and 10 are designed to improve our understanding of the influence of sinuosity on in-channel velocity profiles. The River La Suela cross-section is located in a straight portion of the reach and therefore has a sinuosity of 1. Scenarios 9 and 10 involve increasing the sinuosity in a left-bearing bend to 1.5 and 2.5 respectively. Figure 4.30 provides the depth-averaged velocity profiles for these. On the right or outside bend – there is no change in velocity profile. On the left or inside of the bend the velocities are reduced – and the reduction corresponds to the magnitude of the

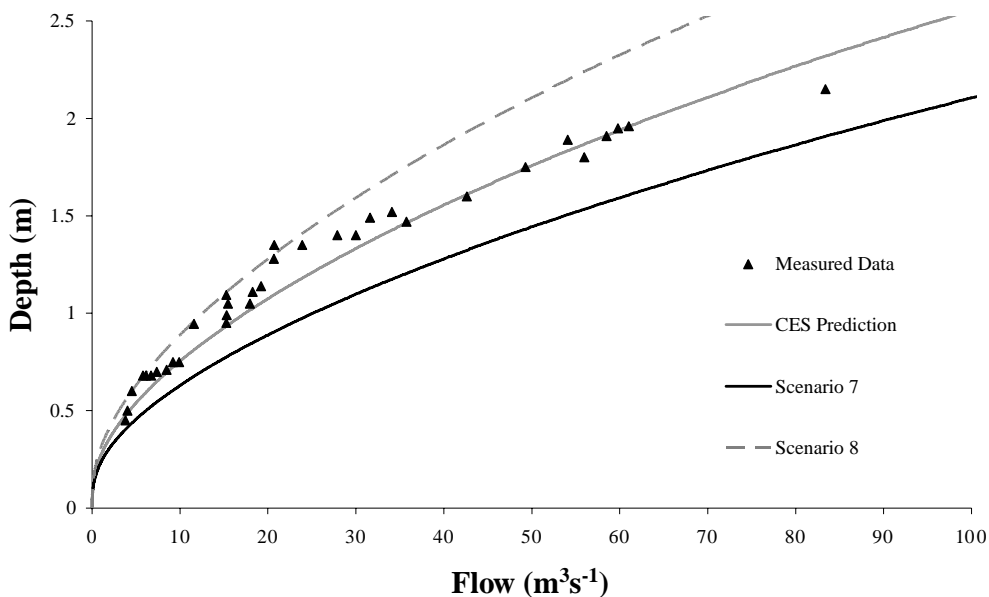


Figure 4.28 Scenario 7 and 8 stage-discharge prediction for the River La Suela.

Table 4.2 Summary of predicted and measured flow rates for 1.52 m and 1.75 m flow depths.

	@ 1.52 m depth		@ 1.75 m depth	
	Flow rate ($m^3 s^{-1}$)	Change in flow rate (%)	Flow rate ($m^3 s^{-1}$)	Change in flow rate (%)
Measured	34	-11	49	-1
Original CES	38	0	50	0
Scenario 1 – double bed roughness	22	-43	30	-40
Scenario 2 – halve bed roughness	69	80	86	74
Scenario 3 – double bank roughness	38	-2	48	-3
Scenario 4 – halve bank roughness	41	7	54	8
Scenario 5 – concrete-lined channel	65	70	84	69
Scenario 6 – concrete-lined rectangular	69	79	86	73
Scenario 7 – double bed slope	55	44	71	43
Scenario 8 – halve bed slope	28	-28	36	-28
Scenario 9 – sinuosity 1.5	39	2	50	1
Scenario 10 – sinuosity 2.5	37	-4	47	-5

sinuosity. This is typically reversed for overbank flows, with the higher main channel velocities observed in the outside of the bend (as observed in the Flood Channel Facility data). For this case, the impact on the overall flow rate is small (<5% for both cases, Table 4.2).

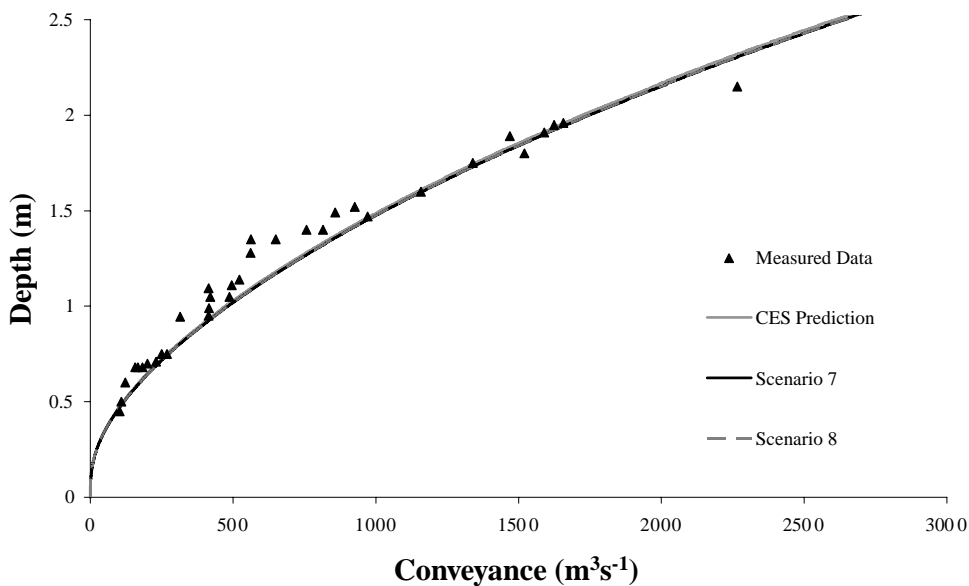


Figure 4.29 Scenario 7 and 8 conveyance prediction for the River La Suela.

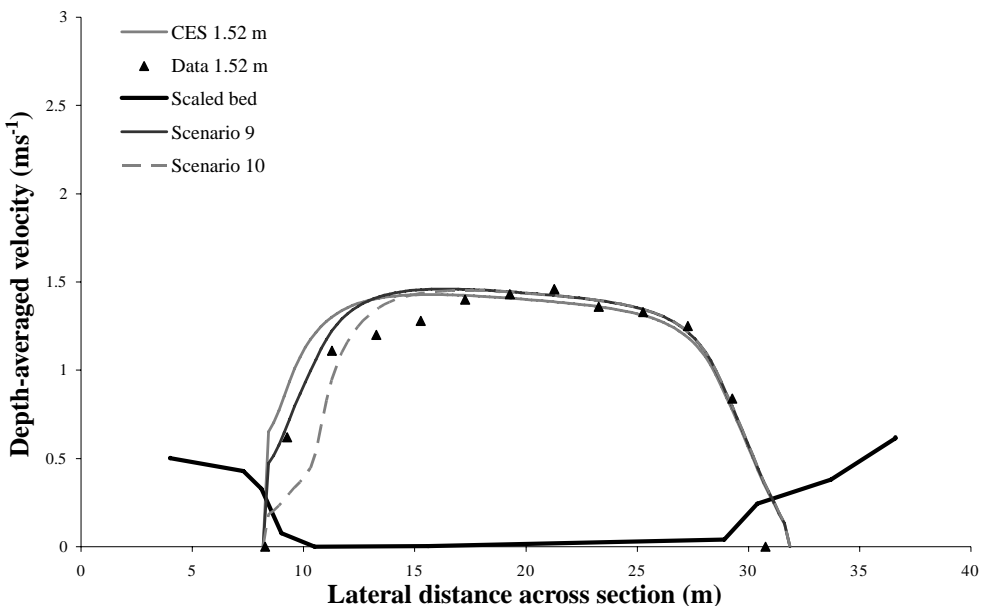


Figure 4.30 Scenario 9 and 10 depth-averaged velocity predictions for 1.52 m flow depth ($Q_{\text{CES}} = 38 \text{ m}^3\text{s}^{-1}$; $Q_{\text{data}} = 34 \text{ m}^3\text{s}^{-1}$; Scenarios $Q_9 = 39 \text{ m}^3\text{s}^{-1}$; $Q_{10} = 37 \text{ m}^3\text{s}^{-1}$).

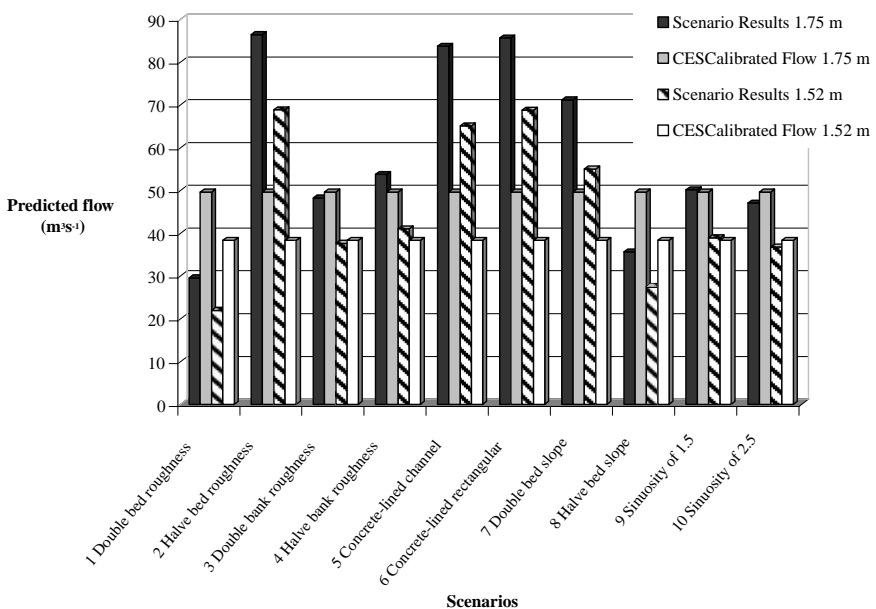


Figure 4.31 Summary of predicted and measured flow rates for 1.52 m and 1.75 m flow depths.

iv Summary flow results all scenarios

Table 4.2 provides a summary of the predicted and measured flows for Scenarios 1 to 10 at flow depths of 1.52 m and 1.75 m. It also indicates the percentage difference in flow rate relative to the calibrated CES flow rate. Figure 4.31 provides a corresponding visual impression of these results.

From this, it is apparent that Scenarios 1, 2, 5, 6, 7 and 8 have the largest influence on the flow rate for the La Suela i.e. altering the bed roughness, concrete-lining the channel and altering the bed slope. Scenarios 3, 4, 9 and 10 have the least impact i.e. altering the bank roughness and the sinuosity. Although these outcomes are specific to the River La Suela and are likely to be different for other channel types (e.g. irregular, compound, narrow/wide, vegetation, boulders, alluvial etc.), they serve to show the qualitative changes that might be expected.

4.2.6 Application of the CES to a mountain stream with boulders

Aim

CES stage-discharge simulations are carried out for two mountain rivers, the River Waiwakaiko (New Zealand) and the River Tomebamba (Ecuador). These are used to demonstrate the use of the CES for mountain streams with boulders and to propose an alternative roughness law to the current CES prediction of ' f ' (Chapter 3,

Colebrook-White law) where large boulders are present. The alternative approach is based on that of Abril and Knight (2004).

Approach for boulders

Abril and Knight (2004) proposed an alternative approach for evaluating boulder roughness in mountain rivers based in part on the work of Ramette (1992), where,

$$f_{mc} = 8 \left[5.75 \log \left(\frac{12H_{mc}}{3d_{90} + \varepsilon_r} \right) \right]^{-2} \quad (4.1)$$

and d_{90} (m) is the sediment dimension, ε_r is a coefficient representing the bed form roughness and f_{mc} is evaluated from,

$$f = f_{mc} \left(0.669 + 0.331D_r^{-0.719} \right) \quad (4.2)$$

H_{mc} is taken as the maximum local cross-section depth and ε_r is zero for the channels considered.

The CES supports simulations for a wide range of channel types e.g. different section and plan form shapes, sizes, vegetation types, substrate cover, etc. An important component of the calculation is the ability to adapt the model as appropriate to the particular site characteristics. For example, where the roughness varies significantly within a cross-section, the model allows for a description of the local roughness values and these are taken into account in the calculation. However, there are some areas which are more challenging, where the basic science is still emerging, for example:

- 1 vegetation which changes its behaviour (e.g. form, resistance) as a function of velocity and depth;
- 2 alluvial channels where the bed roughness is characterised by bed form growth and wash-out;
- 3 very large channels (e.g. Alto Parana, Argentina, flows upwards of $20,000 \text{ m}^3 \text{s}^{-1}$) where the roughness laws developed for small channel and pipe flow may not be applicable;
- 4 steep mountain streams with large boulders – comparable with flow depth.

The following pages now illustrate topic 4 above further, using data from two mountain rivers.

The River Waiwakaiho site

Stage and discharge measurements were taken at station SH3 along the River Waiwakaiho over the nine year period, January 1980 to 1989. The Waiwakaiho serves a catchment area of 58 km^2 , has a mean annual flood of $327 \text{ m}^3 \text{s}^{-1}$ and an average flow rate of $0.63 \text{ m}^3 \text{s}^{-1}$. The observations were made at three cross-sections along a fairly straight 100 m reach, each approximately 40 m wide and 2 m deep. The water surface slope varied from 0.0091 at low depths to 0.0176 at large depths. The bed

comprises cobbles and boulders, some as large as 2 m in diameter (Figure 4.32), and the banks consist of boulders with occasional scrub. The observed Manning n values vary with depth in the range 0.047 to 0.180.

River and cross-section definition for River Waiwakaiho site

Based on this description the assigned roughness values include (Figure 4.33):

- *Channel bed* – The RA bedrock ($n_{\text{sur}} = 0.025$) and boulders >50% ($n_{\text{irr}} = 0.045$) giving $n_l = 0.051$.
- *Channel banks* – The RA cobbles 64–256 mm ($n_{\text{sur}} = 0.035$).
- *Channel high banks* – The RA sand ($n_{\text{sur}} = 0.02$).

The River Tomebamba site

The River Tomebamba is a natural mountain river located in the Southern Andean region of Ecuador, another tributary to the Paute River. Water level, discharge, velocity and roughness measurements were taken along the Tomebamba River at

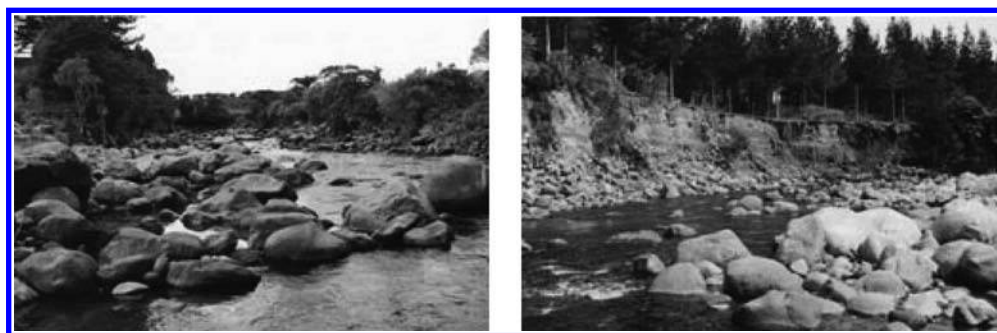


Figure 4.32 River Waiwakaiho at SH3 looking (a) upstream and (b) downstream along the reach (Hicks & Mason, 1998).

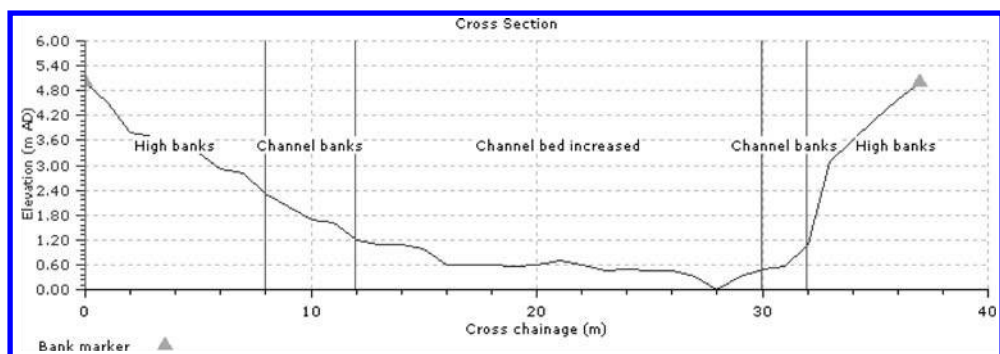


Figure 4.33 River Waiwakaiho cross-section, roughness zones and top-of-bank marker locations.

Monay. The channel is 25 m wide and the reach-averaged longitudinal bed slope is 0.0176. Here, the river bed consists of large boulders, approximately 1.3 m in diameter, and the Manning n values, back-calculated from discharge and water level measurements, range from 0.08 to around 0.15 (Abril & Knight, 2004).

River and cross-section definition for River Tomebamba site

Based on this description the assigned roughness value for the whole section is (Figure 4.34):

- *Channel Cover* – The RA bedrock ($n_{\text{sur}} = 0.025$) and boulders $>50\%$ ($n_{\text{irr}} = 0.045$) giving $n_l = 0.051$.

Results for the River Waiwakaiho and the River Tomebamba

Figure 4.35 provides the CES predicted stage-discharge based on the aforementioned RA values. These are labelled as “uncalibrated” and it is clear the CES roughness is too small, resulting in the flow capacity being over-predicted. The roughness values for the two rivers were increased to better simulate the data. The Waiwakaiho calibrated channel bed roughness is $n_l = 0.5$ (2 m boulders) and the Tomebamba calibrated channel roughness is $n_l = 0.25$ (1.3 m diameter boulders). These calibrated curves (dashed lines) fall closer to the data; although the curve shape of the data is not captured. The reason for this is most likely related to the use of the Colebrook-White law in areas where the boulder size is comparable with depth and different flow mechanisms are taking place. Note that a unit roughness value of 0.25 corresponds to a k_s value of 7.4 m, substantially larger than the 1–2 m boulders.

The boulder approach of Abril and Knight (2004) is also used to simulate the data. Here, the initial d_{90} is taken as 2 m and 1.3 m for the Waiwakaiho and Tomebamba. The curves were then calibrated using the sediment dimension and the final d_{90} 's are 2.1 m and 2 m for the Waiwakaiho and Tomebamba. Figure 4.35 shows how the shape of the curve follows the data more closely than the Colebrook-White approach.

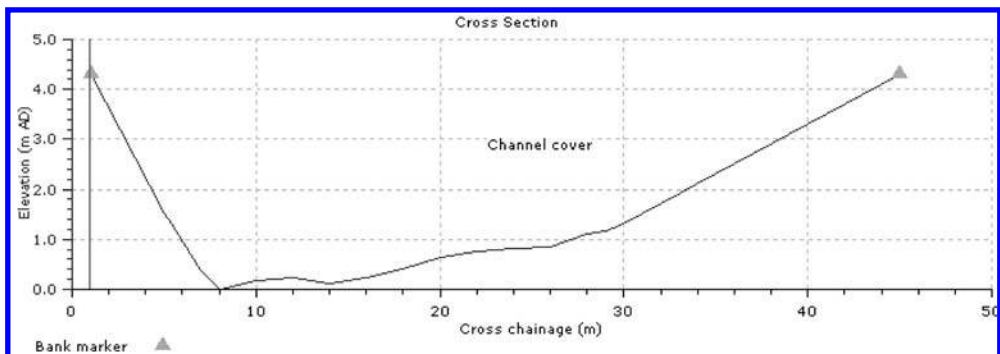


Figure 4.34 River Tomebamba cross-section, roughness zones and top-of-bank marker locations.

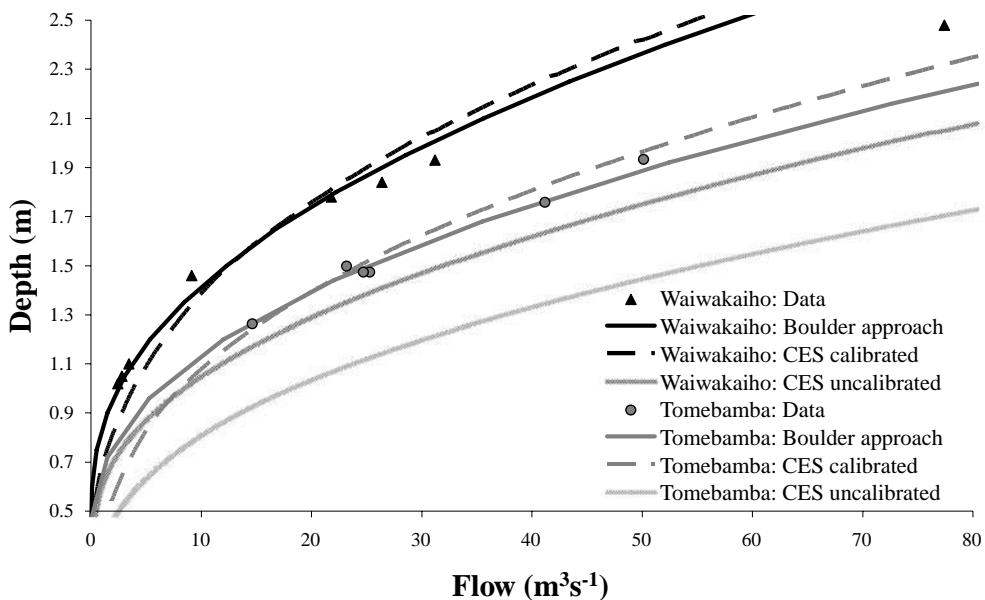


Figure 4.35 Stage-discharge predictions for the River Waiwakaiho and the River Tomebamba using different roughness calculations.

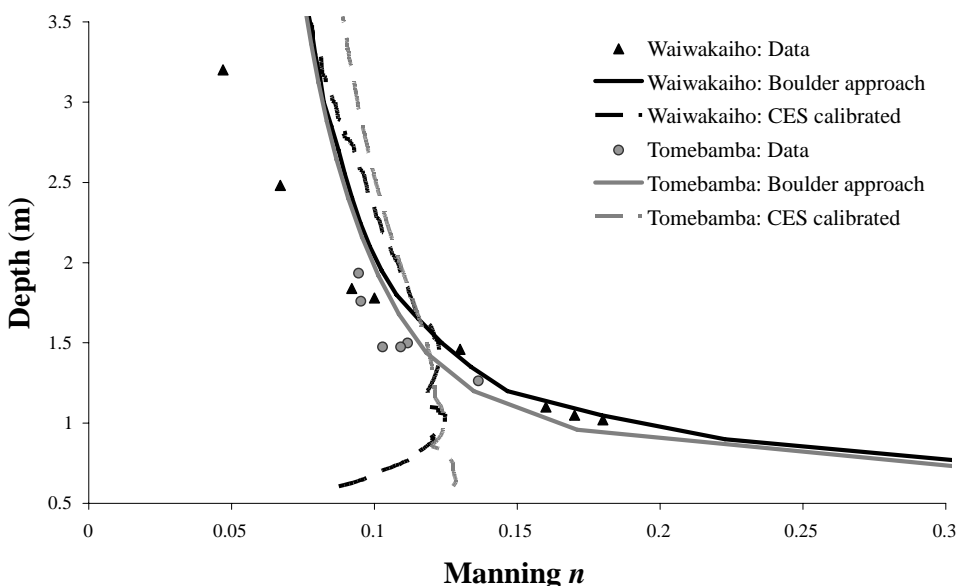


Figure 4.36 Back-calculated Manning n values for the River Waiwakaiho and the River Tomebamba using different roughness calculations.

At flow depths greater than 2 m, both approaches provide poor predictions which may be due to the particular boulder layout at the site or, more fundamentally, that the boulder formulae may only be applicable for a limited range e.g. flow up to the level of the sediment diameter, d_{90} . If the boulder approach is adopted in the CES, a transitional roughness rule between the two approaches should be explored.

Figure 4.36 provides the back-calculated Manning n values for both approaches. As before, the boulder approach best captures the shape of the data.

4.3 USE OF BACKWATER MODULE FOR ESTIMATING WATER LEVELS ALONG THE RIVER MAIN

Aim

This example demonstrates the use of the CES-AES backwater calculation to calculate water levels along a reach of the River Main with:

- i an inflow of $60 \text{ m}^3\text{s}^{-1}$ and a downstream control of 36 mAD; and
- ii an inflow of $10 \text{ m}^3\text{s}^{-1}$ with normal depth conditions at the downstream end.

For condition (i), the channel section 600 m along the reach needs to convey the 100 year return period storm ($Q_{100} = \sim 60 \text{ m}^3\text{s}^{-1}$) below a water level of 38 mAD, despite the new downstream control at 36 mAD.

For condition (ii), the water levels 1400 m along the reach need to be maintained above 35 mAD for flows above $10 \text{ m}^3\text{s}^{-1}$, to ensure the land drainage pumps can operate. Below this flow, the land drainage pumps are automatically turned off. This is explored for the 12 month period prior to installation of the new 36 mAD downstream control. Thereafter, the water levels will be sufficient to ensure pump operation.

The River Main reach

A 1.6 km reach of the River Main in County Antrim, Northern Ireland, is used for this example (see Chapter 2, Section 2.2.2 for a full description). The inflow to the reach is just downstream of Lisnafillan weir and the reach extends to Gracehill Bridge. The cross-sections are located at approximately 50 meter intervals and the topographical survey data includes channel and floodplain information, measured at right angles to the main flow direction, and measured as far across the floodplain as possible.

Bridge End Bridge is located about 400 m downstream of Lisnafillan weir and the roughness values for the reach are based on the calibrated values for this site (Section 4.2.3).

Note 1: This reach of the River Main has a series of fish groyne structures (approximately every 500–700 m) which control the depths at low flows. These are excluded from the current CES-AES model – but could readily be introduced as additional reach-averaged cross-sections with ‘short reaches’ or as downstream controls.

Note 2: This reach of the River Main includes 2 bridge structures. These are excluded from the current example but may be introduced using the AES.

Results for the River Main

An initial run is undertaken to assess the water levels along the reach at a more common flow rate of $40 \text{ m}^3 \text{s}^{-1}$. Figure 4.37 provides the model output for this initial run, with inflow $40 \text{ m}^3 \text{s}^{-1}$, and a downstream level of 36 mAD. The surface profile is more-or-less parallel to the ground profile in the upstream reach and in the downstream reach it approaches the controlled level of 36 mAD. The velocity profile indicates the higher velocities in the upstream reaches (in the region $1.25\text{--}2.0 \text{ ms}^{-1}$) and lower velocities ($<1.25 \text{ ms}^{-1}$) further downstream due to the control. The water levels approximately 600 m and 1400 m downstream of Lisnafillan weir are 37.7 mAD and 36.1 mAD respectively.

Figure 4.38 provides the model outputs for condition (i). The downstream water level is controlled at 36 mAD (assuming no drowning) and the 100 year return period storm, $Q_{100} = 60 \text{ m}^3 \text{s}^{-1}$, is set as the inflow to the reach. The water level 600 m downstream of Lisnafillan weir is 37.9 mAD, which is lower than the required 38 mAD for condition (i). The lower and upper credible scenarios (dashed lines) give water levels of 37.7 mAD and 38.0 mAD respectively at this location. As these are close to the required water level of 38 mAD, some additional resource may be invested to better understand any sources of uncertainty. If the water levels are subsequently considered uncertain, possible options may be explored in the CES e.g. improved vegetation maintenance through altering roughness, dredging through altering channel cross-sections etc.

Figure 4.39 provides the model outputs for condition (ii). The inflow to the reach is $10 \text{ m}^3 \text{s}^{-1}$ and normal depth conditions are present at the downstream end. These correspond to a downstream flow depth of 34.3 mAD. The water surface profile

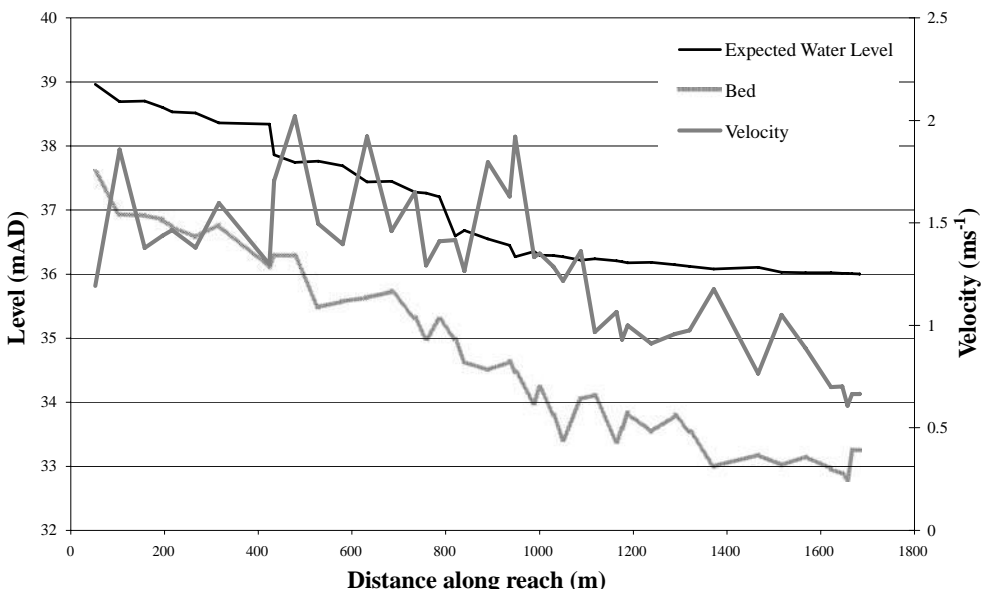


Figure 4.37 Long-section of the River Main reach showing the water surface and velocity profiles for a $40 \text{ m}^3 \text{s}^{-1}$ inflow to the reach and 36 mAD downstream control.

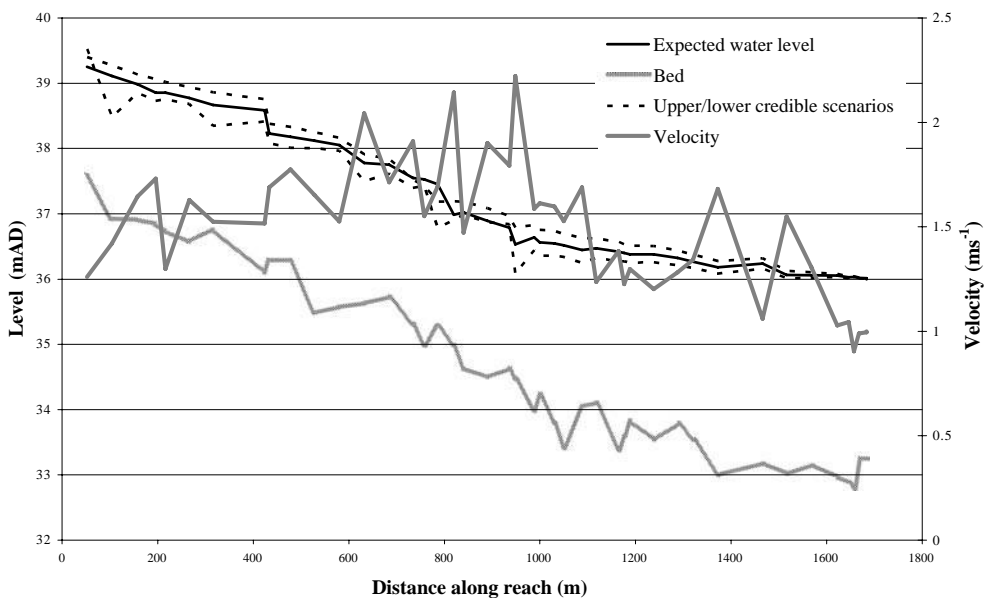


Figure 4.38 Long-section of the River Main reach showing the water surface, upper and lower credible scenarios and velocity profiles for a $60 \text{ m}^3 \text{s}^{-1}$ inflow to the reach and 36 mAD downstream control.

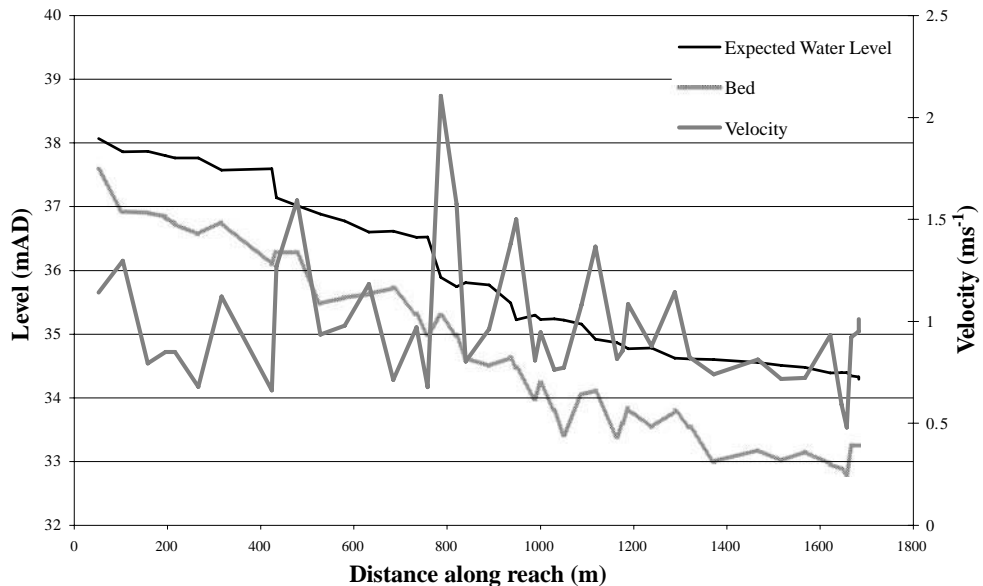


Figure 4.39 Long-section of the River Main reach showing the water surface and velocity profiles for a $10 \text{ m}^3 \text{s}^{-1}$ inflow to the reach with normal depth at downstream end (34.3 mAD).

follows the ground profile more closely as would be expected at low flows, where the effect of the local longitudinal gradient is more dominant. The velocities throughout the reach are in the range 0.5 to 1.5 ms⁻¹ as there is no downstream control to reduce these at the downstream end. The velocity peaks (2.1 ms⁻¹) at ~800 m downstream, which is most likely a result of the local topography i.e. bed level and cross-section shape. At 1400 m downstream of Lisnafillan weir, the expected, upper and lower water levels are all 34.6 mAD. This is well below the required 35 mAD for the drainage pumps and it will be necessary to explore different solutions for this e.g. turn the land drainage pump off at a higher flow rate, introduce a temporary downstream control of ≥35 mAD prior to the planned 36 mAD control.

4.4 ESTIMATING AFFLUX AT BRIDGES

4.4.1 Field scale verification of bridge backwater analysis at Pea Creek, Alabama

Aim

To predict the backwater associated with bridge afflux at a field site where comparisons can be made with survey data (available at http://ms.water.usgs.gov/publications/backwater_HA/HA-608.html).

Pea Creek

The field site is a heavily vegetated floodplain near Louisville, Alabama. It is one of the field sites that was included in the USGS study of backwater at bridges, begun in 1969, that collected detailed topographic and water level surveys plus flow data for 35 floods at 11 sites in the southern USA. This data set remains one of the primary sources of field observations for the study of bridge afflux. Measurements from the Pea Creek site were made for two flood events in December 1971 and published in the Hydrologic Investigations Atlas HA-608 (Colson *et al.*, 1978). The study area is shown in Figures 4.40 and 4.41.

Roughness definition

The Pea Creek is a tributary to the swamp and creek systems of southern Alabama. Floodplains in the region are densely covered with trees (Figure 4.42 shows typical floodplain cover). Underlying substrates are typically silt, sand and clay deposits. Channels are incised into the broad floodplains and so the Roughness Advisor has been used to set unit roughness zones for channel and floodplain zones.

- *Channel bed* – The RA silt with trailing bank side plants is adopted, resulting in a unit roughness of $n_l = 0.053$.
- *Floodplain* – The RA floodplain heavy stands of trees (with depths below branches) is adopted on sand substrate, with resulting $n_l = 0.102$. The reasoning is that the entire floodplain is densely wooded, but there are unlikely to have been significant trailing leafy branches for the vegetation types observed in the field, especially on the date of the modelled event.

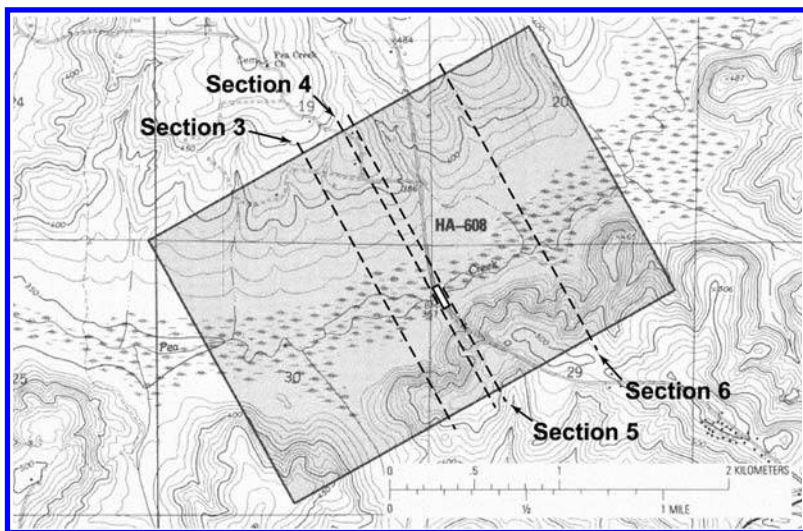


Figure 4.40 Pea Creek site map. Grey box shows extent of study area. Dotted lines show approximate along-stream locations of USGS cross section survey data, section 3 is downstream. Road bridge is situated between sections 4 and 5 (After USGS, 1979).



Figure 4.41 Pea Creek wooded floodplain and road bridge (Photo: USGS).

- *Channel and floodplain roughness at bridge sections* – The AES bridge calculations use Manning's n to represent flow resistance, rather than the unit roughness parameter of the CES (see Section 3.2.5). The bridge unit requires a three panel roughness specification (left overbank, main channel and right overbank),



Figure 4.42 Choctawhatchee/Pea River channel and vegetation (Photograph: Alabama Clean Water Partnership. Reproduced with the permission of StormCenter Communications, Inc.; http://wsfa.envirocast.net/index.php?pagename=ow_watershed_choctawhatchee_river).

separated by ‘left’ and ‘right’ bank markers. Although the Manning’s n and unit roughness are conceptually different quantities, for a short, straight, relatively uniform reach the distinction between the CES and the conveyance calculations based on Manning’s equation is less important. Hence for the short, straight reach within the bridge the unit roughness values have been adopted.

- *Bridge roughness* – The AES calculates energy losses associated with flow acceleration in the transition reaches upstream and downstream of the bridge, plus energy loss associated with friction within the structure. The bridge at Pea Creek is a deck bridge supported by 16 timber pile bents with centres at 4.57 m spacing. It is assumed that each support is made of 4 wooden piles arranged in a 2×2 pattern. The AES treats piers as if they extend continuously from the upstream face to the downstream face of the bridge, which is a common type of structure in the UK. This is unlikely to be the case for the Pea Creek bridge, where the user of more complex hydraulic modelling software would be likely to choose a method based on conservation of momentum to represent form and drag losses around the bridge piers. However, in the simpler AES, only changes in the cross sectional flow area and frictional energy losses are accounted for, and so an ‘effective’ value

of roughness is needed. In this case, the CES floodplain value has been adopted on the basis that, as a crude approximation, dense tree stands on the floodplain may have created similar resistance to flow as closely spaced timber pile supports within the channel.

Cross section definition

Floodplain and bridge cross section data are as published by Colson *et al.* (1978). The floodplain is in general around 300–400 m wide, but contracts to about 75 m at the bridge.

- *River cross sections* – CES cross sections are set up using USGS channel survey data at the locations shown in Figure 4.40. A simple roughness zonation is adopted, with the RA roughness zones for floodplain and channel used, as shown in Figure 4.43 for Section No. 5, which is located approximately 77 m upstream of the bridge (upstream face).
- *Bridge section* – The AES bridge section is shown in Figure 4.44. The bridge length (upstream to downstream faces) is 8 m and the overall valley gradient is very shallow, hence the AES option to use the same cross section and structure profile for both upstream and downstream faces is selected. The soffit elevation is given as 111.8 m above datum and the road elevation as 112.3 mAD.

Results for Pea Creek bridge

Conveyance rating curves for the modelled reach are shown in Figure 4.45. The bridge section is clearly visible showing reduced conveyance at a given elevation owing to the obstruction to flow within the bridge section combined with the frictional resistance. There is, as expected, a sharp change in the curve between soffit and road level, with little change in conveyance. Above the road level, the increase in conveyance with elevation at the bridge section is roughly parallel with the curves for unobstructed sections.

The USGS Hydrologic Investigations Atlas HA-608 includes detailed measurements for an event on 21 December 1972 (Table 4.3), where the discharge, measured

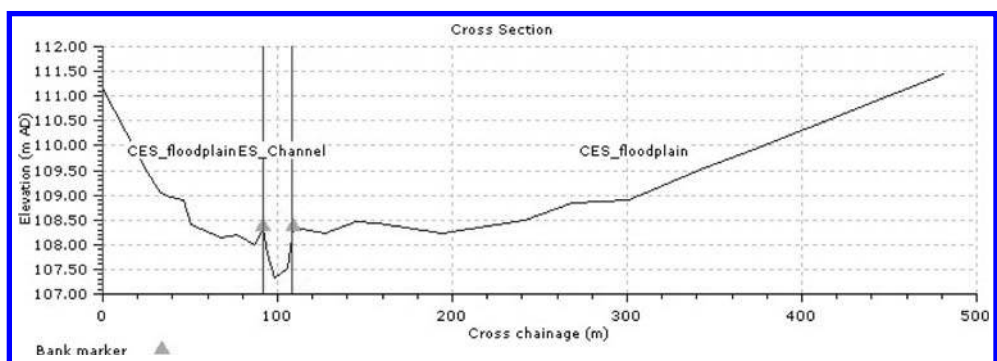


Figure 4.43 Cross-section for Pea Creek site for Section No. 5.

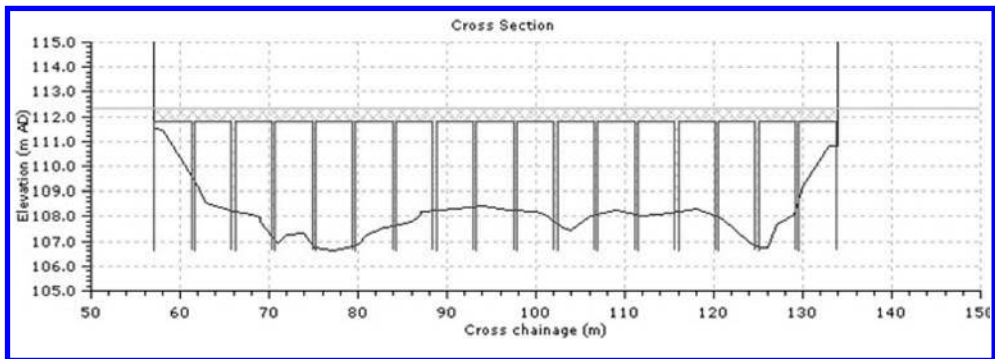


Figure 4.44 Pea Creek AES bridge section.

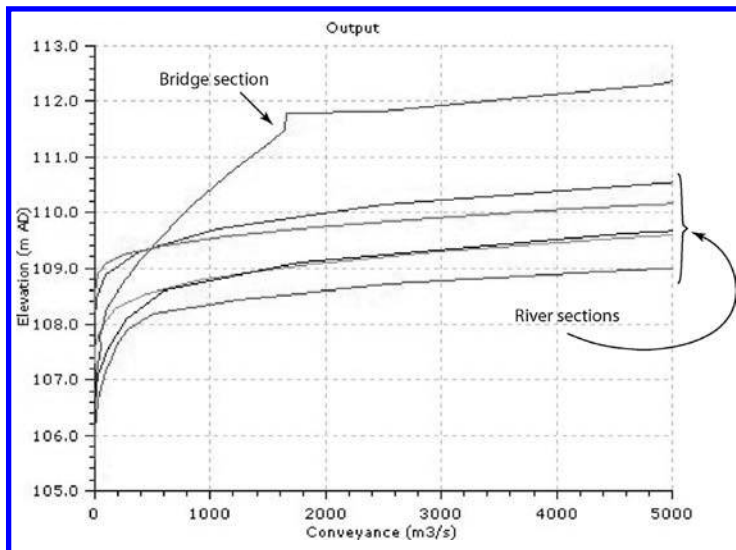


Figure 4.45 CES-AES conveyance curves for Pea Creek.

by velocity area gauging from the bridge, was $50.5 \text{ m}^3\text{s}^{-1}$. The corresponding level of the flood outline surveyed by the USGS at Section No. 3 is 108.5 mAD. This provides a downstream boundary condition for the backwater analysis.

The CES-AES backwater analysis produces water surface profiles as shown in Figure 4.46. The afflux is clearly visible in the comparison of the profile for the reach including the bridge with a second profile where the bridge structure is removed from the model. The modelled water levels can be compared with the surveyed water levels from the flood outline of 21 December 1972.

The surveyed water levels are derived from ground elevations at the mapped flood outline. In some cases, these are uncertain because the outline was between survey points, with no knowledge of the ground elevations in between. In addition, there are

Table 4.3 Surveyed and modelled flood levels for the 21 December 1972 event at Pea Creek.

Section	Flood level from maximum flood outline	Modelled flood level
3	108.50	108.50 (downstream boundary condition)
4	109.05 (uncertain)	108.68
Bridge	109.23	109.29
5	109.53	109.53
6	109.93	109.60

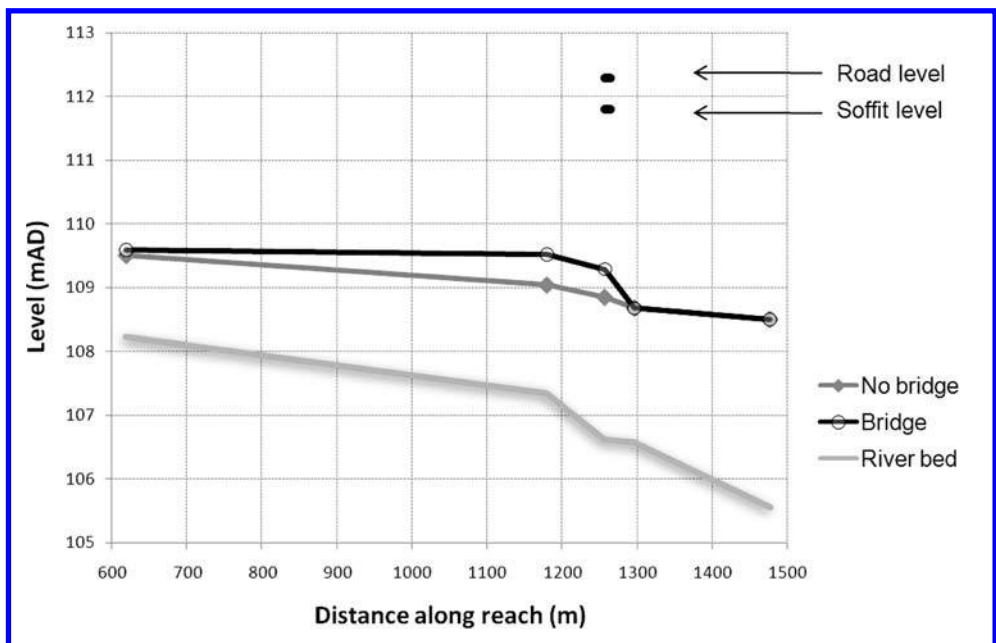


Figure 4.46 Backwater profiles for Pea Creek.

numerous surveyed water levels, assumed to be from water marks on trees, which show uncertainty in identifying a cross section average flood water level. Given the uncertainty in the estimate of flood levels from the measurements, it seems that the CES-AES backwater profile offers a good approximation of the water surface profile in the vicinity of the bridge. In particular, the comparison at Section No. 5, close the location of the afflux, shows very close agreement. Figure 4.47 shows the water surface profiles calculated for the minimum and maximum credible roughness values generated by RA.

This example gives details of one field data test of the AES. Further comparisons between afflux data modeled using AES and field measurements by USGS (1978) have been given by Mantz and Benn (2009).

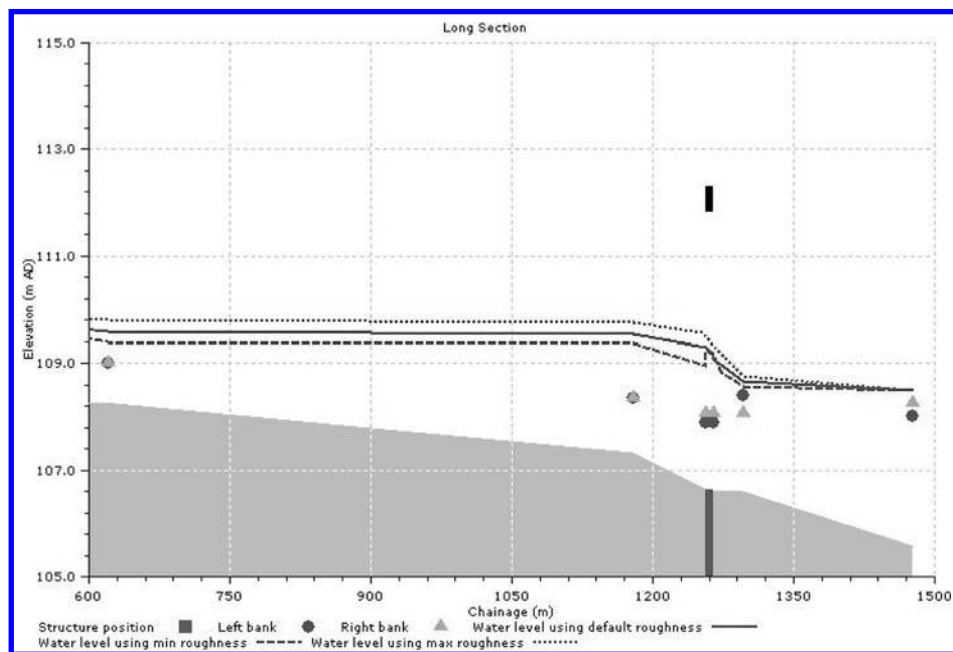


Figure 4.47 Backwater profile for Pea Creek for minimum, default and maximum roughness cases.

4.4.2 Field scale bridge backwater analysis on the River Irwell, UK

Aim

To predict the backwater associated with bridge afflux at a field site on a river in northern England.

Holme Bridge on the River Irwell

The River Irwell flows through Salford close to the city of Manchester in northern England. The Irwell has numerous small tributaries, some of them originating as steep watercourses flowing into small, upland floodplains before joining upstream of Salford. The case study is a twin arched masonry bridge downstream of the town of Rawtenstall. The floodplain and channel gradient is ~ 0.003 for the reach containing the bridge. The floodplain is about 150 m wide and the main channel approximately 25 m wide. The channel is incised at the bridge. The bridge is one of 40 included in a detailed hydrodynamic river model. There are no direct observations available for flows and water levels at the bridge site, but the river is gauged nearby allowing for confident estimates of design flow rates and corresponding water levels are available from the hydrodynamic model for comparison. The upstream and downstream faces of the bridge are shown in Figures 4.48(a) and (b) respectively.



Figure 4.48(a) Holme Bridge, upstream (Photo: JBA Consulting/Maltby Land Surveys) (See colour plate section).



Figure 4.48(b) Holme Bridge, downstream (Photo: JBA Consulting/Maltby Land Surveys) (See colour plate section).

Roughness definition

The reach is an upper branch of the Irwell. The valley has shallow soils underlain by bouldery deposits and bedrock. The floodplain around the bridge is rough grassland with sparse tree cover. The river bank is similar in character to the floodplain. Cross sections upstream and downstream of a bridge in CES-AES require three roughness panels (representing main channel and floodplains on the left and the right). The Roughness Advisor has therefore been used to set roughness zones for the main channel and the floodplain.

- *Channel bed* – The RA coarse gravel with riffles is adopted, resulting in a unit roughness of $n_l = 0.031$.
- *Floodplain* – The RA floodplain light brush with trees is adopted, with resulting $n_l = 0.060$.
- *Channel and floodplain roughness at bridge sections* – The AES bridge calculations use Manning's n to represent flow resistance, rather than the unit roughness parameter of the CES. The bridge unit requires a three panel roughness specification (left overbank, main channel and right overbank), separated by 'left' and 'right' bank markers. Although the Manning's n and unit roughness are conceptually different quantities, for a short, straight, relatively uniform reach the distinction between the CES and the conveyance calculations based on Manning's equation is less important. Hence for the short, straight reach within the bridge the unit roughness values have been adopted.
- *Bridge roughness* – The AES adopts Manning's n values to represent the friction within the arch. In this case a value of $n = 0.020$ is adopted appropriate to an unglazed masonry or brick surface in good condition.

Cross section definition

Floodplain and bridge cross section data were collected by survey.

- *River cross sections* – CES cross sections are set up using the channel survey data at the locations shown in [Figure 4.49](#). A simple roughness zonation is adopted, with the RA roughness zones for floodplain and channel used, as shown in [Figure 4.50](#) for the CES sections located approximately 123 m upstream of the bridge and 89 m downstream.
- *Bridge section* – The AES bridge section is shown in [Figure 4.51](#). The bridge length (upstream to downstream faces) is 3.5 m. The cross section and structure profiles are the same for both upstream and downstream faces. The two arch openings differ slightly in shape but the soffit elevation is approximately 156 m above datum for both. The road elevation is set to equal 157.5 mAD (in fact representing the solid parapet).

Results for Holme Bridge

Conveyance rating curves for the modelled reach are shown in [Figure 4.52](#). The bridge section is clearly visible showing reduced conveyance at a given elevation owing to the



Figure 4.49 Typical bankside and floodplain vegetation around the study reach (Photo: JBA Consulting/Maltby Land Surveys).

obstruction to flow within the bridge section combined with the frictional resistance. There is, as expected, a sharp change in the curve between soffit and road level, with changes in conveyance above road level roughly parallel with the curves for unobstructed sections.

Three ‘design’ flow conditions were analysed using CES-AES, corresponding to flood flows for the return periods of $T = 2, 10$ and 100 years (or annual exceedance probabilities of 50%, 10% and 1%, respectively). The downstream boundary conditions were taken from outputs of the large hydrodynamic river model that included the Holme Bridge. This was a model built using the ISIS Flow software package, with Holme Bridge represented using the arch bridge method of Brown (1988).

The CES-AES backwater analysis produces water surface profiles as shown in Figure 4.53 for each of the three ‘design flows’. In each case, the plot shows the water surface profile computed for the model including the bridge (heavy lines) and also a profile computed after removing the bridge structure from the model. The afflux is hence clearly visible by comparing each pair of profiles.

The afflux is clearly seen to increase with increasing flow rate and hence blockage ratio, as the water level rises into the arch openings. At low water levels, the arch bridge has little effect on the flow because only the relatively slender pier causes an obstruction and the bridge structure contributes relatively little to the frictional energy losses through the section. When water rises above the level of the lowest arch springer

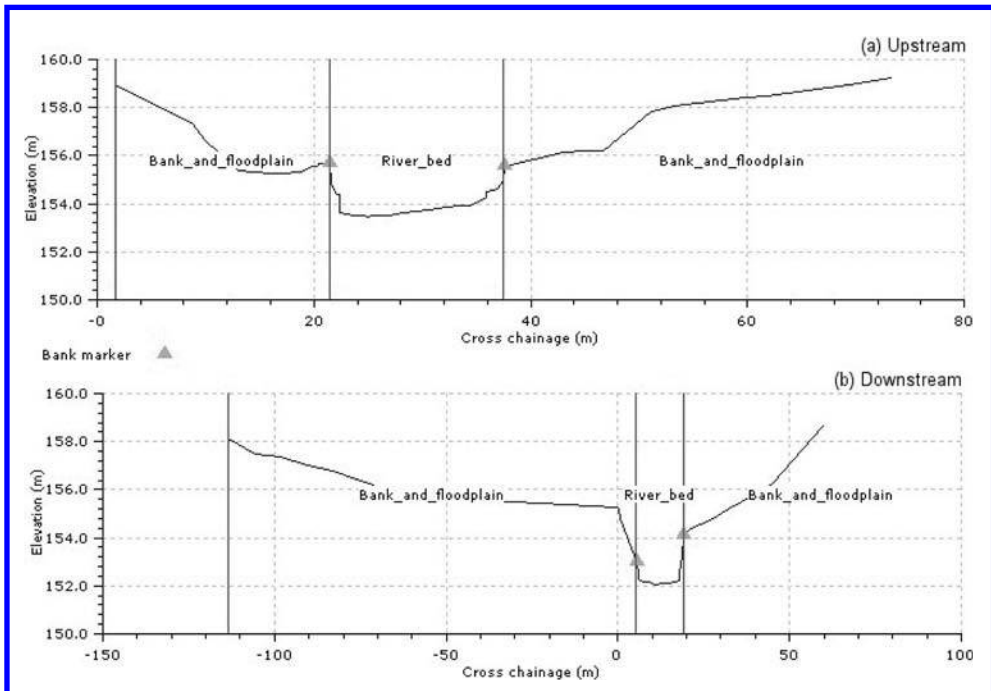


Figure 4.50 CES channel cross sections (a) 123 m upstream and (b) 89 m downstream of bridge section.

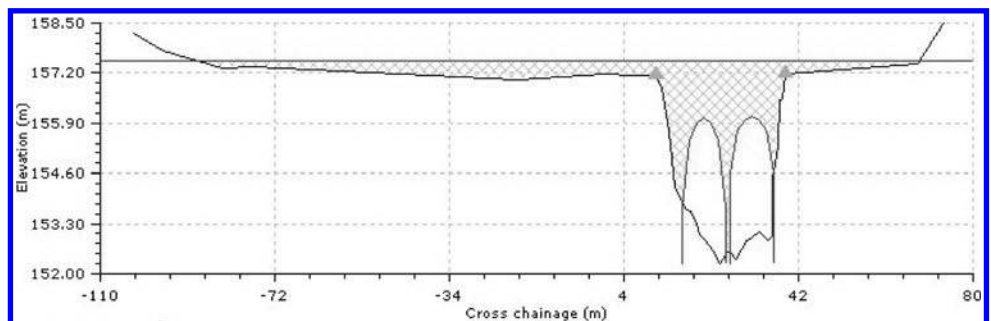


Figure 4.51 Holme Bridge AES bridge section.

then the structure begins to have an effect on the water surface profile. The water surface just rises to soffit level in the modelled 100-year flow condition and so the friction losses caused by the bridge structure are large.

There are no field measurements available to test these results, but it is of interest to compare them with the outputs of the ISIS hydrodynamic model for the same design flow conditions. Table 4.4 shows the flow and water level at the downstream section, the water levels computed at the bridge section in the ISIS simulation and the results

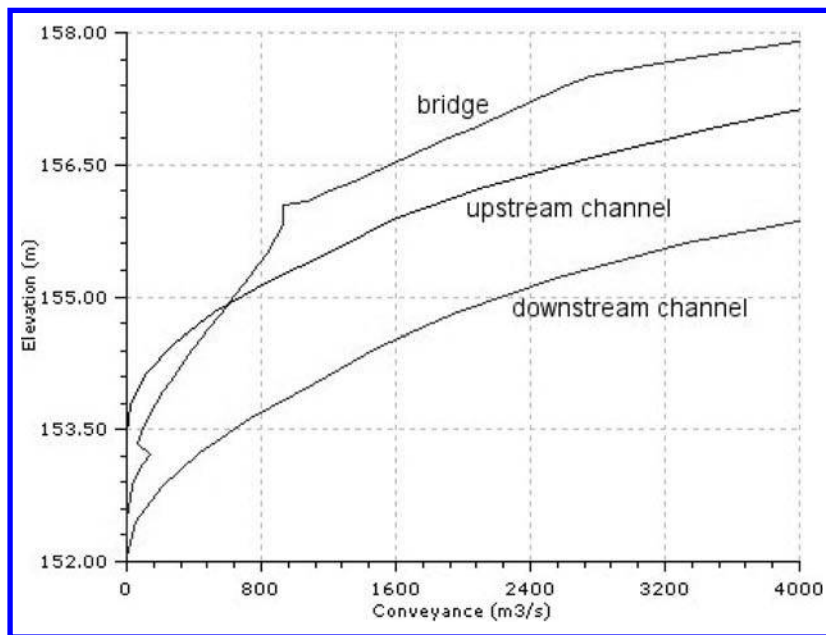


Figure 4.52 CES-AES conveyance curves for Holme Bridge.

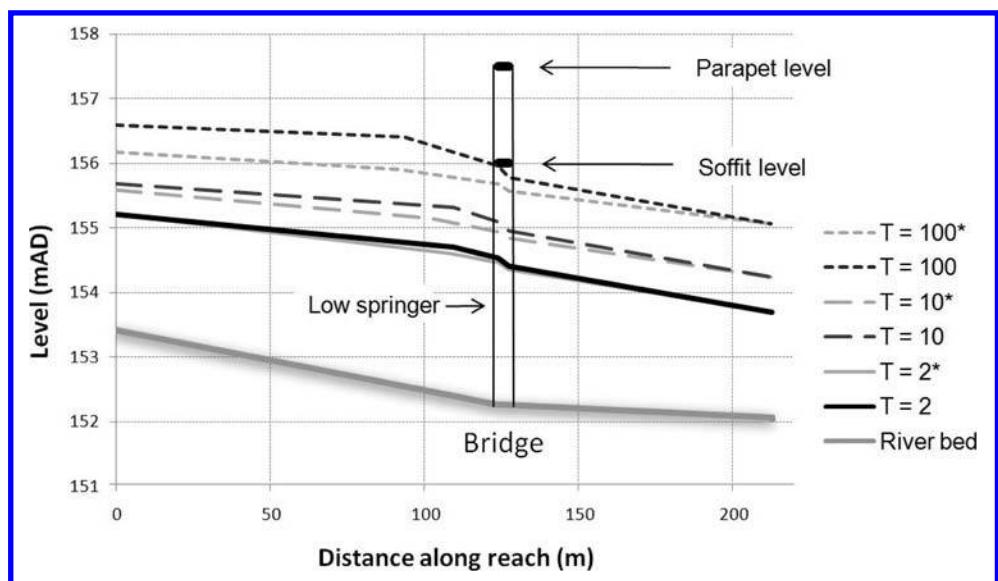
Figure 4.53 Backwater profiles for Holme Bridge for three design flow conditions or return period $T = 2, 10$ and 100 years. For the profiles labelled with an asterisk (*) the bridge was removed from the model.

Table 4.4 Surveyed and modelled flood levels for T = 2, 10 & 100 years at Holme Bridge.

Return period (years)	Flow rate (m^3s^{-1})	Downstream water level (mAD)	ISIS bridge section water level (mAD)	CES-AES water level, downstream bridge face (mAD)	CES-AES water level, upstream bridge face (mAD)
2	45	153.72	154.20	154.41	154.54
10	71	154.24	154.72	154.95	155.10
100	117	155.07	155.60	155.78	155.96

from CES-AES for the downstream and upstream bridge faces. The ISIS bridge unit is based on an empirical dimensionless correlation analysis of afflux, calibrated with laboratory data, and of the same general form as the similarity model used in the AES analysis of transition lengths and energy loss coefficients. This model contains no bridge length scale and is therefore unable to represent the backwater profile through the bridge waterway.

The comparison shows that the CES-AES water levels are similar to those computed using ISIS, but slightly higher. A discrepancy of this size can be judged in the light of extensive tests against scaled laboratory data (Atabay, 2008) that have shown the ISIS ‘ARCH’ bridge unit to have uncertainties in the range of approximately 0.5 to 1.0 meters when estimating an afflux of scale 0 to 3.0 meters.

4.5 ESTIMATING AFFLUX AT CULVERTS

4.5.1 Shallow culvert backwater analysis in a long reach

Aim

To demonstrate backwater analysis for a channel reach including a culvert.

Culvert site

The example is based on the River Main reach described in earlier examples. The reach is 750 m long, and is initially configured for backwater analysis without a structure in place. There are 19 river sections, labelled from 67 (downstream) to 87 (upstream) and a 20 m long culvert is added 560 m downstream. Results are illustrated for a number of example culvert configurations.

Cross section and roughness definition

The channel cross sections immediately upstream and downstream of the culvert are shown in Figure 4.54. The channel upstream and downstream has RA unit roughness values $n_l = 0.102$ for the floodplain, $n_l = 0.045$ for the river banks and $n_l = 0.025$ for the main channel. The culvert roughness, expressed in terms of Manning’s n , is $n = 0.010$.

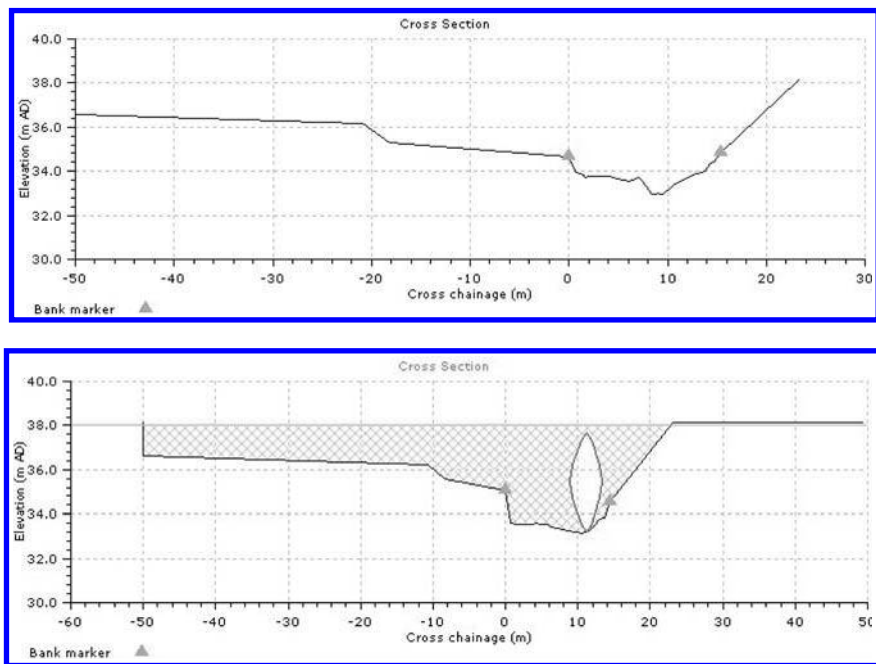


Figure 4.54 Downstream channel and structure cross sections for a pipe culvert in the River Main reach.

Culvert structure

The structure is modelled as a pipe culvert, with a circular concrete inlet set into a headwall (CIRIA type 'A') and square inlet edge. The openings are placed on alignment with the deepest part of the channel. The barrel diameter is 4.5 m.

Results

Conveyance curves are obtained by running a backwater analysis for the reach and plotting the CES-AES output curves, including the results of the afflux calculations (Figure 4.55). It can be seen that, as expected, the conveyance through the culvert is restricted at a given elevation because of the reduction in available flow area. The pipe culvert displays the expected reversal of the conveyance curve as the water level elevation rises into the arch formed in the upper half of the pipe. Above road level, the conveyance increases rapidly with elevation as the channel cross section area expands rapidly above the road.

Water surface profiles are shown in Figure 4.56 for two different downstream boundary conditions, in each case comparing the profiles obtained with and without the culvert. Figure 4.56(a) shows a case where floodplain flow is assumed at the downstream boundary. Here, the culvert overtops the road and the resulting combined pressure and weir flow results in an afflux upstream of approximately 2 m. Figure 4.56(b) shows a flow just within bank at the downstream section. In this case

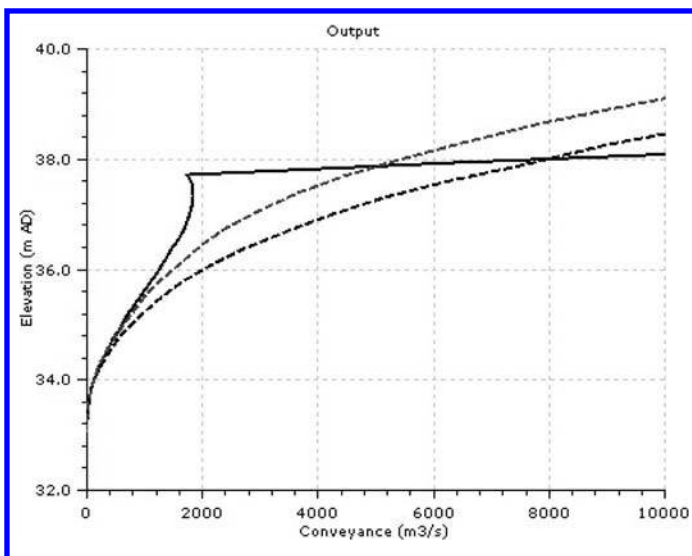


Figure 4.55 Conveyance curves for a pipe culvert in the River Main reach. Solid line shows culvert conveyance at inlet. Dark dashed line shows conveyance in the channel downstream of the culvert, light dashed line upstream.

there is free surface flow through the barrel of the culvert and a smaller afflux of approximately 1 m. Note that there is an increase in velocity through the culvert barrel, as shown by the velocity traces in the CES-AES long section output (Figure 4.57).

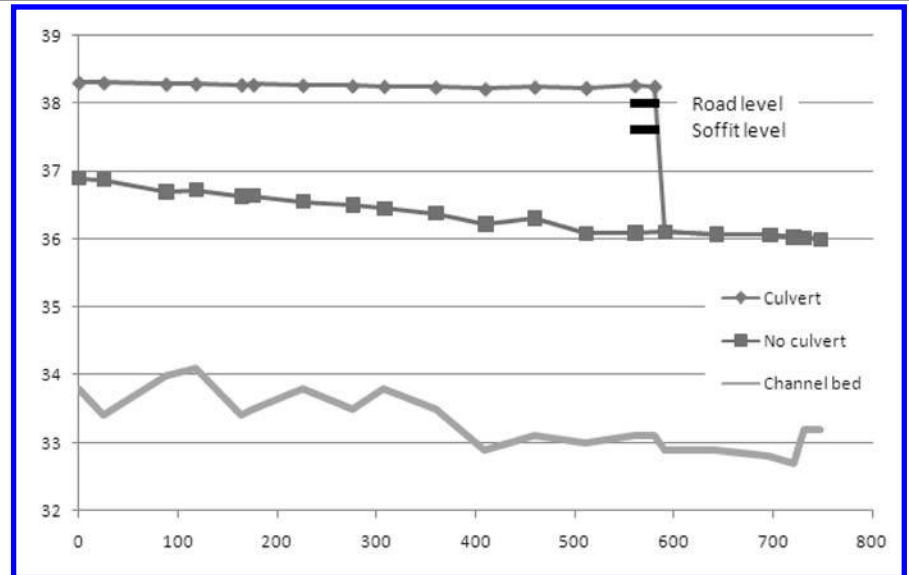
4.5.2 Exploratory culvert design and maintenance calculations in CES-AES

Aim

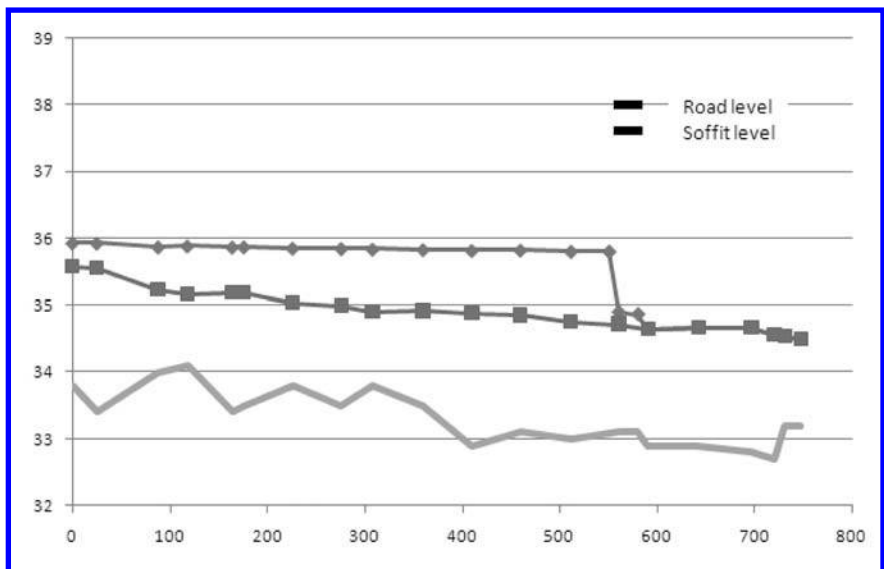
To demonstrate analysis of a trial culvert design. The analysis includes hypothetical scenarios for blockage and deterioration of the culvert barrel condition. The calculations are presented to illustrate an exploratory analysis for a hypothetical culvert design.

Culvert site

The example illustrates simple, exploratory trial calculations for a culvert crossing of a minor road. The required length of the culvert is 12 m and the project requires a box section culvert design. The culvert site is located between two river cross sections in a uniform reach with natural downstream channel control and an average slope of approximately 0.005. The analysis therefore assumes normal depth flow conditions in the reach. The CES-AES model has only three sections. The downstream river section is labelled 1 and the upstream section is labelled 4. Sections 2 and 3 are contained within the culvert unit in CES-AES.



(a)



(b)

Figure 4.56 Water surface profiles for pipe culvert in the River Main reach (a) out of bank flow = $75 \text{ m}^3\text{s}^{-1}$, downstream water level = 36 mAD, (b) in bank flow = $19.7 \text{ m}^3\text{s}^{-1}$, downstream water level = 34.5 mAD. Horizontal axis is distance along stream in meters.

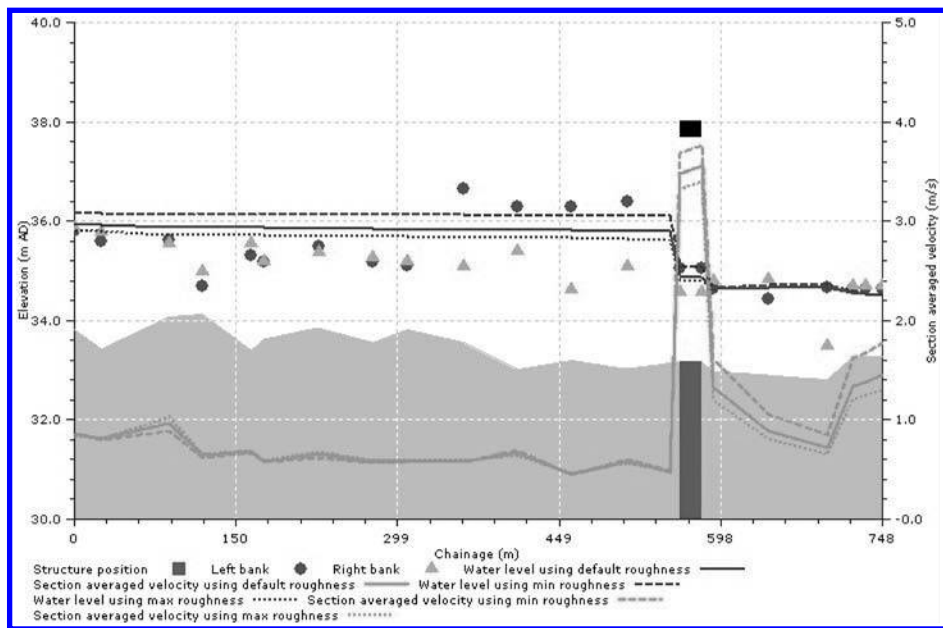


Figure 4.57 Long section backwater profile for reach with 20 m long pipe culvert, showing increased velocity through the culvert barrel.

Table 4.5 Design flow estimates.

Return period (years)	Flow ($m^3 s^{-1}$)
10	3.5
25	4.6
50	5.5
100	8.6

Hydrological analysis has provided design flows for four return periods, as shown in Table 4.5. The area upstream is farmland although there is a car park at the edge of the floodplain. The design should keep any increase in flood water levels to no more than 0.10 m for the 10-year return period flow.

Cross section and roughness definition

The channel cross section downstream of the culvert is shown in Figure 4.58. The main channel comprises medium sized cobbles and so the RA unit roughness values $n_l = 0.102$ is adopted. The floodplain is well grazed pasture and so the RA turf vegetation with no irregularities is adopted with unit roughness $n_l = 0.021$. The CES river cross sections upstream and downstream of the culvert unit have to include three roughness zones, and so there is no separate bank roughness. The banks are assumed

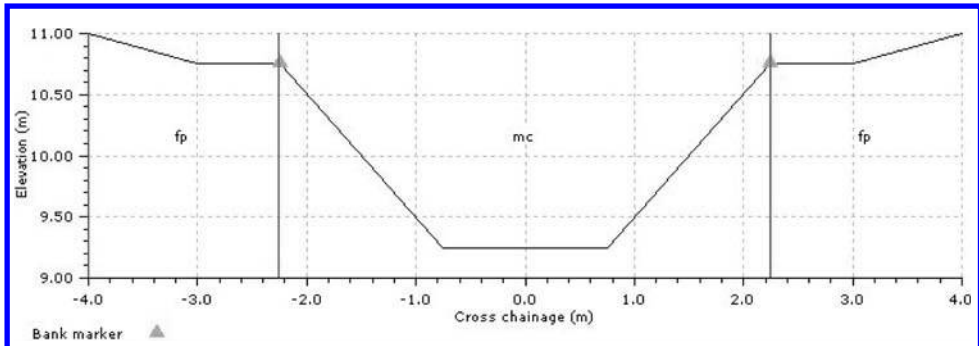


Figure 4.58 Downstream channel cross section. Bed level is 9.25 m.

to have similar roughness to the main channel owing to a combination of substrate and some trailing bank side vegetation.

Culvert structure trial calculations

An estimate of the depth of flow in the channel through the culvert site is obtained from the Conveyance Generator outputs for Section 1. Figure 4.59 shows the flow rating curve for the downstream section. The water level is 10.25 mAD, which corresponds to a flow depth of 1.0 m. The section averaged velocity rating is shown in Figure 4.60. The velocity corresponding to the flow depth of 1.0 m is obtained directly using the outputs interrogator as 1.40 ms^{-1} .

An approximate trial size for the culvert barrel is determined as follows. The section averaged velocity in the culvert should be greater than the channel velocity to discourage excessive siltation. An increase of 20% is desired in this case, giving a design velocity of 1.7 ms^{-1} . The discharge is equal to the cross section averaged downstream velocity multiplied by the flow area. The area required to convey the design flow with a velocity of 1.7 ms^{-1} is therefore $3.5/1.7 = 2.1 \text{ m}^2$. The depth of flow in the culvert should be similar to the normal depth in the channel, which is 1.0 m. A suitable vertical dimension for the barrel would be 1.3 m, allowing for 0.3 m freeboard. With an assumed flow depth of 1.0 m, the required width of the box section would be 2.1 m. Hence the trial culvert barrel dimensions will be a span of 2.1 m and a rise of 1.3 m.

The culvert barrel will be pre-fabricated concrete. Manning's roughness coefficient n would typically be in the range 0.012 to 0.015 for a new concrete culvert. To allow for some minor degradation in use a design value of 0.018 is adopted. The structure is modelled in AES as a box culvert, with a rectangular concrete inlet including headwall and wingwalls and square inlet edges. A similar structure is shown in Figure 4.61 during high flow conditions. The culvert opening data is shown in Figure 4.62.

Exploratory analysis of the trial design

The trial design is analysed by applying the design flow conditions and generating a backwater profile. Results for the 10 year return period flow are shown in Figure 4.63.

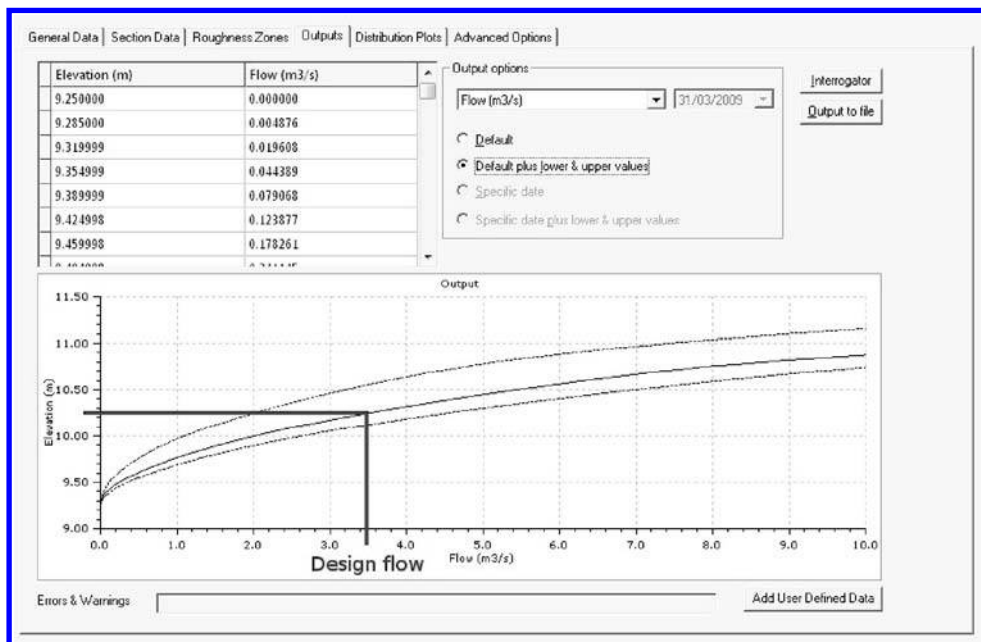


Figure 4.59 Conveyance generator flow rating curve for the downstream section, showing downstream water level for a design flow for the 10-year return period of $3.5 \text{ m}^3 \text{s}^{-1}$.

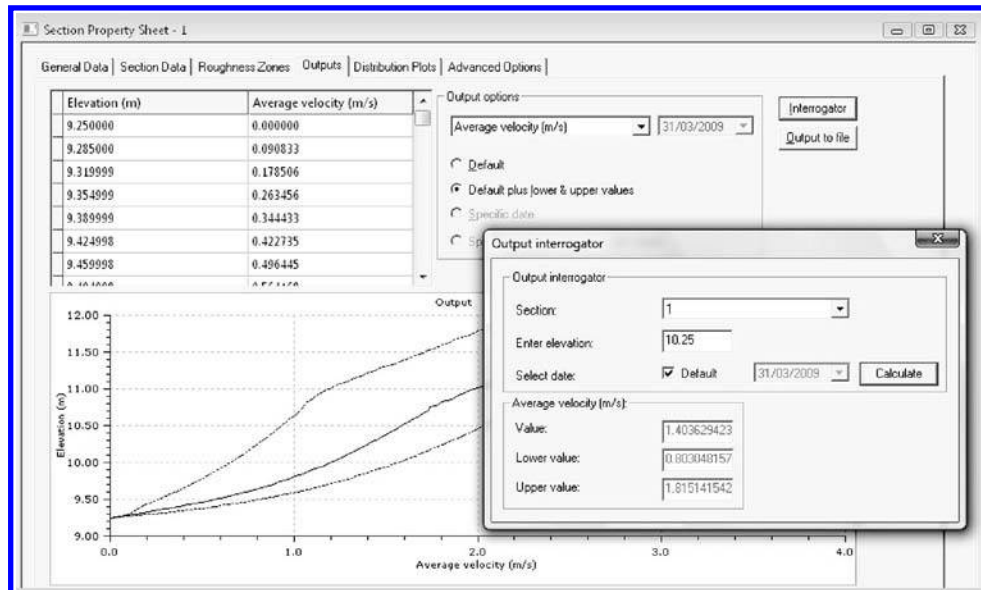


Figure 4.60 Conveyance generator velocity rating curve for the downstream section and 'Interrogator', showing section averaged velocity for a water level of 10.25 mAD.



Figure 4.61 Culvert inlet during high flow conditions. (Photo: John Riddell).

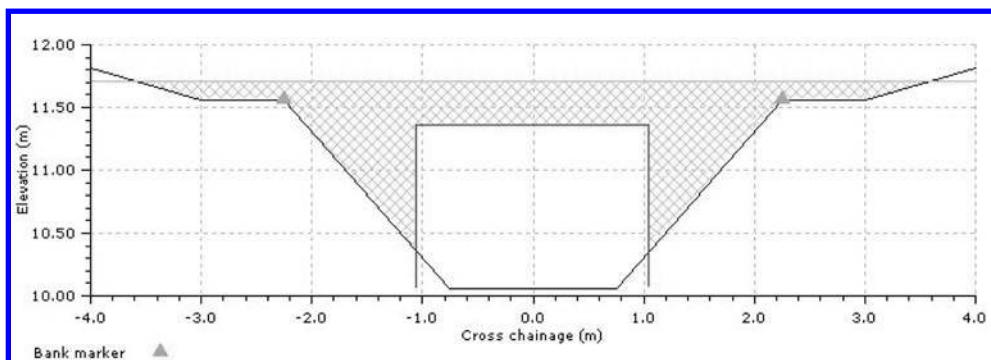


Figure 4.62 Culvert trial opening data in AES.

It can be seen that the culvert causes only a very small increase in water levels upstream of approximately 0.03 m, much less than the stipulated value of 0.1 m. Figure 4.63 also shows water surface profiles for the credible uncertainty bounds around the default roughness, as encoded within CES-AES. The range of uncertainty about water levels is much greater than the indicated change in water levels resulting from the introduction of the culvert, confirming the trial design.

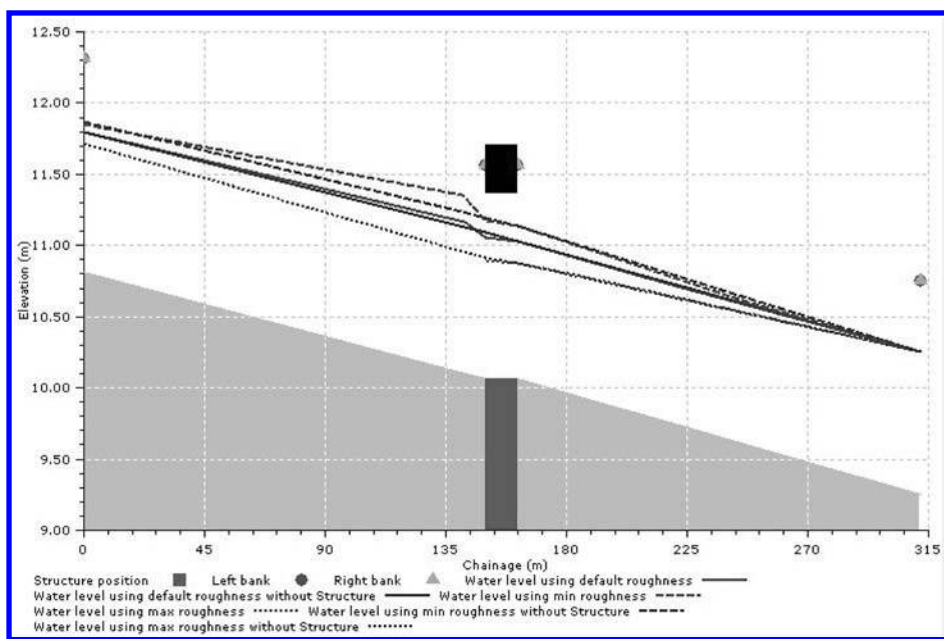


Figure 4.63 Water surface profiles showing best estimate and uncertainty bounds for the trial design, with and without culvert for downstream water level 10.25 m.

Figure 4.64 shows water surface profiles for the 10 year, 50 year and 100 year design flows, both with and without the culvert. At higher flows, the culvert clearly has a greater impact on upstream water levels. For the 50 year design flow the upstream water level just reaches the soffit and a large afflux is produced. For the 100 year flow, the structure is overtopped, flooding the road. The analysis of these larger flow events helps in understanding the robustness of the design. For example, should there be a possibility of development of housing or retail property in the area upstream of the road crossing then the performance of the culvert under higher flow conditions becomes much more important.

Over time there could be deterioration of the condition of the culvert barrel leading to an increase in flow resistance and hence a possible increase in the afflux upstream. An increased roughness value of Manning's $n = 0.035$ has been applied in the AES to test this scenario for future culvert condition. It is also possible that blockage could occur during a high flow event. A simple way to approximate the effects of blockage in AES is to adjust the structure cross section data to reflect a reduction in flow area through the culvert. One such scenario is illustrated in Figure 4.65 where the culvert barrel and opening dimensions have been reduced to a span of 1.6 m and a rise of 1.0 m, which could represent a combination of obstructions within the barrel and floating debris at the inlet. This is a highly simplified representation, but useful for an indicative analysis within the CES-AES.

The impacts of the two culvert condition scenarios are shown in Figure 4.66, which plots rating curves derived from CES-AES backwater profiles for a position

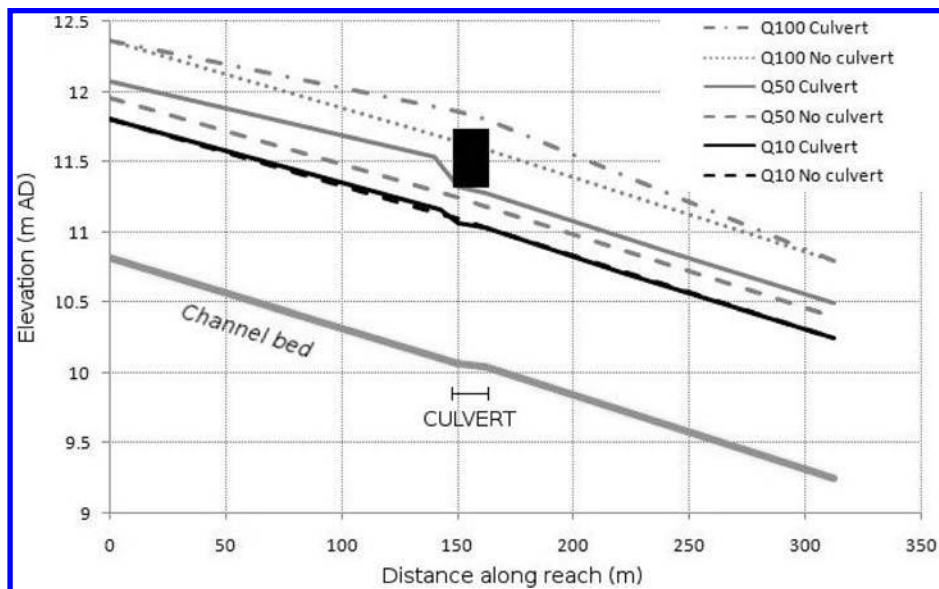


Figure 4.64 Water surface profiles for trial design for design flows with return periods of 10, 50 and 100 years (Q10, Q50 and Q100, respectively).

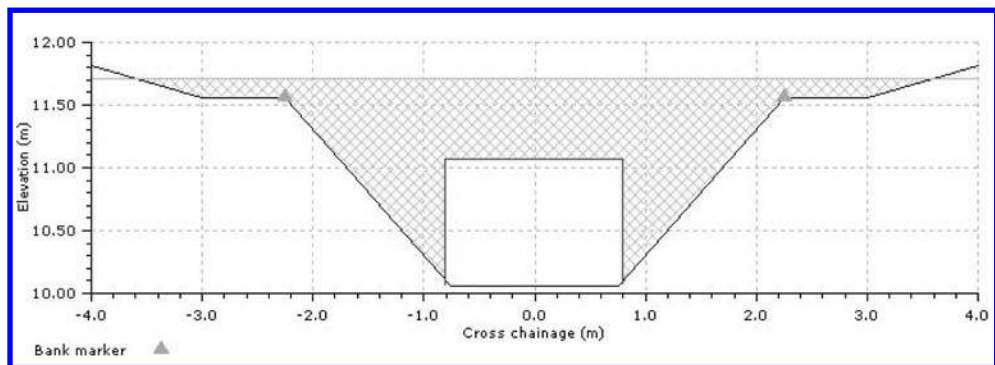


Figure 4.65 Possible blockage scenario represented by a reduction in culvert barrel dimensions.

50 m upstream of the culvert entrance. It can be seen that the modelled scenario for poor barrel condition (increased friction) causes an increased afflux compared to the original trial design, but that this effect diminishes once the structure becomes drowned. This is because the change in barrel friction is less significant once weir flow ensues over the road level. However, the blockage case causes a large increase in water levels for all design flows as a result of the much greater total obstruction to flow in the channel.

Note that the example presents a simplified approach and should not be relied upon as a basis for design calculations. It is intended to demonstrate use of CES-AES

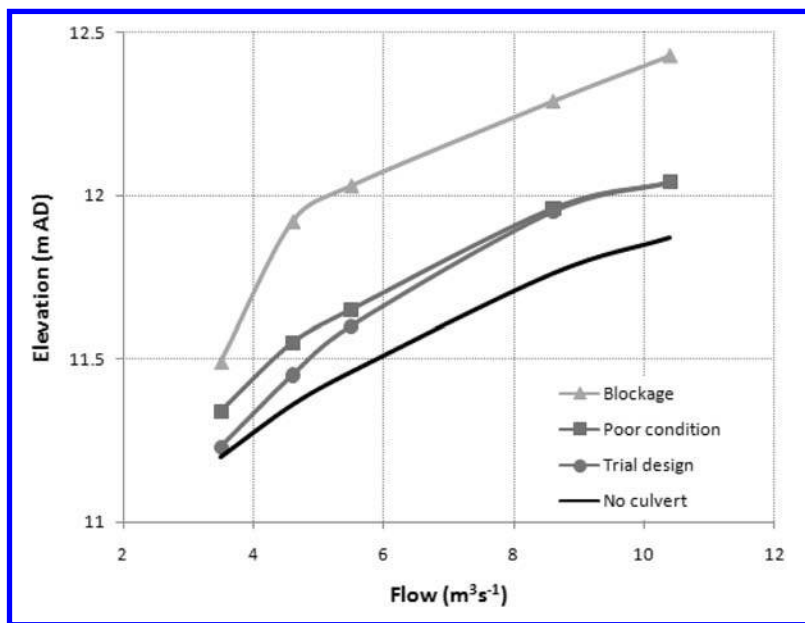


Figure 4.66 Flow rating curves for a position 50 m upstream of the culvert entrance showing two culvert condition scenarios.

as a simple tool to aid understanding of a proposed culvert structure. More detailed calculations are required for a design study.

4.6 DEALING WITH VEGETATION AND MAINTENANCE OF WEEDY RIVERS

Channels provide an important habitat for plants, which in turn provide a range of useful functions such as creating sheltered areas with reduced velocities for fauna, altering the temperature, light penetration and oxygen concentration to promote a variety of species and encouraging siltation. These plants are a vital source of shelter and food for fish, invertebrates and some birds. Where water spills overbank, the drying and wetting of the berms promotes vegetation growth of wetland plants. Vegetation also plays an important role in preventing scour and protecting bed and banks through the binding action of the roots. Channel maintenance is, therefore, multi-faceted, incorporating a range of requirements such as providing sufficient capacity to convey flood flows; reducing the seasonal cutting requirements (and hence expenses) where possible; utilising the bank and scour protection function of the vegetation and promoting the natural habitat.

Guidance on channel management provides current ‘best practice’ for vegetation cutting (e.g. EA, 1998a&b; EA, 2003; CAPM, 1997; Buisson *et al.*, 2008). This typically involves clearing the vegetation in part of the river, for example, cutting

along the channel centre or one of the banks. These variations in pattern give rise to spatial variations in channel roughness, and the roughness is also linked to the density, type, height and stiffness of the vegetation (Fisher, 2001; Defra/EA, 2003b).

There are a number of existing methods for evaluating the reduced conveyance due to the presence of vegetation (e.g. Cowan, 1956; Whitehead *et al.*, 1992; Gordon *et al.*, 1992; Fisher, 2001). These include approaches such as reducing the cross-section or bankside Manning n value according to a simple rule, adapting the Manning equation to account for a reduced flow area due to blockages as well as more complex approaches which aim to relate plant resistance to the biomechanical properties of plants such as form, stiffness, shape and drag (e.g. Petryk & Bosmajian, 1975; Kouwen & Li, 1980; Naden *et al.*, 2006) or to velocity and depth (e.g. Palmer, 1945; Ree & Palmer, 1949; Garton & Green, 1983; Naden *et al.*, 2004; Statzner *et al.*, 2006). In most cases, the main channel and floodplain sections are treated as single units, and the output is an average velocity for each region. As the capacity for aquatic vegetation to support life may be quantified (e.g. invertebrates, Wright *et al.*, 2002), it is possible to estimate the impact to populations of improved conveyance through habitat loss.

The CES conveyance methodology provides scope to describe the local variations in vegetation roughness and it resolves the local depth-averaged velocities and flow depths with due consideration of lateral shearing and boundary layer development. This information can be used to advise on optimum cutting regimes, vegetation patterns, plant types and percentage cut and provides increased confidence in the prediction of the overall channel flow capacity. This is illustrated through examples:

- River Cole in Birmingham – exploration of different cutting regimes;
- River Avon in Enford – exploration of different cutting regimes to satisfy both ecological and flood risk objectives;
- River Hooke in Maiden Newton – exploration of channel deepening.

4.6.1 Exploration of cutting regimes for the River Cole

Aim

The River Cole site is used to explore the impact on flow and depth-averaged velocity for different vegetation cutting regimes at a flow depth of 1.4 m. These include:

- Scenario 1: no cutting i.e. vegetation across the entire channel;
- Scenario 2: vegetation cut in the channel centre (50% of existing vegetation at cross-section location – in Summer);
- Scenario 3: vegetation cut on the right bank (70% of existing vegetation at cross-section location – in Summer); and
- Scenario 4: vegetation cut on both banks (70% of existing vegetation at cross-section location – in Summer).

A comparison is made with the results produced using one of the existing best practice approaches (EA, 1997), the HR Wallingford (Whitehead *et al.*, 1992) method.

HR Wallingford approach

The empirically derived HR Wallingford (HRW) approach is for inbank flow only. It involves evaluating an increased Manning n value, n_{total} , to allow for the additional retardance due to vegetation in the channel. This is evaluated from:

$$n_{\text{total}} = n_{\text{clear}} + 0.0239 \left(\frac{K_w}{UR} \right) \quad (4.3)$$

where n_{clear} is the Manning n value when the channel is clear, K_w is the fraction of the surface area covered by vegetation and U is the average velocity of the clear section. This n_{total} is then used in the Manning equation to evaluate the flow capacity and velocity with vegetation.

The River Cole site

The River Cole in Birmingham is a straight trapezoidal channel, which was overwidened for flood control purposes. It consists of a mainly gravel bed with some silt especially amongst the emergent vegetation. In the summer, it has submerged and floating channel vegetation in the main channel and emergent vegetation on both banks. The emergent vegetation traps silt and creates berms, which cause self-meandering within the channel in the Summer. Pool riffle sequences create some variation in depth along the channel and urban-debris is common ([Figure 4.67](#)). The average water surface slope is 0.00174.



Figure 4.67 The River Cole site in Birmingham showing the channel vegetation, pools and riffles and urban trash (Defra/EA, 2004).

Roughness and cross-section definition

The Roughness Advisor values for the ‘as is’ case i.e. Scenario 1 are as follows (Figure 4.68):

- *Channel bed* – The RA coarse gravel 20–64 mm ($n_{\text{sur}} = 0.027$), submerged fine-leaved plants (medium) ($n_{\text{veg}} = 0.1$) and pools ($n_{\text{irr}} = 0.2$) are adopted giving $n_l = 0.106$.
- *Channel banks* – The RA coarse gravel 20–64 mm ($n_{\text{sur}} = 0.027$) and emergent reeds ($n_{\text{veg}} = 0.15$ but taken as 0.09 – average value – as do not appear very thick) are adopted giving $n_l = 0.094$.
- *Floodplain* – The RA sand ($n_{\text{sur}} = 0.02$) and height-varying grass ($n_{\text{veg}} = 0.041$) are adopted giving $n_l = 0.046$.

Results for the River Cole site

Scenario 1 is essentially the ‘as is’ case i.e. if no vegetation cutting takes place. Figure 4.69 provides the CES predicted stage-discharge and the measured data. There are only a few low flow measurements and one high flow ($16.7 \text{ m}^3 \text{s}^{-1}$ @ 1.49 m) measurement available. The curve does not capture the local variations of these measurements, but it does pass from the low flows to the high flows. The upper and lower uncertainty scenarios are wide, which is indicative of the uncertainty associated with the submerged and emergent vegetation roughness information. Figure 4.70 provides the back-calculated Manning n values and the corresponding Manning n values from the measured flows. Although the detail is not captured, the trend of the CES curve moves from lower Manning n values at high flows to higher Manning n values at low flows.

The CES flow predictions for scenarios 1 to 4 at a depth of 1.4 m are summarised in Table 4.6 and the corresponding depth-averaged velocity profiles are shown in Figure 4.71.

For the HRW method, K_w is taken as 0.70, 0.36, 0.52 and 0.34 for scenarios 1 to 4 respectively. This is derived from the percentage of the cross-section covered by vegetation for each case at a flow depth of 1.4 m. The n_{clear} is taken as 0.061, giving

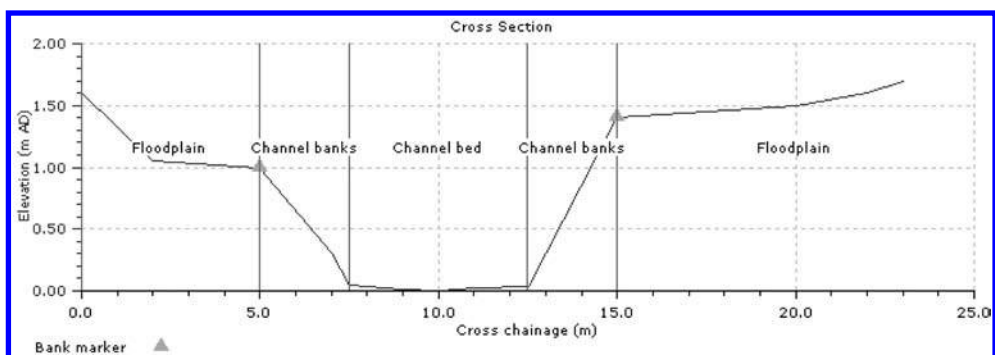


Figure 4.68 River Cole cross-section, roughness zones and top-of-bank marker locations.

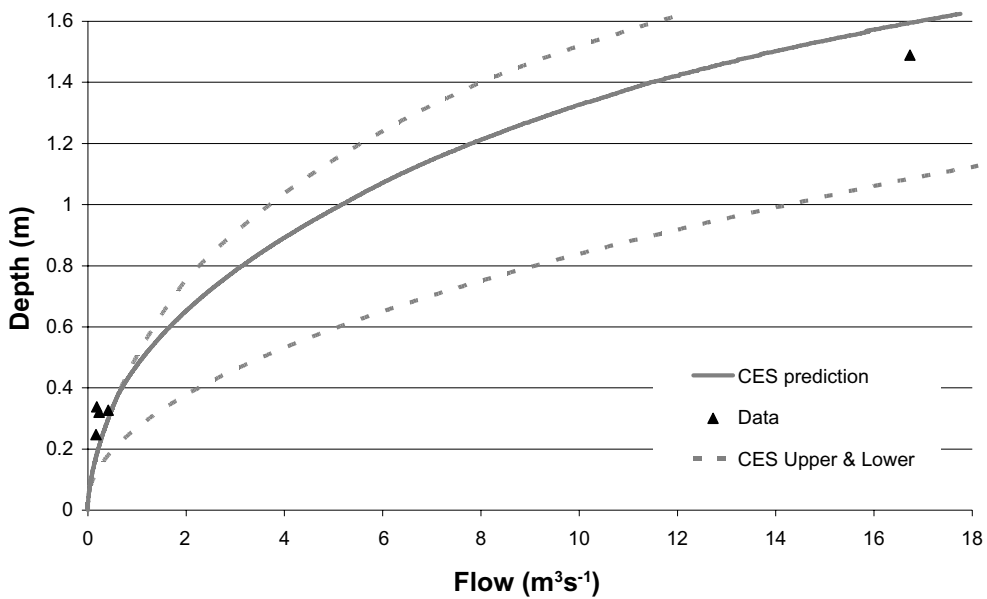


Figure 4.69 Stage-discharge prediction for the River Cole with no channel cutting and comparison to data (data from Defra/EA, 2004).

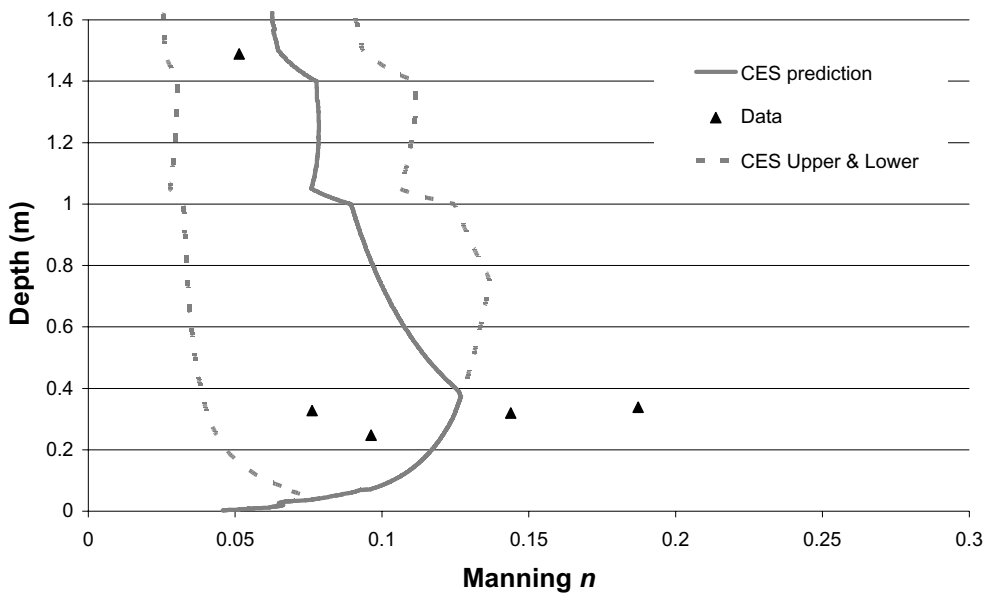


Figure 4.70 Back-calculated Manning n values for the River Cole and comparison to data (data from Defra/EA, 2004).

Table 4.6 Summary of flow predictions using the CES and HRW approach at depth 1.4 m.

Vegetation cutting scenario	Flow ($m^3 s^{-1}$)		Percentage difference relative to Scenario 1 (%)		Percentage difference in CES HRW value (%)
	CES	HRW	CES	HRW	
Scenario 1: no cutting	11.4	11.4	0	0	0
Scenario 2: main channel cut	12.8	16.5	44	12	23
Scenario 3: right bank cut	12.1	12.6	10	6	4
Scenario 4: right left bank cut	12.8	14.2	24	13	9

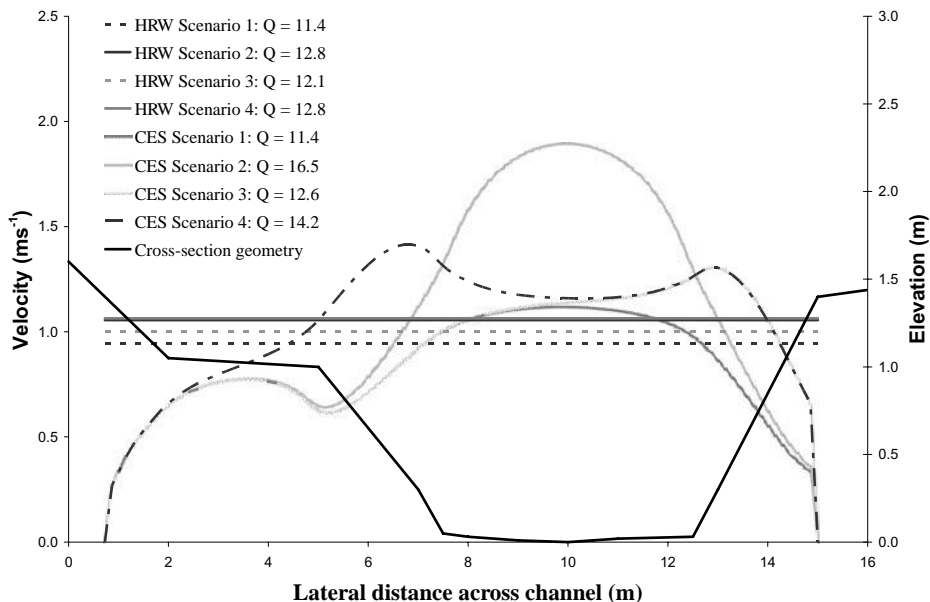


Figure 4.71 Depth-averaged velocity predictions for the River Cole using the CES and the HRW approach.

n_{total} as 0.078, selected to ensure the flow rate for the HRW method and the CES method are identical for Scenario 1, the ‘as is’ case, i.e. $Q_{\text{HRW}} = Q_{\text{CES}} = 11.4 \text{ m}^3 \text{s}^{-1}$. The HRW flow rates are provided in Table 4.4 and the average velocities are shown in Figure 4.71.

The following is observed:

- *Vegetation type* – the CES enables a user to select the vegetation roughness associated with the particular plant species (e.g. emergent reeds), including the time of year (e.g. June) and upper and lower scenarios – providing improved confidence in the outputs. Existing methods such as HRW method do not relate the Manning n values to vegetation morphotypes.

- *Vegetation location* – The CES enables users to identify the exact location in the cross-section where the vegetation is present e.g. banks, main channel. This information is used to evaluate the local unit flow rate and velocities (Figure 4.71) across the section – providing improved confidence in the final overall flow rate. The HRW approach assumes a single Manning's n value for the entire cross-section regardless of different vegetation types and locations within the section and hence average velocities are provided (Figure 4.71). The plan form cover is accounted for through a simple coefficient, K_w .
- *Vegetation cutting, location, nature & timing* – The CES enables users to select the precise location where vegetation is cut, the nature of the cutting (e.g. cut 70% of the vegetation at the location) and the timing of the cut (e.g. June) which influences the resulting unit roughness value. This additional detail provides improved confidence in the results.
- *Flow predictions* – The CES predicted flow capacities are up to 20% larger than those calculated using the HRW method and they provide a clear hierarchy of the cutting regimes with a main channel cut as the most favourable in this case (44% increased flow capacity) followed by cutting on both channel banks (24% increased flow capacity). This information can be considered together with associated costs to ascertain the preferred option.
- *Velocity predictions* – The CES approach provides information on the local velocity variations in the cross-section which is not provided by the more traditional approaches. This information may be used to inform, for example, habitat design, risk to people inclusive during maintenance activities, scour potential.

Further analyses for the River Cole may involve taking the optimum cut, channel bed, and determining the optimum time of year for the cut (current results pertain to a June cut).

To prove the potential added value of the CES outputs outlined above, it is recommended that this information is used in practice to inform a vegetation cutting regime, and the flow capacity should be monitored and compared to that achieved through previous practice.

4.6.2 Exploration of different cutting regimes for the River Avon

Aim

Different cutting regimes are explored for the River Avon to determine the improvement in conveyance with vegetation removal and the potential impact on invertebrate population (Wright *et al.*, 2002). This demonstrates how the trade-off between flood risk management (e.g. greater flow and reduced levels) and ecological (e.g. increased habitat and hence life supported) objectives may potentially be explored.

The River Avon site, roughness and cross-section definition

The Avon comprises a simple channel, 9.2 m wide, with a bankfull depth of ~0.6 m and an average bed slope of 0.0005. The bed consists of gravels and the in-channel

section has an abundance of water crowfoot (*Ranunculus pectinatus pseudofluitans*) vegetation (Figure 4.72), a submerged fine-leaved plant. The assigned Roughness Advisor values are (Figure 4.73):

- *Gravel* – The RA gravel 7–20 mm ($n_{\text{sur}} = 0.025$) is adopted.
- *Ranunculus & gravel* – The RA gravel 7–20 mm ($n_{\text{sur}} = 0.025$) and submerged fine-leaved plants ($n_{\text{veg}} = 0.10$) are adopted giving $n_l = 0.103$.

Results for the River Avon

Discharge predictions (Figure 4.74) are made for 0, 10, 20, 30, 40, 50, 60, 70, 80, 90 and 100% vegetation coverage, with the gravel coverage at the channel centre for each. The dashed lines show the uncertainty scenarios, which are increasing for increasing vegetation coverage, as this is the primary source of uncertainty in the roughness values. The number of invertebrates supported by the vegetation cover is shown. These are based on densities of *Ranunculus pseudofluitans* (Wright *et al.*, 2002) and are calculated for a 20 m reach. Combining the flow, invertebrate and vegetation information enables different ‘what ifs’ to be explored. For example, if the vegetation is cut-back from the existing 42% cover to say, 20%, this provides a ~25% increase in bankfull flow capacity but this is at the expense of a 30,000 drop in total invertebrate life supported. These values are, of course, indicative and other influences should also be considered, for example, there may be a further trade-off



Figure 4.72 River Avon site at Enford, Pewsey, Wiltshire (O'Hare *et al.*, 2008; Courtesy Centre for Ecology and Hydrology).

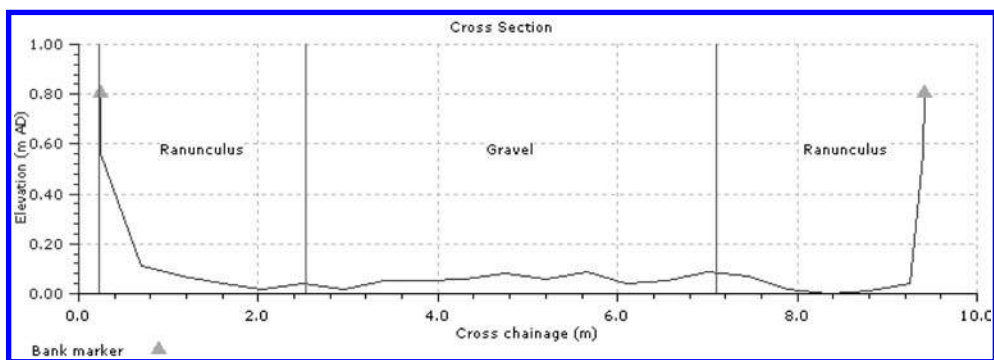


Figure 4.73 River Avon cross-section, roughness zones and top-of-bank marker locations for 50% vegetation present (survey data – O'Hare et al., 2008).

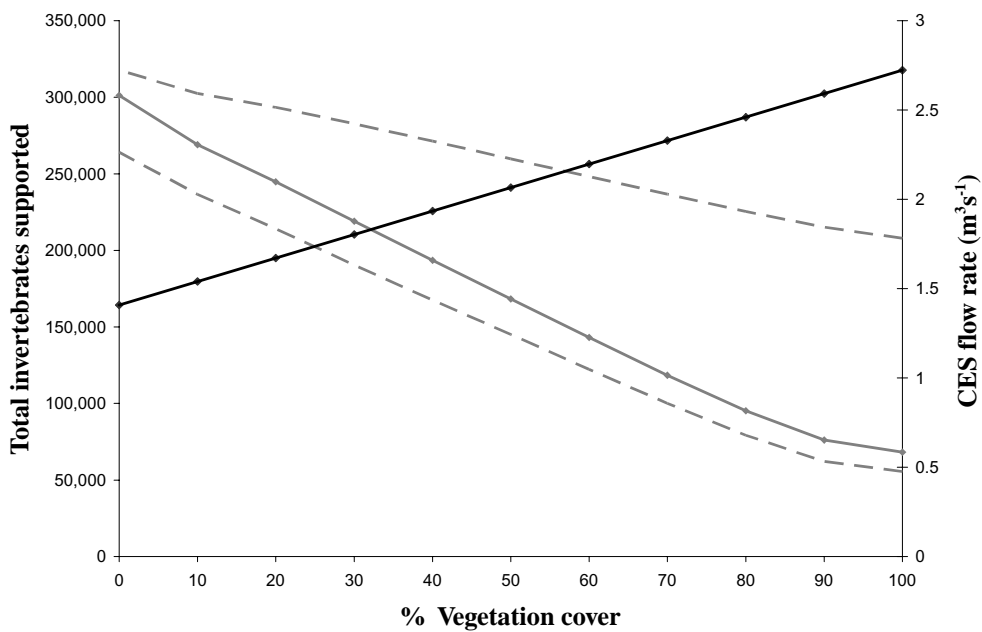


Figure 4.74 Change in number of invertebrates supported and total flow rate with percentage vegetation cover (Mc Gahey et al., 2008).

between vegetation abundance and species diversity. This information can be further enriched through, for example, exploration of different cutting options such as removal of growth on a particular bank and the impact on water levels and flow capacity.

4.6.3 Exploration of channel deepening for the River Hooke

Aim

The River Hooke is used to explore the impact of dredging on local flow depths and depth-averaged velocity profiles, assuming no downstream controls. The existing channel has gravel and water crowfoot scattered throughout the section. The maintenance option will involve removal of the water crowfoot and deepening of the channel section along the central margin.

The River Hooke site, roughness and cross-section definition

The site is found in the village of Maiden Newton, in the Frome catchment, directly upstream of a LOCAR monitoring point, where discharge and other environmental parameters are recorded at high resolution. The channel vegetation is dominated by water crowfoot (*Ranunculus peltatus pseudofluitans*, [Figure 4.75](#)). Directly upstream of the sampling area is a vegetated mid-channel bar, seen on the left of the photograph. The site has been subject to flooding in the past and a flood relief channel has been built just upstream of the mid-channel bar. Water level, velocity,



Figure 4.75 River Hooke site at Maiden Newton (O'Hare et al., 2008; Courtesy Centre for Ecology and Hydrology).

vegetation and roughness measurements are available. The water level slope is 0.0108 at flow depths of 0.32 m.

The ‘as is’ assigned roughness values are:

- *Substrate only* – The RA gravel 7–20 mm ($n_{\text{sur}} = 0.025$)
- *Shallow with vegetation* – The RA gravel 7–20 mm ($n_{\text{sur}} = 0.025$) and June value for submerged water crowfoot or fine-leaved plants in shallow water 0.2–0.6 m ($n_{\text{veg}} = 0.25$) are adopted giving $n_l = 0.251$.

Results for the River Hooke

[Figure 4.76](#) shows the measured and predicted depth-averaged velocities for the River Hooke. There is much scatter amongst the data, which is not unexpected considering the scattered nature of the vegetation. In the channel centre (chainage 2.5 m–5 m) the measured velocities are low reflecting the influence of the upstream mid-channel bar. The CES velocity profile may be improved if the precise location of the vegetation is defined within the CES cross-section. For this case, the average vegetation values for June in shallow (0.2 m–0.6 m) flow are adopted, and the simulated flow rate is within 2% of the measured data.

The cross-section is then altered to simulate channel deepening ([Figure 4.77](#)) with only gravel present in the deepened section. The resulting CES predicted flow capacity

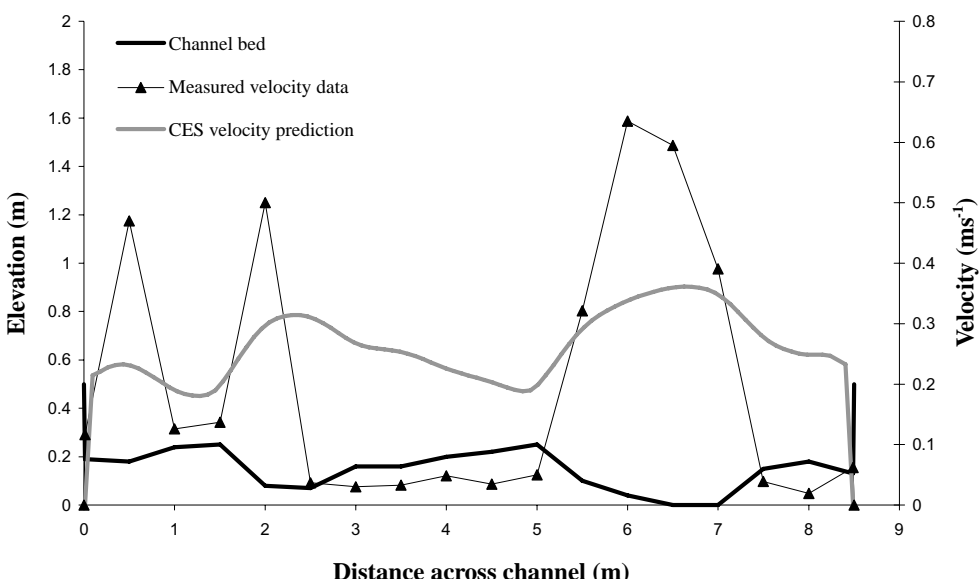


[Figure 4.76](#) Depth-averaged velocity predictions for the River Hooke at flow depth 0.32 m giving a $Q_{\text{CES}} = 0.42 \text{ m}^3 \text{s}^{-1}$ and $Q_{\text{data}} = 0.41 \text{ m}^3 \text{s}^{-1}$ (data – O’Hare *et al.*, 2008).

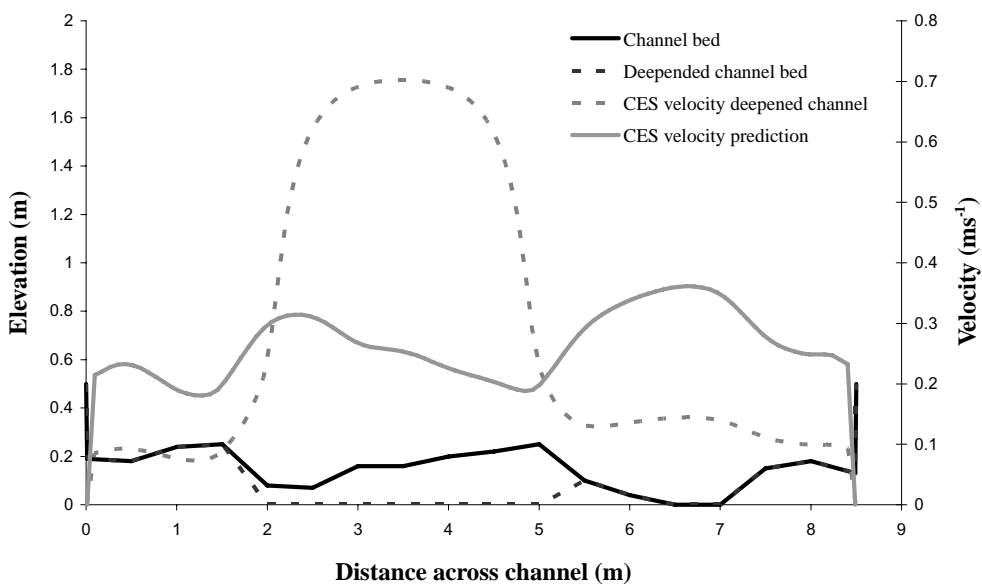


Figure 4.77 Depth-averaged velocity predictions for the River Hooke at flow depth 0.32 m before and after channel deepening and vegetation removal.

at a depth of 0.32 m is $1.8 \text{ m}^3\text{s}^{-1}$, a 330% increase on the CES flow prediction for the ‘as is’ channel section. The velocities in the left-hand margin are, as expected, substantially higher reaching 0.7 ms^{-1} . These velocities may be used to inform scour potential and habitat change for the reach.

Further issues on flows in rivers

ABSTRACT

This chapter considers some further practical issues in river engineering and suggests how the CES-AES software might be used to investigate them. The issues considered relate to river ecology, sediment transport, geomorphology, trash screens and blockages to culverts. A brief overview is given of 1-D, 2-D and 3-D approaches to modelling river flows, and sets the CES-AES software in this context. The chapter concludes with some high level flow charts that indicate how the software might be adapted for other specific research purposes.

5.1 ECOLOGICAL ISSUES

Channel design should be considered in terms of the wider system and its functioning, balancing the ecological biodiversity needs with those of flood risk management. The relationship between channel properties, water levels and habitat provides an opportunity to maximise the biodiversity value of channels (Buisson *et al.*, 2008). Essential to this is the need to incorporate habitats for plants, invertebrates, amphibians, fish, birds, mammals and reptiles where possible, whilst still enabling flood flows to be conveyed with the appropriate standard of protection. For example, aquatic plants in channels provide important environmental benefits (O'Hare *et al.*, 2007), since they increase water depth during summer months, providing wetted habitat for invertebrate and fish species (Hearne *et al.*, 1994). They also boost habitat complexity by providing shelter and varied flow conditions which support large numbers of invertebrates and juvenile salmonid fish (Armitage & Cannan, 2000; Wright *et al.*, 2002). The implications are that all channel design and maintenance should be carried out with sensitivity to wildlife. Thus channel management requires a multi-disciplinary approach, with inputs from a range of experts such as ecologists, water quality specialists, environmentalists and fluvial engineers as well as operating authorities (e.g., in the UK – Local Authorities, Government Agencies, Internal Drainage Boards).

A useful overview of existing legislation, policy and guidance supporting this for drainage channels is provided in Buisson *et al.* (2008). Perhaps most important in the context of European and UK flood risk management are:

- *Water Framework Directive's (2000/60/EEC)* – The primary environmental objectives are to achieve “good ecological and good chemical status” for surface water bodies in general or good ecological potential for the specific case of heavily modified and artificial water bodies. It also seeks that in general “no deterioration” in status of the water body which will require management of the quality, quantity and structure of aquatic environments.
- *Habitats and Species Directive (92/43/EEC)* – This aims to promote the maintenance of biodiversity by requiring Member States to take measures to maintain or restore natural habitats and wild species at a favourable conservation status, introducing robust protection for those habitats and species of European importance. These requirements are now transposed to national laws in the UK, for example, Conservation Regulations 1994, Conservation Regulations for Northern Ireland 1995.
- *The UK Biodiversity Action Plans (1994)* – These are the Governments response to becoming a signatory of the Convention on Biological Diversity. The plan combines new and existing conservation initiatives with an emphasis on a partnership approach. It contains 59 objectives for conserving and enhancing species and habitats as well as promoting public awareness and contributing to international conservation efforts. 391 Species Action Plans and 45 Habitat Action Plans have been published for the UK's most threatened species and habitats, and around 150 Local BAPs have been published (See: <http://www.ukbap.org.uk>).
- *Making Space for Water (MSfW)* – Initiatives such as the UK Government's MSfW advocate flood risk management solutions that satisfy a wider range of objectives such as hydro-morphological, ecological and even social needs.
- *Outcome Measures* – The UK Government has established a framework of flood risk management outcome measures to allocate resources and to guide the activities of flood operating authorities so they reflect MSfW and Government policy in general. These include specific outcome measures for nationally important wildlife sites (Sites of Special Scientific Interest – SSSIs) and for UK Biodiversity Action Plan habitats.

Others include Environmental Impact Assessment; Salmon and Freshwaters Act 1975; Birds Directive 1979; Wildlife and Countryside Act 1981; Habitats Regulation 1994; Land Drainage Act 1994; Natural Environment and Rural Communities Act 2006; UK Priority Species and Habitats 2007.

Software tools such as the CES, the Physical Habitat Simulator (PHABSIM) and River Habitat Simulator (RHABSIM) provide support through enabling exploration of ‘what-if’ scenarios. Information on local velocities, flow depths and sediment concentrations (Section 5.2) are essential inputs for identifying the likely habitat regime, and for re-engineering channels to support a particular species. Typical measures include (Fisher, 2001):

- creating pool and riffle sequences to alter velocities;
- planting different vegetation morphotypes to create different flow regimes;

Table 5.1 Example habitat information for various UK channel species (adapted from Natural England) (See colour plate section).

Species	Description	Appearance	Habitat	Example UK habitat
Bullhead (<i>Cottus gobio</i>)	The bullhead is the only freshwater cottid found in the UK. A small species, it rarely exceeds 15 cm in length & 28 g in weight. It is easily identified by its large head, with eyes on the top & a dorso-ventrally flattened tapering body.		Sheltered streams with tree roots & vegetation for adults. Young prefer shallow water & stoney riffles. Moderate velocities i.e. 10-40 cm s ⁻¹ , most commonly ~22 cm s ⁻¹ . Water depths not critical, provided > 5 cm.	
Atlantic salmon (<i>Salmo salar</i>)	Distinctive & recognizable, well known for agility, strength & persistence. It can leap ~3 m into the air from deep water. Adult males reach up to 1.5 m in length & 36 kg in weight, while females are a maximum of ~120 cm & 20 kg.		Overhanging & submerged vegetation, undercut banks, submerged objects such as logs & rocks, floating debris, deep water, surface turbulence, cobbles & boulders. Water depths 20-40 cm, velocity 60-75 cm s ⁻¹ .	
British river lamprey (<i>Lampetra fluviatilis</i>)	The average adult length is ~30 cm & weight ~60 g but specimens over 40 cm can be found. It is a migratory species, which grows to maturity in estuaries & then moves into fresh water to spawn in clean rivers & streams.		No barriers e.g. weirs. For spawning gravel & interstitial currents. After hatching sandy silt beds. Average stream gradients 0.2–0.6 m km ⁻¹ . Water depth in nursery areas is typically 0.1–0.5 m. Spawning depths 20–150 cm.	
Desmoulain's whorl snail (<i>Vertigo moliniana</i>)	Body is greyish-white with a darker grey to black head & tentacles. The shell is dextrally coiled (inouth on right), ovate to elongate in shape, with a tapering spire & ~5 rounded whorls. Its shell height & breadth is 2.2–2.7 mm & 1.3–1.65 mm.		Climbing species in emergent vegetation e.g. fens & marshes, lakes, ponds, river floodplains. High population: h > 0.25 m (water level above ground); Med population: h > 0 m; Low population: h < 0 m (inundation rare).	
Eurasian otter (<i>Lutra lutra</i>)	Large, warm-blooded top predators. Insulated against many small-scale environmental factors that impact survival of riparian invertebrates & plants (temperature, rates of flow, water chemistry, etc.).		Otters do not avoid structures e.g. weirs, bank reinforcements unless they impact food availability or pipes with no headroom. Diving has been observed in 2–7 m flow depths. In most UK rivers, otters are capable of foraging throughout the water column.	

- altering timing and nature of vegetation cutting to best suit species;
- cutting bankside vegetation to enhance exposure to natural light;
- channel deepening (dredging);
- creation of wet and dry berms;
- reducing soluble, insoluble and floating pollution; and
- introducing weirs to reduce the flow, including the use of fish (Defra/EA, 2003c) passes to ensure upstream movement of fish.

The CES enables users to describe the local vegetation and roughness cover and to resolve the local depths and velocities whereas more traditional approaches (e.g., PHABSIM) are based on section-averaged calculations of flow and velocity (e.g., Chezy, Manning). This more localised information can be used with habitat information, for example:

- *response curves* – velocity/depth versus species preferences; and
- *LIFE scores* (see Extence & Balbi; 1999) – methods for linking benthic macro-invertebrate data to prevailing flow regimes (example given in Section 4.6.2)

in support of channel design.

Table 5.1 provides some examples from Natural England of species velocity, depth and substrate preferences. This may be used together with CES predictions to identify or promote particular habitat regimes.

5.2 SEDIMENT AND GEOMORPHOLOGICAL ISSUES

Despite being based on a rigid-bed assumption, the conveyance methodology within CES may be used to deal with some loose-boundary topics such as sediment transport and geomorphology. This arises primarily from its capability in being able to estimate the lateral distribution of boundary shear stress around the wetted perimeter of a prismatic channel of any shape, as well as the distribution of depth-averaged velocity. Since τ_b is one of the key parameters that govern sediment behaviour, this is a particularly useful extension of the CES software. Furthermore, many natural channels are characterised by a mobile bed, with bed features such as ripples, dunes, plane bed and antidunes, resulting from sediment entrainment and deposition. Sediment issues also feature in many drainage channels and watercourses. The links between τ_b (or friction factor, f), velocity and bed forms that develop after initiation of motion from a flat bed condition in an alluvial channel are shown schematically in Figure 5.1. This is taken from Raudkivi (1998), and described in an introduction to alluvial resistance by Knight (2006c) and Morvan *et al.* (2008).

Figure 5.2, taken from Shen (1971), shows the impact that such bedforms can have on the stage-discharge relationship, using data from the Padma River in Bangladesh. The lateral distribution of boundary shear stress ($\rho g H S_v$, versus y , where S_v is the valley slope) is shown in the inset diagram at low and high stages. At a relatively low stage, the bedforms vary across the channel beginning with ripples near the left hand bank, then dunes, to transitional plane bed and back to dunes again near the right hand bank, in keeping with the bed shear/local velocity and bed forms indicated in Figure 5.1.

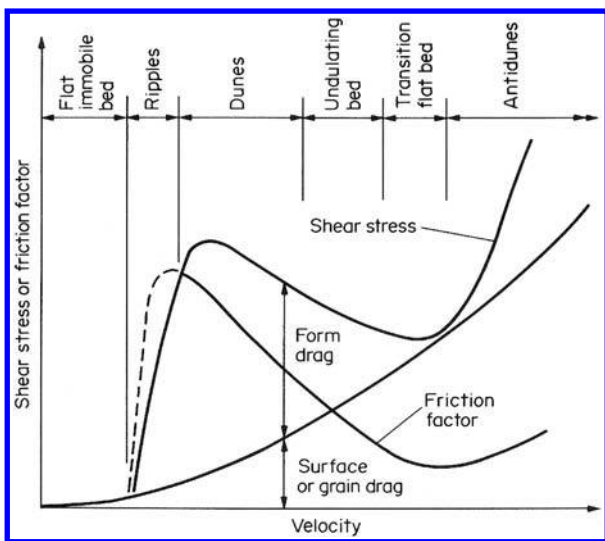


Figure 5.1 Variation of bed shear stress and friction factor with velocity and bedforms for a sand bed river (after Raudkivi, 1998).

Since the local bed shear stress is mainly governed by the local depth of flow, H , the distribution is naturally related somewhat to the geometry of the cross section. At high stage, the bedforms change, in this example by generally a single category, and become dunes, plane bed, antidunes and plane bed again. The effect of this on resistance, and hence the H v Q relationship, is profound. Since dunes have a high resistance, and plane bed (i.e., transitional flow at Froude Numbers approaching unity) have a relatively low resistance, as shown in Figure 5.1, the corresponding H v Q relationship is seen to flatten out at high flows, leading to a more or less constant stage of 27 feet. This is much lower than might have been anticipated had only the low to medium flow data, up to say 75,000 cfs (cubic feet per second) [i.e., $2,124 \text{ m}^3 \text{s}^{-1}$], been used in a regression equation and then subsequently used to extrapolate the H v Q relationship up to flows of say 300,000 cfs [i.e., $8,495 \text{ m}^3 \text{s}^{-1}$]. That estimate would then have been higher than that which actually occurred, arising from the significant proportion of the wetted perimeter experiencing plane bed (i.e., low resistance) conditions at high stages. This illustrates the care that needs to be taken when estimating resistance for sand bed rivers and the difficulties in extrapolating H v Q relationships without taking into account all the relevant physical factors.

There is a large amount of literature on the subject of sediment mechanics, including the flow conditions associated with initiation of motion (e.g., Shields, 1936; Liu, 1957), equilibrium channel conditions (e.g., Ackers, 1992a; Bettess & White, 1987; Blench, 1969; Cao, 1995; Cao & Knight, 1996; Chang, 1988; White *et al.*, 1982), sediment transport rates and concentrations (e.g., Du Boys, 1879; Einstein, 1942; Bagnold, 1966; Engelund & Hansen, 1966; White, 1972; Ackers & White 1973; Chang, 1988; Ackers, 1990), bedforms and resistance (e.g., van Rijn, 1982 &

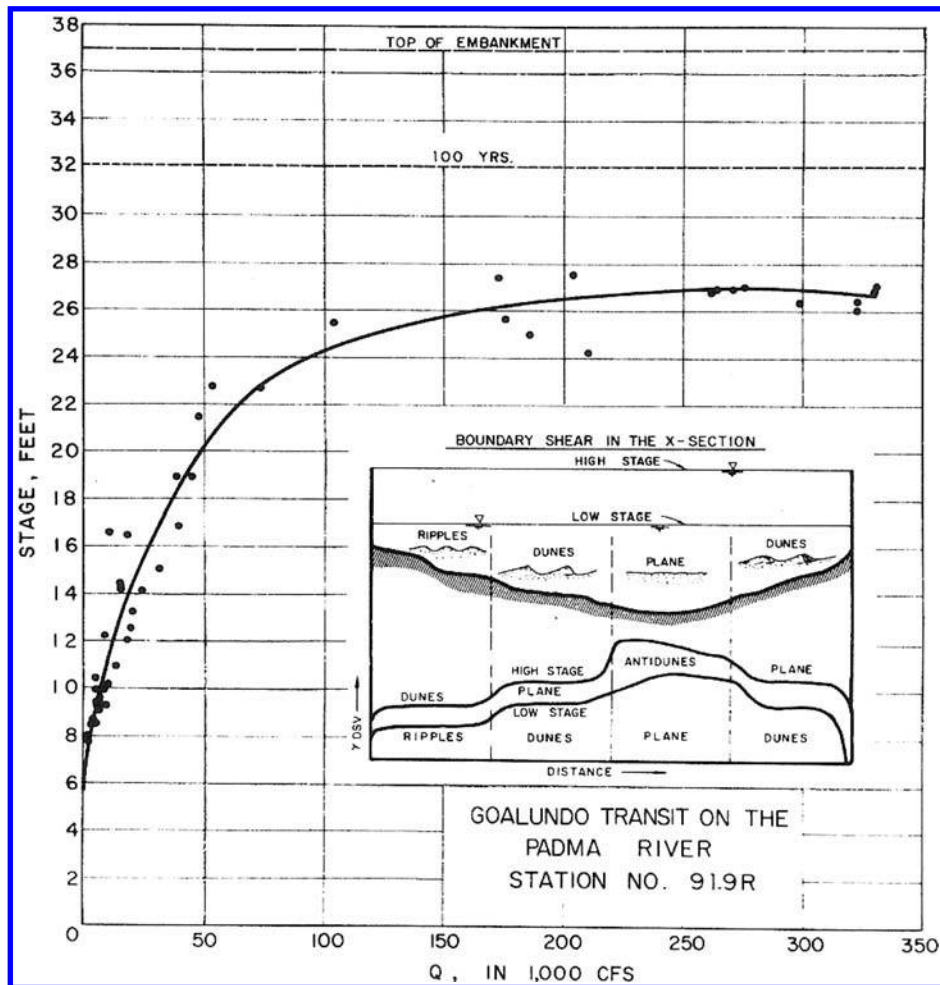


Figure 5.2 Stage-discharge relationship and bedforms in the Padma River, Bangladesh, at low and high discharges (after Shen, 1971).

1984; White *et al.*, 1980) and general behaviour as given in various textbooks (e.g., Chang, 1988; Garde & Ranga-Raju, 1977; Raudkivi, 1998; Shen, 1971; Simons & Senturk, 1992; Thorne *et al.*, 1997; Yalin & da Silva, 2001; Yang, 1987).

With regard to sediment transport rates, most methods typically rely on a resolution of the boundary flow conditions, using bed shear stress, shear velocities, velocity and velocity gradients adjacent to the channel bed as well as the sediment properties such as sediment size, density and fall velocity. This section is now aimed at demonstrating the use of the CES in estimating sediment transport rates, using one of the more recent sediment transport approaches by Ackers & White (1973) and Ackers (1990 & 1993c).

In 1973, Ackers and White first proposed their total material load formulae, which are based on physical considerations and dimensionless analysis. It assumes that for sediment moving as a bed load, transport correlates with grain shear stress, and the grain shear stress becomes less significant while total shear stresses become more significant for finer sediments. Three dimensionless quantities, the sediment transport parameter G_{gr} , the particle mobility number F_{gr} and the particle size number D_{gr} , are defined as

$$G_{gr} = \frac{q_s b}{qd_{50}} \left(\frac{u_*}{U} \right)^{n_{ac}} = C_{ac} \left(\frac{F_{gr}}{A_{ac}} - 1 \right)^{m_{ac}} \quad (5.1)$$

$$F_{gr} = \frac{u_*^{n_{ac}}}{\sqrt{gd_{50}(\rho/\rho_s - 1)}} \left(\frac{U}{\sqrt{32} \log_{10}(10b/d_{50})} \right)^{(1-n_{ac})} \quad (5.2)$$

$$D_{gr} = d_{50} \left(\frac{g(\rho/\rho_s - 1)}{v^2} \right)^{1/3} \quad (5.3)$$

where q_s ($\text{m}^3 \text{s}^{-1} \text{m}^{-1}$) is the volume of sediment transported per second per unit channel width and ρ_s is the sediment density. The coefficients in these formulae, which vary with D_{gr} , were originally based on over 1000 experiments. More recently, these have been updated to include additional data (Ackers, 1990 & 1993), and these coefficients are shown in [Table 5.2](#) according to the value of D_{gr} . A review of the performance of several sediment transport formulae, including that of Ackers & White, is given in Chang (1988).

It should be noted that nearly all sediment transport equations have been derived for inbank flow conditions, typically in a single channel. Their application to overbank flows therefore requires special treatment, as some studies suggest (e.g., Atabay, 2001; Atabay *et al.*, 2004; Atabay *et al.*, 2005; Ayyoubzadeh, 1997; Brown, 1997; Knight *et al.*, 1999; Knight & Brown, 2001; Ikeda & McEwan, 2009; Tang & Knight, 2001). An example is now given to illustrate how the CES can be of use in sediment transport investigations, for both inbank and overbank flows.

The CES shear velocity and unit flow rate outputs may be used to solve these formulae at each point in the cross-section, to evaluate the lateral distribution of q_s . Then by lateral integration of q_s , the total sediment transport rate Q_s ($\text{m}^3 \text{s}^{-1}$) may be obtained, where

$$Q_s = \int_0^B q_s dy \quad (5.4)$$

Table 5.2 Coefficients to be used in the Ackers & White sediment transport equations, (5.1)–(5.3).

Coefficient	$D_{gr} > 60$	$1 < D_{gr} < 60$
n_{ac}	0	$1 - 0.56 \log D_{gr}$
m_{ac}	1.78	$1.67 + 6.83/D_{gr}$
A_{ac}	0.17	$0.14 + 0.23/\sqrt{D_{gr}}$
C_{ac}	0.025	$\log_{10} C_{ac} = 2.79 \log_{10} D_{gr} - 0.98(\log_{10} D_{gr})^2 - 3.46$

It is thus possible to determine the unit sediment charge x_s (ppm) i.e. the unit mass flux of sediment per unit mass of flow per unit time from

$$x_s = \frac{q_s}{q} \left(\frac{\rho_s}{\rho} \right) 10^6 \text{ (ppm)} \quad (5.5)$$

and the sediment charge X_s (ppm) i.e. the total mass flux of sediment per mass flux of fluid per unit time from

$$X_s = \frac{Q_s}{Q} \left(\frac{\rho_s}{\rho} \right) 10^6 \text{ (ppm)} \quad (5.6)$$

Sediment transport is highly non-linear and using an average main channel velocity such as that derived from Divided Channel Methods (DCM) or Ackers' coherence (COHM) approach (Section 2.5), rather than the depth-averaged velocity distribution, may result in substantially different sediment transport rates. In particular, the average main channel velocity does not capture the reduced sediment transport rates at the channel banks, tending to over-predict the average velocity and hence the overall sediment transport. The CES methodology improves the local shear velocity approximation from the more general formula (Eq. (2.31) in Section 2.2.3),

$$U_* = \sqrt{gRS_f} \quad (5.7)$$

as it is based on the locally resolved boundary shear stress, where $U_* = \sqrt{\tau_o/\rho}$.

A hypothetical case is now considered to demonstrate the use of the CES output. This is based on the FCF Phase A Series 2 channel, assuming a sediment d_{50} of 0.8 mm, a sediment density of 2650 kg m^{-3} and a constant flow depth of 0.198 m. Figure 5.3 shows the distribution of X_s with Q for the main channel only, as well as the distribution of X_s assuming no main channel floodplain interaction. This illustrates the importance of capturing the retarding effect of the slower moving floodplain flow on the faster moving main channel flow. The x_s and X_s predictions show similar distributions to those produced by the SKM model of Abril (1997) and Knight & Abril (1996) and the X_s distribution shows a similar trend to that of Ayyoubzadeh (1995), where the COHM method of Ackers was used to account for the floodplain main channel interactions.

As demonstrated, although the CES methodology was primarily intended for predicting the overall flow rate, outputs such as the local boundary shear stress and shear velocities mean it is particularly useful for estimating sediment transport rates for both inbank and overbank flows (Abril & Knight, 2002 & 2004; Atabay *et al.*, 2004; Brown 1997; Knight & Brown, 2001; Ikeda and McEwan, 2009). Further development and applications of the CES may include: predicting incipient motion based on the critical shear stress or Shields' (1936) function; establishing the transverse sediment gradient for channels with varying sediment sizes; incorporating the bed form roughness as a function of the critical velocity or boundary shear stress; erosion and automatic updating of cross-section geometry based on boundary shear stress distribution. Some of these advances could be incorporated in the current calculation set-up, for example, as a post-processing routine or as a core engine enhancement, e.g., an update to the f value provided by Colebrook-White.

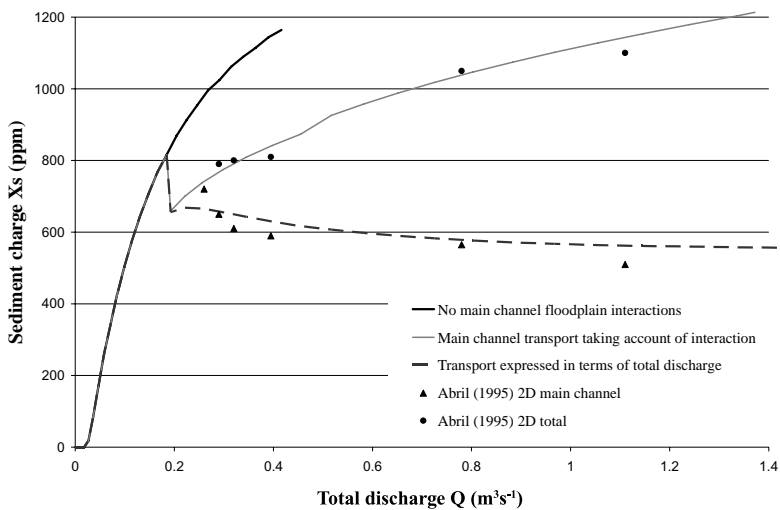


Figure 5.3 The predicted sediment charge X_s for the FCF Phase A Series 2 channel with a d_{50} of 0.8 mm (after Mc Gahey, 2006).

Some work has already been attempted on determining channel shape and bank erosion for inbank flows, as illustrated by Cao & Knight (1998) and Yu & Knight (1998). Geomorphological issues related to overbank flows are dealt with more fully in Ikeda and McEwan (2009), as are sediment processes, computer simulations and design considerations. Work in the FCF on the behaviour of graded sediments in meandering channels is described by Wormleaton *et al.* (2004 & 2005). For information on scour at bridges, see Melville & Coleman (2000).

5.3 TRASH SCREEN AND BLOCKAGE ISSUES

A bridge or culvert structure obstructs flow in the channel, causing an increase in upstream water levels relative to the levels that would be expected for the same channel in the absence of the structure. This afflux can be analyzed using CES-AES and may be considered as part of the hydraulic performance of the structure for specified design conditions. However, additional blockage can increase the afflux, leading to higher than expected upstream water levels. Blockages can occur in several ways, including:

- Collection of floating debris at the abutments/piers or soffit. This is often referred to as 'temporary blockage' because the debris can be removed. Removal more often than not requires human intervention, rather than the flow clearing the debris away;
- Collection of floating debris at a trash screen placed over the inlet of a culvert;
- Collection of floating ice, referred to as 'ice jams';
- Accumulation of bed load at the inlet, outlet, or within a culvert barrel;
- Abrupt blockage by large objects such as shopping trolleys.

There are many causes of blockage, but all are a combination of a source of debris that can cause a blockage and a means of trapping that debris. [Table 5.3](#) provides a list of the most common factors.

The quantitative assessment of blockage potential remains difficult. There is some empirical evidence to support predictive relationships for certain types of blockage. Accumulations of large, floating woody debris (drift) were analyzed by the US Geological Survey (Diehl, 1997) in a Federal Highway Administration study based on 2,577 reported drift accumulations and field investigations of 144 drift accumulations in large, wooded catchments. The maximum width of drift accumulations for any bridge span is about equal to the length of large logs delivered to the bridge. [Figure 5.4](#) shows data used to estimate a ‘design log length’ that could be used in assessing blockage risk for a given structure. This empirical data is valuable but it is also specific to the particular environment, blockage mechanism and bridge types studied.

Table 5.3 Common factors causing blockage of bridges and culverts.

<i>Factors contributing to debris source potential</i>	<i>Factors contributing to blockage potential</i>
Stream slope	Width/height
Urbanisation	Opening ratio
Vegetation	Shape
Sinuosity of stream	Skew
Upstream structures	Length
Channel width	Existence of piers/multiple culverts
Trash screens	Trash screens
Access to the channel	Trash booms
Time since last flood	Availability of skilled operators
Upstream channel maintenance regime	Auto screen raking
Upstream land use and riparian management	
High rainfall intensity	

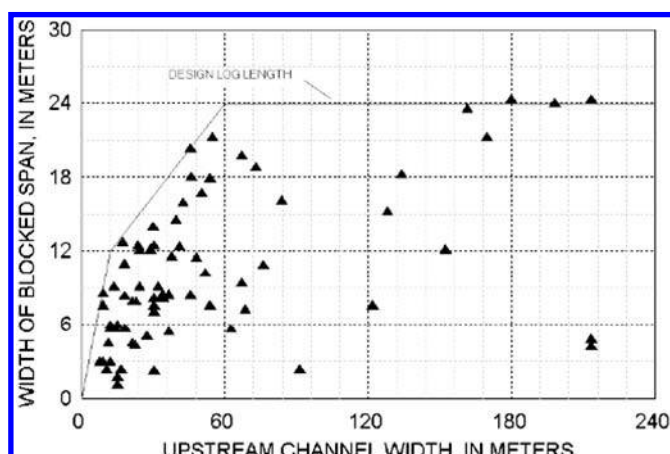


Figure 5.4 Effective width of drift-blocked spans outside the Pacific Northwest (Diehl, 1997).

In the UK, a “Blockage Risk Assessment” method was developed for the Environment Agency South West Region in 1997–8. This method is reviewed by Benn *et al.* (2004). Its main elements are:

- A spreadsheet based “blockage risk model” requiring various basic structural, hydrological and debris type attributes to which individual probability risks can be assigned;
- A decision tree analysis which directs the user to various actions depending on the blockage probability;
- Guidance on the application of hydraulic models to model blockage.

The study identified several major problems with identifying blockage risk. One is the lack of data and the second is that the probability distributions of the variables describing the influence of blockage are not independent, and the associated probabilities are subjective. This problem is not unique to blockage, and requires a consistent risk management framework aligned with the treatment of other risk issues.

Research underway within the Flood Risk Management Research Consortium (FRMRC2, <http://www.floodrisk.org.uk>) is gathering further field data on blockage and seeking to develop a probabilistic method for predicting the onset and degree of blockage potential at pinch points in the flooding system, such as bridges and culverts.

Trash screens (for example see Figure 5.5) are often placed over the entrance of a culvert either to reduce the amount of debris entering the culvert barrel, where it could cause blockage, or as a security screen to prevent unauthorised access. While a trash screen may prevent blockage within the culvert barrel, where it is difficult to clear debris, it may simply move the location of the blockage from the barrel of the culvert or inlet to the screen.



Figure 5.5 Trash screen on the River Sheaf in Sheffield. The screen can be cleared by a mechanical grab suspended from the gantry visible above the inlet. (Photo: JBA Consulting, Maltby Land Surveys).

Debris can accumulate on a screen, which may be cleared manually or using a mechanical system. Debris accumulation can also be linked to poor inlet conditions (e.g., badly aligned wing-walls, zones of ineffective flow, and piers or other ‘obstructions’).

Future development of the CES-AES may include a blockage and trash screen module. In the meantime, a pragmatic approach to represent blockage is to adjust a culvert or bridge cross section so as to reduce the available flow area, either by increasing channel bed levels or reducing the opening span and soffit dimensions. Estimates of head loss associated with a screen, h_s , can be calculated based on the change in velocity head associated with the reduction in flow area through the spaces between the bars using

$$h_s = K_{sc} \left(\frac{U_{sc}^2 - U_{mc}^2}{2g} \right) \quad (5.8)$$

where U_{mc} is the section average velocity in the main channel, U_{sc} is the average velocity through the spaces between bars, g is acceleration due to gravity and K_{sc} is an energy loss coefficient. The average velocity through the screen can be computed as $U_{sc} = Q/A_{sc}$ where Q is the discharge and A_{sc} is the flow area between the bars. CIRIA (1997) recommended $K_s \approx 1.5$. Representation of trash screens and blockage in hydraulic models remains an area of on going research. Experimental measurements and numerical modelling indicate that head loss coefficients increase with increasing blockage and that it may be possible to identify dimensionless relationships between flow variables for trash screens (Tsikata *et al.*, 2009) which may assist with the calibration of simplified empirical models for 1-D analysis.

5.4 WIDER MODELLING ISSUES

Having now described the CES-AES and its use, it is appropriate to set it in the context of other 1-D, 2-D & 3-D software systems. This Section deals briefly with some of the wider issues, such as the different types of computational model that are available, their basis and mathematical formulation, their commonly perceived use and purpose, together with a discussion on the different data and calibration requirements for each type of model, especially as the dimensionality increases from 1-D to 3-D. Although an introduction to the use of models in investigating and solving practical river engineering problems has already been given in Sections 2.2.1 & 2.2.2, the reader should refer to specialists textbooks for more information. Those that are particularly relevant to river engineers are, for example, texts by Abbot & Basco (1989), Batchelor *et al.* (2000), Cunge *et al.* (1980), Garcia-Navarro & Playan (2007), Ikeda & McEwan (2009), Nezu & Nakagawa (1993), Versteeg & Malalaskera (1995) and Vreugdenhil (1989).

5.4.1 Types of model

Table 5.4 shows a sample of the codes that are used in practice, or research, for modelling fluid flows. The list is not meant to be comprehensive, but is simply aimed at

Table 5.4 Some 1-D, 2-D & 3-D river modelling codes.

<i>I-D models</i>	<i>2-D models</i>	<i>3-D models</i>
ISIS	ISIS2D	CFX
MIKE11	MIKE21	PHOENICS
HEC-RAS	RMA2	FLUENT
SOBEK	TELEMAC2D	TELEMAC3D
InfoWorks RS 1D	InfoWorks RS 2D	DELFT FLOW3D
NOAH	DIVAST SSIM LISFLOOD TUFLOW	
Research codes	Research codes	Research codes

showing the range of some standard models and the extent of progress in Computational Fluid Dynamics (CFD) over the last few decades. Whereas 1-D codes were just starting in the 1960s, today they are commonplace and 2-D & 3-D codes are now frequently used in solving practical problems. This does not imply that 2-D & 3-D codes have superseded the use of all 1-D models, as each type of model has its own particular use, functionality and purpose. As seen later on, 1-D models are particularly useful in dealing with many river issues since rivers themselves are, by nature, long single-thread systems that convey water in a predominately downstream direction. It is also shown that the results obtained from higher dimensionality 3-D models are not necessarily more accurate and, furthermore, involve considerable effort and cost in obtaining them (Wright *et al.*, 2004). The purpose here is to identify where the CES-AES software fits into this framework and to consider briefly the issues that arise when using software of different spatial dimensionality, i.e., 1-D, 2-D or 3-D. Before discussing these issues an overview of the equations used in each spatial dimension is given, with particular emphasis placed on 1-D unsteady flow models, so that a direct comparison may be made between these and the CES-AES, even though it contains some 2-D and 3-D flow characteristics and is for steady flow only.

i One-dimensional model equations

As noted in Section 2.2.4, the 1-D equation for flow in an open channel relates the gravitational and frictional forces with the local and convective accelerations. Rather than expressing them in terms of h and U as functions of x and t , as in Eqs. (2.36)–(2.38), in 1-D river modelling codes it is customary to express the continuity and momentum equations in terms of A and Q as functions of x and t . These are known as the St Venant equations, and may be expressed in the form:

$$\frac{\partial A}{\partial t} + \frac{\partial Q}{\partial x} = q^* \quad (5.9)$$

$$\frac{\partial Q}{\partial t} + \frac{\partial}{\partial x} \left(\beta \frac{Q^2}{A} \right) + gA \left(\frac{\partial h}{\partial x} + S_f - S_o \right) = 0 \quad (5.10)$$

where the symbols have their usual meaning, and where q^* = lateral inflow/outflow per unit length and β = momentum correction coefficient. Equations (5.9) & (5.10) thus constitute two equations for two unknowns (A & Q) and may be solved numerically to give A and Q as functions of x and t . The area, A , and discharge, Q , are then known at all points along the river and with time. Examples of unsteady flow where such results might be useful are those involving flood simulations along rivers (flood routing) or tidal motion in long narrow estuaries. Knowing A and Q for all x and t , allows the depth, h , or water level, η , to be determined since the A v h relationship is known at every cross-section. Likewise, the velocity, U , may be calculated at every time step and cross section, since $U = Q/A$. The 1-D nature of the equations thus reflects the mainly one-dimensional flow in a river or estuary. An assessment of the relative importance of the various terms in Eq. (5.10) is given by Knight (1981), based on measurements in the Conwy estuary.

The classification of 1-D flows based on Equations (2.36) and (2.38) in Chapter 2 may now be clarified and linked to the St Venant equations above. Reverting to U and h as variables, then Eq. (2.36) gives the following classification for 1-D flows:

$$S_f = S_o - \frac{\partial h}{\partial x} - \frac{U}{g} \frac{\partial U}{\partial x} - \frac{1}{g} \frac{\partial U}{\partial t} \quad (5.11)$$

steady uniform flow → |

steady non-uniform flow → |

unsteady non-uniform flow → |

Chapter 2 has indicated how uniform flow and non-uniform flow (also known as gradually varied flow) occur in steady flow, and Eq. (5.11) now indicates how unsteady flow adds one extra term into the momentum equation, the so-called local acceleration, $(1/g)(\partial U/\partial t)$. The 3rd and 4th terms on the right hand side of Eq. (5.11) are known as the convective and local accelerations respectively. This method of classifying flows should be distinguished from an alternative method of classification based on Eq. (2.38), which relates particularly to unsteady flows, as follows:

$$Q = Q_n \left[1 - \frac{1}{S_o} \frac{\partial h}{\partial x} - \frac{U}{gS_o} \frac{\partial U}{\partial x} - \frac{1}{gS_o} \frac{\partial U}{\partial t} \right]^{1/2} \quad (5.12)$$

kinematic wave → |

diffusion wave → |

full dynamic wave → |

For the purposes of comparing these two classifications, based on Equations (5.11) & (5.12), with the St Venant equations, (5.9) & (5.10), consider 1-D flow in a frictionless, horizontal prismatic rectangular channel, with no lateral inflow, so that $S_f = 0$, $S_o = 0$, $q^* = 0$ and $A = bh$, where $b = \text{constant}$. Then, by ignoring the convective acceleration term (the second term in Eq. (5.10)), elimination of the terms $\partial A/\partial t$ and $\partial h/\partial x$ by cross differentiation reduces the pair of equations to a single equation, giving the water surface elevation, η , as:

$$\frac{\partial^2 \eta}{\partial t^2} - gh \frac{\partial^2 \eta}{\partial x^2} = 0 \quad (5.13)$$

This represents a simple progressive wave, since a solution to Eq. (5.13) is of the form:

$$\eta = a \cos(kx - ct) \quad (5.14)$$

where a = amplitude of the wave, $k = 2\pi/\lambda$; λ = wavelength; $\omega = 2\pi/T$; T = wave period, and η = height of the water surface above a datum level ($= b + z$ as before) and c = wave celerity (speed), given by $\pm\sqrt{(gh)}$ in shallow water. Thus at its simplest, unsteady 1-D flow in open channels may be conceived as the movement of a wave-form along a channel. This idea also links up with the concept of flood routing in rivers, based on Eq. (5.12). However the movement of a flood wave is not simply progressive.

Kinematic waves may be regarded as those that translate without distortion of shape, given by combining the first term in Eq. (5.12) with Eq. (5.9). Assuming that A and b are related to Q by single valued functions, then

$$\frac{\partial A}{\partial t} = \frac{\partial A}{\partial Q} \frac{\partial Q}{\partial t} = \frac{\partial Q}{\partial t} \frac{dA}{dQ} \quad (5.15)$$

Substituting Eq. (5.15) into Eq. (5.9) gives

$$\frac{\partial Q}{\partial t} + \frac{dQ}{dA} \frac{\partial Q}{\partial x} = 0 \quad \text{or} \quad (5.16)$$

$$\frac{\partial Q}{\partial t} + c \frac{\partial Q}{\partial x} = 0 \quad (5.17)$$

where dQ/dA is the kinematic wave speed, c , given by

$$c = \frac{dQ}{dA} = \frac{1}{B} \frac{dQ}{dh} \quad (5.18)$$

The solution to Eq. (5.17), the ‘kinematic wave’ equation, provided c is constant, is

$$Q = f(x - ct) \quad (5.19)$$

where f is any function. Eq. (5.19) is thus seen to represent any shape of wave, travelling in a positive x direction with a speed or celerity, c , given by Eq. (5.18), without change in shape. This involves the inverse of the gradient of the stage-discharge relationship, $1/(dh/dQ)$, and the water surface width, B . Since the CES can provide the stage-discharge relationship for rivers with any prismatic cross-sectional shape, this maybe demonstrates another use to which the software may be put, as described later in Section 5.4.3.

However, in reality the effect of friction tends to attenuate and delay the passage of a flood wave, so that the simple wave form suggested by Eq. (5.19) becomes distorted as the wave translates (moves) along the river. The non-uniformity of the cross-section shape with stage is also particularly important in this respect. To account for this, the

first two terms in Eq. (5.12) may be combined with Eq. (5.9) to give the so-called convective-diffusion equation, usually presented in the ‘standard’ form as

$$\frac{\partial Q}{\partial t} + c \frac{\partial Q}{\partial x} = D \frac{\partial^2 Q}{\partial x^2} \quad (5.20)$$

in which c = kinematic wave speed, given again by Eq. (5.18) and D = diffusion coefficient, given by

$$D = \frac{Q}{(2BS_o)} \quad (5.21)$$

It follows from Eq. (5.20) that the discharge in a channel during a flood event has the characteristics of a wave that now translates and attenuates. It should be noted that in the context of river engineering, both c and D in (5.20) are functions of the discharge Q , making the solution of Eq. (5.20) somewhat difficult. However, Cunge (1969) has shown that the Variable Parameter Muskingum-Cunge (VPMC) method is similar to the Preissmann finite-difference scheme used in solving the St Venant equations (Preissmann, 1961). VPMC uses 4 points in $x-t$, like the Preissmann box scheme but the leading term of the numerical truncation error is tuned to match the diffusion term. This then relates Equations (5.9) & (5.10) with (5.20) and allows for kinematic wave routing methods to be used in practice for channels with bed slopes greater than around 0.002 (See Knight, 2006c, for further details). It also gives a theoretical basis for varying the travel time constant, K , and the distance weighting parameter, ε , in the basic routing equations used in the original Muskingum method (Bedient & Huber, 1988; Shaw, 1994):

$$I - O = \frac{dS}{dt} \quad (5.22)$$

$$S = K[\varepsilon I + (1 - \varepsilon) O] \quad (5.23)$$

where I = inflow, O = outflow and S = storage. In the Constant Parameter Muskingum-Cunge method (CPMC), the travel time and distance weighting parameters are regarded as constants, to be determined for a particular river by back analysis of flood level data for at least one typical flood event. In the Variable Parameter Muskingum-Cunge (VPMC) the K and ε values vary for each reach, stage and time step, thus modelling the flood wave more accurately. See Tang *et al.* (1999a & b, 2001) and Knight (2006c) for further details.

ii Two-dimensional model equations

The shallow wave water equations are generally used in 2-D models expressed by Morvan *et al.* (2008) in terms of one mass conservation equation and two momentum conservation equations:

$$\frac{\partial h}{\partial t} + \frac{\partial h U_d}{\partial x} + \frac{\partial h V_d}{\partial y} = Q_l \quad (5.24)$$

$$\frac{\partial bU_d}{\partial t} + \frac{\partial bU_d^2}{\partial x} + \frac{\partial bU_dV_d}{\partial y} + gb\frac{\partial h}{\partial x} = gb(S_{ox} - S_{fx}) \quad (5.25)$$

$$\frac{\partial bV_d}{\partial t} + \frac{\partial bU_dV_d}{\partial x} + \frac{\partial bV_d^2}{\partial y} + gb\frac{\partial h}{\partial y} = gb(S_{oy} - S_{fy}) \quad (5.26)$$

with

$$S_{fx} = \frac{n^2 U_d \sqrt{U_d^2 + V_d^2}}{b^{7/3}} \quad \text{and} \quad S_{fy} = \frac{n^2 V_d \sqrt{U_d^2 + V_d^2}}{b^{7/3}} \quad (5.27)$$

where U_d and V_d are the depth-averaged velocities in the x and y directions respectively. Other terms can be included to represent the effects of turbulence. If the turbulent terms are omitted they are in effect lumped together with the numerical truncation errors and any other calibration coefficient, rather than truly reflecting the physical process. The determination of n is therefore not straightforward and this raises a number of issues, as discussed by Cunge *et al.* (1980), Samuels (1985) and Morvan *et al.* (2008).

Equations (5.24)–(5.26) thus constitute three equations for three unknowns (U_d , V_d and b) and may be solved numerically to give these as functions of x , y and t . In this case, rather than use cross-section data, a mesh of $\{x, y\}$ co-ordinates are required to represent the river and any associated floodplains. The individual velocity vectors may be combined to give the magnitude and direction of the depth-averaged velocity at any point with time. This is one advantage of such a model compared with the CES-AES, in which the direction of flow is assumed to be always in the streamwise direction. A 2-D model is therefore more suitable where details of flows over floodplains are required, or where the geometry of a river is such that the flow is complex, as in the case of bends or braided rivers for example. However, the 2-D model, as expressed in Equations (5.24)–(5.26), cannot deal with secondary flows, plan form vorticity or Reynolds stresses, which the CES-AES can do in an approximate, but effective manner.

iii Three-dimensional model equations

In 3-D models, the three time-averaged RANS equations, together with one equation for mass conservation, are used determine all three velocity components $\{UVW\}$ at every point $\{xyz\}$, together with the depth, b , as a function of $\{xy\}$ in plan form, with time, t . In essence, 4 equations are solved to give the 4 unknowns $\{U, V, W \& b\}$ as functions of $\{x, y, z \& t\}$. A 3-dimensional mesh is therefore now required to represent the model river, with special treatment being taken for the free surface (initial water level throughout the domain, as well as how it is controlled during the computation). See Ikeda & McEwan (2009), Nezu and Nakagawa (1993), Rodi (1980) and Versteeg & Malalaskera (1995) for further details.

Such models are inevitably mathematically complex, and also require a large number of ancillary equations to deal with the turbulent structures, in what is known as the ‘turbulence closure’ problem. It is referred to as a ‘problem’ because of the difficulty in describing turbulence in fluid flows, based on our incomplete knowledge of the physical reality, as well as our inability to describe such turbulence in a mathematical

set of equations that are universally agreed. Turbulence closure relates the unknown turbulent processes to the larger scale resolved motions. For further information on turbulent energy, cascades and spectra see Tennekes & Lumley (1972) and Versteeg & Malalaskera (1995).

The turbulence closure issue has been addressed by many researchers, usually by formulating an equation (or set of equations), that purports to represent the turbulence. These additional equations may be of many types. The simplest is a zero equation model, based either on the eddy viscosity principle, first proposed by Boussinesq in 1877, or the mixing length hypothesis, first proposed by Prandtl in 1925. The CES-AES in fact uses the same eddy viscosity approach to deal with one aspect of turbulence, as already indicated in Eq. (2.59) or Eq. (3.18). Other types of equations to deal with turbulence closure problem are: a two-equation model, involving differential equations that represent the relationship between energy production and dissipation; a Reynolds stress model that accounts for all three internal turbulent stresses; or, an algebraic stress model that in a somewhat simpler manner accounts for the anisotropy of the Reynolds stresses. Finally, some have even suggested that the time-averaged RANS equations may not even be the right starting place for certain types of problem and that double-averaged equations (i.e., averaging over time and space) should be used instead (Nikora *et al.*, 2008). As an alternative to RANS based models, large eddy simulation (LES) models or Direct Numerical Simulation (DNS) may be used to actually account for the individual turbulent fluctuations. The present position is best summed up by the authors of two books, written some 70 years apart, as cited in Nakato & Ettema (1996, pages 457–458) by one of the present authors:

“Were water a perfectly non-viscous, inelastic fluid, whose particles, when in motion, always followed sensibly parallel paths, Hydraulics would be one of the most exact of the sciences. But water satisfies none of these conditions, and the result is that in the majority of cases brought before the engineer, motions and forces of such complexity are introduced as baffle all attempts at a rigorous solution. This being so, the best that can be done is to discuss each phenomenon on the assumption that the fluid in motion is perfect, and to modify the results so obtained until they fit the results of experiments, by the introduction of some empirical constant which shall involve the effect of every disregarded factor. It is worthwhile here impressing on the student of the science that, apart from these experimentally-deduced constants, his theoretical results are, at the best, only approximations to the truth, and may, if care be not taken in their interpretation, be actually misleading. On the other hand, it may be well to answer the criticism of those who would cavil at such theoretical treatment, by pointing out that the results so obtained provide the only rational framework on which to erect the more complete structure of hydraulics.”

(A.H. Gibson, 1908)

“Turbulent motions contribute significantly to the transport of momentum, heat and mass in most flows of practical interest and therefore have a determining influence on the distribution of velocity, temperature and species concentration over the flow field. It is the basic task of engineers working in the field of fluid mechanics to determine these distributions for a certain problem, and if the task is

to be solved by a calculation method, there is no way around making assumptions about the turbulent transport processes. Basically this is what turbulence modelling is about: because the turbulent processes cannot be calculated with an exact method, it must be approximated by a turbulence model which, with the aid of empirical information, allow the turbulent transport quantities to be related to the mean flow field.”

(W. Rodi, 1980)

As can be readily appreciated from these comments, as well as from the governing equations, that as one moves from 1-D to 3-D models, so does the level of complexity increase markedly. This is especially so in the ancillary equations required to describe the turbulence in mathematical terms. Another feature of 3-D models is the large number of physical constants that need to be known in order to calibrate, or indeed validate, the model at all. This then suggests that for practical purposes, one should decide on the purpose for using a model, before embarking on any modelling at all. One should then select the most appropriate model carefully, commensurate with the purpose in mind, the model’s technical fitness for the task, as well as the ease with which it may be used.

5.4.2 Implications involved in model selection, calibration and use

It is worth stressing again that higher dimensionality of model does not necessarily lead to better accuracy in the results. In certain cases the opposite may be true. The principle of Occam’s razor should always be applied – that of starting with the simplest by assuming the least. *Pluralitas non est ponenda sine necessitate*; “Plurality should not be posited without necessity.” (William Occam, 1285–1347). The principle gives precedence to simplicity; of two competing theories, the simplest explanation of an entity is to be preferred. The principle may also be expressed as “Entities are not to be multiplied beyond necessity.” [Encyclopaedia Britannica, 2003].

In the context of modelling flows in rivers, this suggests caution before embarking on 3-D modelling for solving every type of river engineering problem. As has been seen for flood routing, a 1-D model might be quite adequate for estimating travel times of floods in a river with fairly regular floodplain geometry. However, where a river meanders significantly, and any overbank flow is not aligned with the flow in the main river channel, then a 2-D depth averaged model will be more appropriate and might be sufficient for the purposes of estimating the magnitude and direction of the velocities at various points in the river valley. The trend in Europe and more recently in the UK is a move towards coupled 1-D and 2-D models, where the 1-D model simulates flow in the main river channel and the 2-D model captures the floodplain flow effects. Where detailed flow patterns are required, as for example in pump fore-bays at river intakes, or in heat dissipation and re-circulation modelling studies for a power station, then a 3-D model might be the only possible and sensible option.

Little mention has been made so far about boundary conditions in 1-D, 2-D & 3-D models. These not only differ according to the type of differential equations being solved, but also influence the solution methodology, the results and the data required

to run the model at all. For example, in 1-D unsteady flow models, the boundary condition upstream is normally that of an input hydrograph $\{Q v t\}$ and the boundary condition downstream is frequently that of a fixed depth or a $\{h v Q\}$ relationship. Initial conditions will also be required throughout the domain, e.g., starting values for depths and discharges (or velocities) at all cross sections. In 2-D models, similar requirements apply, but at open boundaries the velocity field must be specified as well, which may initially be unknown. The same applies in 3-D models where wall functions are used to mimic the boundary conditions at mesh points very close to the wall, and cyclic boundary conditions might be applied at open ends to improve convergence and reduce the run time. For further information on boundary conditions, see Cunge *et al.* (1980), Samuels (1985) and Vreugdenhil (1989).

The numerical approach used in solving any governing differential equation, possibly based on finite-difference, finite-element or finite-volume methods, also needs to be appreciated and understood. The consistency, convergence, stability and accuracy of any adopted numerical method needs to be known, and possibly also the techniques used in investigating them. Such techniques are often based on Fourier series in complex exponential form, but are clearly beyond the scope of this book. See Abbot & Basco (1989), Cunge *et al.* (1980) and Preissmann (1961) for further information.

In 1-D models, it should be noted that even the governing St Venant equations may be discretized in different ways, and that this will inevitably affect the numerical results, as shown by Whitlow and Knight (1992). In 2-D and 3-D models it is imperative to vary the mesh size and to observe at what point of resolution any two solutions agree. In 3-D models, it is not only important to vary the mesh size, but also to check on key parameters at strategic points in the mesh, monitoring them at certain time steps as the computation proceeds. This is because the numerical procedure may take many thousands of iterations to fully converge to a solution, even when solving for a steady flow case. For example, the turbulent intensity or Reynolds stress at a certain point in the mesh is influenced by values at adjacent points in the mesh. Since the solution technique is iterative, the parameters at a single point (e.g., 3 velocity components, $\{UVW\}$, mean pressure, 3 turbulent intensities, 3 Reynolds stresses, etc.) may take a long time to converge at that particular point, and at every other point in the mesh (often thousands). The numerical solution for the whole domain is then not complete until similar convergences are obtained at all points in the mesh, to a pre-determined and specified accuracy for each particular variable or parameter.

From the preceding paragraph it is clear that the data required for different types of model varies according to their dimensionality and complexity. A 1-D model will generally only require cross section data at specified intervals, chosen to reflect the terrain, as indicated by Samuels (1990), and more recently by Casellarin *et al.* (2009). Channel roughness (and its representation) is arguably the single most important issue to resolve prior to successful modelling. In 1-D models, the use of channel cross sections makes it relatively easy to compare results with known mean velocities, since $U = Q/A$. In 2-D models, the data required for calibration increases significantly, since two components of velocity are required at every point in the mesh, giving both magnitude and direction locally. Furthermore, in 2-D models the water surface itself may no longer be considered as planar, as for example occurs in bend flow or in the vicinity of bridges. In 3-D models the data requirements multiply even more significantly,

with mean and turbulent parameters required at every location in an {xyz} co-ordinate system.

In most practical case studies there is simply not enough hydraulic or turbulence data at sufficiently detailed spatial and temporal scales to be meaningful. This makes the calibration stage particularly difficult, and reliance has then to be placed on the software user's experience. The dimensionality of the model also affects the run time and data handling. Modern CFD packages usually come with a number of post processing packages, enabling the results to be analysed in several ways. The use of graphs and charts to plot secondary flow cells, strength of vorticity, shear stresses on internal elements, colours to visualize velocity fields within each cross section, etc., make it possible to undertake assessments and any comparisons quickly and efficiently. Comparisons may not always be between measured and numerical results, on account of the scarcity of measured data, but often between different computer runs with differing flow or geometric features. Not to be forgotten are comparisons with any analytical results, if they are available, and with any suitable benchmark laboratory data.

The concept of 'equifinality' is an important one in model calibration, as noted by Beven & Freer (2001), who state that

"... the concept of equifinality is that the uncertainty associated with the use of models in prediction might be wider, than has hitherto been considered, since there are several (many?) different acceptable model structures or many acceptable parameter sets scattered throughout the parameter space all of which are consistent in some sense with the calibration data. The range of any predicted variables is likely to be greater than might be suggested by a linearised analysis of the area of parameter space around the "optimum". This suggests that the predictions of all the acceptable models should be included in the assessment of prediction uncertainty, weighted by their relative likelihood or level of acceptability."

The use of models outside their calibration range also raises issues in assessing uncertainty. See Beven, (2006), Hall & Solamatine (2008), Samuels (1995) and Sharifi *et al.* (2009a & b) for further details.

5.4.3 The CES-AES software in context

The CES-AES software may now be reviewed in the light of the two preceding Sections. Firstly it needs to be stressed that the model is for steady flow and is more than a 1-D model, since it has certain 3-D flow features embedded in it. It does therefore not fit neatly into the classification given in Table 5.4. It may be described as a type of lateral distribution model (LDM) for both inbank and overbank flows, as it simulates these in a unified manner by treating the flow as in Nature, as a continuum. The same three calibration parameters f , λ and Γ are used in both types of flow, thus unifying the methodology. It perhaps might be regarded then as a 1.5-D model with 3-D features.

These 3-D features are the ability to model secondary flows for inbank flow via Γ , lateral diffusion via a dimensionless eddy viscosity, λ , planform vorticity in overbank flow via Γ , and boundary shear stresses via a local friction, f . The model was developed on the basis of large scale experiments carried out in the Flood Channel Facility (FCF), and validated against an extensive range of experimental data, including detailed

turbulence data on Reynolds stresses, lateral distributions of velocity and boundary shear stress at the same flows in comparable geometries, making the determination of local and zonal friction factors possible, and varying floodplain roughness. The CES has also been tested against a number of full scale rivers in the UK and overseas, for which there is measured data, as well as other laboratory data. See Mc Gahey *et al.* (2006 & 2008).

The Roughness Advisor (RA) distinguishes the CES-AES from other software, as the resistance term is known to be one of the dominant terms in the St. Venant equations, requiring special care. The addition of an Afflux Estimation System (AES) allows the user to include the second most important feature affecting water levels and contributing to head losses, namely bridges and culverts. Together with the Uncertainty Estimator (UE), it allows the CES-AES to be applied to practical river engineering problems with a degree of confidence not matched by comparable systems.

The AES combines many novel features by treating bridges and culverts in a comprehensive way, with multiple arches and backwater effects. One particularly distinguishing feature is that the experimental data for bridge afflux were obtained from experimental flows in compound channels, rather than basing it on flows in simple rectangular channels, as previous authors have done. This is more representative of the actual conditions occurring in practice. The data used herein for both bridge afflux and compound channels are thoroughly documented and available via the two websites www.flowdata.bham.ac.uk and www.river-conveyance.net.

The examples in Chapter 2, showing how 4 or 6 panels can produce lateral distributions of depth-averaged velocity and boundary shear stress in trapezoidal channels of a comparable standard as produced by any 3-D model, but with much less effort, are remarkable. The number of panels or slices in the depth-averaged model naturally increases when the CES is applied to flows in rivers, especially where the need is to investigate velocity fields due to different vegetation patterns. The ability to estimate lateral distributions of boundary shear stress are particularly useful when dealing with sediment behaviour in rivers and channels. This is perhaps one of the most significant uses to which the CES-AES might be put in the future.

Despite being designed initially for steady flow, some elements of the CES-AES make it applicable to unsteady flows, noticeably the use of the conveyance, K , via Eqs (2.41) and (3.48), and subsequent discharge estimation, provided the correct water surface slope is used. The prediction of an accurate stage-discharge relationship also feeds into the estimation of a reliable wave speed- discharge relationship (c v Q) via Eq. (5.18), as demonstrated by Tang *et al.* (2001).

5.5 SOFTWARE ARCHITECTURE AND CALCULATION ENGINES

The conveyance and afflux estimation projects both included a requirement to produce a software tool that implemented the new estimation method. This led to the development of the CES-AES software that is available for download at www.river-conveyance.net. This software is intended to be a relatively simple application that provides the user with a simple and intuitive means of using the new conveyance and afflux methods on any appropriate set of data.

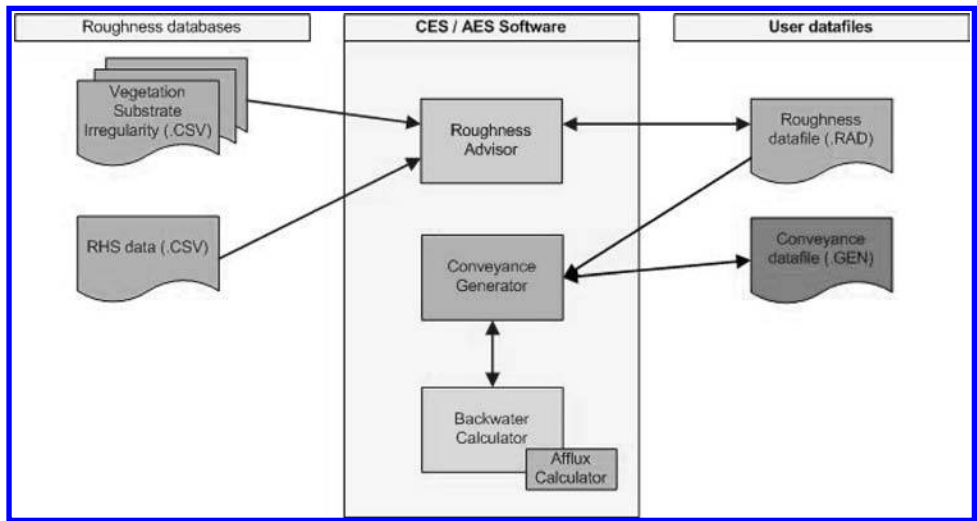


Figure 5.6 Overall structure of the CES-AES software.



Figure 5.7 Roughness calculation engine.

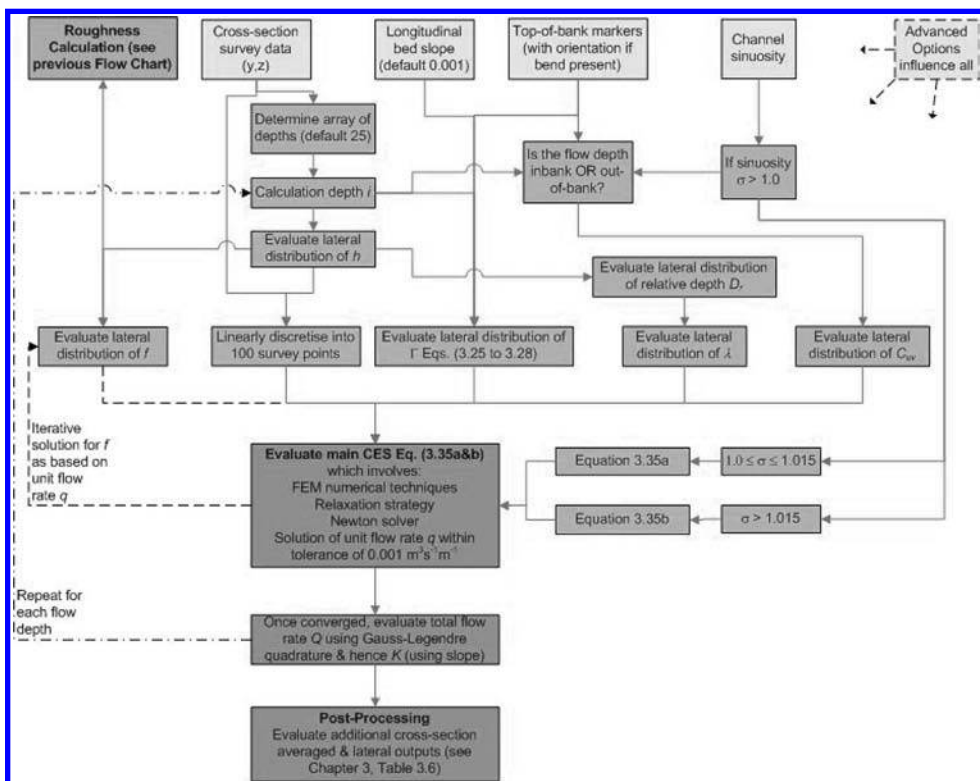


Figure 5.8 Conveyance calculation engine.

The overall structure of the software from a user perspective is shown in Figure 5.6. The software incorporates 3 main elements, the roughness advisor, the conveyance generator and the backwater calculator. Afflux is calculated as part of a backwater as this provides the necessary downstream water level for the afflux method. Data specific to the site of interest is stored in two data files. The .RAD file contains the user specific data relating to vegetation, substrate and irregularity for each of the roughness zones of interest. This file is saved by the user and stores the output of the roughness calculations carried out within the roughness advisor. The .GEN file contains the geometrical data for the channel and any bridge and culvert structures, as well as information on which roughness zones are used for calculating the section conveyance. Together the .GEN and .RAD files contain all of the data relevant to a particular site.

The raw data for the roughness advisor is provided from a number of databases that capture the outputs of the roughness review carried out for the original conveyance estimation project. These databases are in a simple .CSV format and this was selected to allow users the flexibility to edit and update the files if they have access to improved or alternative roughness data, though for most purposes the data should be considered as fixed.

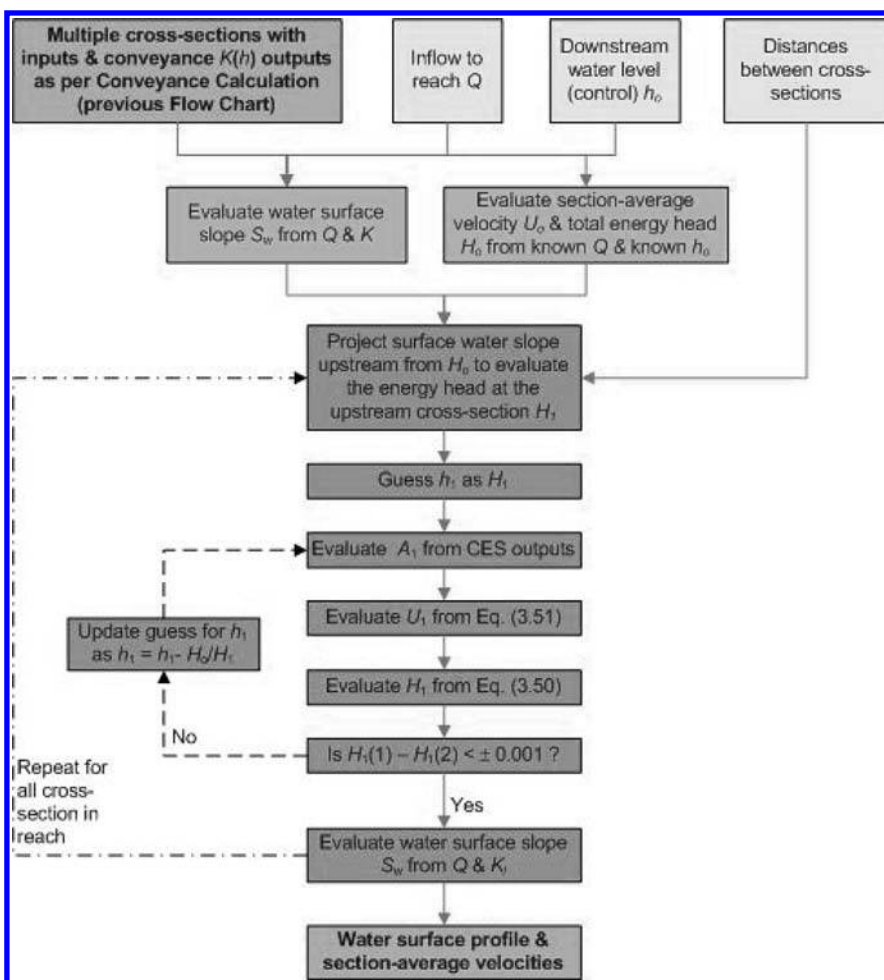


Figure 5.9 Backwater calculation engine (case without structures).

Figures 5.7, 5.8, 5.9 and 5.10 show the flow charts that define the operation of the calculation engines for roughness, conveyance and backwater.

The majority of users of the CES-AES will run the software through the standard user interface. However, it was anticipated in both the conveyance and afflux projects that the source code for the calculation methods would be made available for the purposes of further research. The software design allows for this by separating all the main control and calculation code from the user interface. This is essential, as the user interface contains compiled proprietary code that cannot be distributed. The current structure of the software when compiled is shown in a simplified form in Figure 5.11. The main software procedures are all handled by the Convey.DLL module, including file access, data structure and manipulation, roughness calculation, backwater calculation and interfacing to the conveyance and afflux calculation modules. This structure

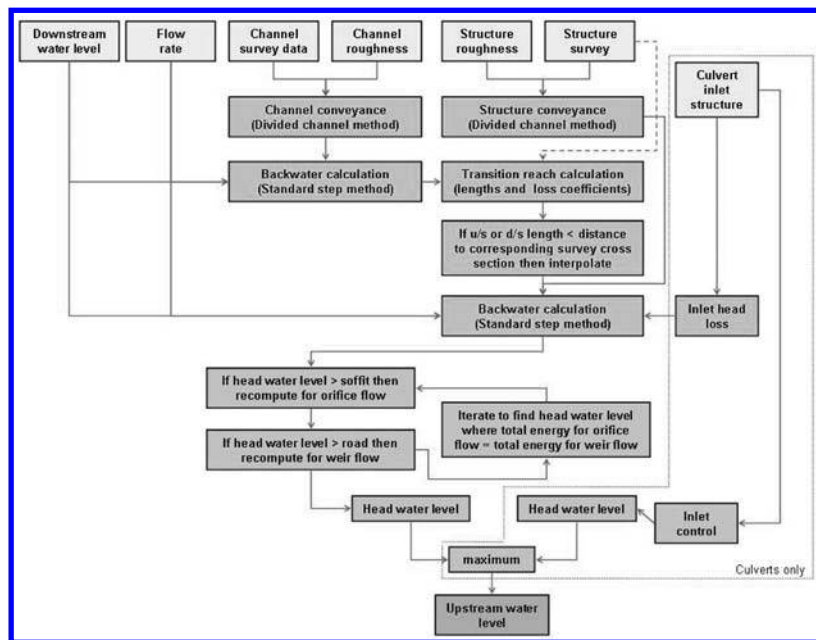


Figure 5.10 Afflux calculation engine.

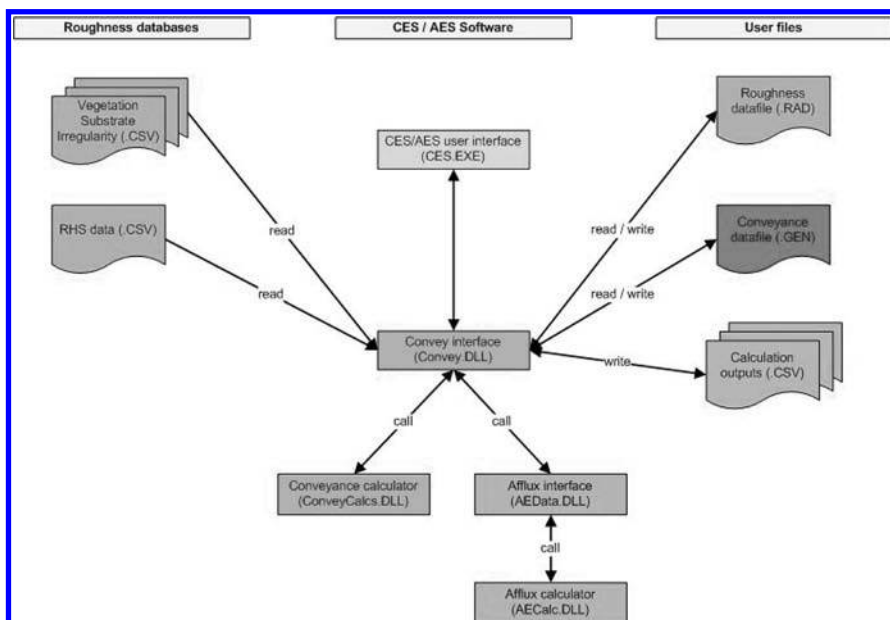


Figure 5.11 Underlying structure of the CES-AES software.

effectively allows a programmer with access to the source code to replace the standard user interface with a simple interface of his or her own, and run all of the underlying calculation code.

The Afflux calculation is accessed through an interface (AEData). This structure was adopted as it allowed the afflux calculator to be developed independently from the CES software, with interaction taking place through the agreed software interface.

In practice, the overall structure shown is more complicated at the level of the source code itself, with the code sub-divided into classes in line with good software development procedures. The code has been written in three different languages. The core conveyance calculation engine (ConveyCalcs) is currently written in C for maximum portability, whilst the afflux interface and engine are written in VB. All other parts of the software are written in C++. It is probable that future updates to the software may result in changes to this structure though these will not remove the capability of running the calculation modules from outside the user interface.

Customisation of the software can be carried out at three levels. Firstly, the user can modify the default parameters that are used in the conveyance calculation. The Advanced Option box shown in Figure 5.12 provides a means for users to alter many of the model parameters via the CES-AES User Interface (Table 5.5).

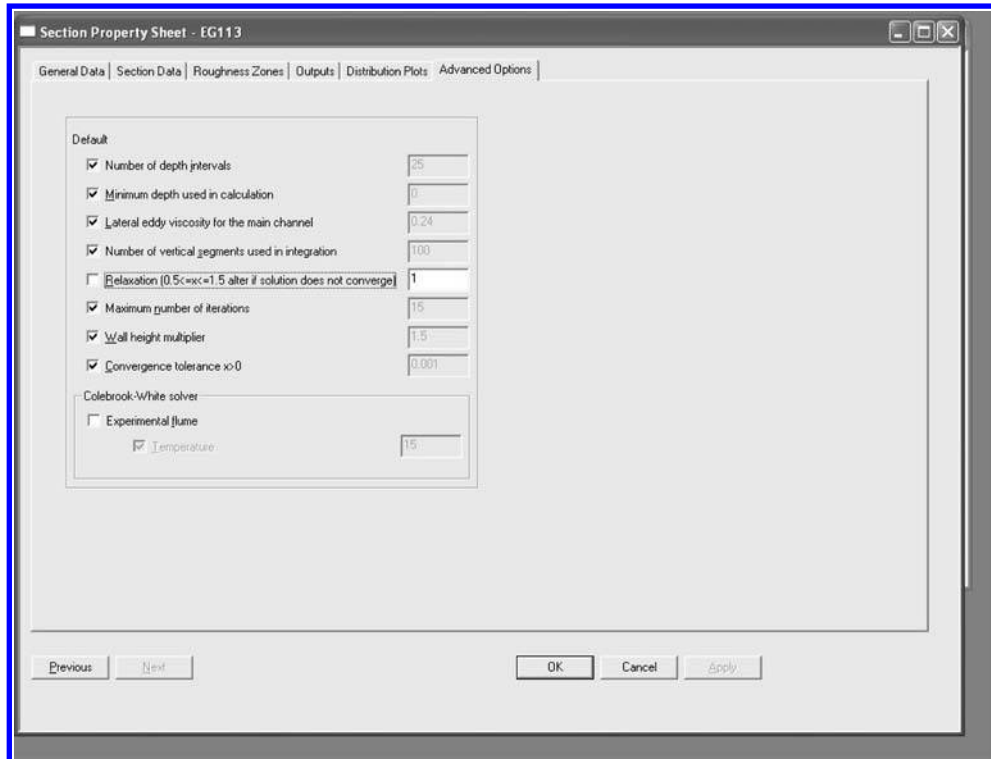


Figure 5.12 Advanced options for conveyance calculation method.

Table 5.5 Advanced options and default values.

Advanced options	Default value	Allowable range
Temperature	15°C	>0
Number of depth intervals	25	100
Minimum depth used in calculation	Lowest bed elevation	Any depth below maximum entered elevation
Lateral main channel eddy viscosity λ_{mc}	0.24	0.1–0.5
Number of vertical segments used in integration	100	500
Relaxation parameter	1	$0.5 \leq \text{Relaxation} \leq 1.5$
Convergence tolerance	0.001	0.001–1.000
Maximum number of iterations	20	50
Wall height multiplier	1.5	10
Experimental flume	Off	On/off

Secondly, the user may modify the default roughness databases used by the software. These changes might take the form of adjustments to the default roughness values, incorporation of new photographs or addition of new materials and roughnesses. The file formats are fully documented and this documentation can be downloaded from the CES-AES Website.

Thirdly, it will be possible for researchers to investigate changes to the core calculation routines in the software through modification of the software source code. For example, the management models used to implement cutting of vegetation might be modified in the light of improved knowledge of the re-growth rates of various vegetation types. The existing cutting routines are found in the CManagementModel class and the C++ code that implements this is available as ManagementModel.cpp.

At the time of writing, the mechanism by which source code for the CES and AES calculation may be made available had yet to be finalised. However, it is expected that it will be made available under licence to other software houses and bona fide researchers. Further information will be available through the CES-AES website at www.river-conveyance.net.

Concluding remarks

ABSTRACT

These concluding remarks draw together some of the key points made in earlier chapters and highlight the more important issues involved in modelling flows in rivers. Suggestions are made about future work that is required in the area of modelling as well as possible developments in the CES-AES software. The need for accurate measurements of certain hydraulic and turbulence parameters at full scale is especially highlighted. These should be carried out in conjunction with the development and rigorous testing of improved computer-based modelling tools, tested on a selected number of rivers and against benchmark laboratory data.

6.1 CONCLUDING REMARKS

As outlined in the Preface, the principal driver for the development of the Conveyance Estimation System and the Afflux Estimation System (CES-AES) software, as well as the underpinning research described throughout this book, was the need for better computer-based tools for flood risk management. Although predominately developed with the needs of the UK in mind, the subject matter is relevant to all rivers, water-courses and open channels, as shown by the application of the current software to a number of international rivers. These were carefully selected to extend both the range of discharge, as well as the type of river (mountain boulder to lowland) and substrate. Fuller accounts of the application of the CES component to a wide range of international rivers are given by Mc Gahey (2006) and Mc Gahey *et al.* (2006 & 2008).

The global scale of flooding, as outlined by Berz (2000), is highlighted in [Chapter 1](#) and the examples drawn from Europe and Asia are used to illustrate the wide range of problems that flooding causes. Having established the international nature of floods, as well as the importance of making sound estimates of the conveyance capacity of channels and water levels under flood flow conditions, new drivers are described that impinge on the work of the hydraulics engineer. These derive from recent international legislation and planning directives, such as the European Water Framework Directive (2000) and the European Directive on the Assessment and Management of Flood Risks (2007), or similar legislation that has been enacted in Japan, the USA and other countries.

In the light of the European legislation, as well as the requirement for better flood risk mapping, the CES-AES software deliberately focuses on the determination of water level in rivers, rather than discharge, since it is the water level that relates particularly strongly to: 1) damage to infrastructure and property, 2) national and local economies, and 3) loss of life. Furthermore, since the water level in rivers and watercourses are predominately influenced by channel roughness and hydraulic structures, especially bridges and culverts, the two elements that feature strongly in the software are those of flow resistance and afflux. The development of ancillary tools, such as the Uncertainty Estimator (UE) and the Roughness Advisor (RA), are aimed at providing the best possible estimates of channel roughness and flow resistance (two related but separate concepts). The Roughness Advisor was developed from a very extensive knowledge of data world-wide, again making it suitable for application both within the UK and internationally. The development of this particular practical component of this toolset is described more fully elsewhere by Mc Gahey *et al.* (2009).

Another important focus and distinguishing feature of the CES-AES is that it deals with both inbank and overbank flows as a continuum, rather than as disparate types of flow. This is, after all, how rivers behave naturally, and one would therefore expect any modelling software to mimic this natural process. Although overbank flows introduce more complex flow structures, these are handled in a similar way as for inbank flows, through the use of the same three hydraulic calibration parameters for each panel, f , λ and Γ , representing local friction, eddy viscosity and secondary flows, thus unifying the methodology. Further parameters related to wave speed, sediment transport and dispersion may also be added, creating a holistic approach to modelling river flows, as illustrated in more detail elsewhere by Knight (2006c). Although the CES-AES is restricted to simulating steady flows with a fixed bed, this still allows many types of practical problems to be solved. Unsteady flow phenomena and flow over loose boundaries, such as sediments, may be readily treated by further development of the CES in the future, allowing alluvial resistance formulae to be used, together with channel adjustment algorithms for channel widening, deepening or slope changes.

One particularly useful feature, often not found in comparable software, is the ability of the CES-AES to provide lateral distributions of depth-averaged velocity, U_d , and boundary shear stress, τ_o , as well as conveyance and water levels. The lateral distributions of U_d are particularly useful for calibration purposes, since they mimic what is often measured when river gauging, as well as being useful in studies related to the maintenance of vegetation. The distribution of τ_o around the wetted perimeter is likewise particularly useful, as it is the most important parameter required for any studies into sediment behaviour and geomorphology.

The title of the book was deliberately chosen to highlight the practical emphasis given throughout, despite the significant scientific nature of some elements in certain chapters. The authors believe that it is no longer possible to treat even one-dimensional (1-D) flow as ‘simple’, since turbulent flows are inherently three-dimensional and should be recognised as such. Thus the examples in Chapter 2, although beginning with relatively straightforward hydraulics, based on Manning’s equation, soon take the reader into the difficulties of modelling flows in rivers and watercourses using the Reynolds-Averaged Navier-Stokes equations, or RANS for brevity. At the same time, an attempt is made to illustrate the physical processes at work in river flows, without ‘blinding the reader with too much science’. It is hoped that the judicious use of case

studies throughout that chapter, without all the details of the RANS equations or the CES-AES methodology being explained, is helpful. It is often said that we learn by repetition, rather like peeling layers from an onion, each ‘layer’ adding to and building on our existing knowledge, taking us deeper into the subject matter. It is for this reason that the full description of the CES-AES methodology is delayed until [Chapter 3](#), with detailed examples of the use of the software reserved until [Chapter 4](#).

The use of examples throughout the book reflects this repetitive, ‘layer’ by ‘layer’ approach, beginning with some simple hydraulics calculations and concepts in [Chapter 2](#) (Examples 1–5), followed by examples of flows in rectangular and trapezoidal channels, analysed by the Shiono & Knight method (SKM). The SKM is introduced at an early stage, as it is not only a pre-cursor to the CES approach, but also may be used at a spreadsheet level by the reader, as shown by the various examples given. These are followed by further ‘layers’, typically case studies of flows in engineered channels and natural rivers, selected to illustrate and aid understanding of flow structures and fluid flow behaviour, rather than just computational techniques. Particular emphasis is placed on understanding the physical processes and the role of the calibration parameters used within the computational model, a feature which is often overlooked in books on computational hydraulics and sometimes even by modellers alike. It is often said that river engineering is an ‘art’ as well as a ‘science’, and that modelling needs therefore to take into account two distinct elements: ‘theoretical fluid mechanics’ and a multitude of ‘practical issues’.

This is illustrated by [Figure 6.1](#), taken from Nakato & Ettema (1996), in which river engineering is envisaged as the joining together of two river banks, one named ‘theoretical fluid mechanics’ and the other ‘practical problems’. On the left hand side (looking downstream), the shapes of the zones represent various practical river problems and their inter-related nature. To deal with a specific problem or practical issue, one has to understand its relationship with other problems, gain that knowledge, cross the river by one of the bridges, pick up the appropriate knowledge on the right hand bank (again looking downstream), return by another bridge and deal with the particular practical problem or issue in question. In doing so, one may have to repeat the journey several times, or recollect previous journeys, thus slowly building up a more complete picture of the river system itself. The two river banks should not therefore be regarded as opposites, but as complementary. Sometimes a false dichotomy develops between people who tend to inhabit one side of the river or the other, perhaps stereotyped by the outdated ‘division’ between practitioners and theoreticians, each regarding the other side as either aliens or at worst useless. However, rivers always have two banks, and the most fruitful advances in river engineering have occurred when the two sides meet, exchange views and deal with common issues. It should be noted that the various areas of theoretical knowledge also have various regions too. The river bank alongside the continuity and Navier-Stokes equations has sheet piling, indicating that the bank is firm and well established. It has been there since 1845. However, the sheet piling barely extends into the turbulence region, where the ground appears to be marshy and not well developed. The high rise buildings nearby indicate enormous growth, activity and development in this region, as typified by the growth in the subject of Computational Fluid Dynamics (CFD) and advanced experimental studies in turbulence. A complete understanding of turbulence is however for future generations to achieve.

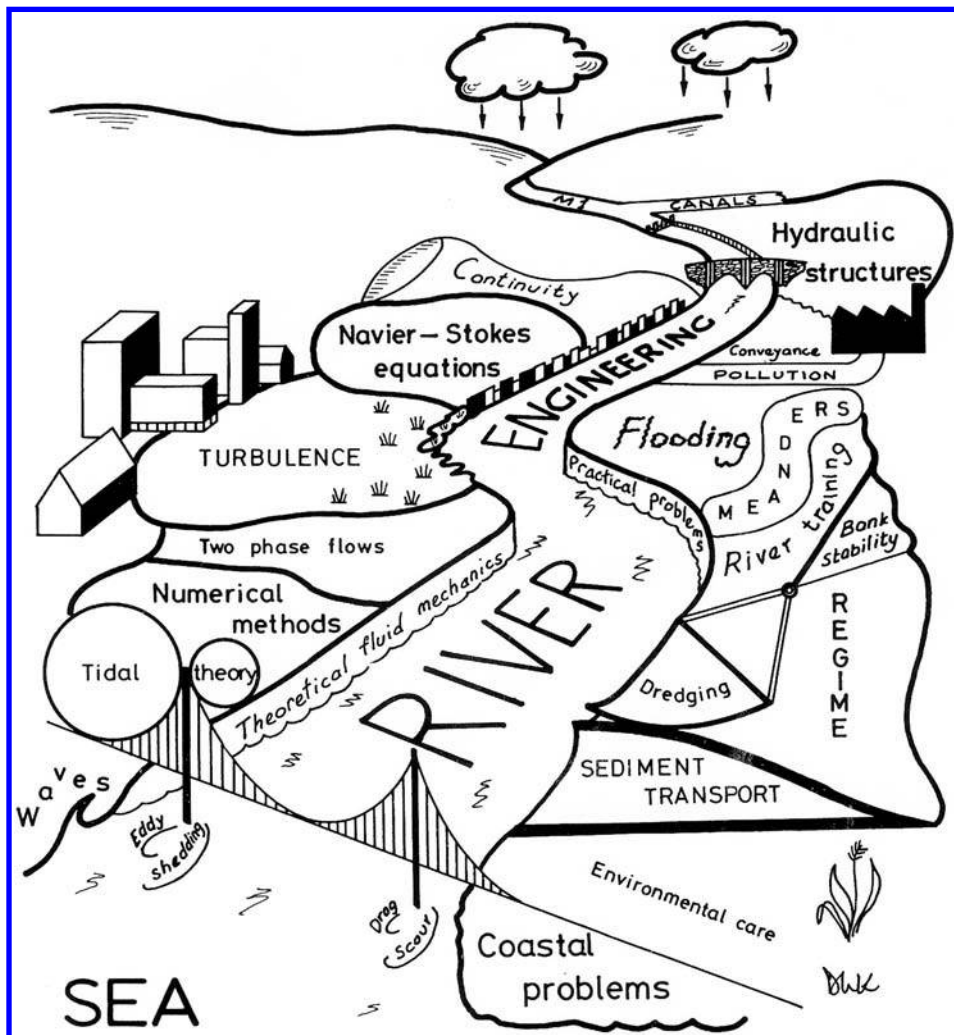


Figure 6.1 The art and science of river engineering (after Knight) [reproduced from Nakato & Ettema, (1996), page 448].

Despite our lack of knowledge of certain aspects of turbulence, the Reynolds-Averaged Navier-Stokes (RANS) equations have been used herein as the basis for the SKM as well as for the CES-AES software, as they are well established, even if the constituent equations for turbulence are not. Greater effort is needed in the area of turbulence measurements in open channels, especially in natural rivers at full scale. At present such data are relatively scarce, mainly due to cost considerations. Does an isometric view of the river between the banks in Figure 6.1 needs to be drawn, zoned and annotated by what is required below the free surface?

[Figure 6.1](#) also reminds the reader that the effective use of any software in river engineering depends as much on the knowledge of the end-user as the software developer. Modelling should never be regarded as simply a matter of feeding numbers into a computer without fully understanding either the nature of the river flow one is attempting to model, or the simulation algorithms that approximate the turbulence. Furthermore it should be recognised that the particular practical problem or issue being investigated may be only one amongst many, as illustrated in [Figure 6.1](#), where ‘conveyance’ is shown as just one relatively small region.

A common danger in interpreting model output is to believe that the visualisations (e.g. vector plots, velocity fields, etc.), are a true representation of the physical process. What is seen can be an artefact of the visualisation algorithms and not a true reflection of the solution of the numerical procedures in the hydrodynamic simulation. For example, post-processing of raw outputs may have smoothed results or introduced false flow structures. The numerical results themselves will also mask the true complexity of the turbulent flows in nature. There is sometimes a tendency for users to give greater weight to more detailed pictorial output from a 2-D or 3-D model, than from a 1-D model or measurements. A useful aid for understanding physical flow processes is the DVD from Cambridge University Press, (for further information, see website: <http://www.cup.es/uk/catalogue.asp?isbn=0521721695>).

Having introduced the reader in [Chapter 2](#) to some important fluid flow concepts, equations and a possible solution methodology via the SKM, as introductory ‘layers’, the worked examples may be considered as the next few ‘layers’. These emphasise the distinction between roughness and fluid flow resistance, the various types of friction factor (global, zonal and local), the way that the SKM deals with both inbank and overbank flows within a unified methodology, the use of calibration parameters, the complex nature of flows through bridges and culverts, as well as some of the more common difficulties in modelling flows. After this introductory phase, a major series of ‘layers’ then follows in [Chapter 3](#), beginning with a systematic exposition of flow structures in rivers and at bridges and culverts. At the same time the methodology behind the CES-AES is fully described, omitting unnecessary detailed application to actual rivers, bridges and culverts, to deepen understanding of the 3-D nature of various fluid flow structures, as well as highlighting how the different components are integrated within a single system to simulate water levels and flow behaviour.

One of these ‘layers’ is particularly important, namely Section 3.2.3, in which the CES methods, outputs and solution techniques are re-capitulated concisely. Tables 3.4 and 3.5 summarise the parameters used and the key assumptions, together with their implications and significance. Appendix 1 gives further details of all the equations used. Section 3.2.5 deals with the afflux methods employed within the AES in a similar way. These layers are the ‘heart’ of the onion, so to speak, and should be studied carefully. Software manuals and explanatory notes are sometimes notorious in not stating clearly and concisely the nature of the methodology used, together with any implicit assumptions. In addition to this, it is hoped that in due course an ‘open-code’ version of the CES-AES will be released so that engineers and research scientists can amend, replace or add in their own particular components. This attempt at ‘transparency’ is aimed at helping users to not only understand the CES-AES thoroughly, but also to use it more effectively and perhaps even to develop it further in the future.

Having now peeled the onion, so to speak, down to its heart, there are still two further Chapters that follow. Continuing with the food metaphor, one might therefore regard these as the more interesting chapters in a ‘recipe book’ in which, following the earlier chapters on basic cooking skills, kitchen equipment, nutrition and food types, one now begins to apply it and get some benefit. In the same manner, these later Chapters illustrate how the CES-AES may be used in practice, beginning with an overview in Section 4.1, and followed by many specialist sections. These contain numerous examples, some relating to estimating stage-discharge relationships in different types of river, and others to estimating lateral distributions of velocity and boundary shear stress. Some of these examples show comparisons between the back-calculated Manning’s n values with measured values. Others show the effect of changes in the stage-discharge relationships arising from changes in roughness, slope or sinuosity. The uses to which these are put, as well as the uncertainties are illustrated throughout the Chapter. Furthermore, the cross-section data for nine representative rivers from the UK, South America and New Zealand are given in Appendix 3 for those interested in repeating the calculations themselves. Sections 4.3 and 4.4 deal with estimating afflux at bridges and culverts and illustrate the use of the AES by applying it to a wide range of cases, again some from the UK and some from overseas. This Chapter thus caters for those interested in international cuisine, and it is hoped that others may add their recipes to enrich the book in the future.

If [Chapter 4](#) is regarded as illustrating ‘established’ recipes, based on experience, then [Chapter 5](#) may be regarded as one of ‘experimental’ recipes, based on novel uses for the CES-AES. The two ideas or ‘recipes’ that have already been tried involve ecological and geomorphological issues, which serve to show the potentially wide range of application for the software. Section 4.6 has already indicated how the lateral distributions of depth-averaged velocity, U_d , can be used in assessing vegetation and the maintenance of weedy rivers, as well as cutting regimes, and the link between invertebrates and weed cover. These distributions might also be used to assess other ecological issues, such as balancing the conflicting requirements of flood risk management, when the maximum discharge capacity is usually needed, with that of biodiversity, when a more varied velocity distribution is required to support different flora and fauna. Habitat information such as response curves (velocity/depth preferences) and LIFE scores can be used with the CES-AES outputs to identify preferred habitats. An example of both deepening and dredging has been given for the River Hooke in Section 4.6.3.

The second application is more strongly related to the lateral distributions of boundary shear stress, τ_o , as this parameter is frequently required in calculations involving sediment motion, as well as in many geomorphological assessments. Section 5.2 shows how both the stage-discharge and sediment rating curves may be estimated, for both inbank and overbank flows, again indicating a continuum. The CES approach may also be applied to other sediment issues, such as the determination of a channel shape for threshold conditions, the effects of widening or deepening the channel cross-section on the velocity field, as well as the design of stable channels and their correspondence with analytical regime formulae. See Cao & Knight (1996 & 1998), Knight & Yu (1995) and Yu & Knight (1998) for further details. The recent

book by Ikeda & McEwan (2009) also contains useful information on the modelling of sediment behaviour in meandering rivers with overbank flow.

It is always important to appreciate what any software ‘is’ and what ‘it is not’. It must be stressed that the CES-AES is not a universal tool aimed at solving all flow and water level problems in rivers and drainage channels and watercourses. It has been designed specifically as a relatively simple tool, dealing with practical issues of water level estimation in steady flow only, stage-discharge relationships, backwater effects, afflux at bridges and culverts, all of which are frequently encountered in engineering practice. It may be operated as a stand-alone piece of software, or embedded within other more complex river engineering modelling systems (e.g. as in ISIS and InfoWorks RS), allowing the non-expert and the experienced river engineer alike to use it, hopefully with relative ease. The limitations are listed in Sections 1.3 and 3.2.3, and the various examples illustrate its capabilities and potential, as well as some of its shortcomings and limitations.

Ancillary tools such as the Roughness Advisor (RA) and the Uncertainty Estimator (UE) are included in the book as they offer practical help in decision making over arguably the most important calibration parameter, the roughness. They also may be used in assessing the output from the combined influence of all three calibration parameters. The practical emphasis is highlighted again by the focus on stage-discharge relationships, since these are frequently used in making decisions in flood risk management, as well as in other areas of river engineering. The subject index highlights these, as do many of the worked examples.

In addition to a comprehensive list of references, mention should also be made of the data sources, described in Section 2.7 and also contained in the websites www.flowdata.bham.ac.uk and www.river-conveyance.net. It should be noted that the studies in the Flood Channel Facility (FCF) have featured significantly in the development of the CES-AES, as have other experimental studies. Without such data and their subsequent analysis, the concepts and equations presented herein would not have materialised. It is suggested that further progress in the ability to model flows in rivers successfully could therefore be made by designing carefully focussed experiments, some to be undertaken in the field and others in laboratories. These should be undertaken to specified standards of accuracy, and then combined with other quality-assured data from other researchers and practitioners, creating a resource that will benefit all. This reiterates the comments made by Chezy in the 1760s, as noted by Mervyn Bramley in his Foreword to this book!

6.2 FUTURE DEVELOPMENTS

From the experience already gained from using the CES-AES, together with new science, a number of future developments and research areas have been recommended to ensure the scientific relevance of the CES-AES is maintained (EA/Defra, 2009). These recommendations are intended to deal with known deficiencies in elements of the theoretical background and methodology, incorporating emerging science, and developing related tools and aids. The review identifies upwards of 70 prioritised recommendations, prioritised following extensive consultation with a wide range of

stakeholders in relation to benefits and value for money, which are categorised as either “enhancements to the science” or “enhancements to the software features”. Some of the high priority aspects recommended for inclusion in the short-term are:

Updating the Roughness Advisor to reflect new science and roughness information – Roughness has the most significant contribution to the uncertainty in conveyance (Khatibi *et al.*, 1997; Latapie, 2003; Mc Gahey, 2006) and of the different roughness types, vegetation roughness includes the greatest natural variability (Sellin & van Beesten, 2004; Defra/EA, 2003b). Much work (Dawson, 1978; Westlake & Dawson, 1982; Baattrup-Pedersen & Riis, 2004; Naden *et al.*, 2006; O’Hare *et al.*, 2008) has been undertaken on understanding this variability, including the seasonal variations and regrowth following cutting, through measurement of biomass, plan form cover and cross-sectional area occupied by plants. Available measurements are largely for two key species, emergent reeds (*Sparganium erectum*) and submerged fine-leaved plants (*Ranunculus pectinatus*), which are two of the most commonly occurring weeds in managed channels in England and Wales. There is information available to derive seasonal uncertainty distributions for vegetation roughness and to extend these to other vegetation morphotypes.

Other RA improvements include, for example, updating the photographic database to ensure each roughness type has ample photographic evidence; improving roughness values for pools and riffles based on recent findings at the River Restoration Centre (Janes *et al.*, 2005); and updating the embedded River Habitat Survey information (Raven *et al.*, 1998) to reflect the recently completed survey (2003–09 based on EA, 2003), including additional fields such as substrate type and trash present.

Developing a Channel Maintenance Module – There is a significant amount of literature and guidance available on channel maintenance (e.g. CAPM, 1997; EA, 1997; EA, 1998a & b; Fisher, 2001; Buisson *et al.*, 2009). Whilst the CES-AES provides a vital tool for supporting the exploration of “what-if” scenarios to investigate different channel management options, the process of investigating these is not straightforward. User experience is that navigation within the tool can be time-consuming, is not always intuitive and many of the outputs require further manipulation to provide them in a useful format for decision making. A CES-AES Channel Maintenance Module would improve the navigation of options within the current CES-AES tool to aid exploration of different “what-if” scenarios; process and summarise outputs to provide user-friendly graphs and tables which highlight the merits of the different scenarios; and incorporate a database of standard vegetation cuts (e.g. cut along one bank, cut 50% of inbank vegetation) with simple explanatory images.

Extending the existing capability to deal with different culvert inlet shapes and multiple barrels – There are a range of opening types available in the CES-AES for bridges and culverts, with some flexibility to define the shapes of the openings; however more complex types such as multiple culvert openings with different shapes and invert levels or bridges with relief culverts cannot be represented directly. In addition, the road or parapet level of bridges is assumed to be horizontal and approach road embankments cannot be represented. Whilst some of the issues are related to how the AES represents opening and cross section geometry, it is also becoming apparent that the coefficients used to compute energy losses for these configurations may require

updating in light of more recent research (e.g. Hotchkiss *et al.*, 2008; Kells *et al.*, 2008; Tullis *et al.*; 2008 for single inlets; Charbeneau, 2006 for multiple barrels). Thus, the CES-AES culvert inlet coefficients, which deal with idealised shapes and are based on the original US methods as adapted in the CIRIA guidance (Ramsbottom *et al.*, 1997), could be improved to better represent inlets as they occur in nature. Accommodating more complex multi-barrel structures raises questions about the lateral distribution of velocity in the flow. A possible approach would be to use an approximate 2-D model such as the CES to determine the spatial velocity distribution of the undisturbed flow and hence to estimate the spatial velocity of the disturbed flow due to the presence of a structure using a simple adjustment, based on, for example, the observed flow behaviour (e.g. Charbeneau, 2006; Haderlie & Tullis, 2008).

Developing a blockage and trash screen module – The issues surrounding blockages and trash screens are detailed in Section 5.3. A CES-AES Blockage and Trash Screen Module would involve developing a hydraulic loss unit for dealing with trash screens (including percentage blocked) and more general channel blockage (e.g. woody debris) and a means to determine the impact on upstream water levels, building on current methods (e.g. EA, 2009) where they continue to offer utility and designed to link with ongoing research in this area (e.g. FRMRC2, <http://www.floodrisk.org.uk/>). Key challenges involve determining the distance upstream of a blocked culvert or trash screen at which the maximum afflux occurs and defining the point at which a channel is considered blocked.

Harmonisation of the CES-AES methods – The AES model for bridges and culverts incorporates a backwater calculation based on an energy balance through the structure to account for energy extracted from the main flow. This makes use of conveyance rating curves calculated both for the river channel as it would be in the absence of the structure (the ‘undisturbed channel’) and for the structure at its upstream and downstream faces. The AES computes the required physical parameters such as cross sectional flow area and wetted perimeter as functions of flow depth for a range of opening geometries. In particular, it works for closed shapes such as arches and pipes, which is essential when modelling the conveyance for a bridge or structure. This calculation is based on a Divided Channel Method using Manning *n* resistance parameters for three panels, consistent with the original experimental research (1950s). The Divided Channel Method and CES calculation typically provide different solutions at the transition section and the use of two distinct approaches has raised questions from users regarding the need for both. Harmonisation of the CES-AES methods will involve adapting and incorporating the CES calculation for the reaches with structures. An important change will be modifying the current CES algorithm for boundary treatment to deal with closed shapes such as circular culverts and arches and appropriate adaptation of the structure coefficients.

A targeted programme of data acquisition – is needed to ensure data on aquatic vegetation (e.g. seasonal measurements to build a long-term record), flow properties (e.g. flow, velocity, turbulence) and evidence of debris following storms (initiated in FRMRC2) is collated. The value of these measurements cannot be overstated as they are fundamental to method development, testing and validation, providing evidence

of the true flood risk system behaviour. A philosophy of “measure more, model less” is essential to the ongoing development of tools such as the CES-AES.

Development of a habitat module – Section 5.1 highlights the importance of ecological functioning and habitat design when considering channel design and maintenance. A CES-AES Habitat Module would provide a CES-AES post-processing tool to enable users to make-use of detailed flow, velocity and shear stress information together with habitat data, for example, response curves or LIFE scores (Section 5.1) in support of identifying preferred channel management options. It would include a database of habitat information and facilitate processing of this, together with CES-AES outputs, into user-friendly graphs and tables.

Methods for extension of rating curves – Rating curves often do not cover high flood flows because of the difficulties in measuring flows under flood conditions and in some instances the gauge stations may be drowned. The extension of ratings is therefore of vital importance in planning and designing flood defence measures. Current best practice guidance (Ramsbottom & Whitlow, 2003) and tools provide a range of regression analysis techniques to fit polynomials to gauged data from within the measurable range, and hence extrapolation of these to predict water levels at flood flows. Emphasis is placed on selecting the most appropriate method for the site. For example, the hydraulic principles of extending inbank and out-of-bank rating curves are different and the site may be treated differently if a structure such as a weir is present. A further challenge in implementing the various approaches is that the surveyed cross-sections do not always extend across the entire inundated area, and there is therefore uncertainty about the true channel shape at large depths. This work would involve extending the data records at key sites to capture flood flows and using these to develop, test and validate methods consistent with the CES-AES for the extension of ratings.

Development of a sediment transport module – Section 5.2 introduces the importance of sediment and geomorphology issues. A CES-AES Sediment Transport Module would include a post-process tool offering a suite of analysis techniques based on, for example, methods of Du Boys (1879), Einstein (1942), Bagnold (1966), Engelund & Hansen (1966), Ackers & White (1973), Chang (1988) and Ackers (1990–93). These would make use of the CES-AES outputs such as the local velocity, shear stress and shear velocity to determine the sediment concentrations and loads. The user support in determining the preferred channel regime will build on work currently underway in the UK on Sediments and Habitats Phase II – Additional Studies and would link closely with the aforementioned Habitat and Channel Maintenance Modules.

Some of the medium-to-long term research areas include:

- Revamp the embedded CES conveyance calculation, for example, a 2-layer model for main channel and floodplain;
- Improved understanding of flow, vegetation and sediment interaction;
- Incorporate the variation of resistance with the passage of the flood;
- Incorporate an embedded model to deal with alluvial friction e.g. ripples, dunes, antidunes;

-
- Embed the CES-AES in a dynamical model which automatically updates the channel bed based on regime theory;
 - Incorporate the impact of climate change, for example, for long-term vegetation growth patterns.

Finally, it should be noted that whilst the research community continue to press the boundaries of science and computational methods, in practice there is considerable value in minimising model complexity, commensurate with producing realistic and acceptable output. As noted earlier, 1-D models, with key 3-D flow processes embedded, can be a cost-effective and efficient way of solving many river engineering problems. The CES-AES software is one such model that offers novel opportunities for learning about basic open channel flow processes as well as for gaining experience in practical problem solving in, for example, extension of rating curves, flood risk management, as well as in certain areas of ecology and geomorphology. Thus we expect that the CES-AES will find a role in education and be a vehicle for transferring knowledge from the research domain into professional use. In conclusion, we are convinced that there is a long-term need for 1-D modelling approaches in practice, as Antoine Chezy pointed out so many years ago.

Appendix I

The finite element approximations for the CES equations

Final CES conveyance equations

$$gHS_o - \psi \frac{f}{8} \frac{q^2}{H^2} + \frac{\partial}{\partial y} \left(\lambda \left(\frac{f}{8} \right)^{1/2} Hq \frac{\partial}{\partial y} \left(\frac{q}{H} \right) \right) - \left(\frac{(1.015 - \sigma)}{0.015} \Gamma + \frac{(\sigma - 1.0)}{0.015} C_{uv} \frac{\partial}{\partial y} \left(\frac{q^2}{H} \right) \right) = 0$$

$\sigma = 1.0$ inbank; $1.0 \leq \sigma \leq 1.015$ overbank

$$gHS_o - \psi \frac{f}{8} \frac{q^2}{H^2} + \frac{\partial}{\partial y} \left(\lambda \left(\frac{f}{8} \right)^{1/2} Hq \frac{\partial}{\partial y} \left(\frac{q}{H} \right) \right) - C_{uv} \frac{\partial}{\partial y} \left(\frac{q^2}{H} \right) = 0$$

$\sigma > 1.0$ inbank; $\sigma > 1.015$ overbank

(3.35a&b)

In the above equation set, the Γ term is a multiple of the hydrostatic pressure term, and it is therefore not dealt with explicitly here. Thus, consider the terms in Equation 3.35b,

$$gHS_o - \psi \frac{f}{8} \frac{q^2}{H^2} + \frac{\partial}{\partial y} \left(\lambda \left(\frac{f}{8} \right)^{1/2} Hq \frac{\partial}{\partial y} \left(\frac{q}{H} \right) \right) - C_{uv} \frac{\partial}{\partial y} \left(\frac{q^2}{H} \right) = 0$$

(1)

(2)

(3)

(4)

The finite element approximations are given by:

Term 1

$$\sum_{\text{elements}} \int_{y_i}^{y_{i+1}} gS_o \left(\sum H_i \phi_i \right) \phi_j dy \quad [\text{Vector Term 1a}]$$

Term 2

$$\sum_{\text{elements}} \int_{y_i}^{y_{i+1}} -\frac{(\sum \beta_i \phi_i) (\sum f_i^n \phi_i) (\sum q_i^n \phi_i)^2}{8(\sum H_i \phi_i)^2} \phi_j dy \quad [\text{Vector Term 2a}]$$

$$\sum_{\text{elements}} \int_{y_i}^{y_{i+1}} -\frac{(\sum \beta_i \phi_i) (\sum f_i^n \phi_i) (\sum q_i^n \phi_i) (\sum \Delta q_i^n \phi_i)}{4(\sum H_i \phi_i)^2} \phi_j dy \quad [\text{Matrix Term 2b}]$$

$$\sum_{\text{elements}} \int_{y_i}^{y_{i+1}} -\frac{(\sum \beta_i \phi_i) (\sum q_i^n \phi_i)^2 \left(\sum \frac{\partial f}{\partial q} \Big|_i \phi_i \right) (\sum \Delta q_i^n \phi_i)}{8(\sum H_i \phi_i)^2} \phi_j dy$$

[Matrix Term 2c]

Term 3

$$\begin{aligned} & \sum_{\text{elements}} \int_{y_i}^{y_{i+1}} -\frac{\lambda}{\sqrt{8}} \left(\sum q_i^n \phi_i \right) \left(\sum f_i^n \phi_i \right)^{1/2} \\ & \times \left[\left(\sum q_i^n \frac{\partial \phi_i}{\partial y} \right) - \frac{(\sum q_i^n \phi_i) \left(\sum H_i \frac{\partial \phi_i}{\partial y} \right)}{(\sum H_i \phi_i)} \right] \frac{\partial \phi_j}{\partial y} dy \end{aligned}$$

[Vector Term 3a]

$$\sum_{\text{elements}} \int_{y_i}^{y_{i+1}} -\frac{\lambda}{\sqrt{8}} \left(\sum q_i^n \phi_i \right) \left(\sum f_i^n \phi_i \right)^{1/2} \left(\sum \Delta q_i^n \frac{\partial \phi_i}{\partial y} \right) \frac{\partial \phi_j}{\partial y} dy$$

[Matrix Term 3b]

$$\sum_{\text{elements}} \int_{y_i}^{y_{i+1}} -\frac{\lambda}{\sqrt{8}} \left[\frac{(\sum q_i^n \phi_i) (\sum f_i^n \phi_i)^{1/2} (\sum \Delta q_i^n \phi_i) \left(\sum H_i \frac{\partial \phi_i}{\partial y} \right)}{(\sum H_i \phi_i)} \right] \frac{\partial \phi_j}{\partial y} dy$$

[Matrix Term 3c]

$$\begin{aligned} & \sum_{\text{elements}} \int_{y_i}^{y_{i+1}} -\frac{\lambda}{\sqrt{8}} \left(\sum \Delta q_i^n \phi_i \right) \left(\sum f_i^n \phi_i \right)^{1/2} \\ & \times \left[\left(\sum q_i^n \frac{\partial \phi_i}{\partial y} \right) - \frac{(\sum q_i^n \phi_i) \left(\sum H_i \frac{\partial \phi_i}{\partial y} \right)}{(\sum H_i \phi_i)} \right] \frac{\partial \phi_j}{\partial y} dy \end{aligned}$$

[Matrix Term 3d]

$$\sum_{\text{elements } y_i} \int_{y_i}^{y_{i+1}} -\frac{\lambda}{2\sqrt{8}} \frac{(\sum \Delta q_i^n \phi_i) (\sum q_i^n \phi_i) \left(\sum \frac{\partial f}{\partial q} \Big|_i \phi_i \right)}{(\sum f_i^n \phi_i)^{1/2}} \\ \times \left[\left(\sum q_i^n \frac{\partial \phi_i}{\partial y} \right) - \frac{(\sum q_i^n \phi_i) \left(\sum H_i \frac{\partial \phi_i}{\partial y} \right)}{(\sum H_i \phi_i)} \right] \frac{\partial \phi_j}{\partial y} dy$$

[Matrix Term 3e]

Term 4

$$\sum_{\text{elements } y_i} \int_{y_i}^{y_{i+1}} -\frac{2C_{uv} (\sum q_i^n \phi_i)}{(\sum H_i \phi_i)} \left(\sum q_i^n \frac{\partial \phi_i}{\partial y} \right) \phi_j dy \quad [\text{Vector Term 4a}]$$

$$\sum_{\text{elements } y_i} \int_{y_i}^{y_{i+1}} \frac{2C_{uv} (\sum q_i^n \phi_i)^2}{(\sum H_i \phi_i)^2} \left(\sum H_i^n \frac{\partial \phi_i}{\partial y} \right) \phi_j dy \quad [\text{Vector Term 4b}]$$

$$\sum_{\text{elements } y_i} \int_{y_i}^{y_{i+1}} -\frac{2C_{uv} (\sum \Delta q_i^n \phi_i)}{(\sum H_i \phi_i)} \left(\sum q_i^n \frac{\partial \phi_i}{\partial y} \right) \phi_j dy \quad [\text{Matrix Term 4c}]$$

$$\sum_{\text{elements } y_i} \int_{y_i}^{y_{i+1}} -\frac{2C_{uv} (\sum q_i^n \phi_i)}{(\sum H_i \phi_i)} \left(\sum \Delta q_i^n \frac{\partial \phi_i}{\partial y} \right) \phi_j dy \quad [\text{Matrix Term 4d}]$$

$$\sum_{\text{elements } y_i} \int_{y_i}^{y_{i+1}} \frac{2C_{uv} (\sum q_i^n \phi_i) (\sum \Delta q_i^n \phi_i)}{(\sum H_i \phi_i)^2} \left(\sum H_i^n \frac{\partial \phi_i}{\partial y} \right) \phi_j dy \quad [\text{Matrix Term 4e}]$$

Appendix 2

Summary of hydraulic equations used in the AES

Transition lengths

$$\frac{L_{(C,E)}}{D_N} = b_0 + b_1 Fr + b_2 J_D + b_3 Fr^2 + b_4 J_D^2 + b_5 Fr J_D$$

Coefficient	Contraction		Expansion	
	$k_1(m^{-1})$	k_2	$k_1(m^{-1})$	k_2
b_0	0.0190	-8.9	0.0712	-26.2
b_1	-0.213	50.8	-0.294	197.8
b_2	0.190	26.6	0.0569	15.2
b_3	0.565	-36.2	-0.872	-22.2
b_4	-0.170	-20.4	0.0170	9.9
b_5	0.418	-39.1	0.394	-2.8

Transition energy losses

$$h_t = LS_f + C \left| \alpha_2 \frac{U_2^2}{2g} - \alpha_1 \frac{U_1^2}{2g} \right|$$

Transition energy loss coefficients

Subcritical flow	Supercritical flow
$C_C = 0.1$	$C_C = 0$
$C_E = \min \left\{ 0.3, 0.1 \frac{B}{B^*} + 0.1 \right\}$	$C_E = 0$

Pressure flow

$$Q = C_d b_N Z (2g \Delta h)^{1/2}$$

Overtopping flow

$$Q = C B_{RD} H^{3/2}$$

Appendix 3

Cross-section survey data

Table 3.1 River Trent, Yoxall.

Y	Z
0	2.59
1	2.4
2	2.42
5	2.35
8	2.36
11	2.36
14	2.34
17	2.4
20	2.42
23	2.43
26	2.41
29	2.4
32	2.43
33.5	2.44
36	2.59
39	2.24
42	2.29
45	2.17
48	1.77
51	0.33
54	0.14
57	0.02
60	0.05
63	0
66	0.04
69	0.23
72	0.71
74	1.61
76	1.7
78	1.94
79	2.04
79.7	2.25
79.9	2.59

Table 3.2 River Colorado.

Y	Z
-60	3.8
7.5	3.6
10	1.2
14	1.36
17	1.3
20	1.2
23	1.1
26	1
29	0.9
32	0.9
35	0.8
38	0.7
41	0.6
44	0.56
47	0.56
50	0.4
53	0.34
56	0.34
59	0.3
62	0.2
65	0
68	0.2
71	1.1
73.6	3.6
150	3.8

Table 3.3 River Main, Bridge End Bridge.

Y	Z
0	4.54
5.3	1.41
13.5	0.92
14.4	0
26.6	0
27.6	0.97
35.7	1.38
40.8	4.89

Table 3.4 River Severn, Montford Bridge.

Y	Z
7	7.74
13	6.94
18	6.62
23	6.46
28	6.32
31	6.21
33	5.87
36	5.46
38	4.91
39	4.15
40	3.63
41	3.22
42	1.84
43	1.36
44	1.05
45	0.29
47	0.17
50	0.06
53	0.01
56	0.02
59	0
62	0.07
63	0.53
64	1.63
65	3.13
66	3.68
67	4.05
68	4.37
69	4.93
70	5.73
72	5.91
76	6
80	6.1
84	6.16
88	6.26
92	6.37
96	6.46
100	6.54
104	6.59
108	6.74
112	6.8
116	6.87
120	6.9
124	6.9
128	6.99
133	7.02
136	7.74

Table 3.5 River La Suela.

Y	Z
4	2.51
7.3	2.14
8.1	1.64
9	0.38
10.5	0
15.6	0.02
28.9	0.2
30.4	1.22
33.7	1.9
36.6	3.07

Table 3.6 River Waiwakaiho.

Y	Z
0	5
1	4.5
2	3.8
3	3.7
4	3.6
5	3.3
6	2.9
7	2.8
8	2.3
9	2
10	1.7
11	1.6
12	1.2
13	1.1
14	1.1
15	1
16	0.6
18	0.6
19	0.55
20	0.6
21	0.7
22	0.6
23	0.45
24	0.5
25	0.45
26	0.45
27	0.3
28	0
29	0.3
30	0.5
31	0.55
32	1.1
33	3.1
34	3.6
35	4.1
36	4.6
37	5

Table 3.7 River Tomebamba.

Y	Z
1	4.3
5	1.53
5.4	1.33
7	0.39
8	0
10	0.17
12	0.23
14	0.13
16	0.24
18	0.42
20	0.64
22	0.75
24	0.83
26	0.86
28	1.1
29	1.16
30	1.33
31	1.53
45	4.3

Table 3.9 (Continued).

Y	Z
1.60	0.04
2.05	0.02
2.50	0.04
2.95	0.02
3.40	0.05
3.85	0.05
4.30	0.06
4.75	0.08
5.20	0.06
5.65	0.09
6.10	0.04
6.55	0.05
7.00	0.09
7.45	0.07
7.90	0.02
8.35	0.00
8.80	0.01
9.25	0.04
9.40	0.56
9.41	0.80

Table 3.8 River Cole.

Y	Z
0.0	1.60
2.0	1.05
5.0	1.00
7.0	0.30
7.5	0.05
8.0	0.03
9.0	0.01
10.0	0.00
10.5	0.01
11.0	0.02
12.5	0.03
13.0	0.30
15.0	1.40
20.0	1.50
22.0	1.60
23.0	1.70

Table 3.10 Holme Bridge.

Y	Z
-102.704	158.229
-96.285	157.797
-83.447	157.333
-77.028	157.375
-64.190	157.279
-19.257	157.039
0.000	157.192
5.638	157.143
10.815	157.126
12.180	156.836
13.713	155.649
14.978	154.274
17.546	153.644
18.629	153.624
19.367	153.400
19.800	153.275
20.392	153.026
21.842	152.880
23.503	152.577
24.860	152.260
26.410	152.561
27.271	152.570
28.540	152.389
29.498	152.652
30.586	152.877

Table 3.9 River Avon.

Y	Z
0.24	0.80
0.25	0.56
0.70	0.11
1.15	0.07

(Continued)

(Continued)

Table 3.10 (Continued).

Y	Z
31.840	152.959
33.570	153.098
35.269	152.878
36.428	152.972
36.429	153.275
36.429	153.646
36.431	154.556
36.695	154.589
37.722	155.329
37.955	156.485
38.432	156.529
39.069	157.168
67.870	157.452
76.076	158.986

Table 3.11 (Continued).

Y	Z
5.630	33.524
5.990	33.490
6.220	33.446
6.920	33.369
7.220	33.355
8.440	33.271
8.780	33.266
9.330	33.202
9.690	33.179
10.460	33.164
10.780	33.185
11.150	33.273
12.150	33.426
12.310	33.508
12.880	33.732
13.340	33.863
13.740	33.862
14.490	34.550
23.130	38.158
49.240	38.126

Table 3.11 River Main culvert.

Y	Z
-50.001	38.126
-50.000	36.642
-10.750	36.196
-8.310	35.599
0.000	35.046
0.750	33.584
0.900	33.583
1.340	33.570
1.820	33.551
2.160	33.543
2.510	33.553
2.870	33.547
3.350	33.553
3.790	33.548
4.220	33.577
4.700	33.552

Table 3.12 Trial culvert design – Section I (downstream).

Y	Z
-4.000	11.000
-3.000	10.750
-2.250	10.750
-0.750	9.250
0.750	9.250
2.250	10.750
3.000	10.750
4.000	11.000

(Continued)

Table 3.13 Trial culvert design – Section chainage, upstream to downstream.

Label	Distance (m)	Comment	Bed slope
4	0	Upstream	0.005
3	150	Culvert inlet	0.005
2	162	Culvert outlet	0.005
1	312	Downstream	0.005

References

- Abbot, M.B.: *Hydroinformatics*, Avebury Technical, Aldershot, (1991).
- Abbot, M.B. and Basco, D.R.: *Computational fluid dynamics: an introduction for engineers*, Longman Scientific & Technical, J. Wiley, (1989), pp. 1–425.
- Abril, J.B.: Numerical modelling of turbulent flow and sediment transport by the finite element method, *MPhil. Thesis, Department of Civil Engineering, The University of Birmingham*, England, (1995).
- Abril, J.B.: Numerical modelling of turbulent flow, sediment transport and flood routing by the finite element method, *PhD Thesis, Department of Civil Engineering, The University of Birmingham*, UK, (1997), pp. 1–334.
- Abril, J.B.: Updated RFMFEM finite element model based on the SKM for depth-averaged river flow simulation, *EPSRC Technical Report GR/R54880/01*, The University of Birmingham (2001).
- Abril, J.B. and Knight, D.W.: Sediment transport simulation of the Paute river using a depth-averaged flow model, *River Flow 2002, Proc. Int. Conf. on Fluvial Hydraulics*, Louvain-la-Neuve, Belgium, Sept., Vol. 2, Balkema, (2002), pp. 895–901.
- Abril, J.B. and Knight, D.W.: Stage-discharge prediction for rivers in flood applying a depth-averaged model, *Journal of Hydraulic Research*, IAHR, 42, No. 6, (2004), pp. 616–629.
- Ackers, P.: Resistance of fluids flowing in channel and pipes, *Hydraulics Research Paper 1*, HMSO, London, (1958), pp. 1–39.
- Ackers, P., White, W.R., Perkins, J.A. and Harrison, A.J.: *Weirs and flumes for flow measurement*, J. Wiley, (1978), pp. 1–327.
- Ackers, P.: Sediment transport: the Ackers and White theory revised, *Report SR 237, HR Wallingford*, UK, (1990).
- Ackers, P.: Hydraulic design of straight compound channels, *SR Report SR 281, HR Wallingford*, October, Vols. 1 & 2, (1991), pp. 1–131 & 1–139.
- Ackers, P.: 1992 Gerald Lacey Memorial Lecture – Canal and river regime in theory and practice: 1929–92, *Proc. Instn Civ. Engrs Wat., Marit. & Energy*, 96, Sept., Paper 10019, (1992a), pp. 167–178.
- Ackers, P.: Hydraulic design of two stage channels, *Proc. Instn Civ. Engrs Wat., Marit. & Energy*, 96, Dec., Paper 9988, (1992b), pp. 247–257.
- Ackers, P.: Stage-discharge functions for two-stage channels: The impact of new research, *Journal Instn Water & Environmental Management*, Vol. 7, No. 1, February, (1993a), pp. 52–61.

- Ackers, P.: Flow formulae for straight two-stage channels, *Journal of Hydraulic Research*, IAHR, Vol. 31, No. 4, (1993b), pp. 509–531.
- Ackers, P.: Sediment transport in open channels: Ackers and White update, *Proc. Instn. Civil Engineers, London, Water, Maritime & Energy*, 101 Water Board Technical Note 619, (1993c), pp. 247–249.
- Ackers, P. and White, W.R.: Sediment transport – new approach and analysis, *Proc. Hydraulic Eng. Div.*, ASCE, Vol. 99, No. 11, (1973), pp. 2041–2060.
- Al-Hamid, A.A.I.: Boundary shear stress and velocity distributions in differentially roughened trapezoidal channels, *PhD thesis*, The University of Birmingham, England, UK, (1991).
- Anastasiadou-Partheniou, L. and Samuels, P.G.: Automatic calibration of computational river models, *Proceedings of ICE Water and Maritime Engineering*, Vol. 130, Issue 3, September, (1998), pp. 154–162.
- Anderson, M.G., Walling, D.E.S. and Bates, P.D.: *Floodplain processes*, J. Wiley, (1996), pp. 1–658.
- Argawal, V.C., Garde, R.J. and Ranga Raju, K.G.: Resistance to flow and sediment transport in curved alluvial channels, *Fourth Congress, Asian and Pacific Division*, IAHR, Thailand, 11–13 September, (1984), pp. 207–218.
- Armitage, P.D. and Cannan, C.E.: Annual changes in the summer patterns of meso-habitat distribution and associated faunal assemblages. *Hydrological Processes*, 14, (2000), pp. 3161–3179.
- Ashworth, P.J., Bennett, S.J., Best, J.L. and McLelland, S.J.: *Coherent flow structures in open channels*, J. Wiley, (1996), pp. 1–733.
- Atabay, S.: Stage-discharge, resistance and sediment transport relationships for flow in straight compound channels, *PhD thesis*, Department of Civil Engineering, The University of Birmingham, (2001).
- Atabay, S.: Accuracy of the ISIS bridge methods for prediction of afflux at high flows, *Water and Environment Journal*, CIWEM, 22, No. 1, (2008), pp. 1–10.
- Atabay, S. and Knight, D.W.: Bridge afflux experiments in compound channels, *Report supplied to jba*, Department of Civil Engineering, The University of Birmingham (2002).
- Atabay, S., Knight, D.W. and Seckin, G.: Influence of a mobile bed on the boundary shear in a compound channel, *River Flow 2004*, Proc. 2nd Int. Conf. on Fluvial Hydraulics, 23–25 June, Napoli, Italy [Eds M. Greco, A. Carravetta & R.D. Morte], Vol. 1, (2004), pp. 337–345.
- Atabay, S., Knight, D.W. and Seckin, G.: Effects of overbank flow on fluvial sediment transport rates, *Water Management*, Proceedings of the Instn. of Civil Engineers, London, 158, WM1, March, (2005), pp. 25–34.
- Ayyoubzadeh, S.A.: Hydraulic aspects of straight-compound channel flow and bed load sediment transport, *PhD thesis*, Department of Civil Engineering, The University of Birmingham, (1997).
- Baatruo-Pedersen, A. and Riis, T.: Impacts of different weed cutting practices on macrophyte species diversity and composition in a Danish stream, *River Research Applications*, 20, (2004), pp. 103–114.
- Bagnold, R.A.: An approach to the sediment transport problem from general physics, Professional Paper 422-I, US Geological Survey, Washington, (1966).

- Baptist, M.J.: Modelling floodplain biogeomorphology, *PhD Thesis, Technical University, Delft*, (2005), pp. 1–195.
- Barnes, H.H.: Roughness characteristics of natural channels, *US Geological Survey, Water-Supply Paper 1849*, Washington D.C., (1967), pp. 1–214.
- Barr, D.I.H.: Two additional methods of direct solution of the Colebrook-White function, *Proc. Inst. of Civil Engineers*, Vol. 59, (1975), p. 827.
- Barr, D.I.H.: Osborne Reynolds' turbulent flow resistance formulae, *Proc. Institution of Civil Engineers, Part 2*, Vol. 67, (1979), pp. 743–750.
- Batchelor, G.K., Moffatt, H.K. and Worster, M.G.: *Perspectives in fluid dynamics: a collective introduction to current research*, Cambridge University Press, (2000), pp. 1–631.
- Bazin, H.: French translates to “A new formula for the calculation of discharge in open channels”, Memoire No. 41, *Annales des Ponts et Chaussees*, Vol. 14, No. 7, (1897), pp. 20–70.
- Bedient, P.B. and Huber, W.C.: *Hydrology and floodplain analysis*, Addison Wesley, Reading, Massachusetts, US, (1988), pp. 1–650.
- Benn, J.R. and Bonner, V.R.: Scoping study into hydraulic performance of bridges and other structures, including the effects of blockage, at high flows, *Report for the Environment Agency*, JBA, December, (2001).
- Benn, J.R., Mantz, P., Lamb, R., Riddell, J. and Nalluri, C.: Afflux at Bridges and Culverts: Review of current knowledge and practice, *Environment Agency R & D Technical Report W5A-061/TR1*, (2004), ISBN 1-844-32291-2, p. 111.
- Berz, G.: Flood disasters: lessons from the past – worries for the future, *Proc. Instn. of Civil Engineers, Water, Maritime and Energy Division*, London, Vol. 142, Issue 1, March, (2000), pp. 3–8.
- Bettess, R. and White, W.R.: Extremal hypotheses applied to river regime, In *Sediment transport in gravel bed rivers* [Eds C.R. Thorne, J.C. Bathurst & R.D. Hey], J. Wiley & Sons, (1987), pp. 767–789.
- Bettess, R.: Sediment transport and alluvial resistance in rivers, *Report by HR Wallingford to MAFF/EA*, MAFF/Defra project FD0112 and W5i 609, (2001).
- Beven, K.: A manifesto for the equifinality thesis, *Journal of Hydrology*, 320, (2006), pp. 18–36.
- Beven, K. and Freer, J.: Equifinality, data assimilation, and uncertainty estimation in mechanistic modelling of complex environmental systems using the GLUE methodology, *Journal of Hydrology*, 249, (2001), pp. 11–29.
- Biery, P.F. and Delleur, J.W.: Hydraulics of single span arch bridge constrictions, *Journal of the Hydraulics Division*, American Society of Civil Engineers, New York, February, Vol. 88, No. 2, March, (1962), pp. 75–108.
- Biglari, B. and Sturm, T.W.: Numerical modeling of flow around bridge abutments in compound channel, *Journal of Hydraulic Engineering*, American Society of Civil Engineers, New York, February, Vol. 124, No. 2, (1998), pp. 156–164.
- Blalock, M.E. and Sturm, T.W.: Minimum specific energy in compound open channel flow, *Journal of the Hydraulics Division*, ASCE, Vol. 107, No. HY6, (1981), pp. 699–717.
- Blasius, P.R.H.: Das Aehnlichkeitgesetz bei Reibungsvorgangen [In *Flüssigkeiten, Forschungsheft 131*], Vereins Deutscher Ingenieure, Berlin, (1913), pp. 1–41.

- Blench, T.: *Mobile bed fluviology*, University of Alberta Press, (1969), pp. 1–222.
- Bos, M.G., Replogle, J.A. and Clemmens, A.J.: *Flow measuring flumes for open channels*, J. Wiley, (1984), pp. 1–321.
- Bousmar, D.: Flow modelling in compound channels: momentum transfer between main channel and prismatic and non-prismatic floodplains, *PhD Thesis, Universite Catholique de Louvain*, (2002).
- Bousmar, D. and Zech, Y.: Momentum transfer for practical flow computation in compound channels, *Journal of Hydraulic Engineering*, ASCE, Vol. 125, No. 7, July, (1999), pp. 696–706.
- Bousmar, D. and Zech, Y.: Velocity distribution in non-prismatic compound channels, *Proc. ICE, Water Management*, Vol. 157, (2004), pp. 99–108.
- Bousmar, D., Wilkin, N., Jacquemart, J.H. and Zech, Y.: Overbank flow in symmetrically narrowing floodplains, *Journal of Hydraulic Engineering*, ASCE, Vol. 130, No. 4, April, (2004), pp. 305–312.
- Bradley, J.N.: Hydraulics of bridge waterways, *Hydraulic Design Series, Edition 2*, Department of Transport, Federal Highway Administration, Washington, D.C., (1978).
- Bronstert, A.: Overview of current perspectives on climate change, [Chapter 3](#) in *River Basin Modelling for Flood Risk Mitigation* [Eds D.W. Knight & A.Y. Shamseldin], Taylor & Francis, (2006a), pp. 59–75.
- Bronstert, A.: The effects of climate change on flooding, [Chapter 4](#) in *River Basin Modelling for Flood Risk Mitigation* [Eds D.W. Knight & A.Y. Shamseldin], Taylor & Francis, (2006b), pp. 77–791.
- Brown, F.A.: Sediment transport in river channels at high stage, *PhD thesis, Department of Civil Engineering, The University of Birmingham*, (1997).
- Brown, P.M.: Afflux at British bridges, *Report No. 60*, HR Wallingford, October, (1985).
- Brown, P.M.: Afflux at arch bridges, *Report No. 182*, HR Wallingford, December, (1988).
- Brundrett, E. and Baines, W.D.: The production and diffusion of vorticity in duct flow, *Jnl. Fluid Mech.*, Vol. 19, (1964), pp. 375–394.
- Buisson, R.S.K., Wade P.M., Cathcart, R.L., Hemmings, S.M., Manning, C.J. and Mayer, L.: *The Drainage Channel Biodiversity Manual: Integrating Wildlife and Flood Risk Management*, Association of Drainage Authorities and Natural England, Peterborough, (2008), pp. 1–189.
- Burnham, M.W. and Davis, D.W.: Effects of data errors on computed steady-flow, *Journal of Hydraulic Engineering*, ASCE, 116(7), (1990), pp. 914–929.
- Cao, S.: Regime theory and a geometric model for stable alluvial channels, *PhD thesis, Department of Civil Engineering, The University of Birmingham*, (1995).
- Cao, S. and Knight, D.W.: Regime theory of alluvial channels based upon the concepts of stream power and probability, *Proc. Instn. of Civil Engineers, Water, Maritime and Energy Division*, London, Vol. 118, Sept., (1996), pp. 160–167.
- Cao, S. and Knight, D.W.: Design for hydraulic geometry of alluvial channels, *Journal of Hydraulic Engineering*, ASCE, Vol. 124, No. 5, May, (1998), pp. 484–492.
- CAPM: Aquatic Weed Control Operation – Best Practice Guidelines, *Centre for Aquatic Plant Management Report W111*, (1997).

- Casellarin, A., di Baldassarre, G., Bates, P.D. and Brath, A.: Optimal cross-sectional spacing in Preissmann scheme 1-D hydrodynamic models, *Journal of Hydraulic Engineering*, ASCE, Vol. 135, February, (2009), pp. 96–105.
- Cebeci, T. and Bradshaw, P.: *Momentum transfer in boundary layers*, Hemisphere Publishing Co. McGraw-Hill, (1977), pp. 1–407.
- Chadwick, A., Morfett, J. and Borthwick, M.: *Hydraulics in Civil and Environmental Engineering*, Spon Press, Taylor & Francis Group, (2004), pp. 1–644.
- Chang, H.H.: Energy expenditure in curved open channels, *Journal of Hydraulic Engineering*, ASCE, Vol. 109, No. 7, (1983), pp. 1012–1022.
- Chang, H.H.: Regular meander path model, *Journal of Hydraulic Engineering*, ASCE, Vol. 110, No. 10, October, (1984), pp. 1398–1411.
- Chang, H.H.: *Fluvial processes in river engineering*, J. Wiley, (1988).
- Chanson, H.: *The Hydraulics of Open Channel Flow: An Introduction*, Arnold, (1999), pp. 1–495.
- Charbeneau, R.J., Henderson, A.D. and Sherman, L.C.: Hydraulic Performance Curves for Highway Culverts, *Journal of Hydraulic Engineering*, ASCE, 132(5), (2006), pp. 474–481.
- Chezy, A., 1768: See ‘Antoine Chezy, histoire d'une formule d'hydraulique’ by G. Mouret, *Annales des Ponts et Chaussees*, Vol. II, (1921) and ‘On the origin of the Chezy formula’ by C. Herschel, *Journal Association of Engineering Societies*, Vol. 18, (1768), pp. 363–368.
- Chlebek, J.: Modelling of simple prismatic channels with varying roughness using the SKM and a study of flows in smooth non-prismatic channels with skewed floodplains, *PhD thesis, Department of Civil Engineering, The University of Birmingham*, UK, (2009), pp. 1–527.
- Chlebek, J. and Knight, D.W.: A new perspective on sidewall correction procedures, based on SKM modelling, *RiverFlow 2006*, September, Lisbon, Portugal, Vol. 1, [Eds Ferreira, Alves, Leal & Cardoso], Taylor & Francis, (2006), pp. 135–144.
- Chlebek, J. and Knight, D.W.: Observations on flow in channels with skewed floodplains, *RiverFlow 2008*, [Eds M.S. Altinakar, M.A. Kokpinar, I. Aydin, S. Cokgar & S. Kirkgoz], Cesme, Turkey, Vol. 1, (2008), pp. 519–527.
- Chow, V.T.: *Open Channel Hydraulics*, McGraw-Hill, (1959), pp. 1–680.
- CIRIA: *Culvert design guide*, [Eds Ramsbottom, D., Day, R. and Rickard, C.], *Construction and Industry Research and Information Association, Report 168*, London, (1997), pp. 1–189.
- CIWEM: River Engineering – Part II, Structures and Coastal Defence Works, *Water Practice Manual 8*, [Ed T.W. Brandon], the Chartered Institution of Water and Environmental Management, London, (1989), pp. 1–332.
- Colebrook, C.F.: Turbulent flow in pipes, with particular reference to the transition region between the smooth and rough pipe laws, *Journal of the Institution of Civil Engineers*, 11, (1939), pp. 133–156.
- Colebrook, C.F. and White, C.M.: Experiments with fluid friction in roughened pipes, *Proc. Roy. Soc., A*, Vol. 161, (1937), pp. 367–381.
- Colson, B.E., Ming, C.O. and Arcement, G.J.: Backwater at bridges and densely wooded flood plains, Bogue Chitto near Johnston Station, Mississippi, *USGS Hydrologic Atlas Series No. 591*, (1978).

- Cowan, W.L.: Estimating hydraulic roughness coefficients, *Journal of Agricultural Engineering*, Vol. 37, (1956), pp. 473–475.
- Cunge, J.A.: On the subject of a flood propagation computation method (Muskingum method), *Journal of Hydraulic Research*, IAHR, Vol. 7, No. 2, (1969), pp. 205–230.
- Cunge, J.A., Holly, F.M. and Verwey, A.: *Practical aspects of computational river hydraulics*, Pitman Publishing Ltd, 1–420 (reprints available from Institute of Hydraulic Research, The University of Iowa, IA 52242-1585, US, (1980), pp. 1–420.
- Darby, S. (lead writer), Alonso, C., Bettess, R., Borah, D., Diplas, P., Julien, P., Knight, D.W., Li, L., Pizzuto, P., Quick, M., Simon, A., Stevens, M., Thorne, C.R. and Wang, S.: River width adjustment. Part II: Modelling, *Journal of Hydraulic Engineering*, ASCE, Task Committee on Hydraulics, Bank Mechanics and the Modelling of River Width Adjustment, Sept., 124(9), (1998), pp. 903–917.
- Darcy, H.: Sur des recherches expérimentales relatives au mouvement des eaux dans les tuyaux, *Comptes rendus des séances de l'Academie des Sciences, Mallet-Bachelier*, Paris, (1857), pp. 1–268 [and atlas “Experimental Research Relating to the Movement of Water in Pipes”].
- Davies, A.J.: *The finite element methods – a first approach*, Clarendon Press, Oxford, (1980).
- Dawson, F.H.: The seasonal effects of aquatic plant growth on the flow of water in a stream, European Weed Research Society, EWRS 5th Symposium on Aquatic Weeds, Amsterdam, (1978), pp. 71–78.
- de Bruijn, K.M., Klijn, F., Mc Gahey, C., Mens, M.P.J. and Wolfert, H.: Long-term strategies for flood risk management, Scenario definition and strategic alternative design, *FLOODsite report T14-08-01*, Delft Hydraulics, Delft, the Netherlands, (2008).
- Defalque, A., Wark, J.B. and Walmsley, N.: Data density in 1-D river model, *Report SR 353, HR Wallingford*, March, (1993), pp. 1–78.
- Defra/EA: Reducing uncertainty in river flood conveyance: scoping study, R & D Technical Report, prepared by Evans, E.P., Pender, G., Samuels, P.G. and Escarameia, M. for the Environment Agency Project W5A-057, HR Wallingford, UK, (2001), pp. 1–127.
- Defra/EA: Risk, Performance and Uncertainty in Flood and Coastal Defence: A Review, *R & D Report FD2302/TR1, Environment Agency R & D Dissemination Centre*, c/o WRc, Swindon, SN5 8YF, (2002), pp. 1–124.
- Defra/EA: Reducing uncertainty in river flood conveyance, Interim Report 2: Review of Methods for Estimating Conveyance, Project W5A-057, prepared by HR Wallingford for the Environment Agency, UK, (2003a), pp. 1–88.
- Defra/EA: Reducing uncertainty in river flood conveyance, Roughness Review, Project W5A-057, prepared by HR Wallingford for the Environment Agency, UK, (2003b), pp. 1–218.
- Defra/EA: The investigation and specification of flow measurement structure design features that aid the migration of fish without significantly compromising flow measurement accuracy, with the potential to influence the production of suitable British Standards, R & D Technical Report to EA prepared by HRW, Project W6-084, Environment Agency, UK, (2003c).

- Defra/EA: Reducing uncertainty in river flood conveyance, Interim Report 3: Testing of Conveyance Methods in 1D River Models, Project W5A-057, prepared by HR Wallingford for the *Environment Agency*, UK, (2004a), pp. 1–237.
- Defra/EA: Reducing uncertainty in river flood conveyance, Conveyance Manual, Project W5A-057, prepared by HR Wallingford for the *Environment Agency*, UK, (2004b), pp. 1–115.
- Defra/EA: Recommendations for maintaining the scientific relevance of the Conveyance and Afflux Estimation System, prepared by HR Wallingford (C. Mc Gahey & P. Samuels) for *Environment Agency*, R & D Project SC070032, April, (2009), pp. 1–115.
- Diehl, T.H.: Potential Drift Accumulation at Bridges, *US Department of Transportation*, Federal Highway Administration Research and Development, Turner-Fairbank Highway Research Center, Virginia, Publication No. FHWA-RD-97-028, (1997).
- Drazin, P.G. and Riley, N.: *The Navier-Stokes equations: a classification of flows and exact solutions*, London Mathematical Society, Lecture Note Series, 334, Cambridge University Press, (2006), pp. 1–196.
- Du Boys, P.F.D.: Le Rhone et le rivier a lit affouillable, *Annales des Ponts et Chausses*, Vol. 18, No. 5, (1879).
- EA: Environmental options specifications for flood maintenance, *Environment Agency* Report, March, (1997), pp. 1–40.
- EA: Environmental Guidelines for Vegetation Management in Channel and on Banks, *Environment Agency*, Technical Report W135, (1998a).
- EA: Management of vegetation on raised embankments, *Environment Agency*, Technical Report W133, (1998b).
- EA: *Scoping Study for Reducing Uncertainty in River Flood Conveyance*, (Available from Environment Agency R&D Dissemination Centre, WRc, Frankland Road, Swindon, Wilts SN5 8YF), (2001).
- EA: Environmental options for flood defence maintenance works, *Environment Agency* Report, Peterborough, November, (2003), pp. 1–46.
- EA: River Habitat Survey in Britain and Wales – Field Survey Guidance Manual, published by the *Environment Agency*, (2003), pp. 1.1–5.13.
- EA: *Hydraulic Performance of River Bridges and Other Structures at High Flows*, Phase 1 Scoping Report, R & D Project: W5A-065, Environment Agency, Rio House, Waterside Drive, Aztec West, Almondsbury, Bristol BS32 4UD, (2004).
- EA: Environment Agency's Hi-Flows site, Retrieved 5 September 2005 from the World Wide Web: <http://www.environment-agency.gov.uk/hiflowsuk/>, (2005).
- Einstein, H.A.: Formulas for the transportation of bedload, *Trans. of ASCE*, Vol. 107, (1942), pp. 561–577.
- Einstein, H.A.: Der Hydraulische oder Profil-Radius, *Schweizerische Bauzeitung*, Zurich, 103, (1934), pp. 89–91.
- Einstein, H.A. and Banks, R.B.: Fluid resistance of composite roughness, *Trans. American Geophysical Union*, Vol. 31, No. 4, (1950), pp. 603–610.
- Einstein, H.A. and Li, H.: Secondary currents in straight channels, *Trans. American Geophysical Union*, Vol. 39, (1958), pp. 1085–1088.
- Elder, J.W.: The dispersion of marked fluid in a turbulent shear flow, *Journal Fluid Mechanics*, Vol. 5, No. 4, (1959), pp. 544–560.

- Elliott, S.C.A. and Sellin, R.H.J.: SERC Flood Channel facility: skewed flow experiments, *Journal of Hydraulic Research*, IAHR, Vol. 28, No. 2, (1990), pp. 197–214.
- Engelund, F. and Hansen, H.: Investigations of Flow in Alluvial Streams, *Journal of Hydraulics Division*, Vol. 92, HY2, (1966), pp. 315–326.
- Ervine, D.A., Babaeyan-Koopaei, K. and Sellin, R.H.J.: Two-dimensional solution for straight and meandering overbank flows, *Journal of Hydraulic Engineering*, ASCE, Vol. 126, No. 9, September, (2000), pp. 653–669.
- Ervine, D.A. and Baird, J.I.: Rating curves for rivers with overbank flows, *Proc. ICE Part 2: Research and Development*, Vol. 73, June, (1982), pp. 465–472.
- Ervine, D.A. and Ellis, J.: Experimental and computational aspects of overbank floodplain flow, *Trans. of the Royal Society of Edinburgh: Earth Sciences*, Vol. 78, (1987), pp. 315–475.
- Escarameia, M., May, R.W.P., Jiming, M. and Hollinrake, P.G.: Performance of sluice gates for free and submerged flows, *Draft Report SR 344*, unpublished, March, HR Wallingford, (1993).
- European Commission: Directive 2000/60/EC of the European Parliament and of the Council, *Establishing a framework for Community action in the field of water policy*, published in the Official Journal of the European Union, L 327, 22 December, (2000), pp. 1–73.
- European Commission: Directive 2007/60/EC of the European Parliament and of the Council, *On the assessment and management of flood risks*, published in the Official Journal of the European Union, L 288/27, 6 November, (2007).
- Evans, E.M., Ashley, R., Hall, J., Penning-Rowsell, E., Saul, A., Sayers, P., Thorne, C. and Watkinson, A. Foresight. Future flooding. *Scientific Summary: Vol. I – Future risks and their drivers*, Office of Science and Technology, London, UK (2004).
- Extence, C.A. and Balbi, D.M.: River flow indexing using British Benthic macro-invertebrates: a framework for setting hydroecological objectives, *Regulated Rivers: Research and Management*, Vol. 15, (1999), pp. 543–574.
- FEH: *Flood Estimation Handbook*, Vols. 1–5, Centre for Ecology and Hydrology, Wallingford, Oxon, UK, [ISBN 0-948540-94], (1995).
- FHWA: *Hydraulic design of highway culverts*, US Department of Transportation, Federal Highway Administration, Washington D.C., (2001).
- Fisher, K.: Handbook for assessment of hydraulic performance of environmental channels, Report SR 490, HR Wallingford, UK, (2001), pp. 1–180.
- Fleming, G.: *Flood risk management*, Thomas Telford, London, (2002), pp. 1–250.
- Franke, P.G. and Valetin, F.: The determination of discharge below gates in case of variable tailwater conditions, *Journal of Hydraulic Research* Vol. 7, No. 4, (1969), pp. 433–447.
- Fukuoka, S.: *Floodplain risk management*, Balkema, (1998), pp. 1–357.
- Fukuoka, S. and Fujita, K.: Prediction of flow resistance in compound channels and its application to design of river courses, *Jnl. Hydr., Coast. and Envir. Eng.*, JSCE, Vol. 411, No. 12, (1989), pp. 63–72 (in Japanese).
- Ganguillet, E. and Kutter, W.R.: Versuch zur augstellung einer neuen allgemeinen furmel für die gleichformige bewegung des wassers in canalen und flussen, *Zeitschrift des Österreichischen Ingenieur – und Architecten-Vereines* 21, (1), 6–25 and (2), (1869), pp. 46–59. Translated into English by: Hering, R. and Trautwine, J.C. (1888 and 1891). *A General Formula for the Uniform Flow of Water in Rivers and Other Channels*, New York, NY: J. Wiley & Sons.

- Garcia-Navarro, P. and Playan, E.: *Numerical Modelling of Hydrodynamics for Water Resources*, Taylor & Francis (2007), pp. 1–389.
- Garde, R.J. and Ranga-Raju, K.G.: *Mechanics of sediment transportation and alluvial stream problems*, Wiley Eastern Ltd, (1977), pp. 1–483.
- Garton, J.E. and Green, J.E.P.: Vegetation lined channel design procedures, *Transaction ASAE*, Vol. 26, No. 2, (1983), pp. 436–439.
- Gibson, A.H.: *Hydraulics and its applications*, Constable and Company, London, (1908), pp. 1–813.
- Gibson, A.H.: On the depression of the filament of the maximum velocity in a stream flowing through an open channel, *Proc. Royal Society of London, Series a*, Vol. 82, (1909), pp. 149–159.
- Gordon, N.D., Mc Mahon, M.D. and Finlayson, B.L.: *Stream hydrology: an introduction for ecologists*, J. Wiley and Sons, Chichester, (1992).
- Gouldby, B.P. and Kingston, G.: Uncertainty and sensitivity method for flood risk analysis, *FLOODsite research report*, HR Wallingford, (2007).
- Gouldby, B.P. and Samuels P.G.: Language of risk, project definitions. *FLOODsite report T32-04-01*, (2005, updated 2009), pp. 1–56.
- Graf, W.H.: *Hydraulics of Sediment Transport*, McGraw-Hill, New York, (1971), pp. 1–513.
- Grass, A.J., Stuart, R.J. and Mansour-Tehrani, M.: Vortical structures and coherent motion in turbulent flow over smooth and rough boundaries, *Trans. Physical Sciences and Eng.*, Vol. 336, No. 1640, Turbulent flow structure near walls, Part 1, (1991), pp. 35–65.
- Green, M., Dale, M., Gebre, H. and Knight, D.W.: The impact of climate change on the threshold of flooding for an urban UK river, *Defra/EA Annual Conference on River Engineering*, Telford, (2009) (in press).
- Greenhill, R.: An Investigation into compound meandering channel flow, *PhD Thesis, Department of Civil Engineering, University of Bristol*, UK, (1992).
- Guan, Y., Altinakar, M.S. and Krishnappan, B.G.: Modelling of lateral flow distribution in compound channels, *Proceedings River Flow 2002*, compiled by Y. Zech & D. Bousmar, Louvain, Belgium, Vol. 1, (2002), pp. 169–175.
- Haderlie, G.M. and Tullis, B.P.: Hydraulics of Multi-barrel culverts under Inlet Control. *J. Irrigation and Drainage Eng.*, ASCE, 134(4), (2008), pp. 507–514.
- Hall, J. and Solomatine, D.: A framework for uncertainty analysis in flood risk management decisions, *Int. Journal of River Basin Management*, Vol. 6, No. 2, (2008), pp. 85–98.
- Hall, J., Harvey, H., Solomatine, D. and Lal Shrestha, D.: Development of framework for the influence and impact of uncertainty, *FLOODsite Task 20 Report T20-08-04*, (2008), available at: www.floodsite.net, pp. 1–168.
- Hamill, L.: Improved flow through bridge waterways by entrance rounding, *Proc. Instn Civil Engrs Mun. Engineering*, 121, March, (1997), pp. 7–21.
- Hamill, L.: *Bridge hydraulics*, Spon, (1999), pp. 1–367.
- Hearne, J., Johnson, I. and Armitage, P.: Determination of ecologically acceptable flows in rivers with seasonal changes in the density of macrophyte. *Regulated Rivers – Research & Management*, 9, (1994), pp. 117–184.
- HEC: Flow transitions in bridge backwater analysis, River Analysis System, Research Document 42, *US Army Corps of Engineers*, Hydrologic Eng. Center, Davis, (1995), pp. 1–67.

- HEC: Bridge hydraulic analysis with HEC-RAS, Technical Paper 151, *US Army Corps of Engineers*, Hydrologic Eng. Center, Davis, (1996), pp. 1–17.
- HEC: *River Analysis System, Version 3.1.2*, US Army Corps of Engineers Hydrologic Engineering Center, Davis, CA, US, (2004).
- HEC-RAS: River Analysis System, User's Manual, Version 4, *US Army Corps of Engineers*, Hydrologic Eng. Center, Davis, March, (2008), pp. 1–747, available at: <http://www.hec.usace.army.mil/software/hec-ras/hecras-document.html>.
- Henderson, F.M.: *Open Channel Flow*, Macmillan, (1966), pp. 1–522.
- Hicks, D.M. and Mason, P.D.: Roughness characteristics of New Zealand Rivers, *National Institute of Water & Atmospheric Research Ltd*, September, (1998), pp. 1–329.
- Hine, D. and Hall, J.W.: Analysing the robustness of engineering decisions to hydraulic model and hydrological uncertainties, in Harmonising the Demands of Art and Nature in Hydraulics: *Proc. 32nd Congress of IAHR, Venice*, 1–6 July (2007).
- Hinze, J.O.: Experimental investigation on secondary currents in turbulent flow through a straight conduit, *Applied Science Research*, Vol. 28, (1973), pp. 453–465.
- Hoffmans, G.J.C.M. and Verheij, H.J.: *Scour Manual*, A.A. Balkema, Rotterdam, (1997).
- Horton, R.E.: Separate roughness coefficients for channel bottoms and sides, *Engineering News-Rec.*, 111, (1933), pp. 652–653.
- Hotchkiss, R.H., Thiele, E.A., Nelson J. and Thompson, P.L.: Culvert Hydraulics: Comparison of current computer models and recommended improvements, Transportation Research Record: *Journal of the Transportation Research Board*, No. 2060, (2008), pp. 141–149.
- Huthoff, F., Roos, P.C., Augustijn, D.C.M. and Hulscher, S.J.M.H.: Interacting divided channel method for compound channel flow, *Journal of Hydraulic Engineering*, American Society of Civil Engineers, New York, August, Vol. 134, No. 8, (2008), pp. 1158–1165.
- ICE: *Learning to live with rivers*, Final report of the Institution of Civil Engineers' Presidential Commission to review the technical aspects of flood risk management in England and Wales, [by Fleming, G., Frost, L., Huntingdon, S., Knight, D.W., Law, F.M. & Rickard, C.], November, (2001), pp. 1–83.
- Ikeda, S.: Self-formed straight channels in sandy beds, *Journal of Hydraulics Division*, ASCE, Vol. 107, No. 4, (1981), pp. 389–406.
- Ikeda, S.: Role of lateral eddies in sediment transport and channel formation, *Proc. Seventh Intl. Symposium on River Sedimentation*, [Eds A.W. Jayawardena, Lee, J.H.W. & Wang, Z.Y.] Hong Kong, December 1998, Balkema, (1999), pp. 195–203.
- Ikeda, S., Kawamura, K., Toda, Y. and Kasuya, I.: Quasi-three dimensional computation and laboratory tests on flow in curved open channels, *Proc. of River Flow 2002*, Editors Bousmar & Zech, Balkema, Louvain La-Neuve, Belgium, Vol. 1, (2002), pp. 233–245.
- Ikeda, S. and Kuga, T.: Laboratory study on large horizontal vortices in compound open channel flow, *Annual Jnl. of hydraulic Eng.*, JSCE, Vol. 45, (1997), pp. 493–498.

- Ikeda, S. and McEwan, I.K.: *Flow and sediment transport in compound channels: the experiences of Japanese and UK research*, IAHR Monograph Series, International Association of Hydraulic Engineering Research, Madrid, Spain, (2009), pp. 1–333.
- Imamoto, H. and Ishigaki, T.: Secondary flow in compound open channel flow, *Proc. HydroComp 89*, Dubrovnik, Yugoslavia, 13–16th June, (1989), pp. 235–243.
- Infoworks RS V5.7: Online Help Manual, InfoWorks RS software, Copyright Wallingford Software, (2004).
- IPCC: *Intergovernmental Panel on Climate Change, Climate Change 2001, Impacts, Adaptation and Vulnerability*, Cambridge University Press, (2001).
- ISIS V2.3: Online help manual, <http://www.wallingfordsoftware.com/products/isis/>, HR Wallingford/Halcrow, (2004).
- ISO: *Measurement of liquid flow in open channels. Part 1: Establishment and operation of a gauging station*, ISO 1100-1, International Standards Organization, Geneva, Switzerland, (1996), pp. 1–20.
- ISO: *Measurement of liquid flow in open channels. Part 2: Determination of the stage-discharge relation*, ISO 1100-2, International Standards Organization, Geneva, Switzerland, (1998), pp. 1–25.
- ISO: *Liquid flow measurement in open channels – Round-nose horizontal broad-crested weirs*, ISO 4374, International Standards Organization, Geneva, Switzerland, (1990), pp. 1–18.
- ISO: *Hydrometric determinations – Flow measurement in open channels using structures – Flat-V weirs*, ISO 4377, International Standards Organization, Geneva, Switzerland, (2002), pp. 1–35.
- ISO: *Hydrometry Open channel flow measurement using thin-plate weirs*, ISO 1438, International Standards Organization, Geneva, Switzerland, (2008), pp. 1–59.
- James, C.S.: Evaluation of methods for predicting bend loss in meandering channels, *Journal of Hydraulic Research*, ASCE, Vol. 120, No. 2, February, (1994), pp. 245–253.
- James, C.S. and Wark, J.B.: Conveyance estimation for meandering channels, Report SR329, HR Wallingford, UK, (1992), pp. 1–91.
- Janes, M., Fisher, K., Mant, J. and de Smith, L.: River Rehabilitation Guidance for Eastern England Rivers, prepared by *The River Restoration Centre* for the EA, November, (2005).
- Kaatz, K.J. and James, W.P.: Analysis of alternatives for computing backwater at bridges, *Journal of Hydraulic Engineering*, American Society of Civil Engineers, New York, April, Vol. 123, No. 9, (1997), pp. 784–792.
- Karcz, I.: Secondary currents and the configuration of a natural stream bed, *Journal of Geophysical Research*, Vol. 71, (1966), pp. 3109–3116.
- Kells, J.A.: Hydraulic performance of damaged-end corrugated steel pipe culverts, Canadian *Journal of Civil Engineering*, 35, (2008), pp. 918–924.
- Keulegan, G.H.: Laws of turbulent flow in open channels, *Journal National Bureau of Standards*, Washington, D.C., Research Paper 1151, Vol. 21, (1938), pp. 707–741.

- Khatibi, R.H., Williams, J.R. and Wormleaton, P.R.: Identification problem of open-channel friction factors, *Journal of Hydraulic Engineering*, American Society of Civil Engineers, New York, December, Vol. 123, No. 12, (1997), pp. 1078–1088.
- Kindsvater, C.E. and Carter, R.W.: Tranquil flow through open-channel constrictions, *Transactions of the American Society of Civil Engineers*, New York, 120, (1955), pp. 955–992.
- Kindsvater, C.E., Carter, R.W. and Tracy, H.J.: Computation of peak discharge through constrictions, *Circular 284, US Geological Survey*, Washington D.C., (1953).
- Kitagawa, A.: Past and recent developments of flood control in the Tone River, [In *Floodplain Risk Management*, S. Fukuoka (Ed)], Balkema, (1998), pp. 61–74.
- Kline, S.J., Reynolds, W.C., Schraub, F.A. and Runstadler P.W.: The structure of turbulence in boundary layers, *Journal of Fluid Mechanics*, Vol. 30, (1967), pp. 741–773.
- Knight, D.W.: Some field measurements concerned with the behaviour of resistance coefficients in a tidal channel, *Estuarine, Coastal and Shelf Science*, Academic Press, London, No. 12, (1981), pp. 303–322.
- Knight, D.W.: Issues and directions in river mechanics – closure of sessions 2, 3 and 5, In '*Issues and directions in hydraulics*', [Ed T. Nakato & R. Ettema], An Iowa Hydraulics Colloquium in honour of Professor John F Kennedy, Iowa Institute of Hydraulic Research, Iowa, US, Balkema, (1996), pp. 435–462.
- Knight, D.W.: Flow and sediment transport in two-stage channels, *Proc. 2nd IAHR Symposium on River, Coastal and Estuarine Morphodynamics*, RCEM2001, Japan, (2001), pp. 1–20.
- Knight, D.W.: Introduction to flooding and river basin modelling, [Chapter 1](#) in *River Basin Modelling for Flood Risk Mitigation* [Eds D.W. Knight & A.Y. Shamseldin], Taylor & Francis, (2006a), pp. 1–19.
- Knight, D.W.: River flood hydraulics: theoretical issues and stage-discharge relationships, Chapter 17 in *River Basin Modelling for Flood Risk Mitigation* [Eds D.W. Knight & A.Y. Shamseldin], Taylor & Francis, (2006b), pp. 301–334.
- Knight, D.W.: River flood hydraulics: calibration issues in one-dimensional flood routing models, Chapter 18, in *River Basin Modelling for Flood Risk Mitigation* [Eds D.W. Knight & A.Y. Shamseldin], Taylor & Francis, (2006c), pp. 335–385.
- Knight, D.W.: Modelling overbank flows in rivers – data, concepts, models and calibration, [Chapter 1](#) in *Numerical Modelling of Hydrodynamics for Water Resources* [Eds P. Garcia-Navarro & E. Playan], Taylor & Francis, (2008a), pp. 3–23.
- Knight, D.W.: A review of some laboratory and field data for checking models of rivers with inbank and overbank flows, *Advances in Hydro-Science and Engineering*, Vol. VIII, *Proc. 8th International Conference on Hydro-science and Engineering*, ICHE, [Eds S.S.Y. Wang, M. Kawahara, K.P. Holtz, T. Tsujimoto & Y. Toda], Nagoya, Japan, Sept., Abstract book pp. 201–202 and full paper in CD pp. 812–821, (2008b).
- Knight, D.W. and Abril, B.: Refined calibration of a depth-averaged model for turbulent flow in a compound channel, *Proc. Instn. of Civil Engineers, Water, Maritime and Energy Division*, London, Vol. 118, Issue 3, Sept., Paper 11017, (1996), pp. 151–159.

- Knight, D.W. and Brown, F.A.: Resistance studies of overbank flow in rivers with sediment using the Flood Channel Facility, *Journal of Hydraulic Research*, IAHR, Vol. 39, No. 3, (2001), pp. 283–301.
- Knight, D.W. and Demetriou, J.D.: Flood plain and main channel flow interaction, *Journal of Hydraulic Engineering*, ASCE, Vol. 109, No. 8, August, (1983), pp. 1073–1092.
- Knight, D.W., Demetriou, J.D. and Hamed, M.E.: Boundary shear in smooth rectangular channels, *Journal of Hydraulic Engineering*, ASCE, Vol. 110, No. 4, April, (1984), pp. 405–422.
- Knight, D.W. and Macdonald, J.A.: Open channel flow with varying bed roughness, *Journal of the Hydraulics Division*, ASCE, Vol. 105, No. HY9, Proc. Paper 14839, Sept., (1979), pp. 1267–1183.
- Knight, D.W. and Samuels, P.G.: Localised flow modelling of bridges, sluices and hydraulic structures under flood flow conditions, *Proc. 34th MAFF Conference of River and Coastal Engineers*, Keele University, June, (1999), pp. 1.2.1–1.2.13.
- Knight, D.W. and Samuels, P.G.: Examples of recent floods in Europe, *Journal of Disaster Research*, Fuji Technology Press, Tokyo, Japan, Vol. 2, No. 3, (2007), pp. 190–199.
- Knight, D.W. and Sellin, R.H.J.: The SERC Flood Channel Facility, *Journal of the Institution of Water and Environmental Management*, Vol. 1, No. 2, October, (1987), pp. 198–204.
- Knight, D.W. and Shamseldin, A.: *River Basin Modelling for Flood Risk Mitigation* [Eds D.W. Knight & A.Y. Shamseldin], Taylor & Francis, (2006), pp. 1–607.
- Knight, D.W. and Shiono, K.: Turbulence measurements in a shear layer region of a compound channel, *Journal of Hydraulic Research*, IAHR, Vol. 28, No. 2, 175–196, (Discussion in IAHR Journal, 1991, Vol. 29, No. 2, (1990), pp. 259–276).
- Knight, D.W. and Shiono, K.: River channel and floodplain hydraulics, in *Floodplain Processes*, (Eds Anderson, Walling & Bates), [Chapter 5](#), J. Wiley, (1996), pp. 139–181.
- Knight, D.W. and Tang, X.: Zonal discharges and boundary shear in prismatic channels, *Journal of Engineering and Computational Mechanics*, Proceedings of the Instn. of Civil Engineers, London, Vol. 161, EM2, June, (2008), pp. 59–68.
- Knight, D.W. and Yu, G.: A geometric model for self formed channels in uniform sand, *26th IAHR Congress*, London, International Association for Hydraulic Research, September, HYDRA 2000, Vol. 1, Thomas Telford, (1995), pp. 354–359.
- Knight, D.W., Al-Hamid, A.A.I. and Yuen, K.W.H.: Boundary shear in differentially roughened trapezoidal channels, In *Hydraulic and Environmental Modelling: Estuarine and River Waters* (Eds R.A. Falconer, K. Shiono & R.G.S. Matthew), Ashgate Press, (1992), pp. 3–14.
- Knight, D.W., Omran, M. and Abril, J.B.: Boundary conditions between panels in depth-averaged flow models revisited, *Proceedings of the 2nd International Conference on Fluvial Hydraulics: River Flow 2004*, Naples, 24–26 June, Vol. 1, (2004), pp. 371–380.
- Knight, D.W., Omran, M. and Tang, X.: Modelling depth-averaged velocity and boundary shear in trapezoidal channels with secondary flows, *Journal of Hydraulic Engineering*, February, ASCE, Vol. 133, No. 1, January, (2007), pp. 39–47.

- Knight, D.W., Shiono, K. and Pirt, J.: Prediction of depth mean velocity and discharge in natural rivers with overbank flow, *Proc. Int. Conf. on Hydraulic and Environmental Modelling of Coastal, Estuarine and River Waters*, (Eds R.A. Falconer, P. Goodwin, R.G.S. Matthew), Gower Technical, University of Bradford, September, Paper 38, (1989), pp. 419–428.
- Knight, D.W., Yuen, K.W.H. and Al-Hamid, A.A.I.: Boundary shear stress distributions in open channel flow, in *Physical Mechanisms of Mixing and Transport in the Environment*, (Eds K. Beven, P. Chatwin & J. Millbank), J. Wiley, [Chapter 4](#), (1994), pp. 51–87.
- Knight, D.W., Brown, F.A., Valentine, E.M., Nalluri, C., Bathurst, J.C., Benson, I.A., Myers, W.R.C., Lyness, J.F. and Cassells, J.B.: The response of straight mobile bed channels to inbank and overbank flows, *Proc. Instn. of Civil Engineers, Water, Maritime and Energy Division*, London, Vol. 136, Dec., (1999), pp. 211–224.
- Kolkman, P.A.: Discharge relationships and component head losses for hydraulic structures, in *Discharge characteristics, Hydraulic Design Considerations, Hydraulic Structures Design Manual 8*, 55–151, edited by Miller, D.S, International Association for Hydraulic Research, Balkema, (1994).
- Kouwen, N. and Li, R.M.: Biomechanics of vegetative channel linings, *Journal of Hydraulic Engineering*, ASCE, Vol. 106, (1980), pp. 1085–1103.
- Krishnamurthy, M. and Christensen, B.A.: Equivalent roughness for shallow channels, *Journal of Hydraulics Division*, ASCE, Vol. 98, HY12, (1972), pp. 2257–2262.
- Lamb, R., Mantz, P., Atabay, S., Benn, J. and Pepper, A.: Recent advances in modelling flood water levels at bridges and culverts, *Proceedings of 41st Defra Flood and Coastal Risk Management Conference*, 4–6 July, York, (2006), pp. 3a.1.1–3a.1.9.
- Lambert, M.F. and Myers, W.R.C.: Estimating the discharge capacity in straight compound channels, *Proc. Instn. of Civil Engineers, Water, Maritime and Energy*, Paper 11530, Vol. 130, June, (1978), pp. 84–94.
- Larock, B.E.: Gravity-affected flow from planar sluice gates, *Journal of the Hydraulics Division*, Proceedings of the American Society of Civil Engineers, HY4, July, (1969), pp. 1211–1226.
- Latapie, A.: Testing of a New Method for Conveyance Estimation in Natural Rivers, MSc Thesis, *Heriot-Watt University*, Edinburgh, (2003), pp. 1–81.
- Laurensen, E.M.: Friction slope averaging in backwater calculations, *Journal of Hydraulic Engineering*, ASCE, Vol. 112, No. 12, December, (1985), pp. 1151–1163.
- Leggett, D.J. and Elliott, C.: Improving the Implementation and Adoption of Flood and Coastal Defence R & D Results, *R & D Technical Report W5G-003*, Environment Agency, Rio House, Waterside Drive, Aztec West, Almondsbury, Bristol BS32 4UD, (2002).
- Leopold, L.B., Bagnold, R.A., Wolman, M.G. and Brush L.M.: Flow resistance in sinuous or irregular channels, *USGS Professional Paper 282-D*, Washington D.C., (1960), pp. 111–134.
- Liao, H. and Knight, D.W.: Analytic stage-discharge formulas for flow in straight prismatic channels, *Journal of Hydraulic Engineering*, ASCE, Vol. 133, No. 10, October, (2007a), pp. 1111–1122.

- Liao, H. and Knight, D.W. Analytic stage-discharge formulae for flow in straight trapezoidal open channels, *Advances in Water Resources*, Elsevier, Vol. 30, Issue 11, November, (2007b), pp. 2283–2295.
- Lighthill, M.J.: Introduction – boundary layer theory, *Laminar Boundary Layers*, Chapter 2, [Editor I Rosenhead], Clarendon, (1963).
- Liu, H.K.: Mechanics of sediment ripple formation, *Journal of Hydraulics Division*, Vol. 83, HY2, April, (1957).
- Lotter, G.K.: Considerations on hydraulic design of channels with different roughness of walls, Trans. All-Union Scientific Research Institute of Hydraulic Eng., Leningrad, Vol. 9, (1933), pp. 238–241.
- Manning, R.: On the flow of water in open channels and pipes, *Trans. Inst. Civil Engineers of Ireland*, Dublin, 20, (1891), pp. 161–207.
- Mantz, P.A. and Benn, J.R.: Computation of afflux ratings and water surface profiles, *Water Management*, Proc. Instn. of Civil Engineers, London, 162, WM1, February, (2009), pp. 41–55.
- Mantz, P.A., Lamb, R. and Benn, J.R.: Afflux Estimation System Hydraulic Reference, *Environment Agency Science Report SC030218/SR*, (2007), pp. 1–142.
- Matthai, H.F.: Measurement of peak discharge at width contractions by indirect method, *Techniques of Water Resources Investigations of the United States Geological Survey*, A4, Book 3, Applications of Hydraulics, US Govt. Printing Office, Washington D.C., (1967).
- May, R.W.P, Ackers, J.C. and Kirby, A.M.: Manual on scour at bridges and other hydraulic structures, *CIRIA Report C551*, Construction and Industry Research and Information Association, London, (2002), pp. 1–225.
- Mc Gahey, C.: A practical approach to estimating the flow capacity of rivers, PhD Thesis, Faculty of Technology, *The Open University (and British Library)*, May, (2006), pp. 1–371.
- Mc Gahey, C. and Samuels, P.G.: A practical approach to uncertainty in conveyance estimation, *Proc. of the 39th Defra Flood and Coastal Management Conf.*, The University of York, 29th June–1st July, (2004), pp. 10.3.1–10.3.12.
- Mc Gahey, C., Ramsbottom, D., Panzeri, M. and Millington, R.: National flood hazard mapping for Scotland – an innovative approach, *Proceedings of the 40th Defra Flood and Coastal Management Conference*, The University of York, 5th–7th July, (2005), pp. 2.4.1–2.4.11.
- Mc Gahey, C., Samuels, P.G. and Knight, D.W.: A practical approach to estimating the flow capacity of rivers – application and analysis, *River Flow 2006*, September, Lisbon, Portugal, Vol. 1, (2006), pp. 303–312.
- Mc Gahey, C., Samuels, P.G., Knight, D.W. and O'Hare, M.T.: Estimating river flow capacity in practice, *Journal of Flood Risk Management*, CIWEM, Vol. 1, (2008), pp. 23–33.
- Mc Gahey, C., Samuels, P.G. and Knight, D.W.: Practical toolset for estimating channel roughness, accepted to *Water Management*, Proc. Instn. of Civil Engineers, London, (2009), (in press).
- Melville, B.W. and Coleman, S.E.: *Bridge scour*, Water Resources publications, LLC, Colorado, US, (2000), pp. 1–550.
- MIKE11 V3.11: General reference manual, 1st edition, Danish Hydraulic Institute, (1995).

- Miller, D.S.: *Discharge Characteristics*, Hydraulic Structures Design Manual No. 8, IAHR, Balkema, (1994), pp. 1–249.
- Miller, J.B.: *Floods: people at risk, strategies for prevention*, United Nations, New York, (1997).
- Montes, J.S.: *Hydraulics of Open Channel Flow*, ASCE Press, New York, US, [ISBN 0-784-40357-0], (1998), pp. 1–712.
- Moody, L.F.: Friction factors for pipe flow, *Transactions of the American Society of Mechanical Engineers*, ASME, Vol. 66, (1944), pp. 671–684.
- Morvan, H., Knight, D.W., Wright, N.G., Tang, X. and Crossley, M.: The concept of roughness in fluvial hydraulics and its formulation in 1-D, 2-D & 3-D numerical simulation models, *Journal of Hydraulic Research*, IAHR, Vol. 46, No. 2, (2008), pp. 191–208.
- Muto, Y.: Turbulent flow in two-stage meandering channels, PhD Thesis, *Department of Civil Engineering, Bradford University*, UK, (1997).
- Myers, W.R.C.: Momentum transfer in a compound channel, *Journal of Hydraulic Research*, IAHR, Vol. 16, No. 2, (1978), pp. 139–150.
- Myers, W.R.C. and Lyness, J.J.: Flow resistance in rivers with floodplains, final report on research grant GR/D/45437, *University of Ulster*, (1989).
- Myers, W.R.C. and Brennan, E.K.: Flow resistance in compound channels, *Journal of Hydraulic Research*, IAHR, Vol. 28, No. 2, (1990), pp. 141–155.
- Myers, W.R.C., Knight, D.W., Lyness, J.F., Cassells, J. and Brown, F.A.: Resistance coefficients for inbank and overbank flows, *Proc. Instn. of Civil Engineers, Water, Maritime and Energy Division*, London, Vol. 136, June, (1999), pp. 105–115.
- Myers, W.R.C. and Lyness, J.F.: Discharge ratios in smooth and rough compound channels, *Journal of Hydraulic Engineering*, American Society of Civil Engineers, Vol. 123, Issue 3, March, (1997), pp. 182–188.
- Naden, P.S., Rameshwaran, P. and Vienot, P.: Modelling the influence of instream macrophytes on velocity and turbulence, *Proceedings 5th International Symposium on Ecohydraulics – Aquatic Habitats Analysis and Restoration*, Editors D.G. de Jalon Lastra & P.V. Martinez, Madrid, Spain, (2004), pp. 1118–1122.
- Naden, P.S., Rameshwaran, P., Mountford, O. and Robertson, C.: The influence of macrophyte growth, typical of eutrophic conditions, on river flow, velocities, and turbulence production, *Hydrological Processes*, 20, (2006), pp. 3915–3938.
- Nagler, F.A.: Obstructions of bridge piers to the flow of water, *Transactions of the American Society of Civil Engineers*, 82, (1918), pp. 334–395.
- Nakato, T. and Ettema, R.: *Issues and directions in hydraulics*, Balkema, (1996), pp. 1–495.
- National Rivers Authority: *Design of straight and meandering channels*, NRA R & D Report 13, Environment Agency, Rio House, Waterside Drive, Aztec West, Almondsbury, Bristol BS32 4UD, (1994).
- Navratil, O., Albert, M.B. and Gresillon, J.M.: Using a 1D steady flow model to compare field determination methods of bank-full stage, *Proceedings of River Flow 2004* [Eds Greco, Caravetta & Della Morte], Naples, June, Balkema, (2004), pp. 155–161.
- Neill, C.R.: (1973), *Guide to bridge hydraulics*, University of Toronto Press for Roads and Transportation Association of Canada, Toronto, (1973), pp. 1–191.
- Newton, I.: *Methodus fluxionum et serierum infinitarum*, (1644–1671).

- Nezu, I. and Nakagawa, H.: *Turbulence in Open-Channel Flows*, IAHR Monograph Series, A.A. Balkema, Rotterdam, (1993), pp. 1–281.
- Nezu, I. and Nakayama, T.: Space-time correlation structures of horizontal coherent vortices in compound open-channel flows by using particle-tracking velocimetry, *Journal of Hydraulic Research*, Vol. 35, No. 2, (1997), pp. 191–208.
- Nezu, I., Onitsuka, K. and Iketani, K.: Coherent horizontal vortices in compound open-channel flows, *Hydraulic Modeling* (ed. V.P. Singh, et al.), Water Resources Publications, Colorado, US, (1999), pp. 17–32.
- Nezu, I. and Rodi, W.: Experimental study on secondary currents in open channel flow, *Proc. of 21st IAHR Congress*, Melbourne, 2, (1985), pp. 115–119.
- Nikora, V.: Hydrodynamics of rough-bed turbulent flows: spatial averaging perspective, *River Flow 2008* [Eds M.S. Altinakar, M.A. Kokpinar, I. Aydin, S. Cokgar & S. Kirkgoz], Kubaba Services, Turkey, (2008), pp. 11–19.
- Nikuradse, J.: Translates to: Laws of flow in rough pipes, *Verein deutscher Ingenieure, Forschungsheft*, No. 361, Berlin, (1933).
- NIRA: National flood map for Northern Ireland, Proposed Methodology Report, prepared by RPS-KMM & HR Wallingford for *Northern Ireland Rivers Agency*, June, (2005), pp. 1–37.
- Novak, P., Moffat, A.I.B., Nalluri, C. and Narayanan, R.: *Hydraulic structures*, E & FN Spon, (2007), pp. 1–700.
- O'Hare, M.T., Stillman, R.A., Mc Donnell, J. and Wood, L.: The effects of mute swan grazing on a keystone macrophyte, *Freshwater Biology* Published article online: 23 Aug, (2007), doi: 10.1111/j.1365-2427.2007.01841.x.
- O'Hare, M.T., Scarlett, P., Henville, P., Ryaba, T., Cailes, C. and Newman, J.: Variability in Manning's n estimates for vegetated rivers – Core Site Study: Intra- and Inter- Annual Variability, *An Aquatic Plant Management Group Report*, Centre for Ecology & Hydrology, UK, (2008), pp. 1–33.
- Okada, S. and Fukuoka, S.: Land-form features in compound meandering channels and classification diagram of flood flows based on sinuosity and relative depth, *River Flow 2002* [Eds D. Bousmar & Y. Zech], Balkema, (2002), pp. 205–212.
- Okada, S. and Fukuoka, S.: Plan shape features in compound meandering channels and classification diagram of flood flows based on sinuosity and relative depth, *Journal of Hydroscience and Hydraulic Engineering*, Vol. 231, No. 1, May, (2003), pp. 41–52.
- Omran, M.: Modelling stage-discharge curves, velocity and boundary shear stress distributions in natural and artificial channels using a depth-averaged approach, *PhD thesis, Department of Civil Engineering, The University of Birmingham*, (2005).
- Omran, M. and Knight, D.W.: Modelling the distribution of boundary shear stress in open channel flow, *RiverFlow 2006*, September, Lisbon, Portugal, Vol. 1, [Eds Ferreira, Alves, Leal & Cardoso], Taylor & Francis, (2006), pp. 397–404.
- Omran, M., Knight, D.W., Beaman, F. and Morvan, H.: Modelling equivalent secondary current cells in rectangular channels, *RiverFlow 2008*, [Eds M.S. Altinakar, M.A. Kokpinar, I. Aydin, S. Cokgar & S. Kirkgoz], Cesme, Turkey, Vol. 1, (2008), pp. 75–82.
- Oshikawa, H., Hashimoto, A., Tsukahara, K. and Komatsu, T.: Impacts of recent climate change on flood disaster and preventive measures, *Journal of Disaster Research*, Vol. 23, No. 2, (2008), pp. 131–141.

- Palmer, V.J.: A method for designing vegetated waterways, *Agriculture Engineering*, Vol. 26, No. 12, (1945), pp. 516–520.
- Pavlovskii, N.: On a design for uniform movement in channels with non-homogenous walls, *All-Union Scientific Research Institute of Hydraulic Engineering*, Leningrad, Vol. 3, (1931), pp. 157–164.
- Perkins, H.J.: The formation of streamwise vorticity in turbulent flow, *Journal of Fluid Mechanics*, Vol. 44, Part 4, (1970), pp. 721–740.
- Petryk, S. and Bosmajian, G.: Analysis of flow through vegetation, *Journal of Hydraulic Division*, ASCE, Vol. 101, No. 7, (1975), pp. 871–884.
- Pitt, M.: *Learning lessons from the 2007 floods*, Defra/Environment Agency, June, (2008), pp. 1–462.
- Powell, R.W.: Resistance to flow in rough channels, *Eos Transactions AGU*, Vol. 31, (1950), pp. 575–582.
- Prandtl, L.: Bericht über Untersuchungen zur ausgebildeten Turbulenz, *Z. Angew. Math., Meth.*, Vol. 5, (1925), pp. 136–139.
- Preissmann, A.: Propagation of translatory waves in channels and rivers, *Proceedings of 1st Congress of French Association for Computation*, AFCAL, Grenoble, France, (1961), pp. 43–442.
- Press, W.H., Teukolsky, S.A., Vetterling, W.T. and Flannery, B.P.: *Numerical recipes in Fortran 90 – the art of parallel scientific computing*, Vol. 2, Cambridge University Press, (1996).
- Rajaratnam, N.: Free flow immediately below sluice gates, *Journal of the Hydraulics Division*, ASCE, Vol. 3, No. 4, April, (1977), pp. 345–351.
- Rajaratnam, N. and Humpries, J.A.: Free flow upstream of vertical sluice gates, *Journal of Hydraulic Research*, Vol. 20, No. 5, (1982), pp. 427–437.
- Rajaratnam, N. and Muralidhar, D.: Boundary shear distribution in rectangular open channels, *La Houille Blanche*, No. 6, (1969), pp. 603–609.
- Rajaratnam, N. and Subramanya, K.: Practical problems of sluice-gate flow, *Water Power*, March, (1969), pp. 112–115.
- Raju, K.G.R., Asawa G.I., Rana O.P.S. and Pillai A.S.N.: Rational assessment of blockage effect in channel flow past smooth circular cylinders, *Journal of Hydraulic Research*, IAHR, Vol. 21, No. 4, (1983), pp. 289–302.
- Rameshwaran, R. and Willetts, B.B.: Conveyance prediction for meandering two-stage channel flows, *Proceedings ICE Journal for Water, Maritime and Energy*, Paper 11765, Vol. 136, Sept., (1999), pp. 153–166.
- Ramette, M.: Hydraulique et morphologie des rivières: quelques principes d'étude et applications, Compagnie Nationale du Rhône, *Formation Continue*, France, (1992).
- Ramsbottom, D., Day, R. and Rickard, C.: *Culvert Design guide*, CIRIA Report 168, Construction and Industry Research and Information Association, London, (1997), pp. 1–189.
- Ramsbottom, D. and Whitlow, C.: Extension of rating curves at gauging stations: best practice guidance manual, Prepared for the Environment Agency, R & D Manual W6-061/M, October, (2003), pp. 1–247.
- Raudkivi, A.J.: *Loose Boundary Hydraulics*, A.A. Balkema, Rotterdam, Netherlands, (1998), pp. 1–538.

- Raven, P.J., Holmes, H.T.H., Dawson, F.H., Fox, P.J.A., Everard, M., Fozzard, I. and Rouen K.J.: River habitat quality: the physical character of rivers and streams in the UK and the Isle of Man, *River Habitat Report No. 2*, Environment Agency, (1998), pp. 1–90.
- Ree, W.O. and Palmer, V.J.: Flow of water in channels protected by vegetative linings, Bulletin No. 967, Soil Conservation Service, US Department of Agriculture, Washington, (1949), pp. 1–115.
- ReFEH: revised *Flood Estimation Handbook*, Vols. 1–5, Centre for Ecology and Hydrology, Wallingford, Oxon, UK, (2007).
- Rehbock, T.: (1922). See Theodor Rehbock, (1864–1950), in *Hydraulics and Hydraulics Research : A Historical Review*, [Ed Gunther Garbrecht], International Association for Hydraulic Research, Balkema, (1987), pp. 281–291.
- Reinius, E.: Steady uniform flow in open channels, Bulletin 60, Division of Hydraulics, Royal Institute of Technology, Stockholm, Sweden, (1961).
- Reynolds, A.J.: *Turbulent flows in engineering*, Wiley, (1974), pp. 1–462.
- Rezaei, B.: Flow in channels with non-prismatic floodplains, *PhD Thesis, Department of Civil Engineering, The University of Birmingham*, (2006).
- Rhodes, D.G. and Knight, D.W.: Lateral shear in wide compound duct, *Journal of Hydraulic Engineering*, ASCE, Vol. 121, No. 11, (1995), pp. 829–832.
- Roberts, J.D., Free-Hewish, R.J. and Knight, D.W.: Modelling of hydraulic drag forces on submersible bridge decks, *Proc. 4th Road Engineering Association of Asia and Australasia (REAA)*, Jakarta, Indonesia, August, (1983), pp. 1–11.
- Rodi, W.: Turbulence models and their application in hydraulics, *State of the Art Paper, Int. Association for Hydraulic Research, IAHR*, Delft, Netherlands, (1980), pp. 1–104.
- Rouse, H.: *Elementary Mechanics of Fluids*, Wiley, New York, (1946), pp. 1–376.
- Rozovskii, I.L.: Flow of water in bends or open channels, *The Academy of Science of the Ukraine SSR*, translated from Russian by the Israel Program for Scientific Translations, Jerusalem, Israel, (1957).
- Samuels, P.G.: Modelling of river and flood plain flow using the finite element method, *PhD Thesis, Department of Mathematics, University of Reading, HR Wallingford Report SR61*, November, (1985).
- Samuels, P.G.: Lateral shear layers in compound channels, *Proceedings International Conference on Fluvial Hydraulics*, Budapest (also published at HR Wallingford, UK), (1988).
- Samuels, P.G.: Some analytical aspects of depth averaged flow models, *Proc. Intl. Conf. Hydraulic and Environmental Modelling of Coastal, Estuarine and River Waters*, Bradford, England, 19–21st September, (1989a).
- Samuels, P.G.: Backwater length in rivers, *Proc. Instn Civ. Engrs*, Part 2, Vol. 87, December, (1989b), pp. 571–582.
- Samuels, P.G.: Cross-section location in 1-D models, *Proc. Int. Conf. on River Flood Hydraulics*, (Ed W.R.White), J. Wiley & Sons, Wallingford, September, Paper K1, (1990), pp. 339–348.
- Samuels, P.G.: Uncertainty in Flood Level Prediction, XXVI Biannual Congress of the IAHR, HYDRA2000, London, Sept. 1995, Vol. 1 of *Proceedings published by Thomas Telford*, (1995).

- Samuels, P.G.: Risk and Uncertainty in Flood Management, Chapter 25 in *River Basin Modelling for Flood Risk Mitigation* [Eds D.W. Knight & A.Y. Shamseldin], Taylor & Francis, (2006), pp. 481–517.
- Samuels, P.G., Dijkman, J. and Klijn, F.: An Analysis of the Current Practice of Policies on River Flood Risk Management in Different Countries, *Irrigation and Drainage*, Vol. 55, S141–156, (2006).
- Sayers, P.B., Hall, J.W. and Meadowcroft, I.C.: Towards risk-based flood hazard management in the UK. *Proceedings of ICE – Civil Engineering*, Vol. 150, Special Issue 1, (2002), pp. 36–42.
- Sayre, W.W. and Albertson, M.L.: Roughness spacing in rigid open channels, *Journal of Hydraulic Division*, ASCE, Vol. 87, HY3, (1961), pp. 121–150.
- Schlichting, H.: *Boundary layer theory*, McGraw-Hill, (1979), pp. 1–817.
- Schmidt, A.R. and Yen, B.C.: Theoretical development of stage-discharge ratings for subcritical open-channel flows, *Journal of Hydraulic Engineering*, American Society of Civil Engineers, New York, Vol. 134, No. 9, September, (2008), pp. 1245–1256.
- Seckin, G., Yurtal, R. and Haktanir, T.: Contraction and expansion losses through bridge constrictions, *Journal of Hydraulic Engineering*, American Society of Civil Engineers, New York, Vol. 124, No. 5, May, (1998), pp. 546–549.
- Seckin, G., Haktanir, T. and Knight, D.W.: A simple method for estimating flood flow around bridges, *Water Management*, Proceedings of the Instn. of Civil Engineers, London, 160, Issue WM4, December, (2007), pp. 195–202.
- Seckin, G., Knight, D.W., Atabay, S. and Seckin, N.: Effect of the Froude number on the assessment of the bridge afflux, *Water Management*, Proceedings of the Instn. of Civil Engineers, London, Vol. 161, Issue WM2, April, (2008a), pp. 97–104.
- Seckin, G., Knight, D.W., Atabay, S. and Seckin N.: Improving bridge afflux prediction for overbank flows, *Water Management*, 161(5), (2008b), pp. 253–260.
- Seed, D.J., Samuels, P.G. and Ramsbottom, D.M.: Quality assurance in computational river modelling, *First Interim report SR 374*, HR Wallingford, (1993).
- Sellin, R.H.J.: A laboratory investigation into the interaction between the flow in the channel of a river and that over its floodplain, *La Houille Blanche*, Vol. 19, No. 7, (1964), pp. 793–801.
- Sellin, R.H.J.: Hydraulic performance of skewed two-stage flood channel, *Journal of Hydraulic Research*, IAHR, Vol. 33, No. 1, (1995), pp. 43–64.
- Sellin, R.H.J. and van Beesten, D.P.: Conveyance of a managed vegetated two-stage river channel, *Journal of Water Management*, The Institution of Civil Engineers, Vol. 157, No. 1, (2004), pp. 21–33.
- Sellin, R.H.J., Ervine, A.E. and Willetts, B.B.: Behaviour of meandering two-stage channels, *Water Maritime and Energy*, Proc. Institution of Civil Engineers, Vol. 101(2), (1993), pp. 99–111.
- SEPA: Second generation flood map for Scotland – methodology report, Report EX5098, prepared by HR Wallingford for the *Scottish Environment Protection Agency*, January, (2006), pp. 1–110.
- Sharifi, S., Knight, D.W. and Sterling, M.: A novel application of a multi-objective evolutionary algorithm in open channel flow modelling, *Journal of Hydroinformatics*, IWA Publishing, 11.1, (2009), pp. 31–50.
- Shaw, E.M.: *Hydrology in practice*, Chapman and Hall, London, (1994), pp. 1–569.

- Shen, H.W.: *River mechanics*, Vols. I & II, Colorado State University, Fort Collins, (1971), pp. 1–897.
- Shields, A.: Anwendung Aenlich Keitsmechanik und der Trubulenz-schung auf Die Geschiebebewegung, *Mitteilungen de Preussischen Veruchsanstalt fur Wasserbau und Schiffbau*, Berlin, Germany, (1936).
- Shiono, K. and Knight, D.W.: Two-dimensional analytical solution for a compound channel, *Proc. 3rd Int. Symposium on Refined Flow Modelling and Turbulence Measurements*, Tokyo, Japan, July, (1988), pp. 503–510.
- Shiono, K. and Knight, D.W.: Mathematical models of flow in two or multi stage straight channels, *Proceedings International Conference on River Flood Hydraulics*, (Ed. W.R.White), Wiley & Sons Ltd., Paper G1, (1990), pp. 229–238.
- Shiono, K. and Knight, D.W.: Turbulent open channel flows with variable depth across the channel, *Journal of Fluid Mechanics*, Vol. 222, (1991), pp. 617–646 (and Vol. 231, October, p. 693).
- Shiono, K. and Muto, Y.: Complex flow mechanisms in compound meandering channels with overbank flow, *Jnl. of Fluid Mechanics*, Vol. 376, (1998), pp. 221–261.
- Shiono, K., Al-Romaih, J.S. and Knight, D.W.: Stage-discharge assessment in compound meandering channels, *Journal of Hydraulic Engineering*, ASCE, Vol. 125, No. 1, Jan., (1999a), pp. 66–77.
- Shiono, K., Muto, Y., Knight, D.W. and Hyde, A.F.L.: Energy losses due to secondary flow and turbulence in meandering channels with overbank flow, *Journal of Hydraulic Research*, IAHR, Vol. 37, No. 5, (1999b), pp. 641–664.
- Simons, D.B., and Senturk, F.: Sediment transport technology, Water Resources Publications, Colorado, US, (1992).
- Spooner, J. and Shiono, K.: Modelling of meandering channels for overbank flow, *Water, Maritime and Energy*, Proc. ICE, Vol. 156, September, (2003), pp. 225–233.
- Statzner, B., Lamouroux, N., Nikora, V. and Sagnes, P.: The debate about drag and reconfiguration of freshwater macrophytes: comparing results obtained by three recently discussed approaches, *Journal of Freshwater Biology*, Vol. 51, (2006), pp. 2173–2183.
- Stearns, F.P.: On the current meter, together with a reason why the maximum velocity of water flowing in open channels is below the surface, *Trans. of ASCE*, Vol. 12, No. 216, (1883), pp. 331–338.
- Stokes, G.G.: On the theories of internal friction of fluid motion and of the equilibrium and motion of elastic solids, *Cambridge Philosophical Society*, Vol. 8, (1845), pp. 287–305.
- Strickler, A.: Translates to: Some contributions to the problem of the velocity formula and roughness factors for rivers, canals and closed conduits, *Mitteilungen des Eidgenossischen Amtes fur Wasserwirtschaft*, Bern Switzerland, No. 16, (1923).
- Sturm, T.W.: *Open Channel Hydraulics*, McGraw-Hill Series in Water Resources and Environmental Engineering, New York, [ISBN 0-070-62445-3], (2001), pp. 1–493.
- Tagg, A.F., and Samuels, P.G.: Modelling flow resistance in tidal rivers, *Proc. Int. Conf. on Hydraulic and Environmental Modelling of Coastal, Estuarine and River Waters*, Bradford, September, (1989), pp. 441–452.

- Tang, X. and Knight, D.W.: Experimental study of stage-discharge relationships and sediment transport rates in a compound channel, *Proc. 29th IAHR Congress, Hydraulics of Rivers, Theme D*, Vol. II, September, Beijing, China, Tsinghua University Press, (2001), pp. 69–76.
- Tang, X., Knight, D.W. and Samuels, P.G.: Volume conservation in variable parameter Muskingum-Cunge method, *Journal of Hydraulic Engineering*, ASCE, Vol. 125, No. 6, June, (1999a), pp. 610–620.
- Tang, X., Knight, D.W. and Samuels, P.G.: Variable parameter Muskingum-Cunge method for flood routing in a compound channel, *Journal of Hydraulic Research*, IAHR, Vol. 37, No. 5, (1999b), pp. 591–614.
- Tang, X., Knight, D.W. and Samuels, P.G.: Wave speed-discharge relationship from cross-section survey, *Proc. Instn. of Civil Engineers, Water and Maritime Engineering*, London, 148, June, Issue 2, (2001), pp. 81–96.
- Tang, X. and Knight, D.W.: Analytical models for velocity distributions in open channel flows, *Journal of Hydraulic Research*, IAHR, (2009), (in press).
- Tennekes, H. and Lumley, J.L.: *A first course in turbulence*, Massachusetts Institute of Technology Press, US, (1972), pp. 1–300.
- Theodorsen, T.: Mechanism of turbulence, *2nd Midwestern Conf. on Fluid Mechanics*, Ohio State University, (1952), pp. 1–18.
- Thijsse, J.T.: Formulae for the friction head loss along conduit walls under turbulent flow, *Proc., 3rd IAHR Congress*, Grenoble, France, Vol. 3, No. 4, (1949), pp. 1–11.
- Thorne, C.R., Hey, R.D. and Newson, M.D.: *Applied fluvial geomorphology for river engineering and management*, J. Wiley, (1997), pp. 1–376.
- Thorne, C.R., (chair), Alonso, C., Bettess, R., Borah, D., Darby, S., Diplas, P., Julien, P., Knight, D.W., Li, L., Pizzuto, P., Quick, M., Simon, A., Stevens, M. and Wang, S.: River width adjustment. Part II : Processes and mechanisms, *Journal of Hydraulic Engineering*, ASCE, Task Committee on Hydraulics, Bank Mechanics, and Modelling of River Width Adjustment, 124(9), (1998), pp. 881–902.
- Toebes, G.H. and Sooky, A.A.: Hydraulics of meandering rivers with flood-plains, *Journal of Waterways and Harbours Division*, ASCE, Vol. 93, (1967), pp. 213–236.
- Tominaga, A., Nezu, I., Ezaki, K. and Nakagawa, H.: Turbulent structure in straight open channel flows, *Journal of Hydraulic Research*, IAHR, 27(1), (1989), pp. 149–173.
- Tominaga, A. and Knight, D.W.: Numerical evaluation of secondary flow effects on lateral momentum transfer in overbank flows, *River Flow 2004, Proc. 2nd Int. Conf. on Fluvial Hydraulics, 23–25 June, Napoli, Italy* [Eds M. Greco, A. Carravetta & R.D. Morte], Vol. 1, (2004), pp. 353–361.
- Townend, I.H., Elliott, C. and Sayers, P.B.: Controlled dissemination and uptake of research, *Proceedings of 42nd Defra Flood and Coastal Risk Management Conference*, 3–5 July, New York, (2007), pp. 5a.1.1–5a.1.10.
- Tsikata, J.M., Katopodis, C. and Tachie, M.F.: Experimental study of turbulent flow near model trashracks, *Journal of Hydraulic Research*, IAHR, Vol. 47, No. 2 (2009), pp. 275–280 doi:10.3826/jhr.2009.3381, pp. 275–280.

- Tullis, B.P., Anderson, D.S. and Robinson, S.C.: Entrance loss coefficients and inlet control head-discharge relationships for buried-invert culverts, *Journal of Irrigation and Drainage Eng.*, ASCE, 134(6), (2008), pp. 831–839.
- USBPR: Hydraulics of Bridge Waterways, US Dept. of Transportation, FHWA, *Hydraulic Design Series No.1*, published electronically in 1978, (1978).
- USGS: Backwater at bridges and densely wooded flood plains, *Hydrologic Atlas Series No. 590–611*, (1978).
- Vanoni, V.A.: Transportation of suspended sediment by water, *Trans. of ASCE*, Vol. 111, (1946), pp. 67–133.
- van Prooijen, B.C.: Transverse momentum exchange in compound channel flows, *Proc. XXX IAHR Conf.*, John F Kennedy Student Paper Competition, Thessaloniki, Greece, 2003.
- van Prooijen, B.M.: Shallow mixing layers, *PhD Thesis, Department of Civil Engineering*, Delft University of Technology Report 04-1, ISSN 0169-6548, (2004).
- van Prooijen, B.C., Battjes, J.A. and Uijttewaal, W.S.J.: Momentum exchange in straight uniform compound channel flow, *Journal of Hydraulic Engineering*, ASCE, 131(3), (2005), pp. 175–183.
- van Rijn, L.C.: The prediction of bedforms and alluvial roughness, *Proc. Euromech 156, Mechanics of sediment transport* [Eds B. Sumer & A. Muller], 12–14 July, Istanbul, Turkey, Balkema, (1982), pp. 133–135.
- van Rijn, L.C.: Sediment transport, Part III: bedforms and alluvial roughness, *Journal of Hydraulic Engineering*, Vol. 110, HY12, December, (1984), pp. 1733–1754.
- Versteeg, H.K. and Malalaskera, W.: *An introduction to computational fluid dynamics: the finite volume method*, Longman Scientific & Technical, (1995), pp. 1–257.
- Vidal, J.P., Moisan, S., Faure, J.B. and Dartus, D.: River model calibration, from guidelines to operational support tools, *Environmental Modelling & Software* (available on-line via Science Direct), Vol. 22, Issue 11, November, (2007), pp. 1628–1640.
- Vreugdenhil, C.B.: *Computational hydraulics: an introduction*, Springer-Verlag, Berlin, (1989), pp. 1–182.
- Wang, S.: On the reliability and accuracy of computational models for Hydroscience and Engineering investigations, *US-China Workshop on Advanced Computational Modelling in Hydroscience and Engineering*, Oxford, Mississippi, US, 19, September, (2005).
- Wark, J.B.: Discharge assessment in straight and meandering compound channels, *PhD Thesis, Department of Civil Engineering, University of Glasgow*, UK, (1993).
- Westlake, D.F. and Dawson, F.H.: Thirty years of weed cutting on a chalk-stream. EWRS 6th Symposium on Aquatic Weeds (1982).
- Weisbach, J.: *Lehrbuch der Ingenieur- und Maschinen-Mechanik*, Braunschweig, (1845).
- White, W.R.: Sediment transport in channels – a general function, SR 102, HR Wallingford, UK, (1972).
- White, W.R., Bettess, R. and Paris, E.: Analytical approach to river regime, *Journal of the Hydraulics Division*, ASCE, Vol. 108, HY10, October, (1982), pp. 1179–1193.

- White, W.R., Paris, E. and Bettess, R.: The frictional characteristics of alluvial streams: a new approach, *Proc. Inst. of Civil Engineers, London*, Vol. 69, No. 1, Sept., (1980), pp. 737–750.
- Whitehead, E., Brown, P. and Hollinrake, P.: The hydraulic roughness of vegetated channels, Report SR305, *HR Wallingford*, UK, (1992), pp. 1–38.
- Whitlow, C.D. and Knight, D.W.: An investigation of the effect of different discretisations in river models and a comparison of non-conservative and conservative formulation of the de St. Venant equations, In *Hydraulic and Environmental Modelling: Estuarine and River Waters* (Eds R.A. Falconer, K. Shiono & R.G.S. Matthew), Ashgate Press, (1992), pp. 115–126.
- Wormleaton, P.R.: Determination of discharge in compound channels using the dynamic equation for lateral velocity distribution, *Proc. Int. Conf. on Fluvial Hydraulics*, Belgrade, Hungary, June, (1988), pp. 98–103.
- Wormleaton, P.R.: Floodplain secondary circulation as a mechanism for flow and shear stress redistribution in straight compound channels, In *Coherent Flow Structures in Open Channels* [Eds Ashworth, Bennett, Best & McLelland], Chapter 28, J. Wiley, (1996), pp. 581–608.
- Wormleaton, P.R. and Merrett, D.J.: An improved method of calculation for steady uniform flow in prismatic main channel/floodplain sections, *Journal of Hydraulic Research*, IAHR, Vol. 28, No. 2, (1990), pp. 157–174.
- Wormleaton, P.R., Allen, J. and Hadjipanagos, P.: Discharge assessment in compound channel flow, *Journal of the Hydraulics Division*, Proc. ASCE, Vol. 108, HY9, Sept., (1982), pp. 975–993.
- Wormleaton, P.R., Allen, J. and Hadjipanagos, P.: Flow distribution in compound channels, *Journal of the Hydraulics Division*, Proc. ASCE, Vol. 111, HY2, February, (1985), pp. 357–361.
- Wormleaton, P.R., Hey, R., Sellin, R.H.J., Bryant, T.B., Loveless, J. and Catmur, S.E.: Behaviour of Meandering Overbank Channels with Graded Sand Beds, *Journal of Hydraulic Engineering*, American Society of Civil Engineers, 131(8), (2005), pp. 665–681.
- Wormleaton, P.R., Sellin, R.H.J., Bryant, T.B., Loveless, J., Hey, R. and Catmur, S.E.: Flow Structures in a Two-Stage Channel with Mobile Bed, *Journal of Hydraulic Research*, IAHR, 42(2), (2004), pp. 145–162.
- Wright, J.F., Gunn, R.J.M., Winder, J.M., Wiggers, R., Vowles, K., Clarke, R.T. and Harris, I.: A Comparison of the Macrophyte Cover and Macroinvertebrate Fauna at three Sites on the river Kennet in the mid 1970s and late 1990s, *The Science of the Total Environment*, 282–283, (2002), pp. 121–142.
- Wright, N.G., Crossley, A.J., Morvan, H.P. and Stoesser, T.: Detailed validation of CFD for flows in straight channels, *Proc. of the 2nd Intl. Conf. on Fluvial Hydraulics*, River Flow 2004, Naples, 24–26 June, Vol. 2, (2004), pp. 1041–1048.
- WSPRO.: Bridge waterways analysis: Research report, by Shearman, J.O. and Kirby, W.H., Schneider, V.R. and Flippo, H.N., Report No. FHWA/RD-86/108, NTIS, VA, US, (1986).
- Wu, B. and Guo, J.J.: Limit ratio for choking phenomenon, *2nd Int. Conf. On Flooding and Flood Defences*, Beijing, China, September, (2002), pp. 1–7.

- Wu, B. and Molinas, A.: Choked flows through short transitions, *Journal of Hydraulic Engineering*, American Society of Civil Engineers, New York, Vol. 127, No. 8, August, (2001), pp. 657–662.
- Yalin, M.S. and Ferreira da Silva, A.M.: *Fluvial processes*, IAHR Monograph, (2001), pp. 1–197.
- Yang, C.T.: *Sediment transport, theory and practice*, McGraw-Hill, (1987), pp. 1–396.
- Yarnell, D.L.: Bridge piers as channel obstructions, *Technical Bulletin No. 442, US Dept. of Agriculture*, Washington, D.C., November, (1934).
- Yen, B.C.: *Channel flow resistance: centennial of Manning's formula*, Colorado, US, Water Resources Publications, (1991), pp. 1–453.
- Yen, C.L. and Overton, D.E.: Shape effects on resistance in floodplain channels, *Journal of the Hydraulics Division*, ASCE, Vol. 99, No. 1, (1973), pp. 219–238.
- Yu, G. and Knight, D.W.: Geometry of self-formed straight threshold channels in uniform material, *Proc. Instn. of Civil Engineers, Water, Maritime and Energy Division*, London, Vol. 130, March, Paper 11398, (1998), pp. 31–41.
- Yuen, K.W.H.: A study of boundary shear stress, flow resistance and momentum transfer in open channels with simple and compound trapezoidal cross section, *PhD thesis, Department of Civil Engineering, The University of Birmingham*, (1989).
- Yuen, K.W.H. and Knight, D.W.: Critical flow in a two stage channel, *Proc. Int. Conf. on River Flood Hydraulics*, (Ed. W.R. White), Wallingford, September, J. Wiley & Sons, Paper G4, (1990), pp. 267–276.
- Zegzhda, A.P.: Teoriia podobiia I metodika rascheta gidrotekhnicheskikh modelei (Translates as: Theory of Similarity and Methods of Design of Models for Hydraulic Eng.), Gosstroizdat, Leningrad, (1938).
- Zienkiewick, O.C.: The finite element method, 3rd Edition, *McGraw-Hill Book Co. Ltd.*, UK, (1977).

Author index

- Abbot, M.B. 25, 266, 274, 305
Abril, J.B. 45, 65, 67, 68, 107, 112, 113, 120, 122, 123, 214, 216, 262, 263, 305, 316, 317
Ackers, P. 10, 42, 60, 63, 69, 106, 111, 117, 118, 124, 142, 259–62, 292, 305, 306
Albertson, M.L. 116, 324
Al-Hamid, A.A.I. 51, 306, 317, 318
Anastasiadou-Partheniou, L. 44, 306
Anderson, M.G. 105, 306, 317
Argawal, V.C. 111, 306
Armitage, P.D. 255, 306, 313
Ashworth, P.J. 60, 105, 306, 328
Atabay, S. 69, 71, 85, 88, 90, 140, 233, 261, 262, 306, 318, 324
Ayyoubzadeh, S.A. 261, 262, 306
Baatruo-Pedersen, A. 290, 306
Bagnold, R.A. 259, 292, 306, 318
Baines, W.D. 96, 308
Baird, J.I. 111, 312
Balbi, D.M. 258, 312
Banks, R.B. 106, 311
Baptist, M.J. 110, 307
Barnes, H.H. 106, 307
Barr, D.I.H. 107, 307
Basco, D.R. 266, 274, 305
Batchelor, G.K. 266, 307
Bazin, H. 106, 307
Bedient, P.B. 270, 307
Benn, J.R. 8, 69, 226, 265, 307, 318, 319
Berz, G. 1, 2, 283, 307
Bettess, R. 14, 259, 307, 310, 326–8
Beven, K. 275, 307, 318
Biery, P.F. 69, 71, 90, 307
Biglari, B. 69, 307
Blalock, M.E. 75, 307
Blasius, P.R.H. 107, 307
Blench, T. 259, 308
Bonner, V.R. 69, 307
Bos, M.G. 42, 69, 308
Bosmajian, G. 244, 322
Bousmar, D. 29, 82, 102, 112, 308, 313, 314, 321
Bradley, J.N. 72, 74, 81, 90, 308
Bradshaw, P. 75, 309
Brennan, E.K. 69, 320
Bronstert, A. 28, 308
Brown, F.A. 261, 262, 308, 317, 318, 320
Brown, P.M. 69, 90, 92, 153, 230, 308, 328
Brundrett, E. 96, 308
Buisson, R.S.K. 184, 243, 255, 256, 290, 308
Burnham, M.W. 165, 308
Cannan, C.E. 255, 306
Cao, S. 259, 263, 288, 308
CAPM 243, 290, 308
Carter, R.W. 81, 84, 90, 316
Casellarin, A. 28, 274, 309
Cebeci, T. 75, 309
Chadwick, A. 15, 309
Chang, H.H. 33, 111, 259, 260, 261, 292, 309
Chanson, H. 15, 309
Charbeneau, R.J. 291, 309
Chezy, A. 31, 105, 106, 111, 112, 115, 258, 289, 293, 309
Chlebek, J. 29, 47, 52, 82, 102, 309
Chow, V.T. 15, 22–4, 36, 42, 58, 60, 69, 72, 75, 85, 106, 138, 199, 309
Christensen, B.A. 106, 318
CIRIA 143, 147, 158–60, 234, 266, 291, 309, 319, 322
CIWEM 72, 85, 306, 309, 319
Colebrook, C.F. 31, 32, 107, 115–20, 138, 214, 216, 262, 307, 309
Coleman, S.E. 263, 319
Colson, B.E. 221, 224, 309
Cowan, W.L. 106, 244, 310
Cunge, J.A. 15, 25, 28, 119, 120, 266, 270, 271, 274, 310, 326
Darby, S. 26, 310, 326
Darcy, H. 31, 33, 46, 50, 105–7, 115, 117, 310
Davies, A.J. 135, 136, 310
Davis, D.W. 165, 308
Dawson, F.H. 290, 310, 325, 327
de Brujin, K.M. 166, 310
Defalque, A. 28, 164, 310
Defra/EA 6, 11, 12, 14, 29, 71, 108–10, 113, 116, 122, 127–9, 162, 185, 244, 245, 247, 258, 290, 310, 311, 313
Delleur, J.W. 69, 71, 90, 307

- Demetriou, J.D. 60, 67, 111, 317
 Diehl, T.H. 264, 311
 Drazin, P.G. 45, 113, 311
 Du Boys, P.F.D. 259, 292, 311
EA 5, 6, 11, 12, 14, 29, 71, 108–10, 113, 116, 122, 127–9, 162, 185, 190, 243–5, 247, 258, 290, 291, 307, 310, 313, 315, 323
 Einstein, H.A. 37, 106, 112, 259, 292, 311
 Elder, J.W. 120, 121, 311
 Elliott, C. 11, 318
 Elliott, S.C.A. 29, 100, 102, 312
 Ellis, J. 112, 312
 Engelund, F. 259, 292, 312
 Ervine, D.A. 111–3, 122–5, 312, 324
 Escarameia, M. 75, 310, 312
 Ettema, R. 25, 272, 285, 286, 316, 320
 European Commission 5, 28, 87, 312
 Evans, E.M. 166, 312
 Extence, C.A. 258, 312
FEH 45, 312, 323
 Ferreira da Silva, A.M. 260, 329
FHWA 70, 143, 144, 158, 160, 311, 312, 327, 328
 Fisher, K. 244, 256, 290, 312, 315
 Fleming, G. 11, 312, 314
 Franke, P.G. 42, 312
 Freer, J. 275, 307
 Fukuoka, S. 29, 97, 100, 103, 312, 316, 321
 Fujita, K. 97, 100, 312
 Ganguillet, E. 106, 312
 Garcia-Navarro, P. 266, 313, 316
 Garde, R.J. 260, 306, 313
 Garton, J.E. 244, 313
 Gibson, A.H. 95, 272, 313
 Gordon, N.D. 244, 313
 Gouldby, B.P. 162, 166, 313
 Graf, W.H. 116, 313
 Grass, A.J. 93, 94, 313
 Green, J.E.P. 244, 313
 Green, M. 28, 313
 Greenhill, R. 112, 313
 Guan, Y. 123, 313
 Guo, J.J. 77, 328
 Haderlie, G.M. 291, 313
 Hall, J. 161, 162, 166, 275, 312–4, 324
 Hamed, M. 111, 317
 Hamill, L. 41, 69, 70, 72, 76–8, 80, 83, 84, 90, 92, 313
 Hansen, H. 259, 292, 312
 Hearne, J. 255, 313
 HEC-RAS 71, 72, 91, 112, 129, 147, 148, 153, 161, 171, 267, 314
 Henderson, F.M. 15, 36, 69, 72, 75, 116, 138, 314
 Hicks, D.M. 29, 57–9, 106, 215, 314
 Hine, D. 166, 314
 Hinze, J.O. 96, 314
 Hoffmans, G.J.C.M. 104, 314
 Horton, R.E. 106, 112, 314
 Hotchkiss, R.H. 291, 314
 Huber, W.C. 270, 307
 Humphries, J.A. 42, 322
 Huthoff, F. 60, 314
ICE 11, 314, 324, 325
 Ikeda, S. 1, 26, 97–9, 103, 120, 261–3, 266, 271, 289, 314, 315
 Imamoto, H. 97, 315
 Infoworks RS 9, 112, 113, 129, 133, 161, 171, 185, 267, 289, 315
 IPCC 166, 315
 Ishigaki, T. 97, 315
ISIS 9, 112, 113, 161, 171, 185, 230, 231, 233, 267, 289, 306, 315
 ISO 68, 69, 315
 James, C.S. 10, 111, 112, 121, 315
 James, W.P. 69, 91, 315
 Janes, M. 290, 315
 Kaatz, K.J. 69, 91, 315
 Karcz, I. 95, 315
 Kells, J.A. 291, 315
 Keulegan, G.H. 116, 315
 Khatibi, R.H. 167, 290, 316
 Kindsvater, C.E. 81, 84, 90, 316
 Kingston, G. 166, 313
 Kitagawa, A. 98, 103, 316
 Kline, S.J. 94, 316
 Knight, D.W. 1, 5, 8, 9, 26, 28, 29, 37, 38, 40, 44–7, 51, 52, 55, 57, 58, 60, 64–9, 71, 75, 82, 85, 87, 88, 90, 93, 97, 105, 107, 111–3, 115, 117, 120–3, 125, 130, 137, 140, 214, 216, 258, 259, 261–3, 268, 270, 274, 284–6, 288, 305, 306, 308–10, 313, 314, 316–21, 323–6, 328, 329
 Kolkman, P.A. 42, 318
 Kouwen, N. 244, 318
 Krishnamurthy, M. 106, 318
 Kuga, T. 97, 314
 Kutter, W.R. 106, 312
 Lamb, R. 88, 307, 318, 319
 Lambert, M.F. 60, 67, 111, 318
 Larock, B.E. 42, 318
 Latapie, A. 167, 206, 290, 318
 Laurensen, E.M. 29, 35, 318
 Leggett, D.J. 11, 318
 Leopold, L.B. 111, 318
 Li, H. 37, 311
 Li, R.M. 244, 318
 Liao, H. 3, 4, 47, 68, 318, 319
 Lighthill, M.J. 94, 319
 Liu, H.K. 259, 319
 Lotter, G.K. 106, 111, 112, 319
 Lumley, J.L. 272, 326
 Lyness, J.F. 27, 60–3, 318, 320
 MacDonald, J.A. 51, 117, 317
 Malalaskera, W. 266, 271, 272, 327
 Manning, R. 9, 16, 17, 19, 20, 24, 30, 32, 34, 35, 50, 57–60, 62, 63, 66, 105, 106, 111–3, 115, 117, 134, 135, 146, 147, 149, 150, 154, 160, 171, 188, 195, 199, 200, 202, 203, 205, 215–8, 222, 223,

- 229, 233, 238, 241,
244–9, 258, 284, 288,
291, 308, 319, 321, 329
- Mantz, P.A. 8, 69, 88, 226,
307, 318, 319
- Mason, P.D. 29, 57–9, 106,
215, 314
- Matthai, H.F. 81, 84, 90,
319
- May, R.W.P. 69, 312, 319
- McEwan, I.K. 1, 26, 261–3,
266, 271, 289, 315
- Mc Gahey, C. 8, 45, 59,
61–3, 68, 110, 111, 113,
118–21, 124, 126, 135,
167, 185, 187, 206, 210,
251, 263, 276, 283, 284,
290, 310, 311, 319
- Melville, B.W. 263, 319
- Merrett, D.J. 60, 111, 328
- MIKE11 112, 267, 319
- Miller, D.S. 72, 318, 320
- Miller, J.B. 1, 320
- Molinas, A. 77, 329
- Montes, J.S. 149, 150, 320
- Moody, L.F. 31, 32, 107,
320
- Morvan, H. 26, 30, 67, 258,
270, 271, 320, 321, 328
- Muralidhar, D. 97, 322
- Muto, Y. 96, 97, 100, 101,
320, 325
- Myers, W.R.C. 27, 60–3, 67,
69, 111, 318, 320
- Naden, P.S. 244, 290, 320
- Nagler, F.A. 71, 90, 320
- Nakagawa, H. 26, 37, 93,
94, 96, 105, 121, 201,
266, 271, 321, 326
- Nakato, T. 25, 272, 285,
286, 316, 320
- Navratil, O. 29, 320
- National Rivers Authority
10, 12, 320
- Neill, C.R. 42, 320
- Newton, I. 23, 137, 139, 320
- Nezu, I. 26, 37, 93, 94,
96–8, 105, 121, 201, 266,
271, 321, 326
- Nikora, V. 272, 321, 325
- Nikuradse, J. 31, 39, 106,
116, 119, 321
- NIRA 185, 321
- Novak, P. 42, 321
- Occam, W. 273
- O'Hare, M.T. 250–3, 255,
290, 319, 321
- Okada, S. 29, 103, 321
- Omran, M. 45, 47, 54–7, 97,
122, 123, 317, 321
- Oshikawa, H. 28, 321
- Overton, D.E. 111, 329
- Palmer, V.J. 244, 322, 323
- Pavlovskii, N. 106, 322
- Perkins, H.J. 96, 322
- Petryk, S. 244, 322
- Pitt, M. 5, 183, 322
- Playan, E. 266, 313, 316
- Powell, R.W. 106, 322
- Prandtl, L. 31, 38, 39, 95–7,
107, 114, 272, 322
- Preissmann, A. 270, 274,
309, 322
- Press, W.H. 138, 322
- Rajaratnam, N. 42, 75, 97,
322
- Raju, K.G.R. 153, 306, 313,
322
- Rameshwaran, R. 111, 320,
322
- Ramette, M. 214, 322
- Ramsbottom, D. 42, 69, 72,
78, 85, 86, 291, 292, 309,
319, 322, 324
- Ranga Raju, K.G. 260, 306,
313, 322
- Raudkivi A.J. 104, 258–60,
322
- Raven, P.J. 109, 290, 323
- Ree, W.O. 244, 323
- ReFEH 45, 323
- Rehbock, T. 90, 323
- Reinius, E. 116, 323
- Reynolds, A.J. 75, 93, 201,
323
- Rezaei, B. 29, 82, 102, 323
- Rhodes, D.G. 107, 121, 323
- Riley, N. 45, 113, 311
- Riis, T. 290, 306
- Roberts, J.D. 87, 323
- Rodi, W. 97, 271, 273, 321,
323
- Rouse, H. 116, 323
- Rozovskii, I.L. 96, 111, 323
- Samuels, P.G. 1, 5, 8, 28, 29,
36, 44, 69, 75, 85, 119,
120, 124, 126, 130, 137,
- 138, 162, 163, 169, 189,
271, 274, 275, 306, 310,
311, 313, 317, 319, 323–6
- Sayers, P.B. 162, 312, 324,
326
- Sayre, W.W. 116, 324
- Schlichting, H. 31, 37, 45,
75, 107, 113, 324
- Schmidt, A.R. 68, 324
- Seckin, G. 69, 88, 90, 140,
306, 324
- Seed, D.J. 44, 324
- Sellin, R.H.J. 9, 29, 30, 44,
82, 87, 98, 100, 102, 290,
312, 317, 324, 328
- Senturk, F. 260, 325
- SEPA 185, 324
- Shamseldin, A. 1, 5, 308,
316, 317, 324
- Sharifi, S. 47, 275, 324
- Shaw, E.M. 270, 324
- Shen, H.W. 258, 260, 325
- Shields, A. 259, 262, 325
- Shiono, K. 8, 9, 38, 45, 46,
60, 87, 96, 97, 100, 101,
107, 111–3, 122, 123,
285, 317, 318, 325, 328
- Simons, D.B. 260, 325
- Solomatine, D. 161, 313
- Sooky, A.A. 97, 111, 326
- Spooner, J. 112, 123, 325
- Statzner, B. 244, 325
- Stearns, F.P. 95, 325
- Stokes, G.G. 94, 325
- Strickler, A. 106, 117, 325
- Sturm, T.W. 69, 75, 149,
307, 325
- Subramanya, K. 42, 322
- Tagg, A.F. 8, 325
- Tang, X. 29, 45, 55, 111,
112, 122, 125, 261, 270,
276, 317, 320, 326
- Tennekes, H. 272, 326
- Theodorsen, T. 94, 95, 326
- Thijssse, J.T. 116, 326
- Thorne, C.R. 26, 260, 307,
310, 312, 326
- Toebes, G.H. 97, 111, 326
- Tominaga, A. 47, 54–6, 97,
326
- Townend, I.H. 11, 326
- Tracy, H.J. 90, 316
- Tullis, B.P. 291, 313, 327
- Tsikata, J.M. 266, 327

- USBPR 70, 71, 74, 150–2,
327
- USGS 70, 82, 84, 85, 88–92,
221, 222, 224–6, 309,
318, 327
- Valetin, F. 42, 312
- Vanoni, V.A. 95, 327
- van Beesten, D.P. 30, 290,
324
- van Prooijen, B.C. 98, 100,
112, 327
- van Rijn, L.C. 259, 327
- Verheij, H.J. 104, 314
- Versteeg, H.K. 266, 271,
272, 327
- Vidal, J.P. 44, 327
- Vreugdenhil, C.B. 266, 274,
327
- Wang, S. 26, 310, 314, 316,
326, 327
- Wark, J.B. 10, 63, 112, 114,
121, 310, 315, 327
- Westlake, D.F. 290, 327
- Weisbach, J. 31, 33, 46, 106,
115, 117, 327
- White, C.M. 31, 32, 107,
115–20, 138, 214, 216,
262, 307, 309
- White, W.R. 259–61, 292,
305–7, 323, 325, 327–9
- Whitehead, E. 244, 328
- Whitlow, C.D. 274, 292,
322, 328
- Willettts, B.B. 111, 322, 324
- Wormleaton, P.R. 60, 67,
111, 120, 263, 316, 328
- Wright, J.F. 244, 249, 250,
255, 328
- Wright, N.G. 267, 320, 328
- WSPRO 70, 141, 328
- Wu, B. 77, 328, 329
- Yalin, M.S. 260, 329
- Yang, C.T. 260, 329
- Yarnell, D.L. 71, 90, 329
- Yen, B.C. 16, 26, 30, 59, 60,
68, 106, 107, 111, 116,
324, 329
- Yu, G. 263, 288, 317, 329
- Yuen, K.W.H. 37, 54–6, 75,
317, 318, 329
- Zech, Y. 29, 112, 308, 313,
314, 321
- Zegzhda, A.P. 116, 329
- Zienkiewick, O.C. 135, 136,
329

Subject index

- afflux 59–86, 88
Afflux Estimation System (AES) 6, 8–9, 12, 14, 88–92, 171, 186–9, 266, 275–6, 280 examples 156, 221–43 governing equations 146–57, 299–300 methods 140–61 software 178–81 software architecture 276–82
- backwater 7, 36–7, 42–3, 138–9, 141–4, 149, 150, 155, 158–60, 184–5, 188–9, 218–21, 221, 227, 233, 279
backwater module (BM) 6, 7, 69, 170, 175–7, 179, 181, 279
bankfull flow 27, 29, 60–1, 65–6, 124, 127, 128, 131, 143, 186, 190–2, 198, 203, 249, 250
blockage 235, 263–6, 291
boundary layers 37, 81, 93–4
boundary shear stress 33, 38, 51, 113–5, 123, 134–5, 262
boundary shear stress distributions 7, 37–8, 52–6, 60, 97, 258, 276, 288
braided channels 103, 128–9
bridges 3, 13, 41–4, 69–77
 afflux 69–70
 eccentricity, e 81–2
 flow modes 141–3
 governing equations 146–57, 299–300
 opening ratio, M 79–81
 opening types 147
 skewness, ϕ 82–4
 transition lengths 151–5
 transition losses 155–7
- calibration 26, 44–5, 47, 52–3, 123, 156, 165, 169, 172, 186, 188–9, 273–5
CAPM 243, 290
Chezy equation 31, 105–6, 111–2, 115, 258, 289
CIRIA 143, 147, 158–60, 234, 266, 291
CIWEM 72, 85
climate change 28, 87, 166, 201, 293
COHerence Method (COHM) 60, 124, 262
coherent structures 97–100, 122
Colebrook White equation 31, 32, 107, 115–9, 138, 214–6
compound channels 9, 10, 27, 69, 72, 85, 89, 97, 101–2, 111
controls 42
conveyance 35, 110
Conveyance Estimation System (CES) 110–33, 169–81
 governing equations 113, 129–30, 295–7
 hydrostatic pressure term 114
 boundary friction 114–9
 conversion of n to k_s 116
 conversion of k_s to f 119
 parameter, f 46–7, 52–4, 56, 67, 114–5, 131, 275
 parameter, λ 46–7, 52–4, 119–20, 131, 186, 275
 parameter, Γ 46–7, 49, 52–4, 122–4, 128, 131, 186, 275
 software 169–181
 software architecture 276–82
Conveyance Generator (CG) 6, 170, 175
critical depth, h_c 17, 19, 22, 36
culverts 66, 77–9
 blockages 86, 263
 energy losses 157
 flow modes 144–5
 governing equations 146–57, 299–300
- Darcy-Weisbach equation 31, 115, 117
data 44, 87–92, 301–4
 and websites www.flowdata.bham.ac.uk, www.river-conveyance.net
Defra/EA 6, 11–2, 14, 29, 71, 108–10, 113, 116, 122, 127–9, 162, 185, 244, 245, 247, 258, 290

- depth-averaged velocity 39, 41, 46–8, 112, 130, 135
 depth-averaged eddy viscosity, $\bar{\varepsilon}_{yx}$ 46
 dimensionless eddy viscosity, λ 46, 48, 119–20, 131
 Divided Channel Method (DCM) 60, 67, 110, 146, 148, 262, 291
- EA 4, 190
 ecological issues 255–8
 eddy viscosity, ε 46
 energy 15, 20–2, 33–5
 energy correction coefficient, α 39–40, 134–5
 Environment Agency (EA) 4–6, 9, 11–2, 164, 183, 190, 243, 265
- FEH 45
 FHWA 70, 143–4, 158, 160
 floodplains 10, 27, 60, 66, 72, 88, 101–2, 128–9
 floods 1–5, 28, 60, 89–91, 283
 FLOODSITE 87, 89
 Flood Channel Facility (FCF) 9, 10, 44, 87, 112, 116, 121, 123, 127, 211, 275, 289
 Flood Estimation Handbook (FEH) 45
 flow structures 29, 37–8, 59, 93–105
 FORESIGHT 87, 89
 friction factor, f 31–3, 46, 60, 67, 276, 287
 global 60, 67, 276
 local 60, 67, 114–5, 275
 zonal 60, 67, 276
 Froude Number (Fr) 17, 19, 35, 134, 154, 200
- geomorphological issues 258–63
 governing equations: CES 113, 129–30, 295–7; AES 146–57, 299–300
 Gradually Varied Flow (GVF) 35–7, 268
- HEC-RAS 112, 147–52, 267
 hydraulic jump 20–5, 75, 141, 144, 153
- ICE 11
 inbank flow 37–8, 47, 57–9, 60, 65, 103, 120, 122, 123, 127, 189–90, 245, 261
 insurance 168, 184–5
 IPCC 166
 ISIS 9, 112–3, 161, 171, 185, 230–3, 267
 ISO 68–9
 isovels 38
- lateral momentum transfer 29, 102, 103
 main channel 27, 60, 66–7, 95–105
 Manning equation 9, 16, 20, 24, 112–3, 115, 135, 244–5
 Manning's n 16, 19, 32, 57–9, 62–3, 66, 105–6, 117, 134, 188, 195, 199–200, 202–3, 205, 215–8, 222–3, 229, 233, 241, 244–9, 288, 291
 meandering channels 9, 11, 30, 45, 60, 96–103, 111, 122, 124–8, 175, 186, 206
 modelling 6, 9, 15, 24–9, 37, 42, 44, 45, 47, 57, 65, 69, 86, 112–3, 128–9, 161, 164, 171, 175, 184–5, 266–75, 284–5, 287, 291, 293
 momentum 15, 20–1, 23–5, 33, 39, 40, 41, 70, 82, 85–6, 98–103, 105, 111, 134, 267–8, 270, 272
 momentum function 23–4
 momentum correction coefficient, β 21, 39, 40, 134
 Moody diagram 31–2, 107
- National Rivers Authority (NRA) 10, 12
 natural channels 8, 41, 46–7, 57–60, 117–9, 121, 123–5, 258
 Navier-Stokes equations 19, 45, 96, 112–3, 284–6
 Nikuradse roughness size, k_s 31, 39, 106, 116, 119
 non-prismatic channels 29, 36, 102
 normal depth, h_n 16–9, 36, 69, 81, 138–40, 141, 144, 152, 155, 218
- overbank flow 26, 37–8, 45–6, 59–68, 82, 87, 97, 103, 123–4, 127–8, 190, 211, 261–3, 273, 275, 284, 287–9
- PHABSIM 256, 258
 power 22, 23
 Prandtl's logarithmic velocity laws 31, 38–9, 114
 prismatic channels 24, 26–7, 33, 36, 40, 45, 60, 82, 85, 122–3, 258, 268–9
- RANS equations 45, 112–3, 130, 271–2, 285–6
 rating curves 7, 34, 148, 157–8, 224, 229, 243, 288, 291, 292, 293
 rectangular channels 19–24, 47–9, 50–4
 ReFEH 45
 research ideas 289–93
 resistance laws 29–33, 105–7
 Chezy equation 31, 106
 Colebrook-White equation 31, 107, 115
 Darcy-Weisbach equation 31, 106, 115
 Manning equation 16, 31, 106

- Reynolds Number (Re) 7, 31–2, 115, 134, 201
RHABSIM 256
 rivers: Avon, UK 42, 138
 Avon, Enford, UK 244, 249–51
 Blackwater, Hampshire, UK 30, 177–9
 Cole, Birmingham, UK 244, 244–9
 Colorado, La Pampas, Argentina 192–5
 Hooke, Maiden Newton, UK 244, 252–4
 Irwell, Salford, UK 227–33
 Main, County Antrim, UK 27, 60–3, 68, 146, 175–7, 195–201, 218–21, 233
 Ngunguru, New Zealand 57–9
 Pea Creek, Alabama, USA 221–6
 Penk, Penkrige, UK 186–7
 Severn, UK 2, 4, 27, 28, 64–9, 138, 201–5
 Suela, Cordoba, Argentina 205–13
 Tomebamba, Ecuador 213–18
 Trent, Yoxall, Staffordshire, UK 189–91
 Waiwakaiho, New Zealand 213–8
 River Habitat Survey (RHS) 6, 109, 174, 195, 290
 roughness 15, 29, 93–5, 105, 183, 214
 roughness & resistance 15, 26, 29–33, 105–10, 200, 205, 214, 217
 roughness values 16, 19, 20, 32, 53, 56, 58–9, 63, 65–8, 108, 118–9, 120, 171–4, 187, 190, 192, 195–6, 200, 202, 205–6, 208, 214–7, 221, 229, 233, 245–7, 250, 253
 unit roughness 6, 62, 68, 105–10, 116–8, 167, 171–4, 187, 190, 192, 195–6, 202, 205–6, 208, 215–6, 221, 229, 233, 245, 246, 250, 253
 Roughness Advisor (RA) 6–7, 12, 29, 105–10, 121, 170–4, 184, 276–8, 284, 290
 rounding 80–1, 84
 schematization 26–9
 secondary flows 38–9, 45–6, 55–6, 95–7, 122–8
 secondary flow term, Γ 46–7, 53–4, 122–4, 128, 131, 186
 shear velocity 7, 32–3, 39, 46, 114–5, 134–5, 261–2, 292
 Shiono & Knight Method, (SKM) 8, 45–6, 47, 49, 54–6, 112, 113
 basic equations 45–7, 113
 examples 50–7, 58–9, 61–3, 67–8
 parameter, f 46–7, 52–4, 56, 67, 114–5, 131, 275
 parameter, λ 46–7, 52–4, 119–20, 131, 186, 275
 parameter, Γ 46–7, 49, 52–4, 122–4, 128, 131, 186, 275
 Single Channel Method (SCM) 16, 51, 60, 110
 slopes 33
 bed slope 16, 33–5, 114, 184
 energy slope 33–5, 110
 friction slope 33–5, 110
 water surface 33–5, 110, 184
 specific energy 15, 20–1, 22–3, 34, 75–6
 Stage-discharge relationships 9, 57–9, 61–2, 68, 175, 183, 186, 189–221, 247, 260–3, 269, 288–9
 trapezoidal channels 11, 16–8, 27, 38, 40, 47, 50, 54–7, 85, 116
 trash screens 263–6
 turbulence 9, 44, 67, 93, 105, 107, 113–4, 119, 122, 201, 271–3, 275, 285–6
 types of model 266–73
 uncertainty 63, 161–9, 275, 290
 within CES 166–9, 170, 189
 representation 176, 183
 Uncertainty Estimator (UE) 6–7, 63, 276, 284, 289
 unit roughness 6, 62, 68, 105–10, 116–8, 167, 171–4, 187, 190, 192, 195–6, 202, 205–6, 208, 215–6, 221, 229, 233, 245, 246, 250, 253
 USBPR 70–1, 74, 150–2
 USGS 70, 82, 84, 85, 88–92, 221–6
 velocity 17, 31, 34, 37–41, 45–6, 134, 139, 177
 velocity distributions, lateral 6, 26, 29, 37–8, 45–9, 55, 61, 67, 95, 177, 189–221, 248, 253–4
 velocity distributions over a vertical 37–9, 94–5
 vorticity 29, 46, 93–105
 planform 46, 97–100, 275
 streamwise 46, 96, 103
 Water Framework Directive (WFD) 5, 256, 283
 worked examples 16–7, 19, 20, 22, 50, 52–4, 189, 192, 195, 201, 205, 213, 218, 221, 227, 233, 235, 244, 249, 252